Cell Journal (Yakhteh)

Guide for Authors

Aims and Scope: The "Cell Journal (Yakhteh)" is a peer review and quarterly English publication of Royan Institute of Iran. The aim of the journal is to disseminate information through publishing the most recent scientific research studies on exclusively Cellular, Molecular and other related topics. **Cell J**, has been certified by the Ministry of Culture and Islamic Guidance since 1999 and also accredited as a scientific and research journal by HBI (Health and Biomedical Information) Journal Accreditation Commission since 2000 which is an open access journal. **This journal holds the membership of the Committee on Publication Ethics (COPE) and the International Committee of Medical Journal Editors (ICMJE).**

1. Types of articles

The articles in the field of Cellular and Molecular can be considered for publications in **Cell J.** These articles are as below:

A. Original articles

Original articles are scientific reports of the original research studies. The article consists of English Abstract (structured), Introduction, Materials and Methods, Results, Discussion, Conclusion, Acknowledgements, Author's Contributions, and References **(Up to 40).**

B. Review articles

Review articles are the articles written by well experienced authors and those who have excellence in the related fields. The corresponding author of the review article must be one of the authors of at least three published articles appearing in the references. The review article consists of English Abstract (unstructured), Introduction, Conclusion, Author's Contributions, and References **(Up to 70).**

C. Systematic reviews

Systematic reviews are a type of literature review that collect and critically analyzes multiple research studies or papers. The Systematic reviews consist of English Abstract (unstructured), Introduction, Materials and Methods, Results, Discussion, Conclusion, Acknowledgements, Author's Contributions, and References **(Up to 70).**

D. Short communications

Short communications are articles containing new findings. Submissions should be brief reports of ongoing researches. The short communication consists of English Abstract (unstructured), the body of the manuscript (should not hold heading or subheading), Acknowledgements, Author's Contributions, and References **(Up to 30).**

E. Case reports

Case reports are short discussions of a case or case series with unique features not previously described which make an important teaching point or scientific observation. They may describe novel techniques or use equipment, or new information on diseases of importance. It consists of English Abstracts (Unstructured), Introduction, Case Report, Discussion, Conclusion , Acknowledgements, Author's Contributions, and References **(Up to 30).**

F. Editorial

Editorial should be written by either the editor in chief or the editorial board.

G. Imaging in biology

Images in biology should focus on a single case with an interesting illustration such as a photograph, histological specimen or investigation. Color images are welcomed. The text should be brief and informative.

H. Letter to the editors

Letter to editors are welcome in response to previously published **Cell J** articles, and may also include interesting cases that do not meet the requirement of being truly exceptional, as well as other brief technical or clinical notes of general interest.

I. Debate.

2. Submission process

It is recommended to see the guidelines for reporting different kinds of manuscripts here. This guide explains how to prepare the manuscript for submission. Before submitting, we suggest authors to familiarize themselves with **Cell J** format and content by reading the journal via the website (www.celljournal.com). The corresponding author ensures that all authors are included in the author list and agree with its order, and they must be aware of the manuscript submission.

A. Author contributions statements

It is essential for authors to include a statement of responsibility in the manuscript that specifies the contribution of every one of them. This participation must include conception and design of the manuscript, data acquisition or data analysis and interpretation, drafting of the manuscript and/or revising it for critically important intellectual content, revision and final approval of the manuscript and statistical analysis, obtaining funding, administrative, technical, or material support, or supervision. Authors who do not meet the above criteria should be acknowledged in the **Acknowledgments section.**

B. Cover letter

Each manuscript should be accompanied by a cover letter, signed by all authors specifying the following statement: "The manuscript has been seen and approved by all authors and is not under active consideration for publication. It has neither been accepted for publication nor published in another journal fully or partially (except in abstract form). I hereby assign the copyright of the enclosed manuscript to **Cell J.** Corresponding author must confirm the proof of the manuscript before online publishing. Also, is it needed to suggest three peer reviewers in the field of their manuscript.

C. Manuscript preparation

Authors whose first language is not English encouraged to consult a native English speaker in order to confirm his manuscripts to American or British (not a mixture) English usage and grammar. It is necessary to mention that we will check the plagiarism of your manuscript by iThenticate Software. The manuscript should be prepared in accordance with the "International Committee of Medical Journal Editors (ICMJE)". Please send your manuscript in two formats Word and Pdf (including: title, name of all the authors with their degree, abstract, full text, references, tables and figures) and Also send tables and figures separately in the site. The abstract and text pages should have consecutive line numbers in the left margin beginning with the title page and continuing through the last page of the written text. Each abbreviation must be defined in the abstract and text when they are mentioned for the first time. Avoid using abbreviation in the title. Please use the international and standard abbreviations and symbols

It should be added that an essential step toward the integration and linking of scientific information reported in published literature is using standardized nomenclature in all fields of science and medicine. Species names must be italicized (*e.g., Homo sapiens*) and also the full genus and species written out in full, both in the title of the manuscript and at the first mention of an organism in a paper.

It is necessary to mention that genes, mutations, genotypes, and alleles must be indicated in italics. Please use the recommended name by consulting the appropriate genetic nomenclature database, e.g., HUGO for human genes. In another words; if it is a human gene, you must write all the letters in capital and italic (*e.g., OCT4, c-MYC*). If not, only write the first letter in capital and italic (*e.g., Oct4, c-Myc*). **In addition, protein designations are the same as the gene symbol but are not italicized.**

Of note, Cell J will only consider publishing genetic association study papers that are novel and statistically robust. Authors are advised to adhere to the recommendations outlined in the STREGA statement (http://www.strega-statement.org). The following criteria must be met for all submissions:

1. Hardy-Weinberg Equilibrium (HWE) calculations must be carried out and reported along with the P-values if applicable [see Namipashaki et al. 2015 (Cell J, Vol 17, N 2, Pages: 187-192) for a discussion].

2. Linkage disequilibrium (LD) structure between SNPs (if multiple SNPs are reported) must be presented.

3. Appropriate multiple testing correction (if multiple independent SNPs are reported) must be included.

Submissions that fail to meet the above criteria will be rejected before being sent out for review.

Each of the following manuscript components should begin in the following sequence:

Authors' names and order of them must be carefully considered (full name(s), highest awarded academic degree(s), email(s), and institutional affiliation(s) of all the authors in English. Also, you must send mobile number and full postal address of the corresponding author).

Changes to Authorship such as addition, deletion or rearrangement of author names must be made only before the manuscript has been accepted in the case of approving by the journal editor. In this case, the corresponding author must explain the reason of changing and confirm them (which has been signed by all authors of the manuscript). If the manuscript has already been published in an online issue, an erratum is needed.

Title is providing the full title of the research (do not use abbreviations in title).

Running title is providing a maximum of 7 words (no more than 50 characters).

Abstract must include Objective, Materials and Methods, Results, and Conclusion (no more than 300 words).

Keywords, three to five, must be supplied by the authors at the foot of the abstract chosen from the Medical Subject Heading

(MeSH). Therefore; they must be specific and relevant to the paper.

The following components should be identified after the abstract:

Introduction: The Introduction should provide a brief background to the subject of the paper, explain the importance of the study, and state a precise study question or purpose.

Materials and Methods: It includes the exact methods or observations of experiments. If an apparatus is used, its manufacturer's name and address should be stipulated in parenthesis. If the method is established, give reference but if the method is new, give enough information so that another author can perform it. If a drug is used, its generic name, dose, and route of administration must be given. Standard units of measurements and chemical symbols of elements do not need to be defined.

Statistical analysis: Type of study and statistical methods should be mentioned and specified by any general computer program used.

Ethical considerations*:* Please state that informed consent was obtained from all human adult participants and from the parents or legal guardians of minors and include the name of the appropriate institutional review board that approved the project. It is necessary to indicate in the text that the maintenance and care of experimental animals complies with National Institutes of Health guidelines for the humane use of laboratory animals, or those of your Institute or agency.

Clinical trial registration: All of the Clinical Trials performing in Iran must be registered in Iranian Registry of Clinical Trials (www.irct.ir). The clinical trials performed abroad, could be considered for publication if they register in a registration site approved by WHO or www.clinicaltrials.gov. If you are reporting phase II or phase III randomized controlled trials, you must refer to the CONSORT Statement for recommendations to facilitate the complete and transparent reporting of trial findings. Reports that do not conform to the CONSORT guidelines may need to be revised before peer-reviewing.

Results: They must be presented in the form of text, tables, and figures. Take care that the text does not repeat data that are presented in tables and/or figures. Only emphasize and summarize the essential features of the main results. Tables and figures must be numbered consecutively as appeared in the text and should be organized in separate pages at the end of the manuscript while their location should be mentioned in the main text.

Tables and figures: If the result of your manuscript is too short, it is better to use the text instead of tables & figures. Tables should have a short descriptive heading above them and also any footnotes. Figure's legend should contain a brief title for the whole figure and continue with a short explanation of each part and also the symbols used (no more than 100 words). All figures must be prepared based on cell journal's guideline in color (no more than 6 Figures and Tables) and also in GIF or JPEG format.

Of Note: Please put the tables & figures of the result in the results section not any other section of the manuscript.

Supplementary materials would be published on the online version of the journal. This material is important to the understanding and interpretation of the report and should not repeat material within the print article. The amount of supplementary material should be limited. Supplementary material should be original and not previously published and will undergo editorial and peer review with the main manuscript. Also, they must be cited in the manuscript text in parentheses, in a similar way as when citing a figure or a table. Provide a legend for each supplementary material submitted.

Discussion: It should emphasize the present findings and the variations or similarities with other researches done by other researchers. The detailed results should not be repeated in the discussion again. It must emphasize the new and important aspects of the study.

Conclusion: It emphasizes the new and important aspects of the study. All conclusions are justified by the results of the study.

Acknowledgements: This part includes a statement thanking those who contributed substantially with work relevant to the study but does not have authorship criteria. It includes those who provided technical help, writing assistance and name of departments that provided only general support. You must mention financial support in the study. Otherwise; write this sentence "There is no financial support in this study".

Conflict of interest: Any conflict of interest (financial or otherwise) and sources of financial support must be listed in the Acknowledgements. It includes providers of supplies and services from a commercial organization. Any commercial affiliation must be disclosed, regardless of providing the funding or not.

References: The references must be written based on the Vancouver style. Thus the references are cited numerically in the text and listed in the bibliography by the order of their appearance. The titles of journals must be abbreviated according to the style used in the list of Journals Indexed in PubMed. Write surname and initials of all authors when there are six or less. In the case of seven or more authors, the names of the first six authors followed by "et al." must be listed. You can download Endnote file for Journal references style: endnote file

The reference of information must be based on the following order:

Article:

Surname(s) and first letter of name &middle name(s) of author(s) .Manuscript title. Journal title (abbr).publication date (year); Volume & Issue: Page number.

Example: Manicardi GC, Bianchi PG, Pantano S, Azzoni P, Bizzaro D, Bianchi U, et al. Presence of endogenous nicks in DNA of ejaculated human spermatozoa and its relationship to chromomycin A3 accessibility. Biol Reprod. 1995; 52(4): 864-867.

Book:

Surname(s) and first letter of name & middle name(s) of author(s).Book title. Edition. Publication place: publisher name; publication date (year); Page number.

Example: Edelman CL, Mandle CL. Health promotion throughout the lifespan. 2nd ed. ST Louis: Mosby; 1998; 145-163.

Chapter of book:

Surname(s) and first letter of name & middle name(s) of author(s).Chapter title. In: Surname(s) and first letter of name & middle name(s) of editor(s), editors. Book title. Edition. Publication place: publisher name; publication date (year); Page number.

Example: Phillips SJ, Whisnant JP. Hypertension and stroke. In: Laragh JH, Brenner BM, editors. Hypertension: pathophysiology, diagnosis, and management. 2nd ed. New York: Raven Press; 1995; 465-478.

Abstract book:

Example: Amini rad O.The antioxidant effect of pomegranate juice on sperm parameters and fertility potential in mice. Cell J. 2008;10 Suppl 1:38.

Thesis:

Name of author. Thesis title. Degree. City name. University. Publication date (year).

Example: Eftekhari Yazdi P. Comparison of fragment removal and co-culture with Vero cell monolayers on development of human fragmented embryos. Presented for the Ph.D., Tehran. Tarbiyat Modarres University. 2004.

Internet references

Article:

Example: Jahanshahi A, Mirnajafi-Zadeh J, Javan M, Mohammad-Zadeh M, Rohani M. Effect of low-frequency stimulation on adenosineA1 and A2A receptors gene expression in dentate gyrus of perforant path kindled rats. Cell J. 2008; 10 (2): 87-92. Available from: http://www.celljournal.org. (20 Oct 2008).

Book:

Example: Anderson SC, Poulsen KB. Anderson's electronic atlas of hematology.[CD-ROM]. Philadelphia: Lippincott Williams & Wilkins; 2002.

D. Proofs are sent by email as PDF files and should be checked and returned within 72 hours of receipt. It is the authors' responsibility to check that all the text and data as contained in the page proofs are correct and suitable for publication. **We are requested to pay particular attention to author's names and affiliations as it is essential that these details be accurate when the article is published.**

E. Pay for publication: Authors do not have to pay any Manuscript Processing Charge or Open Access Publication Fee. **Before publishing author's article, it would be the author's responsibility to pay for the expenses, if the editor feels the level of English used in the manuscript requiresediting.**

F. Ethics of scientific publication: Manuscripts that have been published elsewhere with the same intellectual material will refer to duplicate publication. If authors have used their own previously published work or work that is currently under review, as the basis for a submitted manuscript, they are required to cite the previous work and indicate how their submitted manuscript offers novel contributions beyond those of the previous work. Research and publication misconduct is considered a serious breach of ethics.

The Journal systematically employs iThenticate, plagiarism detection and prevention software designed to ensure the originality of written work before publication. Plagiarism of text from a previously published manuscript by the same or another author is a serious publication offence. Some parts of text may be used, only where the source of the quoted material is clearly acknowledged.

3. General information

A. You can send your manuscript via online submission system which is available on our website. If the manuscript is not prepared according to the format of **Cell J**, it will be returned to authors.

B. The order of article appearance in the Journal is not demonstrating the scientific characters of the authors.

C. Cell J has authority to accept or reject the manuscript.

D. The received manuscript will be evaluated by associate editor. **Cell J** uses a single-blind peer review system and if the manuscript suits the journal criteria, we will select the reviewers. The reviwers of the manuscript must not share information of the review with anyone without permission of the editors and authors. If three reviewers pass their judgments on the manuscript, it will be presented to the editorial board of **Cell J.** If the editorial board has a positive judgment about the manuscript, reviewers' comments will be presented to the corresponding author (the identification of the reviewers will not be revealed). The executive member of journal will contact the corresponding author directly within 3-4 weeks by email. If authors do not receive any reply from journal office after the specified time, they can contact journal office. Finally, executive manager will respond promptly to authors' request.

The Final Checklist

The authors must ensure that before submitting the manuscript for publication, they have to consider the following parts:

1. Title page should contain title, name of the author/coauthors, their academic qualifications, designation & institutions they are affiliated with, mailing address for future correspondence, email address, phone, and fax number.

2. Text of manuscript and References prepared as stated in the "guide for authors" section.

3. Tables and figures should be uploaded separately except in the main manuscript. Figures must be sent in color and also in GIF or JPEG format with 300 dpi resolutions.

4. Cover Letter should be uploaded with signature of all authors.

5. Ethical committee letter should be inserted at the end of cover letter.

The Editor-i ini, Ph.D.

Cell Journal (Yakhteh),

P.O. Box: 16635-148, Iran

Tel/Fax: + 98-21-22510895

Emails: Celljournal@royaninstitute.org

info@celljournal.org

Dr. Saeed Kazemi Ashtiani

IN THE NAME OF GOD

Gone But not Forgotten

In the memory of the late Director of Royan Institute, Founder of Stem Cells Research in Iran and Chairman of ***Cell Journal*** *(Yakhteh)*. May he rest in peace.

PUBLISHED & SPONSORED BY:
Publication of Royan Institute (ACECR)

Indexed in:
1. Thomson Reuters (ISI); *Impact Factor: 2.046*
2. PubMed
3. PubMed Central (PMC)
4. National Library Medicine (NLM)
5. Biosis Preview
6. Index Medicus for the Eastern Mediterranean Region (IMEMR)
7. Regional Information Center for Sciences and Technology (RICeST)
8. Index Copernicus International
9. Cambridge Scientific Abstract (CSA)
10. EMBASE
11. Scopus
12. Cinahl Database
13. Google Scholar
14. Chemical Abstract Service (CAS)
15. Proquest
16. Directory of Open Access Journals (DOAJ)
17. Open Academic Journals Index (OAJI)
18. Directory of Research Journals Indexing (DRJI)
19. Scientific Information Database (SID)
20. Iranmedex
21. Islamic World Science Citation Center (ISC)
22. Magiran
23. Science Library Index
24. Biological Abstracts
25. Essential Science Indicators
26. EuroPub

Editorial Office Address (Dr. Ahmad Hosseini):
Royan Institute, P.O.Box: 16635-148,
Tehran, Iran
Tel & Fax: (+9821)22510895
Website: www.celljournal.org
Emails: info@celljournal.org
celljournal@royaninstitute.org

Printing Company:
Naghshe e Johar Co.
No. 103, Fajr alley, Tehranpars Street,
Tehran, Iran.

Cell Journal (Yakhteh), Vol 22, No 4, Janury-March (Winter) 2021, Serial Number: 88, Pages: 401-574

CONTENTS

Original Articles

Letter to The Editor

Original Article

The Immunomodulatory Effect of Radiofrequency Electromagnetic Field on Serum Cytokine Levels in A Mouse Model of Hindlimb Unloading

Sima Aghajari, M.Sc.[1#], Sayed Mohammad Javad Mortazavi, Ph.D.[2#], Mehdi Kalani, Ph.D.[3, 4], Samaneh Nematolahi, Ph.D.[5], Parham Habibzadeh, M.D.[6, 7], Shirin Farjadian, Ph.D.[3*]

1. Department of Radiology, Shiraz University of Medical Sciences, Shiraz, Iran
2. Department of Medical Physics, Shiraz University of Medical Sciences, Shiraz, Iran
3. Department of Immunology, Shiraz University of Medical Sciences, Shiraz, Iran
4. Professor Alborzi Clinical Microbiology Research Center, Shiraz University of Medical Sciences, Shiraz, Iran
5. Department of Biostatistics, Shiraz University of Medical Sciences, Shiraz, Iran
6. R&D Department, Persian BayanGene Research and Training Center, Shiraz, Iran
7. Student Research Committee, Shiraz University of Medical Sciences, Shiraz, Iran

#The first two authors equally contributed to this work.

Corresponding Address: Department of Immunology, Shiraz University of Medical Sciences, Shiraz, Iran
Email: farjadsh@sums.ac.ir

Received: 13/March/2019, Accepted: 8/July/2019

Abstract

Objective: Astronauts are exposed to a wide range of environmental stresses during spaceflights that reduce their immune responses and make them more susceptible to infections and malignancies. Exposure to a low dose of a certain stress induces an adaptive response, which leads to resistance to higher doses of the same or other types of stress. We designed this study to investigate the effect of radiofrequency electromagnetic field (RF-EMF)-induced adaptive response on immune system modulation in a mouse model of hindlimb unloading (HU) as a ground-based animal model of spaceflight conditions.

Materials and Methods: In this experimental study, serum levels of T helper (Th)-mediated cytokines were determined by the multiplex cytometric bead assay in four groups of mice (n=10 per group): HU mice, RF-EMF-treated mice, HU mice pre-exposed to RF-EMF; and untreated controls. Mice were exposed to 2450 MHz RF-EMF with SAR 0.478 W/kg for 12 hours/day for three successive days.

Results: Tumor necrosis factor-alpha (TNF-α), interleukin-9 (IL-9) and IL-22 were significantly decreased in HU mice. Comparison between HU mice and RF-EMF-treated mice showed an opposite change in IL-6, while IL-9, IL-22, IFN-γ and TNF-α decreased in both groups. However, just interferon gamma (IFN-γ) was significantly decreased in HU mice that were pre-exposed to RF-EMF compared to the control group.

Conclusion: The effect of RF-EMF in elevating IL-6 and reducing IL-9 in opposite directions in HU mice suggest a modulating effect of RF-EMF on HU-induced changes in these cytokines, as Th2 and Th9 eventually returned to normal levels and balances in cytokine ratios were also restored in HU mice pre-exposed to RF-EMF.

Keywords: Cytokine, Flow Cytometry, Hindlimb Suspension, Radio Wave

Cell Journal(Yakhteh), Vol 22, No 4, January-March (Winter) 2021, Pages: 401-405

Citation: **Aghajari S, Mortazavi SMJ, Kalani M, Nematolahl S, Habibzadeh P, Farjadian S. The immunomodulatory effect of radiofrequency electromagnetic field on serum cytokine levels in a mouse model of hindlimb unloading. Cell J. 2021; 22(4): 401-405. doi: 10.22074/cellj.2021.6856.**

Introduction

During spaceflight, astronauts encounter a variety of environmental changes (1) such as microgravity (2) and exposure to radiation and solar energetic particles (3, 4). Along with circadian rhythm disturbances (5) and altered nutritional intake (6), these changes may lead to dysregulation of physiological functions. Impaired immune responses to infectious agents and malignant cells may be life-threatening to space travelers (7, 8).

The fine-tuning of immune responses is mediated by cytokines secreted mainly by T helper (Th) cells. While Th2-mediated humoral immunity plays a major role against extracellular pathogens, cellular immunity mediated by Th1 cells acts as an essential response to viruses and tumor cells. Furthermore, Th17 cells contribute to the clearance of extracellular microorganisms by neutrophilic inflammation. These cells also promote mucosal and epithelial barrier functions. Th9 is crucial for defense against helminthes, and Th22 cells found mainly in the epidermis play an important role in chronic inflammatory skin disorders (9).

There is some evidence of immune deregulation during extended space missions (10, 11). Spaceflight represents a unique situation that results in numerous changes in the human body. The study of immune reactivity before, during and after brief or extended flights is essential for understanding integrated responses in the complex environment that astronauts inhabit. Since many experiments cannot be performed in these conditions, ground-based models that simulate spaceflight conditions can help take this research forward. Mouse models of hindlimb unloading (HU) are widely used to mimic the effect of microgravity during spaceflight on mouse physiology (12).

Adaptive response is the exposure to a low dose of a certain stress that leads to resistance to higher doses of the same or other types of stress (13). Adaptive response was first reported by Samson and Cairns (14) in 1977 when they observed bacterial resistance to a high dose of an alkylating mutagen following bacterial growth in a nontoxic dose of the same substance. In 1984, Olivieri et al. (15) also found that human lymphocytes exposed to ^{3}H-thymidine, as a source of low-level chronic radiation, became more resistant to chromosomal aberration that resulted from high doses of X-rays. It was previously shown that laboratory animals pre-exposed to a radiofrequency electromagnetic field (RF-EMF) were more resistant to subsequent high doses of ionizing radiation or infections caused by life-threatening microorganisms (16-18). Zeni et al. (19) observed a remarkable decrease in the frequency of micronuclei formation in lymphocytes of individuals who were pre-exposed to 1950 MHz RF-EMF at a specific absorption rate (SAR) of 0.3 W/kg for 20 hours and then challenged with mitomycin C. Jiang et al. (20, 21) observed a notable reduction in DNA damage in blood and bone marrow leukocytes of mice that were pre-exposed to an adaptation dose of 900 MHz RF-EMF at a power density of 120 mW/cm^2 for 4 hours/day for 3-14 consecutive days, and then exposed to 3 Gy whole-body γ-radiation. In the current study, we compared serum cytokine levels in HU mice with and without RF-EMF-treatment to untreated mice in order to investigate the effects RF-EMF-induced adaptive response on immunomodulation in microgravity conditions.

Materials and Methods

Study design

In this experimental study, 6-week-old male BALB/c mice with a mean body weight of 25-30 g were housed under controlled conditions at a temperature of 23 ± 1˚C, humidity of 50 ± 5% and equal light/dark cycle. The experimental protocols were approved by the Ethics Committee of Shiraz University of Medical Sciences (approval code: IR.SUMS.REC.1394.S59) based on the "Guide for the Care and Use of Laboratory Animals" published by the National Academy Press (22).

After a 7-day isolation period, the animals were randomly allocated to four groups (10 mice per group): untreated mice (G1), mice with HU (G2), RF-EMF-treated mice (G3) and HU mice that were pre-exposed to RF-EMF (G4). Blood samples were collected from each mouse 24 hours after the last intervention in each group. All serum samples were isolated and stored at -20˚C until further use.

Hindlimb unloading mouse model

Hindlimb unloaded mice were prepared as previously described (23). Briefly, one week after inserting a stainless steel ring between the L5 and L6 mouse vertebrae, the tail ring was connected to a bobbin in a rail mounted at the roof of a plastic cage using an S-shaped hook. Each mouse was suspended by the tail with a 20-degree angle of hind limbs to the horizon. During this time, the animals had free access to food and water.

Radiofrequency irradiation

An AD-link Wi-Fi router was used as the source of RF-EMF. During the exposure period, data was shared between the Wi-Fi router and a laptop at a distance of 6 m in an adjoining room. The Wi-Fi router operated at a power level of 1 W and the device was located 30 cm from the animals' cage. Mice were exposed to 2450 MHz RF-EMF at SAR 0.478 W/kg for 12 hours/day for 3 successive days. All experiments were performed in an environment with a negligible background level of electric and magnetic fields.

Cytokine assay

Serum levels of Th-related cytokines that included Th1 (IFN-γ, TNF-α and IL-2), Th2 (IL-4, IL-5, IL-6, IL-10 and IL-13), Th17 (IL-17A, IL-17F and IL-21), Th9 (IL-9) and Th22 (IL-22) were quantified with a multiplex cytometric bead assay using a commercial kit (BioLegend, San Diego, CA, USA) according to the manufacturer's directions. Briefly, a mixture of FITC-labeled antibody-coated beads for each desired cytokine, which could be differentiated by their sizes and fluorescence intensities, was incubated with the mouse serum samples or standards. After capturing the cytokines by the beads, biotin-conjugated anti-mouse antibody and PE-labeled streptavidin were successively added. The results were visualized with a FACSCalibur flow cytometer (eBioscience, San Diego, CA, USA) and the data were analyzed with FlowCytomix Pro-3.0 software (BioLegend).

Statistical analysis

The Shapiro-Wilk test was used to verify normal distribution of the data. The nonparametric Kruskal-Wallis test was used to compare cytokine levels among groups. Then, post hoc pairwise multiple comparisons were performed with Dunn's test. All statistical analyses were done with SPSS 23 (SPSS Inc., Chicago, Illinois, USA) and a two-sided $P \leq 0.05$ was considered statistically significant. GraphPad Prism 6.0 (GraphPad Software Inc., La Jolla, San Jose, CA, USA) was used to generate the graphs.

Results

We investigated the effect of RF-EMF-induced adaptive response on the immune system in HU mice. To this effect, serum levels of Th-related cytokines were determined in HU mice, RF-EMF-treated mice and HU mice that were pre-exposed to RF-EMF in comparison to untreated mice.

Figure 1 shows the significant changes in cytokine levels among the studied groups. As shown, there was a decrease in IL-9 (P=0.007), IL-22 (P=0.006), TNF-α (P=0.029) and IFN-γ (non-significant, NS) levels, whereas IL-6 (NS) levels increased in HU mice compared with the control group (G2 vs. G1). A comparison of RF-EMF-treated mice to the control group (G3 vs. G1) showed an increase in IL-9 (NS) and decrease in IL-22 (P=0.001), TNF-α (NS), IFN-γ (NS) and IL-6 (NS) levels. A comparison between HU mice and RF-EMF-treated mice showed the opposite, an increase in IL-6 (0.001), whereas IL-9, IL-22, IFN-γ and TNF-α levels decreased in both groups. However, only IFN-γ had a

significant decrease in HU mice that were pre-exposed to RF-EMF compared with the control group (G4 vs. G1).

Figure 2 shows the cytokine changes in Th subsets and their ratios. Th1 levels significantly decreased (P=0.033), Th2 slightly increased (NS), and the Th1/Th2 ratio decreased significantly (P=0.008) in G2 compared to G1 mice. Although Th17 showed no change between these two groups, the (Th1+Th17)/Th2 ratio (P=0.009) was significantly decreased in G2 compared to G1. Th subsets and their ratios showed no remarkable differences between G3 compared to G1. However, significant changes, in the opposite directions, were observed in Th2 (P=0.001), Th1/Th2 (P=0.006), Th17/Th2 (P=0.003), (Th1+Th17)/Th2 (P=0.002) and (Th1+Th17)/(Th2+Th22) (P=0.002) between G2 and G3.

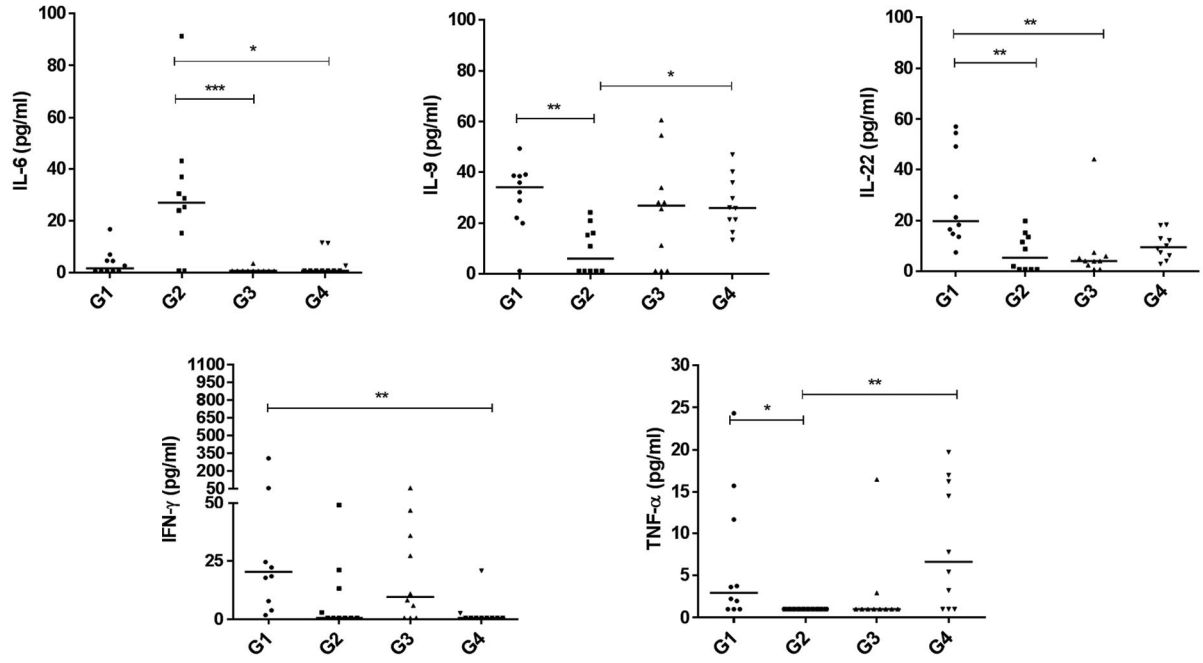

Fig.1: Comparison of cytokine serum levels among four mouse groups (n=10 in each group). Mouse groups are G1; Untreated mice, G2; Hindlimb unloading (HU) mice, G3; Radiofrequency electromagnetic field (RF-EMF)-treated mice, and G4; HU mice that were pre-exposed to RF-EMF.
*; P<0.05, **; P<0.01, and ***; P<0.001.

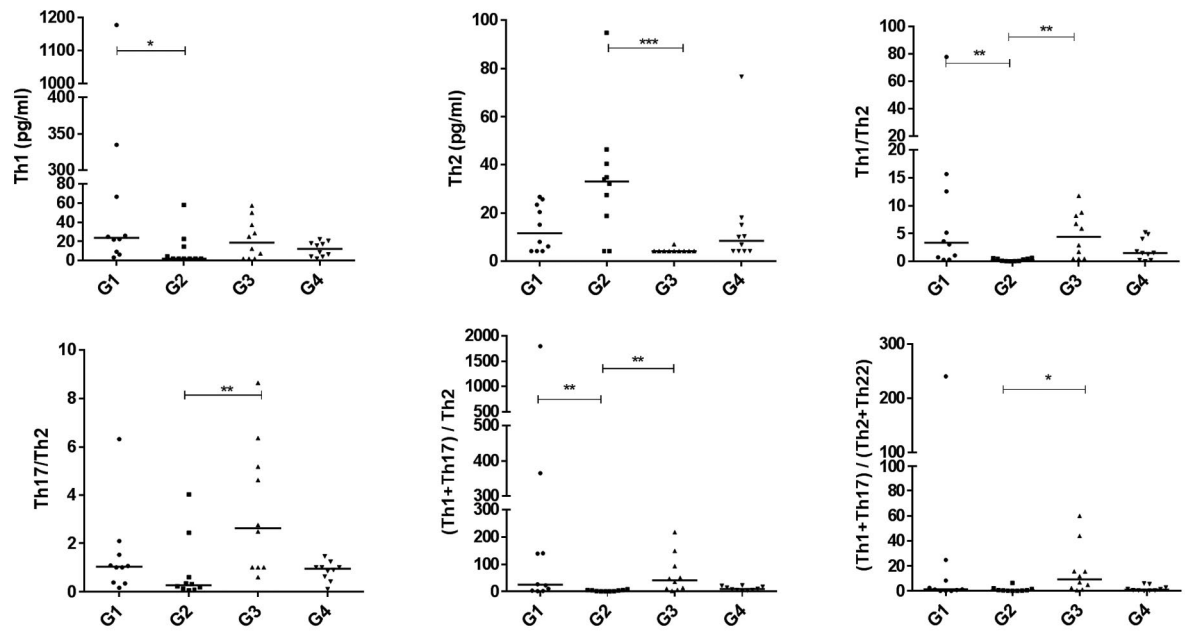

Fig.2: Comparison of cytokines in each T helper (Th) cell subset and their ratios among four mouse groups (n=10 in each group). Mouse groups are G1; Untreated mice, G2; Hindlimb unloading (HU) mice, G3; Radiofrequency electromagnetic field (RF-EMF)-treated mice, and G4; HU mice that were pre-exposed to RF-EMF.
*; P<0.05, **; P<0.01, and ***; P<0.001.

Discussion

We investigated the modulating effect of RF-EMF on HU-induced changes in Th-mediated cytokines by comparing serum cytokine levels in HU mice with and without RF-EMF treatment to untreated mice. Our results showed markedly decreased Th1 levels in HU mice in light of the reduction in IFN-γ and TNF-α. Reactivation of latent viruses in astronauts during long-term spaceflight has previously been reported (24, 25) which might be explained by reduced Th1 responses, although the importance of antibodies in the control of viral infections should not be ignored. In this connection, Gaignier et al. (26) also reported decreased numbers of B cells in the spleen of HU mice and an impaired proliferative response in these cells after mitogen stimulation. However, they used Th1-biased C57BL/6 mice in their experiments instead of the Th2-prone BALB/c mice that we used in the current study (27).

Our results showed a slight increase in Th2 cytokine levels in HU mice, which might be explained by the slight elevation of IL-6. This finding agreed with the results of Jang et al. who found slight change in Th2 cytokines after *in vitro* stimulation of T cells from HU BALB/c mice (28). We found no change in Th17 cytokines in HU mice, which was in line with the results reported by Gaignier et al. (26). In our study, IL-22 levels markedly decreased in HU mice. Although there was no study that directly focused on changes in IL-22 levels in HU mice, Li et al. (29, 30) reported delayed corneal epithelial wound healing in HU mice, which they attributed to decreased levels of IL-22.

In our study, RF-EMF had no crucial effect on IL-9 as well as Th1-, Th2-, and Th17-mediated cytokines; however, there was a strongly decreased IL-22 level in G3 mice compared to the control group.

The opposite changes of IL-6 in G2 compared to G3 mice suggest a modulating effect of RF-EMF on HU-induced changes in this cytokine. This compensatory effect was also observed in IL-9, as eventually Th2 and Th9 returned to normal levels in G4 mice. The modulating effect of RF-EMF on key cytokines might explain the restoration of Th1/Th2, Th17/Th2, (Th1+Th17)/Th2, (Th1+Th17)/(Th2+Th22) and (Th1+Th17)/(Th2+Th9+Th22) balances in G4 mice.

However, concurrent reduction of IFN-γ, TNF-α and IL-22 was observed following HU induction and after RF-EMF treatment in G2 and G3 mice, respectively. The synergistic effect of both conditions was just detected in IFN-γ, which significantly decreased in G4 compared to the control group.

If further experiments in humans confirm the modulatory effect of RF-EMF on microgravity-induced cytokine changes, this method could be used in future long-term crewed space flights, especially journeys to Mars which are planned for the next decade. Due to similarities between space field complications and prolonged head-down bed rest patients, RF-EMF might also be helpful in immunomodulation of these patients.

Conclusion

The effect of RF-EMF in elevating IL-6 and reducing IL-9 in opposite directions in HU mice suggests a modulating effect of RF-EMF on HU-induced changes in these cytokines, as Th2 and Th9 eventually returned to normal levels and balances in cytokine ratios were also restored in HU mice pre-exposed to RF-EMF.

Acknowledgements

This work was performed in partial fulfillment of the requirements for the M.Sc. degree in Radiobiology (Sima Aghajary), and financially supported by a grant from Shiraz University of Medical Sciences (grant number: 8736). We thank S. Kouhi for his technical assistance in the animal laboratory and K. Shashok (AuthorAID in the Eastern Mediterranean) for improving the use of English in the manuscript. There is no conflict of interest in this study.

Authors' Contributions

S.A.; Planned and carried out the experiments. S.M.J.M.; Developed the theory, supervised the project and reviewed the manuscript. M.K.; Contributed to sample preparation, helped carrying out the experiment, and writing the manuscript. S.N.; Calculated the sample size, did statistical analyses, and helped in figure design. P.H.; Presented idea, preliminary study design and reviewed the manuscript by support of supervisors. S.F.; Supervised the project, conceived and planned the experiments, re-checked all analyses, tables and figures, corrected the manuscript draft, and reviewed the final version. All authors read and approved the final manuscript.

References

1. Wang KX, Shi Y, Denhardt DT. Osteopontin regulates hindlimb-unloading-induced lymphoid organ atrophy and weight loss by modulating corticosteroid production. Proc Natl Acad Sci. 2007; 104(37): 14777-14782.
2. Aponte VM, Finch DS, Klaus DM. Considerations for non-invasive in-flight monitoring of astronaut immune status with potential use of MEMS and NEMS devices. Life Sci. 2006; 79(14): 1317-1333.
3. Shearer WT, Zhang S, Reuben JM, Lee BN, Butel JS. Effects of radiation and latent virus on immune responses in a space flight model. J Allergy Clin Immunol. 2005; 115(6): 1297-1303.
4. Uri JJ, Haven CP. Accomplishments in bioastronautics research aboard International Space Station. Acta Astronaut. 2004; 56(9-12): 883-889.
5. Mallis MM, DeRoshia CW. Circadian rhythms, sleep, and performance in space. Aviat Space Environ Med. 2005; 76(6 Suppl): B94-B107.
6. Cena H, Sculati M, Roggi C. Nutritional concerns and possible countermeasures to nutritional issues related to space flight. Eur J Nutr. 2003; 42(2): 99-110.
7. Sonnenfeld G. The immune system in space and microgravity. Med Sci Sports Exerc. 2002; 34(12): 2021-2027.
8. Crucian B, Sams C. Immune system dysregulation during spaceflight: clinical risk for exploration-class missions. J Leukoc Biol. 2009; 86(5): 1017-1018.
9. Raphael I, Nalawade S, Eagar TN, Forsthuber TG. T cell subsets and their signature cytokines in autoimmune and inflammatory diseases. Cytokine. 2015; 74(1): 5-17.
10. Cervantes JL, Hong BY. Dysbiosis and Immune Dysregulation in Outer Space. Int Rev Immunol. 2016; 35(1): 67-82.
11. Stowe RP, Sams CF, Pierson DL. Effects of mission duration on

neuroimmune responses in astronauts. Aviat Space Environ Med. 2003; 74(12): 1281-1284.
12. Adams GR, Caiozzo VJ, Baldwin KM. Skeletal muscle unweighting: spaceflight and ground-based models. J Appl Physiol (1985). 2003; 95(6): 2185-2201.
13. Dimova EG, Bryant PE, Chankova SG. Adaptive response: some underlying mechanisms and open questions. Genet Mol Biol. 2008; 31(2): 396-408.
14. Samson L, Cairns J. A new pathway for DNA repair in Escherichia coli. Nature. 1977; 267(5608): 281-283.
15. Olivieri G, Bodycote J, Wolff S. Adaptive response of human lymphocytes to low concentrations of radioactive thymidine. Science. 1984; 223(4636): 594-597.
16. Mortazavi SM. Space radiobiology and the new era of induced radioresistance: should traditional concepts be moved to science history museums? Technol Health Care. 2012; 21(4): 285-289.
17. Mortazavi SMJ, Motamedifar M, Mehdizadeh AR, Namdari G, Taheri M. The effect of pre-exposure to radiofrequency radiations emitted from a GSM mobile phone on the suseptibility of BALB/c mice to Escherichia coli. J Biomed Phys Eng. 2012; 2(4): 139-146.
18. Mortazavi S, Mosleh-Shirazi M, Tavassoli A, Taheri M, Mehdizadeh A, Namazi S, et al. Increased radioresistance to lethal doses of gamma rays in mice and rats after exposure to microwave radiation emitted by a GSM mobile phone simulator. Dose Response. 2012; 11(2): 281-292.
19. Zeni O, Sannino A, Romeo S, Massa R, Sarti M, Reddy AB, et al. Induction of an adaptive response in human blood lymphocytes exposed to radiofrequency fields: Influence of the universal mobile telecommunication system (UMTS) signal and the specific absorption rate. Mutat Res. 2012; 747(1): 29-35.
20. Jiang B, Nie J, Zhou Z, Zhang J, Tong J ,Cao Y. Adaptive response in mice exposed to 900 MHz radiofrequency fields: primary DNA damage. PLoS One. 2012; 7(2): e32040.
21. Jiang B, Zong C, Zhao H, Ji Y, Tong J ,Cao Y. Induction of adaptive response in mice exposed to 900MHz radiofrequency fields: application of micronucleus assay. Mutat Res. 2013; 751(2): 127-129.
22. The National Academies Collection: Reports funded by National Institutes of Health. Guide for the care and use of laboratory animals. 8th ed. Washington (DC): National Academies Press (US); 2011.
23. Ferreira JA, Crissey JM, Brown M. An alternant method to the traditional NASA hindlimb unloading model in mice. J Vis Exp. 2011; (49). pii: 2467.
24. Pierson DL, Stowe RP, Phillips TM, Lugg DJ, Mehta SK. Epstein-Barr virus shedding by astronauts during space flight. Brain Behav Immun. 2005; 19(3): 235-242.
25. Mehta SK, Stowe RP, Feiveson AH, Tyring SK, Pierson DL. Reactivation and shedding of cytomegalovirus in astronauts during spaceflight. J Infect Dis. 2000; 182(6): 1761-1764.
26. Gaignier F, Schenten V, De Carvalho Bittencourt M, Gauquelin-Koch G, Frippiat JP, Legrand-Frossi C. Three weeks of murine hindlimb unloading induces shifts from B to T and from Th to Tc splenic lymphocytes in absence of stress and differentially reduces cell-specific mitogenic responses. PLoS One. 2014; 9(3): e92664.
27. Schulte S, Sukhova GK, Libby P. Genetically programmed biases in Th1 and Th2 immune responses modulate atherogenesis. Am J Pathol. 2008; 172(6): 1500-1508.
28. Jang TY, Jung AY, Kim YH. Effect of long-term antiorthostatic suspension in a murine model of acute lung injury. Clin Exp Otorhinolaryngol. 2016; 9(4): 332-338.
29. Li Z, Rivera CA, Burns AR, Smith CW. Hindlimb unloading depresses corneal epithelial wound healing in mice. J Appl Physiol (1985). 2004; 97(2): 641-647.
30. Li Z, Burns AR, Miller SB, Smith CW. CCL20, γδ T cells, and IL-22 in corneal epithelial healing. FASEB J. 2011; 25(8): 2659-2668.

Enhancement of The Stability of Human Growth Hormone by Using Tris(hydroxymethyl)aminomethane: Molecular Docking and Experimental Analysis

Siyavash Mirzaei, Ph.D.[1], Hamid Mobedi, Ph.D.[2*], Hamid Gourabi, Ph.D.[1], Mohammad Hosein Sanati, Ph.D.[3], Sakine Khezli, M.Sc.[2], Hamid Omidian, Ph.D.[4], Masoume Ighaeie, Ph.D.[5]

1. Department of Genetics, Reproductive Biomedicine Research Center, Royan Institute for Reproductive Biomedicine, ACECR, Tehran, Iran
2. Department of Novel Drug Delivery Systems, Iran Polymer and Petrochemical Institute, Tehran, Iran
3. Medical Genetics Department, National Institute of Genetic Engineering and Biotechnology (NIGEB), Tehran, Iran
4. Department of Pharmaceutical Sciences, Nova Southeastern University, Pharmaceutical Sciences, Davie, Florida, USA
5. Computational Nano Physical Chemistry Laboratory, Department of Chemistry, Azerbaijan Shahid Madani University, Tabriz, Iran

Corresponding Address: P.O.Box: 14965-115, Department of Novel Drug Delivery Systems, Iran Polymer and Petrochemical Institute, Tehran, Iran
Email: h.mobedi@ippi.ac.ir

Received: 23/April/2019, Accepted: 15/July/2019

Abstract

Objective: It is so difficult to formulate human growth hormone (hGH) in a solution with high stability and new drug delivery system (NDDs) due to physiochemical instability. The purpose of this study was to investigate the possibility of using Tris as a hGH stabilizer.

Materials and Methods: In this experimental study, the role of tris(hydroxymethyl)aminomethane (Tris) was evaluated as a hGH stabilizing agent in phosphate buffer, as a practical aqueous solution and a media to release NDDs. High-performance liquid chromatography (HPLC) and enzyme-linked immune sorbent assay (ELISA) were applied to investigate the stability of hGH in solutions and dynamic light scattering (DLS) was used to measure the effect of Tris on the hydrodynamic size of hGH in aqueous solutions. Ultra violet (UV) spectrophotometry was used to check the hGH spectrum. In computational study, formation of ligand-protein complex of the Tris-hGH, and the intermolecular interactions between Tris and hGH were studied by molecular docking modeling.

Results: The results demonstrated that Tris at the optimum concentration, increases hGH stability in aqueous solutions. Also, molecular docking modeling confirmed that amino acid residues such as tyrosine (Tyr), proline (Pro), glutamic acid (Glu), aspartic acid (Asp), leucine (Leu), and phenylalanine (Phe) in hGH structure, were linked with Tris as a ligand.

Conclusion: It seems that interactions between hGH and Tris are the most important reason for increment of the physicochemical stability of hGH in aqueous solutions containing Tris.

Keywords: Human Growth Hormone, Molecular Modeling, Protein Stability, Tris(hydroxymethyl)aminomethane

Cell Journal(Yakhteh), Vol 22, No 4, January-March (Winter) 2021, Pages: 406-414

Citation: **Mirzaei S, Mobedi H, Gourabi H, Sanati MH, Khezli S, Omidian H, Ighaeie M. Enhancement of the stability of human growth hormone by using tris(hydroxymethyl)aminomethane: molecular docking and experimental analysis. Cell J. 2021; 22(4): 406-414. doi: 10.22074/cellj.2021.6903.**

Introduction

The protein of human growth hormone (hGH) has 191 amino acids and a molecular weight of 22 KDa. This protein is secreted and stored by somatotropic cells in the side section of the pituitary gland (1). Patients who suffer from GH deficiency, Prader-Willi, and Turner syndrome, receive a daily injection of this hormone (2). So, there is a strong need for new dosage forms that can facilitate hGH delivery, reduce the number of injections, and increase treatment efficacy and patients' compliance (2-4). However, hGH instability in new drug delivery systems (NDDSs), aqueous solutions remain a major hurdle. So far, many studies have been done to increase the stability of hGH in solutions.

The most suitable stability for hGH in solution and NDDSs, is generally provided by the addition of antioxidants, osmolytes, acid neutralizers and biological buffers (5-9). In aqueous media, hGH stability is affected by buffer species, concentration, temperature, pH, ionic strength, and physical stress. These factors can produce unwanted crosslinking, oxidation, deamination, and consequently aggregation. An appropriate buffer for protein media, should preferably release its components from the protein domain (to enhance water surface tension), remove free radical, reduce the mobility of the water molecules, and suppress nucleophilic substitution on disulfide bonds (5, 10).

Biological buffers such as tris(hydroxymethyl) aminomethane (Tris) ($C_4H_{11}NO_3$) and other tris derivatives are among additives used to stabilize proteins (11). Tris is a biocompatible weak base (molecular weight 121 Da) (12) that protects proteins against chemical degradation, denaturation, unfolding, and ultimately, aggregation by interacting with the protein, or similar to osmolytes, it induces proteins stabilization (10, 12).

In the previous studies, the stability of some proteins such as bovine serum albumin (BSA) and interleukin was increased in aqueous solutions at high temperatures

in the presence of Tris (11, 13). It has become evident that the hydroxyl groups in Tris form hydrogen bond with glutamic acid, aspartic acid, alanine, glycine, tryptophan and cysteine amino acids in proteins and peptides, and protect them against chemical degradation (14). It was also shown that a greater hydrogen bonding can be achieved by increasing concentrations of Tris (11, 14). Changes in protein stability in the presence of Tris, at least in part, depend on intermolecular interactions that can be studied by empirical experiments as well as computer modeling. Intermolecular interactions that can be studied by empirical experiments as well as computer modeling. Molecular docking is a computer modeling approach used to predict the preferred orientation of binding to provide a stable conformation. The preferred orientation knowledge is utilized for prediction of the binding affinity between two molecules using scoring functions. Two approaches are commonly employed within the docking modeling association. One approach is to simulate the ligand and the protein as complementary surfaces. The second approach describes the docking process in which the energies of interaction in the ligand-protein pair are calculated (15). Investigation of the Tris effects on hGH stability and intermolecular interactions between hGH and Tris, was the aim of this study.

Materials and Methods

Materials

hGH was purchased in the form of powder with excipient ratio of 1:6 from GeneScience Pharmaceuticals (China). Tris(hydroxymethyl)aminomethane (Tris) was purchased from Sigma-Aldrich (USA), and n-propyl alcohol (analytical grade) was obtained from Merck, Germany.

Sample preparation

In this experimental study, to compare hGH stability in phosphate and Tris buffers (0.05 M, pH=7.4), hGH solutions (1 mg/ml) were prepared and kept at two temperatures 5 ± 2°C (refrigerator temperature) and 37 ± 1°C (body temperature). The solutions were sampled and analyzed by High-performance liquid chromatography (HPLC) and enzyme-linked immune sorbent assay (ELISA), for 5 days and 24 hours, respectively. To investigate the effects of Tris on hGH stability in phosphate buffer, the hGH solutions (1 mg/ml) were prepared in phosphate buffer at the concentration of 0.05 M and pH=7.4, containing 0.0, 3.0, 4.0, and 6.0 mM of Tris and kept at 37 ± 1°C. The samples' turbidity was tested after 48 hours. The hGH solutions (1 mg/ml) in Tris buffers (0.01, 0.03, 0.05, 0.07, 0.09 M and pH=7.4) and phosphate buffers (0.05 M, pH=7.4) containing of 0.00, 0.01, 0.03, 0.05, 0.07, 0.09 M Tris were prepared and kept at 37°C for 24 hours. to investigate the effects of Tris on hGH hydrodynamic size, DLS test was performed.

To detect potential interactions between hGH and Tris, reference standard hGH solutions 1(mg/ml) containing 0.00, 0.05, and 0.1 M of Tris were prepared in distilled water and analyzed by UV spectrophotometry.

Experimental analysis and evaluation

ELISA Kit: hGH concentration in solutions was measured using an ELISA Kit (Accubind, Monobind, USA). The absorbance was measured at the wavelength of 450 nm using a microplate photometer (Rodon, Titertek Multiskan, Netherlands).

HPLC: Analysis was performed according to the United State Pharmacopeia (USP) 40 by HPLC (smart line manager 5050, Knauer, Germany) with column C4 (4 mm×25 cm, 5 µm, 300 A°) (phenomenex, China), at 45°C with mobile phase containing a mixture of 71% Tris buffer (0.05 M, pH=7.5) and 29% n-propyl alcohol and the flow rate was set at 0.5 ml/minute.

Dynamic light scattering (DLS): hGH aggregation and agglomeration was investigated using DLS (Omni, Brookhaven, USA) and turbidity tests.

UV spectrophotometer: hGH structural changes were tracked using a UV analyzer (UV-1650PC, Shimadzu, Japan).

Computational analysis and evaluation methods

Density functional theory calculation

In the computational study, a full geometric optimization of the electronic ground state of Tris was obtained by applying the DFT (16, 17) using the Becke's three-parameter hybrid exchange functional (B3) (18) and the Lee-Yang-Parr correlation functional (LYP) (19). A fairly large basis set with two sets of polarization functions denoted the 6-311G (2p, 2d) basis was used (16). All calculations were carried out using Gamess-US Package (20).

Molecular docking

Computational docking can be used to predict bound conformation and free energies for a small ligand molecule binding a macromolecular target. Docking is used to study intermolecular interactions and their mechanisms (21).

The interaction of Tris, as a ligand, with hGH, as a macromolecule, was investigated. The Auto dock 4.2 was used to locate the appropriate conformations and binding orientations of one molecule of Tris into the hGH binding pocket. The lamarckian genetic algorithm (LGA) implemented in the Auto Dock program, was employed (22). The ligand (Tris) structure was optimized by DFT calculations. This optimized structure and hGH protein data bank [PDB code: 1Hgu (N-Hydroxyguanidine)] (23) were subjected to docking analysis. By adding the polar hydrogen atoms, the Kollman united atom charges, atomic solvation parameters, and fragmental volumes were assigned to the protein, using Auto Dock Tools (24). The grid spacing was 0.375Å, and each grid map consisted of 50×36×52 grid points. Lennard-Jones parameters 12- 6 and 12-10, supplied by the program, were used to

model vander Waals interactions and hydrogen bonds, respectively. For ligand, random starting positions, random orientations, and torsions were used. The docking was performed with an initial 150 individuals' population, a maximum of 270,000 generations, and maximum of 25 million energy evaluations. A maximum of 300 conformers was considered in the docking modeling process. Using a root mean square deviation (RMSD) less than 0.2 nm as a threshold, the resulting conformations were clustered. After the simulation was completed, the docked structure was analyzed and the interaction was investigated. The binding distance between the donors and acceptors and the hydrogen bond interactions were measured for the best conformers. Interactions, position, spacing of amino acids with each other within the complex of Tris and hGH, were also studied using a PyMOL package (25).

Statistical analysis

In statistical analysis, to compare the data obtained from different samples, a t test (Paired Two Sample for Mean values) was performed using Microsoft Office Excel version 2016. A $P<0.05$ was considered statistically significant.

Results

Human growth hormone stability in the phosphate and Tris buffers

hGH chemical degradation such as oxidation and deamidation, and physical degradation (e.g. aggregation, agglomeration or unfolding), which lead to biological deactivation of hGH, in Tris and phosphate buffers (0.05 M, pH=7.4) at two temperatures of 5 ± 2˚C and 37 ± 1˚C, were investigated by HPLC (26, 27) and ELISA analysis (28), respectively (Fig.1).

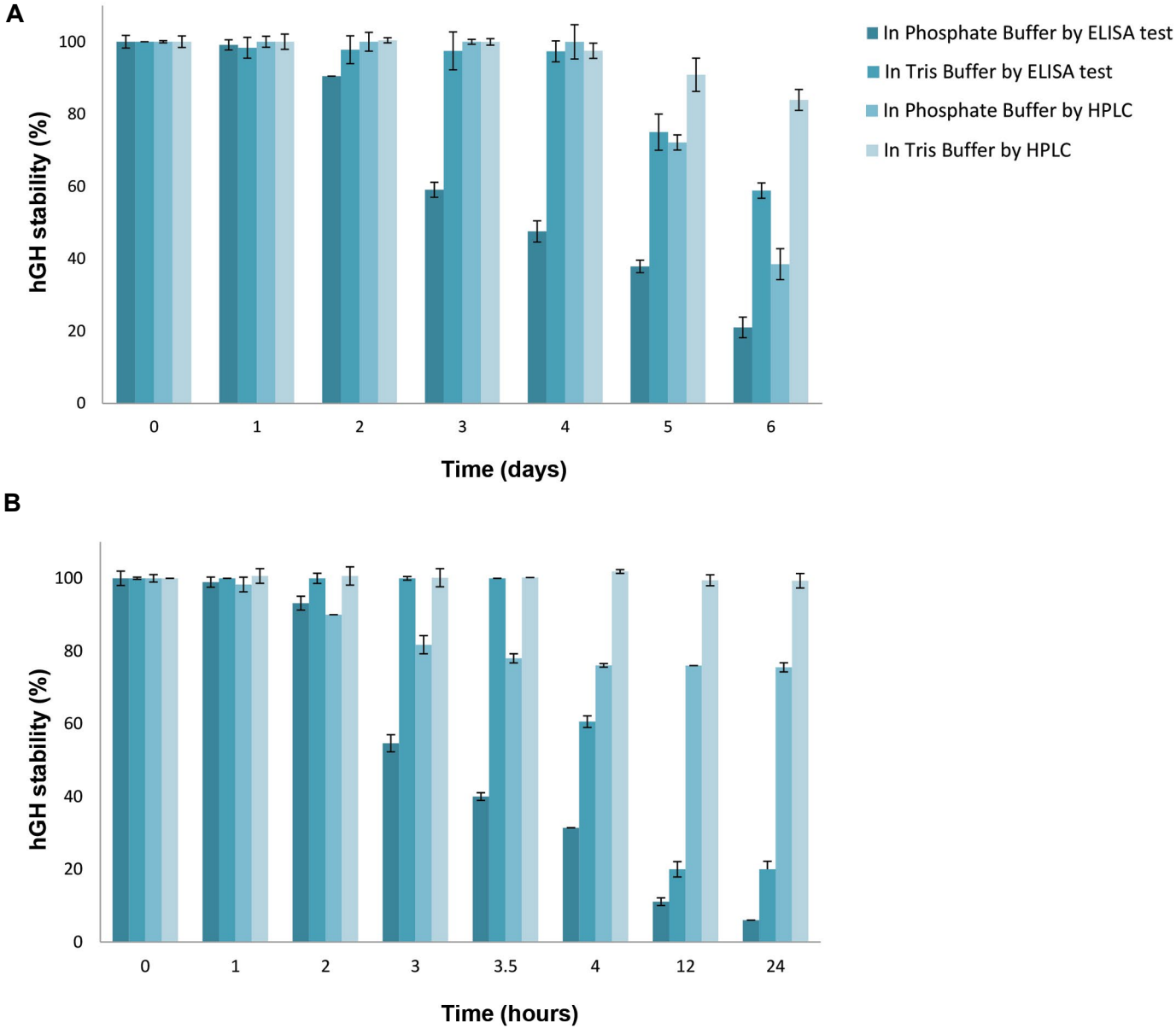

Fig.1: hGH stability in Tris and phosphate buffers (0.05 M, pH=7.4) analyzed by HPLC and ELISA tests. **A.** At 5 ± 2°C and **B.** At 37 ± 1°C. hGH; Human growth hormone, HPLC; High performance liquid chromatography, and ELISA; Enzyme-linked immunosorbent assay.

HPLC analysis of hGH stability in phosphate buffer at 5 ± 2°C, showed that the stability of hGH in the phosphate buffer remained unchanged for four days; however, the results of ELISA analysis showed a decrease in the stability following the second day. In other words, hGH chemical degradation was found insignificant for four days, so decreased stability detected by ELISA test can be attributed to the physical degradation.

In Tris buffer, both HPLC and ELISA results confirmed that hGH stability remained unchanged for four days at 5 ± 2°C. Therefore, the difference in hGH stability between phosphate buffer and Tris buffer confirmed that Tris could enhance hGH stability twice as much. By comparison of the results of hGH stability study at 5 ± 2°C in Tris and phosphate buffers, it was demonstrated that hGH stability remained unchanged for two days and then, significantly decreased in phosphate buffer ($P \leq 0.035$, Fig.1A).

The 24-hour physical and chemical stability data obtained by HPLC and ELISA analysis at 37 ± 1˚C, showed that hGH remained stable in phosphate buffer for 1 hour. hGH stability in this buffer decreased after one hour due to initiation of chemical degradations; however, after 2 hours, physical degradation also increased hGH instability as shown by ELISA results (Fig.1B).

The obtained HPLC and ELISA results in terms of hGH stability in Tris buffer showed that hGH chemical degradation was suppressed for 24 hours and hGH degradation after 3.5 hours, was related to physical degradation. Therefore, comparison of hGH stability between Tris buffer and phosphate buffer (37 ± 1˚C) in 3.5 hours, demonstrated a greater chemical stability for hGH in Tris buffer, and showed that hGH physical degradation rate in Tris buffer was lower than that in phosphate buffer (Fig.1B). Statistical analysis showed differences in hGH stability between Tris and phosphate buffer at 37 ± 1°C from hour 2 to 24 ($P=0.0209$).

Effect of Tris on human growth hormone stability in aqueous solution

Since chemical and physical degradations can lead to protein aggregation, changes in the stability of a protein can be evaluated by monitoring protein aggregation. For this purpose, the effect of Tris on hGH stability was studied by adding Tris to phosphate buffer containing hGH. Aggregated hGH's size and percent in phosphate buffer solution of hGH, was evaluated using qualitative turbidity and DLS tests performed at 37 ± 1°C. Following the addition of Tris, the color of the solution was changed from off-white to completely transparent at Tris concentration of 3.0 up to 6.0 mM at 37 ± 1˚C after 48 hours. This color change was due to reductions in hGH physical degradation, such as unfolding, and aggregation, and chemical degradation (Fig.2).

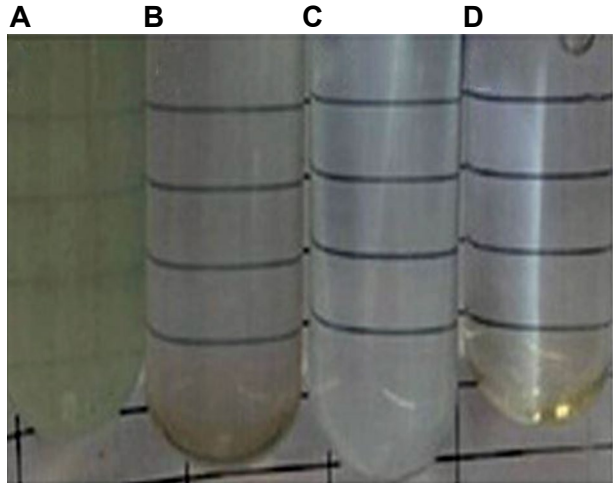

Fig.2: Human growth hormone (hGH) solution in phosphate buffer (pH=7.4), after 48 hours at 37 ± 1˚C. **A.** Solution containing 0.0 mM Tris, **B.** Solution containing 3.0 mM Tris, **C.** Solution containing 4.0 mM Tris, and **D.** Solution containing 6 mM Tris.

The DLS test results indicated that adding Tris at the optimum concentration to the hGH solutions (Tris buffer and phosphate buffer containing Tris), increased the stability of this protein and prevented its aggregation (Fig.3). Based on these results, hydrodynamic size of hGH was in the range of 4 to 5 nm (in dimer form, hGH size is 8-10 nm) in both Tris and phosphate buffers (0.05 M, pH=7.4) at t=0 (Fig.3A). In Tris buffers (pH=7.4) of different concentrations, the average of aggregated protein diameter size decreased with increasing concentrations (0.01 to 0.05 M) of Tris from. Although hGH has the minimum average diameter size in Tris buffer 0.05 M, but with increasing concentration (from 0.05 to 0.09 M) of Tris, hGH aggregation and diameter size was increased (Fig.3B-F).

In phosphate buffer containing hGH and Tris, by increasing Tris concentration from 0 up to 0.03 M in solutions, the aggregated hGH diameter decreased to the diameter of the dimeric protein. However, by increasing Tris concentration from 0.03 up to 0.09 M, the aggregated protein diameter increased again (Fig.3G-L). Therefore, the minimum diameter of aggregated hGH was observed in Tris buffer 0.05 M, and phosphate buffer 0.05 M containing 0.03 M Tris, after 24 hours at 37˚C.

Investigation of Tris and human growth hormone interaction

Chemical interactions between hGH and Tris were investigated using UV spectrometry and molecular modeling. The preliminary results confirmed the interactions between the two molecules (Fig.4A-C). The amino acids of hGH that can potentially create hydrogen bonds with Tris, are introduced by Molecular Docking modeling in Table 1.

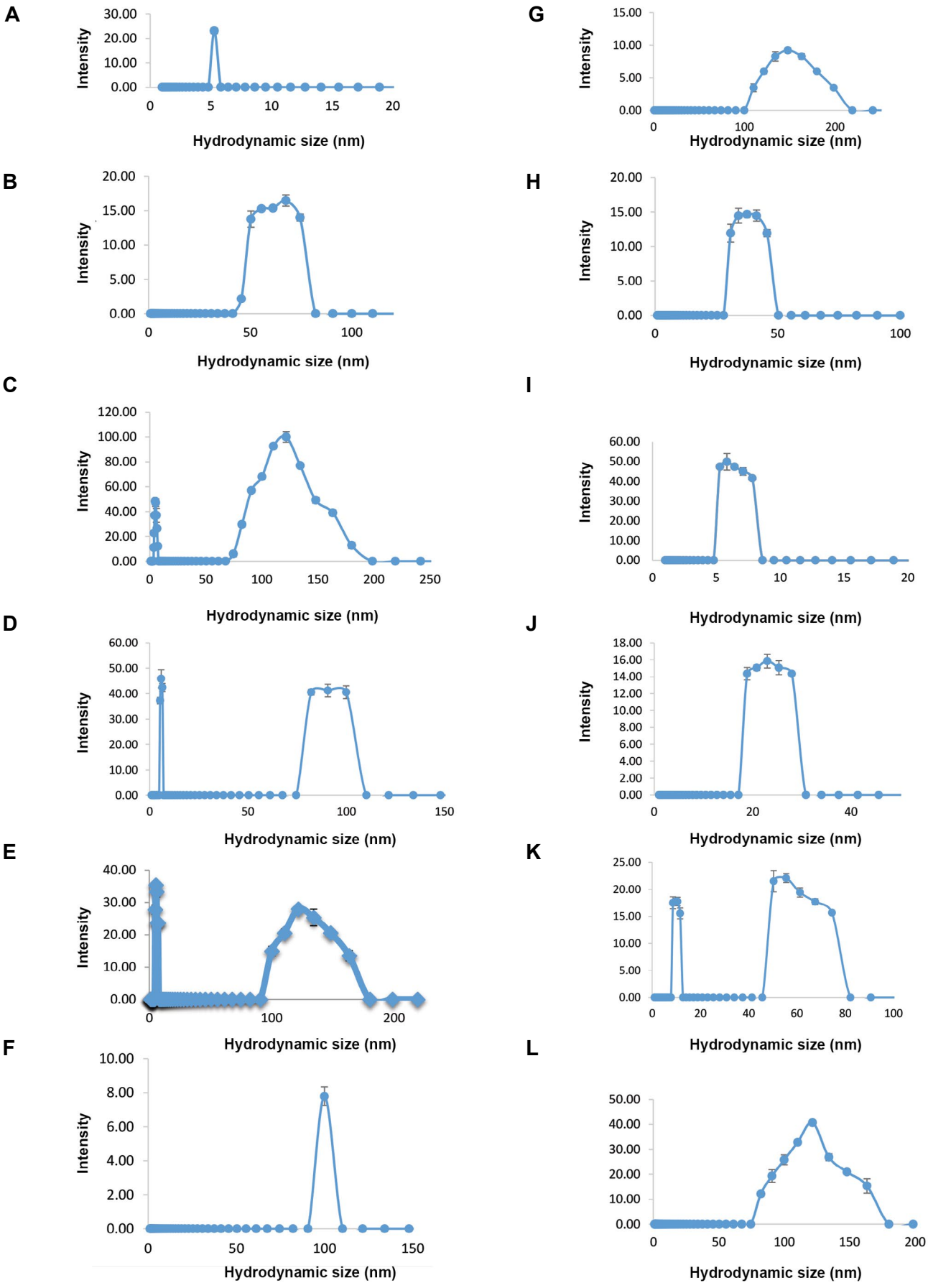

Fig.3: Particle size distribution of human growth hormone (hGH) protein in different phosphate and Tris buffer solutions, pH=7.4. **A.** At t=0, **B-F**. In Tris buffer 0.01, 0.03, 0.05, 0.07, and 0.09 M, **G-L.** In phosphate buffer containing 0.00, 0.01, 0.03, 0.05, 0.07, 0.09 M Tris after 24 hours at 37˚C.

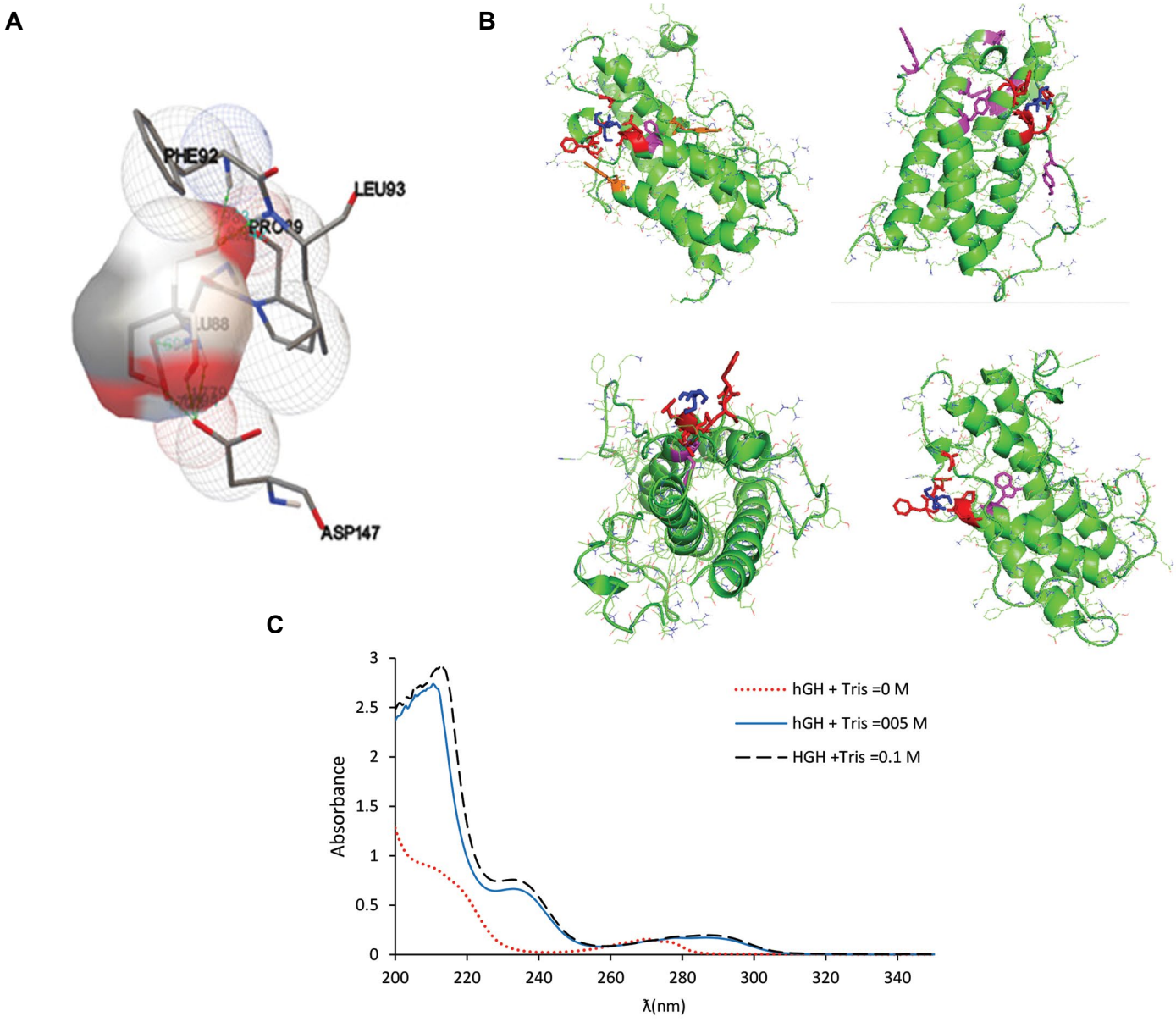

Fig.4: Interactions between human growth hormone (hGH) and Tris. **A.** Interaction from the close view (structure of the first conformation from the first cluster). **B.** Interactions between Tris (blue) and hGH amino acids involved in hydrogen bonds (red) and tryptophan (purple) at 3 different positions. **C.** Ultra violet (UV) spectrums related to hGH solutions containing 0, 0.05 and 0.1 M Tris.

Table 1: Some results of Docking simulation

The cluster	The number of conformation in cluster	The lowest binding energy	The amino acids involved in hydrogen bonding
1	212	-6.22	PRO89, GLU88, ASP147, LEU93, PHE92
2	45	-5.86	GLU32, GLU29, TYR28, LYS41
3	3	-5.05	GLU118, LYS115, GLU119
4	28	-4.85	GLU33, GLu29, Glu32
5	3	-4.74	GLU119, GLU118
6	4	-4.57	GLU119, ASP118, Asp112
7	1	-4.46	ILE36, GLN40
8	1	-4.41	ASP109, ASP112, TYR111, VAL110
9	2	-4.09	TYR164, TYR28, LYS 41
10	1	-3.43	THR60, GLU65

In addition to performed these tests by the present team, Studies by other researchers were suggested, Tris as an osmolyte can increase the hGH stability by changing in folded and unfolded hGH levels of Gibbs free energy (Fig.5).

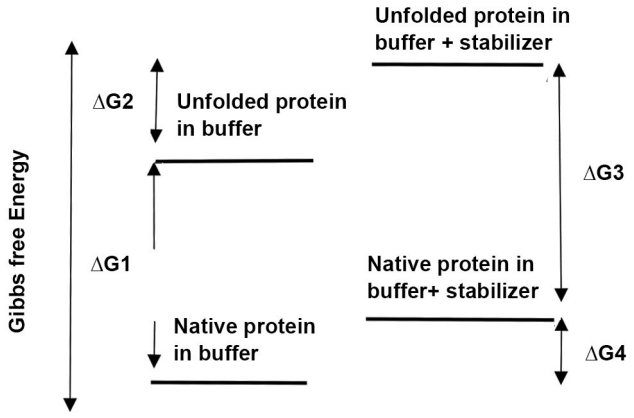

Fig.5: Transfer of natural protein to unfolded protein in buffer solution (ΔG1); the reaction of unfolded protein in aqueous solution to the unfolded protein in buffer with stabilizer (ΔG2); the transfer of natural protein to unfolded protein in buffer with stabilizer (ΔG3); and the reaction of natural protein in aqueous solution to natural protein in solution with stabilizer (ΔG4).

Discussion

With increasing concentrations of Tris, at lower concentrations (to 0.05 M in Tris buffer and to 0.03 M in phosphate buffer), the stability of hGH increased and at higher salt concentrations, increasing Tris concentrations led to decreasing hGH's stability. Increases in hGH stability at low Tris concentration can be potentially attributed to the following three mechanisms: i. Interactions between Tris and hGH, ii. Salting-in effect of Tris, and/or iii. Preferential exclusion of Tris from protein domain in aqueous solutions.

Tris-hGH interactions: Tris could delay oxidation, deamidation, denaturation and ultimately, aggregation of hGH through electrostatic interactions and hydrogen bonding with hGH's amino acids that are prone to degradation (10, 14).

Possibility of Tris-hGH electrostatic interactions can be explained by hGH and Tris net charge in solutions (29, 30). In solutions with pH=7.4, PI 5.12 and pKa 8, the protein could be negatively charged and Tris could be mainly ionized with the positive charges. Thus, probably, there were hGH-Tris electro-static interactions which could be regarded as the reasons for the increase in hGH stability in the solutions (31).

To investigate the possibility of hydrogen bonding between Tris and hGH, as a reason for improved stability of hGH molecules, the interactions between these two molecules were evaluated using a molecular modeling approach and spectrophotometric methods. Molecular docking is the most common means of analyzing ligand-protein interactions at the molecular level. Therefore, computational docking was used to obtain more details on the possible binding mode of Tris and Tris interaction with hGH residues.

Analysis of docking calculations using RMSD-tolerance of 2.0 Å out of 300 docking implementation, showed that there were 10 clusters of conformers. This included the number of conformations in every cluster, the binding energy of the lowest energy conformation in these clusters (in kcal/moll), and the residues participating in hydrogen bonds interactions. The lowest docked energy value was -6.22 kcal/moll, implying that Tris had affinity towards hGH. The residues participating in hydrogen bonds interactions, were Pro89, Glu88, Asp147, Leo93 and Phe92.

In addition to using molecular docking, UV experiment was also performed to study Tris- hGH interactions. UV technique is a simple method to study intermolecular interactions, structural changes and formation of molecular complexes (26, 32). The UV data confirmed that peaks of the hGH spectrum (tyrosine and tryptophan or phenylalanine) were shifted toward the longer wavelengths in the presence of Tris.

The interaction between tyrosin and phenylalanine with Tris, was proven in the Docking data; however, tryptophan could not directly interact with the ligand. The change in the UV peak of tryptophan in the presence of Tris, was presumably due to the interaction of the tryptophan amino acids with the neighboring amino acids in solutions. Consequently, molecular docking modeling and UV experiments data showed that the possibility of hydrogen bonding between Tris and the hGH.

Previous studies showed that some of the amino acids such as Asp, can cause hydrolytic degradation in hGH (33) or similarly, oxidation of Tyr and Leo can cause hGH degradation (34). Therefore, these electrostatic interactions and hydrogen bonds can prevent destructive chemical interactions.

Salting-in effect of Tris: Changes in hGH stability observed in different concentrations of Tris can be related to the Salting-in and Salting-out effects. In aqueous protein solutions, with increasing salt ions at low concentrations, the protein solubility increases due to the creation of charge-charge bonds between ions and the protein surface. This effect of salt is called salting-in. Salting-in effects are observed up to the optimum concentration, and then, with increasing ions concentration, protein solubility decreases (called salting-out). Salting-in phenomena in Tris buffer happened at concentrations lower than 0.05 M, and in phosphate buffer containing Tris, due to existence of phosphate ions, these phenomena happened at lower Tris concentration (0.03 M).

Increase in hGH's physical stability, at low concentrations of Tris in solutions, is related to prevent protein aggregation (35).

Preferential exclusion from protein domain: Preferential exclusion of Tris from hGH's domain in aqueous solutions, is the third mechanism underlying the increased hGH stability in solutions containing the optimum concentration of Tris like osmolyts molecules (36, 37).

Tris as an osmolyte can increase the hGH stability by changing in folded and unfolded hGH levels of Gibbs free energy (38).

The Gibbs free energy of native and unfolded protein in the aqueous solution containing an osmolyte, may be increased as much as ΔG4 and ΔG2, respectively. Since the ΔG2 is increasing more than ΔG4, the thermodynamic stability of the native protein is increased. In other words, unfolded protein in the solution containing a stabilizer is more unstable than in the solutions without any stabilizer (ΔG3 is more than ΔG1). Therefore, the increased hGH's stability could be mainly due to the decreased stability of the unfolded protein in the presence of Tris at the optimum concentration (38). In spite of increased hGH stability at low concentrations of Tris, its stability decreased at high concentration of this salt, from 0.05 to 0.09 in the Tris buffer and from 0.03 to 0.09 in the phosphate buffer. In these ionic strength, it seems that the net charge of protein was neutralized with near zero, and this increased the hydrophobic protein-protein interactions, leading to hGH aggregation. Also, salting-out effect at high salt concentrations in the protein solutions, leads to protein aggregation; in this phenomenon, salts ions could compete with the water molecules needed to solvate the proteins, that leads to protein aggregation (39).

Finally, it can be claimed that adding Tris to aqueous hGH solutions increases chemical and physical stability of this protein due to creation of Tris-hGH bonds, salting-in effect and Preferential exclusion of Tris, that prevents hGH aggregation. It can be also claimed that stabilization occurs at the optimum tris concentration, pH and appropriate ionic strength.

Conclusion

The main finding of this study was that Tris as a weak base, increased the stability of hGH in aqueous solution at the body and refrigerator temperatures. The chemical degradation of hGH's amino acids was decreased due to hydrogen bonding and electrostatic interactions with Tris in the proper pH and ionic strength. By changing the Gibbs free energy between the native and unfolded hGH, Tris prevented hGH from the aggregation. Therefore, as a stabilizer, Tris can enhance hGH physicochemical stability in solutions.

Acknowledgements

This work financially supported by Royan, Iran Polymer, and Petrochemical Institutes. There is no conflict of interest in this study.

Authors' Contributions

All authors contributed to conception, design of the study, and reviewed the literature. S.Kh.; Did experimental work. S.M., H.M., H.G., S.Kh., M.I.; Made substantial contribution to the discussions, wrote, and reviewed the manuscript. H.O.; Edited the manuscript. M.H.S.; Finalized the manuscript before submission, were responsible for overall supervision. All authors read and approved the final manuscript.

References

1. Dehkhoda F, Lee CMM, Medina J, Brooks AJ . The growth hormone receptor: mechanism of receptor activation cell signaling, and physiological aspects. Front Endocrinol (Lausanne). 2018; 9: 35.
2. Cai Y, Xu M, Yuan M, Liu Z, Yuan W. Developments in human growth hormone preparations: sustained-release, prolonged half-life, novel injection devices, and alternative delivery routes. Int J Nanomedicine. 2014; 9: 3527-3538.
3. Bielohuby M, Zarkesh-Esfahani SH, Manolopoulou J, Wirthgen E, Walpurgis K, Toghiany Khorasgani M, et al. Validation of serum IGF-I as a biomarker to monitor the bioactivity of exogenous growth hormone agonists and antagonists in rabbits. Dis Model Mech. 2014; 7(11): 1263-1273.
4. Smeets ETHC, Schutzler SE, Wei JY, Azhar G, Wolfe RR. Do anabolic nutritional supplements stimulate human growth hormone secretion in elderly women with heart failure? Physiol Rep. 2017; 5(15). pii: e13366.
5. Mohammadpanah H, Rastegar H, Ramazani MR, Jaafari MR. Effects of different buffers and pH on the stability of recombinant human growth hormone. Biosci Biotechnol Res Asia. 2013; 10(1): 193-203.
6. Sharma S, Pathak N, Chattopadhyay K. Osmolyte induced stabilization of protein molecules: a brief review. Journal of Proteins and Proteomics. 2012; 3(2): 129-139.
7. Richter S, Fabris D, Binaschi M, Gatto B, Capranico G, Palumbo M. Effects of common buffer systems on drug activity: the case of clerocidin. Chem Res Toxicol. 2004; 17(4): 492-501.
8. Zamiri C, Groves MJ. Stabilization of somatropin by heparin. J Pharm Pharmacol. 2005; 57(5): 555-564.
9. Zhu G, Mallery SR, Schwendeman SP. Stabilization of proteins encapsulated in injectable poly (lactide- co-glycolide). Nat Biotechnol. 2000; 18(1): 52-57.
10. Zbacnik TJ, Holcomb RE, Katayama DS, Murphy BM, Payne RW, Coccaro RC, et al. Role of buffers in protein formulations. J Pharm Sci. 2017; 106(3): 713-733.
11. Kim SJ, Hahn SK, Kim MJ, Kim DH, Lee YP. Development of a novel sustained release formulation of recombinant human growth hormone using sodium hyaluronate microparticles. J Control Release. 2005; 104(2): 323-335.
12. Saeki K, Kunito T, Sakai M. Effect of Tris-HCl buffer on DNA adsorption by a variety of soil constituents. Microbes Environ. 2011; 26(1): 88-91.
13. Komur B, Akyuva Y, Karaslan N, Isyar M, Gumustas SA, Yilmaz I, et al. Can a biodegradable implanted bilayered drug delivery system loaded with BMP-2/BMP-12 take an effective role in the biological repair process of bone-tendon injuries? A preliminary report. J Pharm (Cairo). 2017; 2017: 7457865.
14. Taha M, Lee MJ. Interactions of TRIS [tris(hydroxymethyl)aminomethane] and related buffers with peptide backbone: thermodynamic characterization. Phys Chem Chem Phys. 2010; 12(39): 12840-12850.
15. Gaba M, Punam G, Sarbjot S. An overview on molecular docking. Int J Drug Dev Res. 2010; 2(2): 219-231.
16. Kohn W, Sham LJ. Self-consistent equations including exchange and correlation effects. Phys Rev. 1965; 140: A1133.
17. Rajagopal AK, Callaway J. Inhomogeneous electron gas. Phys Rev. 1973; 1912-1919.
18. Becke AD. Density-functional thermochemistry. III. The role of exact exchange. J Chem Phys.1993; 98: 5648-5652.
19. Lee C, Yang W, Parr RG. Development of the Colle-Salvetti correlation-energy formula into a functional of the electron density. Phys Rev B Condens Matter. 1988; 37(2): 785-789.
20. Schmidt MW, Baldridge KK, Boatz JA, Elbert ST, Gordon MS,

Jensen JH, et al. General atomic and molecular electronic structure system. J Comput Chem. 1993; 14(11): 1347-1363.
21. Forli S, Huey R, Pique ME, Sanner MF, Goodsell DS, Olson AJ. Computational protein-ligand docking and virtual drug screening with the AutoDock suite. Nat Protoc. 2016; 11(5): 905-919.
22. Morris GM, Goodsell DS, Halliday RS, Huey R, Hart WE, Belew RK, et al. Automated docking using a lamarckian genetic algorithm and an empirical binding free energy function. J Comput Chem. 1998; 19(14): 1639-1662.
23. Zhang G, Kazanietz MG, Blumberg PM, Hurley JH. Crystal structure of the cys2 activator-binding domain of protein kinase C delta in complex with phorbol ester. Cell. 1995; 81(6): 917-924.
24. Weiner SJ, Kollman PA, Case DA, Singh UC, Ghio C, Alagona G, et al. A new force field for molecular mechanical simulation of nucleic acids and proteins. J Am Chem SOC. 1984; 106(3): 765-784.
25. Shafique M, Garg ML, Nandel FS. Gly→Ala point mutation and conformation of Poly-Ala Stretch of PABPN1: a molecular dynamics study. Biophys Chem. 2015; 6(2).
26. Bayol A, Bristow A, Charton E, Girard M, Jongen P. Somatropin and its variants: structural characterization and methods of analysis. Pharmeuropa Bio. 2004; 2004(1): 35-45.
27. Varcheh N, Shafaati A, Zarghi A, Aboofezeli R. Separation of somatropin and its degradation products by high-performance liquid chromatography using a reversed-phase polymeric column. Iran J Pharm Res. 2004; 3(4): 209-213.
28. Rezaei M, Zarkesh-Esfahani SH. Optimization of production of recombinant human growth hormone in Escherichia coli. J Res Med Sci. 2012; 17(7): 681-685.
29. Kim NA, An IB, Lim DG, Lim JY, Lee SY, Shim WS, et al. Effects of pH and buffer concentration on the thermal stability of etanercept using DSC and DLS. Biol Pharm Bull. 2014; 37(5): 808-816.
30. Cao XM, Tian Y, Wang ZY, Liu YW, Wang CX. Effects of protein and phosphate buffer concentrations on thermal denaturation of lysozyme analyzed by isoconversional method. Bioengineered. 2016; 7(4): 235-240.
31. Wilhelmsen TW, Skibeli V, Arntzen FC. Stability study of somatropin by capillary zone electrophoresis. Procedia Chem. 2010; 2: 34-45.
32. Yang Q, Liang J, Han H. Probing the interaction of magnetic iron oxide nanoparticles with bovine serum albumin by spectroscopic techniques. J Phys Chem B. 2009; 113(30): 10454-10458.
33. Geiger T, Clarke S. Deamidation, Isomerization, and racemization at asparaginyl and aspartyl residues in peptides. J Biol Chem. 1987; 262(2): 785-794
34. Steinmann D, Ji JA, Wang YJ, Schöneich C. Oxidation of human growth hormone by oxygen-centered radicals: Formation of Leu-101 hydroperoxide and Tyr-103 oxidation products. Mol Pharm. 2012; 9(4): 803-814.
35. de Wit JN, Kessel Tv. Effects of ionic strength on the solubility of whey protein products. A colloid chemical approach. Food Hydrocoll. 1996; 10(2): 143-149.
36. Arakawa T, Timasheff SN . The stabilization of proteins by osmolytes. Biophys J. 1985; 47(3): 411-414.
37. Hare PD, Cress WA, Staden JV. Dissecting the roles of osmolyte accumulation during stress. Plant, Cell and Environment. 1998; 21: 535-553.
38. Auton M, Rösgen J, Sinev M, Holthauzen LM, Bolen DW. Osmolyte effects on protein stability and solubility: A balancing act between backbone and side-chains. Biophys Chem. 2011; 159(1): 90-99.
39. Méndez ASJ, Muñoz-Iglesias V, Izquierdo-Ruíz F, Prieto-Ballesteros O. Salting-out phenomenon induced by the clathrate hydrates formation at high-pressure. Journal of Physics: Conference Series. 2017; 950: 1-4.

Original Article

A Moderate Increase in Ambient Temperature Influences The Structure and Hormonal Secretion of Adrenal Glands in Rats

Florina Popovska-Perčinić, Ph.D.[1], Milica Manojlović-Stojanoski, Ph.D.[2]*, Lazo Pendovski, Ph.D.[1], Suzana Dinevska Kjovkarovska, Ph.D.[3], Biljana Miova, Ph.D.[3], Jasmina Grubin, Ph.D.[4], Verica Milošević, Ph.D.[2], Vladimir Ajdžanović, Ph.D.[2]

1. Department of Functional Morphology, Institute of Reproduction and Biomedicine, Faculty of Veterinary Medicine, Ss Cyril and Methodius University in Skopje, Lazar Pop Trajkov 5-7, Skopje, Republic of Macedonia
2. Department of Cytology, Institute for Biological Research Siniša Stanković, University of Belgrade, 142 Despot Stefan Blvd., Belgrade, Republic of Serbia
3. Department of Physiology and Biochemistry, Institute of Biology, Faculty of Natural Sciences and Mathematics, Ss Cyril and Methodius University in Skopje, Arhimedova 3, Skopje, Republic of Macedonia
4. Ministry of Education, Science and Technological Development of the Republic of Serbia, Njegoševa 12, Belgrade, Republic of Serbia

**Corresponding Address: Department of Cytology, Institute for Biological Research Siniša Stanković, University of Belgrade, 142 Despot Stefan Blvd., Belgrade, Republic of Serbia*
Email: manojlo@ibiss.bg.ac.rs

Received: 13/May/2019, Accepted: 22/July/2019

Abstract

Objective: As a consequence of global warming, the increase in the average annual temperature is observed, while the living organisms actively adapt to these changes. High environmental temperature initiates numerous physiological, autonomic, and behavioral responses, and activates the stress response. Thus, the aim of the study was to investigate effect of a moderate increase in ambient temperature on the activity of the hypothalamic-pituitary-adrenocortical (HPA) axis by determining histological changes in adrenal glands and hormonal levels in adult male rats.

Material and Methods: In this experimental study, the morpho-functional state of adrenal glands was estimated by stereological evaluation of parameters, including the adrenal volume, adrenocortical cell/nuclear size and number, and the volume density of vascular tissues after four days of exposure to a moderate increase in ambient temperature of 35 ± 1˚C. Novelli histochemical and vascular endothelial growth factor (VEGF) immunohistochemical staining provided insight into the adrenal gland vascular network. Additionally, the adrenal levels of aldosterone, corticosterone, and pituitary adrenocorticotropic hormone (ACTH) were determined as crucial indicators of the hypothalamic-pituitary-adrenocortical (HPA) axis activity.

Results: Prolonged exposure to a moderate increase in ambient temperature for four days resulted in a significant increase in ACTH level up to 24%, which altered adrenal glands both structurally and functionally. The adrenocortical volume and number of cells in all cortical zones were markedly increased ($P<0.05$). A statistically significant increase was shown in the level of aldosterone (16%) and corticosterone (25%) in serum levels of individuals.

Conclusion: Increased activity of the HPA axis reflects the response to a moderate increase in ambient temperature during four days, showing the capacity of the HPA axis to adapt the organism to daily temperature changes.

Keywords: Adrenal Glands, Adrenocorticotropic Hormone, Corticosterone, Pituitary, Temperature

Cell Journal(Yakhteh), Vol 22, No 4, January-March (Winter) 2021, Pages: 415-424

Citation: Popovska-Perčinić F, Manojlović-Stojanoski M, Pendovski L, Dinevska Kjovkarovska S, Miova B, Grubin J, Milošević V, Ajdžanović V. A moderate increase in ambient temperature influences the structure and hormonal secretion of adrenal glands in rats. Cell J. 2021; 22(4): 415-424. doi: 10.22074/cellj.2021.6827.

Introduction

The stress response initiates when afferent connections relay information from inner and outer environment to the hypothalamic nucleus paraventricularis (NPV), and more precisely to neurons that synthesize corticotropin-releasing hormone (CRH) and vasopressin (VP). Exposure to acute and chronic stress leads to the release of these hormones into the hypophyseal portal system in order to stimulate the production and secretion of adrenocorticotropic hormone (ACTH) from pituitary corticotrophs into the systemic circulation, which further regulates steroid production by the adrenal gland cortex (1). The adrenal cortex comprises of three concentric zones which are histologically and hormonally specific. Mineralocorticoids are synthesized in the small and ovoid cells of the zona glomerulosa (ZG) which is located beneath the capsule. Mineralocorticoids are controlled by kidneys and pituitary gland. The glucocorticoids are products of the significant part of the adrenal cortex named zona fasciculata (ZF) that consisted of steroidogenic cells arranged into radial lines and stimulated by pituitary ACTH. Zona reticularis (ZR), which is also regulated by pituitary hormones, is the most inner part of the adrenal cortex that produces androgens and other steroids.

Temperature is one of the most critical environmental factors that primarily determines the physiological responses. Any disturbance in homeostasis, such as temperature extremes instantly activates numerous physiological, autonomic, and behavioral responses.

The hypothalamic-pituitary-adrenocortical (HPA) axis activation and an increase in circulating glucocorticoids represent the central part of the stress response (2). In stress conditions, such as high environmental temperatures, glucocorticoids affect numerous metabolic processes related to energy expenditure and storage. In order to mobilize energy, circulating glucocorticoids stimulate glycogenolysis, lipolysis, and proteolysis, which are vital processes for muscle and neural functions (3). The actions of glucocorticoids under the conditions of thermal stress are adaptive, as usual, and directed to increase energy availability, while the currently unnecessary/unessential physiological functions, such as reproduction or immunological defense, are slowed down or interrupted (4). By reducing metabolic heat production and increasing heat dissipation, organisms are able to efficiently cope with heat stress (5). Exposure to high environmental temperature causes the activation of the renin-angiotensin-aldosterone system in order to sustain water and mineral homeostasis (6, 7). Aldosterone, secreted by adrenal gland cortex, incites reabsorption of ions, principally sodium, to avoid excessive loss of sodium and other electrolytes, indirectly influencing water retention or loss (7). Additionally, hypothalamic VP is another vital hormone that maintains water homeostasis during thermal stress. By acting in the kidney, VP stimulates reabsorption of water, thus regulating blood pressure, while together with aldosterone serves to another physiological mechanism, which is essential for survival in continuously changeable temperature conditions (8).

Keeping in mind fluctuations of the climate parameters, along with the results obtained from relevant official documents in the Western Balkan region, some high-risk changes, including intrusion of subtropical climate to the north, the increase of frequency and intensity of heatwaves, dry days, and extreme precipitation are anticipated. During the near future period, which is already happening (2016-2035), the mean annual temperature increase is expected to reach 0.5-1.0˚C, with a particular emphasis on the summer temperature (June-July-August) increase, that is higher than the mean annual up to 0.5-1.0˚C. Some calculations dramatically indicate that temperature for this season will exceed 5.0˚C increases at the end of the century, in comparison to the present climate (9). Usage of the long-term time series of mean annual air temperature confirms the elevated values for the Western Balkans region. The beginning of warming in this part of South-Eastern Europe during the last twentieth years is reported to start in a period between 1987 and 1997, mostly in 1988, while differences in the average mean annual air temperatures before and after warming are about 1˚C (10). Living organisms are very vulnerable to these changes that alter their safety, life quality, and distribution i.e., survival.

The animal thermal comfort zone is defined as the range of temperature in which animal metabolic and physiologic processes are stable and directed to the storage of carbohydrates, proteins, and fat (7). Our earlier findings showed increased activity of the pituitary corticotrophs as a result of an active resistance during four days of continuous exposure to elevated temperature (11). The consequences of 4-day exposure are characterized as short-term exposure, provoking metabolic, and physiological outcomes (12). Generally, the activation of the sympatho-adrenomedullary system triggers the first reaction on the thermal stressor, and consequently, the activation of the HPA axis (13). In this work, the influence of a moderate increase in ambient temperature on the adrenal gland cortex, during a prolonged time period, was investigated in adult rats exposed to 35 ± 1°C for four days. These temperature conditions exceed the upper-temperature comfort range and characterize the real conditions during summertime in the Western Balkan region, as already elaborated. In mammals (rats), as homoeothermic animals, the predictable response to increased environmental temperature starts with the HPA axis activation and may terminate with reduced growth, disturbances of vital functions, specific alterations in the central nervous system function, or extreme cases, lead to death (14). Thus, this study aimed to determine the histological changes and hormonal secretion of the adrenal glands, representing the activity of the HPA axis, and at the same time, being the indicators of the HPA axis disturbances under the conditions described earlier. Stereological measurements of the adrenal gland, as well as determination of adrenocortical aldosterone, corticosterone, and the pituitary ACTH circulation levels, provide respectable insights.

Materials and Methods

Animals and experimental protocol

In this experimental study, the experiments were conducted on adult male Wistar rats, weighing 260 g-350 g. Animals were kept under standard conditions (12:12 hours light-dark cycle with free access to standard laboratory food and water). The animals were divided into two groups (7 animals per group): control and elevated temperature-exposed (experimental) group. The control group was kept at room temperature (20 ± 2°C), while the experimental group was continuously exposed for four consecutive days to moderately high ambient temperature (35 ± 1°C), in a special heat chamber with regulated air temperature and air humidity of 30-40%, as previously described (11). The specific temperature for the experimental group (35 ± 1°C) was chosen based on some previous investigations (15), established as a moderately high environmental temperature. Besides, the mode of continuous exposure was proposed in other studies (16). It should be mentioned that the climate region of South-Eastern Europe, which we belong to, is well-known for having similar air temperatures during the summer months (15, 17). After four days of exposure,

the animals were sacrificed by a laparotomic procedure under ether narcosis (Diethyl ether Stabil. G.R., Lach-Ner, s.r.o., 27711 Neratovice, Czech Republic). The sacrifice was performed between 8.00-9.00 AM. Subsequently, the blood samples were taken from arterial blood (a. dorsalis) and the plasma was frozen at -70°C for the hormonal analysis, while the adrenal glands were excised, weighed, and prepared for the further histological analyses. All animal procedures were in accordance with the EU Directive 2010/63/EU and approved by the Ethical Committee for the Use of Laboratory Animals of the Institute for Biological Research Siniša Stanković University of Belgrade (approval no. 2-12/12).

Histochemical and immunohistochemical staining

The adrenal glands were removed immediately after euthanasia, weighed, and fixed in 4% paraformaldehyde for 24 hours. After dehydration in ethanol with increasing concentrations, they were cleared in xylene and paraffin-embedded. For the histochemical staining and following the histological examinations and stereological measurements, adrenals were serially sectioned using a rotational microtome (RM 2125RT, Leica Microsystem, Wetzlar, Germany). The adrenal sections, at the thickness of 5 μm, were stained with hematoxylin-eosin and the Novelli method, which enables gaining insight into the tissue vascular profile and the measurement of vascular volume density (18). Hematoxylin-eosin staining procedure started with deparaffinization in xylene (2×5 minutes), rehydration in series of alcohol in decreasing gradient (100% ethanol, 96% ethanol, 70% ethanol; 5 minutes each), and continued with incubation in hematoxylin (3 minutes) followed by washing in tap water. The next step was eosin incubation (5 minutes) followed by brief immersion in 96% ethanol, dehydration in 100% ethanol (5 minutes) and incubation in xylene (2×5 minutes). Finally, the sections were mounted on Canada balsam. For the latter, after deparaffinization and rehydration, adrenal sections were incubated in heated 1N HCl (60˚C, 3 minutes), 1% acid fuchsine (30 seconds) and 1% light green (30 seconds), followed by washing in distilled water, and finally, dehydration and mounting were carried out. As a result, purple erythrocytes were clearly visible against the bright green background of the adrenal cortex. Digital visualization was obtained by a Leitz DM RB light microscope (Leica, Germany) with a DFC320 CCD camera (Leica Microsystems Ltd. Switzerland) and a DFC Twain Software (Leica, Germany).

Immunohistochemically labeled sections of the adrenal gland with vascular endothelial growth factor (VEGF), as an angiogenic peptide, provided insight into the capacity of the capillary network forming/branching. After deparaffinization and rehydration, the antigen retrieval procedure was performed by incubating sections in 0.01 M citrate buffer (pH=6.0) in a microwave (750 W) for 21 minutes (18). Endogenous peroxidase activity was blocked in 0.3% H_2O_2 in methanol for 15 minutes, followed by blocking non-specific staining by 1 hour incubation with 10% normal swine serum (Dako, Denmark). Then, sections were incubated with rabbit polyclonal anti-VEGF antibody (Abcam®, ab46154; Cambridge, MA, USA, 1:100) overnight at 4˚C. After washing in phosphate buffered saline (PBS), sections were incubated with secondary antibodies, polyclonal swine-anti-rabbit IgG/HRP (Dako A/S, Glostrup, Denmark; 1:300) for 1 hour, at room temperature. Antibody localization was visualized by 0.05% 3,3-diaminobenzidine tetrahydrochloride (DAB) and counterstained with hematoxylin.

Stereological measurements and morphometric analyses

The adrenal sections stained with hematoxylin-eosin were used for stereological measurements by a simple counting method (19, 20). Sections were examined under a light microscope with the aid of the Weibel multipurpose lattice M_{42} (42 points, 21 test lines) inserted into the ocular of the microscope. The volume of the adrenal gland, adrenal cortex volume, and volume of individual zones of the cortex [zona glomerulosa (ZG), zona fasciculate (ZF), zona reticularis (ZR)] were determined on serially sectioned adrenal glands. To prevent bias, from each adrenal sample, the first analyzed section was randomly chosen (choosing from 1st to 10th section), and then the measurements were performed on every10th section. Using ×100 magnification and mentioned M_{42} lattice, the total number of points falling on each adrenal cortex zone was counted. The volume of adrenal gland cortex and each zone of the cortex were calculated by multiplying the total number of test points by the area corresponding to one point and the thickness of the ten sections.

In order to measure the individual volume of adrenocortical cells and their nuclei for each adrenal gland zone, a single section containing the zona medullaris was selected, as a proxy of the central part of the gland. The 30-test areas of the ZG and 50-test areas of both the ZF and ZR were analyzed under a light microscope, at ×1000 magnification. The number of counts hitting cytoplasm and nuclei, as well as, the total cell number within the lattice M42 correspond to the size of individual cells or their nuclei, respectively. Earlier karyometric studies (19) estimated the shape coefficient to be 1.382 for the ZF, and 1.500 for the ZG. Since the adrenocortical cells are mononuclear, calculation of the numerical density (N_V) (that corresponded to the number of cells per cubic millimeter) and Na (that corresponded to the number of cells in the plane of tissue sections) allowed the calculation of a single adrenocortical cell/nuclear volume.

The formula of Weibel (19) was used to determine the

numerical density of the nuclei (Nv):

$Nv=(k/\beta)\times(Na^{3/2}/Vv^{1/2})$.

The cellular and nuclear volumes were calculated according to these formulas:

$Vc=1/N_V$, and $Vn=V_Vn/N_V$

where V_Vn represents a nuclear volume density of the specific adrenocortical cell, providing information about the nuclei attendance, while N_V indicates a numerical density.

As the volumes of adrenocortical zones and volumes of single cells in each zone were calculated after conducted measurements, the number of adrenocortical cells for ZG, ZF, and ZR was calculated.

The estimation of the volume density was utilized to determine the percentage of vascular volume in the cortex. Image acquisition, morphometric assessment, and digital imaging were performed under a light microscope (Olympus BX-51, Olympus, Japan) and the newCAST stereological software package [Visiopharm Integrator System (VIS), version 5.3.1.1640, Visiopharm, Denmark]. Four central sections were analyzed per animal, with a spacing of 10 sections apart. The morphometric assessment was performed at a final magnification of ×490. The counting area was defined using a mask tool, while an interactive test grid with uniformly spaced test points for histomorphometric assessment was provided by the newCAST software.

Volume densities (V_V) were calculated as the ratio of the number of points hitting the vascular compartment divided by the number of points hitting the analyzed area i.e., adrenal cortex:

V_V (%)=Pp/Pt×100,

where Pp represents counted points hitting the vascular tissue component and Pt is a total number of points of the test system hitting the adrenal cortex. The volume density of vascular tissues was calculated for each of the four sections, then for each animal, and at the end, the average value was calculated per group.

Hormonal level measurements

For conducting the hormonal analysis, plasma and serum samples were used and stored at -70˚C until assay. The plasma levels of ACTH in both groups (experimental and control) were determined by the IMMULITE method (Diagnostic Products Corporation; Los Angeles, CA, USA) in duplicate samples within a single assay (18). The intra-assay coefficient of variation was 9.6%, while the analytical sensitivity of the assay was 9 pg/mL. Serum aldosterone concentrations were determined by enzyme immunoassay for direct quantitative determination (Aldosterone Elisa Kit, IBL, Germany) with intra-assay CV 7.4% and analytical sensitivity of 128.67 pg/mL. Serum corticosterone concentrations were measured without dilution by immunoassay in duplicate within single assays with an intra-assay CV of 8.0% (sensitivity of 171 pg/ml) (Corticosterone Immunoassay, R&D System Inc., USA).

Statistical analysis

Data provided by stereological measurement and hormonal analysis were subjected to statistical analysis using the STATISTICA® version 5.0 (Stat Soft, Inc., USA) software. The stereological and hormonal data were evaluated by the Student's t test. A $P<0.05$ level of confidence was assumed as the statistically significant result. All results are expressed as means for six animals per group.

Results

Body mass and adrenal gland weights

Exposure to the elevated temperature for four days leads to a significant reduction in body mass by 20%, as well as to a marked increase in absolute and relative adrenal gland weights by 16% and 25% respectively, compared with the control group (Table 1).

Stereological parameters of the adrenal gland and hormonal analyses

Stereological measurements and qualitative histological insight after the rat exposure to elevated temperature revealed a significant increase in adrenal gland volume (14%), volume of adrenal gland cortex (15%) and the individual cortical zones (ZG 18%, ZF 15%, ZR 14%), when compared with the adequate control values (Fig.1).

The volume of adrenocortical cells and their nuclei in each zone of the adrenal gland cortex did not significantly change after a four-day exposure to an elevated temperature in comparison with the control values (Fig.2).

Table 1: The body mass, as well as the absolute and relative adrenal gland weights, after exposure to the elevated temperature for four days

Experimental group	Body mass (g)	Absolute adrenal gland weight (mg)	Relative adrenal gland weight (mg %)
Control	337.5 ± 26.9	20 ± 1.2	6.9 ± 0.6
Elevated temperature-exposed	270.6 ± 11.7*↓	23.2 ± 1.5*↑	8.6 ± 0.6*↑

Results are expressed as mean ± SD. *; P<0.05 vs. control.

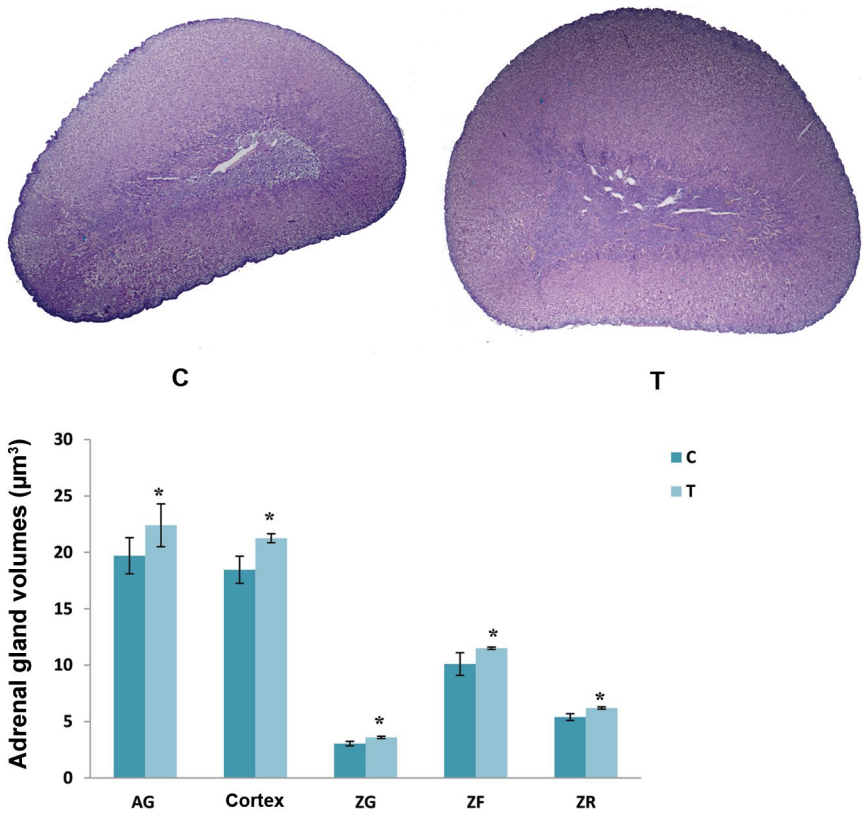

Fig.1: Histological appearance and volumes of the adrenal gland (AG), AG cortex and individual zones within the cortex [zona glomerulosa (ZG), zona fasciculate (ZF) and zona reticularis (ZR)] in the control group (C) and after exposure to the elevated temperature for four days (T). Results are expressed as the mean ± SD. *; P<0.05 vs. control (scale bar: 400 µm).

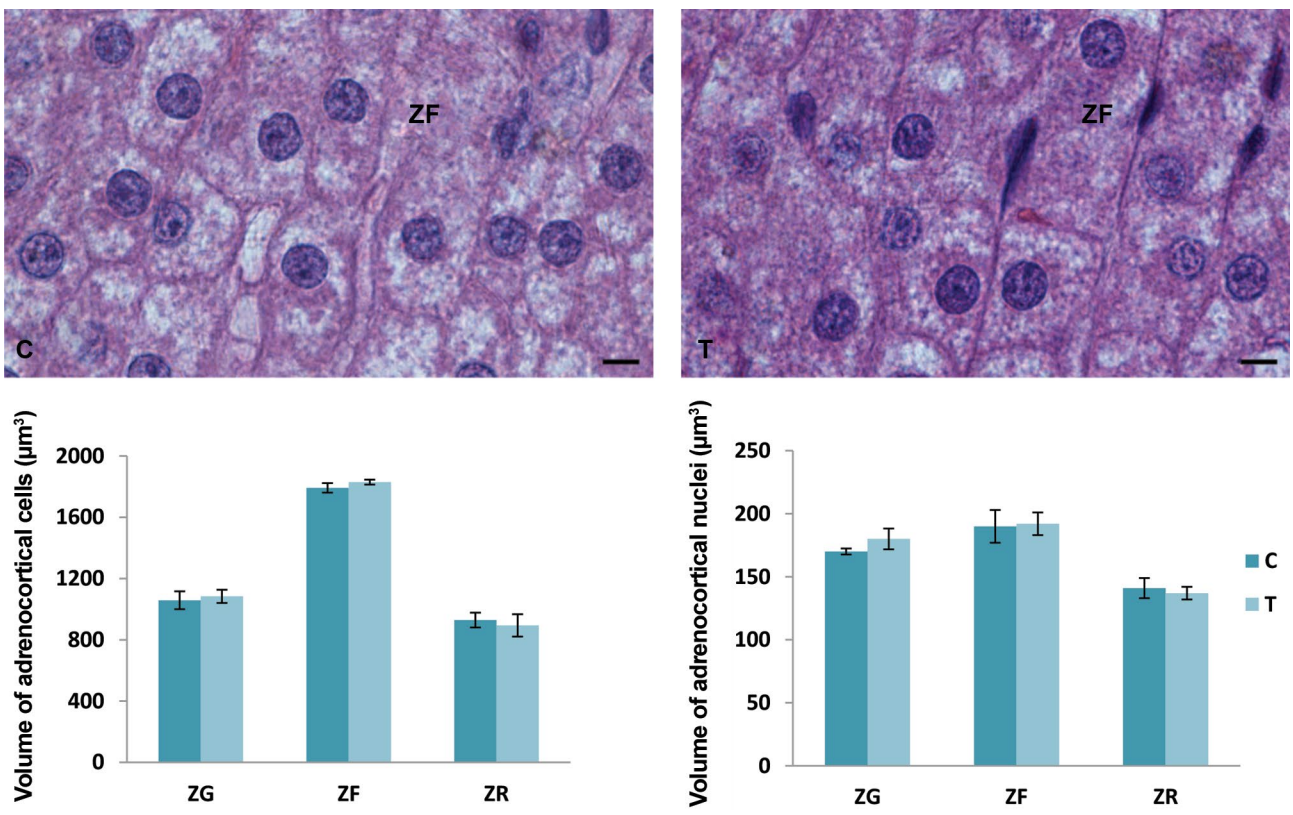

Fig.2: Volumes of the adrenocortical cells and their nuclei in individual zones within the cortex [zona glomerulosa (ZG), zona fasciculate (ZF) and zona reticularis (ZR)] and histological presentation of ZF cells (hematoxylin-eosin staining) in the control group (C) and after exposure to the elevated temperature for four days (T). Results are expressed as mean ± SD (scale bar: 8 µm).

The elevated temperature exposure for four days caused a significant increase in the number of adrenocortical cells in the ZG, ZF, and ZR of adrenal gland cortex compared with the values established in the control group. Namely, a significant increase in the number of adrenocortical cells in ZG was 17%, 9% in ZF and 30% in ZR. The volume density of vascular tissue in the adrenal cortex did not change under the influence of elevated temperature (Fig.3).

The hormonal analysis showed a substantial increase in the plasma ACTH level by 24%, after exposure to elevated temperature in comparison to the control group. Additionally, 4-day exposure to the elevated temperature led to a significant increase in aldosterone by 16%, while the raise of corticosterone concentration was 25% in comparison to the control values (Table 2).

Histological analysis

After the histological examination of hematoxylin/eosin and Novelli-stained sections, the characteristics of a clear zonation pattern in the adrenal cortex was observed (Fig.4A, B). Outermost situated, spherically-organized ZG cells were changed with radially arranged cords of ZF cells and an anastomosing network made of ZR cells that occupied the innermost portion of the cortex. As confirmed after unbiased stereological measurement, only the volume of individual zones differs, while the vascular tissue remained unchanged when the elevated temperature-exposed and control sections were compared.

There were no significant differences in the immunohistochemical appearance and number of VEGF immunopositive cells in the adrenal cortex when the control group and the group exposed to a moderately elevated temperature were compared. VEGF immunostaining was intensive in the cells of ZG in both groups. Moreover, VEGF was expressed in several individual ZF and ZR adrenocortical cells. Cytoplasmic immunopositivity differs among the cells in inner adrenocortical zones: intense immunostaining was noted in some cells, as well as diffuse cytoplasmic immunopositivity. The presence of lipid droplets was also evident in adrenocortical cells (Fig.4C, D)

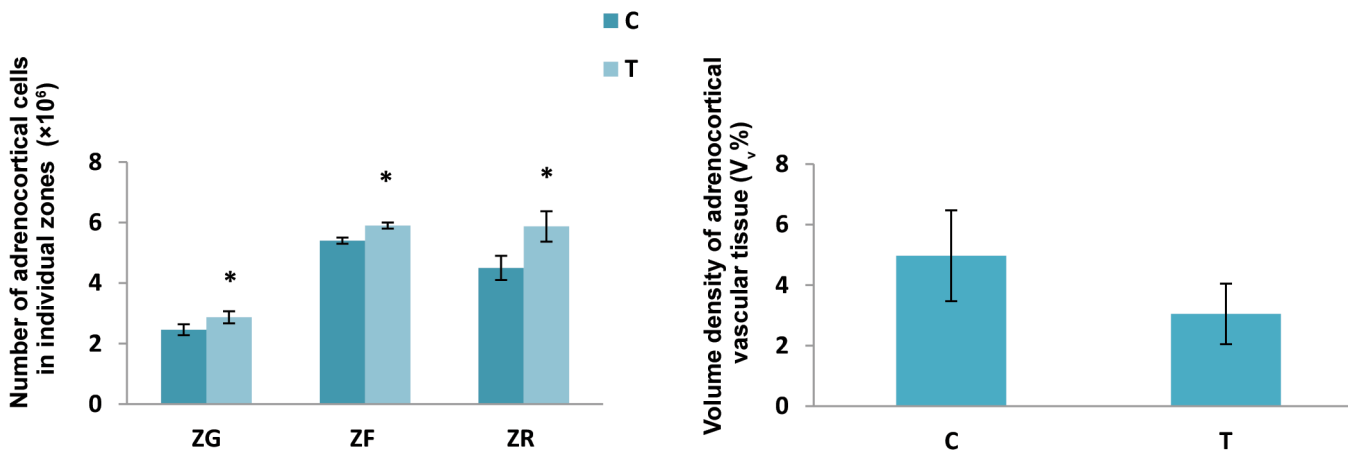

Fig.3: The number of adrenocortical cells in individual adrenocortical zones [zona glomerulosa (ZG), zona fasciculate (ZF), zona reticularis (ZR)] and volume density of vascular tissue in adrenal gland cortex in control animals (C) and after exposure to the elevated temperature for four days (T). Results are expressed as the mean ± SD. *; P<0.05 vs. control.

Table 2: The circulating concentration of pituitary adrenocorticotropic hormone (ACTH), as well as adrenocortical hormones, aldosterone, and corticosterone, in controls and after exposure to the elevated temperature for four days

Experimental group	ACTH (pmol/L)	Aldosterone (nmol/L)	Corticosterone (nmol/L)
Control	25.15 ± 0.88	20 ± 1.2	6.9 ± 0.6
Elevated temperature-exposed	31.12 ± 0.57*↑	23.2 ± 1.5*↑	8.6 ± 0.6*↑

Results are expressed as means ± SD. *; P<0.05 vs. control.

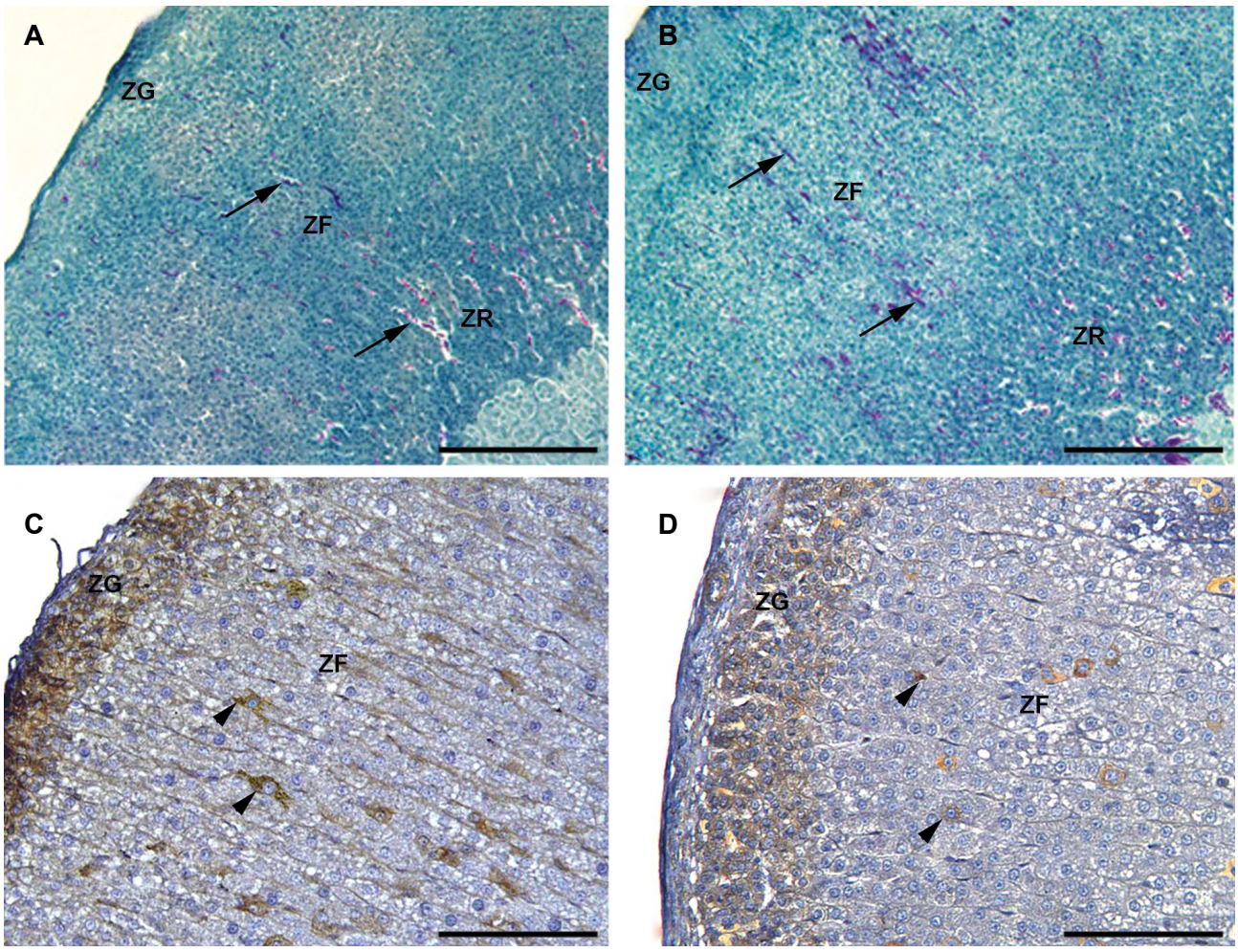

Fig.4: Histological evaluations of the adrenal gland. **A.** The Novelli stained sections of adrenal glands in controls and **B.** After exposure to the elevated temperature for four days. The arrows indicate the blood vessels (scale bar: 200 µm). Immunohistochemical staining of vascular endothelial growth factor (VEGF) in **C.** The adrenal glands in controls and **D.** After exposure to the elevated temperature for four days. Arrow tip indicates VEGF depots (scale bar: 100 µm).
ZG; Zona glomerulosa, ZF; Zona fasciculate, and ZR; Zona reticularis.

Discussion

Actual trend of global warming, being established during the last 50 years, cannot be explained only by natural cycles, but the anthropogenic influence has also been recognized to possess a significant impact. The most significant consequence of the mentioned trend, an increase in the average annual temperature is particularly pronounced during the summer months in South-Eastern Europe (9). In the region of western Balkans, elevated summer temperatures often last several days in continuity, representing a serious challenge to the homeostasis, and living world actively adjusts to the conditions arising from the environment. The function of the HPA axis follows the seasonal and daily temperature rhythm, while the markedly increased activity of the axis reflects the response to a moderate increase in ambient temperature of 35 ± 1°C for four days, as the results of this study clearly show. Circulating ACTH level was significantly increased, thus affecting adrenal glands that respond to both structural and functional alterations. It should also be mentioned that decreased bodyweight, as a consequence of 4-day exposure to moderately high ambient temperature, was established. Previous research noticed the reduction of food intake in rats after heat exposure, probably caused by the inhibition of hypothalamic peptidergic circuitry related to food intake and energy balance (21, 22).

Acute short-term heat exposure (38˚C, 60 minutes) leads to a significant elevation in plasma ACTH, representing the response to hyperthermia, as expected (23). The elevated temperature exposure for four days, performed in the previous histological study (11), has provoked more comprehensive changes in pituitary corticotrophs: weak immunopositivity, confirmed by a decrease in the relative fluorescence intensity of the individual ACTH cells, as well as the reduction of the volume density and the increase in the size of these cells. Thus, morphometric parameters and immunofluorescent features pointed that under described experimental conditions, the intensive synthetic and secretory activity of ACTH cells takes place, followed by a significant rise in blood ACTH concentration (11). In oppose to the acute stress episodes, characterized by the fast reestablishment of homeostasis and returning to the basal level, during constant exposure to a moderate increase in ambient temperature, the

central brain mechanisms of glucocorticoid feedback inhibition are altered. Inhibitory hippocampal neurons drive towards hypothalamic CRH neurons, exerted *via* multi-synaptic pathways, is decreased, so CRH neurons are able to constantly stimulate pituitary ACTH cells functioning (24). Moreover, glucocorticoid feedback inhibition from the amygdala to hypothalamic PVN has been attenuated in chronic stress conditions (25). The elevated temperature exposure for four days obviously activates different pattern of ACTH cell response to the applied chronic stimulus, associated with desensitization of the ACTH cells, that led to constant hormonal levels and consequently to a significant increase in ACTH level in circulation (11).

ACTH is a trophic hormone, which, through the activation of the melanocortin 2 receptor, controls the proliferation of adrenocortical cells and promotes steroidogenesis (26). In the present study, the absolute and relative weight gain of the adrenal gland was clearly shown. The adrenals were stimulated after four days of exposure to elevated temperature. A significant increase in the adrenocortical volume was the consequence of a marked increase in the volume of each adrenocortical zone separately. The unchanged volumes of individual cells and their nuclei, in all cortical zones, were observed in parallel with a significantly increased number of adrenocortical cells. Taking into consideration that the volume density of vascular tissues in the entire cortex was not significantly altered, it could be concluded that the increase in the proliferation rate of adrenocortical cells was an adaptive response to meet the increased physiological demands under the given conditions. Temporal prolongations of the temperature stress for four days, which resulted in the adrenal gland hypertrophy, in fact, has enabled baseline glucocorticoid hypersecretion for an extended period. Intolerance to heat exposure is associated with HPA axis impairment, followed by decreased plasma corticosterone and ACTH levels (27). The intensified process of steroidogenesis after heat exposure, and consequently elevated corticosterone level in circulation, reported here, was accompanied by numerous morphological changes at the level of electron microscopy of adrenocortical cells. Close apposition of specific lipid droplets to the cytoplasmic face of the cell membrane, increased mitochondrial volume density, the close morphological relationship between lipid droplets and mitochondria together with pronounced smooth endoplasmic reticulum, pointed that functional engagement of alleged organelles was needed for intensive steroid hormone synthesis (23). Generally, some lipid droplets contain cholesterol as a steroid hormone precursor, others contain hormone itself or its immediate precursors, as the forms of steroid hormones storage, and release them into the capillary network (28). This is in line with the reports of Nussdorfer (29), who found that the long-term trophic effect of ACTH is involved not only in an increase of the adrenal mass but also in the stimulation of the ZF and organelles involved in the steroidogenic activity of ZF cells. A stimulatory effect of ACTH on adrenocortical ZF cells was characterized by hypertrophy and enhancement of the steroidogenic enzymeactivity (30, 31).

Additionally, ACTH stimulates the proliferation of the adrenocortical cells, mostly in ZG and outer ZF region, and enhances the centripetal migration of newly-formed cells and their accumulation in ZR (32). Consequently, the significantly increased number of ZR cells and ZR volume were established after four days of the elevated temperature exposure in our experiment.

VEGF is the major mediator of angiogenesis and a potent inducer of endothelial fenestration during vascularization of the adrenal gland (33). The ZG, as the place with a massively developed vasculature network, is characterized by VEGF presence in the cytoplasm of all cells, as presented. As in the ZG, the elevated temperature did not have any significant effect on the presence of VEGF-positive adrenocortical cells in ZF and ZR. In parallel, the same percentage of vascular tissue was measured in both examined groups. Thus, the immunohistochemical appearance of the VEGF-positive adrenocortical cells and determined vascular volume density pointed out that ambient temperature of 35 ± 1°C did not significantly influence the circulatory aspect of the adrenal gland. The activated physiological mechanisms caused the blood flow is increased peripherally, in the skin, in order to allow greater heat dissipation in given experimental conditions.

Some earlier reports, elaborating the effect of moderately high ambient temperature (35 ± 1°C), suggesting the decreased serum corticosterone level after 24-48 hours of the heat exposure, through a feedback mechanism resulting from the acute elevated temperature exposure of rats within the first day (15). Such a decrease is followed by an elevation of a serum corticosterone level again (34), which is consistent with our earlier results. Furthermore, normalization or even a decrease in the activity of pituitary-adrenocortical axis after the long-term exposure (28 days) to a moderately high ambient temperature has been reported, suggesting an acclimation of the organism during exposure to a persistent environmental stressor (35).

Our findings of the increased volume of ZG, increased number of the cells in this zone, and increased blood aldosterone concentration probably result from ACTH stimulation in the elevated temperature-exposed group. It was found that although ACTH primarily regulates glucocorticoid production in ZF cells, this pituitary hormone can also provoke the ZG cells activity (36). Some reports found that chronic ACTH and cAMP treatment might induce hyperplasia and mitotic activity in ZG cells (37). Additionally, the strong stimulus for aldosterone synthesis during the elevated temperature exposure and increased aldosterone blood level reported here, supposedly stem from the sodium depletion, which presumed to occur together with the dehydration, in order to preserve mineral homeostasis (7). Increased

synthetic and secretory activity of the ZG cells under elevated temperature regime showed the ultrastructural level, as an increased number of mitochondria and lipid depletion (23). Increased plasma renin and aldosterone concentrations were also found after five days of the continuous heat exposure to a moderate increase in ambient temperature (38). According to Saini et al. (39) elevated aldosterone concentration in men, as a result of increased activity of the renin-angiotensin system, could be a compensatory mechanism against mineral and water losses, which occurs after six days of passive heat exposure. Other studies also showed that under stress conditions, both ACTH and VP secretion increase, which stimulates aldosterone release (31).

Conclusion

The presented results could provide the additional example of the HPA axis capacity to respond to prolonged stimulation of a moderate increase in ambient temperature, enabling the body to adapt to the daily temperature changes and, consequently, successful acclimatize an organism. Future studies will be directed to the elucidation of the concrete mechanisms underlying the changes in the HPA axis activity upon elevation in an ambient temperature.

Acknowledgements

This work financially supported by the Ministry of Science, Education and Technological Development of the Republic of Serbia (grant number 173009). There is no conflict of interest in this study.

Authors' Contributions

F.P.P., L.P., S.D.K., B.M.; The manuscript concept creators have organized and conducted the experiment (work in the animal care unit, daily care and treatment, sacrificing, adrenal glands extraction), processed the experimental material, performed the stereological measurements, biochemical analysis. M.M.S., V.M., V.A.; Written the majority of the manuscript, performed part of the stereological measurements and designed the figures, analyzed and interpreted results of the research group in a broader context of literature. J.G., V.M.; Carefully read and critically revised the manuscript for its scientific merit and intellectual content and supplemented the discussion and literature survey. All authors read and approved the final manuscript.

References

1. Smith SM, Vale WW. The role of the hypothalamic-pituitary-adrenal axis in neuroendocrine responses to stress. Dialogues Clin Neurosci. 2006; 8(4): 383-395.
2. Pacak K, Palkovits M, Yadid G, Kvetnansky R, Kopin IJ, Goldstein DS. Heterogeneous neurochemical responses to different stressors: a test of Selye's doctrine of nonspecificity. Am J Physiol. 1998; 275(4): R1247-R1255.
3. Kuo T, McQueen A, Chen TC, Wang JC. Regulation of Glucose Homeostasis by Glucocorticoids. Adv Exp Med Biol. 2015; 872: 99-126.
4. Joseph DN, Whirledge S. Stress and the HPA axis: balancing homeostasis and fertility. Int J Mol Sci. 2017; 18(10). pii: E2224.
5. Rivas E, Rao M, Castleberry T, Ben-Ezra V. The change in metabolic heat production is a primary mediator of heat acclimation in adults. J Therm Biol. 2017; 70(Pt B): 69-79.
6. Sparks MA, Crowley SD, Gurley SB, Mirotsou M, Coffman TM. Classical renin-angiotensin system in kidney physiology. Compr Physiol. 2014; 4(3): 1201-1228.
7. Sanin YL, Zuluaga CAM, Morales AMT. Adaptive responses to thermal stress in mammals. Rev Med Vet. 2016; 31: 121-135.
8. Frank E, Landgraf R. The vasopressin system-from antidiuresis to psychopathology. Eur J Pharmacol. 2008; 583(2-3): 226-242.
9. Vuković A, Vujadinović Mandić M. Study on climate change in the Western Balkans region. In: Nikčević R, editor. Bosnia and Herzegovina: Regional Cooperation Council Secretariat; 2018.
10. Bonacci O. Increase of mean annual surface air temperature in the Western Balkans during last 30 years. Vodoprivreda. 2012; 44: 75-89.
11. Popovska-Perčinić F, Jarić I, Pendovski L, Ristić N, Trifunović S, Milošević V, et al. The effect of moderate heat on rat pituitary ACTH cells: histomorphometric, immunofluorescent and hormonal study. Acta Vet. 2017(4); 67(4): 495-507.
12. Shido O, Sakurada S, Tanabe M, Nagasaka T. Temperature regulation during acute heat loads in rats after short-term heat exposure. J Appl Physiol (1985). 1991; 71(6): 2107-2113.
13. Jasnic N, Djordjevic J, Djurasevic S, Lakic I, Vujovic P, Spasojevic N, et al. Specific regulation of ACTH secretion under the influence of low and high ambient temperature. The role of catheholamines and vasopressin. J Therm Biol. 2012; 37: 469-474.
14. Sharma HS, Hoopes PJ. Hyperthermia induced pathophysiology of the central nervous system. Int J Hyperthermia. 2003; 19(3): 325-354.
15. Popovska-Perčinić F, Ajdžanović V, Dinevska-Kofkarovska S, Jordanova M, Trifunović S, Šošić-Jurjević B, et al. Morphofunctional characteristics of pituitary corticotropes in an animal model of heat stress. J Med Biochem. 2011; 30(4): 287-292.
16. Ando M, Katagiri K, Yamamoto S, Asanuma S, Usuda M, Kawahara I, et al. Effect of hyperthermia on gluthatione peroxidase and lipid peroxidative damage in liver. J Therm Biol. 1994; 19: 177-185.
17. Mitev S, Dinevska-Kjovkarovska S, Miova B. Effect of acclimation to high environmental temperature on the activity of hepatic glycogen phosphorylase (a+b and a), liver glycogen content and blood glucose level in rats. J Therm Biol. 2005; 30(8): 563-568.
18. Milošević VL, Severs WB, Ristić NM, Manojlović-Stojanoski MN, Popovska-percinic FV, Sosic-Jurievic BT, et al. Soy isoflavone effects on the adrenal gland of orchidectomized adult rats: histological and hormonal study. Histol Histopathol. 2018; 33(8): 843-857.
19. Weibel E. Stereological methods, Vol. 1. Practical methods for biological morphometry. New York: Academic Press; 1979; 1-415.
20. Mahmoudzadeh Sagheb HR, Moudi B. Basic application of stereology in histology and medical sciences. Gene Cells Tissue 2014; 1(3): e24237.
21. Brobeck JR. Food and temperature. Recent Prog Horm Res. 1960; 16: 439-466.
22. Cure M. Plasma corticosterone response in continous versus discontinuous chronic heat exposure in rat. Physiol Behav. 1989; 45(6): 1117-1122.
23. Petrovic-Kosanovic D, Velickovic K, KokoV, Jasnic N, Cvijić G, Čakić-Milošević M. Effect of acute heat stress on rat adrenal cortex-a morphological and ultrastructural study. Cent Eur J Biol. 2012; 7(4): 611-619.
24. Willner P. The chronic mild stress (CMS) model of depression: history, evaluation and usage. Neurobiol Stress. 2017; 6: 78-93.
25. Jankord R, Herman JP. Limbic regulation of hypothalamo-pituitary-adrenocortical function during acute and chronic stress. Ann NY Acad Sci. 2008; 1148(1): 64-73.
26. Lotfi CF, de Mendonca PO. Comparative effect of ACTH and related peptides on proliferation and growth of rat adrenal gland. Front Endocrinol. 2016; 7: 39.
27. Michel V, Peinnequin A, Alonso A, Buguet A, Cespuglio R, Canini F. Decreased heat tolerance is associated with hypothalamo-pituitary-adrenocortical axis impairment. Neuroscience. 2007; 147(2): 522-531.
28. Rhodin JA. The ultrastructure of the adrenal cortex of the rat under normal and experimental conditions. J Ultrastruct Res. 1971; 34(1): 23-71.
29. Nussdorfer GG. Cytophysiology of the adrenal cortex. Int Rev Cytol. 1986; 98:1-405.
30. Nussdorfer GG, Mazzocchi G. Long-term effects of ACTH on rat adrenocortical cells: a coupled stereological and enzymological study. J Steroid Biochem. 1983; 19(6): 1753-1756.

31. Aguilera G, Kiss A, Lu A, Camacho C. Regulation of adrenal steroidogenesis during chronic stress. Endocr Res. 1996; 22(4): 433-443.
32. Stachowiak A, Nussdorfer GG, Malendowicz LK. Proliferation and distribution of adrenocortical cells in the gland of ACTH- or dexamethasone-treated rats. Histol Histopathol. 1990; 5(1): 25-29.
33. de Fraipont F, El Atifi M, Gicquel C, Bertagna X, Chambaz EM, Feige JJ. Expression of the angiogenesis markers vascular endothelial growth factor-A, thrombospondin-1, and platelet-derived endothelial cell growth factor in human sporadic adrenocortical tumors: correlation with genotypic alterations. J Clin Endocrinol Metab. 2000; 85(12): 4734-4741.
34. Kotby S, Johnson H. Rat adrenal cortical activity during exposure to high (34°C) ambient temperature. Life Sci. 1967; 6(11): 1121-1132.
35. Dinevska-Kjovkarovska S, Guladin T, Miova B, Mitev S, Gerazova K. Changes in the hypothalamo-pituitary-adrenocortical and hypothalamo-pituitary-thyroid axes in diabetic rats acclimated to moderate hyperthermic environment. J Therm Biol. 2009; 34(4): 200-205.
36. Spät A, Hunyady L. Control of aldosterone secretion: a model for convergence in cellular signaling pathways. Physiol Rev. 2004; 84(2): 489-539.
37. Payet N, Lehoux JG. Effect of ACTH or zinc treatment on plasma aldosterone and corticosterone levels and on the in vitro steroid output from adrenocortical cells. Can J Biochem. 1982; 60(11): 1058-1064.
38. Brandenberger G, Follenius M, Di Nisi J, Libert JP, Simon C. Amplification of nocturnal oscillations in PRA and aldosterone during continuous heat exposure. J Appl Physiol. 1989; 66(3): 1280-1286.
39. Saini J, Brandenberger G, Libert JP, Follenius M. Nocturnal pituitary hormone and renin profiles during chronic heat exposure. J Appl Physiol. 1993; 75(1): 294-300.

Original Article

Changes in Serum Levels and Gene Expression of *PGC-1α* in The Cardiac Muscle of Diabetic Rats: The Effect of Dichloroacetate and Endurance Training

Hamed Rezaei Nasab, Ph.D.[1]*, Abdolhamid Habibi, Ph.D.[1], Masoud Nikbakht, Ph.D.[1], Mohammad Rashno, Ph.D.[2, 3], Saeed Shakerian, Ph.D.[1]

1. Department of Exercise Physiology, Faculty of Sport Sciences, Shahid Chamran University of Ahvaz, Ahvaz, Iran
2. Department of Immunology, Faculty of Medicine, Ahvaz Jundishapur University of Medical Sciences, Ahvaz, Iran
3. Cellular and Molecular Research Center, Ahvaz Jundishapur University of Medical Sciences, Ahvaz, Iran

Corresponding Address: P.O.Box: 61877-81911, Department of Exercise Physiology, Faculty of Sport Sciences, Shahid Chamran University of Ahvaz, Ahvaz, Iran
Email: hamed.rezai93@yahoo.com

Received: 14/May/2019, Accepted: 24/July/2019

Abstract

Objective: Physical activity leads to changes in the level of gene expression in different kinds of cells, including changes in mitochondrial biogenesis in the myocardium in diabetic patients. Peroxisome proliferator-activated receptor γ coactivator 1α (PGC-1α) is a gene that plays an important role in regulating mitochondrial biogenesis. The purpose of this study was to investigate changes in serum levels and cardiac muscle expression of *PGC-1α* in diabetic rats in response to the administration of dichloroacetate (DCA) and endurance training.

Materials and Methods: In this experimental study, 64 male Wistar rats were selected and randomly divided into eight groups after induction of diabetes with streptozotocin (STZ). The endurance training protocol was performed on a treadmill for 6 weeks. Intraperitoneal injection of DCA of 50 mg/ kg body weight was used for the inhibition of Pyruvate Dehydrogenase Kinase 4 (PDK4) in the myocardium. Gene expression were measured using real-time polymerase chain reaction (PCR). One-way ANOVA and Tukey's test were used to statistically analyze the data.

Results: The results of the study showed that *PDK4* gene expression in the endurance training group, diabetes+endurance training group, diabetes+endurance training+DCA group and endurance training+DCA group was higher compared to the control group. Expression of *PGC-1α* was higher in the endurance training group compared to the control group but was lower compared to the control group in diabetes+endurance training+DCA group and diabetes+DCA group ($P<0.05$).

Conclusion: Considering that *PGC-1α* plays an important role in mitochondrial biogenesis, it is likely that by inhibiting PDK4 and subsequently controlling oxidation of fatty acid (FA) in the heart tissue, oxidative stress in the heart tissue of diabetic patients will be reduced and cardiac efficiency will be increased.

Keywords: Endurance Training, Diabetes, Dichloroacetate, Mitochondrial Biogenesis

Cell Journal(Yakhteh), Vol 22, No 4, January-March (Winter) 2021, Pages: 425-430

Citation: Rezaei Nasab H, Habibi AH, Nikbakht M, Rashno M, Shakerian S. Changes in serum levels and gene expression of PGC-1α in the cardiac muscle of diabetic rats: the effect of dichloroacetate and endurance training. Cell J. 2021; 22(4): 425-430. doi: 10.22074/cellj.2021.6942.

Introduction

Changes in glucose, fat and protein metabolism are usually observed in patients with diabetes. These metabolic abnormalities can lead to a wide range of long-term effects called diabetes complications. Several studies have shown the directly negative effects of diabetes mellitus on the cardiac muscle (1, 2). In addition, cardiovascular diseases are the main cause of death in diabetic patients, not only due to coronary artery disease and high blood pressure but also due to the direct effects of diabetes complications on the heart, independent of other pathologic factors (3).

However, physical activity affects many physiological systems of the body (4), including the structure and function of the myocardium (5). Studies have shown that the myocardium adapts structurally and efficiently to the type of stimulus provided by physical activity, i.e. endurance or strength (6). Tissue changes resulting from physical activity also take place at the level of gene expression (7) including changes in the biogenesis of mitochondria and myosin heavy chains (MHCs) of the myocardium (8, 9). Mitochondrial biogenesis, or increasing the size and number of mitochondria, is a complex process that requires combined function of different mechanisms and the controlled expression of many genes. PGC-1 which is a cell receptor and facilitates the release of mitochondrial proteins, is the most important regulator of mitochondrial biogenesis. PGC-1 has two, alpha and beta, isoforms, both are involved in this process, but alpha is more important (10).

Studies have shown that other members of this family of transcription coactivators are activated in response to environmental stimuli, such as heat and physical activity. They also play an important role in maintaining glucose homeostasis, lipid homeostasis, energy homeostasis and possibly in pathogenic conditions such as obesity, diabetes, neurodegeneration, and heart diseases (11). Since the heart has a very high energy demand and has basically no energy reserves, it needs to constantly produce great amounts of energy in the form of adenosine

triphosphate (ATP) at a high speed to maintain contraction performance and ion homeostasis. Most of the ATP in mitochondria is produced by oxidative phosphorylation, and fatty acids (FA) and carbohydrates are the primary energy substrates. It must be noted that FA account for 50-75% of ATP production in the heart (12, 13). But a diabetic heart cannot completely use glucose due to insulin deficiency, and therefore may be forced to use FA as its energy sources almost exclusively (14). FA metabolism also consumes more oxygen per mole than glucose and thus increases oxidative stress in the heart tissue and reduces cardiac performance (15).

Dichloroacetate (DCA), is imported by cells through the monocarboxylate transporters and mostly a sodium-linked monocarboxylate transporter also named solute carrier family-5 member 8 (SLC5A8), while access to the mitochondrial matrix is achieved by the mitochondrial pyruvate carrier system (16). Studies have shown that glucose incorporation into glycogen was decreased in diabetic rats when DCA was used to activate pyruvate dehydrogenase (PDH); which was accompanied by an increase in glucose oxidation and a reduction of FA oxidation (beta oxidation) in peripheral tissues of diabetic rats (17). The pyruvate dehydrogenase complex (PDC) is a multifunctional complex in the mitochondrial matrix and has the role of gatekeeper in the tricarboxylic acid cycle (TCA) and oxidative phosphorylation. DCA and some of its derivatives play an important role in this mechanism by activating PDC and regulating cell metabolism in response to diabetes and other conditions that increase the beta oxidation of FA e.g. endurance training (18). However, despite studies done on PGC-1α and its effects on diabetes as well as DCA consumption, findings are still very contradictory and, to the best of our knowledge, a study that can investigate the impact of DCA consumption on *PGC-1α* expression and its relation with aerobic training has not been conducted yet. Given the need to develop therapeutic strategies to prevent or treat diabetes complications, we conducted this study to assess whether DCA consumption after endurance training can reduce the complications of the PGC-1α mechanism in diabetic patients.

Materials and Methods

In this experimental study, the Ethical guidelines set by Shahid Chamran University of Ahvaz, Iran, was considered during all stages of the experiment (EE/97.24.3.70001/scu.ac.ir). The present study was designed as a posttest-only with the control groups experiment. In this study, 64 male Wistar rats at 8 weeks of age and weighting 200 ± 12 g were purchased from the Physiology Research Center, Ahvaz Jundishapur University of Medical Sciences, Iran. Rats were kept under the conditions of an even split of 12 hours of light and 12 hours of darkness) at 22 ± 2˚C and 50% humidity, fed with special rat food and water.

After one week of familiarization with the laboratory environment, rats were matched based on weight and were randomly divided into eight groups including healthy control groups (n=7), healthy control group+DCA (n=7), healthy endurance training group (n=7), healthy endurance training group+DCA (n=8), diabetes control group (n=7), diabetes control group+DCA (n=8), diabetes endurance training group (n=8), and diabetes endurance training group+DCA (n=8).

Daily intraperitoneal injections of 50 mg/kg body weight of DCA was used to inhibit PDK4 in the myocardium (19). After 12 hours of food deprivation, induction of diabetes was done by intraperitoneal injection of 50 mg/kg body weight of the STZ solution dissolved in 0.05 M citrate buffer with 4.5 pH (20). The equivalent volume of citrate buffer was also intraperitoneally injected to non-diabetic rats. After 48 hours, with a small lancet cut on the tail vein, a drop of blood was placed on a glucometer strip and the strip was read using a Glucotrend 2glucometer (Roche, Switzerland). Rats whose glucose level was higher than 300 mg/dl were considered diabetic. The rats' blood sugar levels were measured again at the end of the training program to ensure they had not returned to normal (21).

Dichloroacetate

DCA was injected to rats intraperitoneally at 50 mg/kg body weight in the form of 24-hour intervals, dissolved in methyl cellulose 400 cP and combined with calcium gluconate (22).

Endurance training protocol

The protocol was carried out for six weeks (five days/week). First, training groups were trained for seven days with a treadmill (model LE7800; Harvard Apparatus, France) at a speed of 15 m/minutes for 20 minutes. Then, the duration and speed were gradually increased over the course of six weeks, so that in the final week the speed reached 30 m/minutes and the training time reached 50 minutes/day, which was equivalent to 75% of the maximum oxygen consumed. Electric shocks were performed on the rats to make them complete the training during the course of the experiment. Control groups were kept in cages untreated during the training period (Table 1) (23).

72 hours after the last training session, 64 rats were anesthetized by intraperitoneal injection of ketamine (90 mg/kg body weight) and Xylazin (90 mg/kg body weight) and the myocardium was immediately removed and frozen in liquid nitrogen and transferred to -80˚C until used for further analysis.

Table 1: Training protocol

Week	1(acclimatization)	2	3	4	5	6	7
Speed (m/minutes)	15	20	24	24	28	28	30
Time (minuts)	20	30	30	40	40	50	50

Real-time quantitative reverse transcription polymerase chain reaction

Isol-RNA was used to extract mRNA. About 100

milligrams of myocardium tissue was ground and homogenized in one milliliter of Isol-RNA Lysis Reagent. Afterwards, the homogeneous product was centrifuged for 10 minutes at 12000 g and 4˚C, the supernatant was removed, and transferred to a new microtube. In the next step, 200 µl of chloroform was added to the separated supernatant and vigorously stirred for 15 seconds. Then, micro tubes were re-centrifuged for 15 minutes at 12000 g and 4˚C. The aqueous phase was removed and 600 µl of isopropyl alcohol was added and centrifuged at 12000 g to extract total RNA. The concentration of RNA and its purity were calculated by controlling the ratio of 260/280 nm OD where values between 1.8 to 2 were defined as acceptable purity. Synthesis of cDNA was carried out using Takara's cDNA synthesis kit, according to the manufacturer's instructions. Expression of the desired genes was measured using real-time polymerase chain reaction (PCR) and the results were quantified using the $2^{-\Delta\Delta CT}$ formula (24). PCR reactions were performed using AMPLIQON RealQ Plus 2x Master Mix Green High ROX. 40 cycles were considered for each cycle of real-time PCR. And the temperatures of each cycle were set at 94˚C for 20 seconds, 60-58˚C for 30 seconds and 72˚C for 30 seconds. *GAPDH* was used as the reference gene to measure relative gene expression and melting curve analysis was performed to control the specificity of the product. The sequence of the primers used in the study is reported in Table 2.

Blood analysis

The concentration of PGC-1α in the serum was assessed and quantified using an enzyme-linked immunosorbent assay (ELISA) kit according to the manufacturer's instructions (Cusabio- EL018425RA-USA). These concentrations were expressed as picograms per milligram of total protein (pg/ml protein). Detection range was in the domain of 125-8000 pg/ml with 31.25 pg/ml sensitivity (Table 3).

Statistical analysis

Shapiro-Wilk test was used to determine the normality of the data and Levene's test was used to test the homogeneity of the variances. One-way ANOVA and Tukey's test were used to determine the difference between the groups' variables. All statistical analyses were done at a significance level of $P<0.05$ (SPSS Statistics 22).

Results

The results of the study showed that *PDK4* gene expression was higher in the endurance training group (P=0.018), diabetes+endurance training group (P=0.008), diabetes+endurance training+DCA group (P=0.001) and endurance training+DCA group (P=0.026) compared to the control group (Fig.1). *PGC-1α* gene expression in the endurance training group was also higher compared to the control group (P=0.020) but was lower in the diabetes+endurance training+DCA group (P=0.003) and diabetes+DCA group (P=0.001) compared to the control group (Fig.2).

Table 2: Mouse-specific primer pairs used for quantitative reverse transcription polymerase chain reaction

Gene	Primer sequence (5´-3´)	Base per	Accession No.
GAPDH	F: TGATTCTACCCACGGCAAGTT	21	M17701.1
	R: TGATGGGTTTCCCATTGATGA		
PGC-1α	F: TGGAGTCCACGCATGTGAAG	20	NM_013196.1
	R: CGCCAGCTTTAGCCGAATAG		
PDK4	F: TATCGACCCCAACTGCGATG	20	NM_053551.1
	R: TGGATTGGTTGGCCTGGAAA		

Table 3: Physical characteristics and plasma metabolites of groups

Group Variable	CONT	CONT+DCA	TRA	TRA+DCA	DM	DM+DCA	DM+TRA	DM+TRA+DCA
Starting body weight (g)	204 ± 7	207 ± 8	208 ± 9	211 ± 5	205 ± 11	209 ± 6	208 ± 10	209 ± 7
terminal body weight (g)	223 ± 14	198 ± 11	188 ± 10	168 ± 11	216 ± 14	182 ± 12	163 ± 12	149 ± 6
Starting glucose (mg/dl)	104 ± 11	103 ± 6	107 ± 8	108 ± 10	440 ± 81	490 ± 61	412 ± 77	472 ± 58
Terminal glucose (mg/dl)	110 ± 14	111 ± 6	107 ± 8	108 ± 10	407 ± 69	328 ± 52	274 ± 32	178 ± 28
PGC-1α (pg/ml)	75.7 ± 12.6	70.1 ± 10.8	59.6 ± 9.1	73.1 ± 14.8	82.3 ± 13.8	70.3 ± 12.3	64.7 ± 11.7	60.5 ± 10.9

Data are presented as mean ± SD. CONT; Control, DCA; Dichloroacetate, TRA; Training, and DM; Diabetes.

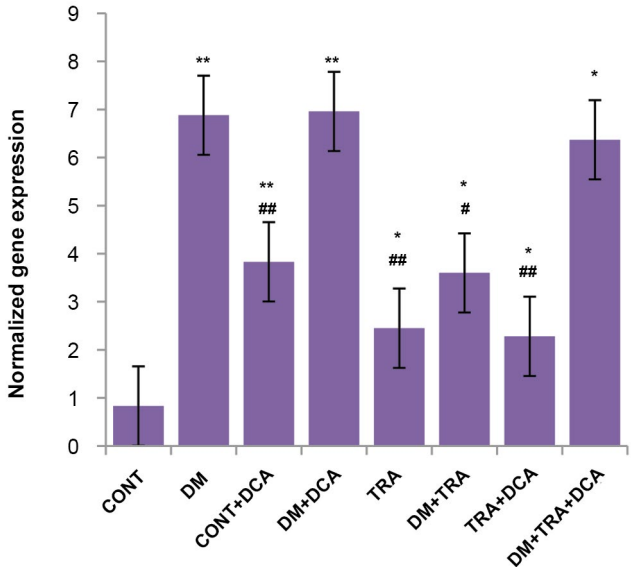

Fig.1: The normalized gene expression of *PDK4* in different groups. From left to right, control group (CONT, n=7); diabetes group (DM, n=7); control+DCA group (CONT+DCA, n=7); diabetes+DCA group (DM+DCA, n=8); healthy group+training group (TRA, n=7); diabetes+training group (DM+TRA, n=8); healthy+training+DCA group (TRA+DCA, n=8); diabetes+training+DCA group (DM+TRA+DCA, n=8). Data are expressed as mean ± SD.
*; P<0.05, **; P<0.01 compared with the control group, #; P<0.05, ##; P<0.01 compared with the diabetic group, and DCA; Dichloroacetate.

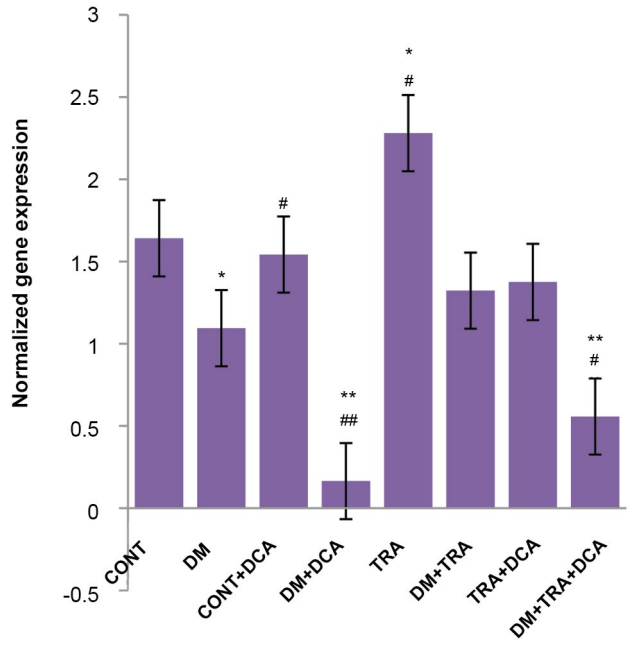

Fig.2: The normalized gene expression of *PGC-1α* in different groups. From left to right, control group (CONT, n=7); diabetes group (DM, n=7); control+DCA group (CONT+DCA, n=7); diabetes+DCA group (DM+DCA, n=8); healthy group+training group (TRA, n=7); diabetes+training group (DM+TRA, n=8); healthy+training+DCA group (TRA+DCA, n=8); diabetes+training+DCA group (DM+TRA+DCA, n=8). Data are expressed as mean ± SD.
*; P<0.05, **; P<0.01 compared with the control group, #; P<0.05, ##; P<0.01 compared with the diabetic group, and DCA; Dichloroacetate.

ELISA results

The results of One-way ANOVA test showed a significant difference in PGC-1α variables (F=72.33, df=7, P=0.001). Also, results of Turkey's test showed that the mean serum levels of PGC-1α in the diabetic+endurance training group, endurance training group and diabetes+endurance training+DCA was significantly lower than the control group (P≤0.01). But the mean serum levels of PGC-1α in the diabetes group was significantly higher than the control group (P≤0.01, Fig.3).

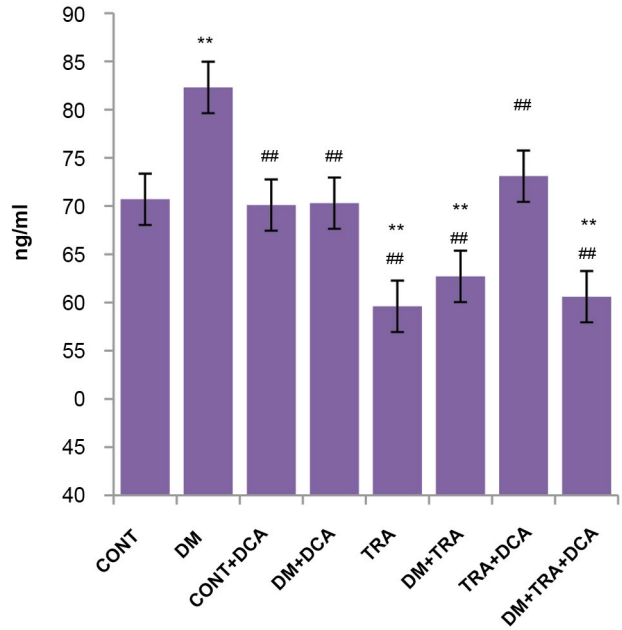

Fig.3: PGC-1α serum levels in different groups. From left to right, control group (CONT, n=7); diabetes group (DM, n=7); control+DCA group (CONT+DCA, n=7); diabetes+DCA group (DM+DCA, n=8); healthy group+training group (TRA, n=7); diabetes+training group (DM+TRA, n=8); healthy+training+DCA group (TRA+DCA, n=8); diabetes+training+DCA group (DM+TRA+DCA, n=8). Data are expressed as mean ± SD.
**; P<0.01 compared with the control group, ##; P<0.01 compared with the diabetic group, and DCA; Dichloroacetate.

Discussion

The purpose of this study was to investigate the effect of *PDK4* inhibition and endurance training on PGC-1α serum levels and gene expression in the cardiac muscle of diabetic rats. The most important results were that after the endurance training, the expression of *PDK4* and *PGC-1α* increased in line with each other. But following inhibition of *PDK4* in the cardiac muscle using DCA, expression of PGC-1α decreased in endurance training+DCA group, the endurance training+diabetes+DCA group, and the diabetes+DCA group. The results also showed that PGC-1α serum levels in the diabetes group was higher than the control group but PGC-1α serum levels in the diabetic+endurance training group, endurance training group and diabetes+endurance training+DCA were lower than the control group. In the present study, DCA as a

halogenated carboxylic acid increased the activity of PDC in the animal muscle (25) competitively by controlling PDK2 and PDK4 (26). DCA is known as an activator of PDC (27). Among the more important features of DCA is its ability to lower the blood sugar level in diabetic rats but not cause changes in the blood glucose levels of non-diabetic ones (28).

On the other hand, PGC-1α plays a main role in regulating cellular energy metabolism (29) and by connecting to *PPAR-γ1* and regulating gene expression, it is linked to mitochondrial biogenesis. In addition, it plays an important role in the metabolism of FA and amino acids, secretion of insulin, insulin sensitivity, and obesity. As has been reported, PGC-1α is involved in the pathogenesis of type 2 diabetes mellitus (30). On the other hand, the amount of PGC-1α in aerobic tissues, including the myocardium, is high (31). Studies have shown that the burden of work-induced physical activity on the heart causes a change in the heart myosin heavy chain (MHC) which is similar to what happens in hypertrophy (32). Endurance activities reduce the level of ATP and increase intracellular calcium which activates two pathways, AMP-activated protein kinase (AMPK) and calcium calmodulin/dependent protein kinase (CaMK) (33). The activation of these two pathways leads to an increase in the synthesis of PGC-1α which, by regulating the expression of contractile and enzymatic proteins that participate in the metabolic network, increases the working capacity and also provides the energy needed for increased heart activity. Endurance activity increases the consumption of ATP and a decrease in the amount of ATP activates the AMPK pathway. In this way, *PGC-1α* gene expression in the heart tissue, that is affected by endurance activity, is increased. One of the main actions of the *PGC-1α* gene is mitochondrial biogenesis and thus supply of oxidative enzymes so its increased expression is consistent with increasing aerobic metabolism of the heart (34). Matsuhashi et al. (35) showed in a study that stable activation of the PDH enzyme through PDK4 inhibition by DCA causes excessive CoA production, meaning increased oxidation in the citric acid cycle and leads to histone acetylation which is one of the most important epigenetic processes that occurs to regulate the expression of genes. Inhibition of the PDK4 enzyme following 6 weeks of DCA injection led to increased *PDK4* expression at the level of mRNA, which this is a natural response to inhibiting this key enzyme in the metabolism of aerobic energy. *PGC-1α* is involved in the upregulation of the expression of genes regulating FA oxidation in the heart and skeletal muscles (36).

Conclusion

The results of this study showed that endurance training increased *PDK4* and *PGC-1α* expressions in the cardiac muscle of diabetic rats by inhibiting *PDK4, PGC-1α* expression decreased in the cardiac muscle of diabetic rats. Given that *PGC-1α* plays an important role in mitochondrial biogenesis, it is likely that by controlling PDK4 and subsequently controlling oxidation of FA (beta oxidation) in heart tissue, oxidative stress in the heart tissues of diabetic patients can be reduced and cardiac efficiency increased.

Acknowledgements

This study was extracted from the thesis for Hamed Rezaei Nasab Ph.D. of Exercise Physiology at Shahid Chamran University of Ahvaz and finacially supported by Shahid Chamran University of Ahvaz, Iran. We thank all the people who have collaborated with us in this research. The authors declare no conflicts of interest.

Authors' Contributions

H.R.N, A.H.H.; Were involved in study design, manuscript preparation, and editing. M.N.; Was involved in animal experiments, preparing first draft and editing. M.R., S.Sh.; Were involved in animal experiments, qRT-PCR, and ELISA assays. All authors read and approved the final manuscript.

Reference

1. Boudina S, Abel ED. Diabetic cardiomyopathy revisited. Circulation. 2007; 115(25): 3213-3223.
2. Boudina S, Abel ED. Diabetic cardiomyopathy, causes and effects. Rev Endocr Metab Disord. 2010; 11(1): 31-39.
3. Ernande L, Derumeaux G. Diabetic cardiomyopathy: myth or reality? Arch Cardiovasc Dis. 2012; 105(4): 218-225.
4. Keteyian SJ, Brawner CA, Savage PD, Ehrman JK, Schairer J, Divine G, et al. Peak aerobic capacity predicts prognosis in patients with coronary heart disease. Am Heart J. 2008; 156(2): 292-300.
5. Fenning A, Harrison G, Dwyer D, Rose'Meyer R, Brown L. Cardiac adaptation to endurance exercise in rats. Mol Cell Biochem. 2003; 251: 51-59.
6. Mihl C, Dassen WRM, Kuipers H. Cardiac remodeling: concentric versus eccentric hypertrophy in strength and endurance athletes. Neth Heart J. 2008; 16(4): 129-133.
7. Iemitsu M, Miyauchi T, Maeda S, Sakai S, Kobayashi T, Fujii N, et al. Physiological and pathological cardiac hypertrophy induce different molecular phenotypes in the rat. Am J Physiol Regul Integr Comp Physiol. 2001; 281(6): R2029-36.
8. Baldwin KM, Haddad F. Effects of different activity and inactivity paradigms on myosin heavy chain gene expression in striated muscle. J Appl Physiol (1985). 2001; 90(1): 345-357.
9. O'Neill BT, Kim J, Wende AR, Theobald HA, Tuinei J, Buchanan J, et al. A conserved role for phosphatidylinositol 3-kinase but not Akt signaling in mitochondrial adaptations that accompany physiological cardiac hypertrophy. Cell Metab. 2007; 6(4): 294-306.
10. Scarpulla RC. Metabolic control of mitochondrial biogenesis through the PGC-1 family regulatory network. Biochim Biophys Acta. 2011; 1813(7): 1269-1278.
11. Lin J, Handschin C, Spiegelman BM. Metabolic control through the PGC-1 family of transcription coactivators. Cell Metab. 2005; 1(6): 361-370.
12. Stanley WC, Recchia FA, Lopaschuk GD. Myocardial substrate metabolism in the normal and failing heart. Physiol Rev. 2005; 85(3): 1093-1129.
13. Taegtmeyer H, Young ME, Lopaschuk GD, Abel ED, Brunengraber H, Darley-Usmar V, et al. Assessing cardiac metabolism: a scientific statement from the American heart association. Circ Res 2016; 118(10): 1659-1701.
14. Boudina S, Abel ED. Diabetic cardiomyopathy revisited. Circulation. 2007; 115(25): 3213-3223.
15. Chong CR, Clarke K, Levelt E. Metabolic remodeling in diabetic cardiomyopathy. Cardiovasc Res. 2017; 113(4): 422-430.
16. Ferrannini E, Mark M, Mayoux E. CV protection in the EMPA-REG OUTCOME trial: a "thrifty substrate" hypothesis. Diabetes Care. 2016; 39(7): 1108-1114.
17. Small L, Brandon AE, Quek LE, Krycer JR, James DE, Turner N, et

al. Acute activation of pyruvate dehydrogenase increases glucose oxidation in muscle without changing glucose uptake. Am J Physiol Endocrinol Metab. 2018; 315(2): E258-E266.
18. James MO, Jahn SC, Zhong G, Smeltz MG, Hu Z, Stacpoole PW. Therapeutic applications of dichloroacetate and the role of glutathione transferase zeta-1. Pharmacol Ther. 2017; 170: 166-180.
19. Sun XQ, Zhang R, Zhang HD, Yuan P, Wang XJ, Zhao QH, et al. Reversal of right ventricular remodeling by dichloroacetate is related to inhibition of mitochondria-dependent apoptosis. Hypertens Res. 2016; 39(5): 302-311.
20. Gajdosik A, Gajdosikova A, Stefek M, Navarova J, Hozova R. Streptozotocin-induced experimental diabetes in male Wistar rats. Gen Physiol Biophys. 1999; 18 Spec No: 54-62.
21. Thomas C, Perrey S, Lambert K, Hugon G, Mornet D, Mercier J. Monocarboxylate transporters, blood lactate removal after supramaximal exercise, and fatigue indexes in humans. J Appl Physiol (1985). 2005; 98(3): 804-809.
22. Ferriero R, Iannuzzi C, Manco G, Brunetti-Pierri N. Differential inhibition of PDKs by phenylbutyrate and enhancement of pyruvate dehydrogenase complex activity by combination with dichloroacetate. J Inherit Metab Dis. 2015; 38(5): 895-904.
23. Sun L, Shen W, Liu Z, Guan S, Liu J, Ding S. Endurance exercise causes mitochondrial and oxidative stress in rat liver: effects of a combination of mitochondrial targeting nutrients. Life Sci. 2010; 86(1-2): 39-44.
24. Cook GA, Lavrentyev EN, Pham K, Park EA. Streptozotocin diabetes increases mRNA expression of ketogenic enzymes in the rat heart. Biochim Biophys Acta Gen Subj. 2017; 1861(2): 307-312.
25. Constantin-Teodosiu D. Regulation of muscle pyruvate dehydrogenase complex in insulin resistance: effects of exercise and dichloroacetate. Diabetes Metab J. 2013; 37(5): 301-314.
26. Patel MS, Korotchkina LG. Regulation of mammalian pyruvate dehydrogenase complex by phosphorylation: the complexity of multiple phosphorylation sites and kinases. Exp Mol Med. 33(4): 2001; 191-197.
27. Hoshino D, Tamura Y, Masuda H, Matsunaga Y, Hatta H. Effects of decreased lactate accumulation after dichloroacetate administration on exercise training-induced mitochondrial adaptations in mouse skeletal muscle. Physiol Rep. 2015; 3(9). pii: e12555.
28. Lloyd S, Brocks C, Chatham JC. Differential modulation of glucose, lactate, and pyruvate oxidation by insulin and dichloroacetate in the rat heart. Am J Physiol Heart Circ Physiol. 2003; 285(1): H163-H172.
29. Boström P, Wu J, Jedrychowski MP, Korde A, Ye L, Lo JC, et al. A PGC1-α-dependent myokine that drives brown-fat-like development of white fat and thermogenesis. Nature. 2012; 481(7382): 463-468.
30. Soyal S, Krempler F, Oberkofler H, Patsch W. PGC-1α: a potent transcriptional cofactor involved in the pathogenesis of type 2 diabetes. Diabetologia. 2006; 49(7): 1477-1488.
31. Lehman JJ, Barger PM, Kovacs A, Saffitz JE, Medeiros DM, Kelly DP. Peroxisome proliferator-activated receptor γ coactivator-1 promotes cardiac mitochondrial biogenesis. J Clin Invest. 2000; 106(7): 847-856.
32. Gupta MP. Factors controlling cardiac myosin-isoform shift during hypertrophy and heart failure. J Mol Cell Cardiol. 2007; 43(4): 388-403.
33. Richter EA, Ruderman NB. AMPK and the biochemistry of exercise: implications for human health and disease. Biochem J. 2009; 418(2): 261-275.
34. Czubryt MP, Olson EN. Balancing contractility and energy production: the role of myocyte enhancer factor 2 (MEF2) in cardiac hypertrophy. Recent Prog Horm Res. 2004; 59: 105-124.
35. Matsuhashi T, Hishiki T, Zhou H, Ono T, Kaneda R, Iso T, et al. Activation of pyruvate dehydrogenase by dichloroacetate has the potential to induce epigenetic remodeling in the heart. J Mol Cell Cardiol. 2015; 82: 116-124.
36. Huss JM, Torra IP, Staels B, Giguere V, Kelly DP. Estrogen-related receptor alpha directs peroxisome proliferator-activated receptor alpha signaling in the transcriptional control of energy metabolism in cardiac and skeletal muscle. Mol Cell Biol. 2004; 24(20): 9079-9091.

Original Article

Correlation of *TCF4, GSK, TERT* and *TERC* Expressions with Proliferation Potential of Early and Late Culture of Human Peripheral Blood Mesenchymal Stem Cells

Zahra Fazeli, Ph.D.[1]*, Masoumeh Rajabibazl, Ph.D.[2], Sepideh Faramarzi, M.Sc.[1], Mir Davood Omrani, Ph.D.[1], Sayyed Mohammad Hossein Ghaderian, M.D., Ph.D.[1], Niloufar Safavi Naini, M.Sc.[1]

1. Department of Medical Genetics, Faculty of Medicine, Shahid Beheshti University of Medical Sciences, Tehran, Iran
2. Department of Clinical Biochemistry, Faculty of Medicine, Shahid Beheshti University of Medical Sciences, Tehran, Iran

Corresponding Address: P.O.Box: 19839-63113, Department of Medical Genetics, Faculty of Medicine, Shahid Beheshti University of Medical Sciences, Tehran, Iran
Email: z.fazeli@sbmu.ac.ir

Received: 23/April/2019, Accepted: 22/June/2019

Abstract

Objective: In the recent years, mesenchymal stem cells (MSCs) were considered as the suitable source of cells for transplantation into the damaged tissues in regenerative medicine. There was low number of these cells in different organs and this characteristic was the main drawback to use them in treatment of diseases. Cellular senescence of the stem cells has been demonstrated to be dependent to the telomerase activity. The aim of present experimental study was to evaluate correlation of the expression of telomerase components and WNT signaling pathway in MSCs derived from human peripheral blood (PB-MSCs).

Materials and Methods: In this experimental study, following the isolation of MSCs from peripheral blood mononuclear cells, RNA was extracted from these cells in the early culture (8-9th days) and late culture (14-17th days). Then, expression of *TERT, TERC, TCF4, GSK* and *CTNNB1* was determined by quantitative reverse transcription polymerase chain reaction (qRT-PCR) based on SYBR Green.

Results: Our data indicated that there was a significantly reduced expression of *TERT* in the late culture of human MSCs derived from peripheral blood ($P<0.05$). Although a negative correlation was observed between *GSK* and *TERC* expression levels in the early culture of MSCs, spearman analysis showed that there was no significant correlation between the expression of telomerase components (*TERC* and *TERT*) and WNT signaling pathway ($P>0.05$).

Conclusion: The obtained results suggested that WNT signaling pathway likely plays a minor role in the maintenance of telomere length and proliferation potential of MSCs.

Keywords: Cellular Senescence, Mesenchymal Stem Cells, Regenerative Medicine, WNT Signaling Pathway

Cell Journal(Yakhteh), Vol 22, No 4, January-March (Winter) 2021, Pages: 431-436

Citation: Fazeli Z, Rajabibazl M, Faramarzi S, Omrani MD, Ghaderian SMH, Safavi Naini N. Correlation of TCF4, GSK, TERT and TERC expressions with proliferation potential of early and late culture of human peripheral blood mesenchymal stem cells. Cell J. 2021; 22(4): 431-436. doi: 10.22074/cellj.2021.6920.

Introduction

Following the characterization of self-renewal and differentiation abilities of mesenchymal stem cells (MSCs), these cells were considered as suitable candidates in the field of tissue engineering and repair of damaged tissues (1). MSCs have been demonstrated to be isolated from different sources including bone marrow, synovium, umbilical cord, adipose tissue and peripheral blood (2, 3). To use MSCs in cell therapy, it is necessary to obtain enough number of MSCs following the long-term culture of these cells. However, the prolonged culture was associated with cellular senescence (4). Identification of the mechanisms regulating MSC senescence could play a key function in preventing the aging in these cells.

Telomere length has been revealed to play an important role in the cellular senescence. Maintaining telomere length by telomerase prevented arrest of cell proliferation (5, 6). Izadpanah et al. (7) demonstrated presence of telomerase activity (TA) in MSCs. Their results indicated that TA was decreased with aging at MSCs. The constitutive expression of telomerase was accompanied with the enhanced proliferation ability of MSCs without any side-effect on their differentiation potential (8). Different studies showed that TA was dependent to the human telomerase reverse transcriptase (*TERT*) expression. TERT expression was regulated mainly at transcription level (9).

Analysis of the MSC expression profile has revealed that several signaling pathways, including WNT signaling, play role in different biological treats (10, 11). WNT signaling pathway has been demonstrated to be involved in several cellular processes including stem cell renewal (12). Following the interaction of WNT with its receptor, the corresponding signal was transduced to the downstream molecule, known as Dsh. This transduction led to the disruption of APC/Axin/GSK3 complex. This event prevented degradation of β-catenin. After translocation of β-catenin from the cytoplasm into the nucleus, this protein formed a complex with TCF4 and then, this complex trigger transcription of the target genes (12, 13). Zhang et al. (14) reported that WNT signaling had an ability to regulate

TERT expression in cancer and somatic cells. They demonstrated that knockdown of β-catenin by shRNA led to TA decrease in cancer cells.

In the study performed by Gry et al. (15), correlation of RNA level with protein was evaluated for different genes. Their results indicated significant correlation of the RNA with protein level in 33% of the cases. The aim of present study was to investigate whether RNA expression of *TERT* and telomerase RNA component (TERC) depend on expression of the WNT signaling pathway genes in the early and late culture of MSCs derived from peripheral blood (PB-MSCs). This finding could increase our understanding about the molecular mechanisms of MSC cellular senescence.

Materials and Methods

Preparation of human mesenchymal stem cells derived from peripheral blood

In this experimental study, 20 ml peripheral blood was collected from three females aged 35-40 years. The Ficoll density gradient method was used to isolate mononuclear cells from the collected human peripheral blood as previously described (16). The obtained cell pellet was cultured in Dulbecco's Modified Eagle Medium: Nutrient Mixture F-12 medium (DMEM-F12, BioIdea, Iran) including 10% fetal bovine serum (FBS, Gibco, USA), 2 mM L-Glutamate (BioIdea, Iran) and 100 U/ml penicillin/streptomycin (Gibco, Germany). After 72 hours, the medium containing non-adherent cells was replaced with the fresh medium. Growth of the cells was monitored under an inverted microscope. The culture cells were usually reached 70-80% confluence after six days (D6). Phenotypic characterization of these cells was confirmed as MSCs by flow cytometry with CyFlow Space (Partec, Germany). This study was performed on MSC cultures after 8-9 days and 14-17 days; they were known as early and late culture, respectively. MSC culture on day 6th was used as control.

Quantitative reverse transcription polymerase chain reaction

Total RNA purification kit (Jena Bioscience, Germany) was used to obtain Total RNA from the cultured cells. In the next step, DNase I (Fermentas, USA) treatment was performed to remove DNA contamination. After that, RevertAid First Strand cDNA Synthesis kit (Thermo Scientific, USA) was used to synthesize cDNA. Next, quantitative reverse transcription polymerase chain reaction (qRT-PCR) was carried out in duplicate using RealQ Plus Master Mix Green (Ampliqon, Denmark). Condition of the reaction was performed as follow: 95˚C for 10 minutes followed by 40 cycles of denaturation at 95˚C for 30 seconds, annealing at 60˚C for 30 seconds, and extension at 72˚C for 30 seconds. The sequences of primer sets are presented in Table 1. Specificity of qRT-PCR products was confirmed by melting curve analysis as well as the electrophoresis of 1.5% agarose gel (Genfanavaran, Iran) stained with Safe stain (Yekta Tajhiz Azma, Iran).

Compliance with ethical standards

All procedures performed in this study including human participants were in accordance with the ethical standards of the institutional and/or national research committee and with the 1964 Helsinki declaration and the relative later amendments or comparable ethical standards. The present study was approved by the Ethics Committee of the School of Medicine Shahid Beheshti University of Medical Sciences (Tehran, Iran, Ethical code: IR.SBMU.MSP.REC.1397.550). The manuscript have been read and confirmed by all authors.

Table 1: The sequence of primers used in the present study

Gene symbol	Primer sequence (5´-3´)	Product length (bp)
HSP90AB1	F: GGAAGTGCACCATGGAGAGGA	157
	R: GCGAATCTTGTCCAAGGCATCAG	
TERT	F: GGAGCAAGTTGCAAAGCATTG	182
	R: TCCCACGACGTAGTACATGTT	
TERC	F: CTGGGAGGGGTGGTGGCCATTT	179
	R: CGAACGGGCCAGCAGCTGACAT	
GSK3B	F: TCGAGAGCTCCAGATCATGAGAA	124
	R: CGGAACATAGTCCAGCACCAGA	
CTNNB1	F: TCTGAGGACAAGCCACAAGATTACA	122
	R: TGGGCACCAATATCAAGTCCAA	
TCF4	F: GCACTGCCGACTACAATAGG	150
	R: CTGCATAGCCAGGCTGATTC	

Statistical analysis

Relative expression level of the studied genes was estimated by using the pfaffl method. The present study was performed in three independent experiments and HSP90AB1 was used as the housekeeping gene to normalize the qRT-PCR data. Student's t test was used to define difference between the early and late cultures of MSC. Correlation between the expression of telomerase components and WNT signaling pathway genes was defined by estimating the Spearman correlation coefficient (r_s). A $P<0.05$ was considered statistically significant. These analyses were performed using Social Science Statistics website (http://www.socscistatistics.com/tests/studentttest/Default2.aspx).

Results

CD marker analysis of the stem cells in the present study indicated that these cells expressed CD184, CD105, CD73 and CD44. No expression was determined in these cells for CD14 and CD45 (Fig.1). Pattern of the surface markers on these cells confirmed identity of these cells as MSCs. These cells showed fibroblast like morphology at the day 6th of culture. Appearance of these cells was changed along with increasing the age. These cells showed flat and wide morphology under inverted microscope at the days 14th -17th of culture (Fig.2).

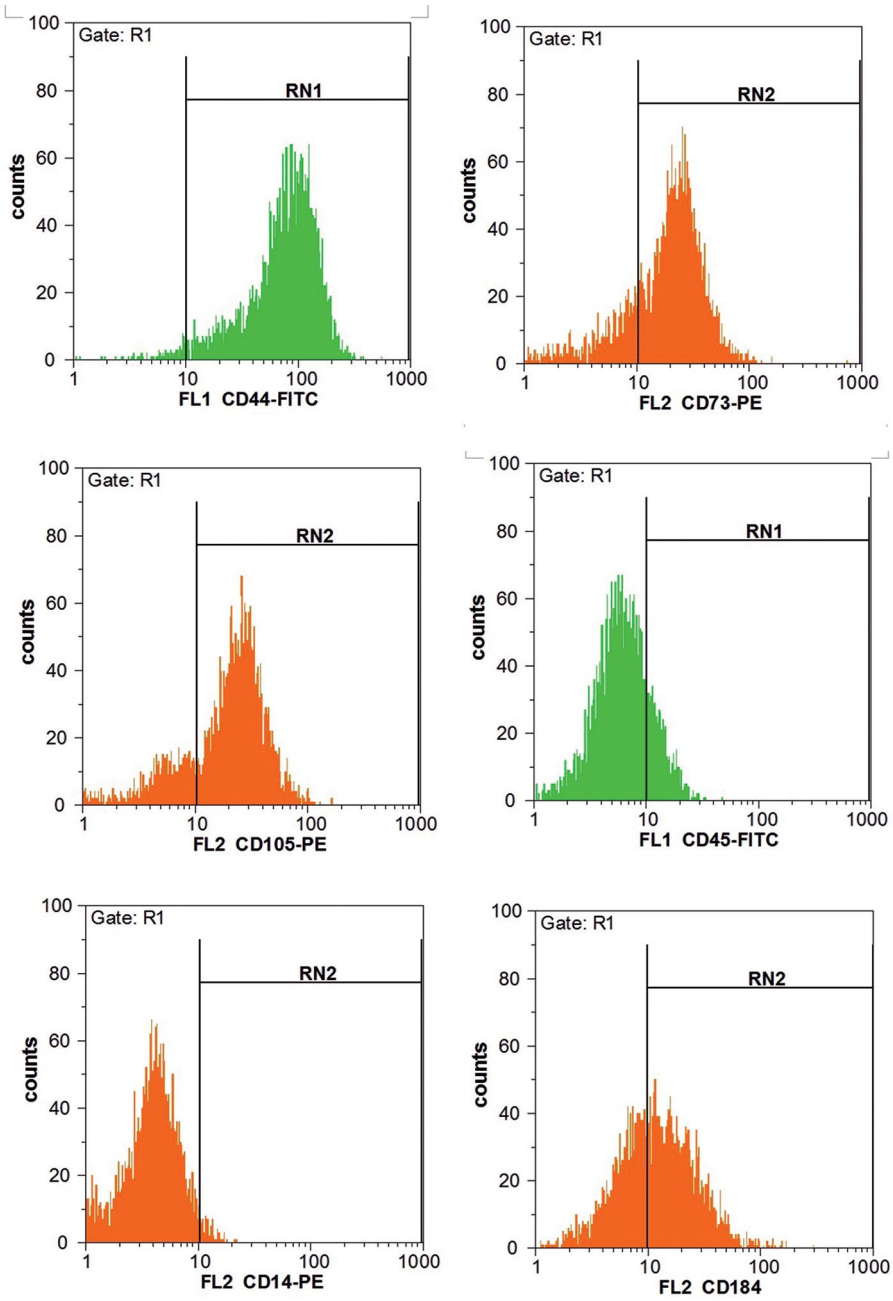

Fig.1: Results obtained from the flow cytometry analysis of peripheral blood-mesenchymal stem cells (PB-MSCs). CD marker expression analyses indicated that these cells were positive for CD184, CD105, CD73 and CD44, while they were negative for CD14 and CD45.

Relative expression level analysis of the studied genes indicated a significant down-regulation of *TERT* in the late culture of MSCs (t test: -2.29, P=0.04, Table 2). The obtained results suggested that low expression of *TERT* and *TERC* in 14-17 days of the culture were accompanied with the diminished *TCF4* expression and enhanced *GSK* expression in 8-9 days of MSCs culture (Fig.3, Table 2). Furthermore, we found that enhanced expression of *TERC* was associated with the enhanced *CTNNB1* and diminished *GSK* expressions in the early MSCs culture (Table 2). Spearman analysis indicated that there was a weak correlation between TERC and CTNNB1, GSK as well as TCF4 expression. However, this correlation was not statistically significant (P>0.05, Table 3).

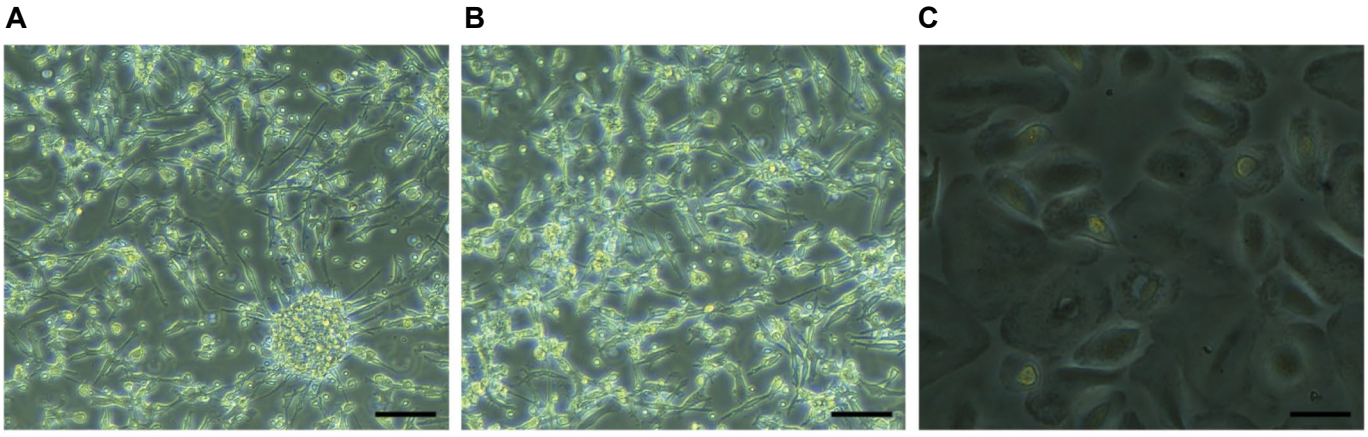

Fig.2: Morphology of peripheral blood-mesenchymal stem cells (PB-MSCs). **A.** These cells showed fibroblast like morphology at day 6th of initial culture, **B.** Their morphology was changed over the time, and **C.** They were appeared flat and wide at the late culture (scale bar: 50 µm).

Table 2: The results obtained from Student's t test (two-sided) analysis for the expression data of the studied genes in early and late mesenchymal stem cells culture

The studied genes	Early term culture		Late term culture	
	t test	P value	t test	P value
TERC	1.82	0.14	-1.43	0.18
TERT	0.17	0.87	-2.29	0.04*
TCF4	0.21	0.85	-0.64	0.54
CTNNB1	1.19	0.30	1.44	0.18
GSK	-1.22	0.29	0.92	0.38

*; Statistically significant.

Table 3: Relationship of telomerase component expressions with WNT signaling pathway using the Shearman correlation coefficient analysis

The WNT signaling pathway genes	Early term culture				Long term culture			
	TERC		TERT		TERC		TERT	
	r_s	P value	r_s	P value	r_s	P value	r_s	P value
TCF4	0.5	1	-0.5	1	0.143	0.803	-0.371	0.497
CTNNB1	-1	0.333	-0.5	1	0.486	0.355	-0.143	0.803
GSK	-0.5	1	0.5	1	0.257	0.658	-0.428	0.419

r_s; Spearman correlation coefficient.

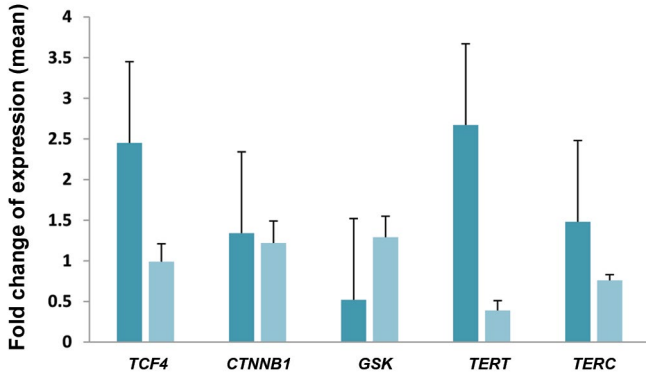

Fig.3: Mean expression levels of *TERT*, *TERC*, *TCF4*, *CTNNB1* and *GSK* in the early mesenchymal stem cells (MSC) culture compared to the late culture. Three independent experiments were performed and the expression levels were normalized to those of *HSP90AB1* gene.

Discussion

In the recent years, MSC was considered as a favorable cellular model in treatment of different diseases. Safety and efficacy of these cells have been confirmed in many clinical trials performed by MSC administrations. However, understanding MSC biological characteristics improved application of these cells in clinic. Zhao et al. (17) showed that activity of telomerase was decreased in long-term culture of MSCs derived from bone marrow of Sprague Dawley rats. They also demonstrated that overexpression of TERT was associated with the enhanced proliferation rate and decreased MSC senescence.

In the present study, we found that expressions of *TERT* and *TERC* were decreased with the aging of human PB-MSCs, which was consistent with the results obtained from MSCs derived from human bone marrow and adipose tissue (18). TA has been demonstrated to be important in different characteristics of stem cell including proliferation and differentiation abilities. Kang et al. (19) showed that transfection of telomerase reverse transcriptase gene into MSCs could enhance life span and differentiation ability.

Some studies indicated that TERC expression could participate in up-regulation or down-regulation of the other genes including the genes involved in glycolytic pathway, angiogenesis and metastasis as well as NF-κB target genes (20-22). Although the results obtained from the spearman correlation analysis indicated that *TERT* expression did not show significant correlation with the expression of WNT signaling pathway genes in the PB-MSCs, we observed negative correlation of *GSK* with *TERT* expression in the studied cells. These results suggested possible function of TERT in the regulation of WNT signaling pathway genes.

Different studies demonstrated that β-catenin phosphorylation, through GSK, contributed to its degradation, resulting in the suppression of WNT signaling pathway (23). Association of the enhanced expression of TERC with the decreased expression of GSK in early culture of MSCs was supported by stabilization and activation of β-catenin in the early culture of MSCs. Furthermore, negative association of *TERC* with *GSK* expression (data not shown) suggested that TERC indirectly regulates activity of β-catenin gene, via GSK, in the early culture of MSCs.

There were several hypotheses about how telomerase could influence expression of the other genes, one of which proposed that telomerase enzyme influences gene expression through alteration of chromatin structure. The other hypothesis indicated that interaction of telomerase with different transcription factors coordinates in the gene transcriptional regulation (23-25). Expression of *TCF4* and *TERT* supported the impact of TERT interaction with TCF4 on the expression of down-stream WNT signaling pathway genes.

Conclusion

Several pathways including WNT signaling pathway have been revealed to be involved in telomerase regulation and self-renewal ability of the stem cells. However, there was no report about the effect of WNT signaling pathway on the expression of telomerase components in the MSCs derived from human PB-MSCs. Our data indicated that activation of WNT signaling in early culture of MSCs may contribute to the enhanced expression of *TERC* and *TERT*, while this signaling pathway appears to have a minor role in the expression of telomerase components and possibly telomerase activity. Taken together, these findings suggested that investigating other signaling pathways could improve our knowledge in the regulation of TERT and TERC.

Acknowledgements

The present study financially supported by "Research Department of the School of Medicine Shahid Beheshti University of Medical Sciences" (grant no.: 12420). There is no conflict of interest in this study.

Authors' Contributions

Z.F.; Performed the study design and wrote the manuscript and also responsible for overall supervision. M.R.; Carried out the data analysis and their interpretation. M.D.O., S.M.H.G.; Contributed to the interpretation of the results and preparation of the discussion. S.F., N.S.N.; Performed the experiments including the preparation of cells and the molecular analysis of the cells. All authors read and approved the manuscript.

References

1. Mahla RS. Stem cells applications in regenerative medicine and disease therapeutics. Int J Cell Biol. 2016; 2016: 6940283.
2. Nancarrow-Lei R, Mafi P, Mafi R, Khan W. A systemic review of adult mesenchymal stem cell sources and their multilineage differentiation potential relevant to musculoskeletal tissue repair and regeneration. Curr Stem Cell Res Ther. 2017; 12(8): 601-610.
3. Rohban R, Pieber TR. Mesenchymal Stem and progenitor cells in

regeneration: tissue specificity and regenerative potential. Stem Cells Int. 2017; 2017: 5173732.
4. Li Y, Wu Q, Wang Y, Li L, Bu H, Bao J. Senescence of mesenchymal stem cells (Review). Int J Mol Med. 2017; 39(4): 775-782.
5. Victorelli S, Passos JF. Telomeres and cell senescence - size matters not. EBioMedicine. 2017; 21: 14-20.
6. Koliada AK, Krasnenkov DS, Vaiserman AM. Telomeric aging: mitotic clock or stress indicator? Front Genet. 2015; 6: 82.
7. Izadpanah R, Trygg C, Patel B, Kriedt C, Dufour J, Gimble JM, et al. Biologic properties of mesenchymal stem cells derived from bone marrow and adipose tissue. J Cell Biochem. 2006; 99(5): 1285-1297.
8. Twine NA, Harkness L, Adjaye J, Aldahmash A, Wilkins MR, Kassem M. Molecular phenotyping of telomerized human bone marrow skeletal stem cells reveals a genetic program of enhanced proliferation and maintenance of differentiation responses. JBMR Plus. 2018; 2(5): 257-267.
9. Leão R, Apolónio JD, Lee D, Figueiredo A, Tabori U, Castelo-Branco P. Mechanisms of human telomerase reverse transcriptase (hTERT) regulation: clinical impacts in cancer. J Biomed Sci. 2018; 25(1): 22.
10. Bhaskar B, Mekala NK, Baadhe RR, Rao PS. Role of signaling pathways in mesenchymal stem cell differentiation. Curr Stem Cell Res Ther. 2014; 9(6): 508-512.
11. Ling L, Nurcombe V, Cool SM. Wnt signaling controls the fate of mesenchymal stem cells. Gene. 2009; 433(1-2): 1-7.
12. Komiya Y, Habas R. Wnt signal transduction pathways. Organogenesis. 2008; 4(2): 68-75.
13. Reya T, Clevers H. Wnt signalling in stem cells and cancer. Nature. 2005; 434(7035): 843-850.
14. Zhang Y, Toh L, Lau P, Wang X. Human telomerase reverse transcriptase (hTERT) is a novel target of the Wnt/β-catenin pathway in human cancer. J Biol Chem. 2012; 287(39): 32494-32511.
15. Gry M, Rimini R, Strömberg S, Asplund A, Pontén F, Uhlén M, et al. Correlations between RNA and protein expression profiles in 23 human cell lines. BMC Genomics. 2009; 10: 365.
16. Fazeli Z, Omrani MD, Ghaderian SM. Down-regulation of nestin in mesenchymal stem cells derived from peripheral blood through blocking bone morphogenesis pathway. J Cell Commun Signal. 2016; 10(4): 273-282.
17. Zhao Q, Wang XY, Yu XX, Zhai YX, He X, Wu S, et al. Expression of human telomerase reverse transcriptase mediates the senescence of mesenchymal stem cells through the PI3K/AKT signaling pathway. Int J Mol Med. 2015; 36(3): 857-64.
18. Truong NC, Bui KH, Van Pham P. Characterization of senescence of human adipose-derived stem cells after long-term expansion. Adv Exp Med Biol. 2019; 1084: 109-128.
19. Kang SK, Putnam L, Dufour J, Ylostalo J, Jung JS, Bunnell BA. Expression of telomerase extends the lifespan and enhances osteogenic differentiation of adipose tissue-derived stromal cells. Stem Cells. 2004; 22(7): 1356-1372.
20. Ghosh A, Saginc G, Leow SC, Khattar E, Shin EM, Yan TD, et al. Telomerase directly regulates NF-κB-dependent transcription. Nat Cell Biol. 2012; 14(12): 1270-1281.
21. Bellon M, Nicot C. Multiple pathways control the reactivation of telomerase in HTLV-I-associated leukemia. Int J Cancer Oncol. 2015; 2(2). pii: 215.
22. Ropio J, Merlio JP, Soares P, Chevret E. Telomerase activation in hematological malignancies. Genes (Basel). 2016; 7(9). pii: E61
23. Zhou J, Ding D, Wang M, Cong YS. Telomerase reverse transcriptase in the regulation of gene expression. BMB Rep. 2014; 47(1): 8-14.
24. Jo D, Park R, Kim H, Jang M, Lee EJ, Jang IS, et al. AMP-activated protein kinase regulates the expression of human telomerase reverse transcriptase. PLoS One. 2018; 13(11): e0207864.
25. Ramlee MK, Wang J, Toh WX, Li S. Transcription regulation of the human telomerase reverse transcriptase (hTERT). Genes (Basel). 2016; 7(8). pii: E50.

Original Article

Differential Expression Patterns of Rspondin Family and Leucine-Rich Repeat-Containing G-Protein Coupled Receptors in Chondrocytes and Osteoblasts

Yeon-Hee Lee, M.Sc.#, Ashish Ranjan Sharma, Ph.D.#, Supriya Jagga, Ph.D., Sang-Soo Lee, M.D., Ph.D.*, Ju-Suk Nam, Ph.D.*

Institute for Skeletal Aging and Orthopedic Surgery, Hallym University-Chuncheon Sacred Heart Hospital, Chuncheon, Korea

#The first two authors equally contributed to this work.

Corresponding Address: Institute for Skeletal Aging and Orthopedic Surgery, Hallym University-Chuncheon Sacred Heart Hospital, Chuncheon, Korea
Emails: 123sslee@gmail.com, jsnam88@hallym.ac.kr

Received: 8/May/2019, Accepted: 5/August/2019

Abstract

Objective: Rspondins (RSPOs) are regarded as the significant modulators of WNT signaling pathway and they are expressed dynamically during developmental stages. Since in osteoarthritis (OA) both cartilage and subchondral bone suffer damages and WNT signaling pathway has a crucial role in their maintenance, the objective of the study was to analyze expression profile of RSPO family and its receptors [leucine-rich repeat-containing G-protein coupled receptors (LGRs)] in OA tissue samples as well as in differentiating chondrocytes and osteoblasts.

Material and Methods: In this experimental study, human early and advanced stage of OA tissue samples were analyzed for the morphological changes of articular cartilage by hematoxylin and eosin (H&E) staining, safranin-O staining and lubricin immunostaining. RSPOs and LGRs expression were confirmed by immunohistochemistry. Human primary chondrocytes and human osteoblast cell line, SaOS-2, were cultured in differentiation medium till day 14 and they were analyzed in terms of expression of RSPOs, LGRs and specific marker for chondrogenesis and osteogenesis by western blotting and quantitative reverse transcription polymerase chain reaction (qRT-PCR).

Results: Advanced stage OA tissue samples showed increased expression of RSPO1 and LGR6 in a region close to subchondral bone. While RSPO2 and LGR5 expression were seen overlapping in the deep region of articular cartilage. Differentiating chondrocytes demonstrated elevated expression of *RSPO2* and *LGR5* from day 7 to day 14, whereas, osteoblasts undergoing differentiation showed enhanced expression of *RSPO1* and *LGR6* from day 2 to day 14. Under tumor necrosis factor alpha (TNFα) stimulatory conditions, RSPO2 and RSPO1 recovered the suppressed expression of inflammatory, chondrogenic and osteogenic markers, respectively. A recovery in the stability of β-catenin was also noticed in both cases.

Conclusions: Spatial expression of RSPOs during progression of OA might be dynamically controlled by cartilage and subchondral bone. Interplay amid chondrocytes and osteoblasts, via RSPOs, might provide probable mechanisms for treating inflammatory pathogenic conditions like OA.

Keywords: Chondrocyte, LGR, Osteoarthritis, Osteoblast, R-spondin

Cell Journal(Yakhteh), Vol 22, No 4, January-March (Winter) 2021, Pages: 437-449

Citation: Lee YH, Sharma AR, Jagga S, Lee SS, Nam JS. Differential expression patterns of rspondin family and leucine-rich repeat-containing G-protein coupled receptors in chondrocytes and osteoblasts. Cell J. 2021; 22(4): 437-449. doi: 10.22074/cellj.2021.6927.

Introduction

Degenerative osteoarthritis (OA) is hallmarked by synovial joints that suffer from degeneration of articular cartilage, causing alteration of cartilage structure and compositions along with changes in subchondral bone architecture (1, 2). Initially, it was proposed that alterations in bone take place secondary to cartilage degeneration, and they do not participate in the process of disease augmentation. Nevertheless, several animal studies have demonstrated that alterations in subchondral bone takes place at the initial stages of OA (3, 4), and that changes in subchondral bone can lead to degeneration of cartilage (5). The intimate physical interface amid cartilage and subchondral bone suggests biochemical and molecular interaction throughout this interface in healthy and osteoarthritic joints (6).

Amplified vascular communicating channels, microcracks and fissures throughout the interface and the asymmetrical bone cartilage anatomy could provide a transport conduit to assist molecular transport. During the OA progress, hydraulic conductance between articular cartilage and subchondral bone increases (7). Effector molecules produced from bone matrix metalloproteinase 2 (MMP2), receptor activator of nuclear factor κ-B ligand (RANKL), hepatocyte growth factor (HGF) or cartilage (i.e. interleukin 1; also known as IL1), metalloproteinases with thrombospondin motifs (ADAMTS) and MMP13 may crossover from one zone to another and they can alter the homeostasis of each other (8). Studies have confirmed that the nutrients from bone may nourish cartilage through the channels that links them, apart from the blood vessels (9, 10). In bovine explant cultures, chondrocyte survival is significantly influenced by subchondral bone (11). While, regulatory factors released from the chondrocytes

in degraded cartilage might contribute to induction of osteoclastogenesis, and thus participate in the loss of subchondral bone during OA (12). Taken together, it may be proposed that interplay between the bone cartilage complexes is a holistic system, whereby multiple factors might contribute to OA pathogenesis.

Among various molecular regulators that affect cartilage and subchondral bone, WNT signaling pathway is crucial for maintaining the biochemical unit of bone and cartilage. Studies have demonstrated that both, inhibition or activation of canonical WNT signaling can have adverse effect on cartilage, including apoptosis of chondrocytes, perturb phenotype of articular chondrocytes, OA-like lesions, overexpression of markers related to hypertrophy and terminal differentiation (13, 14). While, activation of WNT signaling pathway, either by inhibiting WNT antagonists or increasing the stability of β-catenin, can have stimulatory effect on bone formation causing stiffer and thicker bones (15, 16). Since, various agonists and antagonists, which are often secretory in nature -like secreted frizzled-related protein (sFRP), sclerostin (SOST) and Dickkopf (DKK1)- tightly regulate WNT signaling, it is possible that bone and cartilage modulate each other via WNT signaling pathway and create pathological environment like arthritis. Overexpression of WNT signaling pathway agonists, WNT1-inducible signaling pathway protein1 (WISP1) and WNT16, has been described in human cartilage tissue samples after initiation of cartilage damage and synovium of OA (17, 18). Release of agonists can directly induce secretion of the aggrecanase and MMPs in chondrocytes, leading to destruction of cartilage. While, remodeling process in subchondral bone may be compelled toward bone formation resulting in development of osteophytes (19).

Rspondins (RSPOs) contain a thrombospondin type 1 domain/repeat-1 and they are cysteine-rich secretory proteins (20). In mammals, four members (RSPO1, RSPO2, RSPO3 and RSPO4) of RSPO protein family have been identified, having overall resemblance index of 40-60% in sequence homology and organization of domain (21, 22). In a high throughput sequencing study of human fetal brain cDNA library, RSPO3 was identified as the first member of the RSPO family (23). Thereafter, other members of RSPO family were identified from different species (20, 24, 25). To activate WNT signaling pathway, extracellular constituents of the WNT signaling acts synergistically with RSPOs (25-27). It has been observed that during developmental stages, expression of Wnt and RSPO proteins are either close or overlaps with each other, suggesting a probable relationship between RSPOs and WNT signaling pathway (28). Due to the capability of RSPOs to act as a regulator of WNT signaling pathway, several possible roles of these proteins have been suggested (27). Considering the functional role of RSPOs as agonists of WNT signaling, we tried to analyze expression pattern RSPOs along with its receptors [leucine-rich repeat-containing G-protein coupled receptors (LGRs)] during early and advanced stages of OA. An insight into the expression pattern of RSPOs and LGRs could be helpful in understanding the regulation of WNT signaling, as a cross-talk signaling mechanism between bone and cartilage during OA progression.

Materials and Methods

Histochemistry

In this experimental study, cartilage tissue samples from human femoral condyles were acquired from healthy patients (around 58- to 80-years old) undergoing surgery for hip replacements. The Ethical Committee of Hallym University-Sacred Heart Hospital, Chuncheon, South Korea (2009-42) reviewed the experimental procedure and granted permission. To examine the status of explanted cartilage damage, histochemical staining was performed on random samples of femoral condyles cartilage tissue pertaining to early and advanced OA stages. Explanted femoral heads were cleaned under sterilized conditions and harvested cartilage soft tissue was fixed by immersing in a solution of 2% paraformaldehyde (PFA, Merck, USA) for 24 hours. The samples were decalcified in 10% ethylenediaminetetraacetic acid solution (EDTA, Sigma-Aldrich, USA) before embedding in paraffin wax. Prior to staining, the tissues were deparaffinized and rehydrated.

Hematoxylin and eosin staining

The paraffin-embedded samples were deparaffinized, rehydrated and 5 μm thick sectioned samples were cut. Representative sections from all cartilage subtype samples were stained with hematoxylin and eosin (H&E) for the descriptive analysis of morphological details. Light microscope at ×10 magnification (Ziess AxioCam digital camera, Carl Zeiss, Germany) was used to visualize and photograph the stained sections.

Safranin-O staining

Safranin-O staining was carried out as follows. After steeping in Weigert's iron hematoxylin solution for about 10 minutes, the samples were rinsed with normal alkaline tap water for 10 minutes. For 5 minutes, the samples were stained in fast green solution and bathed with 1% acetic acid for 10 seconds. Subsequently, 0.1% Safranin-O solution (Sigma-Aldrich, USA) was used to stain the samples for 5 minutes and they were dehydrated by using a graded series of alcohol. Next, the samples were cleared with xylene. Finally, each sample was mounted with resinous mounting medium for observation and image acquisition. The obtained results were visualized at ×10 magnification by a microscope and pictured by a Ziess AxioCam digital camera.

Immunohistochemistry

Lubricin, RSPOs and LGRs were immune stained using the two-step immunohistochemistry procedure according to the manufacturer's protocol (Santa Cruz Biotechnology, USA). In short, the tissue sections were treated with rabbit polyclonal antibody for lubricin (Santa Cruz

Biotechnology, USA), RSPO1 (Sigma-Aldrich, USA), RSPO2 (Sigma-Aldrich, USA), LGR5 (Sigma-Aldrich, USA), LGR6 (Abcam, England) and β-catenin (Santa Cruz Biotechnology, USA) of 1:500 dilutions at 4˚C. The slides were washed thrice with phosphate-buffered saline (PBS, Wel Gene, Korea) and goat anti-rabbit immunoglobulin G (IgG, Santa Cruz Biotechnology, USA) was treated at room temperature for 30 minutes. Western blot bands were developed for visualization with 3, 3′-diaminobenzidine as the chromogen. Each section was photographed at ×10 magnification by a Zeiss Axio Cam digital camera.

Preparation of primary human chondrocytes

Cartilage samples from human femoral condyles were dissected in 100 mm dish under sterilize environment. Samples were rinsed continually with Dulbecco's Modified Eagle Medium (DMEM, Gibco, USA) including 10% fetal bovine serum (FBS, Gibco, USA) supplemented with 1% Penicillin-Streptomycin (P/S, Gibco). After digestion with Hyaluronidase in dish, sterilized blade was used to dissect the cartilage samples into small fragments. In serum free DMEM media, minced pieces of cartilage were washed twice and treated with protease buffer for one hour at 37˚C and 5% CO_2. Again, in DMEM (serum free), the cartilage fragments were rinsed twice followed by enzymatic digestion with collagenase for nearly 2 hours and 30 minutes at similar condition as mentioned above. After completion of the enzymatic degradation, solution was filtered through cell strainer of 70 µm and stored in a 50 ml tube. Then, the media was centrifuged at a speed of 1500 rpm for 5 minutes and pellet so obtained was rinsed while performing the procedure twice. At the start, cell pellet was resuspended with complete DMEM (20% FBS and 1% P/S). Three days later, DMEM media (10% FBS and 1% P/S) was replaced to maintain the cells.

Pellet culture of the primary human chondrocytes for differentiation

To induce chondrocyte differentiation, aliquots of 5×10^5 cells were centrifuged at 250 g for 5 minutes (29). Then, chondrocyte cells were treated with 1X insulin-transferrin-selenium x supplement premix (ITS-X, Gibco, USA). After 24 hours of incubation period, spherical aggregate of the sedimented cells were observed at the bottom of each tube. 1×10^5 cells were grown in 60 mm dish for control. Primary chondrocytes were differentiated for 1, 7 and 14 days. The cells were cultured under optimal condition of 37˚C and 5% CO_2. Once attached, the cells were cultured and medium was changed after every 3 days.

Cultivation and differentiation of osteoblasts

SaOS-2 cells (Human osteosarcoma cell line, ATCC, HTB-85), were grown in complete DMEM (10% FBS and 1% P/S). To induce differentiation, osteoblasts were grown in osteogenic medium, containing 50 µg/ml ascorbic acid (Sigma-Aldrich, USA) and 10 mM β-glycerophosphate (Sigma-Aldrich, USA). 1×10^5 cells per well were seeded in a 60 mm petri dish and grown at 37˚C and 5% CO_2. After every 3 days of culturing in osteogenic medium, it was replaced. Osteoblasts were then differentiated for 1, 7 and 14 days.

RNA isolation and quantitative reverse transcription polymerase chain reaction

As per the manufacturer's guidelines, TRIzol reagent (Invitrogen, USA) was used to isolate entire RNA. First strand of cDNA was synthesized by using SuperScript II (Invitrogen, USA) and 2 µg of total RNA. For each PCR mixture one-tenth of the cDNA was used in each quantitative reverse transcription PCR (qRT-PCR) supermix (EXPRESS SYBR green, BioPrince, Korea). qRT PCR was done by using a Rotor-Gene Q (Corbett RG3000, Australia). PCR reaction was accomplished by 50 cycles amplification at 95˚C for 20 seconds, 60˚C for 20 seconds and 72˚C for 25 seconds. Relative mRNA expression level of specific genes was standardized to *GAPDH* and quantified by using ΔΔCt method. The human PCR primer sequences utilized in the study are listed in Table 1.

Table 1: Human primer sequences for quantitative reverse transcription polymerase chain reaction

Gene	Primer sequence (5′-3′)
RSPO1	F: AGGCCTGCTTCAAGCCATAACTTCT
	R: GCTCATTTCACATTGCGCAGGACT
RSPO2	F: TGGCTCAGTGTGTGCTGAGAGAAT
	R: AAGGTCACGAGTGAGTAGCGCATT
RSPO3	F: TGCACTGTGAGGTCAGTGAATGGA
	R: AGGTTACCCTTTGCTGAAGGATGC
RSPO4	F: ACCACCAGTGACTTGAGCATCTGT
	R: TGATGGCAGAAGGATAGGCAGTGA
LGR4	F: TTGTGGGCAACTTCAAGCTG
	R: AACCCCAAAATGCACAGCAC
LGR5	F: TGTTTCAGTGGCCTGCATTC
	R: AAGGTCATGGCTTGCAATGC
LGR6	F: AACAACATCAAGGCCATCCC
	R: ATGCCGATCTTCCCACAAAC
GAPDH	F: TTCAGCTCAGGGATGACCTT
	R: ACCCAGAAGACTGTGGATGG

Protein extraction and western blotting

The cells were instantly rinsed with PBS (ice-cold) after removing the media and incubated for 15 minutes with lysis cocktail buffer containing phosphatase and protease inhibitor (Roche Diagnostics, Germany). After centrifugation at 14,000 rpm for 15 minutes, the entire cell lysates were collected (separated from the cells debris). As per manufacturer's protocol, protein assay kit (BioRad, USA) was used to determine protein amount in the samples. For each sample, equal amount of protein was loaded into 10% sodium dodecyl sulfate (SDS)-polyacrylamide gel followed by gel electrophoresis. Then, separated proteins were transferred to polyvinylidene fluoride (PVDF) membranes (Millipore, USA). The blots were incubated with 1:1000 dilutions of primary antibodies: RSPO1, RSPO2, LGR5 and LGR6, Col1α, Col2, osterix, IkBα, β-catenin, β-Actin (Santa Cruz Biotechnology, USA), Sox-9 (Abcam, USA) and Cox-2 (Cell Signaling Technology, USA) in 1 % BSA. Blots were washed three times with TBST (10 mM Tris HCl, 50 mM NaCl, 0.25% Tween 20) and then treated with a horseradish peroxidase-conjugated secondary antibody (Jackson Immunoresearch, USA) followed by two times washing with TBST. Finally, the obtained bands were pictured by using chemiluminescence (ECL) reagents (BioNote Inc., Korea). Antibody against β-actin was considered as a loading control. Densitometric analyses of the western blots were also performed (Fusion FX, Vilver Lourmat, France).

Statistical analysis

All of the statistical data were evaluated by Graphpad Prism 5.0 (GraphPad Software, USA) and assessed by two-tailed Student t test. Value of $P<0.05$, $P<0.01$ and $P<0.001$ was considered to designate statistical significance.

Results

Differential expression of RSPOs and LGRs at early and advanced stages of human OA samples

To observe the pattern of expression of RSPO proteins and its receptors (LGRs) in OA tissue sample from human patients, tissue sections were categorized as early or advanced stage samples and they were immunostained for the proteins like lubricin, RSPOs, LGRs and β-catenin, as described in material and methods. H&E, lubricin and safranin-o staining demonstrated intact cartilage structure in the case of early stage OA samples, while a loss of articular surface, reduced expression of lubricin and decrease in width of cartilage was observed in advanced OA samples (Fig.1A). In advanced stage OA samples, spatial RSPO1 expression was observed close to subchondral bone plate which includes lower area of calcified cartilage and a thin cortical bone tissue layer (Fig.1B). Though, no localized expression of RSPO1 was observed in early stage OA samples. Expression of LGR6 appeared to overlap with the expression of RSPO1 (i.e. near the subchondral bone plate). The spatial expression of RSPO2 was very much localized towards the middle and deep zone of articular cartilage since upper layer of cartilage was found distorted in the advanced stage tissue samples. LGR5 expression was observed close to the area of expression of RSPO2 which is near to middle and deep zone of articular cartilage area. No expression of RSPO2 or LGR5 was visible in the early stage OA samples. Since, RSPOs has the ability to activate WNT signaling pathway, we evaluated expression level of β-catenin in early and advanced stage OA samples. In the advanced stage OA samples, expression level of β-catenin was increased around the overlapped region of RSPO1 and RSPO2.

mRNA expression profile of RSPO proteins and its receptors during differentiation process of chondrocytes

Since RSPO2 showed increased expression level along with its receptor (LGR5) in advanced stages OA tissue samples, we tried to analyze the expression pattern of RSPO family proteins in differentiating chondrocytes. Initially, the primary chondrocytes were cultured as pellet culture and treated with Insulin-Transferrin-Selenium-X supplement 1X (ITS-X) to induce differentiation for 14 days. mRNA was collected at days 2, 7 and 14 of the differentiation process of chondrocytes. qRT-PCR data displayed a substantial increase in the expression of *RSPO2* after 7 days (10 folds) of treatment which followed till day 14 (16 folds), while a small increase in expression pattern of *RSPO3* and *RSPO4* was observed at day 14 (3 folds) of differentiation process. In the case of RSPO receptors, *LGR5* demonstrated a significant increase in the mRNA expression level after 7 days (10 folds) of differentiation process followed till day 14 (15 folds). mRNA expression levels of other two receptors, namely *LGR4* and *LGR6*, did not show any significant change (Fig.2A). Findings obtained from western blot confirmed the mRNA expression results by demonstrating protein expression of RSPO2 in human primary chondrocytes pellet culture after 2 days of differentiation process till day 14. While, RSPO1 protein expression was not observed during this time. Protein expression of LGR5 was also observed to be enhanced during differentiation process of the chondrocytes (Fig.2B). An increment in the protein expression level of chondrogenic markers -like collagen (Col) 2 and master transcription factor, Sox-9 (sex-determining region Y-type high mobility

group box protein; responsible for early chondrocyte differentiation) confirmed induction of differentiation process in the chondrocytes.

mRNA expression profile of RSPO proteins and its receptors during differentiation process of osteoblasts

Osteoblasts are well known for differentiating into osteocytes and contributing to bone formation. This process is tightly regulated by several regulatory molecules like RSPOs. To observe the expression pattern of RSPOs during the process of osteoblast differentiation process, SaOS-2 cells were induced to differentiate by treating β-glycerophosphate (10 mM) and ascorbic acid (50 µg/ml). mRNA from SaOS-2 cells was collected after 2, 7 and 14 days of differentiation process. Expression level of RSPO1, RSPO2, RSPO3 and RSPO4 as well the receptors for RSPOs, *LGR4, LGR5* and *LGR6* were analyzed by qRT-PCR. Among RSPOs, mRNA expression level of *RSPO1* was found to be significantly increased after 7 days (12 folds) of differentiation process till day 14 (20 folds). mRNA expression of the other *RSPOs* were not found to be significantly affected during the day 14 of differentiation. Among the receptors for RSPOs, *LGR6* was found to be elevated after 7 days (3 folds) of differentiation till day 14. *LGR4* and *LGR5* showed no significant alteration in mRNA expression level during differentiation process of osteoblasts (Fig.3A). In order to confirm the expression of RSPOs and its receptor at mRNA levels, we tried to analyze protein level of significantly expressed genes by western blotting. Western blot results demonstrated elevated protein expression of RSPO1 after 2 days of differentiation process in SaOS-2 cells, till day 14. However, protein expression of RSPO2 was not in accordance with the mRNA expression profile in osteoblasts during differentiation. Similar to mRNA expression of LGR6, western blot results also confirmed the expression of LGR6 after 7 days of differentiation process, till day 14. The process of differentiation in osteoblasts was confirmed with an increment in the protein level of osteogenic marker like Col1α and osterix (OSX, an osteoblast-specific transcription factor) from day 2 till 14 of differentiation process in osteoblasts (Fig.3B).

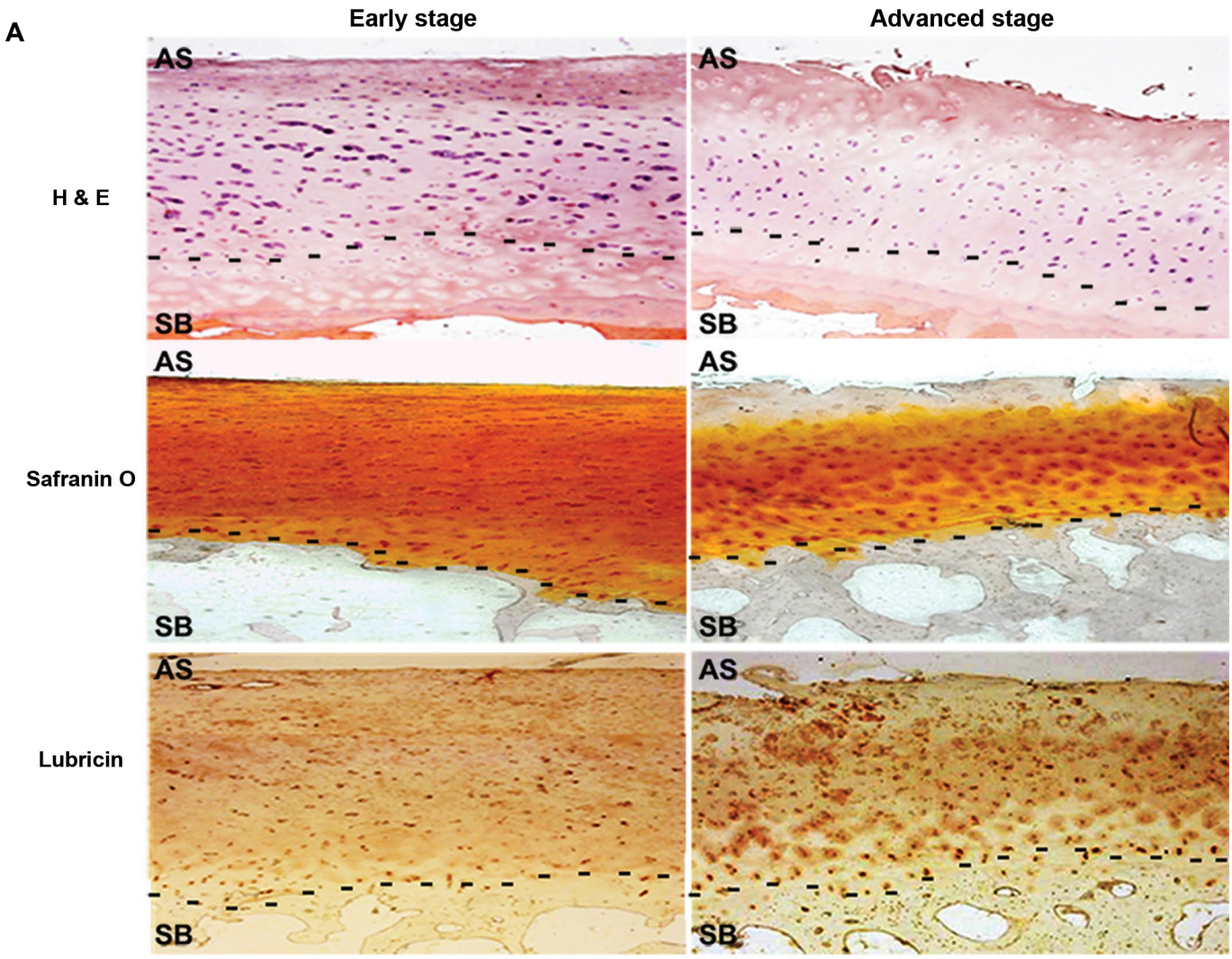

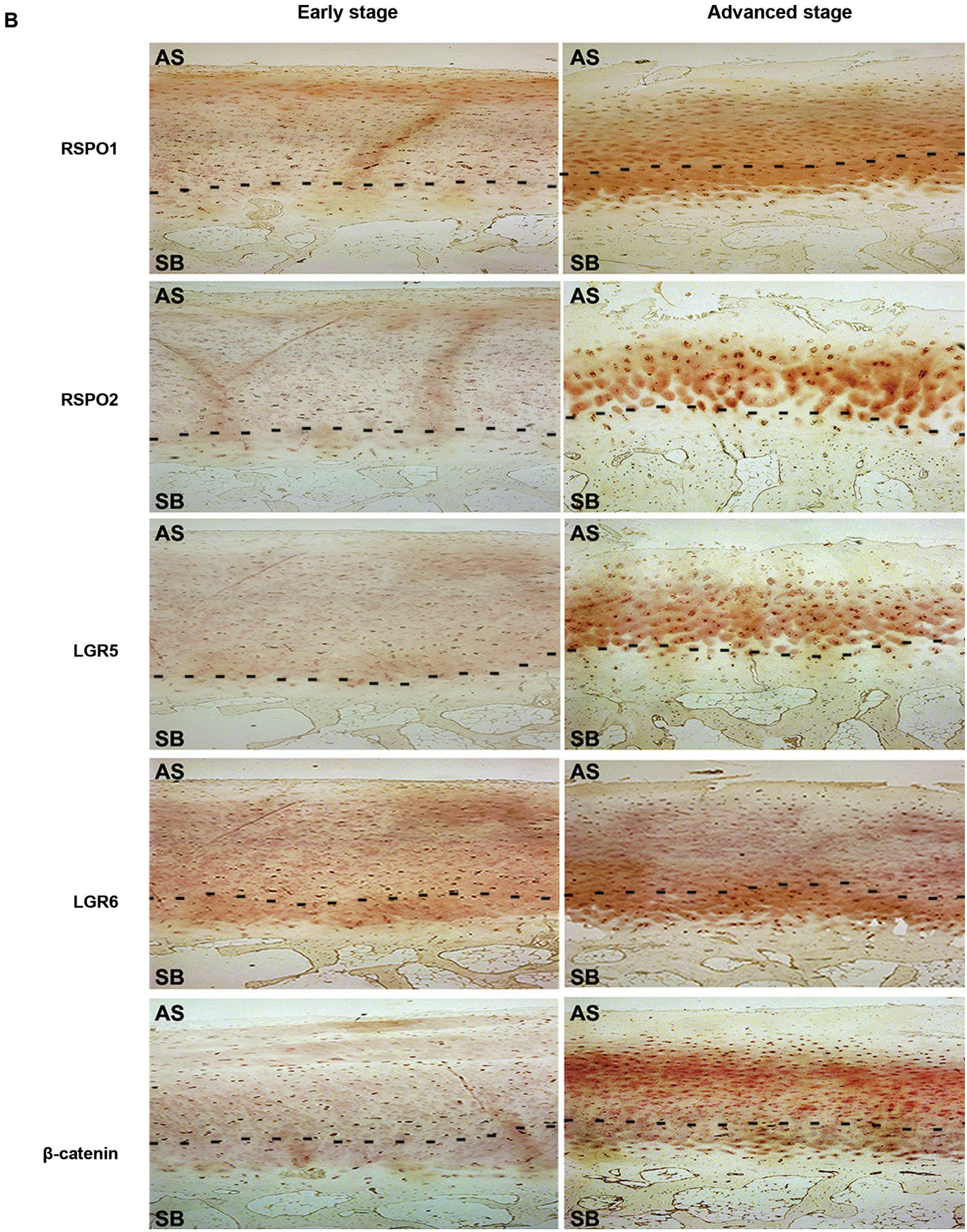

Fig.1: Expression of RSPOs, LGRs and β-catenin in human OA cartilage samples. **A.** H&E staining, safranin-O staining and IHC of lubricin in OA cartilage tissue samples with early and advanced stages obtained from femoral condyles cartilage. **B.** IHC showed that the expression of RSPOs, LGRs and β-catenin is significantly increased in advanced stage of OA cartilage compared to early stage. In these figures, above part of the dotted line represents articular cartilage whereas the lower part represents subchondral bone (approximate estimation, magnification ×10, scale bar: 100 µm). AS; Articular surface, SB; Subchondral bone, RSPOs; Rspondins, LGRs; Leucine-Rich Repeat-Containing G-Protein Coupled Receptors, OA; Osteoarthritis, and IHC; Immunohistochemistry.

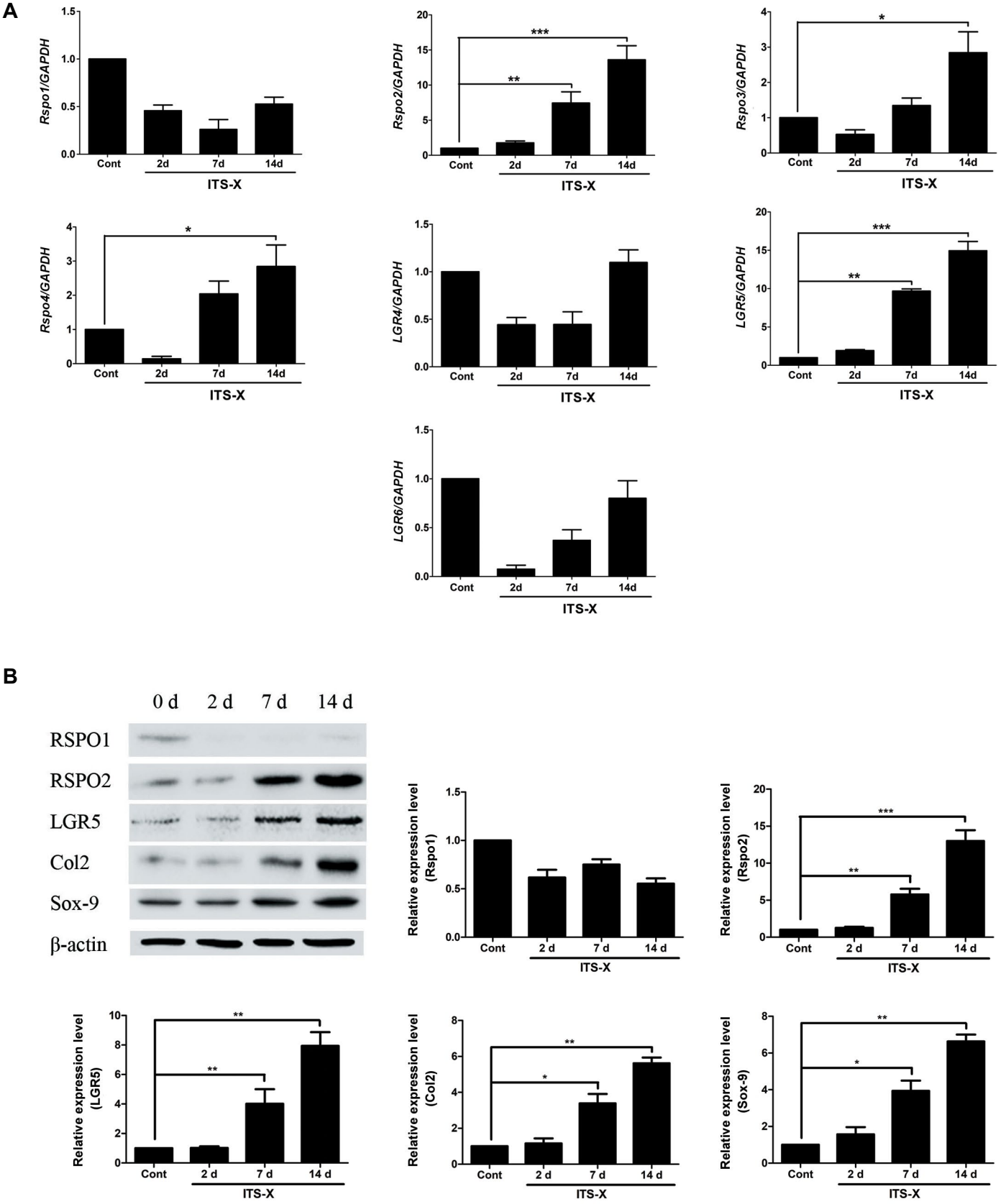

Fig.2: Expression of RSPOs and LGRs in human primary chondrocytes during differentiation. To induce differentiation, chondrocytes were treated with 1X ITS-X supplement. **A.** mRNA levels were measured by qRT-PCR after 2, 7 and 14 days of differentiation. Results are represented as fold-increase relative to *GAPDH* expression. **B.** Protein levels were measured by western blotting after 2, 7 and 14 days of differentiation. Quantitative densitometric analysis of protein was performed by using Fusion FX software. The results were normalized with β-actin expression. Data are shown as the mean ± SD of three independent experiments.
*; P≤0.05, **; P≤0.01, ***; P≤0.001, RSPOs; Rspondins, LGRs; Leucine-Rich Repeat-Containing G-Protein Coupled Receptors, 1X ITS-X; Insulin-Transferrin-Selenium-Ethanolamine, qRT-PCR; Quantitative reverse transcription polymerase chain reaction, Cont; Control, and d; Day.

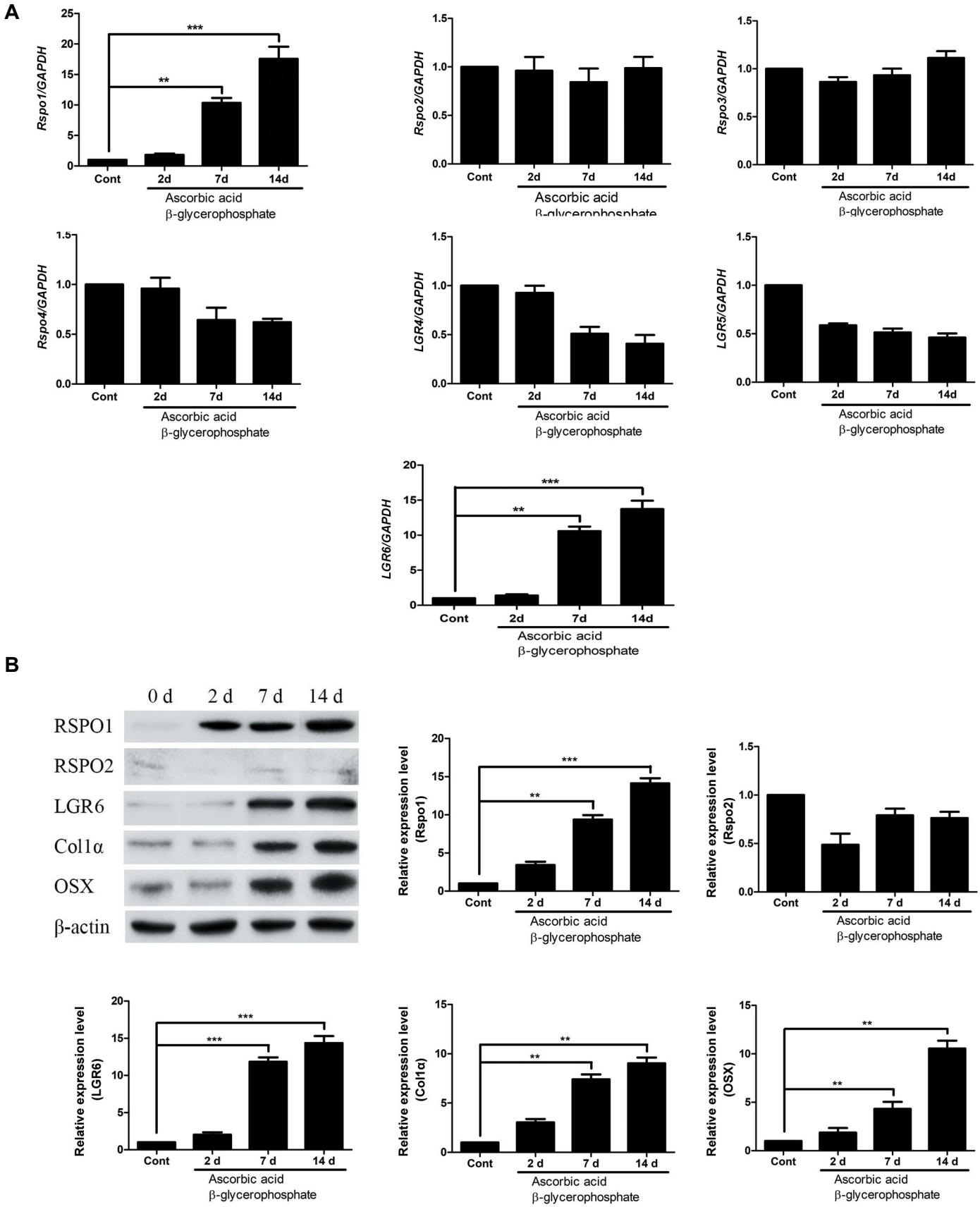

Fig.3: Expression of RSPOs and LGRs in osteoblasts during differentiation. To induce differentiation, osteoblasts were treated with 10 mM β-glycerophosphate and 50 µg/ml ascorbic acid. **A.** mRNA levels were measured by qRT-PCR after 2, 7 and 14 days of differentiation. Results are represented as fold-increase relative to *GAPDH* expression. **B.** Protein levels were measured by western blotting after 2, 7 and 14 days of differentiation. Quantitative densitometric analysis of protein was carried out by using Fusion FX software. The results were normalized with β-actin expression. Data are shown as the mean ± SD of three independent experiments. **; P≤0.01, ***; P≤0.001, RSPOs; Rspondins, LGRs; Leucine-Rich Repeat-Containing G-Protein Coupled Receptors, qRT-PCR; Quantitative reverse transcription polymerase chain reaction, Cont; Control, and d; Day.

Effect of RSPO2 during tumor necrosis factor alpha stimulatory conditions in chondrocytes

Tumor necrosis factor alpha (TNFα) is a known inflammatory marker and is a major cytokine released during inflammatory pathological condition, like arthritis (30). To depict an *in vitro* inflammatory condition, TNFα (10 ng/ml) was induced to chondrocytes after 7 days of differentiation and the protein expression level of inflammatory marker like Cox-2 and stability of IκBα (NFκB signaling activation) were measured by western blotting (Fig.4). Moreover, to observe any effect by RSPO2 on the inflammation induced by TNFα, RSPO2 (100 ng/ml) was treated along with TNFα and expression levels of inflammatory marker were analyzed. Results demonstrated an increased protein level of Cox-2 and diminished IκBα stability in chondrocytes, indicating activation of NFκB signaling by TNFα, as expected. Interestingly, treatment of RSPO2 recovered the effect of TNFα and suppressed the Cox-2 expression, in addition to restoring the stability of IκBα. RSPO2 is known to induce WNT signaling activity and it was evident by the increased stability of β-catenin in chondrocytes. However, TNFα inhibited the β-catenin stability which was restored by the treatment of RSPO2. Effect of TNFα was also evident on the expression level chondrogenic markers, like Col2 and Sox-9, in differentiated chondrocytes which again was recovered after the treatment of RSPO2.

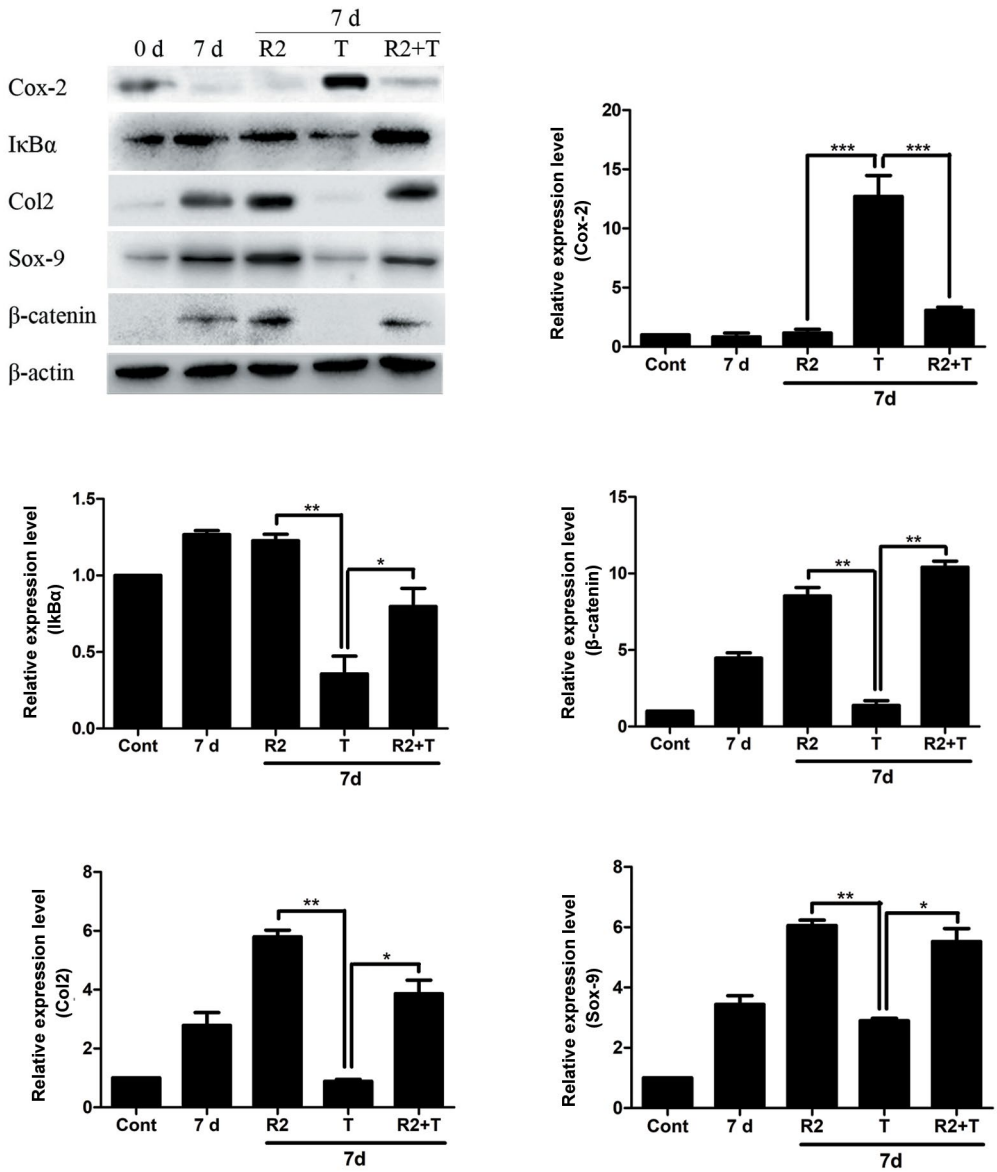

Fig.4: Effect of RSPO2 during chondrocyte differentiation under inflammatory conditions. Primary human chondrocytes were differentiated till day 7 by treating with 1X ITS-X. Thereafter, the cells were treated either with TNFα (T: 10 ng/ml) or along with RSPO2 (R2: 100 ng/ml) recombinant proteins. After 24 hours, protein expression levels of Cox-2, IkBα, Col2, Sox-9 and β-catenin were analyzed by western blotting. Protein expressions were detected by western blot. A relative densitometry analysis of protein bands was performed using Fusion FX software. The results were normalized with β-actin expression. Significant changes between the RSPO2 treated sample with TNF-α (alone) and TNFα with TNFα along with RSPO2 has been depicted. Data are shown as the mean ± SD of three independent experiments. *; P≤0.05, **; P≤0.01, ***; P≤0.001, RSPOs; Rspondin, TNFα; Tumor necrosis factor-alpha, Cont; Control, and d; Day.

Effect of RSPO1 during TNFα stimulatory conditions in osteoblasts

Treatment of SaOS-2 cells with TNFα (10 ng/ml) 7 days after differentiation induced the expression of Cox-2 and decreased the stability of IκBα, implicating activation of NFκB signaling in SaOS-2 cells (Fig.5). The ability of RSPO1 (100 ng/ml) to induce WNT signaling activity was observed even in SaOS-2 cells as the protein level of β-catenin was found to be increased after RSPO1 treatment. Stimulation of RSPO1 to TNFα treated SaOS-2 cells decreased the protein levels of Cox-2, while it restored the stability of IκBα. Moreover, TNFα suppressed protein level of β-catenin, while it was recovered after the stimulation of RSPO1. As marker for differentiation process of osteoblasts, the protein levels of Col1α and OSX was increased in SaOS-2 cells after day 7 of differentiation process. However, treating with TNFα was able to suppress the protein levels of Col1α and OSX in 7 days differentiated SaOS-2 cells. Stimulation of RSPO1 to TNFα treated SaOS-2 cells restored the protein level of both Col1α and OSX.

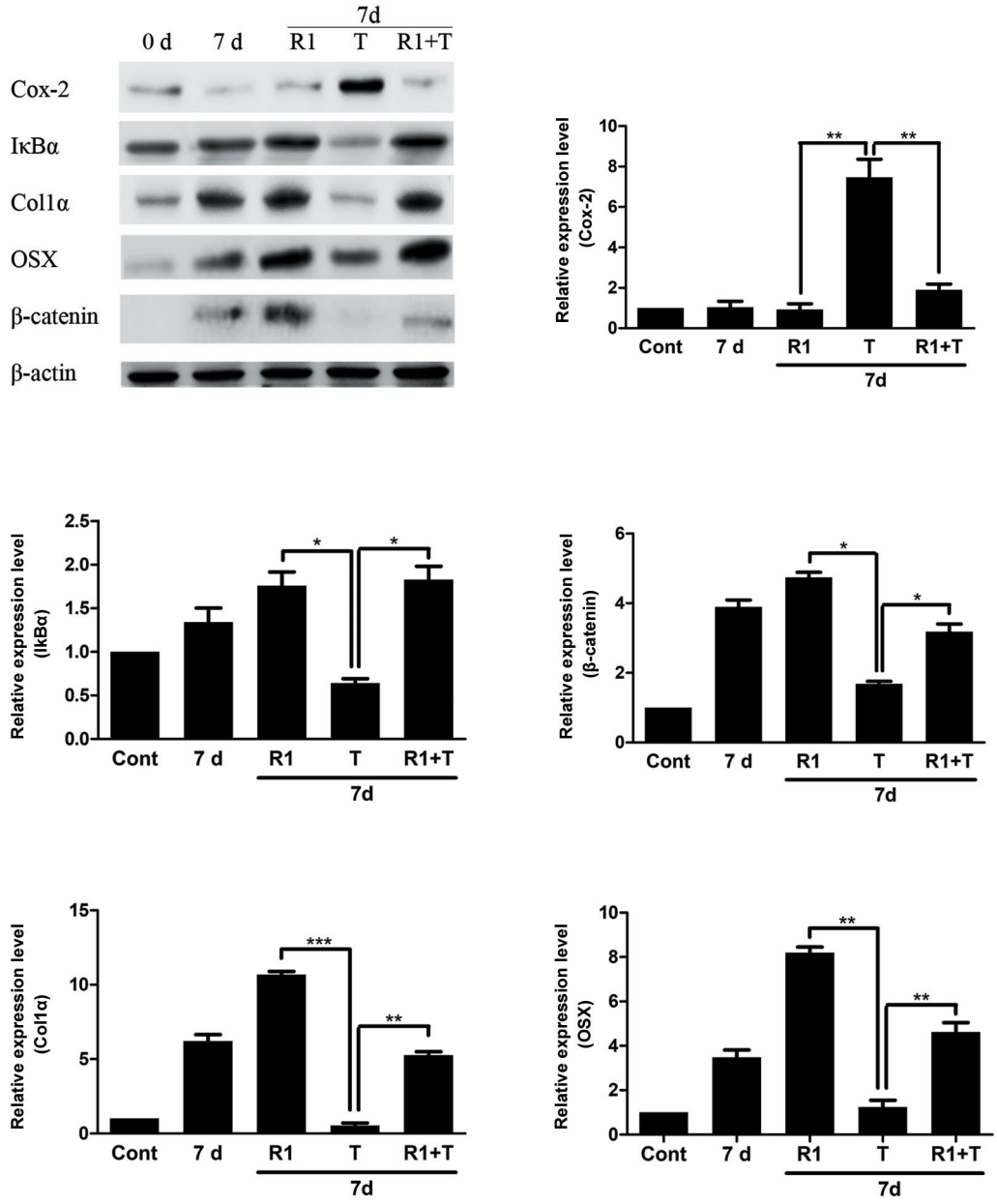

Fig.5: Effect of RSPO1 during osteoblast differentiation under inflammatory conditions. SaOS-2 cells were differentiated till day 7 by treating with 10 mM β-glycerophosphate and 50 µg/ml ascorbic acid. Then, SaOS-2 cells were treated either with TNFα (T: 10 ng/ml) or along with RSPO1 (R1: 100 ng/ml) recombinant proteins. After 24 hours, the protein expression levels of Cox-2, IkBα, Col1α, OSX and β-catenin were analyzed by western blotting. Protein expressions and a relative densitometry analysis were performed by using Fusion FX software. The results were normalized with β-actin expression. Significant changes between the RSPO1 treated sample with TNFα (alone) and TNFα with TNFα along with RSPO1 has been depicted. Data are shown as the mean ± SD of three independent experiments. *; P≤0.05, **; P≤0.01, ***; P≤0.001, TNFα; Tumor necrosis factor-alpha, Cont; Control, and d; Day.

Discussion

OA is marked by a continual damage of articular cartilage accompanied with gradual loss of extracellular matrix, causing pain and functional disabilities in elder people (2). Regardless of extensive research efforts on OA, there is a massive need of effective therapies that can ultimately alter the natural course of this painful disease. With due efforts, recent researches have established that OA is not just a disease of articular cartilage, but the subchondral bone beneath. It also has a vital role in maintaining the health of the osteochondral unit (9). Studies focused on the molecular communications amid bone and cartilage interfaces might provide an understanding into the various mechanisms that control the vital molecular factors and signaling pathways involved in pathophysiology of OA (6, 19). Among the various factors that affects both cartilage and bone, WNT signaling pathway has been found to be activated during OA and it is thought to play critical role in tissue repair and fibrosis (31).

RSPOs are secretory proteins that have an ability to activate WNT signaling pathway and they are often co-expressed with WNTs (21, 27). During mouse development, RSPOs expression overlap with the expression of WNT signaling proteins, suggesting a likely association of RSPOs with the WNT signaling pathway (28). *Rspo* genes are differentially expressed during development of mouse limbs, implicating dynamic role of RSPOs during skeletal development (24, 28, 32). Recently, efforts were made to study the involvement of RSPO proteins in inflammatory arthritis animal model (TNFα transgenic mice) and it was demonstrated that RSPO1 was able to prevent bone and cartilage from inflammation-related damage (33). RSPO family proteins are dynamically expressed with distinct patterns during different mouse embryonic and fetal developmental stages (28). Henceforth, in order to understand the involvement of RSPO proteins in OA, we tried to analyze the expression pattern of RSPOs along with their receptors (LGRs) in early and advanced stage of human OA tissue samples. A progression based dynamic expression of RSPOs might explain its regulatory role during the pathogenesis of OA. Moreover, we tried to understand the pattern of expression of RSPO and LGR family during differentiation process of chondrocytes and osteoblasts, *in vitro*. In endochondral ossification, RSPO2 has been implicated to facilitate differentiation of chondrocytes by augmenting WNT signaling pathway (34). However, in animal OA models, increased stimulation of WNT/β-catenin signaling exerts hypertrophic differentiation in articular chondrocytes, which, in turn, results in enhanced expression of cartilage-degrading metalloproteinase and subsequent aggravation of OA. RSPO2 exerts this effect by binding to its receptor LGR5 (35). In agreement, expression profile of our results demonstrated an overlap between the expression of RSPO2 and LGR5 in advanced stage OA samples. The expression of RSPO2 and LGR was very much localized toward the deep region of articular cartilage. Moreover, *in vitro* data showed the expression of RSPO2 and LGR5 during differentiation process of chondrocytes. Here, it appears that expression of RSPO2 is critical for differentiation of chondrocytes and it is enhanced under pathological conditions, like OA the expression of RSPO2.

Previously, we have shown that RSPO1 can promote osteoblast differentiation process through WNT signaling pathway (36). Increased expression of LGR6 has been identified in the mesenchymal stem cells undergoing osteogenic induction and LGR6 has been suggested as an osteoblastic progenitor marker (37). In accordance to the above studies, we also observed that LGR6 expression overlapped with the expression of RSPO1 in advanced stage OA samples. In addition, the expressions of RSPO1 and LGR6 were detected during differentiation process of osteoblasts, implicating that LGR6 is possibly responsible for recognizing RSPO1 and mediating its effect for WNT signaling stimulation. However, further experiments are needed to ascertain this fact.

Numerous studies have indicated that TNFα plays a critical role, not only during the pathogenesis of inflammatory arthritis but also during degenerative joint disease like OA (30, 38). TNFα is responsible for maintaining the homoeostasis of matrix synthesis and its degeneration in articular cartilage of tandem with other cytokines like IL1, transforming growth factor β. Moreover, TNFα role has been shown in induction of bone loss during inflammatory conditions by affecting WNT signaling pathway (39, 40). In order to mimic the pathological conditions that might prevail during OA, we simply stimulated the chondrocytes and osteoblasts with TNFα and induced inflammatory response in these cells. Interestingly, co-treatment of TNFα along with RSPO2 in chondrocytes and RSPO1 in osteoblasts not only recovered the induction of inflammatory marker like Cox-2, but also suppressed activated NFκB signaling in both of the cell types. Moreover, TNFα, suppressed chondrogenic markers (Col2 and Sox-9) and osteogenic markers (Col1α and OSX), were found to be recovered after co-treatment with RSPO2 and RSPO1, respectively. Additionally, TNFα, suppressing β-catenin stability, was restored by treatment of RSPO2 and RSPO1 in chondrocytes and osteoblasts, respectively. These results point towards a regulatory role of RSPOs in inflammation which might be achieved by activating WNT signaling pathway. TNFα has been shown to induce secretion of WNT antagonists, like DDK1 and SOST, from differentiating osteoblasts affecting their bone forming ability (39). Moreover, the localized expression pattern of RSPO1 (near to subchondral bone area) and RSPO2 (near to deep articular cartilage area) in the OA samples raise a possibility of interplay between chondrocytes and osteoblasts. Though, it appears to be interesting, further studies would be needed to delineate the mechanism by which WNT signaling pathway might interact with the inflammatory mechanism under the regulation of RSPOs. For example, further studies focused on the release of WNT signaling antagonists, in response to TNFα in chondrocytes and

osteoblasts and finding any role of RSPOs in regulating this process would be quite interesting. Limitation of our study is that we have just considered TNFα as a stimulator for inflammation *in vitro*, while inflammation during OA pathogenesis is a multifactorial event, involving a diverse kind of pro-inflammatory factors and cytokines. For instance, other than TNFα, IL1β is the other cytokine that affects both chondrocytes and osteoblasts in joints. Hence, future studies should try to reveal the effect and role of IL1β or a combination of other cytokines in presence of RSPOs. A clear understanding of RSPOs anti-inflammatory role under inflammatory conditions, like OA, would be helpful to suggest novel therapeutic agents in near future.

Conclusion

During pathogenesis of OA, both articular cartilage and subchondral bone shows morphological and biochemical changes. OA does not simply represent an event of wear and tear process, but instead it is an atypical remodeling process leading to joint failure. An intermolecular interaction between articular cartilage and subchondral bone interface is being regarded as the contributing factor for altered structural and functional characteristics of this unit. RSPO family of proteins is known to stimulate WNT signaling pathway. Chondrocytes and osteoblasts need functional role of WNT signaling pathway during their developmental process as well as in pathogenic state. Thus, as key molecules for WNT signaling pathway, RSPOs might play a crucial role during their cross-talk based on their differential expression patterns. Our results in OA tissue samples demonstrate spatial expression of RSPO1 and RSPO2 along with their receptors, respectively LGR6 and LGR5, in early and advanced stage of OA samples. *In vitro* differentiation analysis of chondrocytes and osteoblasts also demonstrated correlation of expression pattern of RSPOs along with its receptors. Interestingly, the ability of RSPOs to recover adverse effect induced by TNFα represents possible role of RSPOs in affecting inflammatory pathways through WNT signaling. However, more detailed studies would be required to ascertain the functional role of RSPOs during inflammation. In brief, RSPOs might be the regulatory molecule and they may explain the relationship amongst cartilage and subchondral bone under pathogenic conditions like OA. A clear insight into the differential expression of RSPOs and their functional role might contribute to identify novel therapeutic targets for the cure of OA in near future.

Acknowledgements

This research financially supported by Hallym University Research Fund and Basic Science Research Program through the National Research Foundation of Korea (NRF) established by the Ministry of Education (NRF-2016R1D1A1B03931318 and NRF-2017R1A2B4012944). There is no conflict of interest in this study.

Authors' Contributions

Y.-H.L., A.R.S.; Performed the experiments, collected and interpreted the data, drafted and edited the manuscript. S.J.; Participated in data analysis, evaluations and editing the manuscript. J.-S.N., S.-S.L.; Conceived the idea, participated in study design and supervised the project. All authors read and approved the final manuscript.

References

1. Lories RJ, Luyten FP. The bone-cartilage unit in osteoarthritis. Nat Rev Rheumatol. 2011; 7(1): 43-49.
2. Buckwalter JA, Martin JA. Osteoarthritis. Adv Drug Deliv Rev. 2006; 58(2): 150-167.
3. Hayami T, Pickarski M, Zhuo Y, Wesolowski GA, Rodan GA, Duong LT. Characterization of articular cartilage and subchondral bone changes in the rat anterior cruciate ligament transection and meniscectomized models of osteoarthritis. Bone. 2006; 38(2): 234-243.
4. Quasnichka HL, Anderson-MacKenzie JM, Bailey AJ. Subchondral bone and ligament changes precede cartilage degradation in guinea pig osteoarthritis. Biorheology. 2006; 43(3,4): 389-397.
5. Lahm A, Uhl M, Edlich M, Erggelet C, Haberstroh J, Kreuz PC. An experimental canine model for subchondral lesions of the knee joint. Knee. 2005; 12(1): 51-55.
6. Sharma AR, Jagga S, Lee SS, Nam JS. Interplay between cartilage and subchondral bone contributing to pathogenesis of osteoarthritis. Int J Mol Sci. 2013; 14(10): 19805-19830.
7. Hwang J, Bae WC, Shieu W, Lewis CW, Bugbee WD, Sah RL. Increased hydraulic conductance of human articular cartilage and subchondral bone plate with progression of osteoarthritis. Arthritis Rheum. 2008; 58(12): 3831-3842.
8. Goldring SR. Role of bone in osteoarthritis pathogenesis. Med Clin North Am. 2009; 93(1): 25-35, xv.
9. Li G, Yin J, Gao J, Cheng TS, Pavlos NJ, Zhang C, et al. Subchondral bone in osteoarthritis: insight into risk factors and microstructural changes. Arthritis Res Ther. 2013; 15(6): 223.
10. Stewart HL, Kawcak CE. The importance of subchondral bone in the pathophysiology of osteoarthritis. Front Vet Sci. 2018; 5: 178.
11. Amin AK, Huntley JS, Simpson AH, Hall AC. Chondrocyte survival in articular cartilage: the influence of subchondral bone in a bovine model. J Bone Joint Surg Br. 2009; 91(5): 691-699.
12. Jiao K, Niu LN, Wang MQ, Dai J, Yu SB, Liu XD, et al. Subchondral bone loss following orthodontically induced cartilage degradation in the mandibular condyles of rats. Bone. 2011; 48(2): 362-371.
13. Zhu M, Chen M, Zuscik M, Wu Q, Wang YJ, Rosier RN, et al. Inhibition of beta-catenin signaling in articular chondrocytes results in articular cartilage destruction. Arthritis Rheum. 2008; 58(7): 2053-2064.
14. Zhu M, Tang D, Wu Q, Hao S, Chen M, Xie C, et al. Activation of beta-catenin signaling in articular chondrocytes leads to osteoarthritis-like phenotype in adult beta-catenin conditional activation mice. J Bone Miner Res. 2009; 24(1): 12-21.
15. Lane NE, Nevitt MC, Lui LY, de Leon P, Corr M; Study of Osteoporotic Fractures Research Group. Wnt signaling antagonists are potential prognostic biomarkers for the progression of radiographic hip osteoarthritis in elderly Caucasian women. Arthritis Rheum. 2007; 56(10): 3319-3325.
16. Sharma G, Sharma AR, Seo EM, Nam JS. Genetic polymorphism in extracellular regulators of Wnt signaling pathway. Biomed Res Int. 2015; 2015: 847529.
17. Dell'accio F, De Bari C, Eltawil NM, Vanhummelen P, Pitzalis C. Identification of the molecular response of articular cartilage to injury, by microarray screening: Wnt-16 expression and signaling after injury and in osteoarthritis. Arthritis Rheum. 2008; 58(5): 1410-1421.
18. Blom AB, Brockbank SM, van Lent PL, van Beuningen HM, Geurts J, Takahashi N, et al. Involvement of the Wnt signaling pathway in experimental and human osteoarthritis: prominent role of Wnt-induced signaling protein 1. Arthritis Rheum. 2009; 60(2): 501-512.
19. Yuan XL, Meng HY, Wang YC, Peng J, Guo QY, Wang AY, et al. Bone-cartilage interface crosstalk in osteoarthritis: potential pathways and future therapeutic strategies. Osteoarthritis Cartilage.

2014; 22(8): 1077-1089.
20. Kamata T, Katsube K, Michikawa M, Yamada M, Takada S, Mizusawa H. R-spondin, a novel gene with thrombospondin type 1 domain, was expressed in the dorsal neural tube and affected in Wnts mutants. Biochim Biophys Acta. 2004; 1676(1): 51-62.
21. Kim KA, Zhao J, Andarmani S, Kakitani M, Oshima T, Binnerts ME, et al. R-Spondin proteins: a novel link to beta-catenin activation. Cell Cycle. 2006; 5(1): 23-26.
22. Sharma AR, Chakraborty C, Lee SS, Sharma G, Yoon JK, George Priya Doss C, et al. Computational biophysical, biochemical, and evolutionary signature of human R-spondin family proteins, the member of canonical Wnt/beta-catenin signaling pathway. Biomed Res Int. 2014; 2014: 974316.
23. Chen JZ, Wang S, Tang R, Yang QS, Zhao E, Chao Y, et al. Cloning and identification of a cDNA that encodes a novel human protein with thrombospondin type I repeat domain, hPWTSR. Mol Biol Rep. 2002; 29(3): 287-292.
24. Kazanskaya O, Glinka A, del Barco Barrantes I, Stannek P, Niehrs C, Wu W. R-Spondin2 is a secreted activator of Wnt/beta-catenin signaling and is required for Xenopus myogenesis. Dev Cell. 2004; 7(4): 525-534.
25. Nam JS, Turcotte TJ, Smith PF, Choi S, Yoon JK. Mouse cristin/R-spondin family proteins are novel ligands for the Frizzled 8 and LRP6 receptors and activate beta-catenin-dependent gene expression. J Biol Chem. 2006; 281(19): 13247-13257.
26. Wei Q, Yokota C, Semenov MV, Doble B, Woodgett J, He X. R-spondin1 is a high affinity ligand for LRP6 and induces LRP6 phosphorylation and beta-catenin signaling. J Biol Chem. 2007; 282(21): 15903-15911.
27. Jin YR, Yoon JK. The R-spondin family of proteins: emerging regulators of WNT signaling. Int J Biochem Cell Biol. 2012; 44(12): 2278-2287.
28. Nam JS, Turcotte TJ, Yoon JK. Dynamic expression of R-spondin family genes in mouse development. Gene Expr Patterns. 2007; 7(3): 306-312.
29. Johnstone B, Hering TM, Caplan AI, Goldberg VM, Yoo JU. In vitro chondrogenesis of bone marrow-derived mesenchymal progenitor cells. Exp Cell Res. 1998; 238(1): 265-272.
30. Pelletier JP, Roughley PJ, DiBattista JA, McCollum R, Martel-Pelletier J. Are cytokines involved in osteoarthritic pathophysiology? Semin Arthritis Rheum. 1991; 20(6 Suppl 2): 12-25.
31. De Santis M, Di Matteo B, Chisari E, Cincinelli G, Angele P, Lattermann C, et al. The role of wnt pathway in the pathogenesis of OA and its potential therapeutic implications in the field of regenerative medicine. Biomed Res Int. 2018; 2018: 7402947.
32. Yoon JK, Lee JS. Cellular signaling and biological functions of R-spondins. Cell Signal. 2012; 24(2): 369-377.
33. Kronke G, Uderhardt S, Kim KA, Stock M, Scholtysek C, Zaiss MM, et al. R-spondin 1 protects against inflammatory bone damage during murine arthritis by modulating the Wnt pathway. Arthritis Rheum. 2010; 62(8): 2303-2312.
34. Takegami Y, Ohkawara B, Ito M, Masuda A, Nakashima H, Ishiguro N, et al. R-spondin 2 facilitates differentiation of proliferating chondrocytes into hypertrophic chondrocytes by enhancing Wnt/β-catenin signaling in endochondral ossification. Biochem Biophys Res Commun. 2016; 473(1): 255-264.
35. Okura T, Ohkawara B, Takegami Y, Ito M, Masuda A, Seki T, et al. Mianserin suppresses R-spondin 2-induced activation of Wnt/beta-catenin signaling in chondrocytes and prevents cartilage degradation in a rat model of osteoarthritis. Sci Rep. 2019; 9(1): 2808.
36. Sharma AR, Choi BS, Park JM, Lee DH, Lee JE, Kim HS, et al. Rspo 1 promotes osteoblast differentiation via Wnt signaling pathway. Indian J Biochem Biophys. 2013; 50(1): 19-25.
37. Khedgikar V, Lehoczky JA. Evidence for Lgr6 as a novel marker of osteoblastic progenitors in mice. JBMR Plus. 2019; 3(2): e10075.
38. Westacott CI, Sharif M. Cytokines in osteoarthritis: mediators or markers of joint destruction? Semin Arthritis Rheum. 1996; 25(4): 254-272.
39. Lee SS, Sharma AR, Choi BS, Jung JS, Chang JD, Park S, et al. The effect of TNFα secreted from macrophages activated by titanium particles on osteogenic activity regulated by WNT/BMP signaling in osteoprogenitor cells. Biomaterials. 2012; 33(17): 4251-4263.
40. Nam JS, Jagga S, Sharma AR, Lee JH, Park JB, Jung JS, et al. Anti-inflammatory effects of traditional mixed extract of medicinal herbs (MEMH) on monosodium urate crystal-induced gouty arthritis. Chin J Nat Med. 2017; 15(8): 561-575.

The Relationship between Functional Promoter Variants of Macrophage Migration Inhibitory Factor and Endometriosis

Zahra Chekini, M.Sc.[1, 2], Maryam Shahhoseini, Ph.D.[3, 4], Reza Aflatoonian, M.D., Ph.D.[2*], Parvaneh Afsharian, Ph.D.[4*]

1. Department of Biology, Science and Research Branch, Islamic Azad University, Tehran, Iran
2. Department of Endocrinology and Female Infertility, Reproductive Biomedicine Research Center, Royan Institute for Reproductive Biomedicine, ACECR, Tehran, Iran
3. Reproductive Epidemiology Research Center, Royan Institute for Reproductive Biomedicine, ACECR, Tehran, Iran
4. Department of Genetics, Reproductive Biomedicine Research Center, Royan Institute for Reproductive Biomedicine, ACECR, Tehran, Iran

Corresponding Addresses: P.O.Box: 16635-148, Department of Endocrinology and Female Infertility, Reproductive Biomedicine Research Center, Royan Institute for Reproductive Biomedicine, ACECR, Tehran, Iran
P.O.Box: 16635-148, Department of Genetics, Reproductive Biomedicine Research Center, Royan Institute for Reproductive Biomedicine, ACECR, Tehran, Iran
Emails: r.aflatoonian@gmail.com, pafshar@royaninstitute.org

Received: 13/March/2019, Accepted: 8/July/2019

Abstract

Objective: Endometriosis is a common gynecological and inflammatory disorder. Macrophage migration inhibitory factor (MIF) is a key pro-inflammatory cytokine that is secreted by accumulated active macrophages in ectopic endometrial tissues. Two promoter polymorphisms of *MIF* [-794(CATT)$_{5–8}$ /-173G/C] were identified to susceptibility and severity of several immune and inflammatory diseases. We aimed to evaluate the possible association between *MIF* promoter polymorphisms and susceptibly to endometriosis and its corolation with mRNA level.

Materials and Methods: This case-control study was performed in Royan Institute from 2015 to 2017. Polymorphisms were evaluated in 106 endometriosis patients and 110 controls. For 17 endometrioma tissues, gene expression studies were conducted during secretory phase of menstrual cycle. Restriction fragment length polymorphism (RFLP) analysis was performed to determine -173G/C polymorphism and -794(CATT)$_{5-8}$ were detected by sequencing. Quantitative polymerase chain reaction (Q-PCR) was carried out to determine MIF expression level.

Results: Homozygote of CATT$_7$ was observed only in endometriosis whilst we did not detect the significant allele and genotype variation in both groups. The homozygotes for -794(CATT)$_{5–8}$ and -173G/C polymorphisms were obtained to estimate the haplotype frequencies. Significantly higher haplotype frequencies were observed for CATT$_5$/G in controls [global P value=0.044]. Additionally, the CATT$_5$/C and CATT$_7$/G haplotypes were not detected in any groups. Expression level of mRNA in ectopic tissue of endometriosis patients with CATT$_{6,7}$/CC haplotype, were significantly higher compared to other haplotypes including CATT$_{5,5}$/GG (2.91 fold, P=0.007), CATT$_{5,5}$/GC (2.48 fold, P=0.047) and CATT$_{6,6}$/GG (2.08 fold, P=0.046).

Conclusion: We report, for the first time, a strong linkage between the decreased repetition of CATT and G allele in control and CATT$_6$/C and CATT$_7$/C haplotypes in endometriosis patients. Increased MIF expression is affected by genetic variants in the *MIF* promoter in ectopic endometrial tissues. This promoter haplotype might play an important role in the development and establishment of endometriosis.

Keywords: Endometriosis, Gene Expression, Haplotype, Macrophage Migration Inhibitory Factor, Polymorphism

Cell Journal(Yakhteh), Vol 22, No 4, January-March (Winter) 2021, Pages: 450-456

Citation: Chekini Z, Shahhoseini M, Aflatoonian R, Afsharian P. The relationship between functional promoter variants of macrophage migration inhibitory factor and endometriosis. Cell J. 2021; 22(4): 450-456. doi: 10.22074/cellj.2021.6858.

Introduction

Endometriosis is an inflammatory, estrogen-dependent disease that is characterized by presence of ectopic endometrial-like tissue outside of the uterine cavity (1, 2). Endometriosis is associated with pelvic pain and infertility in most patients (2). Several theories explained the pathogenesis of the condition (3), but the Sampson's hypothesis is the most-widely accepted one which suggested a retrograde movement of endometrial cells via the fallopian tubes into the peritoneal cavity during menstruation (4). It seems that approximately 90% of women possess retrograde menstruation; however, refluxed endometrial cells are usually cleared by macrophages, natural killer (NK) cells, and lymphocytes but in endometriosis patients, a combination of impaired immunological clearance and aberrant cytokine expression interferes with clearance of the ectopic lesions leading to establishment and development of the disease (5). The impaired immune response is related to reduced cytotoxic activity of NK cells, increased number of T cells and accumulation of activated macrophages (6, 7).

Macrophage migration inhibitory factor (MIF) is a pleiotropic pro-inflammatory cytokine (8, 9) that is produced by T lymphocytes and accumulative macrophages and activates several molecular pathways in the ectopic endometrial tissue (10). The

MIF-induced extracellular mitogen-activated (MAP) kinase pathway causes an increase in prostaglandin E2 (PGE2) and estrogen, also negatively regulates p53 and promotes apoptosis; thus, its inhibition may enhance proliferation (11, 12). Several studies as well as our group suggested that mRNA and plasma levels of MIF are increased in the ectopic and eutopic tissues of endometriosis patients (12-15) but no genetic variation was described.

The *MIF* gene is located in the chromosome 22q11.2 region and consists of three exons (16). Polymorphisms with potential functional relevance were also identified in the *MIF* promoter (17); a single nucleotide polymorphism (SNP) at position -173G/C (rs755622) and a short tandem repeat polymorphism (STRP), -794 $(CATT)_{5–8}$ (rs5844572), were shown by several meta-analyses to increase susceptibility some immune and inflammatory diseases and their severity (18-21).

Since endometriosis is an inflammatory disorder and increased levels of MIF are observed in ectopic tissues, we aimed to evaluate *MIF* promoter variations that could be involved in development of endometriosis and susceptibility towards this disorder. Also, *MIF* mRNA expression levels in ectopic tissues from patients with endometriosis who carried different genotypes for the two promoter variations were determined.

Materials and Methods

Subjects

This case-control study was approved by Ethics Committee of Royan Institute (No.EC/91/1137) and each participant signed an informed consent form. The stage of endometriosis lesions was categorized based on the revised classification of the American Fertility Society (rAFS). In the current study, 106 patients with diagnosed endometriosis, who had undergone laparoscopy from 2015 to 2017 and had endometrioma cysts confirmed by histological tests, were enrolled. The endometrioma tissues were collected during laparoscopic surgery in the secretory phases of menstrual cycle (days 16-19). The 110 controls were recruited from subjects who were not diagnosed with endometriosis, underwent diagnostic laparoscopy or fertile women with no sign of endometriosis in Doppler ultrasonography. None of the participants had endometrial hyperplasia, neoplasia, or inflammatory and autoimmune disorders, and none of them were receiving anti-inflammatory or hormonal medication for at least 3 months before laparoscopy. The subjects' age was between 20 and 40 years old and the control individuals were matched with the endometriosis patients in terms of body mass index (BMI).

Identification of the *MIF* polymorphisms

DNA extraction

DNA was extracted from whole blood anticoagulated with ethylenediamine tetraacetic acid (EDTA)-2Na. Patients' genomic DNA was extracted by using the Gene All® kit (Korea), according to the manufacturer's instructions. Salting-out method was used to obtain the controls' genomic DNA.

Polymerase chain reaction reactions

The polymerase chain reaction (PCR) was used to amplify the studied fragments of *MIF* gene. The PCR included a hot start at 95˚C for 5 minutes, followed by 35 PCR cycles, each including denaturation for 30 seconds at 94˚C, primer annealing (depending on the primer pairs) for 30 seconds, and extension for 60 seconds at 72˚C. A final extension step was conducted at 72˚C for 10 minutes.

Genotyping of the -173G/C polymorphism

Restriction fragment length polymorphism (RFLP) was performed to detect -173G/C SNP. PCR was used to amplify a 303 bp fragment.

Sense primer was:

5′- CCT-CCT-GGC-GAC-TAA-CAT-CGG-TGA-CT-3′
and the anti-sense primer was:

5′- TAC-GTG-CCT-GAC-TTC-TCG-GAC-ACC-ACT -3′.

The annealing temperature was set at 63˚C. The resulting fragment was digested using *AluI* restriction endonuclease (Fermentase Biolabs, MA, USA) for 15 minutes at 37˚C, and the digested fragments were resolved using 1.7% agarose gel stained with ethidium bromide, and visualized using Molecular Imager® Gel Doc™ XR+ (BioRad, California, USA) under ultraviolet (UV) light. The GG genotype revealed a single band (303 bp) because no cutting site for this enzyme, while two small PCR fragments containing 98 and 205 bp represent CC genotype. The RFLP pattern for heterozygous GC was characterized using the following 3 bands: 303, 205 and 98bp. More than 10% of the samples with different genotypes, were randomly selected to be sequenced (Macro gen, Geumcheon-gu, Korea) to confirm the genotypes obtained by PCR- RFLP method.

Microsatellite typing

Oligonucleotide primers (sense primer:

5′-TAT- GGA -TTG-CAC-CTA-TCA-GAG-ACC-3′
and anti-sense primer:

5′-TCT-CAT-AGA-GCC-CTT-GGT-GAAT-3′),

were designed to amplify a 250 bp segment of the -794$(CATT)_{5-8}$ promoter region. The annealing temperature of PCR cycle was 58˚C. Purified PCR products of -794$(CATT)_{5-8}$ and ORF region were sequenced using an ABI automated DNA sequencer (Macro gen, Geumcheon-gu, Korea).

Real-time fluorescent quantitative polymerase chain reaction

Endometriotic tissues were collected from 17

endometrioma lesions in women who were genotyped for the *MIF* promoter. The RNA was isolated using TRIzol (TRI® reagent, Sigma-Aldrich, St Louis, MO, USA) based on the manufacturer's instructions. cDNA was amplified by One-Step Reverse transcriptase (RT)-PCR using a transcriptase kit (Fermentase Biolabs, Ipswich, MA, USA) in the presence of random hexamers. The reaction was incubated at 25˚C for 5 minutes, 42˚C for 60 minutes, and 70˚C for 5 minutes. The RT-PCR products were run on agarose gel. Quantitative real-time PCR was performed in an ABI 7000 Thermal Cycler (Applied Biosystems, Foster City, CA, USA). Each standard PCR reaction contained 2 µl cDNA templates, 1 µl of each primer (final concentration, 0.1 mmol/L), and 10 µl SYBR Green PCR Master Mix (Applied Biosystems, Foster City, CA, USA) containing Taq DNA polymerase buffer, deoxynucleotide triphosphate mix, SYBR green I, $MgCl_2$, and Taq DNA polymerase. After denaturation (for 4 minutes at 95˚C), amplification and quantification were repeated 40 times (10 seconds at 95˚C, 30 seconds at 60˚C, and 30 seconds at 72˚C). The primer pairs (in the 5'-3'direction) used for human *MIF:*
[(sense:

5′-AGA-ACC-GCT-CCT-ACA-GCA-AG-3′

antisense:

5′-GAG-TTG-TTC-CAG-CCC-ACA-TT-3′

and amplicon size: 121bp) and

(sense:

5′-CAA-GAT-CAT-TGC-TCC-TCC-TG-3′

and antisense:

5′-ATC-CAC-ATC-TGC-TGG-AAG-G-3′
and amplicon size: 90bp)]

for *β-Actin* were described in our previous study (15). The specificity of the PCR product was estimated by melting curve analysis. All experiments were carried out in triplicate and the relative expression was evaluated using the $2^{-\Delta\Delta Ct}$ method.

Statistical analysis

Comparison of Hardy-Weinberg equilibrium test results was made and allelic and genotype distributions were compared between endometriosis patients and controls using the Pearson's Chi-square analysis by SHEsis (http://analysis.bio-x.cn) (22). The homozygotes for -794$(CATT)_{5-8}$ and -173G/C were evaluated by SHEsis for haplotype distribution, odds ratios (ORs) and 95% confidence interval (CI) (23). For haplotype analyses, scale significantly was considered global P values<0.05. Clinical features of endometriosis patients were studied and comparisons of *MIF* mRNA levels in endometrioma lesions were made using one-way ANOVA and the Tukey's test, and the results were presented as mean ± standard deviation (SD). Differences were considered statistically significant at P<0.05. All statistical analyses were performed using Statistical Package for the Social Sciences (SPSS Inc., version 22, Chicago, IL, USA) software.

Results

Characteristics of the study population

All endometriosis participants had severe endometriosis (stage III and IV). The two groups matched on age with a mean distribution of 31 ± 3.74 and 31.75 ± 3.52 years in endometriosis patients and controls, respectively. BMI has not significant difference between both groups (25.2 ± 3.52 and 24.8 ± 3.8 Kg/m^2 in endometriosis and control groups, respectively). All participants in the current study have a regular menstruation cycle.

Promoter polymorphisms and haplotype study

Genotype and allele frequencies were in Hardy–Weinberg equilibrium in both groups (P>0.05). As shown in Table 1, the CATT8 allele was not detected neither in endometriosis patients nor in controls. Homozygote of CATT7 was observed only in endometriosis whilst CATT6 and CATT7 alleles were more prevalent in endometriosis patients and CATT5 allele was more prevalent in controls but these differences were not significant (P>0.05). Therefore, at the first step, we studied the -794 $(CATT)_{5-8}$ polymorphisms (Table 1) and found that 53 out of 106 endometriosis patients and 53 subjects out of 110 controls were homozygous. In order to assess the effect of simultaneous occurrence of two promoter polymorphisms (-794$(CATT)_{5-8}$ and -173G/C), we continued to evaluate the frequencies of -173G/C polymorphism in 53 endometriosis patients and 53 controls with homozygous genotypes of -794$(CATT)_{5-8}$ polymorphism (Table 2). The data obtained from -173G/C genotyping in these patients were used for this analysis extracted from our previous related study (24). Finally, considering the results presented in Tables 1 and 2, samples from 43 endometriosis patients and 46 controls who were homozygotes for both -794$(CATT)_{5-8}$ and -173G/C polymorphisms, were investigated to estimate the haplotype frequencies (Table 3). Since the purpose of this study was run a haplotype analysis, it was essential to eliminate heterozygous subjects. The homozygous for -794$(CATT)_{5-8}$ polymorphism was more frequently accompanied by the GG genotype of the -173GC in both groups. With respect to haplotypic frequencies, $CATT_5$/G haplotype was significantly more frequent in controls [global test P=0.044]. We observed similar distributions for $CATT_6$/G haplotype in both groups; however, the carriage of the $CATT_6$/C and $CATT_7$/C haplotypes was associated with higher endometriosis susceptibility, but the difference was not statistically significant (P>0.05). Additionally, the $CATT_5$/C and $CATT_7$/G haplotypes were not detected in any group (Table 3). Therefore, strong linkage between decreased repetition of CATT and G allele was detected.

Table 1: Distribution of genotype and allele frequency of *MIF* -794(CATT)$_{5-8}$ in endometriosis patients and controls

Variant	Endometriosis n=106	Controls n=110	P value
-794(CATT)$_{5-8}$ genotype			
5/5*	3 (2.8)	9 (8.2)	0.339
5/6	40 (37.8)	45 (40.9)	
6/6*	49 (46.2)	44 (40)	
6/7	13 (12.3)	12 (10.9)	
7/7*	1 (0.9)	0	
-794(CATT)$_{5-8}$ allele			
5	46 (21.7)	63 (28.6)	0.227
6	151 (71.2)	145 (65.9)	
7	15 (7.1)	12 (5.5)	

Data are presented as n (%). *; Homozygote subjects identified for further analysis (in total 53 endometriosis patients and 53 controls were included in this analysis).

Table 2: Distribution of genotype and allele frequency of *MIF* -173G/C between -794(CATT)$_{5-8}$ homozygotes in endometriosis patients and controls

Variant	Endometriosis n=53	Controls n=53	P value
-173G/C genotype			
GG*	39 (73.6)	45 (84.9)	0.251
GC	10 (18.9)	7 (13.2)	
CC*	4 (7.5)	1 (1.9)	
-173G/C allele			
G	88 (83)	97 (91.5)	0.063
C	18 (17)	9 (8.5)	

Data are presented as n (%). *; Homozygote subjects identified for further analysis.

Table 3: Distribution of *MIF* -794(CATT)$_{5-8}$ and -173G/C haplotype in endometriosis patients and controls*

Haplotype	Endometriosis n=43	Controls n=46	P value	OR [95% CI]
5G	6 (7)	16 (17.4)	0.04	0.365 [0.136-0.983]
5C	0	0	-	-
6G	72 (83.7)	74 (80.4)	0.352	1.459 [0.656-3.246]
6C	6 (7)	2 (2.2)	0.113	3.462 [0.697-17.646]
7G	0	0	-	-
7C	2 (2.3)	0	-	-

Data are presented as n (%). *; Homozygous of -794(CATT)$_{5-8}$ and -173G/C were included in haplotype frequencies assessment, OR; Odds ratios, and CI; Confidence interval.

Expression of *MIF* correlates with haplotype of *MIF* promoter

To evaluate the promoter haplotype -173G/C and -794(CATT)$_{5\text{-}8}$ and function with *MIF* mRNA expression, we assessed the levels of mRNA using fluorescent quantitative polymerase chain reaction (FQ-PCR) in 17 patients with endometrioma who were also genotyped for promoter polymorphisms. The data were normalized against the mRNA level of the CATT$_5$/G samples. We found an interaction between the -173C and more copies of repetitions of CATT in ectopic endometriotic tissues. Promoter activity and subsequent expression of mRNA in ectopic tissue of patients with CATT$_{6,7}$/CC haplotype were significantly higher compared to other haplotypes including CATT$_{5,5}$/GG (2.91 fold, P=0.007), CATT$_{5,5}$/GC (2.48 fold, P=0.047) and CATT$_{6,6}$/GG (2.08 fold, P=0.046). However, the higher transcriptional activity in individuals carrying CATT$_{6,6}$/GC (2.07 fold, P=0.113) and CATT$_{6,6}$/CC (2.01 fold, P=0.130) was not significantly different from those of subjects carrying CATT$_{6,7}$/CC haplotype (Fig.1).

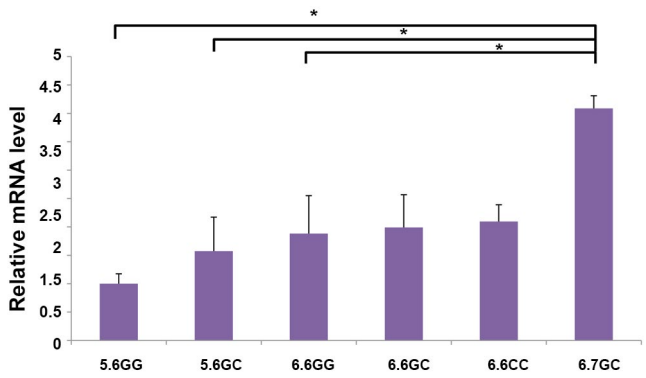

Fig.1: Analysis of *MIF* mRNA levels and evaluation of the promoter haplotype with different *MIF* -794 CATT genotypes (5/5, 5/6, 6/6, and 6/7) together with -173 (GG/GC/CC). Comparison between groups was made by analysis of means ± SEM. Bars show the mean and SEM of experiment performed in triplicate. *; P<0.05.

Discussion

Considering the importance of the *MIF* gene in promoting the inflammatory processes and establishment of ectopic tissues, we investigated possible associations between genetic variants of *MIF* promoter and susceptibility to endometriosis. The results revealed that genetic variants of *MIF*, including the 7 repetitions of the CATT STR in homozygote, were only detected in subjects with endometriosis. Exceptionally, the CATT$_8$ allele, which is a rare allele, was not detected in this study.

Based on our results, the -173C allele is more common in patients carrying -794(CATT)$_{5\text{-}8}$ homozygotes suggesting it as a risk factor for endometriosis. This finding was confirmed by haplotype analysis which revealed that CATT$_6$/C and CATT$_7$/C haplotypes can be considered as moderate risk factors and CATT$_5$/G has an almost protective effect against endometriosis. Additionally, the CATT$_5$/C and CATT$_7$/G haplotypes were not detected in any of the groups.

Geographic variation in -794 STRP also exists and farther from Kenya and Zambia, the frequency distribution of MIF-794 STRP with 5 repeats was lower than other genotypes (25), while in white and Northeast Asian populations, the 6-repeat allele was predominant (26). The western populations with short tandem repeat of MIF CATT$_5$ were less susceptible to autoimmune inflammation (27) and in Northeast Asian populations, the 6-repeat allele was predominant (26). In our study, the most frequent CATT$_5$ allele showed protective properties against endometriosis, which is similar to the effect observed in the Asian population, whereas the 8- repeat of CATT allele was not detected in this study.

Donn et al. (28), for the first time, reported that -173C *MIF* variation is related to inflammatory disorders. Also, Baugh et al. (29), first proposed that -794CATT has five to eight-repeat units and found that short CATT repetitions have a protective effect on rheumatoid arthritis (RA) and suggested that CATT$_7$/C haplotype is related to increased MIF level. Up to now, several meta-analyses investigated possible associations between -173C and CATT$_7$/C, and inflammatory and autoimmune disorders such as tuberculosis (TB), juvenile rheumatoid arthritis (JRA), inflammatory bowel disease (IBD) and cancers (18-21, 30, 31). Another study evaluated associations between haplotype promoter and *MIF* expression level and demonstrated that the 7-repeat at the -794CATT and C allele at the -173 G/C position (7C haplotype) are related to increased *MIF* expression in RA (19). Also, we previously showed the over-expression of *MIF* in ectopic tissues from endometriosis patients (15). The presence of C in the -173 promoter region introduces an AP-4 (activating enhancer binding protein 4) transcription factor binding site (28). AP-4 plays an important role in cellular function by regulation of genes involved in cell growth, survival, immune response and angiogenesis (32). Therefore, the presence of C allele in this region increases the tendency of DNA to bind AP-4 transcription factor.

At the promoter region, the CATT repetition contains several identification regions pituitary-specific factor 1 (Pit-1) binding sites. Pit-1 is a transcription factor in neuroendocrine and mononuclear cells (33, 34). Also, recent studies revealed that inverted CCAAT box binding protein of 90 kDa (ICBP90) is the transcription factor required for interactions between *MIF* microsatellite in several immune system cells and synovial fibroblasts (35). Pit-1 and ICBP90 regulate *MIF* promoter function that is dependent on the length of tandem repetition (34, 35). This may be the reason for the association between the *MIF* CATT$_7$/C genotype (haplotype) and the susceptibility towards endometriosis, because this haplotype causes the simultaneous presence of AP-4, Pit-1 and ICBP90 transcription factors and consequently enhances *MIF* promoter activity. The results showed an increased expression of *MIF* mRNA in individuals

with 6C compared to those with 5G and 7C haplotypes. Thus, observed simultaneous attendance of longer CATT repeats at -794 and the -173C allele in the gene was associated with elevated MIF production and correlated with increased risk of endometriosis. This was confirmed in haplotype analysis which revealed that $CATT_5$/G has strongly protective effect against endometriosis. Taken together, our findings indicate that increment of *MIF* expression is associated with genetic variants of *MIF* promoter in ectopic endometriotic tissues.

Increased MIF activates a cascade of events and strongly stimulates cyclooxygenase 2 (COX2) and prostaglandin E2 (PGE2) expression. This finally leads to increased local synthesis of estrogen in ectopic tissues, which is involved in maintenance and progression of endometriosis (36). Thus, increased MIF is associated with facilitated growth, angiogenesis and development of endometriosis tissue (11, 37).

Conclusion

We believe that the $CATT_5$/G have a protective effect on endometriosis. As well, increased repetitions of CATT and C allele in *MIF* promoter were associated with increased susceptibility to endometriosis in our population and this was related to transcriptional activity of *MIF*. These findings provide the first insight that *MIF* promoter polymorphisms may have a significant effect on susceptibility towards endometriosis; however, further studies are required to determine contribution of MIF to development of endometriosis.

Acknowledgments

We are grateful to Mrs. M. Uromiechi in operation room of Royan Institute for collection of blood samples and ectopic tissues of endometriosis patients who undergone laparoscopy. This study financially supported by a grant from Royan Institute, Reproductive Biomedicine Research Center, Tehran, Iran. The authors declare no conflict of interest.

Authors' Contributions

Z.C.; Conceived and carried out experiments, contributed to collection and assemblying of data, literature review, and manuscript drafting. M.Sh., R.A., P.A.; Contributed to conception, design, and literature review. P.A., R.A.; Administrative support and draft revision. All authors read and approved the final version of the manuscript.

References

1. Bulun SE, Zeitoun K, Takayama K, Noble L, Michael D, Simpson E, et al. Estrogen production in endometriosis and use of aromatase inhibitors to treat endometriosis. Endocr Relat Cancer. 1999; 6(2): 293-301.
2. Burney RO, Giudice LC. Pathogenesis and pathophysiology of endometriosis. Fertil Steril. 2012; 98(3): 511-519.
3. Giudice LC. Endometriosis. N Engl J Med. 2010; 362(25): 2389-2398.
4. Sampson JA. Peritoneal endometriosis due to the menstrual dissemination of endometrial tissue into the peritoneal cavity. Am J Obstet Gynecol. 1927; 14(4): 422-469.
5. Kyama CM, Debrock S, Mwenda JM, D'Hooghe TM. Potential involvement of the immune system in the development of endometriosis. Reprod Biol Endocrinol. 2003; 1(1): 123.
6. Javeed A, Zhao Y, Zhao Y. Macrophage-migration inhibitory factor: role in inflammatory diseases and graft rejection. Inflamm Res. 2008; 57(2): 45-50.
7. Larson DF, Horak K. Macrophage migration inhibitory factor: controller of systemic inflammation. Crit Care. 2006; 10(2): 138.
8. Calandra T, Roger T. Macrophage migration inhibitory factor: a regulator of innate immunity. Nat Rev Immunol. 2003; 3(10): 791-800.
9. Renner P, Roger T, Calandra T. Macrophage migration inhibitory factor: gene polymorphisms and susceptibility to inflammatory diseases. Clin Infect Dis. 2005; 41 Suppl 7: S513-S519.
10. Kats R, Metz CN, Akoum A. Macrophage migration inhibitory factor is markedly expressed in active and early-stage endometriotic lesions. J Clin Endocrinol Metab. 2002; 87(2): 883-889.
11. Carli C, Metz CN, Al-Abed Y, Naccache PH, Akoum A. Up-regulation of cyclooxygenase-2 expression and prostaglandin E2 production in human endometriotic cells by macrophage migration inhibitory factor: involvement of novel kinase signaling pathways. Endocrinology. 2009; 150(7): 3128-3137.
12. Lin W, Chen S, Li M, Wang B, Qu X, Zhang Y. Expression of macrophage migration inhibitory factor in human endometriosis: relation to disease stage, menstrual cycle and infertility. J Obstet Gynaecol Res. 2010; 36(2): 344-351.
13. Kats R, Al-Akoum M, Guay S, Metz C, Akoum A. Cycle-dependent expression of macrophage migration inhibitory factor in the human endometrium. Hum Reprod. 2005; 20(12): 3518-3525.
14. Morin M, Bellehumeur C, Therriault MJ, Metz C, Maheux R, Akoum A. Elevated levels of macrophage migration inhibitory factor in the peripheral blood of women with endometriosis. Fertil Steril. 2005; 83(4): 865-872.
15. Mahdian S, Aflatoonian R, Yazdi RS, Yaghmaei P, Ramazanali F, Afsharian P, et al. Macrophage migration inhibitory factor as a potential biomarker of endometriosis. Fertil Steril. 2015; 103(1): 153-159. e3.
16. Donn RP, Ray DW. Macrophage migration inhibitory factor: molecular, cellular and genetic aspects of a key neuroendocrine molecule. J Endocrinol. 2004; 182(1): 1-9.
17. Donn R, Alourfi Z, Zeggini E, Lamb R, Jury F, Lunt M, et al. A functional promoter haplotype of macrophage migration inhibitory factor is linked and associated with juvenile idiopathic arthritis. Arthritis Rheum. 2004; 50(5): 1604-16410.
18. Areeshi MY, Mandal RK, Dar SA, Jawed A, Wahid M, Lohani M, et al. MIF-173 G> C (rs755622) gene polymorphism modulates tuberculosis risk: evidence from a meta-analysis and trial sequential analysis. Sci Rep. 2017; 7(1): 17003.
19. Bae SC, Lee YH. Circulating macrophage migration inhibitory factor levels and its polymorphisms in systemic lupus erythematosus: a meta-analysis. Cell Mol Biol (Noisy-le-grand). 2017; 63(10): 74-79.
20. Illescas O, Gomez-Verjan JC, García-Velázquez L, Govezensky T, Rodriguez-Sosa M. Macrophage migration inhibitory factor-173 G/C polymorphism: a global meta-analysis across the disease spectrum. Front Genet. 2018; 9: 55.
21. Ma M, Tao L, Liu A, Liang Z, Yang J, Peng Y, et al. Macrophage migration inhibitory factor-794 CATT microsatellite polymorphism and risk of tuberculosis, a meta-analysis. Biosci Rep. 2018; 38(4). pii: BSR20171626.
22. Shi YY, He L. SHEsis, a powerful software platform for analyses of linkage disequilibrium, haplotype construction, and genetic association at polymorphism loci. Cell Res. 2005; 15(2): 97-98.
23. Li Z, Zhang Z, He Z, Tang W, Li T, Zeng Z, et al. A partition-ligation-combination-subdivision EM algorithm for haplotype inference with multiallelic markers: update of the SHEsis (http://analysis. bio-x. cn). Cell Res. 2009; 19(4): 519-523.
24. Chekini Z, Yaran AP, Ansari-Pour N, Shahhoseini M, Ramazanali F, Aflatoonian R, et al. The novel gene-wide haplotype at the macrophage migration inhibitory factor (MIF) locus is associated with endometrioma. Eur J Obstet Gynecol Reprod Biol. 2019 (In Press).
25. Zhong XB, Leng L, Beitin A, Chen R, McDonald C, Hsiao B, et al. Simultaneous detection of microsatellite repeats and SNPs in the macrophage migration inhibitory factor (MIF) gene by thin-film biosensor chips and application to rural field studies. Nucleic Acids Res. 2005; 33(13): e121.
26. Awandare GA, Martinson JJ, Were T, Ouma C, Davenport GC, Ong'echa JM, et al. MIF (macrophage migration inhibitory factor)

promoter polymorphisms and susceptibility to severe malarial anemia. J Infect Dis. 2009; 200(4): 629-637.
27. Grieb G, Merk M, Bernhagen J, Bucala R. Macrophage migration inhibitory factor (MIF): a promising biomarker. Drug News Perspect. 2010; 23(4): 257-264.
28. Donn R, Alourfi Z, De Benedetti F, Meazza C, Zeggini E, Lunt M, et al. Mutation screening of the macrophage migration inhibitory factor gene: positive association of a functional polymorphism of macrophage migration inhibitory factor with juvenile idiopathic arthritis. Arthritis Rheum. 2002; 46(9): 2402-2409.
29. Baugh JA, Chitnis S, Donnelly SC, Monteiro J, Lin X, Plant BJ, et al. A functional promoter polymorphism in the macrophage migration inhibitory factor (MIF) gene associated with disease severity in rheumatoid arthritis. Genes Immun. 2002; 3(3): 170-176.
30. Yang J, Li Y, Zhang X. Meta-analysis of macrophage migration inhibitory factor (MIF) gene-173G/C polymorphism and inflammatory bowel disease (IBD) risk. Int J Clin Exp Med. 2015; 8(6): 9570-9574.
31. Zhang X, Weng W, Xu W, Wang Y, Yu W, Tang X, et al. The association between the migration inhibitory factor− 173g/c polymorphism and cancer risk: a meta-analysis. Onco Targets Ther. 2015; 8: 601-613.
32. Ku WC, Chiu SK, Chen YJ, Huang HH, Wu WG, Chen YJ. Complementary quantitative proteomics reveals that transcription factor AP-4 mediates E-box-dependent complex formation for transcriptional repression of HDM2. Mol Cell Proteomics. 2009; 8(9): 2034-2050.
33. Vallette-Kasic S, Pellegrini-Bouiller I, Sampieri F, Gunz G, Diaz A, Radovick S, et al. Combined pituitary hormone deficiency due to the F135C human Pit-1 (pituitary-specific factor 1) gene mutation: functional and structural correlates. Mol Endocrinol. 2001; 15(3): 411-420.
34. Agarwal S, Cho TY. Biochemical and structural characterization of a novel cooperative binding mode by Pit-1 with CATT repeats in the macrophage migration inhibitory factor promoter. Nucleic Acids Res. 2017; 46(2): 929-941.
35. Yao J, Leng L, Sauler M, Fu W, Zheng J, Zhang Y, et al. Transcription factor ICBP90 regulates the MIF promoter and immune susceptibility locus. J Clin Invest. 2016; 126(2): 732-744.
36. Veillat V, Sengers V, Metz CN, Roger T, Leboeuf M, Mailloux J, et al. Macrophage migration inhibitory factor is involved in a positive feedback loop increasing aromatase expression in endometriosis. Am J Pathol. 2012; 181(3): 917-927.
37. Cao WG, Morin M, Metz C, Maheux R, Akoum A. Stimulation of macrophage migration inhibitory factor expression in endometrial stromal cells by interleukin 1, beta involving the nuclear transcription factor NFκB. Biol Reprod. 2005; 73(3): 565-570.

Original Article

Influence of Follicular Fluid and Seminal Plasma on The Expression of Endometrial Receptivity Genes in Endometrial Cells

Tamouchin Moharrami, Ph.D.[1], Jafar Ai, Ph.D.[2], Somayeh Ebrahimi-Barough, Ph.D.[2], Mohammad Nouri, Ph.D.[3], Maryam Ziadi, M.Sc.[4], Hossein Pashaiefar, Ph.D.[5], Fatemeh Yazarlou, Ph.D.[1], Mohammad Ahmadvand, Ph.D.[5], Soheil Najafi, Ph.D.[6], Mohammad Hossein Modarressi, M.D, Ph.D.[1]*

1. Department of Medical Genetics, Tehran University of Medical Sciences, Tehran, Iran
2. Department of Tissue Engineering and Applied Cell Sciences, Faculty of Advanced Technologies in Medicine, Tehran University of Medical Sciences, Tehran, Iran
3. Stem Cell Research Center, Tabriz University of Medical Sciences, Tabriz, Iran
4. Department of Medical Genetics, Tabriz University of Medical Sciences, Tabriz, Iran
5. Hematology, Oncology and Stem Cell Transplantation Research Center, Tehran University of Medical Sciences, Tehran, Iran
6. Department of Immunology, School of Public Health, Tehran University of Medical Sciences, Tehran, Iran

**Corresponding Address: P.O.Box: 1417613151, Department of Medical Genetics, Tehran University of Medical Sciences, Tehran, Iran*
Email: Modaresi@tums.ac.ir

Received: 5/May/2019, Accepted: 24/July/2019

Abstract

Objective: Endometrial receptivity plays a key role in pregnancy success in assisted reproduction cycles. Recent evidence suggests that seminal plasma (SP) and follicular fluid (FF) influence the uterine endometrium to improve implantation of the embryo and the establishment of pregnancy. In this study, we attempt to assess the influence of FF and SP on the expression levels of main endometrial receptivity genes (*HOXA10, HOXA11, ITGAV, ITGB3* and *LIF*) in endometrial stromal cells.

Materials and Methods: In this experimental study, SP and FF were collected from 15 healthy fertile men and 15 healthy fertile women, respectively. Tissue specimens of the endometrium were obtained from 12 women undergoing hysterectomy for benign conditions. After endometrial stromal cell isolation and culture, dose- and time-dependent cytotoxic effects of pooled FF and SP on 3D-cultured endometrial cells were evaluated. A second independent set of 12 endometrium samples was treated under determined optimum conditions and evaluated for gene expression analysis using quantitative real-time polymerase chain reaction (qRT–PCR).

Results: The results of this study indicated that exposure of endometrial stromal cells to FF resulted in the elevated expression of *HOXA10* (fold change=2.6, P=0.02), *HOXA11* (fold change=3.3, P=0.002), *LIF* (fold change=4.6, P=0.0003), *ITGB3* (fold change=3.5, P=0.012), and *ITGAV* (fold change=2.8, P=0.001) compared to untreated cells. In addition, we found that SP-treated endometrial cells showed increased mRNA levels of only the LIF gene (fold change=2.5, P=0.008) compared to untreated cells.

Conclusion: Human SP and FF may modulate the endometrial receptivity and improve the implantation rate in assisted reproduction cycles through the up-regulation of endometrial receptivity genes.

Keywords: Endometrium, Follicular Fluid, Implantation, Seminal Plasma

Cell Journal(Yakhteh), Vol 22, No 4, January-March (Winter) 2021, Pages: 457-466

Citation: Moharrami T, Ai J, Ebrahimi-Barough S, Nouri M, Ziadi M, Pashaiefar H, Yazarlou F, Ahmadvand M, Najafi S, Modarressi MH. Influence of follicular fluid and seminal plasma on the expression of endometrial receptivity genes in endometrial cells. Cell J. 2021; 22(4): 457-466. doi: 10.22074/cellj.2021.6851.

Introduction

Assisted reproductive technologies (ART) are not only used to overcome fertility issues in infertile cases but are also key tools in preventing genetic abnormalities in fertile couples. However, the efficacy of ARTs is still suboptimal and the low rates of transferred embryo implantation in ART cycles remains the main challenge for achieving successful pregnancies. This limitation partly results from inadequate knowledge about the cellular and molecular basis of germ cells, embryos, and endometrium physiology (1). Despite recent advances in embryo development, selection, and transfer techniques, implantation failure occurring in approximately 75% of cases is a major limiting factor for pregnancy following *in vitro* fertilization (IVF) attempts (2). The receptive endometrium is one of the most important factors for the outcome of pregnancies following ART cycles and optimizing endometrial receptivity is imperative to improving the success rate of ART. During the implantation window, a unique timeframe in which implantation is possible, the endometrium plays a crucial role in successful implantation (3).

Endometrial receptivity and subsequent embryo implantation can only happen after a complex series of histological, cellular and molecular changes in the endometrium. It has been shown that successful embryo implantation depends on an ideal endometrium-embryo cross-talk through the known crucial growth factors and cytokines which are secreted from endometrial cells (4).

Previous studies have indicated that differential expression of a variety of genes including those involved in immune response, the complement cascade pathway, cell adhesion and exosome biogenesis may influence

endometrial receptivity (5). Hence, in the past decade, many global transcriptomic studies have been designed to find potential biomarkers or molecular signatures for a receptive endometrium. There are, however, many disagreeing reports due to differences in the analysis of gene expression and sample selection (6, 7). Moreover, different studies have suggested that the use of supplements such as vitamins, hormones and minerals may improve endometrial receptivity and increase the chance of implantation in ART procedures (8, 9) .

Due to the complex nature of endometrial receptivity, it seems the use of a cocktail of supplements can be more effective than individual supplements. Seminal plasma (SP) and Follicular fluid (FF) can be considered as cocktails of various natural biocompounds. SP is a reach medium comprised of different biologically active factors including cytokines, chemokines, prostaglandins, growth factors, angiogenic factors, vitamins, zinc, etc (10). According to recent proteomic studies, high concentrations of these cytokines and prostaglandins in the SP of fertile men and aberrant concentrations of these components in the SP of infertile men demonstrate that SP constituents may play a key role in human reproduction. Furthermore, most of these important compounds which have been identified in the female reproductive tract (FRT) suggest their involvement in the regulation of FRT functions and successful reproduction (11). From the mechanistic point of view, different studies in mice, pigs and humans have shown that SP may play a critical role in endometrial receptivity and the improvement of implantation chances (12, 13). In addition to SP, FF which provides critical factors for oocyte development, contains important cytokines, hormones and growth factors that may mediate paracrine/autocrine interactions during the process of implantation (14).

During ART cycles such as IVF or ICSI, unlike what happens naturally in the body of mammals, the blastocyst is transferred without any SP and the FF is also discarded during ovum pick-up. As these fluids contain a vast range of natural elements including growth factors that possibly improve receptivity of the endometrium, we hypothesize that using the blastocyst alone might cause limited implantation rates after ART cycles. We evaluated this hypothesis through the study of the *in vitro* influence of SP and FF on the expression levels of the genes *HOXA10, HOXA11, LIF, ITGB3,* and *ITGAV,* whose role in the successful implantation of blastocysts have been established, in endometrial stromal cells.

Materials and Methods

Endometrial tissue collection and processing

In this experimental study, twelve fresh endometrial tissue samples were collected from childbearing-age women (ages 23-35) undergoing hysterectomy for benign conditions. Six of the participants were receiving hysterectomies for fibroids, three for adenomyosis, one for uterine prolapse and one for heavy menstrual bleeding. All of them were in the secretory phase of their menstrual cycle. Malignancy, drug and hormone therapy, and pregnancy were the exclusion criteria for the participants in our study. Written informed consent was obtained from all participants and the study was approved by the Ethics Committee of Tehran University of Medical Sciences (IR.TUMS.MEDICINE.REC.1396.4258). Immediately after sampling, the endometrium specimens were placed in Hank's Balanced Salt Solution (HBSS, Sigma-Aldrich, USA) with 1% penicillin/streptomycin (Pen/Strep, Gibco, USA) and transported to the laboratory within two hours. Tissue samples were then transferred to sterile 10 cm petri dishes and rinsed with phosphate buffered saline (PBS, Merck, Germany). After washing, the tissue samples were transferred to another petri dish containing pre-warmed HBSS and were cut into small pieces with a sterile scalpel. The dissected specimens were transferred into sterile 15 ml tubes containing HBSS and 3 mg/ml collagenase type I (Sigma-Aldrich, USA) for enzymatic digestion. After 60 minutes of incubation at 37˚C, the solutions were re-suspended in Dulbecco's Modified Eagle Medium and Ham's F-12 (DMEM/F12, Gibco, USA) supplemented with 10% fetal bovine serum (FBS, Gibco, USA) for enzyme neutralization. Following complete tissue digestion, cell suspensions were filtered through 70 micron cell strainers to remove the undigested fragments from the suspension. Afterwards, the cell suspensions were filtered through a 40 micron cell strainer to isolate the endometrial stromal cells from endometrial epithelial cells.

For further purification and removal of red blood cells (RBCs), fresh DMEM/F12 culture medium supplemented with 10% FBS was added to the collected cells and centrifuged at 1500 rpm for 10 minutes. After removing the supernatant, the cell pellet was resuspended and added to Ficoll-Paque media solution in 15 ml tubes, then centrifuged for 20 minutes at 1200 rpm. Afterward, the upper layer containing stromal cells was transferred to a new tube and washed twice with PBS (15) including osteocytes and adipocytes. Here, the potency of EnSC in neural differentiation has been investigated. Flow cytometric analysis showed that they were positive for CD90, CD105, OCT4, CD44 and negative for CD31, CD34, CD133. The characterized cells were induced into neural differentiation by bFGF (basic fibroblast growth factor.

Primary cell cultures

The stromal cells were transferred to T_{25} culture flasks containing DMEM/F12, 10% FBS and 1% Pen/Strep and were incubated at 37˚C and 5% CO_2. After 24 hours of incubation, the culture medium and nonadherent cells were discarded and the attached cells were washed twice with PBS, then fresh culture medium was added and incubated at 37˚C and 5% CO_2. The medium was changed

every 3 days until passage 3. Cells of passage 3 were used for the experiments.

Three-dimensional cell culture

Fibrin gel was used to provide a three-dimensional matrix for culturing endometrial stromal cells. The 3D cultures of for MTT (3-(4,5-Dimethylthiazol-2-yl)-2,5-diphenyltetrazolium bromide) assays were carried out in 96-well culture plates while other cultures took place in 24-well plates for optimized treatment. Fibrin gel, were produced by dissolving 3 mg of fibrinogen (Sigma, USA) in 1 ml of M199 medium (Sigma, USA). Stromal cells (2×10^5 cells/ml) were added to the prepared fibrinogen solution and carefully mixed with 2 µl of a thrombin solution (120 U/ml in 1 M sodium buffer, Sigma, USA), 1.5 µl of $CaCl_2$ (1%). Then 100µl of cell containing fibrinogen medium was added to each well of a 96-well cell culture plate. The plate was incubated at 37˚C for 1-2 hours to form a three-dimensional structure. Following fibrin gel formation, 0.1 ml of DMEM/F12 medium supplemented with 10% FBS was added to each well and the plate was returned to the 37˚C incubator. The culture medium was refreshed every 3 days following a previously published protocol (16).

Seminal plasma and follicular fluid preparation

Semen samples were collected from 15 fertile donors, aged 27-41 years old (mean age of 34), with normal spermogram from the Reproductive Health Center of Tabriz Alzahra Hospital. The samples were centrifuged at 3000 rpm for 20 minutes. Supernatants were collected and centrifuged again at 10000 rpm for 15 minutes in order to remove. The supernatants were pooled, filtered through 0.22 µm filters for the prevention of microbial contamination and stored at -20˚C until used.

FF was obtained by puncturing ovarian follicles from 15 ovum donors, aged 23-32 (mean age of 27), at Reproductive Health Center of Tabriz Alzahra Hospital. Macroscopically clear FF samples were centrifuged at 6000 rpm for 20 minutes to remove cellular components. The supernatants were pooled, filtered through 0.22 µm filters and stored at -20˚C until used.

Seminal plasma and follicular fluid toxicity evaluation using the MTT assay

The MTT assay was used to determine the non-toxic doses and effects of semen plasma and FF on viability of the fibrin gel-encapsulated endometrial stromal cells. The MTT assay is a reliable colorimetric reaction, which is widely used to measure cell viability and cytotoxicity. The principle of this assay is the reduction of MTT dye to formazan crystals by the mitochondrial dehydrogenases of viable cells. There is a linear correlation between the amount of formazan and cell viability. So, determination of formazan quantity can be used as an estimate of the population of living cells.

A total of 10^4 endometrial stromal cells isolated from three different samples were encapsulated in fibrin gel (3 mg/ml) in separate wells of 96-well plate. Different concentrations of FF and semen plasma (1%, 5%, 10%, 20%, 50% and 100%) were added to each well as treatment groups. These concentrations were achieved through dilution with DMEM/F12 culture medium containing 2% FBS. The control group was endometrial stromal cells encapsulated in fibrin gel without any treatments.

After treatment with SP for 3, 6, 24, 48 and 72 hours or FF for 3, 6, 24, 48 72, and 96 hours, the culture media were removed and 100 µl of MTT solution (0.5 mg/ml in PBS, Sigma, USA) was added to each well and incubated at 37˚C for 4 hours. Afterward, 100 µl of dimethyl sulfoxide (DMSO, Sigma Aldrich, USA) was added to each well and incubated for 15 minutes in a dark room at room temperature to dissolve the formazan crystals. Finally, absorbance was measured at 570 nm using a spectrophotometric plate reader Asys Expert 96 (Biochrom, UK) according to established guidelines. These experiments were repeated five times. Cell survival was calculated as the percentage of test absorbance compared to the control absorbance.

RNA isolation and quantitative real-time polymerase chain reaction

Total RNA was extracted from cultured endometrial stromal cells using TriPure Isolation Reagent (Roche, Switzerland) according to the manufacturer's instructions.

Concentration and purity of extracted RNA samples were checked with a NanoDrop 2000C spectrometer (Thermo Scientific, USA) and RNA integrity was evaluated by running 1 µl of total RNA samples through 1% agarose gel. A total 1 µg of extracted RNA was retrotranscribed to complementary DNA (cDNA) with random hexamer and oligo dT primers, using a cDNA synthesis kit (Takara, Japan). The final cDNA product was used as the template for qRT-PCR.

Quantitative real-time PCR was done in duplicates on a light cycler 96 real-time PCR system (Roche, Switzerland). The qRT-PCR reactions were run with the following settings: 95˚C for 10 minutes, followed by 45 cycles of 95˚C for 10 seconds and 60˚C for the 30 seconds. At the end of each qRT-PCR run, the melting curve program was run to make sure the PCR product's specificity. Each qRT-PCR reaction contained 10 µl RealQ Plus Master Mix Green (Ampliqon- Denmark), 1 µl (100 ng/µl) of cDNA, 1µl mixed forward and reverse primers and 8 µl ddH_2O. Expression levels of the target genes were evaluated by normalizing to the expression of the *GAPDH* gene as the reference gene. The relative expression levels of target transcripts were calculated through the $2^{-\Delta\Delta Ct}$ method. Primer sequences and characteristics are summarized in Table 1.

Table 1: Primer sequences used for quantitative real-time polymerase chain reaction

Gene name	Transcript	Primer sequence (5´-3´)	Annealing T_m (˚C)	Amplicon size (bp)
HOXA10	NM_018951.4	F: GGATTCCCTGGGCAATTCCA	60	99
		R: AGTGTCTGGTGCTTCGTGTA		
HOXA11	NM_005523.5	F: CCAGAATGAGGCTGCTTTCC	59	173
		R: GAACTCAGGGCTGGATCAGT		
ITGAV	NM_002210.5	F: TGGAGCACCTCTCTTCATGG	60	177
		R: CCATCCTGGTCCAGATCTCC		
ITGB3	NM_000212.2	F: CTCCTCATCACCATCCACGA	59	84
		R: GTTGTTGGCTGTGTCCCATT		
LIF	NM_002309.5	R: ACATCTGGACCCAACTCCTG	59	131
		F: AGAAGAAGAAGCTGGGCTGT		
GAPDH	NM_002046	F: GAAGGTGAAGGTCGGAGTCA	60	109
		R: ATTGAAGGGGTCATTGATGG		

Statistical analysis

The obtained data were analyzed statistically using the SPSS 20.0 software package (SPSS, Chicago, IL, USA). Paired t test was applied to assess statistical significance differences as appropriate. For all statistical analyses, a $P<0.05$ was considered to be statistically significant.

Results

Cytotoxicity assays

Before analyzing of the effects of semen plasma and FF on the expression levels of receptivity genes in endometrial stromal cells, we determined the optimum FF and SP concentrations and treatment time that had no dose- or time-dependent cytotoxic effects on the 3D- cultured endometrial stromal cells obtained from 3 different women.

As shown in Figures 1 and 2, respectively, we found that a 72-hour incubation with 20% FF and a 48-hour incubation with 10% SP resulted in the highest proliferation rate and had no cytotoxic effects on the cultured cells. Therefore, these non-toxic conditions were chosen for subsequent qRT-PCR analyses.

Influence of follicular fluid and seminal plasma on the expression of endometrial receptivity genes

To evaluate the capacity of SP and FF, to modulate expression of endometrial receptivity genes, cultured endometrial stromal cells were exposed to either vehicle control medium alone, 10% SP for 48 hours or 20% FF for 72 hours. mRNA expression levels of *LIF*, *ITGB3*, *ITGAV*, *HOXA11*, and *HOXA10* were analyzed with qRT-PCR.

The exposure of endometrial stromal cells to FF resulted in elevated expression of *HOXA10* (fold change=2.6, P=0.02), *HOXA11* (fold change=3.3, P=0.002), *LIF* (fold change=4.6, P=0.0003), *ITGB3* (fold change=3.5, P=0.012) and *ITGAV* (fold change=2.8, P=0.001) compared to vehicle control medium alone (Fig.3).

In addition, we found that in SP treated endometrial stromal cells, only the mRNA levels of the *LIF* gene was increased (fold change=2.5, P=0.008) compared with vehicle control medium while the expression of *ITGB3*, *ITGAV*, *HOXA11*, and *HOXA10* did not change (Fig.4).

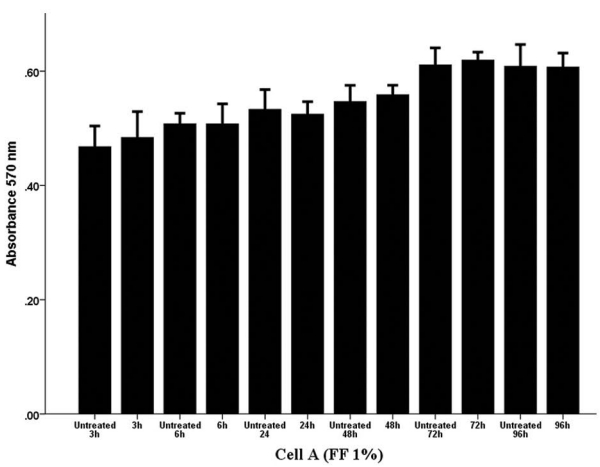

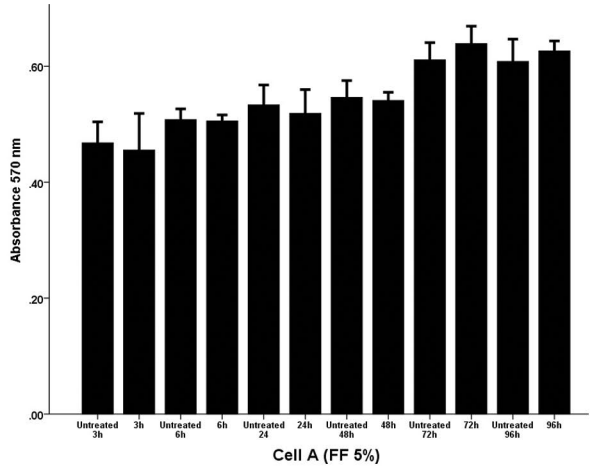

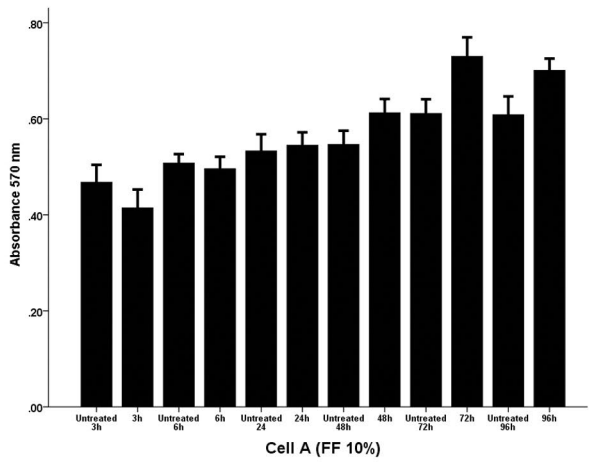

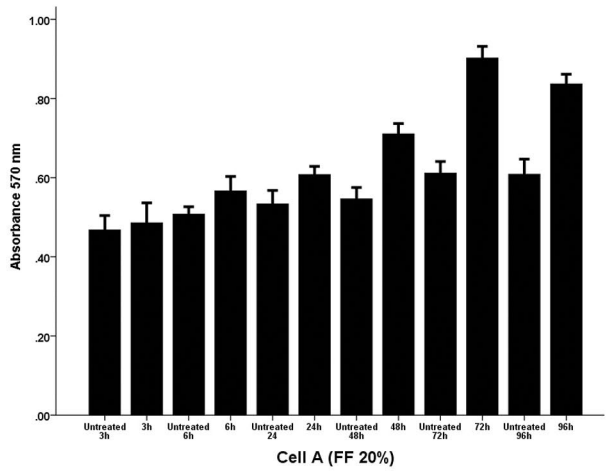

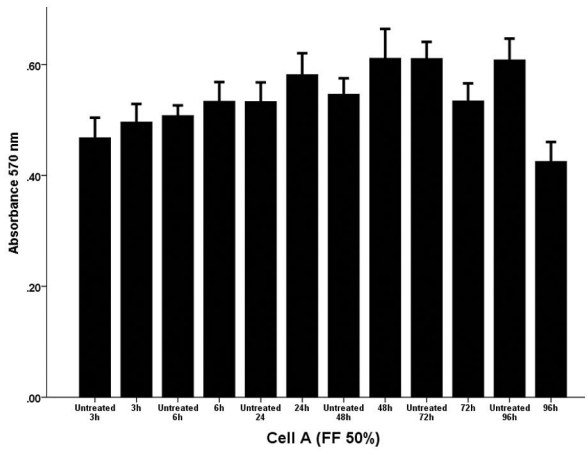

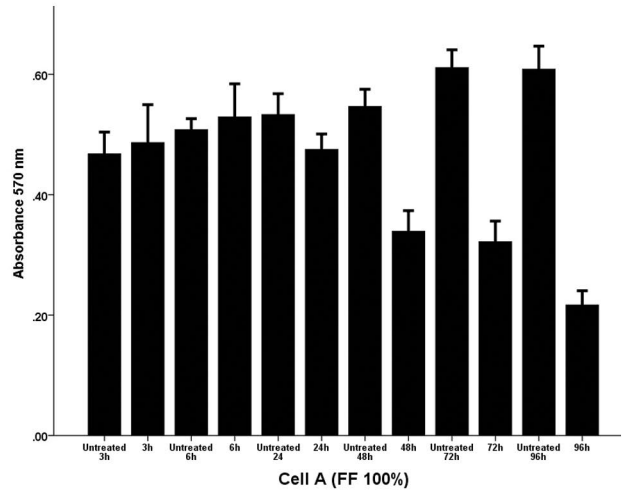

Fig.1: Analysis of the dose- and time-dependent effect of follicular fluid (FF) on the viability of endometrial stromal cells using the MTT assay. The endometrial cells were exposed to different concentrations of FF (0, 1, 5, 10, 20, 50 and 100%) for 3, 6, 24, 48, 72 and 96 hours. The numbers on the bars show mean absorbance at 570 nm.

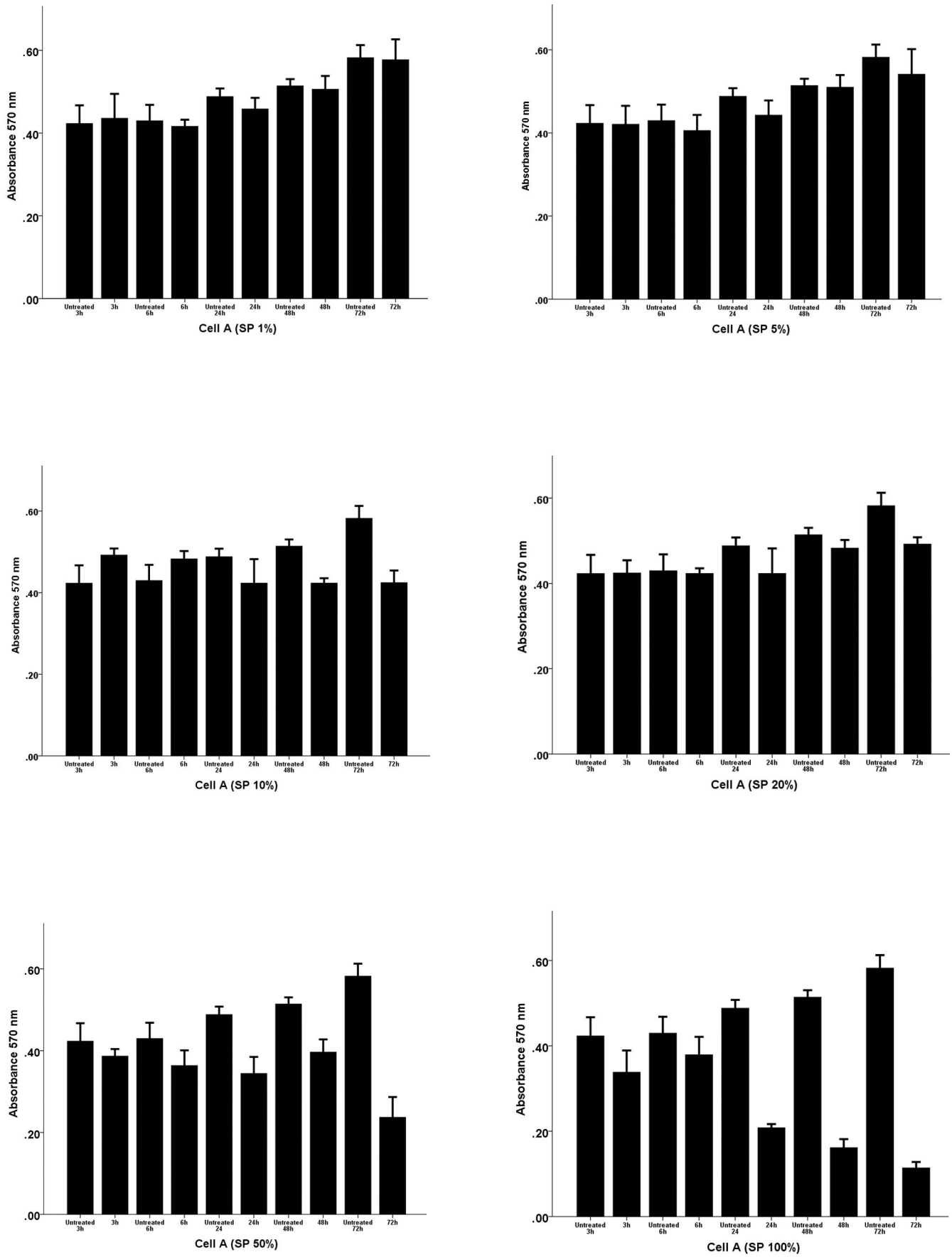

Fig.2: Analysis of the dose- and time-dependent effect of seminal plasma (SP) on the viability of endometrial stromal cells using the MTT assay. The endometrial cells were exposed to the different concentrations of SP (0, 1, 5, 10, 20, 50 and 100%) for 3, 6, 24, 48, and 72 hours. The numbers on the bars show mean absorbance at 570 nm.

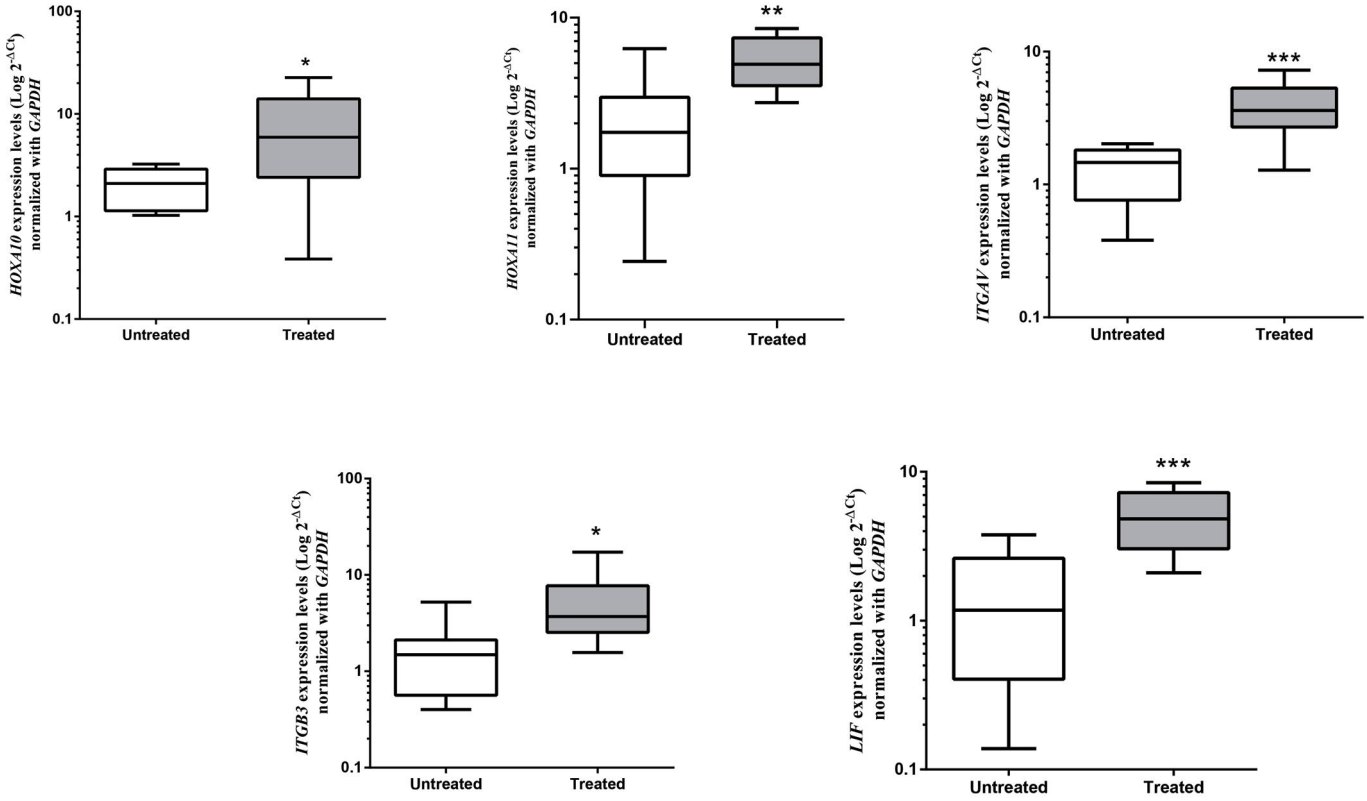

Fig.3: The relative mRNA expression levels of endometrial receptivity genes following follicular fluid (FF) treatment. The line in each box indicates the mean expression level and bars represent confidence interval (CI) 95%. Gene expression levels are indicated in Log scales. *; P≤0.05, **; P≤0.01, and ***; P≤0.001.

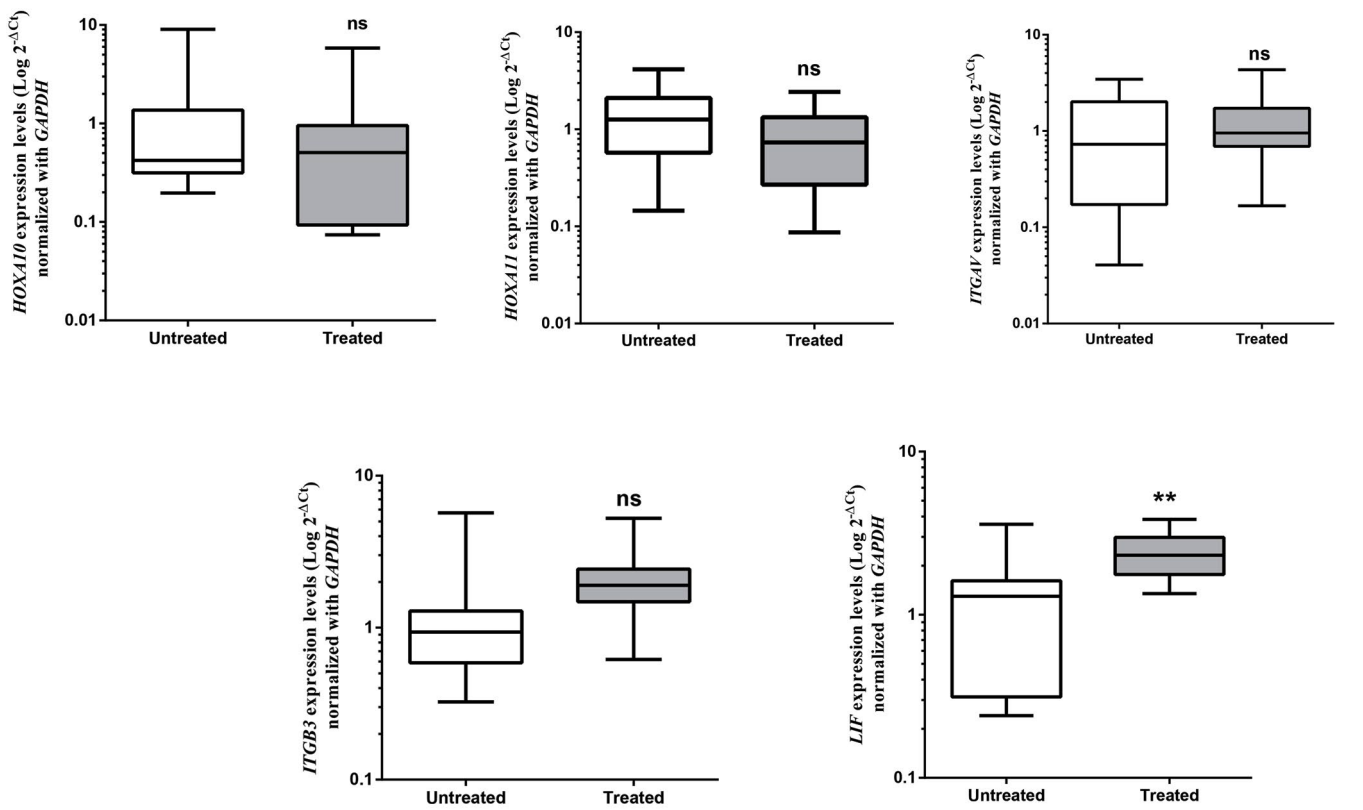

Fig.4: The relative mRNA expression levels of endometrial receptivity genes following seminal plasma (SP) treatment. The line in each box indicates the mean expression level and bars represent confidence interval (CI) 95%. Gene expressions levels are indicated in Log scales. ns; P>0.05 and **; P≤0.01.

Discussion

During the past two decades, ART has become a key medical procedure to help infertile women achieve pregnancy. However, embryo implantation failure in ART cycles remains the main obstacle for achieving a successful pregnancy. The implantation of the blastocyst is a complex process involving reciprocal communication between the embryo and the uterus, which is mainly dependent on the function and receptivity of the endometrium. It is thought that suboptimal endometrial receptivity is the reason for two-thirds of implantation failures. Thus, different clinical strategies have been employed to improve implantation rates following ART cycles (17).

Many different histological, biochemical, and molecular genetics studies have been conducted with the aim of defining endometrial receptivity markers. Identification of these markers can be very useful in using them in diagnostic setting and improving ART methods. Of these markers, molecular markers are of a great importance due to their high sensitivity and specificity (7). That is why many transcriptomic and proteomic investigations have been performed in the past decade to find reliable molecular markers that reflect the level of the endometrium's receptivity (18). Discovery of these markers and the key molecular pathways involved in the implantation process can facilitate improvement of the endometrium receptivity methods (19). However, due to considerable differences among the results of these studies, there is no consensus on the genes that can be used as biomarkers in clinical diagnostic tests for determining of the level of endometrial receptivity (7). Nevertheless, the central roles of some gene families and signaling pathways that are involved in implantation have been established in endometrial cells. These gene families are mainly growth factors, cytokines, chemokines and cell adhesion molecules. The fact that a variety of molecular mechanisms such as disrupted growth factor, cytokine, and hormone signaling are thought to be involved in the suppression of endometrial receptivity biomolecules that lead to a reduced implantation rate further confirms this (20).

It therefore seems that one main approach for enhancing endometrial receptivity can be exposure of the endometrium to a biological cocktail containing various biologically active factors. It is believed that human semen plasma and FF naturally contain the critical signaling components that have major functions in the process of implantation. Furthermore, recent studies have indicated that SP and FF which can enter the uterine cavity during sexual intercourse ovulation respectively, may affect and regulate endometrial signaling mechanisms to induce implantation and increase reproductive success (21).

Several studies have assessed the *in vitro* and *in vivo* effects of SP and FF on the functions and gene expression of the endometrium. Chen et al. (22) examined the *in vitro* effects of SP on the transcriptome of human endometrial cells. Their results indicated that SP exposure leads to up-regulation of genes involved in proliferation, viability, and migration in the endometrial stromal cells. Gutsche et al. (23) indicated that SP has an *in vitro* stimulatory effect on the expression levels of pro-inflammatory cytokines including IL-1b, IL-6 and, LIF in human endometrial cells. In agreement with the previous studies, a recent study by Rodriguez-Caro et al. (24) has proved that *in vitro* interaction between SP extracellular vesicles and endometrial stromal cells may improve endometrial receptivity by inducing prolactin secretion, which is a key hormone in implantation, and enhancing decidualization. A recent systematic review and meta-analysis conducted by Saccone et al. (11) indicated a higher clinical pregnancy rate after intra-vaginal/cervical injection of SP at the time of oocyte pickup suggesting that SP plays an important role on endometrial function and the maternal immune system, and thereby supports implantation. A prospective randomized study by Hashish et al. (25) showed that flushing of the endometrial cavity with FF in patients undergoing intracytoplasmic sperm injection (ICSI) did not significantly improve implantation rates. However, FF is rich in growth factors and its potential for increasing the rate of implantation and subsequent successful pregnancy should be the focus of further research.

To address these challenges, in the current study, we determined the *in vitro* influence of FF and SP on the expression levels of main endometrial receptivity genes with established roles in the implantation process including *HOXA10*, *HOXA11*, *ITGAV*, *ITGB3* and *LIF*, in endometrial stromal cells.

We have applied a fibrin three-dimensional cell culture system for endometrial stromal cells culture to provide information that is more physiologically relevant to cells *in vivo*. This polymer has recently become widely used in tissue engineering. Fibrin gel is naturally formed in the body, through the natural process of fibrinogen mixing with thrombin (26).

We first ensured that the response to FF or SP was not due to their cytotoxic effects by performing precise cytotoxicity assays. We found that a 48 hours incubation with 10% SP and a 72 hours incubation with 20% FF showed they had no dose- or time-dependent cytotoxic effects on the endometrial stromal cells and interestingly, the maximum viability for cells was seen in these conditions.

Exposure of endometrial stromal cells to FF resulted in elevated expression of all of the analyzed genes including an increase of 2.6 fold in *HOXA10*, 3.3 fold in *HOXA11*, 4.6 fold in *LIF*, 3.5 fold in *ITGB3* and 2.8 fold in *ITGAV* expression levels. In addition, we found that SP-treated endometrial cells only showed an increase of 2.5 fold in the mRNA levels of the *LIF* gene compared to untreated controls.

In this study, we selected genes whose essential role in fetus implantation has been proven by different studies, and are involved in the key signaling pathways. *HOXA10* and *HOXA11* are two important members of the homeobox gene family, and encode very important

transcription factors. It has been proven that expression of *HOXA10,* a member of a family of homeobox genes, is critical for FRT development and endometrial receptivity. Moreover, up-regulation of *HOXA10* at the time of implantation improves endometrial receptivity by regulating downstream genes such as ITGB3 (27). A supporting study, Wang et al. (28) reported that 5-Aza-20-deoxycytidine (AZA) might improve endometrial receptivity through the induction of *HOXA10* expression.

Like *HOXA10*, *HOXA11* expression plays an important role in implantation and the down regulation of this gene leads to female infertility. Therefore, up-regulation of both *HOXA10* and *HOXA11* in the receptive endometrium indicate that these genes play important roles in decidualization. Women with abnormal expression of *HOXA10* and *HOXA11* genes show lower rates of implantation indicating that these genes are important for blastocyst implantation because they regulate the expression of molecular and cellular markers needed for embryo implantation (29).

ITGAV and *ITGB3* encode essential cell adhesion molecules. *ITGAV*, a member of the integrin gene family that encodes integrin αv, heterodimerizes with the integrin β3 chain that leads to improvement of angiogenesis and embryo attachment. Accordingly, deregulation of *ITGAV* gene has been reported in a variety of reproductive disorders suggesting its essential role in the human reproduction processes. It is reported that the expression of αvβ3 integrin, a cell surface adhesion molecule, was elevated during implantation in humans and its endometrial expression was reduced in infertile women suggesting that it is important for the process of implantation (30).

The last gene, *LIF,* encodes a multi-functional cytokine that plays a key role in the implantation process. *LIF*, belongs to the IL-6 family and plays a clear role in the process of implantation by regulating a variety of biological processes during blastocyst implantation (31). The absence of *Lif* in mice reduces blastocyst implantation. A recent study by Shokrzadeh et al. (32) indicated that administration of calcitonin during the implantation window improves endometrial receptivity in mice by up-regulating *LIF* and Le-7a miRNAs and down-regulating that of Muc-1. Increased expression of endometrial *LIF* in the secretory phase is essential for implantation in humans, because multiple critical events during implantation are regulated by *LIF* such as promoting the endometrial receptive state, endometrial-embryo interaction, decidualization of stromal cells, and development of the blastocyst. In addition, leukemia inhibitory factor-mediated adhesion molecules require integrin αvβ3 and αvβ5 for the adhesion of trophoblast cells to endometrial cells. Gremlich et al. (33) showed in their study that IVF patients with lower plasma concentrations of *LIF* had an increased risk of implantation failure.

Most previous studies have only investigated the biochemical compounds of FF and its relation with the quality of the ovum. In contrast, the present study investigated the effect of FF on endometrial cells and it was observed that FF induces the expression of the genes that are involved in Embryo implantation. FF is rich in steroidal hormones (34), especially estrogen and progesterone, and previous studies have shown that the expression level of *HOXA10* and *HOXA11* in endometrial cells are upregulated by these hormones (35). It seems that these steroidal hormones have induced the expression of the *HOX* genes that, in turn, have functioned as transcription factors leading to the upregulation of *LIF* in the endometrial cells. Many related studies have suggested *LIF* as a positive regulator of integrins αv and β3. Therefore, *LIF* is a key regulator of the fetus implantation, as it has in turn induced the expression of the adhesion molecules *ITGAV* and *ITGB3* (36).

Unlike the study of Hashish et al. (25) that used FF from a single mature oocyte, we used pooled FF obtained from 15 mature follicles to treat the endometrial stromal cells. Our results showed a higher expression level of endometrial receptivity genes suggesting that FF can be an inexpensive, more readily available source of cytokine and growth factors and may be applicable for improving implantation rates in ART cycles.

In case of SP, unlike with FF, we only observed a significant up-regulation in the level of *LIF* gene. Considering the fact that the cytokine *LIF* has multiple roles in the implantation process and functions as a mediator in some other pathways (37), it seems that it may be necessary to study other *LIF*-related genes. Many studies have indicated the positive effect of SP in the implantation process (23, 38-40) . Therefore, it is necessary to perform systematic studies to investigate the genes that are affected by SP to decipher the underlying molecular mechanisms.

Conclusion

Taken together, our results provide evidence that SP and FF may contribute to the regulation of endometrial function by upregulating endometrial receptivity genes in human endometrial cells. Accordingly, the application of SP and FF can be considered a potential natural supplement to IVF. More research is required to evaluate the clinical importance of SP and FF in the rate of embryo implantation such as intravaginal or intracervical uses of SP and FF in IVF therapies.

Acknowledgments

The current study financially supported by a grant from Tehran University of Medical Sciences, International Campus, Tehran, Iran (grant number: 96-04-103-36874). There is no conflicts of interest in this study.

Authors' Contributions

T.M., M.H.M.; Participated in study design, all experimental work, collection, and interpretation of the data. S.E.-B., J.A.; Contributed to 3D cell culture

experiments and the MTT assay. M.N., M.Z.; Performed semen and FF sample collections and prepared the samples for treatment experiments. F.Y., S.N.; Conducted the molecular experiments and qRT-PCR analysis. H.P., M.A.; Contributed to all statistical analyses and interpretation of the data. All authors performed editing of the final version of this manuscript for submission, and participated in the finalization of the manuscript and approved the final draft.

References

1. Egea RR, Puchalt NG, Escrivá MM, Varghese AC. OMICS: Current and future perspectives in reproductive medicine and technology. J Hum Reprod Sci. 2014; 7(2): 73-92.
2. Allersma T, Farquhar C, Cantineau AE. Natural cycle in vitro fertilisation (IVF) for subfertile couples. Cochrane Database Syst Rev. 2013; (8): CD010550.
3. Macklon NS, Brosens JJ. The human endometrium as a sensor of embryo quality. Biol Reprod. 2014; 91(4): 98.
4. Achache H, Revel A. Endometrial receptivity markers, the journey to successful embryo implantation. Hum Reprod Update. 2006; 12(6): 731-746.
5. Timeva T, Shterev A, Kyurkchiev S. Recurrent implantation failure: the role of the endometrium. J Reprod Infertil. 2014; 15(4): 173-183.
6. Ulbrich SE, Groebner AE, Bauersachs S. Transcriptional profiling to address molecular determinants of endometrial receptivity--lessons from studies in livestock species. Methods. 2013; 59(1): 108-115.
7. Craciunas L, Gallos I, Chu J, Bourne T, Quenby S, Brosens JJ, et al. Conventional and modern markers of endometrial receptivity: a systematic review and meta-analysis. Hum Reprod Update. 2019; 25(2): 202-223.
8. Zhao J, Huang X, Xu B, Yan Y, Zhang Q, Li Y. Whether vitamin D was associated with clinical outcome after IVF/ICSI: a systematic review and meta-analysis. Reprod Biol Endocrinol. 2018; 16(1): 13.
9. Carrascosa JP, Cotán D, Jurado I, Oropesa-Ávila M, Sánchez-Martín P, Savaris RF, et al. The effect of copper on endometrial receptivity and induction of apoptosis on decidualized human endometrial stromal cells. Reprod Sci. 2018; 25(7): 985-999.
10. Mcgraw LA, Suarez SS, Wolfner MF. On a matter of seminal importance. Bioessays. 2015; 37(2): 142-147.
11. Saccone G, Di Spiezio Sardo A, Ciardulli A, Caissutti C, Spinelli M, Surbek D, et al. Effectiveness of seminal plasma in in vitro fertilisation treatment: a systematic review and meta-analysis. BJOG. 2019; 126(2): 220-225.
12. Schjenken JE, Glynn DJ, Sharkey DJ, Robertson SA. TLR4 signaling is a major mediator of the female tract response to seminal fluid in mice. Biol Reprod. 2015; 93(3): 68.
13. Robertson SA. Seminal fluid signaling in the female reproductive tract: lessons from rodents and pigs. J Anim Sci. 2007; 85(13 Suppl): E36-E44.
14. Revelli A, Delle Piane L, Casano S, Molinari E, Massobrio M, Rinaudo P. Follicular fluid content and oocyte quality: From single biochemical markers to metabolomics. Reprod Biol Endocrinol. 2009; 7: 40.
15. Mobarakeh ZT, Ai J, Yazdani F, Sorkhabadi SM, Ghanbari Z, Javidan AN, et al. Human endometrial stem cells as a new source for programming to neural cells. Cell Biol Int Rep (2010). 2012; 19(1): e00015.
16. Bayat N, Ebrahimi-Barough S, Ardakan MM, Ai A, Kamyab A, Babaloo H, et al. Differentiation of human endometrial stem cells into schwann cells in fibrin hydrogel as 3d culture. Mol Neurobiol. 2016; 53(10): 7170-7176.
17. Miravet-Valenciano JA, Rincon-Bertolin A, Vilella F, Simon C. Understanding and improving endometrial receptivity. Curr Opin Obstet Gynecol. 2015; 27(3): 187-192.
18. Altmäe S, Koel M, Võsa U, Adler P, Suhorutšenko M, Laisk-Podar T, et al. Meta-signature of human endometrial receptivity: a meta-analysis and validation study of transcriptomic biomarkers. Sci Rep. 2017; 7(1): 10077.
19. Blesa D, Ruiz-Alonso M, Simón C. Clinical management of endometrial receptivity. Semin Reprod Med. 2014; 32(5): 410-414.
20. Koot YE, Teklenburg G, Salker MS, Brosens JJ, Macklon NS. Molecular aspects of implantation failure. Biochim Biophys Acta. 2012; 1822(12): 1943-1950.
21. Robertson SA, Sharkey DJ. Seminal fluid and fertility in women. Fertil Steril. 2016; 106(3): 511-519.
22. Chen JC, Johnson BA, Erikson DW, Piltonen TT, Barragan F, Chu S, et al. Seminal plasma induces global transcriptomic changes associated with cell migration, proliferation and viability in endometrial epithelial cells and stromal fibroblasts. Hum Reprod. 2014; 29(6): 1255-1270.
23. Gutsche S, von Wolff M, Strowitzki T, Thaler CJ. Seminal plasma induces mRNA expression of IL-1β, IL-6 and LIF in endometrial epithelial cells in vitro. Mol Hum Reprod. 2003; 9(12): 785-791.
24. Rodriguez-Caro H, Dragovic R, Shen M, Dombi E, Mounce G, Field K, et al. In vitro decidualisation of human endometrial stromal cells is enhanced by seminal fluid extracellular vesicles. J Extracell Vesicles. 2019; 8(1): 1565262.
25. Hashish NM, Badway HS, Abdelmoty HI, Mowafy A, Youssef MA. Does flushing the endometrial cavity with follicular fluid after oocyte retrieval affect pregnancy rates in subfertile women undergoing intracytoplasmic sperm injection? A randomized controlled trial. Eur J Obstet Gynecol Reprod Biol. 2014; 176: 153-1537.
26. Blombäck B, Bark N. Fibrinopeptides and fibrin gel structure. Biophys Chem. 2004; 112(2-3): 147-151.
27. Daftary GS, Troy PJ, Bagot CN, Young SL, Taylor HS. Direct regulation of beta3-integrin subunit gene expression by HOXA10 in endometrial cells. Mol Endocrinol. 2002; 16(3): 571-579.
28. Wang L, Tan YJ, Wang M, Chen YF, Li XY. DNA methylation inhibitor 5-Aza-2′-deoxycytidine modulates endometrial receptivity through upregulating HOXA10 expression. Reprod Sci. 2019; 26(6): 839-846.
29. Daftary GS, Taylor HS. Implantation in the human: the role of HOX genes. Semin Reprod Med. 2000; 18(03): 311-320.
30. Elnaggar A, Farag AH, Gaber ME, Hafeez MA, Ali MS, Atef AM. AlphaVBeta3 Integrin expression within uterine endometrium in unexplained infertility: a prospective cohort study. BMC Womens Health. 2017; 17(1): 90.
31. Salleh N, Giribabu N. Leukemia inhibitory factor: Roles in embryo implantation and in nonhormonal contraception. ScientificWorldJournal. 2014; 2014: 201514.
32. Shokrzadeh N, Alivand MR, Abedelahi A, Hessam Shariati MB, Niknafs B. Calcitonin administration improves endometrial receptivity via regulation of LIF, Muc-1 and microRNA Let-7a in mice. J Cell Physiol. 2019; 234(8): 12989-13000.
33. Gremlich S, Chanson A, Urner F, Senn A, Reymondin D, Damnon F, et al. LIF and sIL-2R plasma concentrations in IVF patients on the day of embryo transfer: predictive markers of IVF outcome. J Reprod Immunol. 2012; 94(2): 175-182.
34. de los Santos MJ, García-Láez V, Beltrán-Torregrosa D, Horcajadas JA, Martínez-Conejero JA, Esteban FJ, et al. Hormonal and molecular characterization of follicular fluid, cumulus cells and oocytes from pre-ovulatory follicles in stimulated and unstimulated cycles. Hum Reprod. 2012; 27(6): 1596-1605.
35. Taylor HS, Igarashi P, Olive DL, Arici A. Sex steroids mediate HOXA11 expression in the human peri-implantation endometrium. J Clin Endocrinol Metab. 1999; 84(3): 1129-1135.
36. Chung TW, Park MJ, Kim HS, Choi HJ, Ha KT. Integrin αvβ3 and αvβ5 are required for leukemia inhibitory factor-mediated the adhesion of trophoblast cells to the endometrial cells. Biochem Biophys Res Commun. 2016; 469(4): 936-940.
37. Rosario GX, Stewart CL. The multifaceted actions of leukaemia inhibitory factor in mediating uterine receptivity and embryo implantation. Am J Reprod Immunol. 2016; 75(3): 246-255.
38. Chicea R, Ispasoiu F, Focsa M. Seminal plasma insemination during ovum-pickup--a method to increase pregnancy rate in IVF/ICSI procedure. A pilot randomized trial. J Assist Reprod Genet. 2013; 30(4): 569-574.
39. Saccone G, Di Spiezio Sardo A, Ciardulli A, Caissutti C, Spinelli M, Surbek D, et al. Effectiveness of seminal plasma in in vitro fertilisation treatment: a systematic review and meta-analysis. BJOG. 2019; 126(2): 220-225.
40. Robertson SA. Seminal plasma and male factor signalling in the female reproductive tract. Cell Tissue Res. 2005; 322(1): 43-52.

Original Article

Preimplantation Genetic Screening and The Success Rate of *In Vitro* Fertilization: A Three-Years Study on Iranian Population

Mehdi Totonchi, Ph.D.[1, 2#], Babak Babaabasi, M.Sc.[1#], Hadi Najafi, M.Sc.[1, 3], Mojtaba Rezazadeh Valojerdi, Ph.D.[4], Poopak Eftekhari-Yazdi, Ph.D.[4], Lila Karimian, M.Sc.[4], Navid Almadani, M.D.[1], Anahita Mohseni Meybodi, Ph.D.[1], Morteza Kimiai, M.Sc.[1], Mehri Mashayekhi, M.D.[5], Tahereh Madani, M.D.[5], Hamid Gourabi, Ph.D.[1, 2*]

1. Department of Genetics, Reproductive Biomedicine Research Center, Royan Institute for Reproductive Biomedicine, ACECR, Tehran, Iran
2. Department of Stem Cells and Developmental Biology, Cell Science Research Center, Royan Institute for Stem Cell Biology and Technology, ACECR, Tehran, Iran
3. Departments of Genetics, Faculty of Biological Sciences, Tarbiat Modares University, Tehran, Iran
4. Department of Embryology, Reproductive Biomedicine Research Center, Royan Institute for Reproductive Biomedicine, ACECR, Tehran, Iran
5. Department of Endocrinology and Female Infertility, Reproductive Biomedicine Research Center, Royan Institute for Reproductive Biomedicine, ACECR, Tehran, Iran

#The first two authors equally contributed to this work.

Corresponding Address: P.O.Box: 16635-148, Department of Genetics, Reproductive Biomedicine Research Center, Royan Institute for Reproductive Biomedicine, ACECR, Tehran, Iran
Email: gourabi@royaninstitute.org

Received: 24/February/2019, Accepted: 21/July/2019

Abstract

Objective: *In vitro* fertilization (IVF) is one of the most efficient approaches within the context of assisted reproductive technology (ART) to treat infertility. High pregnancy rates have become the major index of successful IVF in clinical studies. It is not clear yet which factors are certainly responsible for IVF success, as various outcomes were obtained in different IVF centers with different settings. In this study, we aimed to address controversies in the interpretation of promising results of IVF with respect to preimplantation genetic screening (PGS).

Materials and Methods: In this retrospective case series study, we built a dataset containing data from 213 IVF patient candidates for PGS (654 embryos) with blastomere biopsy at day 3 and trophectoderm biopsy in day 5, referred to Royan Institute, Tehran, Iran from 2015 to 2018. Next, the data were analyzed to find influential factors affecting success rate of ART cycles.

Results: Data analyses showed that regardless of PGS indications (ART failures, recurrent miscarriage, chromosomal abnormalities, etc.), the pregnancy rate is influenced by maternal and embryonic factors such as the age of mother as well as quantity and quality of transferred embryos. Furthermore, genotyping of embryos using array comparative genomic hybridization (aCGH) depicted the highest rate of chromosomal aberrations for chromosomes 1, 16 and 19 while the lowest frequency for chromosomes 11 and 17. Similarly, we detected 463 genetically abnormal embryos by aCGH, among which only 41.9% could be detected by classical fluorescent in situ hybridization (FISH) method.

Conclusion: This study not only highlighted the advantages of aCGH over the FISH method in detection of chromosomal abnormalities, but also emphasized the importance of genetic abnormality as an indication for determination of IVF success rate.

Keywords: Array Comparative Genomic Hybridization, Assisted Reproductive Technology, *In Vitro* Fertilization, Preimplantation Genetic Screening

Cell Journal(Yakhteh), Vol 22, No 4, January-March (Winter) 2021, Pages: 467-475

Citation: **Totonchi M, Babaabasi B, Najafi H, Rezazadeh Valojerdi M, Eftekhari-yazdi P, Karimian L, Almadani N, Mohseni Meybodi A, Kimiai M, Mashayekhi M, Madani T, Gourabi H. Preimplantation genetic Screening and the Success rate of in vitro fertilization: a three-years study on Iranian population. Cell J. 2021; 22(4): 467-475. doi: 10.22074/cellj.2021.6784.**

Introduction

Higher pregnancy rate following application of assisted reproduction technology (ART) is probably the main aim of almost all *in vitro* fertilization (IVF) centers. Recent surveys have estimated an average success rate of ~30% for ART, around the world (1, 2). One approach toward higher pregnancy rate is to recognize factors that influence IVF procedure, although it is still a matter of debate (3, 4). In addition to the type of IVF settings, genetic background (such as aneuploidy) of the transferred embryos can potentially affect pregnancy success rate (5). In fact, chromosomal abnormalities of embryo, as the form of either numerical or structural, may possibly cause recurrent ART failure, meaning failure of pregnancy from two or three times good quality embryo transfer (6). Therefore, chromosomal abnormalities need to be considered as an important factor which is responsible for the fate of ART-produced embryo (7). These abnormalities can be "inherited" from a parent (such as translocation) or be "de novo" (new to the embryos) (8). Unlike the inherited chromosomal abnormalities, de novo chromosomal abnormalities may occur during IVF procedure (9) and unexpectedly cause failure of ART (10). Therefore, in addition to the procedures of analyzing

the parents' genotype, introducing an optimal procedure for detection of chromosomal abnormalities of transferred embryos is of great importance (11).

Preimplantation genetic screening (PGS) could be regarded as a risk assessment step for identification of numerical and structural chromosomal abnormalities to ensure genomic integrity of the embryo (2). Some studies explained the benefit of fluorescence in situ hybridization (FISH) (12), oligo-arrays, single nucleotide polymorphism (SNP)-arrays (13), quantitative polymerase chain reaction (qPCR) (12) and bacterial artificial chromosome (BAC)-array for PGS (14). Nevertheless, they are not able to make distinct and comprehensive analyses of the human genome (15). Accordingly, array comparative genomic hybridization (aCGH) was introduced as a reliable and accessible diagnostic approach to assess 24-chromosomal abnormalities in humans (16).

We designed a retrospective case series study to investigate the effect of PGS on IVF outcome as well as the influence of environmental and genetic factors responsible for pregnancy success rate.

Materials and Methods

Study design

The retrospective case series study was conducted among the patients who referred to the Royan Institute Infertility Clinic (Tehran, Iran) as IVF candidates from 2015 to 2018. Overall, 213 individuals were chosen based on the history of previous ART treatment cycles and genetic background for aCGH analysis.

Ovarian stimulation and oocyte retrieval were performed by a standard protocol (i.e. long luteal-phase pituitary down-regulation). Briefly, the patients were prescribed to start injection of 0.5 mg/day buserelin SC (Superfact, Aventis, Germany) in the luteal phase of menstrual cycle. After confirmation of hypothalamic-pituitary-ovarian (HPO) axis suppression (the serum E2 levels of less than 50 pg/ml, no ovarian cyst on transvaginal ultrasound examination and thin endometrium) buserelin dosage was reduced from 0.5 mg/day to 0.25 mg/day and it was sustained until administration of human chorionic gonadotropin (hCG) (for puncture triggering). The controlled ovarian hyperstimulation (COH) was commenced with administration of recombinant follicle-stimulating hormone (FSH, Gonal F, Serono, Switzerland) or human menopausal gonadotropin (HMG, Menogon, Ferring Pharmaceuticals, Germany) 150 IU/day on the second day of menstrual cycle. Serial ultrasound monitoring and measuring serum E2 levels for evaluation of ovarian response and adjusting gonadotropin dosage is required. With reaching three follicles diameter to 18 mm, 10,000 IU of recombinant hCG (Pregnyl, Organon, Netherlands) was administered. Oocyte retrieval, by the transvaginal ultrasound guided approach, was performed 34-36 hours after hCG injection.

Oocytes were classified according to their capability for being IVF recipient. As soon as reaching the thickness of uterus to 8 mm with three-line pattern, the patient was treated with progesterone and the treatment was terminated in the case of no pregnancy. Otherwise, the patient continued progesterone treatment during gestation according to Gyenocologist recommendation.

Afterward, all patients were followed-up after PGS and embryo transfer. Ethical approval was obtained from Royan institute to use patients' data (Ethical code: EC/1393/1082). Variables such as age, history of previous ART failure, recurrent miscarriage (RM), biopsy method, total number of transferred embryos, the day of embryo transfer, embryo quality, infertility etiologies and chromosomal abnormalities of parents were analyzed. Total number of transferred embryos included those for which genotype was performed by aCGH and the others which had good post-IVF quality but had clearly ascertained genotype. Possible IVF confounding factors that may influence the IVF efficiency were also assessed and accurately categorized data were collected.

Karyotyping

Karyotype analysis for parents was performed on trypsin-banded metaphase chromosomes according to the modifications of Verma and Babu (17). The analysis was performed by a standard protocol to generate a resolution of 550 bands per haploid set, from a single cell of the corresponding parents (18). Normally, 30 random metaphase spreads per sample were targeted. In karyotyping, the result was reported based on the latest International System for Human Cytogenetic Nomenclature (ISCN) (19).

Sperm preparation

Semen collection was performed mostly by masturbation. For the intracytoplasmic sperm injection (ICSI) procedure, spermatozoa were prepared by the standard swim-up assay. In final sperm suspension, 10% Albuminar-5 (containing 5% human serum albumin, Blood Research Center, Iran) was added to Ham's-F10 culture medium (Sigma-Aldrich, USA). The prepared spermatozoa were incubated at 37˚C and 6% CO_2 until the usage.

Oocyte and embryo culture

The oocyte-cumulus masses were collected in a drop of Ham's F-10 medium, supplemented with 10% Albuminar-5. Then, the cells were washed in the G-1™ver 3 (Vitrolife, Sweden) supplemented with 10% recombinant serum albumin (rHA, Vitrolife, Sweden). In the next step, they were transferred into a 20 µl fresh G-1™ver 3 medium and kept under mineral oil in the culture dish. The oocytes were then inseminated with 50,000 spermatozoa/ml and incubated at 37˚C, 6% CO_2 for overnight.

To proceed fertilization, we used ICSI technique. The oocytes were immersed in the HEPES (Sigma-Aldrich, USA) Ham's F-10 medium, supplemented with 10% Albuminar-5 and washed in the G-1™ver 3 supplemented with 10% rHA. Then, they were transferred into a 5 µl fresh G-1™ver 3 medium, kept under mineral oil *in vitro*. The embryos were maintained in G-1™ver 3 medium for three days and they were transferred into G2 (G-2™ver 3, Vitrolife, Sweden) from day-3 to day-5. On average, 18 hours post-insemination, the occurrence of fertilization was confirmed. Then, the successfully fertilized oocytes were individually kept in 50 µl drops of embryo culture medium (G.1.2, Vitrolife, Sweden) surrounded by paraffin oil (Sigma-Aldrich, USA) for a maximum period of six days.

Embryo evaluation

The cleavage-stage was evaluated on day-3, as previously described by Gardner and Balaban (20). The quality of embryo was scored based on Veeck's published criteria (21).

Additionally, the quality of embryos was determined according to their appearance characteristics such as shape, size, cell number and integrity of zona pellucida (18). At the time of biopsy, on day-3 post-insemination, the embryos were graded from the highest to lowest quality, A to D, respectively. At the time of transfer, on day-5 post-insemination, embryos were categorized in the following groups: "excellent" (blastocyst, expand blastocyst and hatching blastocyst), "good" (for morula, early and mid-blastocyst) and "poor" (for the other stages). Embryos with spurious appearance were categorized as "not determined (N.D.)".

Clinical pregnancy was confirmed when an intrauterine fetal pole with a positive fetal heartbeat was observed.

Embryo biopsy

Cleavage-stage biopsy

Eight cells embryos with less than 30% fragmentation at 66 ± 2 hours post-ICSI were considered suitable for biopsy. Less than five cells embryos with more than 30% fragmentation were discarded. Zona opening was performed by laser beam (22, 23) and single blastomere was biopsied.

Trophectoderm biopsy

Zona of day-3 embryos was initially drilled by laser beam. Primary criteria for the embryo selection was the same as described for Cleavage-stage biopsy. The embryo culture continued and those developing to the blastocyst stage were biopsied using laser technology as previously described (22, 24). Only well-defined inner cell mass blastocysts with hatching trophectoderm were biopsied. Three to eight trophectoderm cells were biopsied.

After biopsy, the embryos were washed in 1X phosphate buffered saline (PBS, Gibco, USA) and they were transferred to digestion buffer with minimum PBS for further genetic analysis. The lysis and Whole Genome Amplification step was performed by SurePlex®DNA Amplification System (Illumina, USA).

Array comparative genomic hybridization

aCGH enabled us to accurately detect copy number variations in each individual cell removed from blastomeres or trophoblasts. In order to perform this cytogenetic technique, the 24sure Microarray Pack version 3.0 (Illumina, USA) was applied according to the manufacturer's protocol. The array data was read by InnoScan 900 microarray scanner (INNOPSYS, France). The BlueFuse Multi v3.1 (Illumina, USA) was used to analyze the 24sure experiments. We reported the median $\log_2$ ratio for each chromosome as the index of aneuploidy was analyzed by BlueFuse Multi software.

Statistical analyses

Chi-square test was used for comparison of the study groups. In all statistical analyses, a $P<0.05$ was considered statistically significant. Graph plotting and data analysis were done using GraphPad software (version 6) and Microsoft Excel (version 2013). Pearson correlation coefficient (R^2) was performed using GraphPad Prism software (version 6) to analyze correlations between the studied variables.

Results

Indications for preimplantation genetic screening

Indications for PGS such as recurrent miscarriage (RM), ART failure and parental chromosomal aberration, might perhaps justify why PGS was applied following IVF. In this study, patients who had a history of RM, previous ART failures and chromosomal abnormalities were subjected to PGS. Patients with other heterogeneous features (such as mosaicism, advanced maternal age, unexplained infertility, etc.) that were grouped as "others" also underwent PGS. The frequency and percentage of each group are presented as a pie chart. This data shows that most of the patients (80.7%) were subjected to PGS due to ART failure and RM, while patients with chromosomal abnormalities and other features comprised 8.4% and 10% of the total PGS candidates, respectively (Fig.1A).

For a series of 213 cycles, a total of 147 (69%) embryo transfers (ET) were carried out, which resulted in 34.69% and 23.94% of pregnancy rates per ETs and cycles, respectively (Fig.1B). Pregnancy rate between ART failure and RM groups did not show statistically significant difference (Fig.1C).

In addition, clinical pregnancy rates were increased in younger (≤ 35 years old) women (40% versus 29.03% for ART failure, and 40% versus 13.33% for RM groups, Fig.1D, bright bars). Similarly, pregnancies per cycles

showed the same pattern in both ART failure and RM groups (Fig.1D, dark bars). Nevertheless, a significant decline was observed in pregnancy rate among the women with >35 years old who also had RM (Fig.1D).

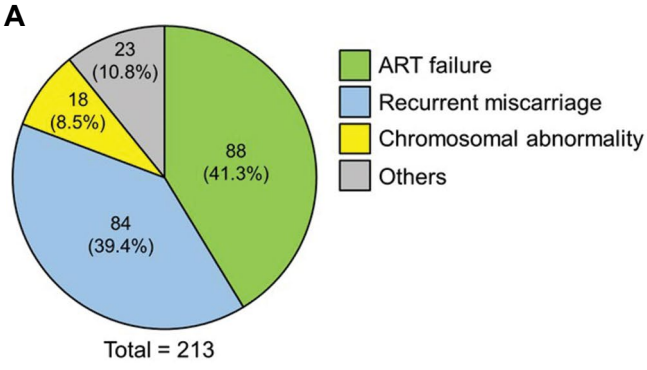

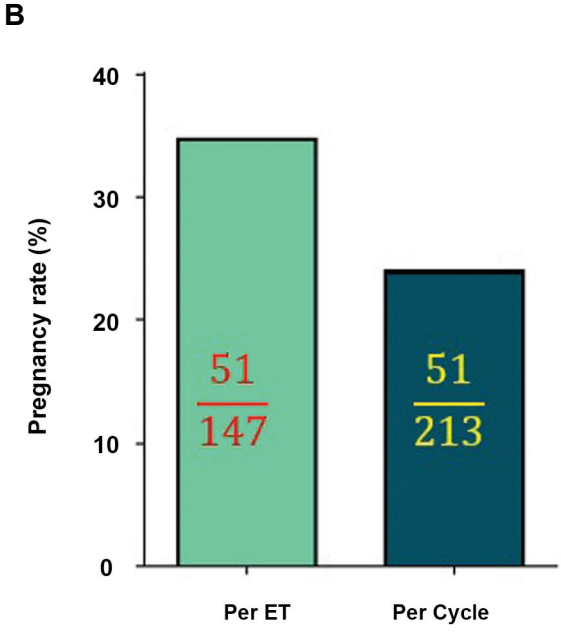

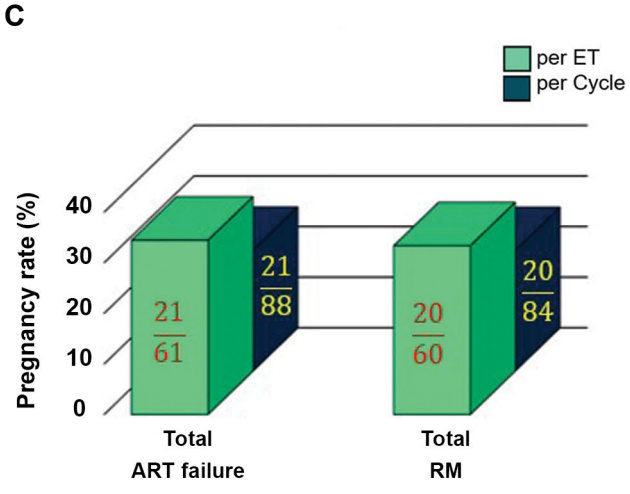

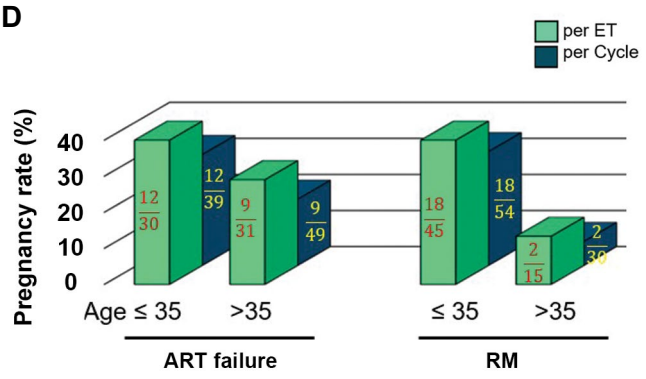

Fig.1: Indications of PGS in IVF patients referred to Royan Institute and its influence on the pregnancy rate. **A.** 213 patients were chosen to undergo PGS by aCGH for several reasons including ART failure (41.3%), recurrent miscarriage (RM, 39.4%) and chromosomal abnormality of parents (8.5%). Some patients who had heterogeneous characteristics (such as advanced age and unexplained infertility) were classified as "others" comprising 10.8% of the population. **B.** Regardless of the indications of PGS, pregnancy success rate was calculated for IVF and reported as pregnancy rate per ET and cycle. **C.** Pregnancy rate (per ET and cycle) for patients with ART failure and RM. **D.** Evaluating the effect of age on IVF success rate, presented as pregnancy rate per ET and cycle for ART failure and RM groups. PGS; Preimplantation genetic screening, IVF; *In vitro* fertilization, aCGH; Array comparative genomic hybridization, ART; Assisted reproductive technology, and ET; Embryo transfer. Patients are categorized by their ages: Ages>35 years ≤35.

The effects of embryo transfers number and fresh/frozen embryos on pregnancy rate

Among 213 patients, 147 subjects had at least one healthy embryo (as confirmed by aCGH) undergoing ET. Patients with only one genetically normal transferred embryo (one-ET group) had a pregnancy rate of 23.91% (22 out of 92 patients), while patients with two ETs showed a significantly higher level of pregnancy rate (52.72%, 29 out of 55 patients, Fig.2A). This increase in the pregnancy rate for two ETs was also observed in both ART failure and RM groups (Fig.2B).

In order to investigate the influence of fresh or frozen embryos on ART success, the pregnancy rates were calculated for these groups. Results showed the same pregnancy rates per-ET/per-cycle in fresh and frozen embryos (Fig.2C). Figure 2 shows the number of patients (cycles) or ETs, together with positive pregnancy.

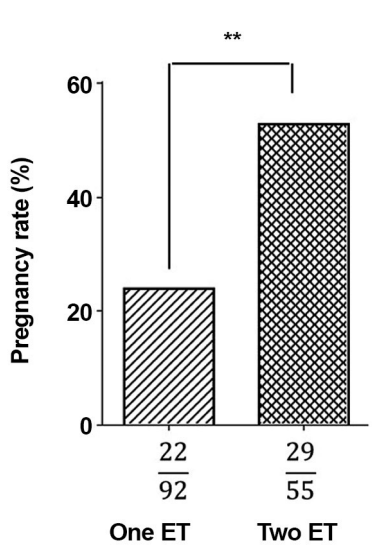

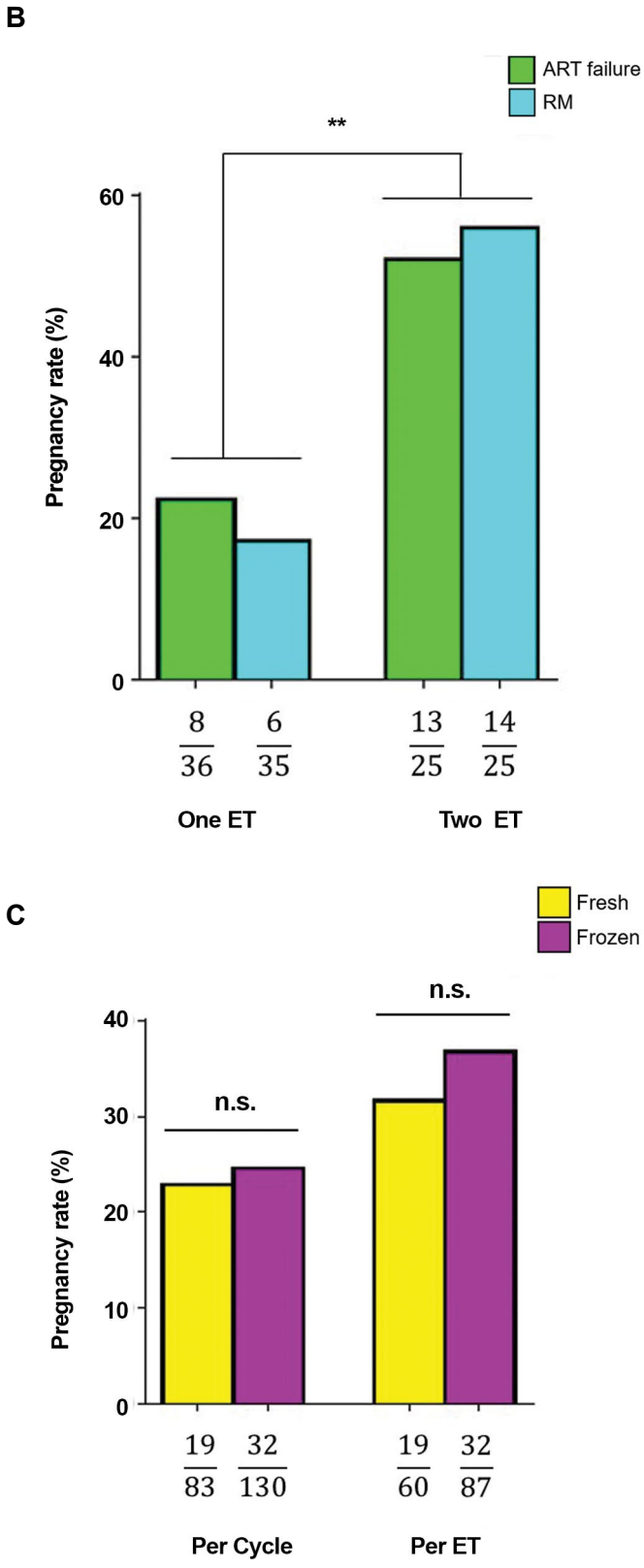

Fig.2: Effect of the number of genetically normal transferred embryos and pregnancy success rate. **A.** Pregnancy rate results were achieved under two conditions: One ET and two ETs. **B.** Pregnancy rate of one ET compared to that of two ETs, separately, for ART failure and RM groups. **C.** Effect of freezing on pregnancy rate was evaluated for the both conditions (one ET and two ETs). Data showed no significant difference in pregnancy rates between fresh and frozen embryos.
ET; Embryo transfer, ART; Assisted reproductive technology, and RM; Recurrent miscarriage.
n.s; Not significant, *; P<0.05, **; P<0.01, and ***; P<0.001.

Analyses of chromosomal abnormality rate in embryos undergoing *in vitro* fertilization

Chromosomal aberration is an inevitable problem during IVF procedure. Therefore, we exploited the advantages of aCGH strategy to explore frequency and type of chromosomal abnormalities occurring during IVF. Analysis of aCGH results showed that the most frequent abnormalities were found in chromosomes 1, 16 and 19 in both ART failure and RM groups. Conversely, chromosomes 17 had the lowest abnormality rates in the two groups (Fig.3A). As it is deduced from Figure 3A, the abnormality rate in both ART failure and RM groups presented a similar pattern. Consistently, a significant positive correlation (R^2=0.51, P<0.0001) was observed between chromosomal abnormality rates with ART failure (x-axis) and RM (y-axis) groups (Fig.3B). The chromosomes 13, 18, 21, 22 and X (numbers surrounded by circles) are the common ones in PGS using the conventional FISH technique.

In order to compare capability of aCGH and FISH methods to detect different types of such chromosomal abnormalities (i.e. whole chromosome insertion/deletion and partial insertion/deletion), the number of embryos containing chromosomal abnormalities commonly testes by FISH technique (13, 18, 21, 22 and X) were calculated. Our data showed from 463 abnormal embryos detected by aCGH, only 194 embryos could likely be detected by conventional FISH technique (Fig.3C). The rate of partial or complete chromosomal abnormality per abnormal embryos was 2.02 (938 abnormal chromosomes in 463 abnormal embryos).

The effect of embryo quality and biopsy methods on *in vitro* fertilization success

In addition to the aforementioned factors, other important variables, such as transferred embryos' quality, may influence the IVF success rate. Thus, all of the tested and transferred embryos were scored based on their quality from "A" to "D" (for the biopsy day) and "poor, good and excellent" (for the transferring day). These scores alongside with IVF assessment results were recorded. The recorded data showed that there is no relationship between the IVF outcome and quality of embryo on the biopsy day (Fig.4A), suggesting that probably grading at the time of biopsy cannot be regarded as a proper measurement to predict IVF outcome. However, assessment at the time of embryo transfer showed a positive relationship between the embryo quality and IVF success (Fig.4B), indicating that embryo grading at this time point is a better determinant for IVF success than scoring on the biopsy day.

In order to investigate influence of the biopsy day (day-3 vs. day-5 of post-insemination) on IVF outcome, pregnancy rate was assessed. The results indicated no significant difference in pregnancy rates between day-3 (23.23%) and day-5 of biopsies (26.67%, Fig.4C).

At both scoring time points, it was difficult to assign a certain quality grade for some embryos with unnatural or unknown phenotypes; therefore, we categorized them as "others" or "not determined" (N.D., Fig.4A, B). However, a pregnancy rate of <10% was observed for these groups. Taken together, these data imply that transferring embryos with higher quality would increase the chance of successful pregnancy.

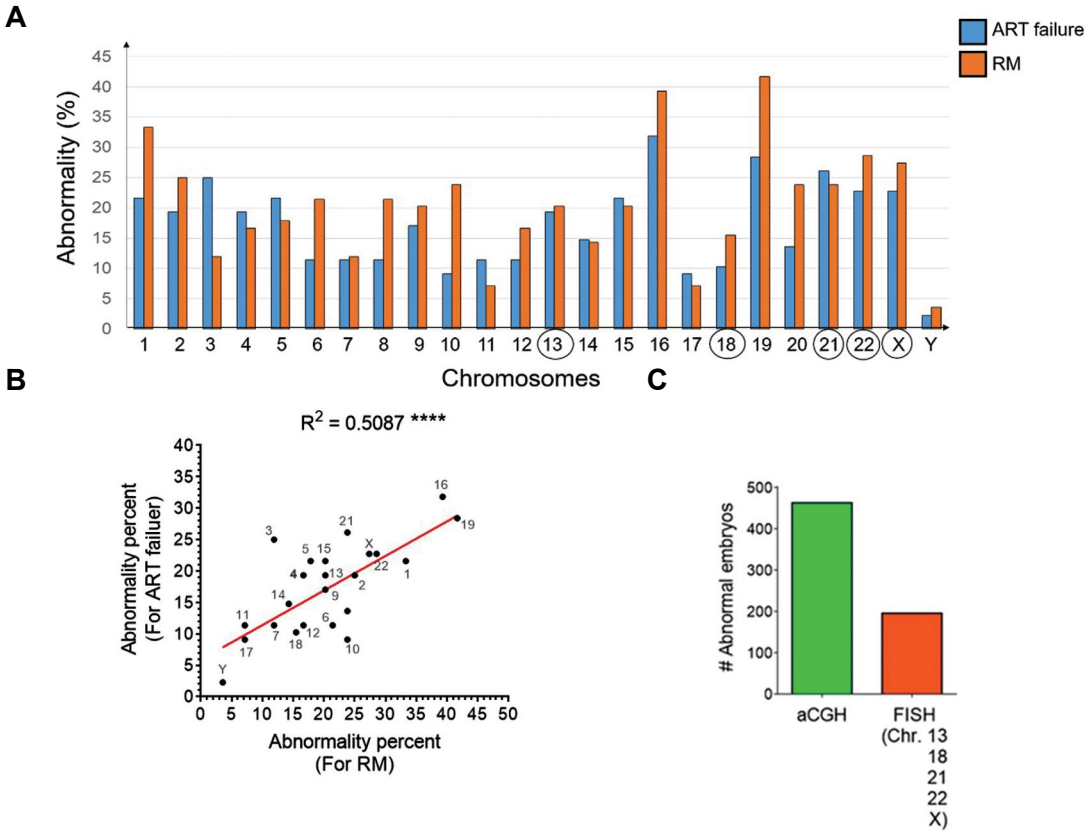

Fig.3: Frequency of chromosomal abnormalities in IVF procedures in addition to efficacies of aCGH and FISH for detection of such abnormalities. **A.** While aCGH surveys the whole genome (24 chromosomes) to detect abnormalities, conventional FISH uses probes that are often specific to chromosomes 13, 18, 21, 22 and X (encircled numbers). Here, aCGH data showed the highest abnormality rate for chromosomes 1, 16 and 19, while the lowest one was found for chromosomes 11 and 17. Chromosomal abnormalities in ART failure and RM groups are presented as blue and orange bars. **B.** Significantly positive correlation between chromosomal abnormality rate in ART failure and RM groups. Each chromosome is shown as a point and abnormality rate of each chromosome for ART failure and RM groups are represented as Y and X axes, respectively. **C.** Comparison of abnormalities, detected by aCGH versus those found by FISH method.
IVF; *In vitro* fertilization, aCGH; Array comparative genomic hybridization, FISH; Fluorescence in situ hybridization, ART; Assisted reproductive technology, and RM; Recurrent miscarriage.

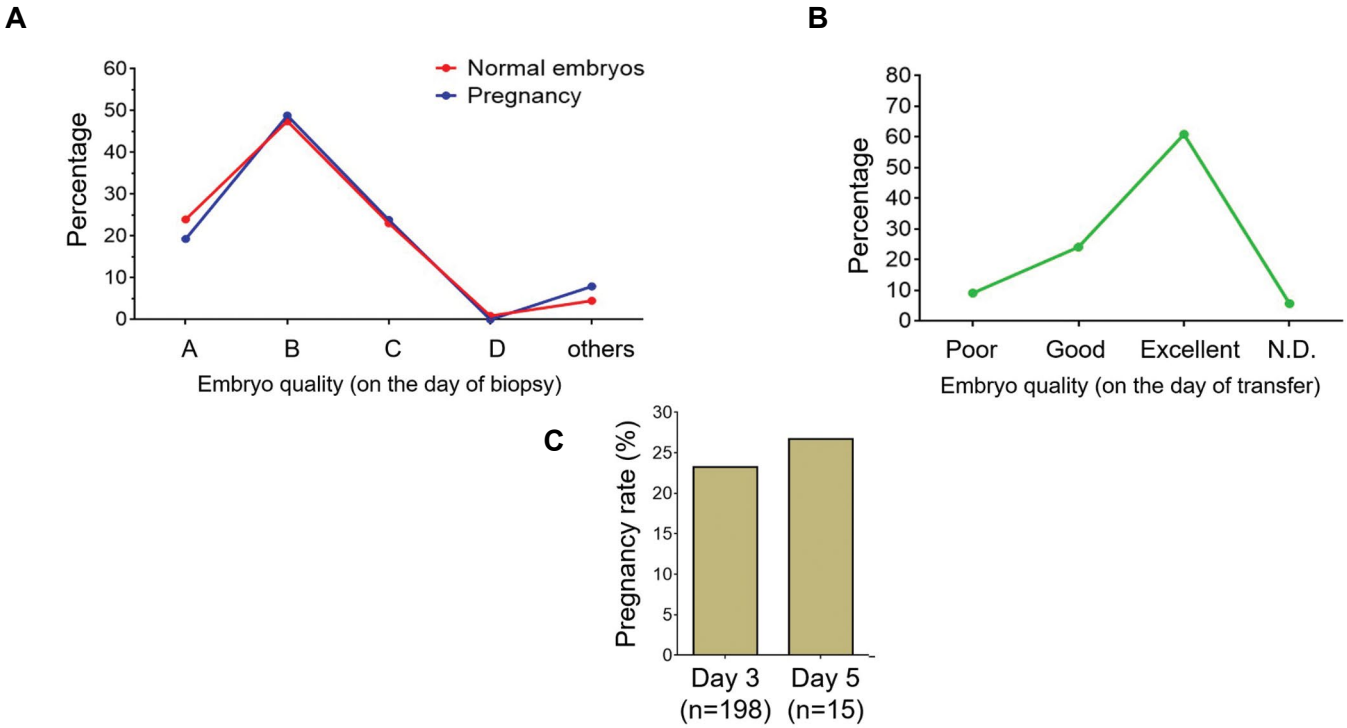

Fig.4: Relationship between the quality of embryos and pregnancy. **A.** Quality of embryos determined on the biopsy days and their relation to the number of normal embryos (red line) and pregnancies (blue line). **B.** Relationship between quality of embryos at the time of transfer and pregnancy frequency (presented in number). **C.** Comparison between the biopsy day (3 or 5) and the rate of pregnancy per embryo transfer (ET).

Discussion

Based on the results of studied cohorts, recognition of the factors that influence the outcome of IVF would benefit clinicians to achieve higher pregnancy rates. Effects of different factors that may influence IVF success rate (mostly referred as clinical pregnancy rate) were investigated in the previous studies (1-4, 25-28). However, since different IVF centers use different approaches, the influence of these factors may vary among different IVF centers. Thus, these variables should be normalized based on various circumstances that exist in different IVF centers.

This retrospective case series study was designed not only to evaluate the factors affecting IVF outcomes, but also to assess the genetic basis of this issue in our IVF center at Royan Institute, Tehran, Iran. Between the years 2015 and 2018, 8650 patients referred to our clinic. Among these patients, only 213 individuals were selected to undergo PGS using the aCGH method, according to the recommendation of the genetic counselor of the center and the final decision of the board of clinicians. Earlier studies concluded that clinical pregnancy rate is generally accepted as the main outcome of IVF (29, 30).

Since PGS candidates had different criteria when referring to PGS laboratory, we were interested in the evaluating relationship of the aforementioned indications with pregnancy rates. Data of this study showed no significant difference between pregnancy rate of the patients with the history of ART failure and RM. Noteworthy, pregnancy rate tended to become lower in aged women, which is consistent with the results reported by previous studies concerning the effect of age on pregnancy rates (25, 31, 32). It was also shown while the pregnancy rate is similar among younger women (≤35 years old) in each category, pregnancy rate differs among older women (>35 years old). Importantly, half of the ≥35 years old women with RM had no normal embryo and the rest showed significantly lower pregnancy rate per transfer. This outcome would suggest that PGS-IVF procedure for women >35 years old who possibly have a history of RM is not as efficient as younger patients. Previous studies indicated decreased IVF success rates in older women through observation of predominantly increased aneuploidy in oocytes (4, 33). Since we discarded embryos with aneuploidy, the observed decrease in pregnancy rate for women of > 35 years old, may be due to the presence of other factors such as lower endometrial receptivity (34).

Apart from age, the number of transferred embryos potentially affects the pregnancy rate (25). We found that patients with two transferred embryos, had higher pregnancy rates (2.2 folds), and the increased pregnancy rate were observed in both ART failure and RM groups. These results are in agreement with previous studies which examined the influence of transferred embryo number and pregnancy rate (35).

Aside from the effect of transferred embryo quantity, there was no significant difference in pregnancy rate between fresh and frozen embryos; however, an insignificant slight increase in pregnancy rate was observed following the use of frozen ones. On the other hand, the other studies provided evidence which is not consistent with our findings, as they reported higher pregnancy rate following the utilization of frozen embryos (36). This inconsistency may be due to the adverse effects of ovarian hyperstimulation and its effects on endometrial receptivity (37, 38). Insignificant increases in pregnancy rate observed for frozen embryos in this study, would suggest that IVF outcome for frozen or fresh embryos presumably depends on different factors, such as freezing and thawing procedures and more importantly the condition of patient endometrium. In addition, the PGS candidates were selected based on having a history of ART failure, RM and chromosomal aberration; thus, other factors may simultaneously have an influence on the result of frozen embryo transfer. Therefore, there would be a controversy between our data and previous reports regarding better pregnancy results of frozen embryo transfer (36).

Another determinant for successful IVF is the embryo quality which can be assessed by genotype and phenotype analyses. In this experiment, 654 embryos from all studied patients (213 subjects) were genotyped using aCGH. Results showed that excluding 191 embryos with a chaotic and noisy outcome, 463 embryos had interpretable and meaningful genotyping data. Out of 463 embryos, 195 had abnormalities in chromosomes 13, 18, 21, 22 and X which potentially would be detected by conventional FISH. This data definitely introduces aCGH as a powerful method (rather than FISH) to screen embryos prior transfer process. Our data suggest that quality assessment of the embryos based on both phenotype and genotype can be a good parameter helping us to select a good embryo for IVF. However, there may be some cases in which good morphology of embryos do not harbor favorable genotypes, suggesting necessity of the aCGH method after quality assessment of the embryos (4, 39). In addition, while aCGH cannot detect polyploidies (e.g. triploidy and tetraploidy) and balanced chromosomal rearrangements (e.g. translocations), using complementary tests such as karyotyping and next generation sequencing (NGS) would be useful; nevertheless, they are expensive and time consuming (40).

Data obtained from aCGH also revealed that chromosomes 19, 16 and 1 were frequently aberrant during IVF treatment, while they could not be detected by routinely applied FISH probes for PGS.

Supportive evidence for similar chromosomal abnormality rates in both ART failure and RM groups was also shown by the existence of a significantly positive correlation between chromosomal abnormality rate of ART failure (X axis) and RM (Y axis).

Phenotypic analyses showed that natural appearance

of the embryo, at the time of transfer, is an important determinant for successful IVF, whereas determination of embryo status at the time of biopsy does not have such a predictive value. This may be due to the altered quality of embryos during their growth between biopsy and transferring time points.

Conclusion

Comprehensive chromosomal screening of IVF embryos in parallel with optimizing other factors (such as controlled ovarian stimulation, embryo culture, endometrial receptivity and etc.) not only can increase the pregnancy success rate, but also reduces patient anxiety regarding the abortion, stillbirth and abnormality in offspring.

Acknowledgements

The authors wish to thank from all those Royan Institute's patients who permitted to use their medical histories in this article. This research granted financially supported by Royan Institute. There is no conflict of interest in this study.

Authors' Contributions

H.G., M.T.; Involved in designing the main idea of the current study, and contributed to perform experimental procedures, and edited the manuscript. B.B., M.K.; Contributed to perform experimental procedures (aCGH) and data gathering. H.N.; Performed statistical analysis and wrote the initial text of the manuscript. M.R.V.,L.K., P.E-Y.; Supervised embryology lab including performing ICSI, embryo culture, biopsy and embryo transfer. N.A.; Genetic counseling during patient selection and interpretation of the demographic data of the patients. A.M.M.; Performed karyotype analysis. M.M., T.M.; Contributed in patient management, ovarian stimulation, oocyte retrieval and embryo transfer. All authors approved the final version of manuscript.

References

1. Dahdouh EM, Balayla J, Garcia-Velasco JA. Impact of blastocyst biopsy and comprehensive chromosome screening technology on preimplantation genetic screening: a systematic review of randomized controlled trials. Reprod Biomed Online. 2015; 30(3): 281-289.
2. Tiegs AW, Hodes-Wertz B, McCulloh DH, Munne S, Grifo JA. Discrepant diagnosis rate of array comparative genomic hybridization in thawed euploid blastocysts. J Assist Reprod Genet. 2016; 33(7): 893-897.
3. van Loendersloot LL, van Wely M, Limpens J, Bossuyt PM, Repping S, van der Veen F. Predictive factors in in vitro fertilization (IVF): a systematic review and meta-analysis. Hum Reprod Update. 2010; 16(6): 577-589.
4. Mateo S, Vidal F, Parriego M, Rodriguez I, Montalvo V, Veiga A, et al. Could monopronucleated ICSI zygotes be considered for transfer? Analysis through time-lapse monitoring and PGS. J Assist Reprod Genet. 2017; 34(7): 905-911.
5. Maxwell SM, Colls P, Hodes-Wertz B, McCulloh DH, McCaffrey C, Wells D, et al. Why do euploid embryos miscarry? A case-control study comparing the rate of aneuploidy within presumed euploid embryos that resulted in miscarriage or live birth using next-generation sequencing. Fertil Steril. 2016; 106(6): 1414-1419. e5.
6. Rubio C, Simón C, Vidal F, Rodrigo L, Pehlivan T, Remohí J, et al. Chromosomal abnormalities and embryo development in recurrent miscarriage couples. Hum Reprod. 2003; 18(1): 182-188.
7. Mastenbroek S, Twisk M, van Echten-Arends J, Sikkema-Raddatz B, Korevaar JC, Verhoeve HR, et al. In vitro fertilization with preimplantation genetic screening. N Engl J Med. 2007; 357(1): 9-17.
8. Du L, Brezina PR, Benner AT, Swelstad BB, Gunn M, Kearns WG. The rate of de novo and inherited aneuploidy as determined by 23-chromosome single nucleotide polymorphism microarray (SNP) in embryos generated from parents with known chromosomal translocations. Fertil Steril. 2011; 96(Suppl 3): S221.
9. Vanneste E, Voet T, Le Caignec C, Ampe M, Konings P, Melotte C, et al. Chromosome instability is common in human cleavage-stage embryos. Nat Med. 2009; 15(5): 577-583.
10. Lee HL, McCulloh DH, Hodes-Wertz B, Adler A, McCaffrey C, Grifo JA. In vitro fertilization with preimplantation genetic screening improves implantation and live birth in women age 40 through 43. J Assist Reprod Genet. 2015; 32(3): 435-444.
11. Chang LJ, Chen SU, Tsai YY, Hung CC, Fang MY, Su YN, et al. An update of preimplantation genetic diagnosis in gene diseases, chromosomal translocation, and aneuploidy screening. Clin Exp Reprod Med. 2011; 38(3): 126-134.
12. Grifo JA, Ward DC, Boyle A. In situ hybridization of blastomeres from embryo biopsy. In: Verlinsky Y, Kuliev A, editors. Preimplantation Genetics. Switzerland: Springer; 1991; 147-152.
13. Van Uum CM, Stevens SJ, Dreesen JC, Drüsedau M, Smeets HJ, Hollanders-Crombach B, et al. SNP array-based copy number and genotype analyses for preimplantation genetic diagnosis of human unbalanced translocations. Eur J Hum Genet. 2012; 20(9): 938-944.
14. Harper JC, Harton G. The use of arrays in preimplantation genetic diagnosis and screening. Fertil Steril. 2010; 94(4): 1173-1177.
15. Hultén MA, Dhanjal S, Pertl B. Rapid and simple prenatal diagnosis of common chromosome disorders: advantages and disadvantages of the molecular methods FISH and QF-PCR. Reproduction. 2003; 126(3): 279-297.
16. Shinawi M, Cheung SW. The array CGH and its clinical applications. Drug Discov Today. 2008; 13(17-18): 760-770.
17. Verma RS, Babu A. Human chromosomes: manual of basic techniques. McGraw-Hill; 1989.
18. Lundin K, Bergh C, Hardarson T. Early embryo cleavage is a strong indicator of embryo quality in human IVF. Hum Reprod. 2001; 16(12): 2652-2657.
19. McGowan-Jordan J, Simons A, Schmid MI. An international system for human cytogenomic nomenclature (2016) reprint of. Cytogenetic and Genome Research. 2016; 149(1-2).
20. Gardner DK, Balaban B. Assessment of human embryo development using morphological criteria in an era of time-lapse, algorithms and 'OMICS': is looking good still important? Mol Hum Reprod. 2016; 22(10): 704-718.
21. Hsu M-I, Mayer J, Aronshon M, Lanzendorf S, Muasher S, Kolm P, et al. Embryo implantation in in vitro fertilization and intracytoplasmic sperm injection: impact of cleavage status, morphology grade, and number of embryos transferred. Fertil Steril. 1999; 72(4): 679-685.
22. Coll L, Parriego M, Boada M, Devesa M, Arroyo G, Rodriguez I, et al. Transition from blastomere to trophectoderm biopsy: comparing two preimplantation genetic testing for aneuploidies strategies. Zygote. 2018; 26(3): 191-198.
23. Boada M, Carrera M, De La Iglesia C, Sandalinas M, Barri PN, Veiga A. Successful use of a laser for human embryo biopsy in preimplantation genetic diagnosis: report of two cases. J Assist Reprod Genet. 1998; 15(5): 302-307.
24. Veiga A, Sandalinas M, Benkhalifa M, Boada M, Carrera M, Santalo J, et al. Laser blastocyst biopsy for preimplantation diagnosis in the human. Zygote. 1997; 5(4): 351-354.
25. Cetin MT, Kumtepe Y, Kiran H, Seydaoglu G. Factors affecting pregnancy in IVF: age and duration of embryo transfer. Reprod Biomed Online. 2010; 20(3): 380-386.
26. Baker VL, Jones CE, Cometti B, Hoehler F, Salle B, Urbancsek J, et al. Factors affecting success rates in two concurrent clinical IVF trials: an examination of potential explanations for the difference in pregnancy rates between the United States and Europe. Fertil Steril. 2010; 94(4): 1287-1291.
27. Sneed ML, Uhler ML, Grotjan HE, Rapisarda JJ, Lederer KJ, Beltsos AN. Body mass index: impact on IVF success appears age-related. Hum Reprod. 2008; 23(8): 1835-1839.
28. Majumdar G, Majumdar A, Lall M, Verma IC, Upadhyaya KC. Preimplantation genetic screening for all 24 chromosomes by microarray comparative genomic hybridization significantly increases im-

plantation rates and clinical pregnancy rates in patients undergoing in vitro fertilization with poor prognosis. J Hum Reprod Sci. 2016; 9(2): 94-100.
29. Check JH, Wilson C, Choe JK, Amui J, Katsoff B. A comparison of pregnancy rates following fresh and frozen embryo transfer according to the use of leuprolide acetate vs ganirelix vs cetrorelix. Clin Exp Obstet Gynecol. 2010; 37(2): 105-107.
30. Kuivasaari P, Hippeläinen M, Anttila M, Heinonen S. Effect of endometriosis on IVF/ICSI outcome: stage III/IV endometriosis worsens cumulative pregnancy and live-born rates. Hum Reprod. 2005; 20(11): 3130-3135.
31. Preutthipan S, Amso N, Curtis P, Shaw RW. Effect of maternal age on clinical outcome in women undergoing in vitro fertilization and embryo transfer (IVF-ET). J Med Assoc Thai. 1996; 79(6): 347-352.
32. Yesodi V, Yaron Y, Lessing JB, Amit A, Ben-Yosef D. The mitochondrial DNA mutation (ΔmtDNA5286) in human oocytes: correlation with age and IVF outcome. J Assist Reprod Genet. 2002; 19(2): 60-66.
33. Kotdawala A, Patel D, Herrero J, Khajuria R, Mahajan N, Banker M. Aneuploidy screening by array comparative genomic hybridization improves success rates of in vitro fertilization: a multicenter Indian study. J Hum Reprod Sci. 2016; 9(4): 223-229.
34. Tamhankar VA, Liu B, Yan J, Li TC. A comparison of pattern of pregnancy loss in women with infertility undergoing ivf and women with unexplained recurrent miscarriages who conceive spontaneously. Obstet Gynecol Int. 2015; 2015: 989454.
35. Pandian Z, Templeton A, Serour G, Bhattacharya S. Number of embryos for transfer after IVF and ICSI: a Cochrane review. Hum Reprod. 2005; 20(10): 2681-2687.
36. Roque M, Lattes K, Serra S, Solà I, Geber S, Carreras R, et al. Fresh embryo transfer versus frozen embryo transfer in in vitro fertilization cycles: a systematic review and meta-analysis. Fertil Steril. 2013; 99(1): 156-162.
37. Bourgain C, Devroey P. The endometrium in stimulated cycles for IVF. Hum Reprod Update. 2003; 9(6): 515-522.
38. Kolibianakis E, Bourgain C, Albano C, Osmanagaoglu K, Smitz J, Van Steirteghem A, et al. Effect of ovarian stimulation with recombinant follicle-stimulating hormone, gonadotropin releasing hormone antagonists, and human chorionic gonadotropin on endometrial maturation on the day of oocyte pick-up. Fertil Steril. 2002; 78(5): 1025-1029.
39. Fesahat F, Kalantar SM, Sheikhha MH, Saeedi H, Montazeri F, Firouzabadi RD, et al. Developmental and cytogenetic assessments of preimplantation embryos derived from in-vivo or in-vitro matured human oocytes. Eur J Med Genet. 2018; 61(4): 235-241.
40. Griffin DK, Ogur C. Chromosomal analysis in IVF: just how useful is it? Reproduction. 2018; 156(1): F29-F50.

Cytokine Gene Expression Alterations in Human Macrophages Infected by *Leishmania major*

Khodaberdi Kalavi, M.Sc.[1, 2], Ogholniaz Jorjani, Ph.D.[2], Mohammad Ali Faghihi, M.D., Ph.D.[3, 4], Seyed Javad Mowla, Ph.D.[1*]

1. Department of Molecular Genetics, Faculty of Biological Sciences, Tarbiat Modares University, Tehran, Iran
2. Department of Laboratory Sciences, School of Allied Medical Sciences, Golestan University of Medical Sciences, Gorgan, Iran
3. Department of Medical Genetics, Shiraz University of Medical Sciences, Shiraz, Iran
4. Department of Psychiatry and Behavioral Sciences, School of Medicine, University of Miami, FL, USA

Corresponding Address: P.O.Box: 14115/175, Department of Molecular Genetics, Faculty of Biological Sciences, Tarbiat Modares University, Tehran, Iran
Email: sjmowla@modares.ac.ir

Received: 14/April/2019, Accepted: 10/June/2019

Abstract

Objective: Leishmaniasis is caused by members of the *Leishmania* species and constitute a group of infective diseases that range from cutaneous lesions to lethal visceral forms. In infected persons, macrophages recognize and eliminate the parasites via phagocytosis. In order to change a hostile environment into an environment adequate for survival and reproduction, the engulfed Leishmania species needs to modulate the function of its host macrophage. The expression patterns of cytokine genes such as interleukin-12 *(IL-12)*, tumour necrosis factor-alpha *(TNF-α), IL-1*, and interferon-gamma (*IFNγ*) represent the immune response. In this study, we employed an RNA-seq approach for human monocyte-derived macrophages infected with *Leishmania major (L. major)* to decipher cytokine gene expression alterations in host macrophages.

Materials and Methods: In this descriptive study, human monocytes were isolated by magnetic activated cell sorting (MACS) and cultured in the presence of monocyte colony stimulating factor (M-CSF) to obtain the macrophages. Monocyte-derived macrophages were then co-cultured with metacyclic promastigotes of *L. major* for 4 hours. RNA isolation was performed using TRIzol reagent. RNA sequencing was performed using the Illumina sequencing platforms. Gene expression analysis was performed using a Bioconductor DESeq2 package.

Results: Our data revealed significant changes in immune response gene expressions in macrophages infected with L. major, with an up-regulation of cytokines and mostly down-regulation of their receptors.

Conclusion: The obtained data could shed more light on the biology of *L. major* and how the host cell responds to leishmaniasis.

Keywords: Chemokines, Cytokines, *Leishmania major,* Macrophages, RNA Sequencing

Cell Journal(Yakhteh), Vol 22, No 4, January-March (Winter) 2021, Pages: 476-481

Citation: **Kalavi KH, Jorjani O, Faghihi MA, Mowla SJ. Cytokine gene expression alterations in human macrophages infected by leishmania major. Cell J. 2021; 22(4): 476-481. doi: 10.22074/cellj.2021.6524.**

Introduction

Leishmaniasis is a worldwide chronic inflammatory disease caused by *Leishmania* species. Leishmaniasis has cutaneous, mucocutaneous and lethal visceral forms. Macrophages phagocytize pathogens such as *Leishmania* species. However, when inside macrophages, the *Leishmania* species adapt and modulate the host microenvironment for better survival and reproduction. Understanding the means used by these pathogens to alter host defence mechanisms for intracellular survival and reproduction could help to define novel diagnostics and therapeutics for leishmaniosis (1).

The host response to infection is regulated by controlled production of cytokines. In mice and humans, resistance against many pathogens, including *Leishmania* species, is associated with T helper type 1 (Th-1) cell cytokine response that includes interleukin 12 (IL-12) and gamma interferon (IFNγ). Susceptibility to infection is associated with production of the Th-2 cytokines IL-4, IL-5, and IL-10 (1). High-throughput technology has made it possible to define and analyse large sets of genes or proteins that modulate in response to host-pathogen interactions. Recent studies that used techniques such as microarray have generated some data. However, the limitations due to hybridization have recently improved with next generation sequencing (NGS) technology (2). Accordingly, several *in vivo* and *in vitro* models of animal and human host cells have been developed, especially monocyte derived macrophages (MDMs).

Leishmania species alter cytokine production in infected host cells towards the pathogen's benefit. Important altered cytokines include IL-12, TNF-α, IL-1, and IFNɣ. Receptor mediated phagocytosis causes alterations such as suppressed production of IL-12. This cytokine immunologically transduces signals to produce and activate qualified Th-1 cells which, in turn, leads to IFNɣ production and natural killer (NK) cell proliferation and activation as the major source of IFNɣ (3). IFNɣ interacts with the IFNɣ receptor (IFNɣR) expressed on the macrophage surface and leads to pathogen disposal by host immune cells (4). In leishmaniasis, the aforementioned parameters are altered.

There are reports on early shifting of Th-2 cells where cytokines produced by these cells suppress the protective

capacities of the immune system. IL-10, produced by this type of cell, is associated with both decreases in nitric oxide (NO), *IFNɣ*, and *IL-12* gene expressions and inhibition of protein kinase C (PKC) in infected macrophages (5). In this direction, *Leishmania* species induce the regulatory T (Treg) cells to suppress anti-leishmania immune responses in cutaneous and visceral animal models and in human leishmaniasis (6). T-regs generally function as immune preventers against effector Th-1 cells and *Leishmania* parasites use this potential to escape from Th-1 related eradication. T-regs down-regulate Th-1 related macrophage activity by secreting IL-10 and transforming growth factor beta (TGF-β) at the site of infection, resulting in changes that are favourable to the pathogen (7).

Chemokines, another specific type of cytokine, plays a crucial role in the anti-leishmaniasis immune response and are modulated by the parasite (8). Chemokines are small polypeptides that contain cysteine residues within the polypeptide chain (9).

Control of leishmaniasis strongly depends on an IL-12 driven Th-1 cell response and IFNɣ production that, in turn, causes facilitated recruitment of effector cells (macrophages, NK cells, CD4+ and CD8+ cytotoxic cells) to the site of infection (10). The chemokine production strategy is very important as it determines cellular recruitments and communications needed to establish a proper immune response. Chemokines act through binding to chemokine receptors, which leads to a variety of biological functions, such as directed cellular migration (11).

Here, we performed an RNA seq approach study using an Illumina sequencing platform to determine transcriptome changes in macrophages infected with *Leishmania major (L. major)*.

Materials and Methods

Study method

The present study was approved by the Ethics Committee of the Guilan University of Medical Sciences (Guilan, Iran, Ethical code: IR.Goums.1397.293). This was a descriptive study of RNA-seq data on human monocyte-derived macrophages infected with *L. major* to decipher gene expression alterations of the cytokines in host macrophages.

Peripheral blood mononuclear cell preparation

Healthy donors donated blood at the Gorgan Blood Bank. The buffy coat fractions in the whole blood bags were used for separation of peripheral blood mononuclear cells (PBMCs). A 1:1 (v:v) phosphate-buffered saline (PBS) and the buffy coat sample were transferred into 50 ml sterile falcon tubes thatwhich contained an equal amount (v:v) of Ficoll solution (density 1.077 g/mL, Baharafshan, Iran). We obtained the separated PBMCs after 25 minutes of centrifugation at 300 g. The PBMC were then washed three times using a sterile PBS solution and were subdivided into fresh sterile tubes.

Monocyte isolation

The magnetic activated cell sorting (MAC) method (Miltenyi Biotec, Germany) was used to obtain monocytes with a high purity.

Macrophage preparation

After cell counts and adjustment to 1 250 000 cells/well, we cultured these cells in Roswell Park Memorial Institute (RPMI 1640) media (Gibco, USA) in sterile T25 (2×6 well) flasks supplemented with 10% fetal bovine serum (FBS, Sigma, USA), 1% penicillin/streptomycin (pen/strep) and 20 ng/ml of monocyte colony stimulating factor (M-CSF, Miltenyi Biotec, Germany). This complex was incubated at 37˚C, with 5% CO_2 under high moisture conditions for 7-9 days with media changes every two days.

Parasite culture

MRHO/IR/75/ER (IR endemic) were cultured in RPMI 1640 and incubated (22-25˚C) for 3-6 days. Promastigotes were collected during the stationary phase, transferred to a sterile Ficoll tube and centrifuged (350 g) for purification.

Macrophage-promastigote co-culture

We used two, 6-well T25 flasks to co-culture 5-7 promastigotes per macrophage in the presence of M-CSF for 4 hours. At the same time, and in parallel, 5-10 polystyrene latex particles (4.16 µl) per cell were used for phagocytosis by the macrophages over 4 hours. In parallel, one plate of uninfected macrophages was collected after 4 hours to be used as the control (9 replicates in 3 groups).

RNA isolation

Total RNA was extracted using TRIzol (Invitrogen, USA) reagent and stored at -75˚C. A Nanodrop was used for 260/280 and 230/260 ratio assessments and 1% agarose gel electrophoresis was performed for determination of the 28S/18S ratio. The RNA integrity number (RIN) of total RNA was assessed using an Agilent 2100 Bioanalyzer system.

cDNA synthesis and RNA-Seq

For transcriptome sequencing (SureSelect, Agilent, USA, 2017), cDNA libraries were prepared from the RNA obtained at two different time points (0 and 4 hours after infection). cDNA synthesis was performed using oligo dTs against a 3′ poly (A) tail according to the manufacturer's instructions. Quality-controlled cDNA were sequenced using an Illumina RNA-Seq workflow method. Single-end reads and the resultant reads were arranged and trimmed. Transcripts were mapped against the human genome, hg38/GRCh38.

Bioinformatics and statistical analyses

High quality sequencing data were analysed using our bioinformatic pipeline that consists of FastQC for quality

controls, Trimmomatic for trimming, and Kallisto for pseudoalignment to the transcriptome. Data analysis was performed with a Bioconductor DESeq2 package for data normalization and DE analysis. P≤0.05 was considered for statistical significance and the 5 FC threshold based on log2 for deferential expression assays. For gene annotation, we used an online software program, the Biological Database Network (bioDBnet) and for log2 fold change conversion, we used a base 2 logarithm (Log2) calculator.

Results

Gene expression integrity assessments

The majority of anti-leishmania effects on host cells occur after phagocytosis. For this reason, we assessed the test and control samples after phagocytosis. We used total RNAs from three repeated micro-bead latex particles ingested by the macrophages to determine the triggering power of inert particles on macrophage gene expression (phagocytosis effect). As shown in Figure 1A, B, the inert particles did not trigger transcriptome changes at 4 hours post-infection (4hpi), which indicated similar expression patterns as the non-infected macrophages.

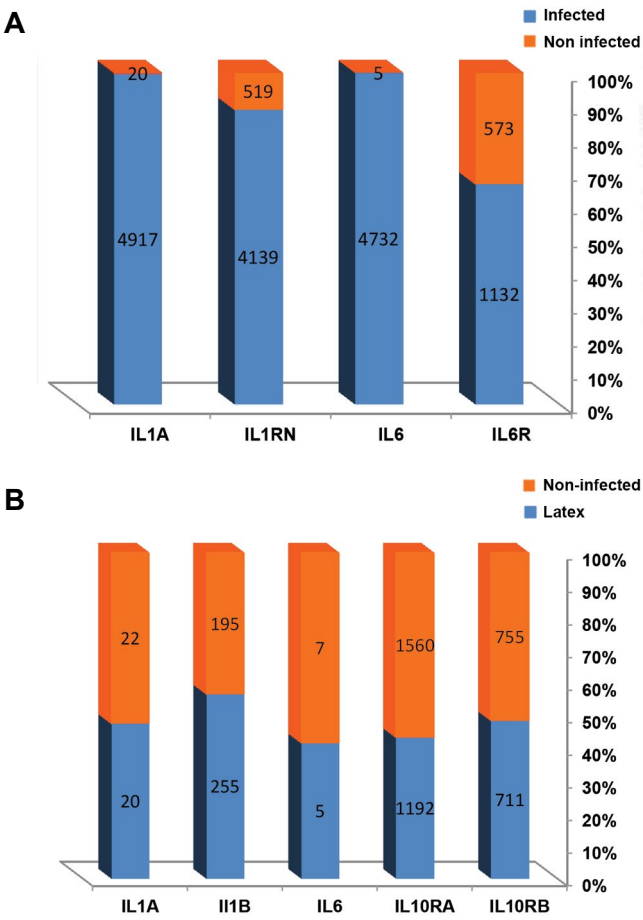

Fig.1: Gene expression pattern showing different expressions of non-infected samples compared to infected samples. As seen in the non-infected cells, the gene expression pattern is almost similar. In infected cells, the gene expression pattern is clearly altered. **A.** The different expression patterns for infected (grey column) and non-infected (red column) cells are shown. **B.** Non-infected cells exhibit a more similar gene expression pattern.

Cytokine gene expressions

Immune response and inflammatory cytokines *IL-1a/b,* tumour necrosis factor alpha (*TNF-α)* and TNF superfamily genes (*IL-6, IL-2, IL-12,* IFNs) were up-regulated with higher transcript reads expressed in the infected macrophages compared with the other samples (Table 1). Chemokines mostly up-regulated and only a few were down-regulated (Fig.2). *IL-1a, b,* TNF-α, and *IL-6s* all up-regulated as a result of pro-inflammatory stress caused by the pathogen (Table 2). *IL-27* was up-regulated, whereas we observed down-regulation of *IL-27R*. Some cytokines such as *IL-1*, *TNF-α* and the IFNs were up-regulated. In particular, *IFNɣ* was up-regulated. IFNs are produced by activated macrophages, T cells, and NK cells. IFNɣ pathway regulation is critical to lipopolysaccharide (LPS) induced and Toll-like receptor (TLR) related pathway responses.

Table 1: Cytokines and their receptor RNA sequence read counts

Cytokine	Latex ingested	Non- infected	Infected
IL-1A	22	20	4917
IL-1B	255	197	8772
IL-1R1	223	1064	1352
IL-1RN	413	526	4139
IL-2	0	0	18
IL-2RA	7	0	148
IL-2RG	568	338	817
IL-3RA	50	42	29
NFIL3	222	217	40
IL-4R	631	578	1168
IL-15	31	12	78
IL-6	5	7	4752
IL-6R	382	573	1132
IL-7R	86	591	1203
IL-10	6	13	47
IL-10RA	1192	1560	4412
IL-10RB	711	775	502
TNF	10	2.5	3114
TNFRSF12A	61	43	67
TNFRSF1B	2806	3900	4819
TNFRSF9	191	188	1543
TNFRSF1A	604	602	439
TNFSF13B	354	265	194
TNFAIP1	160	133	340
TNFAIP3	488	404	7490
TNFAIP8	480	475	3156
TNFAIP6	112	63	5474
TNFSF9	56	25	1033
IL-15RA	2	17	293

Table 2: Cytokines and their receptor fold changes

	Genes	Fold change
Interleukins and their receptors	*IL-2*	55 ↑
	IL-2RB	50 ↑
	IL-12A and B	18 and 117 ↑
	IL-6	678 ↑
	IL-18	4 ↑
	IL-10, IL-24	4 and18 ↑
	IL-23A, IL-27	268 and >100 ↑
	IL-1RN	8 ↑
	IL-15, IL-15RA	7 and 15 ↑
	IL-1A and B	33 and 55 ↑
TNFs and their receptors	*TNFSF8*	2 ↓
	TNFAIP3	17 ↑
	TNFAIP2	13 ↑
	TNFRSF9	8 ↑
	TNFRSF4	12 ↑
	TNFAIP8	6 ↑
	TNFSF1B	1.5 ↓
	TNF-α	176 ↑
IFNs and their receptors	*IFNB1*	55 ↑
	IFNL1	21 ↑
	IFNɣ	5 ↑
	IFNɣR1	3 ↓
	IFNAR1	1.5 ↓
	IFNAR2	1.5 ↓
CSFs	*CSF1*	19 ↑
	CSF2	142 ↑
	CSF3	67 ↑

TNF; Tumour necrosis factor, INF; Interferon, and CSF; Colony stimulating factor.

Growth factors and chemokine cytokine type gene expressions

Growth factors, colony stimulating factors (CSF) *1, CSF2* and *CSF3* were up-regulated in the infected cells (Table 2). Both *CSF-1RB* and *CSF-2R* were insignificantly down-regulated. *CSF-3R* was insignificantly up-regulated. Both *CCL2* and *CCL7* and their receptors were down-regulated. *CCL2* and its receptors, *CCR2* and *CCR4,* act to recruit monocytes and macrophages to the site of infection. The majority of chemokines were significantly up-regulated (Fig.2).

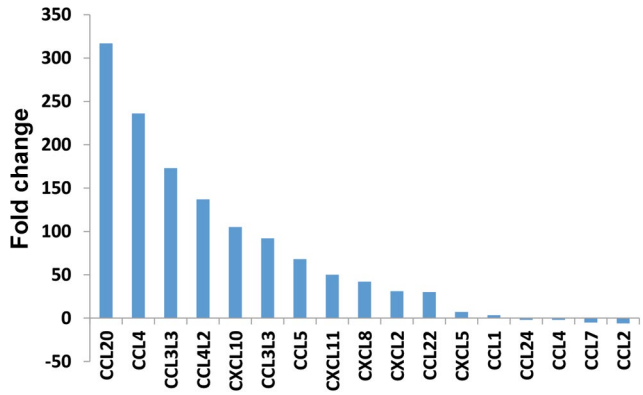

Fig.2: Expression levels of CC chemokine genes are higher than CxC chemokines. CCL2 and CCL7 chemokines were down-regulated. CCL2 seems to be one of the most important targets of *Leishmania major* (*L. major*) that is reprogrammed by this parasite. Most of the chemokine genes showed up-regulated expression patterns; thus, it may indicate the importance of cellular recruitments early infection time point.

Discussion

The expression status of cytokines, as an indicator of the immune response, depends on the type of pathogen and its virulence factors, as well as the genetic background of the host. Thus the immune response to *L. major* continues from the moment it enters the body until it is processed by immune cells such as macrophages. During this process, *L. major* modifies the host defence mechanisms in its favour for better survival and transforms the target cell, such as the macrophage, into a safe environment for itself.

Leishmania species benefit from a variety of tools in achieving this goal. Most notably, the selection of specific receptors from the macrophage-level complement system (CR1,3) and modulation of TLRs to neutralize the highly lethal phagolysosomal system, disruption of exposure of antigens to T cells, and anti-apoptotic changes, especially those that occur with the production and function of cytokines. In fact, *Leishmania* species control host defence mechanisms by activating or suppressing them.

The expressions of many cytokines in the infected host cells are altered by these pathogens. Pro-inflammatory and anti-inflammatory cytokine changes have been the main focus of many reports on cytokine alterations in leishmaniasis (12). The most important of these cytokines are IL-12, IL-6, IL-23, IL-1 alpha and beta, IL-10, IL-18, IL-15, and IL-2, TNF-α, IFNɣ, and TGF-β.

IL-12 is one of the most important cytokines produced by infected macrophages that has a role in Th-1 cell response. It is reported to be suppressed in these aforementioned cells (13). As a key cytokine gene that enables host macrophages to kill or clean up pathogen, *IL-12* is highly expressed by macrophages. However, they lose this killing capability because of inhibitor of serine protease (ISP) produced by the parasite (14). *IL-12, IL-23,*

and *IL-27* genes with structural and functional homology showed significant up-regulation in our study.

Pro-inflammatory cytokine genes *TNF-α, IL-1a, IL-1b, IL-6, IL-8* and *IFNɣ* were significantly up-regulated in our study, and reports of these types of cytokine genes were inconsistent. There is no RNA-seq-based report on this subject. Dillon et al. (15) reported an overall increase in the expression of immune and metabolic response genes, and the involvement of signalling pathways which supported our data. Therefore, because of the lack of such data, this study could be served as a reference for future studies.

In this study, despite some significant increases in the expression of cytokine receptor genes *IL-1R, TNF-Rs, IL-6R, IL-15R,* and *IL-2R*, other receptors had low or even reduced expressions. There is a lack of RNA-seq studies on cytokine receptor genes in leishmaniasis.

In this study, *IL-2*, *IL-15* and their receptor genes had significant upregulation. These two cytokines have a similar function and are involved in the proliferation and survival of Th cells. In addition, the effect of *IL-2* gene expression on macrophage dysfunction with *IL-12* gene expression has been reported (16). This confirms a possible dual role of some of these molecules, which has been reported by Abdoli et al. (17) who assessed the dual role of *IL-10* and *TGF-β* genes in *L. major* species.

An association has been reported between *IL-10*, a suppressive cytokine gene expressed by Treg cells, and leishmaniasis. *IL-10* expression suppresses the Th-1 cellular response to leishmaniasis. In this study, we have observed increased expression of *IL-10* and its receptor genes, and partial upregulation of *TGF-β* and its receptor.

Chemokines and their receptors are another type of cytokine. They play an important role in the processes of directing immune cells to pathogens. *Leishmania* species also play a critical role by altering chemokine expression for their own benefit. Chemokines, on the other hand, carry immune cells to the site of infection or inflammation and perform other biological functions. For example, CCL2, despite attracting monocytes, macrophages, dendritic cells, and memory T cells, also exhibits anti-leishmania effects and may be one of the pathogen targets in the pathway of suppression. In the current study, *CCL2* had a six-fold decrease in expression. On the other hand, lipophosphoglycan (LPG), which is present on surface of *Leishmania* species has inhibitory effects on monocyte migration. *CCL2* induces secretion of molecules such as selectins, ICAM-1, and VCAM-1. In this study, there was a 21-fold increase in *ICAM-1* and a 15-fold increase in *ICAM-5* gene expression. *CCR2,4*, specific *CCL2* receptor genes, were not expressed in this study. *CCL3* and its receptor genes, *CCR1,5*, had increased expression. The *CCL7* chemokine gene had decreased expression in this study. This chemokine is reported to increase functionally at the site of infection and, while recruiting monocytes, shows anti-macrophage function effects (18). Since *CCR1,5* also acts as receptor genes for these chemokines, it seems that their function is not solely dependent on ligand-receptor binding because *CCL7* selectively binds to Th-2 cells and prevents them from acting. We observed a 2-fold increase in *IL-4* expression.

Other *CCL* and *CXCL* genes also had increased expressions in this study. Most of these chemokines are products of IFN*ɣ* signalling pathways. *CXCL10* (*IP10*), which showed increased expression in this study, has antiangiogenic effects related to IL-12 activity associated to IFN*ɣ* (19).

Conclusion

We used an RNA-seq approach to decipher the pattern of gene expression alterations in early immune response and inflammatory pathways in macrophages infected with *L. major*. The obtained data could shed more light on the biology of *L. major* and the host cell response to infection. Our data also demonstrated up-regulation of some important pro-inflammatory cytokines during the early post-infection period.

Acknowledgements

We appreciate Dr. Tohidi for the preparation and culture of *Leishmania major* promastigotes, Dr. Hosseini, the General Director of Golestan Province Blood Banking Organization, Dr. Mohammad Shafiee, and Dr. Alireza Shahryari for their assistance. This work is financially supported by research deputies of Tarbiat Modares University and Golestan University of Medical Sciences. The authors declare no conflict of interests in this study.

Authors' Contributions

K.K., S.J.M.; Designed the study, collected, evaluated, and interpreted the data. O.J.; Standard endemic species collection of *L. major* promastigotes as infective agents essential to this study. M.A.F.; Performed and analysed RNA-seq data. All authors edited and approved the final version of the manuscript before submission.

References

1. Maspi N, Abdoli A, Ghaffarifar F. Pro- and anti-inflammatory cytokines in cutaneous leishmaniasis: a review: Pathog Glob Health. 2016; 110 (6): 247-260.
2. Rai MF, Tycksen ED, Sandell LJ, and Brophy RH. Advantages of RNA-seq compared to RNA microarrays for transcriptome profiling of anterior cruciate ligament tears. J Orthop Res. 2018; 36(1): 484–497.
3. Banerjee S, Bose D, Chatterjee N, Das S, Chakraborty S, Das T, Saha KD. Attenuated Leishmania induce pro-inflammatory mediators and influence leishmanicidal activity by p38 MAPK dependent phagosome maturation in Leishmania donovani co-infected. Sci Rep. 2016; 6(4): 1-14.
4. Ribeiro-Gomes FL, Romano A, Lee S, Roffê E, Peters NC, Debrabant A, Sacks D. Apoptotic cell clearance of Leishmania major-infected neutrophils by dendritic cells inhibits $CD8^+$ T-cell priming in vitro by Mer tyrosine kinase-dependent signalling. Cell Death Dis. 2015; 6(12): 1-12.
5. Messlinge H , Sebald H, Heger L, Dudziak D, Schleicher Ch. Monocyte-derived signals activate human natural Killer cells in response to Leishmania parasites. Front Immunol. 2018; 9 (1): 1-18.
6. Olivier M, Gregory DJ, Forget G. Subversion mechanisms by which Leishmania parasites can escape the host immune response: a

signalling point of view. Clin Microbiol Rev. 2005; 18(2): 293–305.
7. Bhattacharya P, Ghosh S, Ejazi SA, Rahaman M, Pandey K, Ravi Das VN, Das P, Goswami RP, Saha B, Ali N. Induction of IL-10 and TGFβ from CD4+CD25+FoxP3+ T cells correlates with parasite load in indian kala-azar patients infected with leishmania donovani. PLoS Negl Trop Dis. 2016, 10(2): 1-20.
8. Rossi M, Fasel N. How to master the host immune system? Leishmania parasites have the solutions! Int Immunol. 2017, 30(3): 103-111.
9. Bacon K, Baggiolini M, Broxmeyer H, Horuk R, Lindley I, Mantovani A, et al. IUIS/WHO Subcommittee on Chemokine Nomenclature. Chemokine/chemokine receptor nomenclature. J Leukoc Biol. 2001, 70(3): 465-466.
10. Murray HW, Luster AD, Zheng H, Ma X. Gamma interferon-regulated chemokines in Leishmania donovani infection in the liver. Infect Immun. 2016; 85(1): e00824-16.
11. Sousa R, Andrade VM, Bair T, Ettinger NA, Guimarães L, Andrade L, et al. Early suppression of macrophage gene expression by Leishmania braziliensis. Front Microbiol. 2018, 9(10): 1-16.
12. Andargie TE, Ejara ED. Pro- and anti-inflammatory cytokines in visceral Leishmaniasis. J Cell Sci Ther; 2015, 6(3): 1-8.
13. Jayakumar A, Widenmaier R, Ma Xio, McDowell MA. Transcriptional inhibition of interleukin-12 promoter activity in Leishmania spp.-infected macrophages. J Parasitol. 2008; 94(1): 84–93.
14. Goundry A, Romano A, Paula A. Jeremy L. Mottram JC, Myburgh E. Inhibitor of serine peptidase 2 enhances Leishmania major survival in the skin through control of monocytes and monocyte-derived cells. FASEB J. 2018, 32(3): 1315-1327.
15. Dillon LA, Suresh R, Okrah K, Bravo HC, Mosser DM, El-Sayed NM. Simultaneous transcriptional profiling of Leishmania major and its murine macrophage host cell reveals insights into host-pathogen interactions. Genomics. 2015; 16: 1108: 1-15.
16. Ramer-Tait AE, Petersen CA, Jones DE. IL-2 limits IL-12 enhanced lymphocyte proliferation during Leishmania amazonensis infection. Cell Immunol. 2011; 270(1): 32–39.
17. Abdoli A, Maspi N, Ghaffarifar F. Wound healing in cutaneous leishmaniasis: A double edged sword of IL-10 and TGF-β. Comp Immunol Microbiol Infect Dis. 2017, 51: 15-26.
18. Rees PA, Greaves NS, Baguneid M, Bayat A. Chemokines in wound healing and as potential therapeutic targets for reducing cutaneous scarring. Adv Wound Care (New Rochelle). 2015; 4(11): 687-703.
19. Ontoria E, Hernández-Santana YE, González-García AC, López MC, Valladares B, Carmelo E. Transcriptional profiling of immune related genes in leishmania infantum infected mice: identification of potential biomarkers of infection and progression of disease. Front Cell Infect Microbiol. 2018; 8(3): 1-17.

Methylation Status of *MTHFR* Promoter and Oligozoospermia Risk: An Epigenetic Study and in Silico Analysis

Atefeh Rezaeian, M.Sc.[1, 2], Mohammad Karimian, Ph.D.[2*], Abasalt Hossienzadeh Colagar, Ph.D.[2*]

1. Department of Cellular Biotechnology, Cell Science Research Center, Royan Institute for Biotechnology, ACECR, Isfahan, Iran
2. Department of Molecular and Cell Biology, Faculty of Basic Sciences, University of Mazandaran, Babolsar, Iran

Corresponding Addresses: P.O. Box: 4741695447, Department of Molecular and Cell Biology, Faculty of Basic Sciences, University of Mazandaran, Babolsar, Iran
Emails: mdkarimian@gmail.com, ahcolagar@umz.ac.ir

Received: 3/March/2019, Accepted: 21/July/2019

Abstract

Objective: In this study, we evaluated the effects of promoter methylation of *MTHFR* on oligozoospermia risk, followed by an in silico analysis.

Materials and Methods: In a case-control study, semen samples were collected from infertile and healthy control men. *MTHFR* promoter region was amplified by methylation-specific polymerase chain reaction (PCR). Finally, the promoter region of *MTHFR* was analyzed by bioinformatics software.

Results: Our data revealed significant associations of CpG island promoter methylation with oligozoospermia in a case-control study. In silico analysis showed that promoter contains a strong nucleosome exclusion region, a bonafide CGIs, six PROSITE motifs without a defined TATA box and 14 transcription factor (TF) binding sites, which are directly involved in spermatogenesis

Conclusion: Based on our findings, methylation of the *MTHFR* gene promoter region may be a risk factor for oligozoospermia. However, this is a preliminary report representing data for future comprehensive studies to make a clinical conclusion on the potential biomarker role of methylation of this promoter in elevating susceptibility to oligozoospermia.

Keywords: Bioinformatics, DNA Methylation, Male Infertility, Methylenetetrahydrofolate Reductase, Oligozoospermia

Cell Journal(Yakhteh), Vol 22, No 4, January-March (Winter) 2021, Pages: 482-490

Citation: **Rezaeian A, Karimian M, Hossienzadeh Colagar A. Methylation status of MTHFR promoter and oligozoospermia risk: an epigenetic study and in silico analysis. Cell J. 2021; 22(4): 482-490. doi: 10.22074/cellj.2021.6498.**

Introduction

Human infertility is a major health problem in 10-15% of couples worldwide. Male factors are responsible for 50% of infertility causes (1). There are many environmental, genetic and epigenetic risk factors for male infertilities. About 15-30% of the male infertilities are due to genetic abnormalities, such as chromosomal or monogenic disorders, mitochondrial DNA (mtDNA) mutations, micro-deletions on Y chromosome and autosomal deletions, defects in DNA repair mechanism, Y-linked syndromes and some single nucleotide polymorphisms (SNPs). In addition to genetic factors, epigenetics may also affect male infertility (2-4). Epigenetics refers to the heritable alteration in gene expression and activity without any change of DNA sequences (5). Epigenetic modifications such as acetylation, de-acetylation, methylation and demethylation of DNA and proteins lead to different patterns of gene expression (6).

Epigenetics play a crucial role in development and function of sperm, fertilization and post-fertilization events (5). DNA methylation is the most common epigenetic factor which may affect male reproduction (7). DNA methylation occurs by addition of a methyl group in the fifth position of the cytosine ring among the CpG (cytosine-phosphate-guanine) di-nucleotides (8). Hyper-methylation of CpG rich sequences (called CpG islands) in the promoter region usually leads to down-regulation, whereas hypo-methylation generally leads to up-regulation of genes (9).

One of the key enzymes involved in the spermatogenesis process is methylene tetrahydrofolate reductase (MTHFR; OMIM: 607093). MTHFR converts 5, 10-methylenetetrahydrofolate to 5-methyltetrahydrofolate, which donates a methyl group for re-methylation of homocysteine to methionine. Then, methionine provides the methyl group for S-adenosylmethionine, a major methyl group donor for various reactions such as DNA, RNA and protein methylation. On the other hand, 5, 10-methylenetetrahydrofolate is an essential substrate for thymidylate synthase. Therefore, MTHFR is a key enzyme regulating methylation reactions and nucleic acid

synthase (10).

Alteration of *MTHFR* gene expression may also influence spermatogenesis process. *MTHFR* transcript level is lower in human tissues, compared to the testis, showing that MTHFR has a critical role in germ cell maturation (11). High levels of MTHFR in testis ensure that sufficient amounts of folate derivatives move toward the production of methyl group -S adenosyl methionine, as the main donor of methyl group in the methylation reaction. Therefore, alterations in the methyl supplies, raised from *MTHFR* insufficiency, may influence spermatogenesis (12). However, methylation patterns are amazingly similar among the embryonic stem cells, embryonic germ cells, and sperms (13). Promoter methylation of this gene may influence the expression of MTHFR and subsequently male infertility (14).

The human *MTHFR* gene consists of 12 exons and is located on 1p36.3 (10). There are no CAAT and TATA-box elements in the promoter of this gene, but it has multiple binding sites for transcription factors (TFs) including SP1, HINF-3, NF-GMa, c-Rel, UTRF, E2-F1, NF-kB and AP1 (11). Here we investigated promoter methylation in semen samples with reduced sperm count and fertile men, to evaluate its role in oligozoospermia. Also, the bioinformatics approach was applied to validate the laboratory results.

Materials and Methods

Subjects and sample collection

In this case-control study, semen samples were collected from 151 subjects (including 73 oligozoospermic men with age of 36.28 ± 3.49 years and 78 fertile men with age of 37.42 ± 4.11 years). The infertile men who referred to Shahid Beheshti Infertility Center (Kashan, Iran) had no history of cryptorchidism, orchitis, infectious disease, diabetes mellitus, drug abuse, obstruction of the vas deferens, varicocele, abnormal profiles of luteinizing hormone (LH), follicle-stimulating hormone (FSH) and testosterone, abnormal karyotype as well as Y-chromosome microdeletion. In addition, the infertile men's women had no problem in their reproductive systems. The control group was comprised of volunteer men with no history of infertility and at least one healthy offspring who were referred to the same clinic for sperm analysis to approve normal sperm parameters. Semen parameters were analyzed according to World Health Organization, 2010 criteria (15). Therefore, men with less than 15 million/ml sperm count, less than 39% progressive motility, and less than 4% normal form were classified as oligozoospermic, asthenozoospermic and teratozoospermic, respectively. In this study, all of the infertile men were identified as oligozoospermic. Finally, semen samples were collected from all subjects into sterile tubes. Informed written consent was obtained from all of the participants and this study was confirmed by the principles outlined in the Declaration of Helsinki and approved by the Medical Ethics Committee of Kashan University of Medical Sciences (Kashan, Iran, IR.KAUMS.REC.1396.24).

Sperm preparation, DNA isolation, and-specific polymerase chain reaction

An osmotic shock process was employed to avoid sperm contamination with some other cells such as lymphocytes and epithelial cells. To remove the extra cells, sperm mixture was treated with Tris-HCl (50 mM, pH=6.8) at 8˚C for 20 minutes and then the mixture was centrifuged to collect the purified spermatozoa. Genomic DNA was extracted from semen samples with DNG plus DNA extraction buffer (Cinnagen, Iran). We analyzed a single gene promoter in our study. CpG methylation in the promoter region of the *MTHFR* gene was detected by methylation-specific PCR (MSP, also known as MS-PCR) method. For this purpose, the entire sequence of *MTHFR* gene was deduced from NCBI database (Accession no. NG_013351.1). The specific primers for methylated and unmethylated forms of the promoter region were designed by MethPrimer online software (16). The promoter region of *MTHFR* was analyzed by the mentioned software, showing two CpG islands in that region. As depicted in Figure 1, the specific methylated and unmethylated primers were designed on the upstream CpG island. DNA samples were treated with sodium bisulfite using EpiTect Bisulfite Kit (Qiagen, USA) which converts unmethylated cytosine residues to uracil, while it does not affect on the methylated cytosine. Treated DNA was purified by EpiTect spin columns of the aforementioned Kit. MS-PCR was carried out for methylated and unmethylated primers separately in 12.5 µl PCR mixture containing 30 ng of treated DNA, 0.1 µl *Taq* DNA polymerase, 0.12 µl dNTPs mix, 0.17 µM forward primer, 0.17 µM reverse primer and 1.5 µM $MgCl_2$. PCR was performed in an Eppendorf thermal cycler (Mastercycler, Eppendorf, Germany). All of the PCR reagents were ordered from Cinnagen Company. Finally, the amplified fragments were separated by electrophoresis on 8% polyacrylamide gel electrophoresis and stained with silver nitrate ($AgNO_3$; Sigma Aldrich, UK). SssI methyltransferase (New England Biolabs, USA) was applied for methylation of one sperm DNA sample as the methylated positive control.

Statistical analysis

A Chi-square test was used to evaluate the differences in frequency of methylated, unmethylated and heterogeneous samples between case and control

groups. A binary regression logistic was applied to calculate odd ratio (OR) and 95% confidence interval (CI) for evaluation of the association between *MTHFR* promoter methylation and oligozoospermia. When $P<0.05$, the correlation was considered statistically significant. All statistical analyses were performed using the SPSS v.20 software (IBM SPSS, USA).

Computational analysis

An in silico analysis was performed using bioinformatics tools to evaluate the promoter features of *MTHFR*. Promoter and transcription start sites (TSSs) of *MTHFR* gene were diagnosed by Eukaryotic Promoter Database (http://epd.vital-it.ch) and DBTSS online software (http://dbtss.hgc.jp), respectively. The presence of TATA boxes and PROSITE motifs were further investigated using MOTIF software (http://www.genome.jp/tools/motif). *MTHFR* CpG island, transcriptionally competent CpG islands (bona-fide CGIs), and nucleosome-exclusion regions were determined with UCSC Genome browser (http://genome.ucsc.edu/cgi-bin/hgTracks). Methylation-sensitive TF binding sites (TFBS) in the regulatory region was predicted by the cisRED online server (http://www.cisred.org). UCSC genome browser was used to characterize Cis-regulatory module (CRM). To detect TFs binding to CRM, this region was stretched using PReMod database (http://genomequebec.mcgill.ca/PReMod).

Results

Methylation-specific polymerase chain reaction

By using the MS-PCR method we identified methylation patterns of *MTHFR* promoter region. After using the M-*MTHFR-f* and M-*MTHFR-r* primers in MS-PCR, a 186 bp fragment was detected on 8% polyacrylamide gel for methylated samples. Whereas, application of U-*MTHFR-f* and U-*MTHFR-r* primers demonstrated a 178-bp unmethylated fragment on the polyacrylamide gel. Therefore, the heterogeneous samples indicated both 186-bp and 178-bp fragments (Fig.1).

MTHFR-CpG promoter methylation and oligozoospermia

The number of subjects was 151 individuals including 73 patients with oligozoospermia and 78 healthy controls. Characteristics of the oligozoospermia males and fertile controls are shown in Table 1. After MSP analysis, we found methylated (MM), unmethylated (UU) and heterogeneous (MU) status among the subjects. Frequency of methylated, unmethylated, and heterogeneous samples in the patients were 8 (10.96%), 46 (63.01%), and 19 (26.03%), respectively; whereas, these numbers (ratios) in control group were 1 (1.28%), 68 (87.18%), and 9 (11.54%), respectively. The characteristics and semen parameters of 8 patients with hypermethylated *MTHFR* are depicted in Table 1. When we calculated Chi-square, a significant difference was found between case and control groups concerning the methylation methylation status of *MTHFR* promoter. Additionally, OR in 95% CI showed a significant association between methylated ($\chi^2=7.98$, OR=11.83, 95% CI=1.43-97.77, P=0.022) and heterogeneous ($\chi^2=6.85$, OR=3.12, 95% CI=1.30-7.50, P=0.011) statuses of *MTHFR* promoter and oligozoospermia.

Table 1: Characteristics and sperm parameters of the subjects

Variables	Infertile		Fertile	P value*
	All	Methylated *MTHFR*	n=78	
	n=73	n=8		
Age (Y)	36.28 ± 3.49	34.25 ± 2.05	37.42 ± 4.11	0.069
Smoking (Y/N)	16/57	1/7	26/52	0.151
BMI (kg/m^2)	23.41 ± 2.09	22.75 ± 2.12	24.00 ± 2.31	0.103
Seminal volume (mL)	3.19 ± 0.92	3.33 ± 0.95	3.26 ± 0.76	0.603
Sperm count (×10^6/mL)	9.25 ± 3.17	9.38 ± 2.92	60.67 ± 10.10	<0.0001
Motility (% motile)	46.14 ± 7.25	47.13 ± 8.64	57.83 ± 8.88	<0.0001
Morphology (% normal)	41.41 ± 11.39	45.38 ± 9.30	51.95 ± 12.06	<0.0001

The data are expressed as mean ± standard deviation. *; The P value represents comparison of all infertile and fertile subjects.

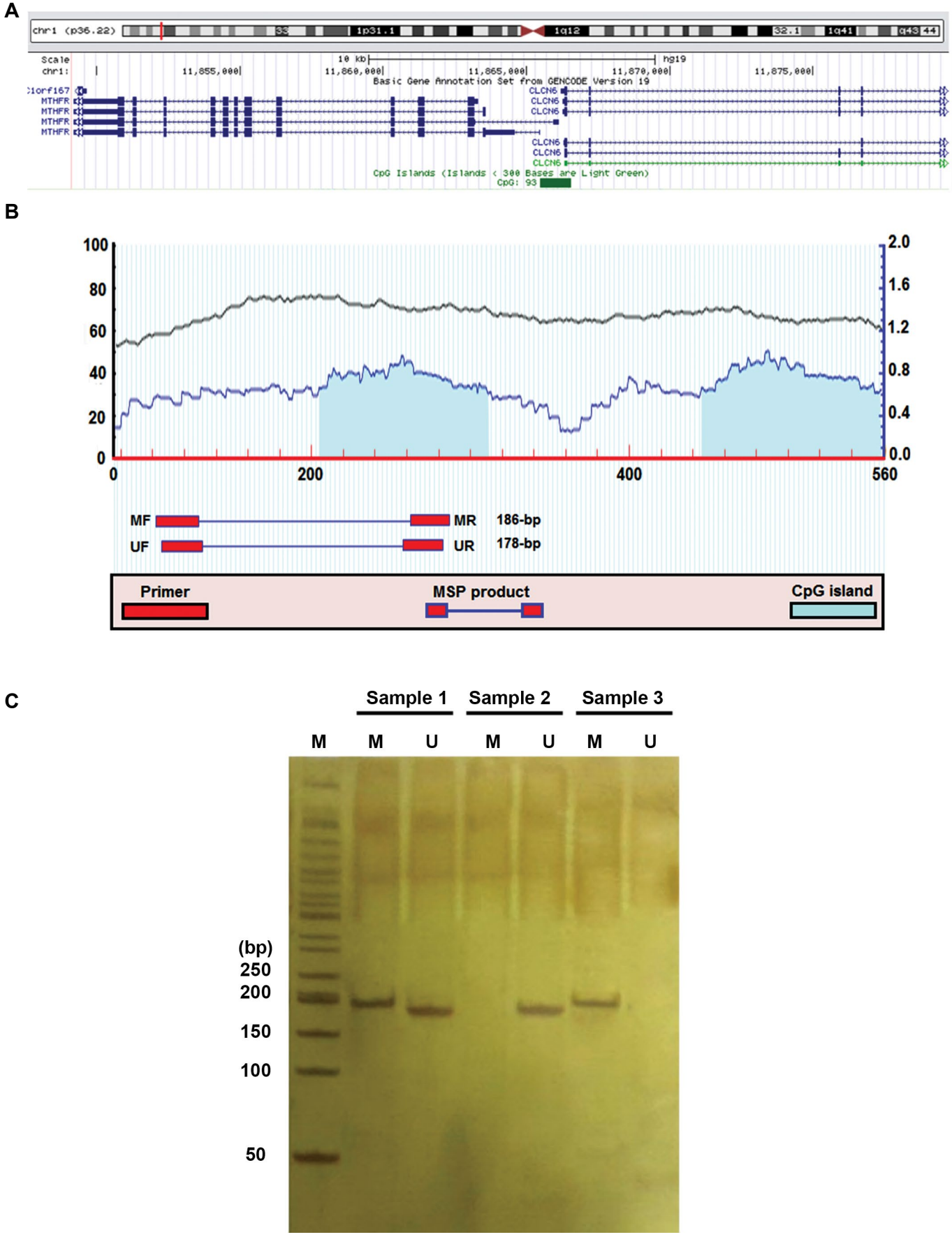

Fig.1: CpG map of *MTHFR* and methylation-specific polymerase chain reaction (PCR) result. **A.** *MTHFR* gene is located on chromosome 1 (1p36.22), the region containing CpG islands demonstrated by the green box. **B.** MethPrimer software indicated presence of two CpG islands in *MTHFR* promoter. The location of methylated and unmethylated primers, as well as the PCR products, was illustrated. Length of methylated and unmethylated PCR products respectively shows 186 and 178 bp. **C.** MS-PCR results showed the heterogeneous samples amplifying both methylated and unmethylated primers (sample 1), while the unmethylated (sample 2) and methylated (sample 3) samples were just amplified with unmethylated and methylated primers, respectively.

In silico analysis

Description of *MTHFR* promoter

Three various promoter sequences were identified in *MTHFR* by Eukaryotic Promoter Database (EPD). There are four different *MTHFR* transcripts with different transcription start sites in the various tissues. Three polypeptides with 657, 698 and 680 residues are encoded by this gene. The data from EPD revealed that the promoter of *MTHFR* is near or in the CpG island. This shows the importance of epigenetic regulation of *MTHFR*. The CpG island with 1104 bp length has 93 CpG dinucleotide, 69.9% C or G, and 16.8% CpG. MOTIF software shows nine PROSITE motifs for the promoter region of *MTHFR* whereas there was not any TATA box in the region.

Analysis of transcription-factor binding sites

ChIP-seq, cisRED and PReMod databases were used for analysis of TFBS in *MTHFR*. ChIP-seq server predicts position and architecture of TF in the genome. The data from this server revealed 44 TFs binding to the promoter region of *MTHFR*, 14 of which are related to spermatogenesis process (Table 2).

The data obtained from cisRED program showed that 13 atomic motifs, as an evolutionarily conserved sequence recognized in the promoter region via a comparative examination of more than 40 vertebrate species and five annotation-based modules, exist in *MTHFR* regulatory region. According to this database, *MTHFR* regulatory region with 1854 bp expands at the 5′ end of CpG island (Fig.2). The module mod000898 in *MTHFR* promoter, predicted by PReMod database, overlaps with 5′ end of CpG island. This module (mod000898) with 418 bp size has score 460 and it exactly overlaps with the amplified fragment in our research. Moreover, the PReMod server showed that Sp1, MAZR, and p300 are the most important TFs which regulate *MTHFR* expression (Fig.3).

Bona fide CpG island

We detected "bona-fide CGIs", a high accuracy method to identify CpG islands by integrating their genetic and epigenetic features, for *MTHFR* gene. Bona-fide CGIs that introduce epigenetic and genetic states (such as open chromatin structure, frequent promoter activity, euchromatin, DNA helix structure, significant conservation, and repeat depletion) was detected at the promoter region of *MTHFR* with the score 573 (Fig.4). As depicted in Figure 4, the bona fide CGIs has not only positional overlap with CpG island, but also even with a larger length than CpG island.

Nucleosome exclusion region

Nucleosome exclusion regions (NXRegions) were predicted by a custom track in UCSC genome browser. The data from this server revealed that there are three regions with the high score of NXRegions in the promoter of *MTHFR* (Fig.4). Also, there were some transcription start sites in these NXRegions.

Table 2: Transcription factor binding site in *MTHFR* promoter involved in spermatogenesis process

Factor	Size	Score	Target description
NFKB	88	139	NFKB acts as a regulator TF in the Sertoli cell-spermatid junctional complexes. In the spermatogenesis processes, selenium incorporate with NFKB has a critical regulator function.
STAT1	1710	149	STAT1 as a member of STAT family has an important role in development, prevention of proliferation and immune response. It acts as a regulator which controls the gene transcription in Sertoli cells
AP1	1792	182	This factor is required through the G1 phase of the cell cycle
c-Myc	2314	386	It acts as a multifunctional protein which has roles in cell cycle, apoptosis and cellular transformation
Max	1926	1000	This factor with other families such as Myc which is an oncoprotein involved in cell proliferation, differentiation and apoptosis
FOSL2	1144	1000	FOS family applies as regulators of cell proliferation, differentiation, and transformation
GABP	1013	886	GA-binding protein (GABP) acts as a regulator of gene expression. It regulates some crucial genes which incorporate in cell cycle, protein synthesis, and cellular metabolism
p300	962	1000	This factor regulates transcription by chromatin remodeling, and it involves in cell proliferation and differentiation
PAX5	740	807	Expression of this factor has been identified in the developing testis, implicates its role in spermatogenesis
SP1	917	832	This well-known factor involved in many cellular processes such as cell development, differentiation, immune defense, apoptosis, chromatin remodeling and response to DNA damage
POU2F2	754	424	This protein has multiple functions such as immune response, embryogenesis, neurogenesis, etc
Sin3Ak-20	772	1000	This protein with histone deacetylases (HDACs) manages gene silencing. Sin3/HDAC is also involved in genomic stability, cell cycle development, embryonic progression, and homeostasis
BHLHE40	274	345	BHLHE40 roles as a transcriptional repressor. It controls cellular progression, development and differentiation
USF-1	216	71	USF1 with p53 takes part in cell fate decisions. It also simplifies the switch of proliferation to differentiation of Sertoli cells in testes

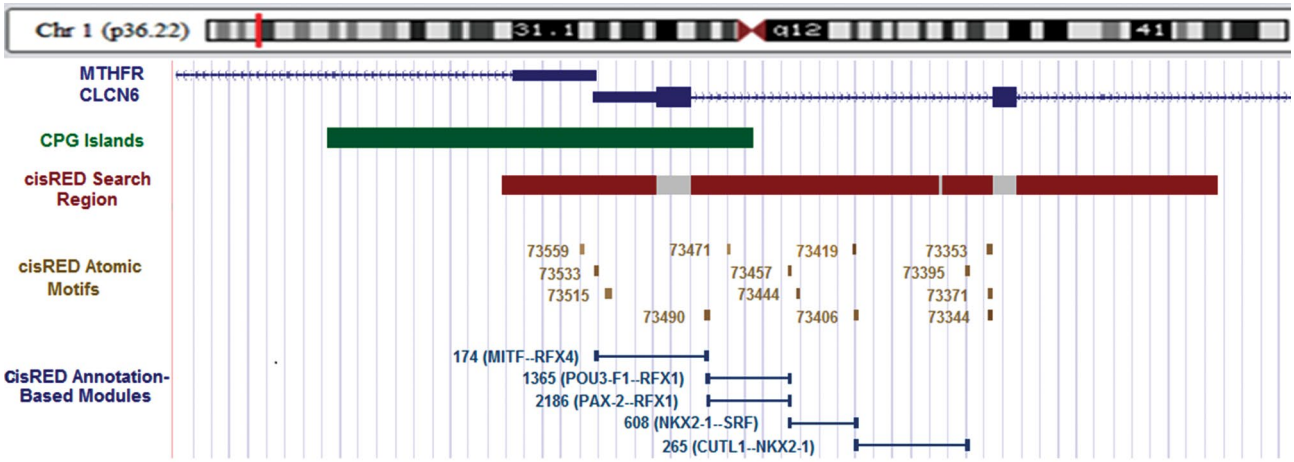

Fig.2: Location of cisRED atomic motifs and cisRED modules in *MTHFR* promoter. The long green bar at the top shows location of CpG island. The red and gray bars indicate a nominal 'search region' within which comparative genomics discovery methods were applied by cisRED. The numbered brown blocks are 'atomic' motifs, i.e. conserved DNA sequence motifs that were identified by discovery methods and post-processing operations. Blue lines show annotation-based modules.

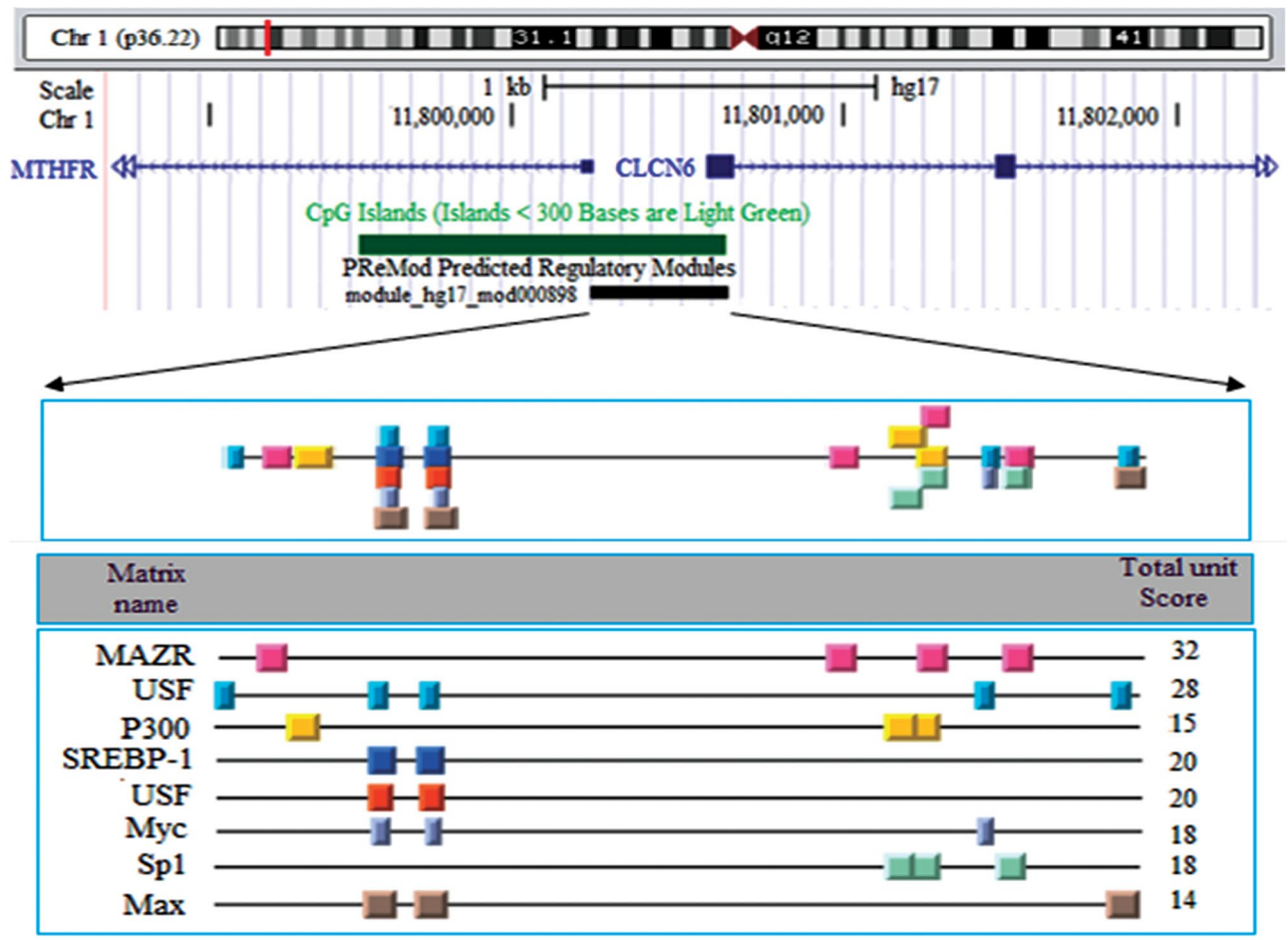

Fig.3: The module mod000898 and related transcription factors predicted by PReMod database. The black bar shows exact position of this module in CpG island and the precise location of transcription factor binding sites in this module is demonstrated by colorful boxes.

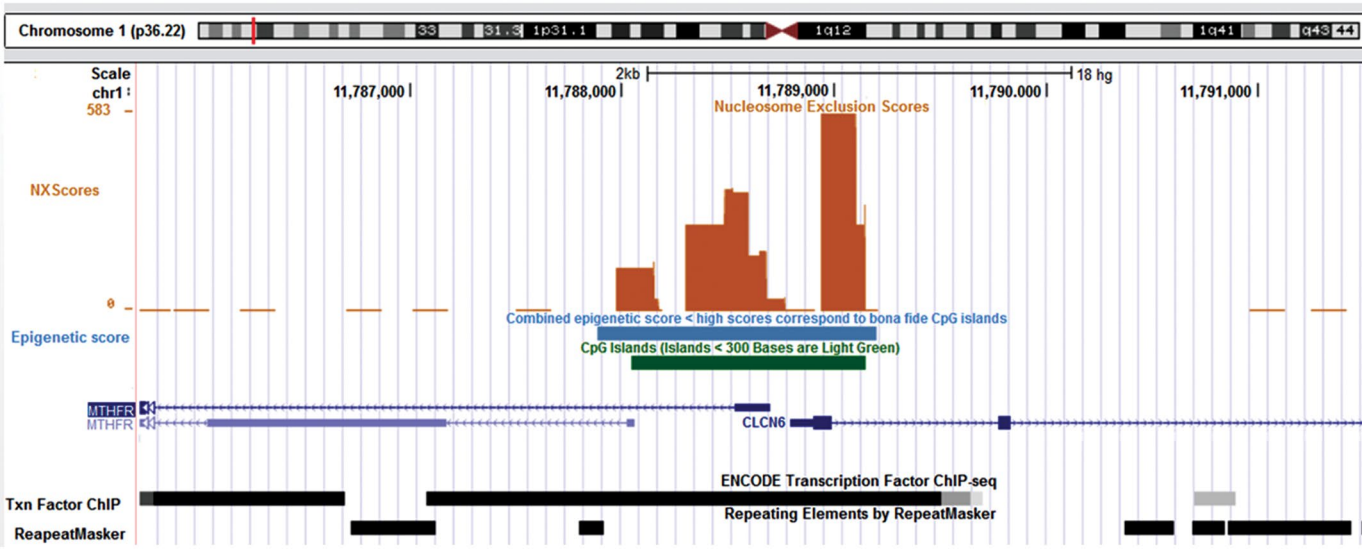

Fig.4: CpG Island, bona fide and nucleosome exclusion score (NXScore) of *MTHFR* promoter. CpG island expands in 5' end of *MTHFR* gene and even beyond it. Bona fide area overlaps with and even broader than CpG island. The NXScore graph implicates low density of nucleosome at the promoter region of *MTHFR*.

Discussion

In this study, we investigated the association of *MTHFR* promoter methylation with oligozoospermia in an Iranian population. Our results indicated that there was a significant association between promoter methylation and oligozoospermia. Consistent findings were also reported in some previous studies. Houshdaran et al. (17) suggested a significant association between abnormal semen parameters and hypermethylation in several genes. They indicated that improper erasure of DNA methylation during epigenetic reprogramming would be the cause of disorder. In the other study, Wu et al. (18) reported hypermethylation of *MTHFR* promoter in sperms and its association with idiopathic male infertility. Moreover, Khazamipour et al. (14) detected hypermethylation of *MTHFR* promoter region in testis biopsies. They reported that more than half of the patients with non-obstructive azoospermia (NOA) were hypermethylated in the *MTHFR* promoter, while the patients with obstructive azoospermia had a normal methylation pattern. Botezatu et al. (19) also reported that *MTHFR* hypermethylation may be associated with male infertility in Romanian population. Rotondo et al. (20) observed a correlation of hypermethylation status of *MTHFR* promoter in semen samples of 55% of infertile couples with recurrent spontaneous abortion (RSA), compared to 8% in non-RSA (NRSA) and 0% the fertile couples. They suggested *MTHFR* methylation as a novel putative risk factor for RSA etiology. All of these studies proved the important role of epigenetic regulation of *MTHFR* in male infertility. However, the geographical, racial and environmental factors may modulate the effects of *MTHFR* promoter methylation.

The testis of an adult male is composed of more than 80% germ cells, chiefly in the meiotic and post-meiotic phases of spermatogenesis (21). Some studies presented the patterns of DNA methylation in different cells throughout spermatogenesis. Oakes et al. (22) mentioned that testicular germ cells established their pattern of methylation genome meiosis, first of all in spermatogonia and after that in early prophase I spermatocytes. Another study reported that DNA methylation is maintained steadily during spermatogenesis and spermiogenesis (6). Farthing et al. (13) evaluated DNA methylation of 26,275 promoters and indicated that the patterns of methylation with hypomethylation states were similar in embryonic stem cells, embryonic germ cells, and sperms. Therefore, based on the mentioned previous study, aberrant DNA methylation pattern of spermatozoa from infertile men reflects methylation status of adult germ cells throughout the seminiferous tubules. In this regard, Rotondo et al. (20) reported that *MTHFR* hypermethylation detected in spermatozoa samples could be representative of the status of adult germinal stem cells.

Folate metabolism has a critical role in DNA synthesis, DNA protection and epigenetic modifications such as histone or DNA methylation. MTHFR is one of the key enzymes which regulate folate metabolism. Dysfunction of the enzyme leads to the adverse effect on spermatogenesis and it may result in infertility. *MTHFR* expression can be regulated by genetic and epigenetic factors. Here, we investigated the role of *MTHFR* promoter methylation as an epigenetic factor in oligozoospermia, followed by computational analyses. We detected an altered pattern of promoter methylation in the oligozoospermic man compared to healthy controls. Our data revealed that there is a significant association between methylated CpG islands in *MTHFR* promoter region and oligozoospermia.

Hypermethylation of this area causes down-regulation in *MTHFR* gene expression. Therefore, it causes folate pathway defects followed by some adverse results, such as homocysteine accumulation, DNA impairment, genome destabilization, defects in sperm proliferation and differentiation. All of these abnormalities may result in oligozoospermia.

Genetic and epigenetic variations may affect gene expression and bioinformatics is a useful tool for evaluation of these effects (23, 24). In this study, we applied a bioinformatics approach to investigate the effects of *MTHFR* promoter methylation in regulating gene expression. Our research revealed strong evidence for the epigenetic regulation of the *MTHFR* promoter. For example, we detected the NXRegion in this promoter. Nucleosomes are one of the basic structures for DNA condensation and they contribute to epigenetic regulation of genes (25). Their interaction with DNA leads to chromatin condensation, whereas promoter region inactive genes are nucleosome free, so that TFs can bind to DNA and start the transcriptional event (26). CpG dinucleotides in DNA are one of the factors which modify strength and condensation of nucleosomes (27). Methylation of CpG dinucleotide could directly affect DNA bendability and nucleosome positioning (28). There is a reliable association between tissue specificity of a coding sequence and tendency of its promoter to exclude nucleosomes. Some computational algorithm predicts *in vivo* nucleosome positioning through a specific gene. Here, we used a custom track that shows NXRegions in the genome sequence. In this software nucleosome exclusion score for *MTHFR* gene was positively correlated with gene expression levels and DNase I hypersensitive sites (29). Peaks in graph generally are associated with transcription start sites. Based on MOTIF software, there is six PROSIT motif in the promoter region of *MTHFR*, but there was not any TATA box in the region. Absence of TATA box in this promoter suggests that it is less conserved compared to a common promoter. The "bona-fide CGIs", is a marker with high accuracy to identify CpG islands by integrating their genetic and epigenetic features. This marker identified this region in *MTHFR* promoter. The length of this area is a determining parameter to ensure that epigenetic properties of a fragment are not missed (30). Furthermore, the promoter region of *MTHFR* is an area which binds to several TFs, 14 of which are directly involved infertility process.

Conclusion

Based on our findings, promoter methylation of *MTHFR* gene may be a risk factor for oligozoospermia. However, further studies with a larger sample size among different ethnicity are needed to obtain more accurate results. There were some limitations in our study which should be considered. Firstly, the study suffered small sample size for the case and control groups. We also did not evaluate the effects of methylation on gene expression. Furthermore, the influence of environmental factors such as folate intake was not assessed.

Acknowledgments

There is no financially support and conflict of interest in this study.

Authors' Contributions

A.R.; Contributed to perform the molecular experiments, data analysis, and writing the initial manuscript. M.K., A.H.; Contributed to the study design, revision and finalization of the manuscript. All authors read and approved the final manuscript.

References

1. Colaco S, Modi D. Genetics of the human Y chromosome and its association with male infertility. Reprod Biol Endocrinol. 2018; 16(1): 14.
2. Rafatmanesh A, Nikzad H, Ebrahimi A, Karimian M, Zamani T. Association of the c.-9C>T and c.368A>G transitions in H2BFWT gene with male infertility in an Iranian population. Andrologia. 2018; 50(1).
3. Li LC, Dahiya R. MethPrimer: designing primers for methylation PCRs. Bioinformatics. 2002; 18(11): 1427-1431.
4. Talebi E, Karimian M, Nikzad H. Association of sperm mitochondrial DNA deletions with male infertility in an Iranian population. Mitochondrial DNA A DNA Mapp Seq Anal. 2018; 29(4): 615-623.
5. Gunes S, Arslan MA, Hekim GNT, Asci R. The role of epigenetics in idiopathic male infertility. J Assist Reprod Genet. 2016; 33(5): 553-569.
6. Dada R, Kumar M, Jesudasan R, Fernández JL, Gosálvez J, Agarwal A. Epigenetics and its role in male infertility. J Assist Reprod Genet. 2012; 29(3): 213-223.
7. Sujit KM, Sarkar S, Singh V, Pandey R, Agrawal NK, Trivedi S, et al. Genome-wide differential methylation analyses identifies methylation signatures of male infertility. Hum Reprod. 2018; 133(12): 2256-2267.
8. Dahl C, Grønbæk K, Guldberg P. Advances in DNA methylation: 5-hydroxymethylcytosine revisited. Clin Chim Acta. 2011; 412(11-12): 831-836.
9. Jones PA. Functions of DNA methylation: islands, start sites, gene bodies and beyond. Nat Rev Genet. 2012; 13(7): 484-492.
10. Nikzad H, Karimian M, Sareban K, Khoshsokhan M, Hosseinzadeh Colagar A. MTHFR-Ala222Val and male infertility: a study in Iranian men, an updated meta-analysis and an in silico-analysis. Reprod Biomed Online. 2015; 31(5): 668-680.
11. Gaughan DJ, Barbaux S, Kluijtmans LA, Whitehead AS. The human and mouse methylenetetrahydrofolate reductase (MTHFR) genes: genomic organization, mRNA structure and linkage to the CLCN6 gene. Gene. 2000; 257(2): 279-289.
12. Garner JL, Niles KM, McGraw S, Yeh JR, Cushnie DW, Hermo L, et al. Stability of DNA methylation patterns in mouse spermatogonia under conditions of MTHFR deficiency and methionine supplementation. Biol Reprod. 2013; 89(5): 125.
13. Farthing CR, Ficz G, Ng RK, Chan CF, Andrews S, Dean W, et al. Global mapping of DNA methylation in mouse promoters reveals epigenetic reprogramming of pluripotency genes. PLoS Genet. 2008; 4(6).
14. Khazamipour N, Noruzinia M, Fatehmanesh P, Keyhanee M, Pujol P. MTHFR promoter hypermethylation in testicular biopsies of patients with non-obstructive azoospermia: the role of epigenetics in male infertility. Hum Reprod. 2009; 24(9): 2361-2364.
15. World Health Organization. WHO laboratory manual for the examination and processing of human semen. 5th ed. WHO Press; 2010.
16. Li LC, Dahiya R. MethPrimer: designing primers for methylation PCRs. Bioinformatics. 2002; 18(11): 1427-1431.
17. Houshdaran S, Cortessis VK, Siegmund K, Yang A, Laird PW, Sokol RZ. Widespread epigenetic abnormalities suggest a broad DNA methylation erasure defect in abnormal human sperm. PLoS One. 2007; 2(12): e1289.
18. Wu W, Shen O, Qin Y, Niu X, Lu C, Xia Y, et al. Idiopathic male infertility is strongly associated with aberrant promoter methylation of

methylenetetrahydrofolate reductase (MTHFR). PLoS One. 2010; 5(11): e13884.
19. Botezatu A, Socolov R, Socolov D, Iancu IV, Anton G. Methylation pattern of methylene tetrahydrofolate reductase and small nuclear ribonucleoprotein polypeptide N promoters in oligoasthenospermia: a case-control study. Reprod Biomed Online. 2014; 28(2): 225-231.
20. Rotondo JC, Bosi S, Bazzan E, Di Domenico M, De Mattei M, Selvatici R, et al. Methylenetetrahydrofolate reductase gene promoter hypermethylation in semen samples of infertile couples correlates with recurrent spontaneous abortion. Hum Reprod. 2012; 27(12): 3632-3638.
21. Oakes CC, La Salle S, Smiraglia DJ, Robaire B, Trasler JM. A unique configuration of genome-wide DNA methylation patterns in the testis. Proc Natl Acad Sci USA. 2007; 104(1): 228-233.
22. Oakes CC, Salle S, Smiraglia DJ, Robaire B, Trasler JM. Developmental acquisition of genome-wide DNA methylation occurs prior to meiosis in male germ cells. Dev Biol. 2007; 307(2): 368-379.
23. Karimian M, Aftabi Y, Mazoochi T, Babaei F, Khamechian T, Boojari H, et al. 2018. Survivin polymorphisms and susceptibility to prostate cancer: A genetic association study and an in silico analysis. EXCLI J. 2018; 17: 479-491.
24. Nejati M, Atlasi MA, Karimian M, Nikzad H, Azami Tameh A. Lipoprotein lipase gene polymorphisms as risk factors for stroke: a computational and meta-analysis. Iran J Basic Med Sci. 2018; 21(7): 701-708.
25. Jiang C, Pugh BF. Nucleosome positioning and gene regulation: advances through genomics. Nat Rev Genet. 2009; 10(3): 161-172.
26. Choi JK, Kim YJ. Epigenetic regulation and the variability of gene expression. Nat Genet. 2008; 40(2): 141-147.
27. Wang JP, Widom J. Improved alignment of nucleosome DNA sequences using a mixture model. Nucleic Acids Res. 2005; 33(21): 6743-6755.
28. Segal E, Widom J. What controls nucleosome positions? Trends Genet. 2009; 25(8): 335-343.
29. Radwan A, Younis A, Luykx P, Khuri S. Prediction and analysis of nucleosome exclusion regions in the human genome. BMC Genomics. 2008; 9: 186.
30. Su J, Zhang Y, Lv J, Liu H, Tang X, Wang F, et al. CpG_MI: a novel approach for identifying functional CpG islands in mammalian genomes. Nucleic Acids Res. 2010; 38(1): e6.

Original Article

Effects of Different Vitrification Solutions and Protocol on Follicular Ultrastructure and Revascularization of Autografted Mouse Ovarian Tissue

Mohammad Mahmoudi Asl, M.Sc.[1], Reza Rahbarghazi, Ph.D.[1], Rahim Beheshti, Ph.D.[2], Alireza Alihemmati, Ph.D.[3], Mohammad Reza Aliparasti, M.Sc.[4], Ali Abedelahi, Ph.D.[5*]

1. Stem Cell Research Center, Tabriz University of Medical Sciences, Tabriz, Iran
2. Department of Veterinary, Shabestar Branch, Islamic Azad University, Shabestar, Iran
3. Department of Anatomical Sciences, Tabriz University of Medical Sciences, Tabriz, Iran
4. Department of Immunology, Tabriz University of Medical Sciences, Tabriz, Iran
5. Department of Reproductive Biology, Faculty of Advanced Medical Sciences, Tabriz University of Medical Sciences, Tabriz, Iran

Corresponding Address: P.O. Box: 5166714766, Department of Reproductive Biology, Faculty of Advanced Medical Sciences, Tabriz University of Medical Sciences, Tabriz, Iran
Email: abedelahia@gmail.com

Received: 20/March/2019, Accepted: 27/July/2019

Abstract

Objective: Many attempts have been made to preserve fertility by improving the cryopreservation of the ovarian tissue. This current studyaimed to improve of direct cover vitrification (DCV) protocol on follicular preservation and angiogenesis in autografted ovarian tissue.

Materials and Methods: In this experimental study, sixty five female Balb/c mice (5-6 week-old) were anesthetized and their ovaries were dissected. The left ovaries were vitrified by DCV solution, thawed by descending concentrations of sucrose, and then autografted subcutaneously. The right ovaries were autografted with no vitrification procedure prior to transplantation. The animals were sacrificed under anesthesia on the 7th day after transplantation to obtain ovarian tissue. Follicular quality was assessed by histological and ultrastructure observations, and angiogenesis was examined by immunohistochemical staining and real-time polymerase chain reaction (PCR) analysis.

Results: The histological and ultrastructure features of the follicles preserved well after vitrification of the ovarian tissue by 10% ethylene glycol (EG) and 10% dimethyl sulfoxide (DMSO). Revascularizationwas manifested prominently in the DCV1-vitrified/grafted ovaries by von Willebrand factor (*vWF*) and alpha smooth muscle actin (*α-SMA*) immunostaining. The ovarian tissue vitrified in DCV1 protocol had higher expression levels of angiopoietin-2 (Ang-2) and vascular endothelial growth factor (*VEGF*) 7 days after autotransplantation (P<0.01).

Conclusion: These findings suggest that DCV with 10% of both EG and DMSO, is an effective cryopreservation solution for preservation of good quality follicles as well an upregulation of angiogenic factors after ovarian tissue transplantation.

Keywords: Angiogenesis, Cryopreservation, Graft, Mouse, Ovary

Cell Journal(Yakhteh), Vol 22, No 4, January-March (Winter) 2021, Pages: 491-501

Citation: **Mahmoudi Asl M, Rahbarghazi R, Beheshti R, Alihemmati A, Aliparasti MR, Abedelahi A. Effects of different vitrification solutions and protocol on follicular ultrastructure and revascularization of autografted mouse ovarian tissue. Cell J. 2021; 22(4): 491-501. doi: 10.22074/cellj.2021.6877.**

Introduction

Ovarian tissue cryopreservation and grafting are appropriate strategies for fertility preservation in women undergoing radiotherapy and chemotherapy (1). The cryopreservation process and cryoprotectant (CP) toxicity are inevitable aspects of ovarian tissue cryopreservation (2). Vitrification is a simple and efficient procedurefor preservation of the follicle quality in cryopreservation of ovarian tissue (3, 4). However, vitrification requires high concentrations of CPs and fast cooling rates, which can cause cell injury and follicle loss (5). Both ethylene glycol (EG) and dimethyl sulfoxide (DMSO) as CP agents have been used commonly in cryopreservation of the ovarian tissue, because of their low toxicity and rapid permeability (6, 7). Youm et al. (7) proposed that combining EG and DMSO through a stepwise increase in concentration could improve follicle preservation quality due to its lowertoxicity. Many attempts have been made to optimize vitrification protocols through assessing appropriate cryopreservation techniques, CP agents and concentrations, cryopreservation devices, equilibration, and warming times (7-10). Recently, many studies have focused on improving cryopreservation protocols by accelerating the cooling rate using ultra-rapid vitrification, such as DCV (10, 11). Our previous study illustrated that DCV is an efficient method for preserving ovarian tissue (12, 13).Transplantation of ovarian tissue is an excellent experimental model for evaluating the effects of CP agents on follicular viability and development.

A subcutaneous grafting site was selected based on Shubert's results (14). He reported that ovarian tissue was transplanted subcutaneously for accessible monitoring of angiogenesis and follicular morphology, which allowed for the preservation of ovarian integrity. The most important process in the early stages of ovarian transplantation is revascularization, which is regulated by angiogenic factors (15). It has been observed, however,

that transplantation of ovarian tissue is subject to hypoxia that leads to follicle loss (16). Therefore, detection of angiogenic factors in vitrified ovaries is crucial for monitoring and evaluating follicular development after transplantation.

Several ligands and receptors participate actively in angiogenesis signaling pathways including VEGF, Ang and tyrosine kinase (17, 18). Angiogenesis is primarily controlled by VEGF, which is produced mainly by theca and/or granulosa cells in ovarian tissue (19-21). VEGF is an endothelial cell mitogen that regulates neovascularization and vascular permeability in grafted ovarian tissue (19), and has been demonstrated to regulate follicular growth as well as folliculogenesis (20, 21). Ang-2 is another angiogenesis factor that destabilizes endothelial-endothelial cell connections, resulting in the migration of endothelial cells and promoting further angiogenesis (22).

In addition, vWF is a glycoprotein expressed exclusively in endothelial cells, and α-SMA is a marker of mature pericyte cells, which stabilize new blood vessels and are considered as early signs of neo-angiogenesis within vitrified/grafted ovaries (18, 23).

There are still many obstacles and limitations in DCV for preserving fertility in patients undergoing chemo- or radiotherapy for cancer. In this regard, the aim of this study was to evaluate the influence of different CP agents on autografted mouse ovarian tissue viability and revascularization using follicular morphology and ultrastructure, expression of angiogenesis factors, and endothelial and pericytes cell markers.

Material and Methods

Chemicals

All chemicals in this experimental study were purchased from Sigma-Aldrich (Sigma Chemical Co., Deisenhofen, Germany) unless otherwise mentioned.

Animals and ovarian tissue preparation

Sixty-five female Balb/c mice (5-6 week- old) were purchased from Tabriz University of Medical Sciencesand housed in standard conditions (12-hours light/12-hours dark, 22-25˚C and 55% humidity), according to the International Animal Care and Use Committee (IACUC) instructions, and were given free access to food and water. The animals were anesthetized with an intraperitoneal injection of ketamine (80 mg/kg IP) and xylazine (10 mg/kg IP).Then the ovaries were dissected through a small dorsolateral incision. The left ovaries were vitrified while the right ovaries were not vitrified as controls. The vitrified/thawed ovaries or non-vitrified ovaries were autografted into subcutaneous pockets in the lateral flank and placed on the lumbar muscles.

Direct cover vitrification procedure

Our direct cover vitrification (DCV) protocol was a modified version of the one used by Zhou et al. (11). The CP and warming solutions were prepared in Dulbecco's phosphate-buffered saline (DPBS).Three concentrations of the CP solution were prepared as follows:

i. 5% EG+5% DMSO+0.5 M sucrose+20% FBS (CP1)
ii. 10% EG+10% DMSO+0.5 M sucrose+20% FBS (CP2)
iii. 15% EG+15% DMSO+0.5 M sucrose+20% FBS (CP3)

The vitrified samples were prepared as follows:

i. Ovaries were vitrified sequentially to the CP1 and CP2 solutions for 12 minutes at room temperature (DCV1).
ii. Ovaries vitrified sequentiallyto the CP1 and CP3 solutions for 12 minutes at room temperature (DCV2).
iii. Ovaries equilibrated vitrified sequentiallyto the CP2 and CP3 solutions for 12 minutes at room temperature (DCV3).
iv. Ovaries vitrified sequentially to the CP1, CP2 and CP3 solutions for 12 minutes at room temperature (DCV4)

The surrounding vitrification medium was removed, and then, ovarian tissue was placed in a 1.8 plastic standard cryovial with a minimum volume of the vitrification solution and liquid nitrogen was applied directly in the cryovial (DCV). The cryovials were placed into a tank of liquid nitrogen (-196 ˚C) and kept for one week.

Thawing process

The cryovials containing vitrified ovaries were thawed in nitrogen vapor for 30 seconds, at room temperature for 30 seconds and then were put into a 38˚C water bath for 60 seconds. The ovarian tissue was suspended in 1 ml descending concentrations of sucrose (1, 0.5 and 0.25 M) and DPBS for 10 minutes. To evaluate the vitrification toxicity, a group of control ovaries were exposed to all stages of vitrification and thawing procedures except for being plunged into liquid nitrogen.

Histological evaluation

The ovaries (n=5 from each groups) were fixed in 10% formalin-buffered solution, dehydrated in serial alcohol washes, clarified with xylene, embedded in paraffin wax, and sequentially sectioned at 5 μm thickness. The 10^{th} section of each ovary was mounted on glass slides (five sections from each sample), stained with hematoxylin-eosin (H&E) solution and observed under a light microscope at a magnification of ×400 in 10 fields for each sample. The ovarian follicles with visible nuclei in the oocyte were noted at various stages of development. Primordial follicles were characterized by a single layer of flattened granulosa cells surrounding the oocyte; primary follicles had a single layer of cuboidal granulosa cells around the oocyte; preantral follicles were characterized by two or more layers of cuboidal granulosa cells and no antrum; and antral follicles were characterized by the presence of an antrum filled with follicular fluid. Follicular quality was assessed as normal, having intact oocyte and regular granulosa cells, or degenerated, with cytoplasmic

vacuolization, detachment of oocyte and granulosa cells and irregular granulosa cells with pyknotic nucleus (24).

Ultrastructureevaluation

Both fresh and vitrified ovaries (n=3 from each groups) were fixed in 2.5% glutaraldehyde (TAAB Laboratories Ltd., Berkshire, UK) in phosphate-buffered saline (PBS, pH=7.4) for 2 hours at room temperature, washed in PBS, then post-fixed in 1% osmium tetroxide (TAAB Laboratories Ltd., Berkshire, UK) in the same buffer for 2 hours at 4˚C. After washing in PBS, the samples were dehydrated in ascending concentrations of ethanol, placed in propylene oxide, and embedded in Epon 812 (TAAB Laboratories Ltd., Berkshire, UK). The samples were sectioned and 0.5 µm sections (semi-thin sections) were stained with toluidine blue and observed under light microscope. Thin sections (70 nm) were prepared using glass blades and placed on copper grids, stained with uranyl acetate and lead citrate (TAAB Laboratories Ltd., Berkshire, UK), and evaluated by transmission electron microscope (Zeiss, Germany). The granulosa cells and oocytes were evaluated by the integrity of the cytoplasmic and nuclear membranes, the number and size of the vesicles and the structure of the cytoplasmic organelles.

Immunohistochemical detection of endothelial and pericyte cells

The endothelial and pericyte cells were stained to identify new blood vessels in vitrified/grafted ovaries (n=3 from each group). The 5-µm paraffin sections (three serial sections from each sample) were deparaffinized with xyloland rehydrated in graded alcohol series (Merck, Germany). The sections were incubated with hydrogen peroxide (3%) inmethanol for 30 minutes at room temperature to block endogenous peroxidase. After autoclaving in the citrate buffer, the slides were incubated with the primary antibodies for 30 minutes:1/100 anti-vWF (Dako, Denmark) for staining endothelial cells, and 1/100 anti-α-SMA (Dako, Denmark) for staining smooth muscle cells. The slides were washed with PBS, and stained with the EnVision+Dual Link System HRP kit (Dako, Denmark), 3-Diaminobenzidine (DAB).

Each specimen was observed under a light microscope (×400) (Nikon, Japan). Single or clusters of endothelial cells positive for yWF (brown dye), were considered indicative of vessels formation. In the current experiment, the results from treatment groups were compared with those of the intact ovarian tissue from the control mice. All immunohistochemical analyses were done in three independent experiments.

Real-time polymerase chain reaction procedure

As angiogenesis-related genes were expected to be expressed following successful transplantation of ovarian tissue in the mice, VEGF and Ang-2 primers were designed for evaluation of the genes. For this purpose, all fresh and vitrified/grafted ovaries were immediately frozen in liquid nitrogen and stored at -196˚C for real-time polymerase chain reaction (PCR) analysis. The ovaries were collected for RNA extraction by Trizol Reagent (Invitrogen, USA) according to the manufacturer's recommendations. The specimens were treated with RNase-free DNase and single-stranded cDNAs and were synthesized by incubating 1 µg of isolated RNA. The real-time PCR analysis was carried out by the Corbett Life Science (Rotor-Gene 6000) System and Fast Start SYBR Green Master (Roche). Primer sequences for VEGF and Ang-2 are outlined in Table 1.

Table 1: Primers used for the real-time polymerase chain reaction assay

Gene name	Primer sequence (5´-3´)	Length (bp)
VEGF-a	F: GACAGAAGGAGAGCAGAAGTCC	223
	R: CATGGTGATGTTGCTCTCTGAC	
Ang-2	F: TGACGAGCTGGAGAAGAAGC	236
	R: TGGAGTTGGGGAAGGTCAGT	
β-microglobulin	F: CCTGGTCTTTCTGGTGCTTG	171
	R: CCGTTCTTCAGCATTTGGAT	

Real-time PCR amplifications were performed using the following program: denaturation of cDNA (1 cycle at 95˚C for 10 minutes), amplification (40 cycles at 95˚C for 15 seconds, 57˚C for 30 seconds and 63˚C for 38 seconds), and melting curve analysis (1 cycle at 60 to 95˚C with 1˚C/seconds). The mRNA expression levels were normalized by β-microglobulin (β-mg) and the quantification was evaluated using the $2^{(-\Delta\Delta Ct)}$ method. The assay was performed in triplicate.

Statistical analysis

Data was analyzed using SPSS 24 (IBM, International Business Machines Corp., New Orchard Road Armonk, New York). Quantitative data is reported as means ± SD. The normality of data was evaluated using theKolmogrov-Smirnov test, and the homogeneity of variance was assessed using Levene's test. Differences between the groups were evaluated using one-way analysis of variance (ANOVA). The results of real-time PCR were analyzed using the independent-samples t test as well as the Wilcoxon test. A value of $P<0.05$ was considered statistically significant.

Ethical consideration

All applicable international, national and institutional guidelines for the care and use of animals were followed by the IACUC of Tabriz University of Medical Sciences (No. 2004-0405). This article does not contain any studies with human participants performed by any of the authors.

Results

Histological examination

The morphology of primordial and primary follicles from vitrified ovarian tissue was well preserved, but some cryoinjury such as detachment of oocytes and granulosa cells was observed in the vitrified/grafted groups (Fig.1). After transplantation, the morphology of preantral and antral follicles was preserved significantly better in the ovaries from vitrified/grafted with DCV1 in comparison with the other vitrified/grafted groups (Fig.1B). Preantral and antral follicles from ovarian tissue vitrified with DCV2, DCV3, and DCV4 after transplantation showed numerous ultrastructural alterations, such as oocyte shrinkage, numerous cytoplasmic vacuoles, stromal fibrosis, and detachment of the oocyte from granulosa cells (Fig.1C-E).

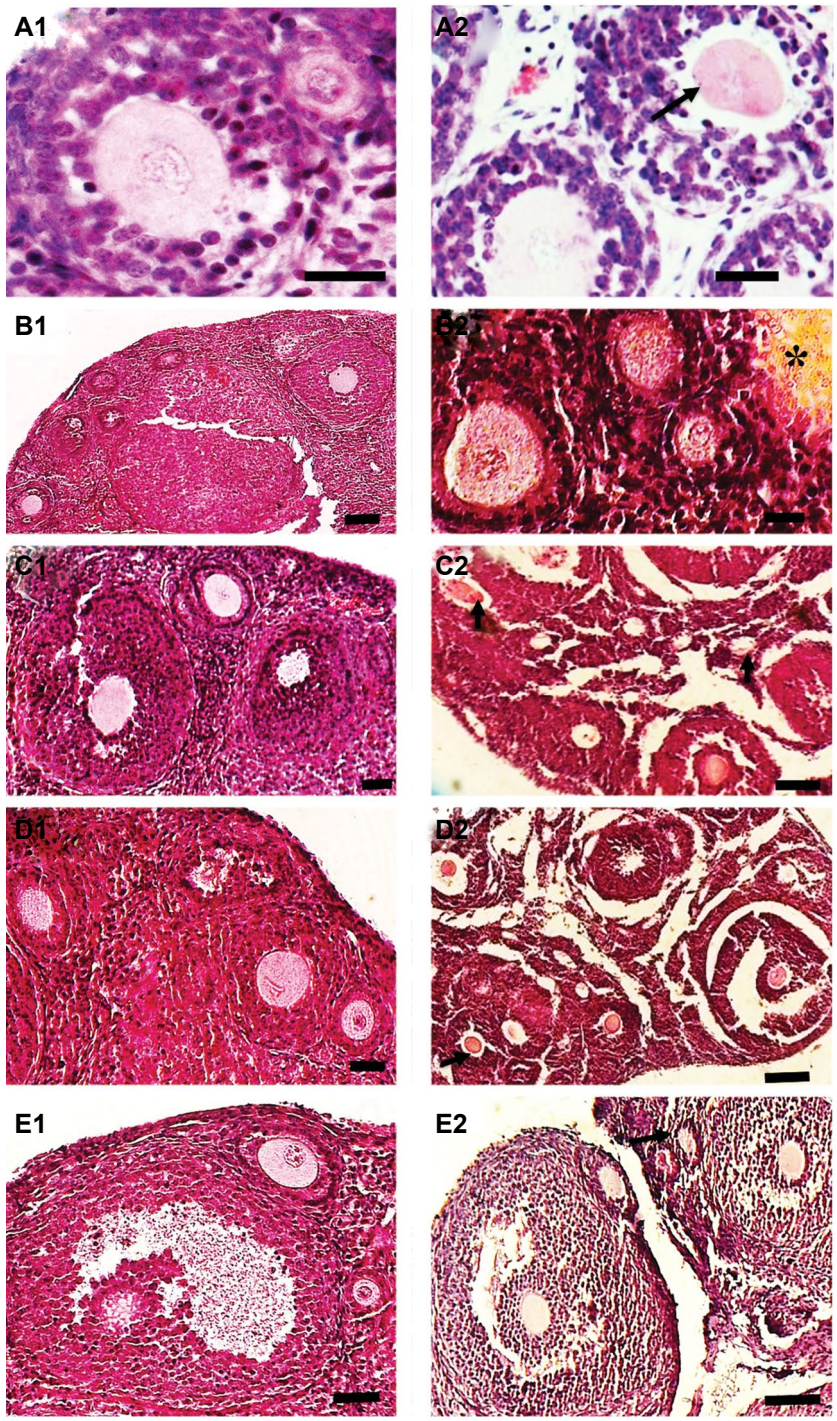

Fig.1: Histological images of mouse ovarian tissue. **A1.** Intact, **A2.** Fresh grafted, **B1.** Vitrified with DCV1, **B2.** Vitrified with DCV1/grafted, **C1.** Vitrified with DCV2, **C2.** Vitrified with DCV2/grafted, **D1.** Vitrified with DCV3, **D2.** Vitrified with DCV3/grafted, **E1.** Vitrified with DCV4, and **E2.** Vitrified with DCV4/grafted. The follicular integrity and stromal tissue structure was well-preserved in the fresh and vitrified ovaries before transplantation. In the ovarian tissues vitrified with DCV2, DCV3 and DCV4 after transplantationmore signs of cryodamage, such as cytoplasmic retraction, shrinkage of the oocyte (black arrow) and fibrotic tissues (star), were observed (scale bar: 50 µm). DCV; Direct cover vitrification.

Ultrastructure analysis

The ultrastructure of the follicles in vitrified ovaries showed a well-developed cytoplasmic organelle, round mitochondria and continuous membranes. The majority of cryoinjuries were observed commonly in preantral and antral follicles from vitrified/grafted ovaries and included nuclei shrinkage, damaged basement membrane of granulosa cells, irregular distribution of cytoplasmic organelles together with the accumulation of vacuoles. The ultrastructure of the preantral and antral follicles from ovarian tissue vitrified/grafted with DCV1 was well preserved and showed great similarity with the control group (Fig.2).

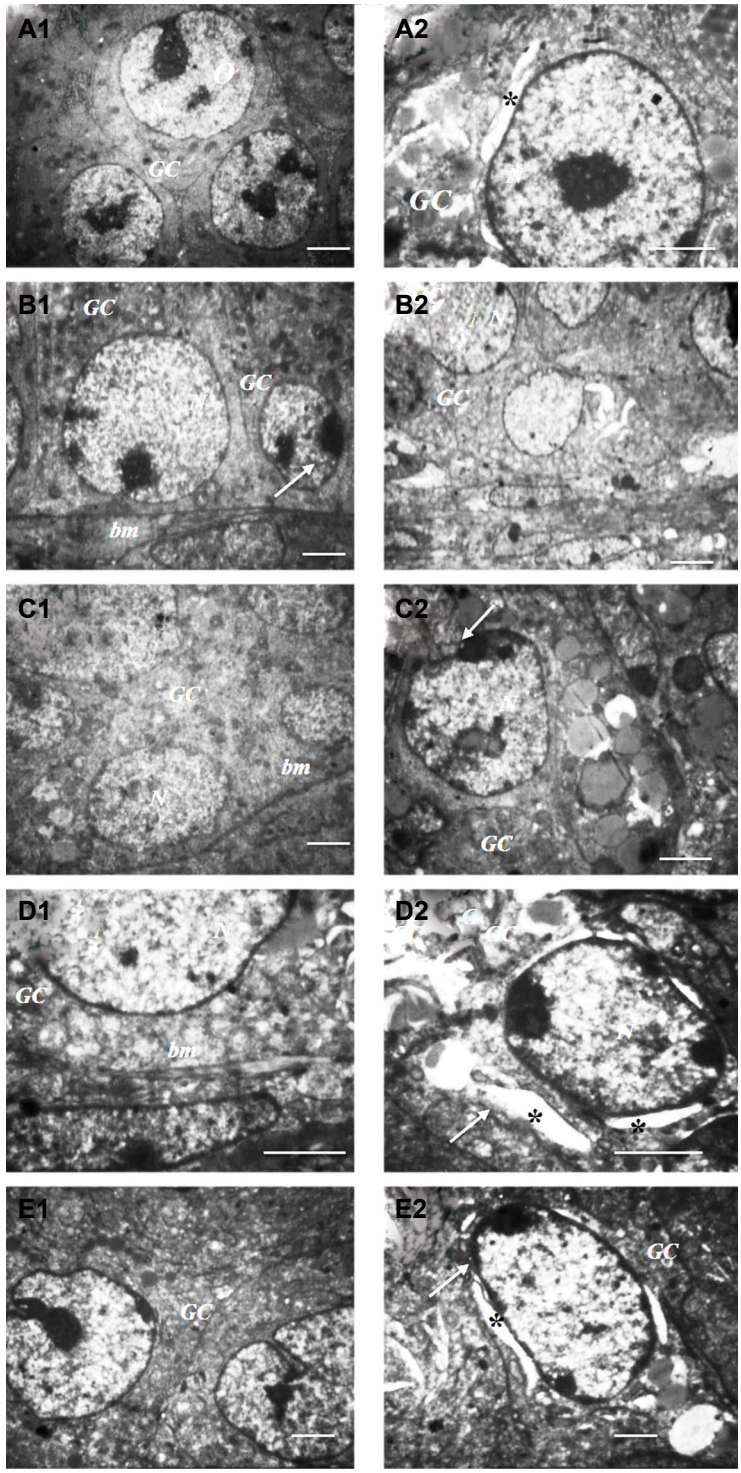

Fig.2: Ultrastructure of the antral follicles in murine ovarian tissue. **A1.** Intact, **A2**. Fresh grafted, **B1**. Vitrified with direct cover vitrification1 (DCV1), **B2**. Vitrified with DCV1/grafted, **C1**. Vitrified with DCV2, **C2.** Vitrified with DCV2/grafted, **D1.** Vitrified with DCV3, **D2.** Vitrified with DCV3/grafted, **E1.** Vitrified with DCV4, and **E2.** Vitrified with DCV4/grafted. The ultrastructures of cytoplasmic organelles in vitrified ovarieswere well-organized before transplantation. Granulosa cells (GC) hadnormal basement membrane (bm) and normal nucleus (N). After transplantation,more signs of damage were observed in vitrified ovaries including nucleus shrinkage in granulosa cells (white arrow) and perinuclear space (PS) (star) (scale bar: 500 µm).

The ultrastructure of the follicles was well-preserved in the control group (Fig.3A) and swollen mitochondria with a few cristae were found in antral follicles from fresh/grafted ovaries (Fig.3B). Mitochondria showed the most signs of malformation and vacuolization in preantral and antral follicles from vitrified/grafted ovaries (Fig.3C-F). Theseirregularly shaped mitochondria were prominent in vitrified/grafted ovaries with DCV2, DCV3 and DCV4 (Fig.3D-F). Damaged zona pellucida was observed in some follicles from vitrified/grafted ovaries, in which wider empty spaces between the oocyte and the granulosa cells were identified (Fig.3G-I). Moreover, numerous blood vessels were detected in vitrified ovarian tissue after transplantation (Fig.3K), but newly formed blood vessels were frequently observed in ovaries vitrified/grafted with DCV1 (Fig.3L-N).

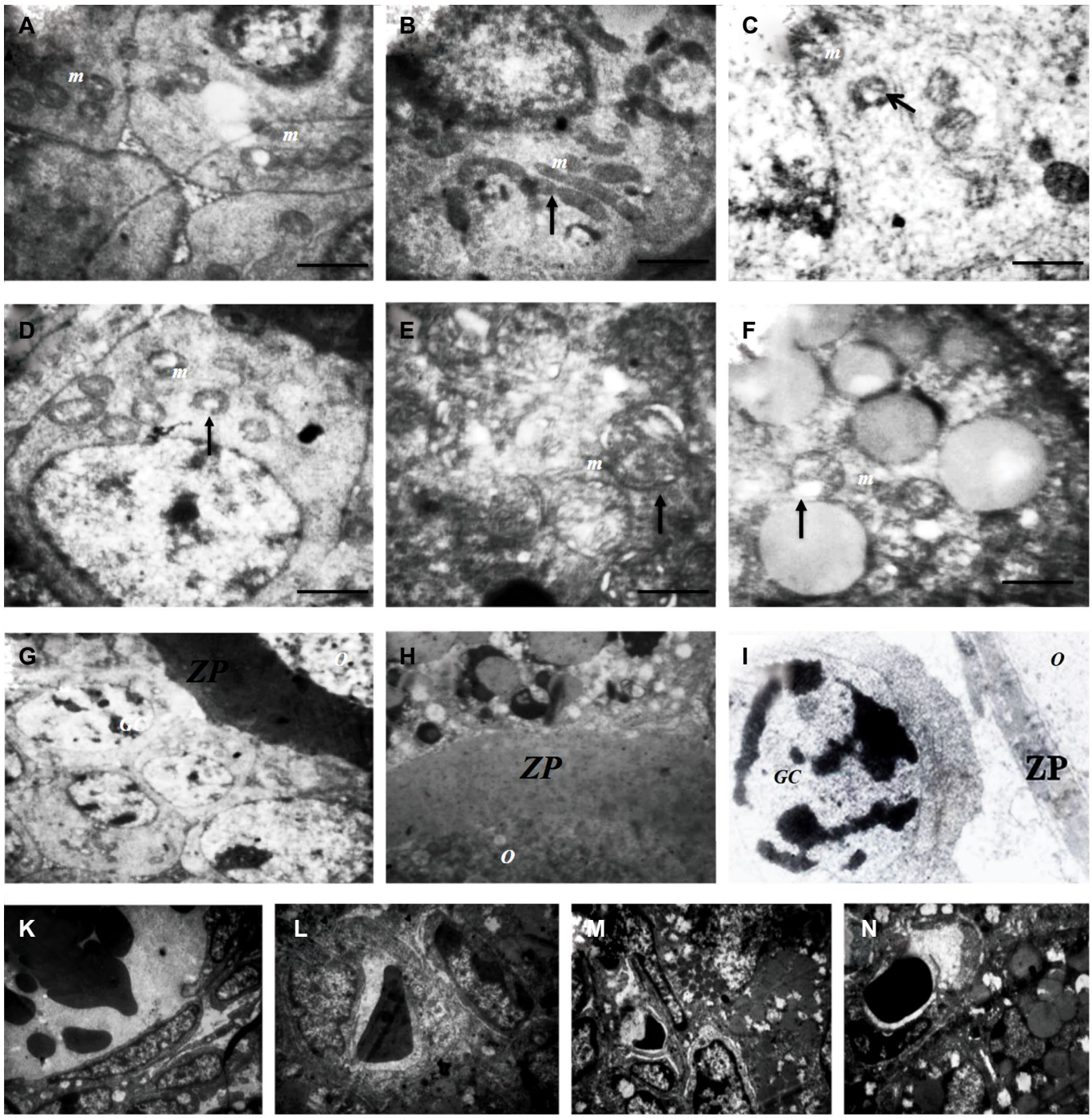

Fig.3: Ultrastructure of the mitochondria in antral follicle in murine ovarian tissue. **A**. Intact, **B.** Fresh grafted, **C.** Vitrified with DCV1/grafted, **D.** Vitrified with DCV2/grafted, **E**. Vitrified with DCV3/grafted, and **F.** Vitrified with DCV4/grafted. Ultrastructure of the zona pellucid (ZP) in the antral follicles: **G**. Vitrified with DCV1, **H.** Fresh grafted, **I.** Vitrified with DCV1/grafted. Ultrastructure of the blood vessels in murine ovarian tissue: **K.** Vitrified with DCV1/grafted, **L.** Vitrified with DCV2/grafted, **M.** Vitrified with DCV3/grafted, and **N.** Vitrified with DCV4/grafted (scale bar: 500 µm). Numerous swollen mitochondria (m) and elongated mitochondria (black arrow) with a few cristae were observed in vitrified ovaries after transplantation. Damaged ZP was observed between oocyte (O) and granulosa cells (GC) inantral follicles. Vascular endothelial cells in the vessel lumen are detected frequently in vitrified ovarian tissue after transplantation.

Immunohistochemical analysis

Re-vascularization was detectable 7 days after autotransplantation of vitrified ovarian tissue, as indicated by the expression of α-SMA as a marker of smooth muscle cells or vWF as a marker of endothelial cells (Fig.4). Immunohistochemical analysis showed that the expression of vWF and α-SMA was more prominent in the ovarian tissue vitrified with DCV1 than in the vitrified ovarian tissue with DCV2, DCV3, and DCV4 after transplantation. This observation indicated that with regard to vascularization DCV1 was the suitable protocol for potent revascularization in vitrified ovarian tissue after transplantation.

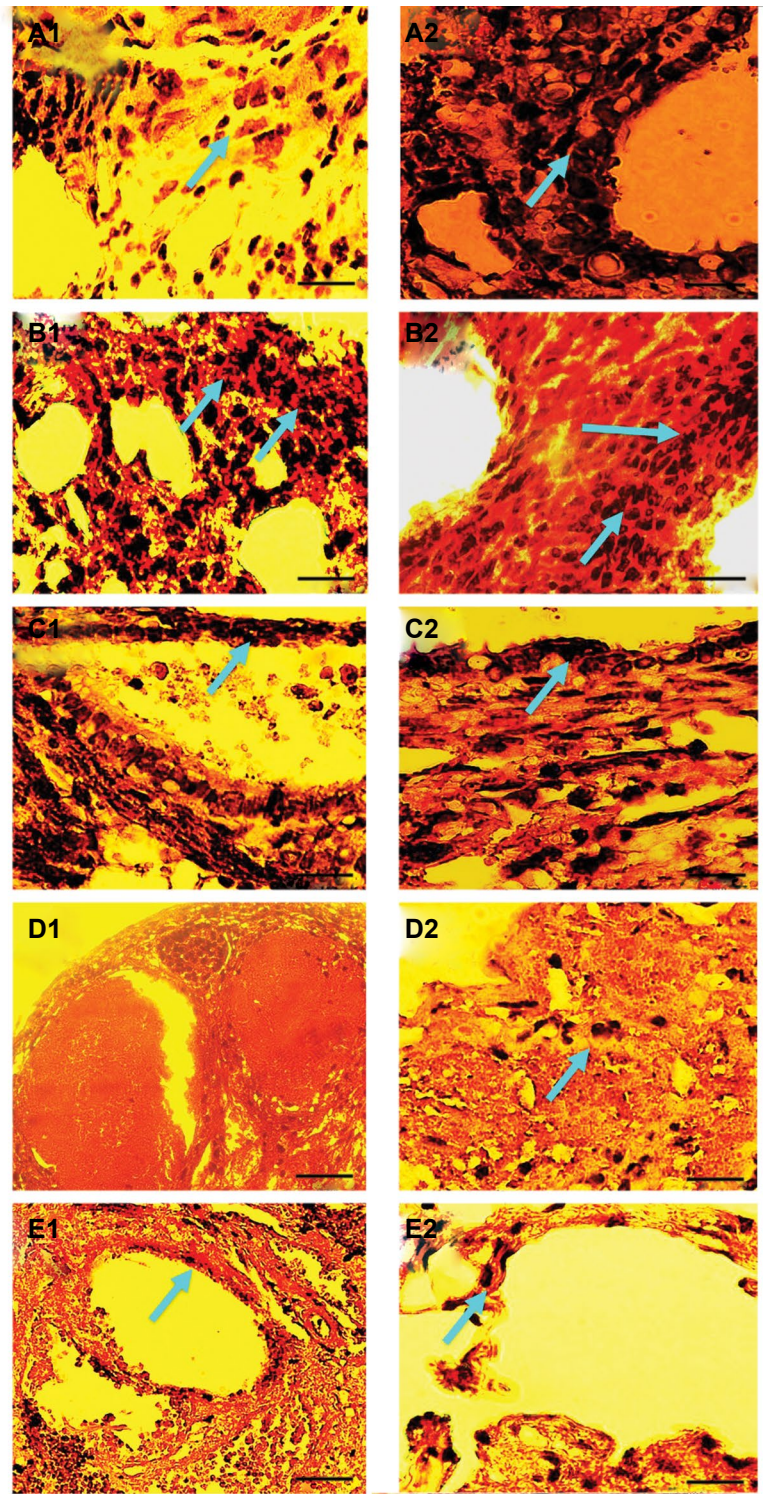

Fig.4: Immunohistochemical staining of new blood vessels in vitrified ovarian tissue after transplantation by the expression of α-SMA and vWF. **A1**. α-SMA and **A2.** vWF expression in non-vitrified/grafted ovaries. **B1.** α-SMA and **B2.** vWF expression in vitrified with DCV1/grafted. **C1.** α-SMA and **C2.** vWF expression in DCV2-vitrified with /grafted. **D1.** α-SMA and **D2.** vWF expression in vitrified with DCV3/grafted. **E1.** α-SMA and **E2.** vWF expression in vitrified with DCV4/grafted ovarian tissue (scale bar: 10 µm). The expression of α-SMA and vWF was more prominent in cryopreserved ovaries with DCV1 following autotransplantation in comparison with the other groups. The positive cells are indicated by blue arrows.

Real-time polymerase chain reaction analysis

The expression levels of *VEGF* and *Ang-2* were detected in order to demonstrate the successful angiogenesis in vitrified/grafted ovarian tissue after transplantation (Fig.5). Real-time PCR analysis showed that *VEGF* and *Ang-2* genes were expressed in all vitrified/grafted ovaries following transplantation. The expression levels of both *VEGF* and *Ang-2* were increased significantly in ovarian tissue vitrified with DCV1 in comparison with the other vitrified ovaries post-transplantation (P<0.01). The levels of *VEGF* and *Ang-2* in DCV1 group did not differ from fresh ovaries.

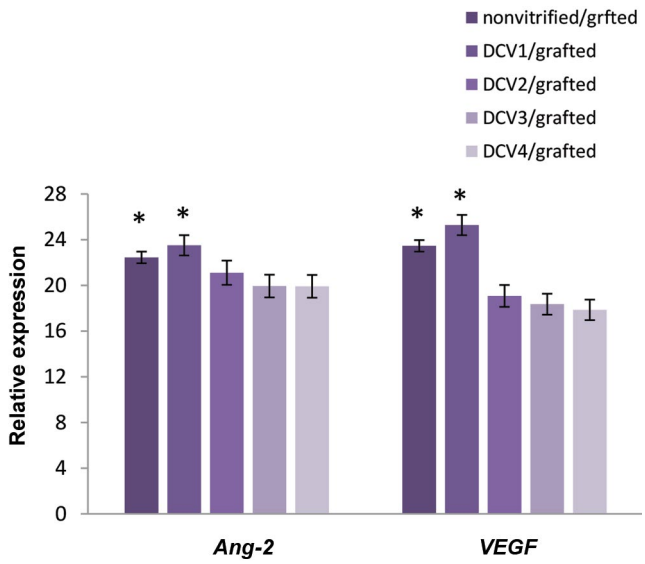

Fig.5: The expression levels of *VEGF* and *Ang-2* in vitrified ovarian tissue after transplantation by real time-polymerase chain reaction (PCR) analysis.*; Both angiogenic genes, *VEGF* and *Ang-2* were expressed at significantly higher levels in the ovarian tissue cryopreserved with DCV1 in comparison to the other groups after autotransplantation (P<0.01).

Discussion

Evaluation of angiogenesis has proven to be a useful tool for the assessment and comparison of the results of different CP agents and protocols on transplanted ovarian tissue. In addition, transplantation of ovaries provides a direct way to examine follicular viability and development during cryopreservation. In this study, it was shown that the histological features and ultrastructure of follicles were better preserved in ovarian tissue vitrified by EG and DMSO in a concentration of 10% after transplantation. Furthermore, high expression levels of VEGF and Ang-2, which are crucial angiogenic factors, were observed in the cryopreserved ovarian tissue after subcutaneous ovary autotransplantation.

The current study illustrated that more histological degeneration was observed in oocyte and granulosa cells from ovaries vitrified/grafted in EG and DMSO mixture at a concentration of 15%. The evidence of degeneration included detachment of the innermost granulosa cells from the oocyte, oocyte shrinkage, and disarrangement of granulosa cells. The consistency that was observed between the ultrastructure and histological data confirmed that the organelles of granulosa cells and oocytes were well-preserved in the ovaries vitrified/grafted in DCV1. The greatest extent of follicular damage occurred during autotransplantation in cryopreserved ovarian tissue when a higher concentration of CP agent was used. These damages included vacuolization, lipid droplet distribution and swollen mitochondria with abnormal cristae. In this study, the grafted ovarian tissue following vitrification with DCV1 showed a remarkable microvessel density compared to the other vitrification protocols due to the reduction in cryoinjury.

Vitrification is a useful technique for cryopreservation of ovarian tissue (3-7). Nonetheless, CP toxicity is a main challenge in vitrification, but it can be limited by manipulating the nature and concentrations of the CP agents as well as the cooling rate (4, 6, 7, 10, 11). A fast cooling rate has been achieved in the DCV protocol, where ovarian tissue is plunged directly into liquid nitrogen. The current study suggests that the optimal vitrification concentration appears to play an important role in ovarian tissue cryopreservation. Therefore, a critical challenge in cryobiology is to obtain an optimal concentration of CP with low biological toxicity (25).

Our study in contrast with the Leonel et al. (26) results indicated that using the mixed cryopreservation technique by a stepwise addition of CP agents provides the best condition for cryopreservation of mouse ovarian tissue. These conflicting results may be explained by differences in protocols, CP solutions and concentrations, exposure times, or species. In the current study, follicular integrity at various stages of development was preserved in the cryopreserved ovarian tissue by using 10% EG and 10% DMSO through sufficient dehydration and penetration into ovarian tissue. However, vitrification procedures need to be optimized to minimize follicular failure after cryopreservation and grafting of ovarian tissue.

In this study, mitochondria were commonly damaged during the vitrification and transplantation of ovarian tissues. The mitochondrial organization is necessary for producing energy, Ca^{2+} signaling, regulating cell viability and cell function (27, 28). Several studies have indicated that the damaged mitochondria following vitrification may lead to in appropriate metabolic activity, reduced ATP levels, or disruption of the cytoskeleton proteins, and thereby result in free radical production (29).

Dare et al. (30) demonstrated that prolonged cryopreservation of the heart increased mitochondrial free radical production and ischemia-reperfusion damage during grafting. Therefore, it is suggested that ischemic and hypoxia conditions are the main causes of follicular loss after ovarian tissue transplantation, due to the production of free radicals (31, 32). It can be assumed

that mitochondrial damage during vitrification and transplantation not only induces free radical production and apoptosis, but also causes ischemic conditions, and thereby leads to delayed revascularization.

In this study, it was found that the microvasculature distribution occurs mainly within the first week after transplantation based on observations of the ultrastructure and immunohistochemical examination. In particular, the markers of the vascular endothelial cells and pericyte cells were prominently found in ovarian tissue vitrified and grafted with EG and DMSO in concentrations of 10%, suggesting that the vascularization had returned to normal levels.

According to real-time PCR results, expression of *VEGF* and *Ang-2* was detected in the vitrifying and grafting ovarian tissues, which explains the promotion of angiogenesis in ovarian tissue post-transplantation. A significantly high level of *VEGF* expression was observed after transplantation in the ovarian tissue vitrified by 10% EG and 10% DMSO. Therefore, *VEGF* seems to be a critical index for predicting the success rate of vitrified/grafted ovaries and may result in the improvement of follicular integrity preservation during transplantation. Furthermore, it was found that the expression of *VEGF* and *Ang-2* was diminished in cryopreserved ovarian tissue that had high concentrations of CP, suggesting that angiogenesis is adversely disrupted by vitrification and transplantation, and thus reduces ovarian function due to the initial ischemia.

It appears that VEGF, Ang-1 and Ang-2 as angiogenic factors are expressed in endothelial cells under normal or pathological conditions (33). The most recognized angiogenic factor expressed in ovarian tissue is VEGF (34). It was hypothesized that high expression levels of VEGF induce the formation of new blood vessels after ovarian tissue transplantation and that Ang-2 promotes neovascularization and stabilizes new blood vessels in the presence of VEGF (35). These findings suggest that there is a positive correlation between the expression of angiogenic factors and the endothelial cell markers in grafted ovaries. Therefore, high expression of VEGF and Ang-2 can predict the success of a cryopreservation protocol and agent on ovarian tissue during vitrification and grafting. In accordance with a study by Lee et al. (16), our current results have demonstrated that ovarian tissue subjected to a combination of vitrification and transplantation procedures may suffer from massive follicular damage during the initial days after ovarian transplantation. Grafting was much more detrimental to ovarian tissue than the vitrification procedure because of delayed tissue revascularization. Moreover, it was observed that large follicles including preantral and antral follicles were much more vulnerable to ischemic damage due to the high level of metabolite activity and delayed revascularization (36).

The main limitation in transplantation is ischemic reperfusion damage (37) and graft site plays a critical role in the revascularization of grafting tissue. Expressed angiogenic factors at a graft site induced the formation of new blood vessels in the grafted ovaries, and the improvement of angiogenesis could be an efficient strategy for evaluating a cryopreservation protocol (14). The results of Schubert et al. (14) suggested that the subcutaneous space is a convenient heterotopic transplantation site for the restoration of ovarian function and provision of follicular growth. In agreement with the results of Yang et al. (38), our data suggested that ovarian tissue autografted to a subcutaneous site could preserve follicular viability and ovarian function as a result of revascularization in the grafted site.

Although the subcutaneous area does not have a high blood supply, it was selected because it was easier to observe and follow up the situation of the grafted ovarian tissue and the transplantation surgery was easy to perform in experiments using murine models (14, 16). Revascularization is very important to minimizing ischemia damage,thereby facilitating angiogenesis and restoring ovarian function after transplantation in vitrified ovaries are crucial. Moreover, angiogenesis and revascularization in the early stage of transplantation are essential for follicular preservation and viability, allowing the follicular cells to provide oxygen and other vital factors (36). The current results are in agreement with previous studies, which illustrated that angiogenesis in vitrified ovaries initiates within 48 hours after transplantation and is elevated during 7 days after transplantation by an increase in expression of angiogenic factors (39).

It has been indicated that VEGF protects granulosa cells from undergoing apoptosis during ovarian cryopreservation and that it maintains the follicular pool (40). Interestingly, the current results suggest that VEGF and Ang-2 have a synergistic effect on the revascularization of cryopreserved ovarian tissue after grafting. Moreover, the expression of VEGF and Ang-2 is critical for the evaluation of optimal CP agents in the cryopreservation of ovarian tissue.

Conclusion

The present study demonstrated that DCV is an effective protocol for cryopreservation of ovarian tissue. In addition, the solution of EG and DMSO in concentrations of 10% is the most efficacious CP agent for preserving follicular viability and development after transplantation of ovarian tissue, because it facilitates angiogenesis and improves revascularization capability through higher expression of angiogenic factors. However, further research is needed to optimize the vitrification processes to preserve follicular integrity in grafted ovaries.

Acknowledgements

This study was funded by a grant from Stem Cell Research Center at Tabriz University of Medical Sciences (Grant No.9327-5). The authors would like to thanks Dr. Daryosh Mohammadnejad and Ayda Azami for technical

assistance in electron microscopy. The authors declare no conflicts of interest in this study.

Authors' Contributions

M.M.A.; Contributed to all experimental work, acquisition of data, and evaluation. R.R.; Contributed to immunohistochemical detection, contributed extensively in interpretation of the data, and also the conclusion. R.B.; Contributed to ovarian tissue preparation and surgical processes. A.R.A.; Contributed to histological and ultrastructure analysis. M.R.A.; Conducted molecular experiments and real-time PCR analysis. A.A.; Were responsible for overall supervision, manuscript drafting and statistical analysis. All authors performed editing and approving the final version of this manuscript for submission, also participated in the finalization of the manuscript and approved the final draft.

References

1. Donnez J, Dolmans MM, Pellicer A, Diaz-Garcia C, Sanchez Serrano M, Schmidt KT, et al. Restoration of ovarian activity and pregnancy after transplantation of cryopreserved ovarian tissue: a review of 60 cases of reimplantation. Fertil Steril. 2013; 99(6): 1503-1513.
2. Mathias FJ, D'Souza F, Uppangala S, Salian SR, Kalthur G, Adiga SK. Ovarian tissue vitrification is more efficient than slow freezing in protecting oocyte and granulosa cell DNA integrity. Syst Biol Reprod Med. 2014; 60(6): 317-322.
3. Ramezani M, Salehnia M, Jafarabadi M. Vitrification and in vitro culture had no adverse effect on the follicular development and gene expression of stimulated human ovarian tissue. J Obstet Gynaecol Res. 2018; 44(3): 474-487.
4. Li YB, Zhou CQ, Yang GF, Wang Q, Dong Y, Morrow T, et al. Modified vitrification method for cryopreservation of human ovarian tissues. Chin Med J (Engl). 2007; 120(2): 110-114.
5. Zhang JM, Li LX, Liu XL, Yang YX, Wan XP. Sucrose affecting successful transplantation of vitrified-thawed mouse ovarian tissues. J Assist Reprod Genet. 2009; 26(2-3): 137-142.
6. Nateghi R, Alizadeh A, JafariAhangari Y, Fathi R, Akhlaghi A. Ethylene glycol and dimethyl sulfoxide combination reduces cryoinjuries and apoptotic gene expression in vitrified laying hen ovary. Biopreserv Biobank. 2017; 15(6): 519-528.
7. Youm HW, Lee JR, Lee J, Jee BC, Suh CS, Kim SH. Optimal vitrification protocol for mouse ovarian tissue cryopreservation: effect of cryoprotective agents and in vitro culture on vitrified-warmed ovarian tissue survival. Hum Reprod. 2014; 29(4): 720-730.
8. Lima GL, Luz VB, Lunardi FO, Souza ALP, Peixoto GCX, Rodrigues APR, et al. Effect of cryoprotectant type and concentration on the vitrification of collared peccary (Pecaritajacu) ovarian tissue. Anim Reprod Sci. 2019; 205: 126-133.
9. Ladanyi C, Mor A, Christianson MS, Dhillon N, Segars JH. Recent advances in the field of ovarian tissue cryopreservation and opportunities for research. J Assist Reprod Genet. 2017; 34(6): 709-722.
10. Chen SU, Chien CL, Wu MY, Chen TH, Lai SM, Lin CW, et al. Novel direct cover vitrification for cryopreservation of ovarian tissues increases follicle viability and pregnancy capability in mice. Hum Reprod. 2006; 21(11): 2794-2800.
11. Zhou XH, Wu YJ, Shi J, Xia YX, Zheng SS. Cryopreservation of human ovarian tissue: comparison of novel direct cover vitrification and conventional vitrification. Cryobiology. 2010; 60(2): 101-115.
12. Ghavami M, Mohammadnejad D, Beheshti R, Solmani-rad J, Abedelahi A. Ultrastructural and morphalogical changes of mouse ovarian tissues following direct cover vitrification with different cryoprotectants. J Reprod Infertil. 2015; 16(3): 138-147.
13. Tayefi-Nasrabadi H, Gavami M, Akbarzadeh A, Beheshti R, Mohammadnejad D, Abedelahi A. Preservation of mouse ovarian tissue follicle morphology and ultra-structure after vitrifying in biotechnological protocols. J Ovarian Res. 2015; 8: 7.
14. Schubert B, Canis M, Darcha C, Artonne C, Smitz J, Grizard G. Follicular growth and estradiol follow-up after subcutaneous xenografting of fresh and cryopreserved human ovarian tissue. Fertil Steril. 2008; 89(6): 1787-1794.
15. Gao J, Huang Y, Li M, Zhao H, Zhao Y, Li R, et al. Effect of local basic fibroblast growth factor and vascular endothelial growth factor on subcutaneously allotransplanted ovarian tissue in ovariectomized mice. PLoS One. 2015; 10(7): e0134035.
16. Lee J, Kong HS, Kim EJ, Youm HW, Lee JR, Suh CS, et al. Ovarian injury during cryopreservation and transplantation in mice: a comparative study between cryoinjury and ischemic injury. Hum Reprod. 2016; 31(18): 1827-1837.
17. Cheraghi O, Dehghan G, Mahdavi M, Rahbarghazi R, Rezabakhsh A, Charoudeh HN, et al. Potent anti-angiogenic and cytotoxic effect of conferone on human colorectal adenocarcinoma HT-29 cells. Phytomedicine. 2016; 23(4): 398-405.
18. Siavashi V, Nassiri SM, Rahbarghazi R, Vafaei R, Sariri R. ECM-Dependence of endothelial progenitor cell features. J Cell Biochem. 2016; 117(8): 1934-1946.
19. Mattioli M, Barboni B, Turriani M, Galeati G, Zannoni A, Castellani G, et al. Follicle activation involves vascular endothelial growth factor production and increased blood vessel extension. Biol Reprod. 2001; 65(4): 1014-1019.
20. Araújo VR, Duarte AB, Bruno JB, Pinho Lopes CA, de Figueiredo JR. Importance of vascular endothelial growth factor (VEGF) in ovarian physiology of mammals. Zygote. 2013; 21(3): 295-304.
21. Asadi E, Najafi A, Moeini A, Pirjani R, Hassanzadeh G, Mikaeili S, et al. Ovarian tissue culture in the presence of VEGF and fetuin stimulates follicle growth and steroidogenesis. J Endocrinol. 2017; 232(2): 205-219.
22. Lin Z, Liu Y, Sun Y, He X. Expression of Ets-1, Ang-2 and maspin in ovarian cancer and their role in tumor angiogenesis. J Exp Clin Cancer Res. 2011; 30: 31.
23. Zanetta L, Marcus SG, Vasile J, Dobryansky M, Cohen H, Eng K, et al. Expression of von Willebrand Factor, an endothelial cell marker, is up-regulated by angiogenesis factors: a potential method for objective assessment of tumor angiogenesis. Int J Cancer. 2000; 85(2): 281-288.
24. Candy CJ, Wood MJ, Whittingham DG. Effect of cryoprotectants on the survival of follicles in frozen mouse ovaries. J Reprod Fertil. 1997; 110(1): 11-19.
25. Courbiere B, Odagescu V, Baudot A, Massardier J, Mazoyer C, Salle B, et al. Cryopreservation of the ovary by vitrification as an alternative to slow-cooling protocols. Fertil Steril. 2006; 86(4 Suppl): 1243-1251.
26. Leonel ECR, Vilela JMV, Carrilho DJ, Lucci CM. Cat ovarian follicle ultrastructure after cryopreservation with ethylene glycol and dimethyl sulfoxide. Cryobiology. 2018; 83: 9-14.
27. Liu L, Hammar K, Smith P, Inoue S, Keefe DL. Mitochondrial modulation of calcium signaling at the initiation of development. Cell Calcium. 2001; 30(6): 423-433.
28. Baril G, Traldi AL, Cognié Y, Lebeouf B, Beckers JF, Mermillod P. Successful direct transfer of vitrified sheep embryos. Theriogenology. 2001; 56(2): 299-305.
29. Zampolla T, Spikings E, Srirangarajah S, Rawson DM, Zhang T. Impact of cryoprotectants and cryopreservation on metabolic activity and cytoskeleton proteins of zebrafish (Danio rerio) ovarian fragments. Cryo Letters. 2011; 32(6): 525-536.
30. Dare AJ, Logan A, Prime TA, Rogatti S, Goddard M, Bolton EM, et al. The mitochondria-targeted anti-oxidant MitoQ decreases ischemia-reperfusion injury in a murine syngeneic heart transplant model. J Heart Lung Transplant. 2015; 34(11): 1471-1480.
31. Abedelahi A, Salehnia M, Allameh A, Davoodi D. Sodium selenite improves the in vitro follicular development by reducing the reactive oxygen species level and increasing the total antioxidant capacity and glutathione peroxide activity. Hum Reprod. 2010; 25(4): 977-985.
32. Jassem W, Fuggle SV, Rela M, Koo DD, Heaton ND. The role of mitochondria in ischemia/reperfusion injury. Transplantation. 2002; 73(4): 493-499.
33. Rahbarghazi R, Nassiri SM, Ahmadi SH, Mohammadi E, Rabbani S, Araghi A, et al. Dynamic induction of pro-angiogenic milieu after transplantation of marrow-derived mesenchymal stem cells in experimental myocardial infarction. Int J cardiol. 2014; 173(3): 453-466.
34. Hazzard TM, Molskness TA, Chaffin CL, Stouffer RL.Vascular endothelial growth factor (VEGF) and angiopoietin regulation by gonadotrophin and steroids in macaque granulosa cells during the peri-ovulatory interval. Molecular Hum Reprod. 1999; 5(12): 1115-1121.
35. Asahara T, Chen D, Takahashi T, Fujikawa K, Kearney M, Magner M, et al. Tie2 receptor ligands, angiopoietin-1 and angiopoietin-2,

modulate VEGF-induced postnatal neovascularization. Circ Res. 1998; 83(3): 233-240.
36. Liu J, Van der Elst J, Van den Broecke R, Dhont M. Early massive follicle loss and apoptosis in heterotopically grafted newborn mouse ovaries. Hum Reprod. 2002; 17(3): 605-611.
37. Bedaiwy MA, Jeremias E, Gurunluoglu R, Hussein MR, Siemianow M, Biscotti C, et al. Restoration of ovarian function after autotransplantation of intact frozen-thawed sheep ovaries with microvascular anastomosis. Fertil Steril. 2003; 79(3): 594-602.
38. Yang H, Lee HH, Lee HC, Ko DS, Kim SS. Assessment of vascular endothelial growth factor expression and apoptosis in the ovarian graft: can exogenous gonadotropin promote angiogenesis after ovarian transplantation? Fertil Steril. 2008; 90(4 Suppl): 1550-1558.
39. Wu D, Lei Y, Tong Y, Tang F, Qian Y, Zhou Y. Angiogenesis of the frozen-thawed human fetal ovarian tissue at the early stage after xenotransplantation and the positive effect of salviae miltiorrhizae. Anat Rec (Hoboken). 2010; 293(12): 2154-2162.
40. Roberts AE, Arbogast LK, Friedman CI, Cohn DE, Kaumaya PT, Danforth DR. Neutralization of endogenous vascular endothelial growth factor depletes primordial follicles in the mouse ovary. Biol Reprod. 2007; 76(2): 218-223.

A VHH-Based Anti-MUC1 Chimeric Antigen Receptor for Specific Retargeting of Human Primary T Cells to MUC1-Positive Cancer Cells

Alireza Rajabzadeh, Ph.D.[1], Fatemeh Rahbarizadeh, Ph.D.[2*], Davoud Ahmadvand, Ph.D.[3], Maryam Kabir Salmani, Ph.D.[4], Amir Ali Hamidieh, M.D.[1, 5*]

1. Department of Tissue Engineering and Applied Cell Sciences, School of Advanced Technologies in Medicine, Tehran University of Medical Sciences, Tehran, Iran
2. Department of Medical Biotechnology, Faculty of Medical Sciences, Tarbiat Modares University, Tehran, Iran
3. Department of Biochemistry, School of Allied Medical Sciences, Iran University of Medical Sciences, Tehran, Iran
4. Department of Stem Cell and Regenerative Medicine, National Institute of Genetic Engineering and Biotechnology (NIGEB), Tehran, Iran
5. Pediatric Cell Therapy Research Centre, Tehran University of Medical Sciences, Tehran, Iran

**Corresponding Addresses: P.O.Box: 14115111, Department of Medical Biotechnology, Faculty of Medical Sciences, Tarbiat Modares University, Tehran, Iran,*
P.O.Box: 1419733151, Paediatric Cell Therapy Research Centre, Tehran University of Medical Sciences, Tehran, Iran
Emails: rahbarif@modares.ac.ir, aahamidieh@sina.tums.ac.ir

Received: 20/April/2019, Accepted: 28/July/2019

Abstract

Objective: Immunotherapy with redirected T cells that express a chimeric antigen receptor (CAR) is a promising prospect in cancer treatment. Most CARs use murine-derived single-chain variable fragments (scFvs) as an antigen targeting moiety, which may lead to host immunogenic responses and engineered T cell disappearance. It seems that development of less immunogenic CARs, such as CARs composed of the camelid variable domain of heavy chain antibodies (VHHs) may likely overcome this obstacle. Here, we improved the expression of the VHH-based anti-MUC1 *CAR* gene construct using a third generation lentiviral vector in primary human T cells and assessed its effect on antigen specific targeting, activation and cytotoxicity of redirected human T cells.

Materials and Methods: In this experimental study, we established a second generation novel CAR (VHH-based anti-MUC1 CAR) that contained a camelid-derived anti-MUC1 VHH followed by an IgG3 hinge, a CD28 transmembrane domain and signalling endodomains of CD28 and CD3ζ. Next, we constructed lentiviral vectors that contained this *CAR* gene construct using an optimized transiently virus production method and transduced it into human T cells. Cell surface expression of CAR, cytokine secretion and cytotoxic activity were assessed in the transduced $CD3^+$ T cells.

Results: The transduced T cells had high levels of surface expression of CAR. T cells that expressed anti-MUC1 CAR showed significantly increased secretion of Th1 cytokines, including IL-2, TNF alpha and IFN-γ, as well as cytotoxic activity upon recognition of MUC1 on tumour cells after co-incubation with T47D or MCF-7 (MUC1-positive) compared with A431 (MUC1-negative) or untransduced T cells.

Conclusion: Our results suggested that, given the unique properties of VHHs to prevent immunogenic responses and tonic signalling, our novel VHH-based anti-MUC1 CAR might be effective for clinical purposes in cancer immunotherapy.

Keywords: Immunotherapy, Single-Chain Antibodies, T-Lymphocytes

Cell Journal(Yakhteh), Vol 22, No 4, January-March (Winter) 2021, Pages: 502-513

Citation: Rajabzadeh A, Rahbarizadeh F, Ahmadvand D, Kabir Salmani M, Hamidieh AA. A VHH-based anti-MUC1 chimeric antigen receptor for specific retargeting of human primary T cells to MUC1-positive cancer cells. Cell J. 2021; 22(4): 502-513. doi: 10.22074/cellj.2021.6917.

Introduction

Adoptive cell-based immunotherapy is a promising approach in the treatment of cancers. In recent years, chimeric antigen receptor (CAR)-T cell based immunotherapies have shown impressive successes in the treatment of hematologic malignancies, especially lymphoma. In 2017, the first two engineered cell-based immunotherapies (CD19-targeted CAR-T cells) were approved by the US Food and Drug Administration (FDA). Kymriah was introduced by Novartis for treatment of B-cell acute lymphoblastic leukaemia (ALL) patients less than 25 years of age and about two months later, Yescarta was introduced by Kite Pharma (Gilead) for patients with relapsed or refractory B-cell lymphoma (1, 2).

Despite the significant advances in CAR-T therapies against hematologic malignancies, the treatment of most solid tumours is still faced with serious challenges (3). One of the main reasons for this failure is the identification of suitable tumour-specific antigens for solid tumours. Contrary to CD19, which is expressed solely on the surface of B-lymphocytes, most tumour antigens for solid tumours are found in healthy tissues, which can be recognized by redirected T cells and lead to "on-target off-tumour" toxicities. For instance, Lamers et al. (4) have observed infiltration of cytotoxic T cells that surrounded the bile duct in renal cell carcinoma patients who received transfusions of anti-CA IX CAR-T cells. They reported that the normal bile duct epithelial cells expressed CA IX.

The physical barrier of solid tumours is another challenge. In solid tumours, unlike hematologic

malignancies, CAR-T cells must successfully migrate from the blood to the tumour site, pass across the tumour stroma, and identify the antigen. Unfortunately, there is often a "chemokine receptor/chemokine mismatch" between CAR-T cells and tumours as well as "poor trafficking" after adoptive CAR-T cell transfer. Another challenge is the presence of an immunosuppressive system around the tumour that blocks the effectiveness of CAR-T cells. The presence of infiltrating regulatory T cells, checkpoint pathways (such as PD-1/PD-L1), inhibitory cytokines (TGF-β and IL-10), and a hostile tumour microenvironment (hypoxia, acidic pH, oxidative stress, etc.) in most solid tumours has presented problems for CAR-T cell therapy. Currently, several novel innovations such as Identification of neoantigens, designing inhibitory CARs (iCARs), dual recognition of different antigens by two CARs (tandem CARs), co-expression of cytokine receptor transgenes in CAR-T cells, and the combination of checkpoint inhibitors with CAR-T cells have been developed to overcome these barriers (3, 5).

In addition, the long-term persistence and proliferation of infused CAR-T cells is a determining factor that dominates the inefficiency observed in CAR-T treatments for solid tumours. Recently, several studies have reported poor persistence of engineered T cells after adoptive infusion due to immunogenicity of the *CAR* transgene (6-8). Development of a host immune response against mouse derived single-chain variable fragments (scFvs) is one of the main reasons for depletion of CAR-T cells after infusion (9). A strategy to reduce CAR immunogenicity and subsequently improve therapeutic efficacy in CAR-T cell therapies would be the use of humanized mouse derived scFvs (10, 11) or totally human scFvs (12-14) in the CAR structure. Unfortunately, the use of humanized scFv does not prevent the development of anti-IgE responses that induce anaphylaxis (8). Furthermore, in a clinical trial, despite the use of humanized scFv TAG-72-binding domain in the CAR construct, anti-CAR immunogenic responses resulted in rapid clearance of infused CART72 cells in most patients (15). An alternative strategy to overcome this obstacle is the employment of camelid variable domain of heavy chain antibodies (VHH) instead of scFv in the CAR anatomy (16, 17). These antibodies, also known as Nanobody®, present an extensive antigen binding repertoire and high binding affinity, despite the lack of a light chain.

In addition to naturally transmitting the stimulatory signals, CARs may constitutively trigger antigen-independent tonic signalling. These frequent signals can lead to T cell exhaustion and negatively affect antitumor efficacy *in vivo*. Antigen-independent tonic signalling, at least in part, is due to self-aggregation characteristics of the scFvs used in CARs. Various strategies have been suggested to reduce antigen-independent signalling, including targeting of CARs to the endogenous TCR alpha (*TRAC*) gene locus, utilization of self-inactivating (SIN) lentiviral vectors instead of gamma-retroviruses, incorporation of 4-1BB in endodomain signalling of CARs and substitution of single-domain antibodies instead of scFv (18). Therefore, the use of VHHs in the CAR structure seems to enhance the functional efficacy of redirected T cells *in vivo*.

Our main objective in designing this study was the stable expression of the VHH-based anti-MUC1 *CAR* gene construct, which we previously constructed in primary human T cells using a third generation lentiviral vector. We also sought to investigate the efficiency of this chimeric receptor on the activation and cytotoxicity of redirected human T cells. Accordingly, we constructed lentiviral particles that contained second-generation VHH-based anti-MUC1 CAR. Subsequently, we described the *in vitro* functional activity of VHH-based anti-MUC1 CAR-T cells by cytolysis of MUC1-positive tumour cells and cytokine production.

Materials and Methods

Cell lines, antibodies and reagents

In this experimental study, human breast cancer cell lines (T47D and MCF-7 cells), human epidermoid squamous carcinoma cell line (A431), and Lenti-X 293T cells were purchased from Iranian Biological Resource Centre (IRBC, Iran). T47D cells were cultured in RPMI 1640 medium (Gibco, Life Technologies, USA). MCF-7, A431 and Lenti-X 293T cells were cultured in Dulbecco's Modified Eagle Medium (DMEM, Gibco, Life Technologies, USA). Both media were supplemented with 10% fetal bovine serum (FBS) and 2 mM L-glutamine (Gibco, Life Technologies, USA). Furthermore, for packaging and production of lentiviral particles, Lenti-X 293T cells were maintained in DMEM (Gibco, Life Technologies, USA) that consisted of 10% FBS and 2 mM L-glutamine. For flow cytometry assessment, APC-conjugated anti-CD3 (BD Pharmingen™) was purchased from BD Biosciences (USA) and FITC-conjugated goat anti-rabbit IgG secondary antibody was purchased from Abcam (Cambridge, MA, USA).

Vectors and preparation of anti-MUCI chimeric antigen receptor gene construct

pLJM1-EGFP (Addgene plasmid #19319) transfer plasmid (a gift from David Sabatini), pRSV-Rev), pMDLg/pRRE and pMD2.G plasmids were used to produce the third generation lentiviral particles. Anti-MUC1 CAR cassette that contained coding sequences for anti-MUCI VHH-IGg3-CD28-CD3ζ was made in our previous study (19). This construct was modified and PCR amplified by oligonucleotide primers

F: 5′-TATAGCTAGCGCCACCATGGCCGAGGTGGAG-3′ and
R: 5′-TATTACCGGTTTCGATCCTCCTCC-3′

designed to introduce the NheI (3′ site) and AgeI (5′ site) restriction sites in the ends of the CAR construct. The modified anti-MUCI construct was subcloned to the pLJM1-EGFP plasmid using digestion and ligation of the NheI/AgeI fragment.

Transfection and viral packaging

First, to determine the optimum transfection condition, 0.8×10^6 Lenti-X 293T cells were seeded onto a 24-well plate and incubated overnight in a 37˚C, 5% CO_2 incubator. The next day, pMDLg/pRRE, pRSV-Rev, pMD2.G and pLJM1-EGFP plasmids were co-transfected to the Lenti-X 293T cells using branched polyethyleneimine (PEI, Sigma-Aldrich, DE) (20) in PEI:DNA ratios of 1:1, 2:1 and 3:1; incubation times of 3, 6 and 24 hours; and various PEI concentrations (0.25 µg/µL, 0.5 µg/µL, 0.75 µg/µL and 1 µg/µL). After 24 hours, we evaluated the transfection rate by (GFP) expression using a fluorescent microscope. Cell viability was appraised by cell counting using the dye exclusion test (trypan blue). For preparation of recombinant viral particles, 2.5×10^6 Lenti-X 293T were cultured on 100 cm^2 plates and incubated overnight in a 37˚C, 5% CO_2 incubator. Afterwards, the pLJM1-CAR recombinant vector along with helper vectors (pRSV-Rev, pMDLg/pRRE, pMD2.G) were co-transfected to the Lenti-X 293T cells by the optimized PEI transfection method. Cell supernatants that contained the virus particles were harvested at 24, 48 and 72 hours after transfection and were centrifuged at 500 × g/4˚C. The supernatants that contained the virus particles were filtered through 0.45 µm filters (Millipore) to remove cell debris, then transferred to sterile capped tubes and concentrated by ultra-centrifugation (20000 × g for 2 hours at 4˚C). The probable virus pellet was resuspended in 100-200 µL of DMEM, from which we obtained aliquots that were stored at -80˚C until the subsequent transduction step.

The infective lentivirus titre was determined by quantitative PCR (21) for the puromycin resistance gene using the following

pur-F: 5′-GCAGCAACAGATGGAAGG-3′ and
pur-R: 5′-GAGGTCTCCAGGAAGGC-3′ primers.

Briefly, after transduction of Lenti-X293T cells, copy numbers of integrated lentiviral vectors were measured by the standard curve of real-time PCR (Rotor-Gene 6000 Series Software 1.7) and the following formula: (DNA amount (ng)$\times6.022\times10^{23}$)/(length (bp)$\times1\times10^9\times650$). The titre of the recombinant anti-MUC1 CAR lentiviral vector, reported in transforming units (TU)/mL, was calculated to be 1.12×10^8 TU/mL.

Human T cell culture and transduction

Peripheral blood samples were obtained from healthy males and non-pregnant females between the ages of 25-35 years in compliance with the Institutional Review Board-approved research protocols of the Tehran University of Medical Sciences (IR.TUMS.VCR.REC.1395.538). All blood samples collected following donor informed consent. Peripheral blood mononuclear cells (PBMC) were isolated by the Ficoll-paque (Sigma, GE) density gradient separation method. Freshly isolated PBMCs were cultured in 2 mL 10% FBS RPMI1640 media supplemented with 100 IU/mL rIL-2 (Miltenyi Biotech, DE) and subsequently mixed with Dynabeads Human T-Activator CD3/CD28 (Gibco by Life Technologies, USA) at a 1:1 (bead:cell) ratio. At 48 to 72 hours after activation, the T cells were transduced with recombinant lentiviral particles at a multiplicity of infection (MOI) of >20 using the spinoculation protocol where the MOI was calculated by viral titre/number of cells. Briefly, 2×10^5 T cells were resuspended in 1 mL of complete media (RPMI 1640, 5% FBS, 2 mM L-glutamine) to which we added the appropriate volume of concentrated virus particles and soluble RetroNectin® (Clontech) for a final concentration of 8 µg/mL. Cell suspensions were centrifuged at 800 × g for 90 minutes at 32˚C. T cells were then resuspended in complete media supplemented with 100 IU/mL rIL-2 and plated in 24-well plates for 72-96 hours (humidified 5% CO_2, 37˚C incubation).

Flow cytometry

In order to detect VHH-based CAR expression on T cells, FITC goat anti-rabbit IgG antibody, specific for VHH (Abcam, Cambridge, UK), was used to stain 2×10^5 transduced T cells. The purity of the activated T cells was verified by APC mouse anti-human (BD Pharmingen™, CA). All samples were examined by BD FACSCanto II equipment. FlowJo software (v10) was utilized for data analysis.

Analysis of cytokine production after co-cultivation of transduced T cells with tumour cells

To examine antigen specific activation and cytotoxicity of the transduced T cells, confluent cells that highly expressed MUC1 (T47D and MCF-7) and also cells with no or slight expression (A431) were co-cultured with transduced T cells at a 10:1 (effector:target) ratio in RPMI 1640 (10% FBS) supplemented with rIL-2 (100 IU/mL) (n=3). The untransduced T cells were co-cultured with cancerous cells and a single culture of tumour cells were used as the negative control in this assay. After 72 hours of incubation, all supernatants were collected and cytokine secretion was measured by the human TNF alpha (Abcam, USA), human IL-2 (Abcam, USA) and IFN-γ (Abcam, USA) ELISA assays according to manufacturer's instructions.

Cell viability assay for tumour cells after co-culturing with anti-MUCI chimeric antigen receptor T cells

Viable MUC1-positive or MUC1-negative cells were analysed after co-culture with either anti-MUCI CAR-T cells or untransduced T cells in a 10:1 ratio by the MTT assay (n=3). For this purpose, after 72 hours, the anti-MUC1 CAR-T cells or untransduced T cells were removed and MTT reagent was added directly into the cell media. Subsequently, the cells were maintained for 3 hours in a humidified 5% CO_2 incubator at 37˚C. Cell supernatant media were aspirated after the incubation time and the formation of a formazan product (dissolved in DMSO) was detected at a 540 nm absorbance wavelength by an ELISA plate reader.

Statistical analysis

Analysis of variance (ANOVA) was used to identify differences between groups. Data were analysed by ANOVA and Tukey's post hoc test using GraphPad Prism software (version 7.05). The data are shown as mean ± SEM or mean ± SD. $P<0.05$ was considered statistically significant.

Results

Preparation of variable domain of heavy chain antibodies-based anti-MUC1 chimeric antigen receptor construct

The VHH-based anti-MUC1 CAR construct has been generated previously (19). This gene construct is comprised of a sequence coding camelid VHH antibody, an IgG3 domain (hinge), the transmembrane sequence of human CD28 and signalling enodomains that include CD28 and CD3ζ. The anti-MUCI VHH-IgG3 hing-CD28-CD3ζ construct was successfully cloned into the pLJM1-EGFP plasmid. Sub-cloning was verified by restriction enzyme digestion and DNA sequencing according to the Sanger sequencing method (16). The recombinant vector was determined to be 9732 bp that resulted in fragments of 648 bp, 903 bp and 8145 bp when digested by the BsrG1 restriction enzyme. Undigested recombinant plasmids were observed in a supercoil form (Fig.1).

Transfection optimization, production of recombinant lentivirus particles that contained variable domain of heavy chain antibodies-based anti-MUC1 chimeric antigen receptor

The optimal PEI:DNA ratio, transfection incubation time and PEI concentration were identified to limit PEI toxicity side effects as well as to maximize transfection efficacy.

As shown in Figure 2, 24 hours incubation of the PEI-DNA complex, regardless of the PEI:DNA ratio, led to the death of the Lenti-X 293T cells and no green fluorescence expression. In the 3 hour incubation time, both the 1:1 and 2:1 PEI:DNA ratios resulted in low levels of fluorescence (Fig.2A), while the 3:1 PEI:DNA ratio was cytotoxic (Fig.2D). The 6 hour incubation of Lenti-X 293T cells with the PEI-DNA complex showed the highest level of fluorescence at the 1:1 PEI:DNA ratio (Fig.2B), while the PEI:DNA ratios above 1:1 caused cell death (Fig.2D). Figure 3 shows the viability profiles and transfection efficiency of the transfectants in various PEI concentrations where the condition of transfection was considered the 1:1 PEI:DNA ratio at the 6 hour incubation time. Cell viability density in cells treated with PEI concentrations (µg/µL) of 0.25, 0.5, 0.75 and 1 did not show any significant difference (Fig.3E), while the highest level of GFP expression was shown at the 1 µg/µL PEI concentration (Fig.3A-D). Hence, the 1:1 PEI:DNA ratio, incubation time of 6 hours and PEI concentration of 1 µg/µL were selected for next step of transient virus production. Transfection efficacy for the recombinant lentiviral vector was considered based on transfection of the empty vector that contained GFP as the positive control and by using the optimized protocol. The transfection rate of the GFP-vector was >80% and was calculated by using a fluorescent microscope and counting the cells that emitted fluorescence.

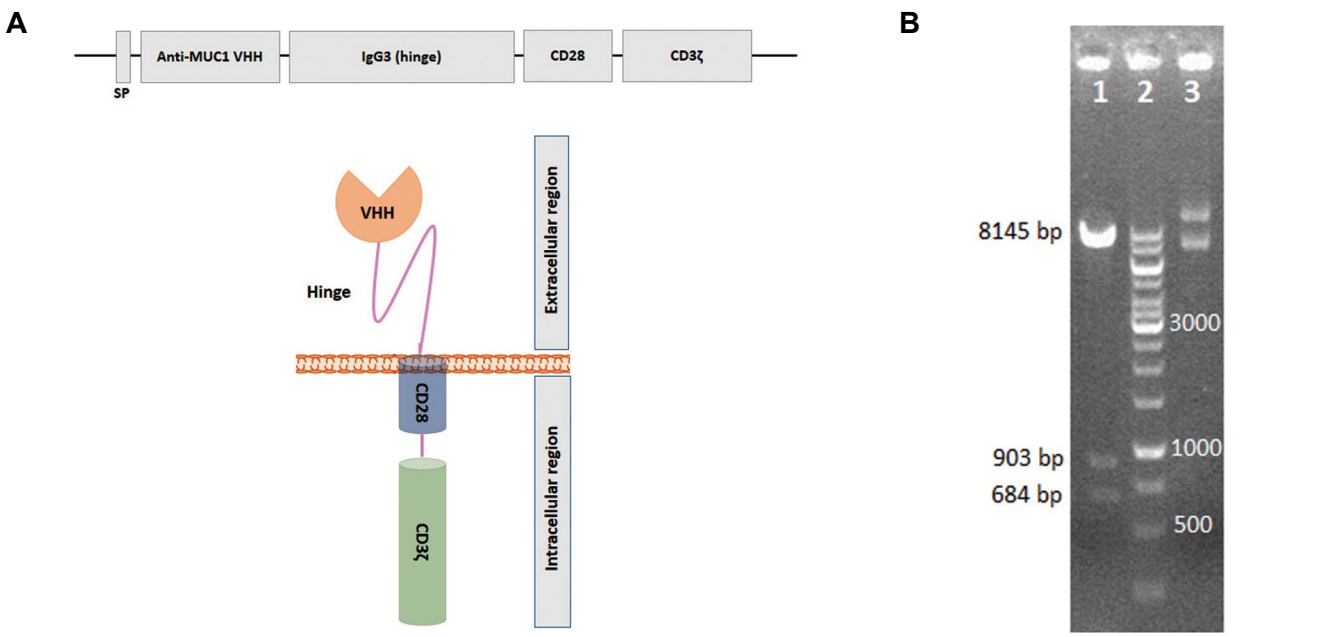

Fig.1: Design and sub-cloning confirmation of variable domain of heavy chain antibodies (VHH)-based anti-MUC1 chimeric antigen receptor (CAR). **A.** Schematic representation of VHH-based anti-MUC1 CAR that contains signal peptide (SP), the anti-MUC1 VHH, IgG3 hinge, and CD28 and CD3ζ, as intracellular domains. **B.** Insertion of VHH-based anti-MUC1 *CAR* gene construct into the pLJM1 vector was confirmed by the enzymatic digestion test. The recombinant vector digested by BsrG1 restriction enzyme produced 684 base pair (bp), 903 bp and 8145 bp fragments (line 1). Line 2; DNA ladder and Line 3; Undigested pLJM1-anti-MUC1 CAR plasmid.

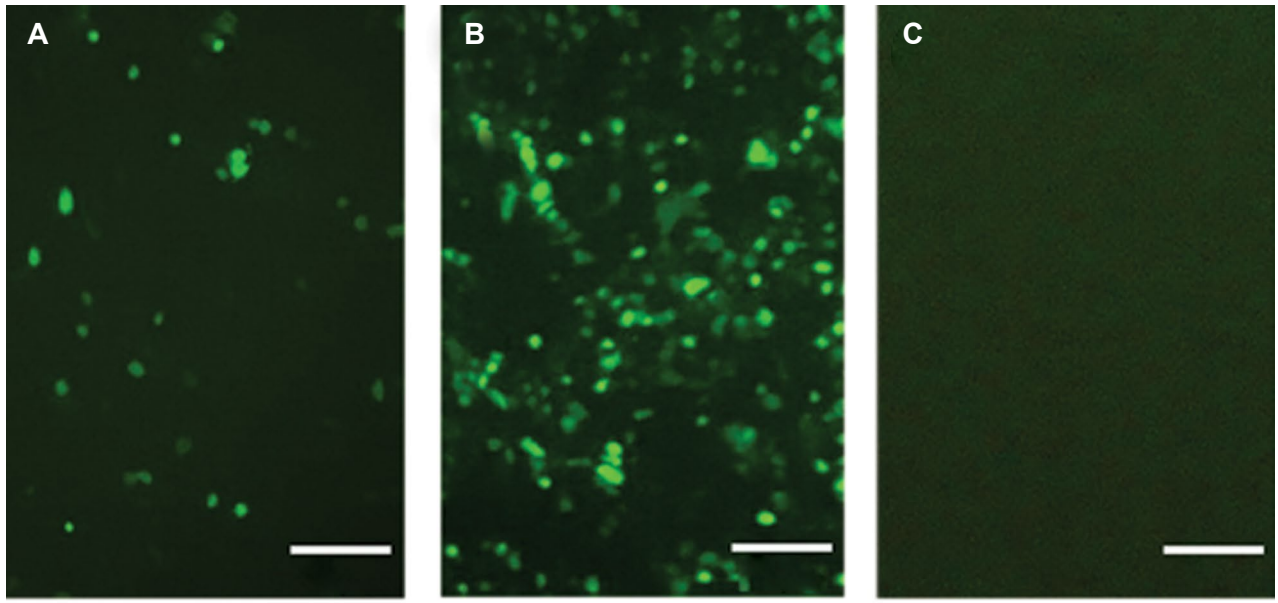

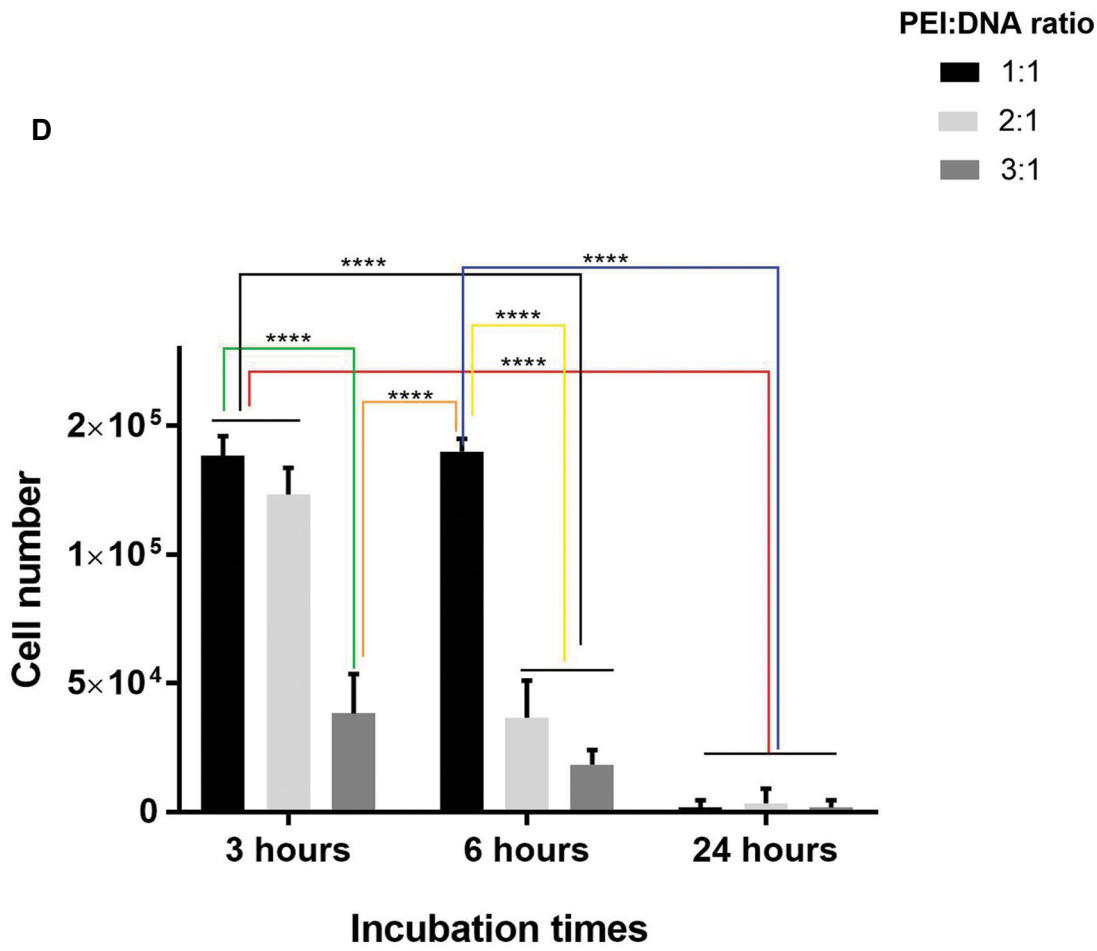

Fig.2: Optimization of the polyethyleneimine (PEI):DNA ratio and incubation time for optimal transfection of Lenti-X 293T cells. **A-C.** The transfection efficiency of pLJM1-EGFP vector (empty backbone) was verified based on fluorescence microscopy of green fluorescence protein (GFP) expression. The upper images show the effectiveness of vector transfection at **A**. 3, **B.** 6 and **C.** 24 hour incubation times of PEI-DNA complexes (1:1 ratio). **B.** The maximum levels of GFP fluorescence was observed at the 6 hour incubation time (scale bars: 50 µm). **D.** The graph indicates number of viable cells after PEI-based transfection at various incubation times and PEI:DNA ratios. The results show that the 24 hour incubation time of PEI or PEI:DNA 3:1 ratio are cytotoxic. Error bars represent the SD of 3 samples. ****; P<0.001 was considered statistically significant.

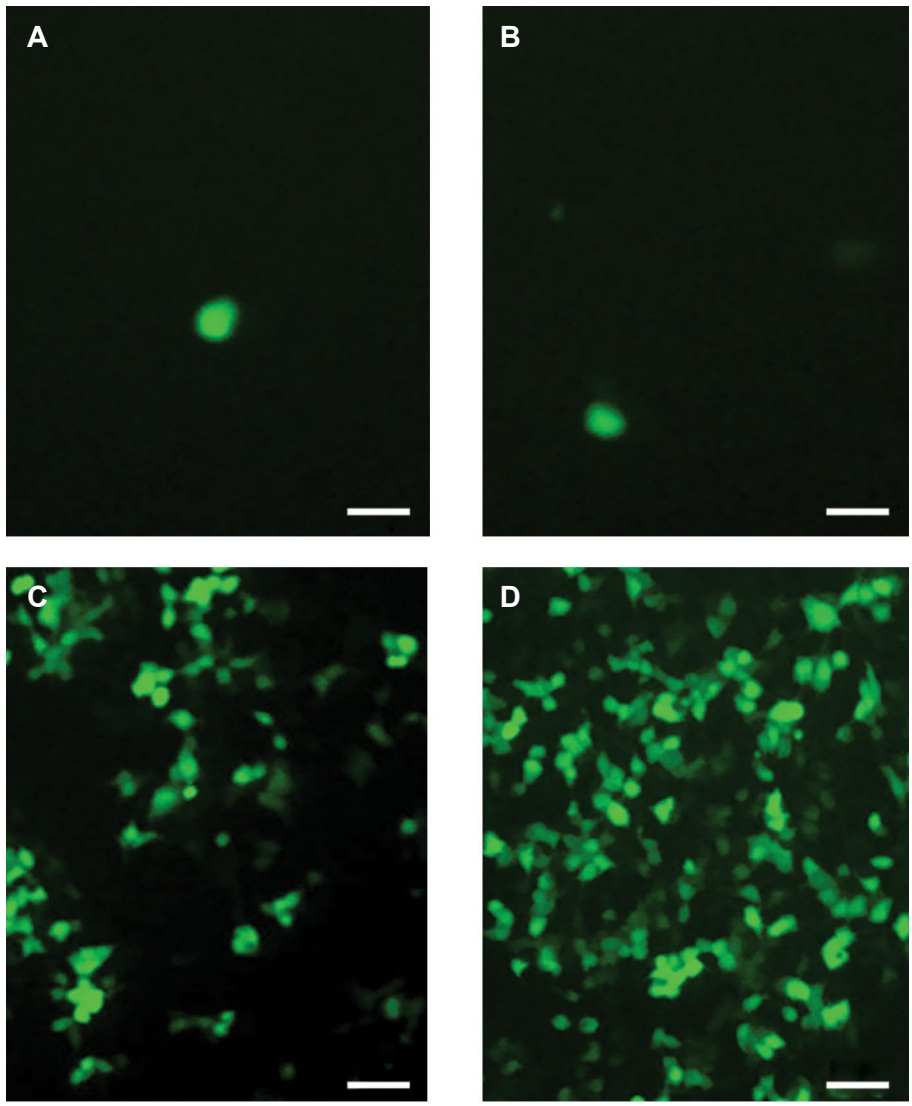

E

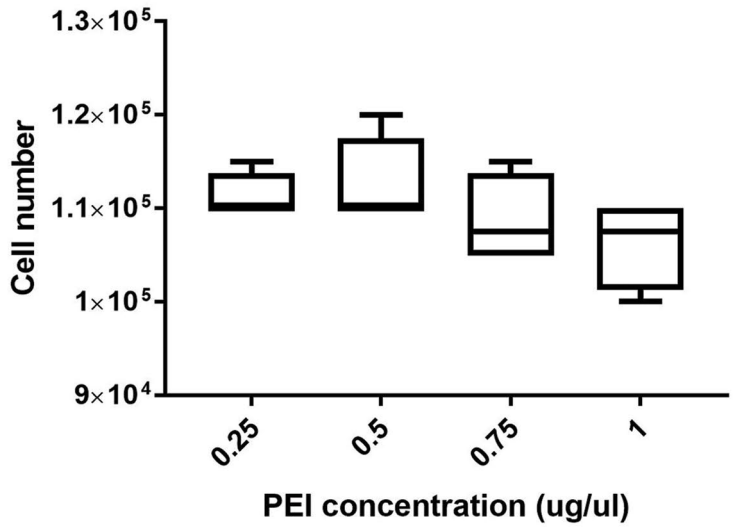

Fig.3: The effect of various concentration of polyethyleneimine (PEI) on transfection efficiency and viability of Lenti-X 293T cells in PEI:DNA at a 1:1 ratio and 6 hour incubation time. The effect of **A.** 0.25 µg/µl, **B.** 0.5 µg/µl, **C.** 0.75 µg/µl and 1 µg/µl of PEI concentrations on transfection on pLJM1-EGFP (empty backbone) as shown by green fluorescence protein (GFP) expression. **D.** The images indicate the highest levels of GFP expression at the 1 µg/µl PEI concentration (scale bars: 50 µm). **E.** The graph indicates the numbers of viable cells after transfection of the pLJM1-EGFP vector into Lenti-X 293T cells using various concentrations of PEI. Error bars represent the SD of 4 samples.

Transduction of recombinant lentiviral particles into human primary CD3+ T cells

After stimulation of PBMCs, flow cytometry data revealed positive detection of the CD3 marker on the stimulated PBMCs. The results showed that the cell population of CD3+ T cells was almost 90%. (Fig.4A).

Flow cytometry results of transduced T cells showed a high percentage of simultaneous expression of anti-MUC1 CAR and CD3 surface marker on these cells (84.9%), which were called anti-MUC1 CAR-T cells (Fig.4B, C).

Cytokine secretion of anti-MUC1 chimeric antigen receptor-T cells

Cytokine production is a functional hallmark of CAR-T cells. Therefore, production of cytokines IL-2, TNF alpha and IFN-γ were measured using ELISA after co-culturing the modified T cells with MUC1 positive (T47D and MCF-7) or MUC1 negative (A431) tumour cell lines. The results revealed that the MUC1-redirected CAR-T cells could produce TNF alpha, IFN-γ and IL-2 in response to recognition of MUC1 expressed on the tumour cells (Fig.5). The co-culture of T47D tumour cells significantly triggered the production of IL-2 (1388 ± 81.32 pg/mL, 28-fold, Fig.5A), TNF alpha (503 ± 4.24 pg/mL, 9-fold, Fig.5D) and IFN-γ (253 ± 5.65 pg/mL, 10-fold, Fig.5G) from MUC1-specific CAR-T cells, but not the untransduced T cells. Furthermore, MUC1-specific CAR-T cells significantly increased secretion of IL-2 (597.5 ± 38.89 pg/mL, 15-fold, Fig.5B), TNF alpha (359 ± 1.41 pg/mL, 6-fold, Fig.5E) and IFN-γ (182 ± 9.89 pg/mL, 9-fold, Fig.5H) in response to MCF-7, another MUC1 positive tumour cell line. The untransduced T cells did not show significant production of IL-2 (Fig.5B), TNF alpha (Fig.5E) or IFN-γ (Fig.5H) after the co-culture with MCF-7 cells. When MUC1-negative tumour cells (A431) were used as the stimulator, MUC1-specific CAR-T cells showed no significant secretion of IL-2 (30 ± 2.82 pg/mL, 1-fold, Fig.5C), TNF alpha (8 ± 2.82 pg/mL, 1.7-fold, Fig.5F) and IFN-γ (22 ± 2.82 pg/mL, 1.2-fold, Fig.5I). A single culture from each of cell lines was maintained as the negative control.

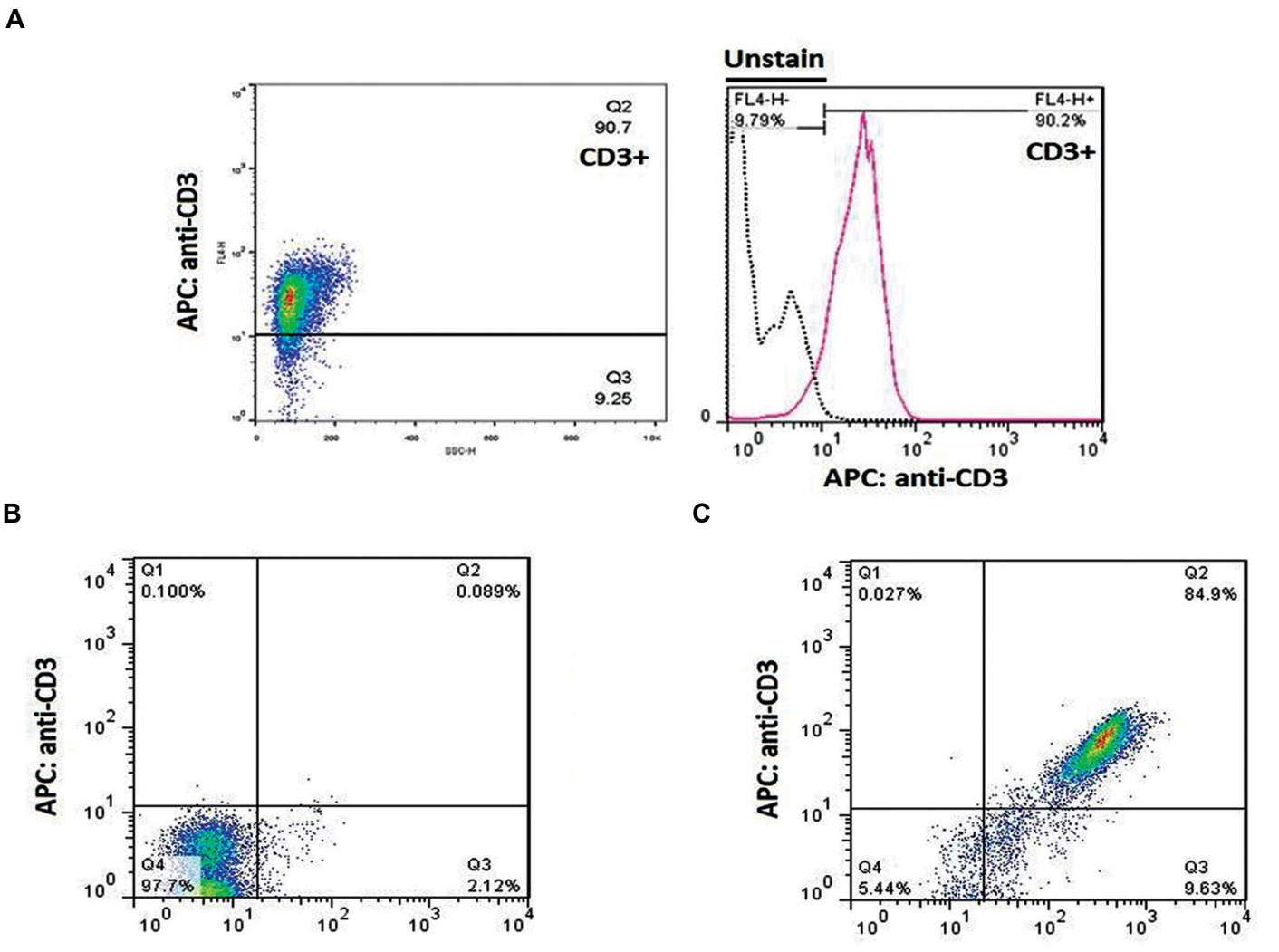

Fig.4: Immunophenotyping of activated CD3+ T cells for detection of chimeric antigen receptor (CAR) expression after transduction of anti-MUC1 CAR recombinant lentiviruses. **A.** Flow cytometry was utilized to characterize peripheral blood mononuclear cells (PBMCs) for the T cell surface marker (CD3) after 72 hours of activation with CD3/CD28 dynabeads. Cells stained with APC-conjugated anti-CD3 antibody. **B.** Indicates unstained flow cytometry of transduced T cells. **C.** Represents CAR expression on CD3+T cells after APC-conjugated anti-CD3 and FITC-conjugated anti-VHH staining.

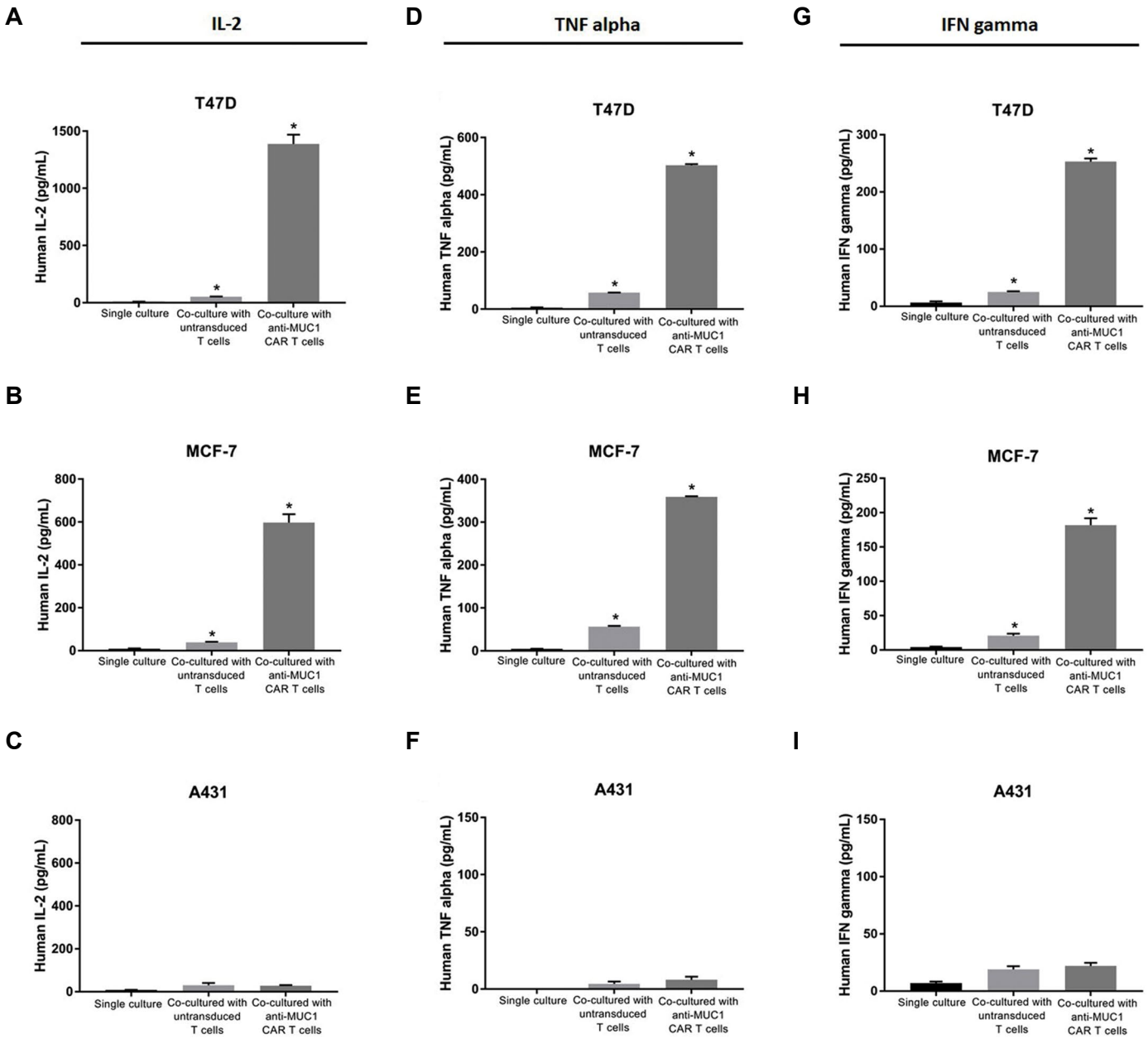

Fig.5: Cytokine production of anti-MUC1 chimeric antigen receptor (CAR)-T cells. Anti-MUC1 CAR-T cells or untransduced T cells co-cultured for 72 hours with MUC1-positive cells (T47D and MCF-7) or MUC1-negative cells (A431). **A-C.** Concentrations of IL-2, **D-F.** TNF alpha and **G-I.** IFN-γ secreted into supernatants was quantified by the enzyme-linked immunosorbent assay (ELISA). A single culture from each of cell lines was maintained as the negative control. The results are shown as the mean ± SD of three samples (n=3). *; P=0.033.

Cytotoxicity of MUC1-redirected chimeric antigen receptor-T cells

We sought to appraise the cytotoxicity of CAR-T cells by assessing cell viability of the target cells after a 72-hour co-culture with transduced or untransduced T cells (Fig.6). MTT assay results indicated that co-culturing of T47D (a MUC1-positive tumour cell line) with anti-MUC1 redirected T cells led to a viability rate of 24.9 ± 9.19%, while T47D cell viability was 85.01 ± 3.18% upon co-culture with untransduced T cells. These results were significantly higher than the viability of T47D cells co-cultured with MUC1-specific CAR-T cells (P<0.01). A negative control of a single culture of T47D cells showed 92.39 ± 3.76% viability (Fig.6A). In addition, as shown in Figure 6B, MCF-7 cells (another MUC1-positive tumour cell line) co-cultured with MUC1-specific CAR-T cells showed significantly lower viability (22.73 ± 5.24%) than the MCF-7 cells co-cultured with untransduced T cells (86.9 ± 17.81%, P<0.05) or MCF-7 single culture cells (92.31 ± 3.45%, P<0.01). There was no difference in the viability of A431 cells (a negative-MUC1 tumour cell line) while co-cultured with anti-MUC1 CAR-T cells (69.1 ± 22.48%) compared to the co-culture with untransduced T cells (70.93 ± 30.61%) or single culture cells (78.4 ± 17.55%), as seen in Figure 6C.

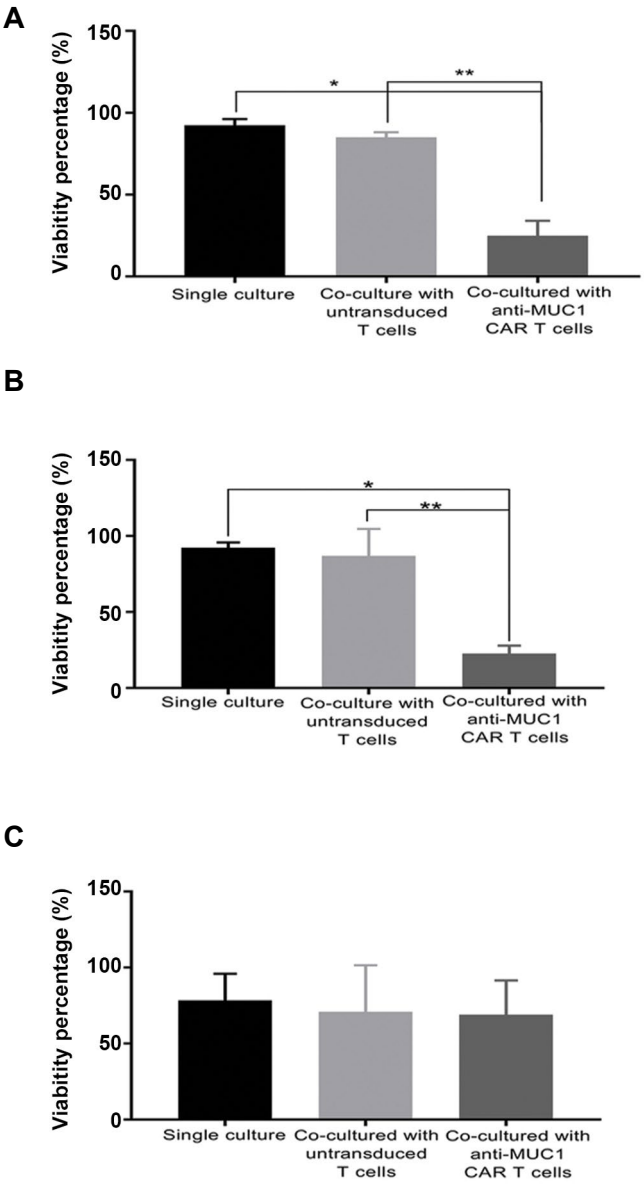

Fig.6: Cytotoxicity mediated by anti-MUC1 chimeric antigen receptor (CAR)-T cells. Viability of MUC1-positve cells [**A.** T47D and **B.** MCF-7) or MUC1-negative cells (**C.** A431) measured by the MTT assay after 72 hours co-incubation with anti-MUC1 CAR-T cells or untransduced T cells. A single culture from each of cell lines was maintained as a negative control. The results are shown as the mean ± SD of three samples (n=3).). *; P=0.033 and **; P=0.002.

Discussion

MUC1 is a heavily glycosylated glycoprotein with an extracellular domain that extends up to 200-500 nm from the cell surface. MUC1 has been found to be overexpressed on the cell surface in multiple epithelial aden(Sahraei, 2012 #64)ocarcinomas, including those of the breast, ovary, and pancreas (22). In malignant cells, MUC1 is re-distributed across the cell surface and loses apical-basal polarity that leads to interaction between MUC1 and few tyrosine kinase receptors such as epidermal growth factor receptor (EGFR) and platelet-derived growth factor-A (PDGFA), which then leads to cell proliferation and enhanced tumorigenesis. Furthermore, MUC1 promotes tumorigenesis through interactions with hypoxia-inducible factor a (HIF1-a) (23), increases angiogenesis (24) and inhibits the GSK3b pathway (25). In recent years, several clinical trials have used CAR technology for MUC1 targeting in solid and non-solid tumours (22).

CAR is composed of three main parts: i. Ligand binding domain that specifically recognizes tumour antigens and commonly is a B cell receptor (BCR)-derived scFv, ii. Extracellular spacer (hinge) which is the connecting region between the ligand binding domain to the transmembrane domain, and iii. Transmembrane and signalling domains. Between the hinge region and signalling endodomains are sequences which are usually derived from CD8, CD28 or CD3ζ (transmembrane). Immediately after this region lies the signalling endodomains that transmit activation and costimulatory signals upon antigen recognition by scFv. According to these signalling endodomains, CARs are classified into three “generations”. Only CD3ζ has been used as a signalling domain in “first generation” CARs. They lack co-stimulatory molecules and are unable to directing engineered T cell activation and expansion effectively upon antigen recognition. “Second generation” CARs are added to intracellular domain often comprising of CD28 or 4-1BB. "Third generation" CARs include CD3ζ and two or more costimulatory domains, such as CD28 and usually OX40 (CD134) or 4-1BB (CD137) (26).

Although the use of third generation CARs has been more effective than second generation CARs based on their anti-tumour effects and persistence in animal studies (27), there were serious adverse events in a clinical trial conducted by Morgan et al. (28) (NCT00924287). They investigated efficacy and safety of third-generation anti-HER2 CAR and unfortunately their study terminated after a patient’s death due to CAR-T cell immunotherapy. The authors considered that the cause of the patient’s death was recognition of HER2-positive healthy lung epithelium by anti-HER2 CAR-T cells and respiratory failure. In contrast, significant toxicity has not been reported after infusion of second generation HER-2 specific CAR-T cells (NCT00902044) as the lack of 4-1BB in the endodomain of the CAR construct prevented excessive CAR-T cell activation (29). Therefore, it seems second generation CARs are a more suitable choice due to higher safety in solid tumour CAR-T cell therapy. Here, we have utilized a second generation MUC1-specific CAR to reduce the possibility of chronic cytotoxicity due to excessive T cell activation.

Most clinical CAR-T cell studies have utilized murine-derived scFvs that lead to the elimination of the scFv-based CAR-expressing T cells by the host anti-mouse or anti-IgE antibodies (30). These anti-CAR immune responses represent a challenge for the CAR-T cell-based treatments because long-term persistent engineered T cells are essential for the effective tumour elimination. A novel approach

to reduce anti-CAR responses is VHH-based CARs. VHHs have high amino acid similarity to human VH family III. Therefore, in comparison with murine scFvs, humanization of these novel targeting antibodies is simpler and more efficient. Regarding the structure of VHH, it can be predicted that most substitutions with human sequence, except for the common key amino acids in the framework region 2 (FR2), can be implemented without altering its function and properties. Therefore, high homology with human antibody along with other features like small size (2.5 nm diameter and about 4 nm height), steric monomeric behaviour and high solubility, make VHHs ideal choices for cancer immunotherapy (31, 32). Hence, in this study, we have used a novel VHH-based anti-MUC1 CAR construct and subsequently transduced human primary T cells by recombinant lentiviruses that contained this gene construct.

To improve the condition of the high titer virus production, first we optimized the condition of transfection for our third generation of lentiviral vectors. Our data showed maximum transfection rate along with minimum toxicity at the 1:1 (PEI:DNA) ratio and 6 hour incubation period. Although reagent cytotoxicity increased with increasing PEI:DNA ratio levels, GFP expression did not increase in ratios higher than 1:1 PEI:DNA. Xie et al. (33) have reported that higher PEI concentrations are needed for an efficient transfection and suggested a 5:1 PEI:DNA ratio for optimum transfection. Differences in cell line type and experimental scale might be responsible for the different results. Next, we calculated recombinant lentivirus copy number by quantitative real-time PCR. The conventional method for determining the viral titer is the evaluation of GFP expression, but since the *EGFP* gene was removed from the pLJM1-EGFP after subcloning the CAR construct, we calculated the titer of the recombinant lentiviruses by evaluating puromycin resistant gene quantitation. Our results indicated that our novel VHH-based anti-MUC1 CAR-T cells could produce cytokines and cytotoxic activity, which are essential for a prosperous T cell based therapy. Successful clinical usage of CAR-T cells depends on high-level expression of CAR on the T cell surface. Our data showed 85% CAR expression on the T cells. Low expression of CAR is among the many challenges of CAR-T cell therapy and is a major obstacle. In several studies that used non-viral methods, the reported CAR expression was <50% (34, 35). Here, we used a third generation lentiviral vector with high MOI to transfer our *CAR* gene construct to human primary T cells. Moreover, we also optimized our T cell transduction method (data not shown). This high anti-MUC1 CAR expression was responsible for specific cytotoxicity and cytokine production observed upon co-cultivation of anti-MUC1 CAR expressing T cells with cancerous cells. Moreover, our results showed significantly reduced survival of MUC1-positive cells after co-culturing with transduced T cells (24.9% and 22.73%), but not in co-culturing with untransduced T cells (85.01% and 86.9%), which showed that specific recognition of the MUC1 antigen by anti-MUC1 CAR on the transduced T cells triggered intracellular signal transduction and activation of redirected human T cells, and led to specific elimination of MUC1-positive cells by these anti-MUC1 CAR-T cells. Accordingly, recognition of MUC1 by our anti-MUC1 VHH antibody was in an antigen-specific manner. In line with this result, we previously demonstrated specific and efficient recognition of a tumor antigen (TAG-72) by CCRF-CEM cells that expressed another VHH-based CAR (anti-TAG-72), which led to proliferation and cytokine release (16).

In several CAR constructs, tonic signalling has led to prolonged expansion, constitutive cytokine release and exhaustion of T cells in the inexistence of target ligand and can be a cause of poor antitumor efficacy (36-38). Ligand-independent tonic signalling may occur due to clustering of CAR surface molecules, owing to the level of CAR surface expression as well as oligomerization and aggregation of the utilized scFvs (18). Structural properties of scFvs such as unfolded VH:VL flexible linker can cause domain swapping between the adjacent scFv molecules and lead to oligomerization (39). Several strategies have been suggested to improve scFv stability and thus prevent the scFvs oligomerization. These strategies include engineering of disulphide bonds in the linker between the VH and VL domains, computational modelling and selection of new target epitopes in antigens. It has been reported that substitution of the targeting domain with a single-chain antibody such as VHHs in the CAR structure may also avoid tonic signalling (18). VHHs are intrinsically incapable of domain swapping and oligomerization. Moreover, their small size enables VHHs to access the cryptic epitopes or large structures (40). It has been shown that the use of an SIN lentiviral vector for CAR expression may reduce tonic signalling and improve antitumor efficacy (36). According to our VHH-based anti-MUC1 CAR construct and the use of an SIN lentiviral vector, our functional assay results showed that, besides the high level of CAR expression, tonic signalling did not occur in the absence of the MUC1 antigen. It has been reported that the incorporation of a CD28 co-stimulatory molecule as the endodomain signalling resulted in tonic signalling of CAR-T cells. Long et al. (37) indicated that the replacement of the CD28 molecule with 4-1BB in a second generation CAR construct reduced T cell exhaustion. This contradicted our findings since our CD28-based anti-MUC1 CAR construct did not show the background cytokine production in co-incubation with MUC1-negative cells. In line with our results, Zhong et al. (27) did not observe any difference between CD28-CAR and 4-1BB CAR in the efficacy of tumour eradication.

Conclusion

Taken together, the present study successfully demonstrated transduction of a second generation VHH-based CAR construct into human primary T cells. VHH-based anti-MUC1 redirected T cells were activated upon recognition of MUC1 expressing cancer cells and showed significant cytokine production and cytotoxic activity. This study supported the idea that VHH-based CARs might be a promising alternative strategy to efficiently target tumour cells and potentially overcome immunogenic and target-independent signalling impediments observed in scFv-based CARs. Although this study was significant in targeting and cytolysis of MUC1 positive cell lines due to VHH-based CAR-T cells specific for TAA-MUC1, *in vivo* experiments must be performed to assess both efficacy and safety.

Acknowledgements

This study financially supported by the Council of Stem Cell Sciences and Technologies of Iran (Rep393) and in part by Tehran University of Medical Sciences and Tarbiat Modares University. There is no conflict of interest in this study.

Authors' Contributions

A.R.; Did the experiment and the data collection. A.R., F.R.; Did the analysis and interpretation of data. F.R., A.A.H.; Contributed to the conception, study design, and manuscript preparation. M.K.S., D.A.; Contributed in interpretation of the data and the conclusion. All authors read and approved the final manuscript.

References

1. Zheng PP, Kros JM, Li J. Approved CAR-T cell therapies: ice bucket challenges on glaring safety risks and long-term impacts. Drug Discov Today. 2018; 23(6): 1175-1182.
2. Mullard A. FDA approves first CAR-T therapy. Nat Rev Drug Discov. 2017; 16(10): 669.
3. D'Aloia MM, Zizzari IG, Sacchetti B, Pierelli L, Alimandi M. CAR-T cells: the long and winding road to solid tumors. Cell Death Dis. 2018; 9(3): 282.
4. Lamers CH, Sleijfer S, van Steenbergen S, van Elzakker P, van Krimpen B, Groot C, et al. Treatment of metastatic renal cell carcinoma with CAIX CAR-engineered T cells: clinical evaluation and management of on-target toxicity. Mol Ther. 2013; 21(4): 904-912.
5. Newick K, Moon E, Albelda SM. Chimeric antigen receptor T-cell therapy for solid tumors. Mol Ther Oncolytics. 2016; 3: 16006.
6. Lamers CH, Willemsen R, van Elzakker P, van Steenbergen-Langeveld S, Broertjes M, Oosterwijk-Wakka J, et al. Immune responses to transgene and retroviral vector in patients treated with ex vivo–engineered T cells. Blood. 2011; 117(1): 72-82.
7. Kershaw MH, Westwood JA, Parker LL, Wang G, Eshhar Z, Mavroukakis SA, et al. A phase I study on adoptive immunotherapy using gene-modified T cells for ovarian cancer. Clin Cancer Res. 2006; 12(20 Pt 1): 6106-6115.
8. Maus MV, Haas AR, Beatty GL, Albelda SM, Levine BL, Liu X, et al. T cells expressing chimeric antigen receptors can cause anaphylaxis in humans. Cancer Immunol Res. 2013; 1(1): 26-31.
9. Turtle CJ, Hanafi LA, Berger C, Gooley TA, Cherian S, Hudecek M, et al. CD19 CAR–T cells of defined CD4+: CD8+ composition in adult B cell ALL patients. J Clin Invest. 2016; 126(6): 2123-2138.
10. Sun M, Shi H, Liu C, Liu J, Liu X, Sun Y. Construction and evaluation of a novel humanized HER2-specific chimeric receptor. Breast Cancer Res. 2014; 16(3): R61.
11. Johnson LA, Scholler J, Ohkuri T, Kosaka A, Patel PR, McGettigan SE, et al. Rational development and characterization of humanized anti–EGFR variant III chimeric antigen receptor T cells for glioblastoma. Sci Transl Med. 2015; 7(275): 275ra22.
12. Lanitis E, Poussin M, Hagemann IS, Coukos G, Sandaltzopoulos R, Scholler N, et al. Redirected antitumor activity of primary human lymphocytes transduced with a fully human anti-mesothelin chimeric receptor. Mol Ther. 2012; 20(3): 633-643.
13. Sommermeyer D, Hill T, Shamah SM, Salter AI, Chen Y, Mohler KM, et al. Fully human CD19-specific chimeric antigen receptors for T-cell therapy. Leukemia. 2017; 31(10): 2191-2199.
14. Song DG, Ye Q, Poussin M, Liu L, Figini M, Powell DJ Jr. A fully human chimeric antigen receptor with potent activity against cancer cells but reduced risk for off-tumor toxicity. Oncotarget. 2015; 6(25): 21533-21546.
15. Hege KM, Bergsland EK, Fisher GA, Nemunaitis JJ, Warren RS, McArthur JG, et al. Safety, tumor trafficking and immunogenicity of chimeric antigen receptor (CAR)-T cells specific for TAG-72 in colorectal cancer. J Immunother Cancer. 2017; 5: 22.
16. Sharifzadeh Z, Rahbarizadeh F, Shokrgozar MA, Ahmadvand D, Mahboudi F, Jamnani FR, et al. Genetically engineered T cells bearing chimeric nanoconstructed receptors harboring TAG-72-specific camelid single domain antibodies as targeting agents. Cancer Lett. 2013; 334(2): 237-244.
17. Jamnani FR, Rahbarizadeh F, Shokrgozar MA, Mahboudi F, Ahmadvand D, Sharifzadeh Z, et al. T cells expressing VHH-directed oligoclonal chimeric HER2 antigen receptors: towards tumor-directed oligoclonal T cell therapy. Biochim Biophys Acta. 2014; 1840(1): 378-386.
18. Ajina A, Maher J. Strategies to address chimeric antigen receptor tonic signaling. Mol Cancer Ther. 2018; 17(9): 1795-1815.
19. Bakhtiari SH, Rahbarizadeh F, Hasannia S, Ahmadvand D, Iri-Sofla FJ, Rasaee MJ. Anti-MUC1 nanobody can redirect T-body cytotoxic effector function. Hybridoma (Larchmt). 2009; 28(2): 85-92.
20. Yang S, Zhou X, Li R, Fu X, Sun P. Optimized PEI-based transfection method for transient transfection and lentiviral production. Curr Protoc Chem Biol. 2017; 9(3): 147-157.
21. Delenda C, Gaillard C. Real-time quantitative PCR for the design of lentiviral vector analytical assays. Gene Ther. 2005; 12 Suppl 1: S36-S50.
22. Taylor-Papadimitriou J, Burchell JM, Graham R, Beatson R. Latest developments in MUC1 immunotherapy. Biochem Soc Trans. 2018; 46(3): 659-668.
23. Sahraei M, Roy LD, Curry JM, Teresa TL, Nath S, Besmer D, et al. MUC1 regulates PDGFA expression during pancreatic cancer progression. Oncogene. 2012; 31(47): 4935-4345.
24. Kitamoto S, Yokoyama S, Higashi M, Yamada N, Takao S, Yonezawa S. MUC1 enhances hypoxia-driven angiogenesis through the regulation of multiple proangiogenic factors. Oncogene. 2013; 32(39): 4614-4621.
25. Huang L, Chen D, Liu D, Yin L, Kharbanda S, Kufe D. MUC1 oncoprotein blocks glycogen synthase kinase 3beta-mediated phosphorylation and degradation of β-catenin. Cancer Res. 2005; 65(22): 10413-1022.
26. Pang Y, Hou X, Yang C, Liu Y, Jiang G. Advances on chimeric antigen receptor-modified T-cell therapy for oncotherapy. Mol Cancer. 2018; 17(1): 91.
27. Zhong XS, Matsushita M, Plotkin J, Riviere I, Sadelain M. Chimeric antigen receptors combining 4-1BB and CD28 signaling domains augment PI3kinase/AKT/Bcl-XL activation and CD8+ T cell–mediated tumor eradication. Mol Ther. 2010; 18(2): 413-420.
28. Morgan RA, Yang JC, Kitano M, Dudley ME, Laurencot CM, Rosenberg SA. Case report of a serious adverse event following the administration of T cells transduced with a chimeric antigen receptor recognizing ERBB2. Mol Ther. 2010; 18(4): 843-851.
29. Ahmed N, Brawley VS, Hegde M, Robertson C, Ghazi A, Gerken C, et al. Human epidermal growth factor receptor 2 (HER2)–specific chimeric antigen receptor–modified T cells for the immunotherapy of HER2-positive sarcoma. J Clin Oncol. 2015; 33(15): 1688-1696.
30. Dotti G, Gottschalk S, Savoldo B, Brenner MK. Design and development of therapies using chimeric antigen receptor-expressing T cells. Immunol Rev. 2014; 257(1): 107-126.
31. Saerens D, Ghassabeh GH, Muyldermans S. Single-domain antibodies as building blocks for novel therapeutics. Curr Opin

Pharmacol. 2008; 8(5): 600-608.
32. Van Bockstaele F, Holz JB, Revets H. The development of nanobodies for therapeutic applications. Curr Opin Investig Drugs. 2009; 10(11): 1212-1224.
33. Xie Q, Xinyong G, Xianjin C, Yayu W. PEI/DNA formation affects transient gene expression in suspension Chinese hamster ovary cells via a one-step transfection process. Cytotechnology. 2013; 65(2): 263-271.
34. Eshhar Z. The T-body approach: redirecting T cells with antibody specificity. Handb Exp Pharmacol. 2008; (181): 329-342.
35. Morita D, Nishio N, Saito S, Tanaka M, Kawashima N, Okuno Y, et al. Enhanced expression of anti-CD19 chimeric antigen receptor in piggyBac transposon-engineered T cells. Mol Ther Methods Clin Dev. 2017; 8: 131-140.
36. Frigault MJ, Lee J, Basil MC, Carpenito C, Motohashi S, Scholler J, et al. Identification of chimeric antigen receptors that mediate constitutive or inducible proliferation of T cells. Cancer Immunol Res. 2015; 3(4): 356-367.
37. Long AH, Haso WM, Shern JF, Wanhainen KM, Murgai M, Ingaramo M, et al. 4-1BB costimulation ameliorates T cell exhaustion induced by tonic signaling of chimeric antigen receptors. Nat Med. 2015; 21(6): 581-590.
38. Gomes-Silva D, Mukherjee M, Srinivasan M, Krenciute G, Dakhova O, Zheng Y, et al. Tonic 4-1BB costimulation in chimeric antigen receptors impedes T cell survival and is vector-dependent. Cell Rep. 2017; 21(1): 17-26.
39. Wörn A, PluÈckthun A. Stability engineering of antibody single-chain Fv fragments. J Mol Biol. 2001; 305(5): 989-1010.
40. Rahbarizadeh F, Ahmadvand D, Sharifzadeh Z. Nanobody; an old concept and new vehicle for immunotargeting. Immunol Invest. 2011; 40(3): 299-338.

Diosgenin and 4-Hydroxyisoleucine from Fenugreek Are Regulators of Genes Involved in Lipid Metabolism in The Human Colorectal Cancer Cell Line SW480

Maryam Mohammad-Sadeghipour, M.Sc.[1, 2], Mehdi Mahmoodi, Ph.D.[2, 3, 4], Mojgan Noroozi Karimabad, Ph.D.[4], Mohammad Reza Mirzaei, Ph.D.[3, 4], Mohammad Reza Hajizadeh, Ph.D.[3, 4*]

1. Student Research Committee, School of Medicine, Kerman University of Medical Sciences, Kerman, Iran
2. Department of Clinical Biochemistry, Afzalipoor Faculty of Medicine, Kerman University of Medical Sciences, Kerman, Iran
3. Department of Clinical Biochemistry, Faculty of Medicine, Rafsanjan University of Medical Sciences, Rafsanjan, Iran
4. Molecular Medicine Research Center, Institute of Basic Medical Sciences Research, Rafsanjan University of Medical Sciences, Rafsanjan, Iran

Corresponding Addresses: P.O.Box: 7718175911, Molecular Medicine Research Center, Institute of Basic Medical Sciences Research, Rafsanjan University of Medical Sciences, Rafsanjan, Iran
Email: hajizadehus@yahoo.com

Received: 1/February/2019, Accepted: 08/May/2019

Abstract

Objective: Diosignin and 4-hydroxy-L-isulosine (4-OH-Ile) are the two active ingredients of Fenugreek (*Trigonella foenum-graecum*). Thus, in this study, we examined the effects of hydroalcoholic extract of fenugreek seeds (HEFS), diosgenin and 4-OH-Ile on the expression of acetyl-CoA carboxylase (*ACC*), fatty acid synthase (*FAS*), peroxisome proliferator-activated receptor gamma (*PPARγ*) and low-density lipoprotein (LDL) receptor (*LDLR*) which are involved in lipid metabolism in SW480 cell line.

Materials and Methods: In this experimental study, SW480 cells were cultured in RPMI-1640 medium and treated with HEFS, diosignin, 4-OH-Ile or orlistat for 24 and 48 hours. Inhibitory concentration of 20% (IC20) was calculated using MTT method and cells were then pre-treated with the IC20 concentrations for 24 and 48 hours before RNA extraction and cDNA synthesis. Changes in the expression of *ACC, FAS, PPARγ* and *LDLR* genes were assayed by employing the real time-polymerase chain reaction (PCR) method.

Results: Our results showed a significant down-regulation in the expression of *ACC* ($P<0.001$ and $P<0.001$ after 24 and 48 hours, respectively) and *FAS* genes ($P<0.001$ and $P<0.001$ after 24 and 48 hours, respectively) in SW480 cells treated with HEFS, diosignin, 4-OH-Ile, or orlistat, but significant up-regulation in the expression of *PPARγ* ($P<0.001$ and $P<0.001$ after 24 and 48 hours, respectively) and *LDLR* ($P=0.005$ and $P=0.001$ after 24 and 48 hours, respectively).

Conclusion: According to the results of the present study, HEFS, diosgenin and 4-OH-Ile up or down-regulate the expression of some predominant genes involved in lipid metabolism pathway, similar to that observed for orlistat. These types of regulatory effects are presumably proper for the treatment of obesity and overweight.

Keywords: Trigonella, Diosgenin, Orlistat, Obesity

Cell Journal(Yakhteh), Vol 22, No 4, January-March (Winter) 2021, Pages: 514-522

Citation: **Mohammad-Sadeghipour M, Mahmoodi M, Noroozi Karimabad M, Mirzaei MR, Hajizadeh MR. Diosgenin and 4-Hydroxyisoleucine from fenugreek are regulators of genes involved in lipid metabolism in the human colorectal cancer cell line SW480. Cell J. 2021; 22(4): 514-522. doi: 10.22074/cellj.2021.6751.**

Introduction

Obesity is one of the greatest public health challenges of the 21st century that is increasing at various rates worldwide (1). Approximately 20% of the global population is obese (about 1.5 billion people) (2). Obesity has an adverse effect on the quality of life and overweight is associated with some disorders such as dyslipidemia, type 2 diabetes mellitus, hypertension, gallbladder disease (3), osteoarthritis and cancers at several sites (mainly endometrial, breast, and colorectal) (4). Overweight is defined as having a body mass index (BMI) between 25 and 29.9 kg/m^2, while obesity is described as a BMI of over 30 kg/m^2 (5). Four weight-loss drugs have recently been approved by the US food and drug administration (FDA), and among them, some drugs (Orlistat, Xenical® and Alli® and Sibutramine) were found to be appropriate for long-term use (6). Orlistat as a reversible inhibitor of gastric and pancreatic carboxylester lipase also reduces the absorption of lipids in the intestine (Fig.1A) (7). In addition to being expensive, these synthetic reagents have considerable side effects on the gastrointestinal tract and their use is restricted to treatment of obesity. Medicinal plants are of great value and importance and are considered for providing health and well-being, both for treatment and prevention of the diseases and therefore, many of the drugs of modern medicine were originated from plant sources (8).

Trigonella foenum-graecum (Fenugreek) is an annual plant belonging to the Leguminosae family, and grows in different climates especially in the Mediterranean

countries and India. The fenugreek seeds have long been consumed for medicinal purposes in many countries (9). The biological and pharmaceutical properties of fenugreek seeds are mainly due to the presence of several components, including alkaloids, sapogenins, mucilages, 4-hydroxy-L-isoleucine (4-OH-Ile) (Fig.1B), galactomannan, diosgenin (Fig.1C) and fiber (10). Findings of a study showed that daily consumption of 1176 mg of fenugreek hydroalcoholic extract by healthy volunteers, resulted in decreased fat intake (9). Fuller and Stephens (11), reported that three bioactive compounds of fenugreek (diosgenin, 4-OH-Ile and fiber) controlled both hyperglycemia and hyperlipidemia. Fenugreek is also a rich source of diosgenin (as a steroidal saponin) which is generated by hydrolysis of saponins (12). 4-OH-Ile is a branched-chain amino acid that exists in plant sources and is especially abundant in fenugreek seeds. Animal studies demonstrated hypoglycaemic and antihyperlipidemic properties for 4-OH-Ile (13).

The absorption of fat by the gut cells has an important role in the maintenance of fat metabolism balance, but its regulation at the molecular level remains largely unknown (14). The gut cells play a role in the production of apolipoproteins and lipoproteins, which are formed of combination of lipids with proteins (15). Different proteins affect the absorption of fat in the gut, including: FAS, a key enzyme in fat biosynthesis (16), and *ACC* which is the key enzyme in fat metabolism, it is a biotin-dependent enzyme that catalyzes the irreversible carboxylation of acetyl-CoA to produce through its two catalytic activities, biotin carboxylase (BC) and carboxyltransferase (CT) (17). So, these cells are highly involved in the synthesis and absorption of fat. Moreover, orlistat, a gastric and pancreatic lipase inhibitor that reduces dietary fat absorption, has been used for nearly ten years (7), and is known as a FAS inhibitor (18). Since our aim was to study the hypolipidemic effects of HEFS and diosignin and 4-OH-Ile compared to orlistat, we preferred to use SW480 cell line.

Although metabolic effects of fenugreek have been widely studied, there is no study yet to address its effects on the gut cells. While most studies done in the SW480 cell line are related to cancer and metastasis and inflammation, there is no study of lipid metabolism in these cells yet. Thus, the current investigation was aimed for the first time, to examine the hypolipidemic effects of hydroalcoholic extract of fenugreek seeds (HEFS) and its two bioactive compounds (diosignin and 4-OH-Ile), in addition to orlistat via evaluation of the expression of acetyl-CoA carboxylase (ACC), fatty acid synthase (FAS), peroxisome proliferator-activated receptor gamma (PPARγ) and low-density lipoprotein (LDL) receptor (LDLR) as the genes responsible for lipid metabolism in the SW480 cell line.

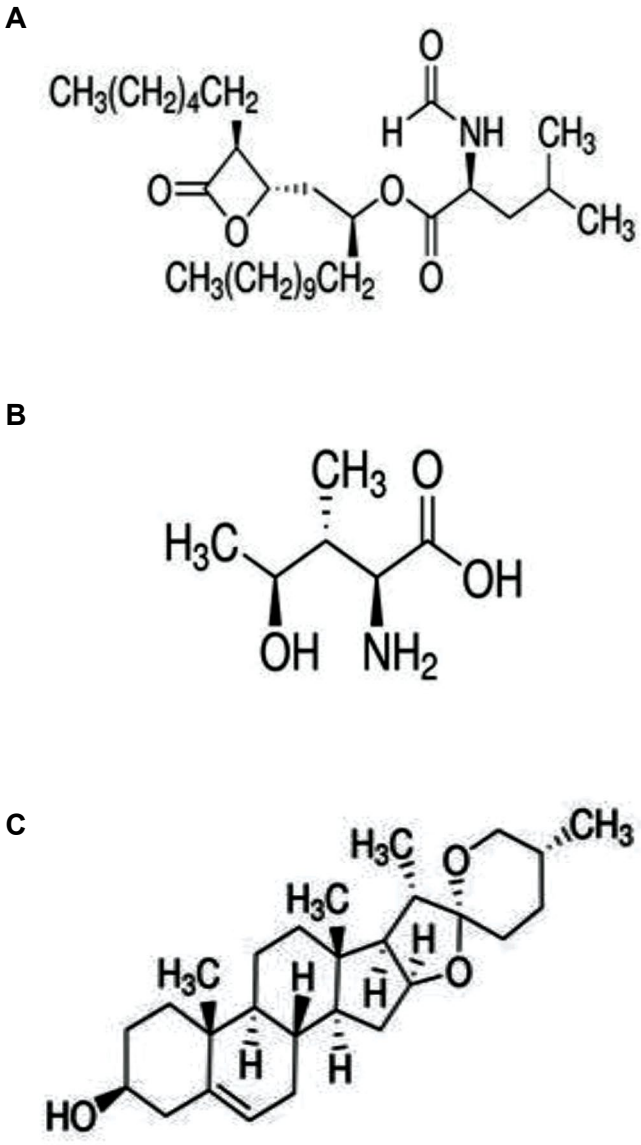

Fig.1: The structure of antihyperlipidemic drug and bioactive compounds of fenugreek respectively. **A.** Orlistat, **B.** 4-hydroxy-L-isoleucine, and **C.** Diosgenin.

Materials and Methods

In this experimental study, a batch of SW480 cell line was purchased from Pasteur Institute (Iran, Tehran). RPMI-1640, fetal bovine serum (FBS), penicillin-streptomycin and trypsin were provided from Gibco-BRL (Grand Island, NY, USA), MTT powder and dimethyl sulfoxide (DMSO) were bought from Merck (USA), diosgenin of 93% purity, 4-OH-Ile (2S3R4S Isoform) of ≥98% (TLC) purity and orlistat of approximately ≥98% purity, were provided from Sigma (USA). RNA extraction and cDNA synthesis kits were purchased from PARS Tous (Iran), and SYBR Green Premix Ex Taq II Kit was obtained from ABI Company (Takara, Japan). This study approved by the Rafsanjan University of Medical Sciences (RUMS) Ethical Committee (IR.RUMS.REC.1395.109).

Extraction of plant materials

The dry milled fenugreek powder (5 g) was packed in

a filter paper and placed into a container filled up to two thirds of its volume with 70% ethanol. The extraction was further performed using a Soxhlet apparatus at 80°C for 100 min (BAKHSHI Laboratory Industrial Co., Iran). The extract was dehydrated by a freeze dryer apparatus (VaCo5-D, Zirbus Technology Co., Germany) at -70°C for 72 hours and the collected dry yellow crystalline powder was stored at -20°C for further use. Different concentrations of the extract were obtained by dissolution in RPMI 1640.

Preparation of diosgenin, 4-OH-Ile, and orlistat

Initial stock solutions of diosgenin, 4-OH-Ile, and orlistat were prepared in ethanol, phosphate-buffered saline (PBS), and DMSO, respectively.

Cell culture

SW480 cells were cultured at 37°C in the presence of 95% O_2 and 5% CO_2 in complete cell culture medium (CCM) comprising RPMI-1640, in addition to 10% FBS and 100 IU/ml of penicillin and 100 µg/ml of streptomycin. Cells were grown to 80% confluence prior to treatment for 24 and 48 hours.

Analysis of cell proliferation by MTT assay

Cell proliferation was assessed by 3-(4,5-dimethylthiazol-2-yl)-2,5-diphenyltetrazolium bromide (MTT) assay. SW480 cells (7×10^3 cells per well) were seeded in 96-well plates with the culture medium containing FBS, allowed to grow and become attached, and then treated with HEFS (0-2000 µg/ml), diosgenin (0-32 µg/ml) 4-OH-Ile (0-16 µg/ml) and orlistat (0-48 µg/ml) for 24 and 48 hours. All the experiments were performed in sextuple assay. After incubation, 10 µl of MTT solution (5 mg/ml in PBS stock solution) was added to each well and incubated at 37°C for 4 hours. The medium was removed, and the purple formazan crystals were dissolved in 150 µl of DMSO. The optical density (OD) was measured at 570 nm using an ELISA reader.

Relative growth rate (%)=(OD treatment/OD control)×100

An average inhibitory concentration of 20% (IC20) will result in 80% cell survival. The IC20 value was partly non-toxic where the SW480 cells exhibited an approximate viability of 80%. This IC20 concentration was considered for future treatment of SW480 cells. Thus, treatments were performed using HEFS 50 µg/ml, and 6.21, 1.37, 4.64 µg/ml of diosgenin, 4-OH-Ile, and orlistat, respectively for 24 and 48 hours. One flask containing cells and complementary culture medium were considered as controls.

RNA extraction and cDNA synthesis

Total cellular RNA content was isolated and the complementary DNA (cDNA) was synthesized employing Pars Tous kit according to the manufacturer's instructions. Both purity and integrity of harvested RNA specimens were analyzed by spectrophotometry and electrophoresis in agarose gel, respectively. The purity was assessed by the A260/280 and A260/230 absorbance ratios obtained using a NanoDrop spectrophotometer. The samples were further used for cDNA synthesis.

Real time-polymerase chain reaction

Specific primers were designed employing primer 3 and BLAST software in NCBI (Table 1). The level (percentage) of changes in the expression of *ACC, FAS, PPARγ,* and *LDLR* genes was evaluated by real time-polymerase chain reaction (RT-PCR) technique with ABI Step One Plus TM Real-Time PCR System (Applied Biosystems, USA) and using the Takara Bio SYBR Green Master Mix Kit (Japan) at a final volume of 20 µl. Thermal cycling conditions were as follows: 95˚C for 30 seconds and 40 cycles at 95˚C for 5 seconds, and continued at *ACC*: 60˚C, *FAS*: 62˚C, *PPARγ*: 58˚C, and *LDLR*: 61˚C for 30-60 seconds. Threshold cycle (CT) data was analyzed by Step One ver.2.3 software. Relative values of the fold changes in the expression of genes were calculated by $2^{-\Delta\Delta Ct}$ where $\Delta_{Ct}=_{Ct}$ (target genes) - Ct (reference gene) and $\Delta\Delta_{Ct}=\Delta_{Ct}$ (treated groups) - Δ_{Ct} (untreated group (control)). Eventually, $2^{-\Delta\Delta CT}$ values were estimated using Excel 2013 (Table 2) (19).

Table 1: Nucleotide sequence of primers used in this study

Gene	Primer sequence (5´-3´)
ACC	F: GGATCCGGCGCCTTACTT
	R: CTCCGATCCACCTCATAGTTGAC
FAS	F: TTGGAAGGCCTGCATCATG
	R: CACCTGGAGGACAGGGCTTA
PPARγ	F: TCAGGGCTGCCAGTTTCG
	R: GCTTTTGGCATACTCTGTGATCTC
LDLR	F: ACTGGGTTGACTCCAAACTTCAC
	R: GGTTGCCCCCGTTGACA
β-Actin	F: GATCAGCAAGCAGGAGTATG
	R: GTGTAACGCAACTAAGTCATAG

Table 2: Inhibitory concentration of 20% (IC20) following 24 and 48 hours of treatment with HEFS, diosgenin, 4-OH-Ile, and orlistat

Treatment	IC20 after treatment (24, 48 hours)
HEFS (µg/ml)	50
Diosgenin (µg/ml)	6.21
4-OH-Ile (µg/ml)	1.37
Orlistat (µg/ml)	4.64

Statistical analysis

Data is presented as mean ± SD of triplex independent experiments. Data were statistically analyzed by the SPSS Statistical Package software version 18.0 for Windows (SPSS Inc. Chicago, IL, USA). The gene expression data was analyzed by one-way ANOVA among different groups. Tukey's post hoc test was used to evaluate differences in each group. Treated groups were compared to the untreated control using one-way ANOVA accompanied by a Dunnett's post hoc test. Independent t test was used to compare the effect of treatment period in each group. The differences were considered significant if $P<0.05$.

Results

Effects of HEFS, diosgenin, 4-OH-Ile and orlistat on the viability of SW480 cells

The *in vitro* cytotoxic effects of HEFS, diosgenin, 4-OH-Ile, and orlistat were evaluated by MTT test. Cell viability following treatment with different concentrations of the mentioned compounds, was assessed by MTT assay and is presented in Figure 2. These results showed that in response to 24 and 48 hours treatment with the mentioned compounds, the viability of SW480 cells was decreased in a concentration-dependent manner ($P<0.001$). Also, 24 hours after the treatment with HFSE, cell viability percentage decreased from 81.61 ± 5.44% at the concentration of 50 µg/mLl to 21.11 ± 1.40% at the concentration of 1000 µg/ml, and 48 hours after the treatment, it decreased from 75.38 ± 3.88% at the concentration of 50 µg/ml to 21.77 ± 2.96% at the concentration of 1000 µg/ml ($P<0.001$, Fig.2).

The results also showed that 24 hours after the treatment with diosgenin, viability percentage decreased from 95.8 ± 2.35% at the concentration of 2 µg/ml to 40.16 ± 2.08% at the concentration of 32 µg/ml, and 48 hours after the treatment, it decreased from 82.66 ± 1.23% at the concentration of 2 µg/ml to 33.91 ± 1.92% at the concentration of 32 µg/ml ($P<0.001$, Fig.2). In addition, 24 hours after treatment with 4-OH-Ile, viability percentage reached 19.25 ± 5.46% at the concentration of 16 µg/ml and 87.66 ± 1.61% at the concentration of 1µg/ml, and 48 hours after the treatment, it changed from 85.41 ± 3.11% at the concentration of 1 µg/ml to 16.75 ± 2.05% at the concentration of 16 µg/ml ($P<0.001$, Fig.2). Furthermore, 24 hours after treatment with orlistat, viability percentage reached 34.16 ± 1.69% at the concentration of 48 µg/ml to 87.57 ± 1.61% at the concentration of 3 µg/ml, and 48 hours after treatment, it was 33.83 ± 1.64% at the concentration of 48 µg/ml and 82.91 ± 1.72% at the concentration of 3 µg/ml ($P<0.001$, Fig.2). Results also indicated that concentrations <50 µg/ml of HEFS, ≤6.21 µg/ml of diosgenin, ≤1.37 µg/ml of 4-OH-Ile and ≤4.64 µg/ml of orlistat had the minimum inhibitory effect on SW480 cell viability after 24 hours or 48 hours of treatment. Therefore, for the future experiments, the IC20 was used and thus, at this concentration, nearly 80% of the cells had survival potential. In Figure 3, the negative control group, the concentration of IC20 and the concentration of IC50 of SW480 cells, are shown.

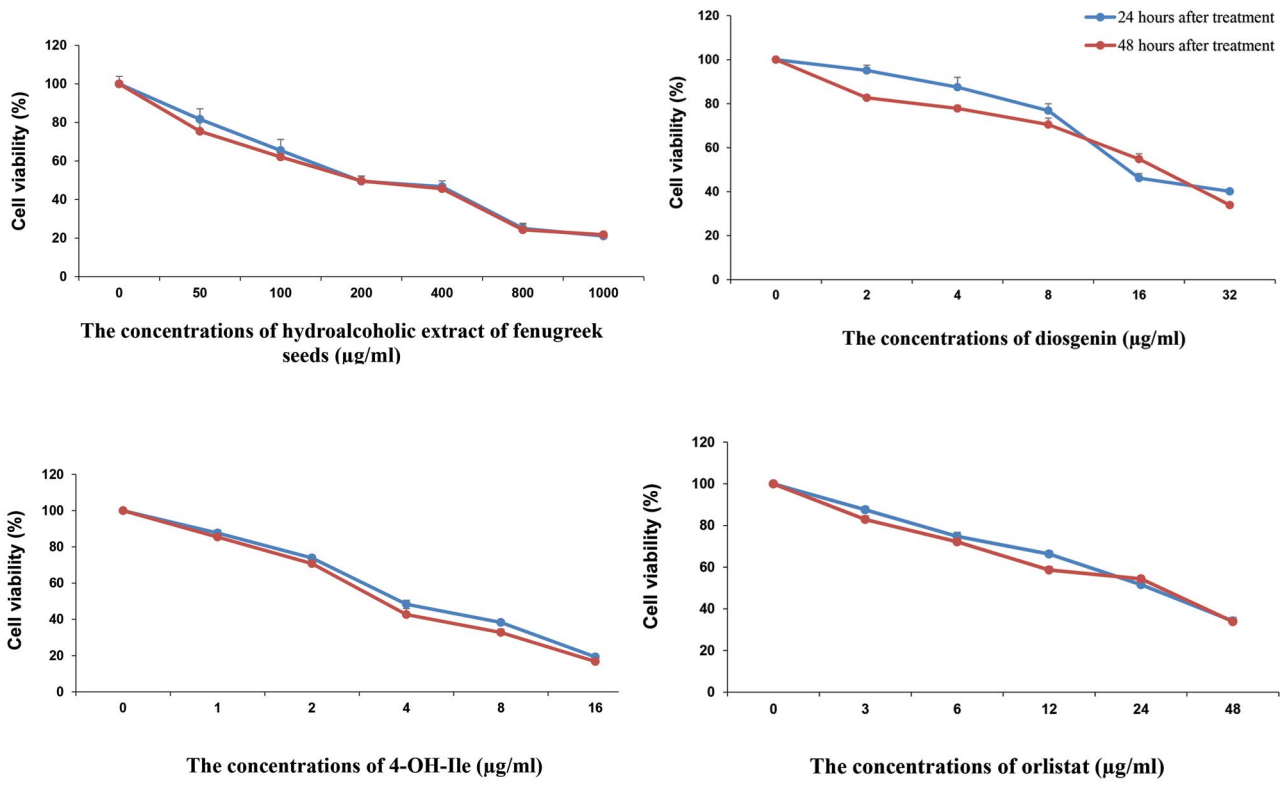

Fig.2: Percentage of SW480 cells viability following 24 and 48 hours of treatment with different concentrations of HEFS, Diosgenin, 4-OH-Ile, and Orlistat (µg/mL) measured by MTT assay. Results were obtained from three independent experiments as individual and triplicate and data are presented as mean ± SD, ($P<0.001$).

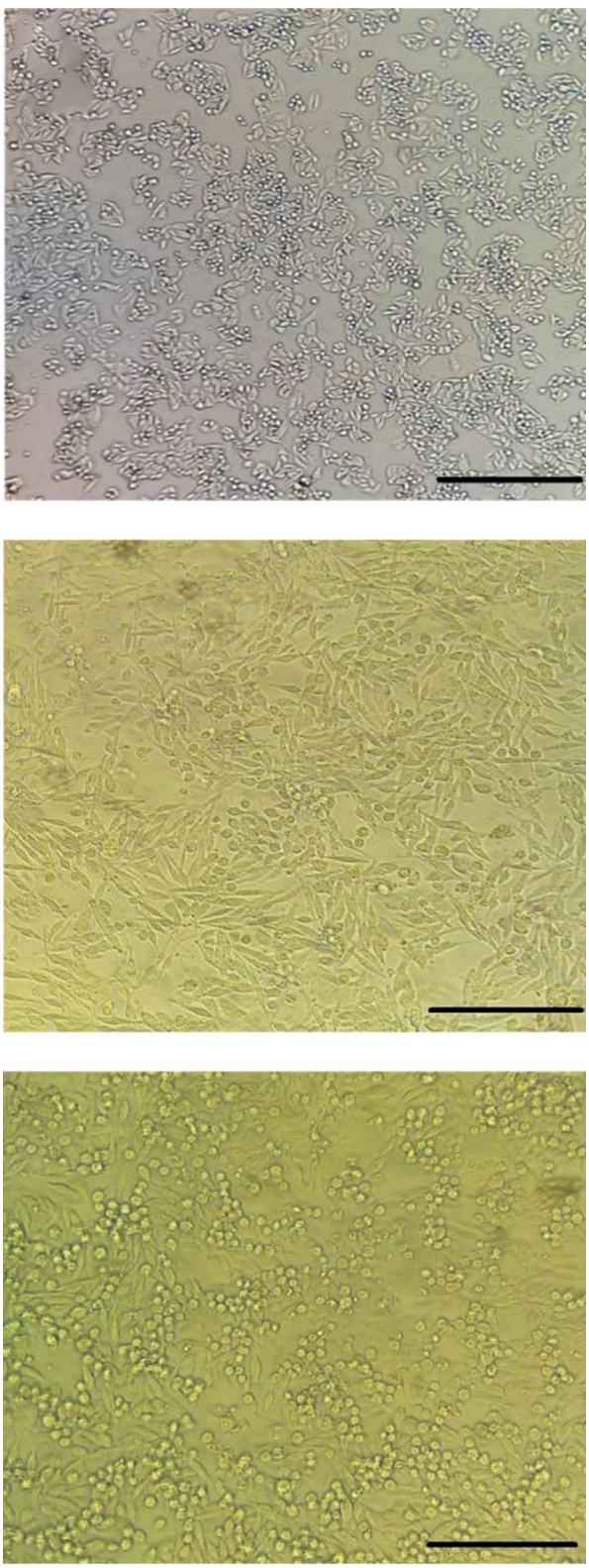

Fig.3: Morphological changes on SW480 cells after exposure with HEFS that were observed with an inverted microscope. **A.** 0 (untreated), **B.** IC20 concentration, and **C.** IC50 concentration (scale bar: A-C: 40 µm). IC; Inhibitory concentration.

HEFS, diosgenin, 4-OH-Ile and orlistat down-regulated the expression of *ACC* and *FAS* genes in SW480 cells

Our RT-PCR results showed that 24 and 48 hours treatment with IC20 concentration of HEFS, diosgenin, 4-OH-Ile, and orlistat significantly downregulated the mRNA level of genes involved in lipid metabolism, including *ACC* (0.48-, 0.34-, 0.44- and 0.25-fold decrease, respectively in 24 hours P<0.001) and (0.24-, 0.30-, 0.33-, and 0.23-fold decrease, respectively in 48 hours P<0.001) compared to the negative control. After orlistat, the most marked reduction in 24 hours was related to diosgenin (P<0.001) and HEFS (P<0.001) in 48 hours (Fig.4A).

IC20 concentration of the compounds significantly downregulated the expression of FAS (0.38-, 0.34-, 0.50-, and 0.20-fold decrease, respectively in 24 hours P<0.001) and (0.25-, 0.22-, 0.27-, and 0.20-fold decrease, respectively in 48 hours P<0.001) compared to the negative control. After orlistat, the most marked reduction in 24 and 48 hours was related to diosgenin (P<0.001) (Fig.4B).

HEFS, diosgenin, 4-OH-Ile and orlistat up-regulated the expression of *PPARγ* and *LDLR* genes in SW480 cells

We also cultured SW480 cells in the presence of the compounds of the expression of *PPARγ* (1.23-, 4.45-, 2.37-, and 1.89-fold decrease, respectively for HEFS, diosgenin, 4-OH-Ile and orlistat in 24 hours P<0.001) and (2.19-, 5.27, 3.44-, and 3.39-fold decrease, respectively for HEFS, diosgenin, 4-OH-Ile and orlistat in 48 hours P<0.001). These results showed that, diosgenin (P<0.001 and P<0.001 for 24 and 48 hours, respectively), 4-OH-Ile (P=0.035 and P=0.022 for 24 and 48 hours, respectively) and orlistat (P=0.028) in 48 hours significantly reduced the expression of *PPARγ* gene compared to the negative control. Also, there was a significant difference between diosgenin and 4-OH-Ile groups (P=0.001 and P=0.002 for 24 and 48 hours, respectively); diosgenin and orlistat groups (P<0.001, and P=0.001 for 24 and 48 hours, respectively). The independent t test results indicated a significant increase in *PPARγ* gene expression after 48 hours of treatment with HFSE and orlistat compared to *PPARγ* expression in 24 hours (P=0.043) and (P=0.003) respectively for HFSE and orlistat). Overall, among the four compounds used in this study the greatest reduction was related to diosgenin in 24 and 48 hours (P<0.001, Fig.4C).

Also, a significant up-regulation was observed in the expression of *LDLR* (2.14-, 2.91-, 2.76-, and 3-fold decrease, respectively in 24 hours P=0.005) and (1.53-, 3.54-, 1.59-, and 3.31-fold decrease, respectively in 48 hours P=0.001) genes compared to the negative control. 48-hour results showed significant differences between HFSE and diosgenin groups (P=0.011); HFSE and orlistat groups (P=0.034); diosgenin and 4-OH-Ile groups (P=0.013); and 4-OH-Ile and orlistat groups (P=0.042). The results showed that among the treated groups, the most marked reduction in 24 hours was related to orlistat (P=0.004), while the greatest diminution was related to diosgenin in 48 hours (P=0.001, Fig.4D).

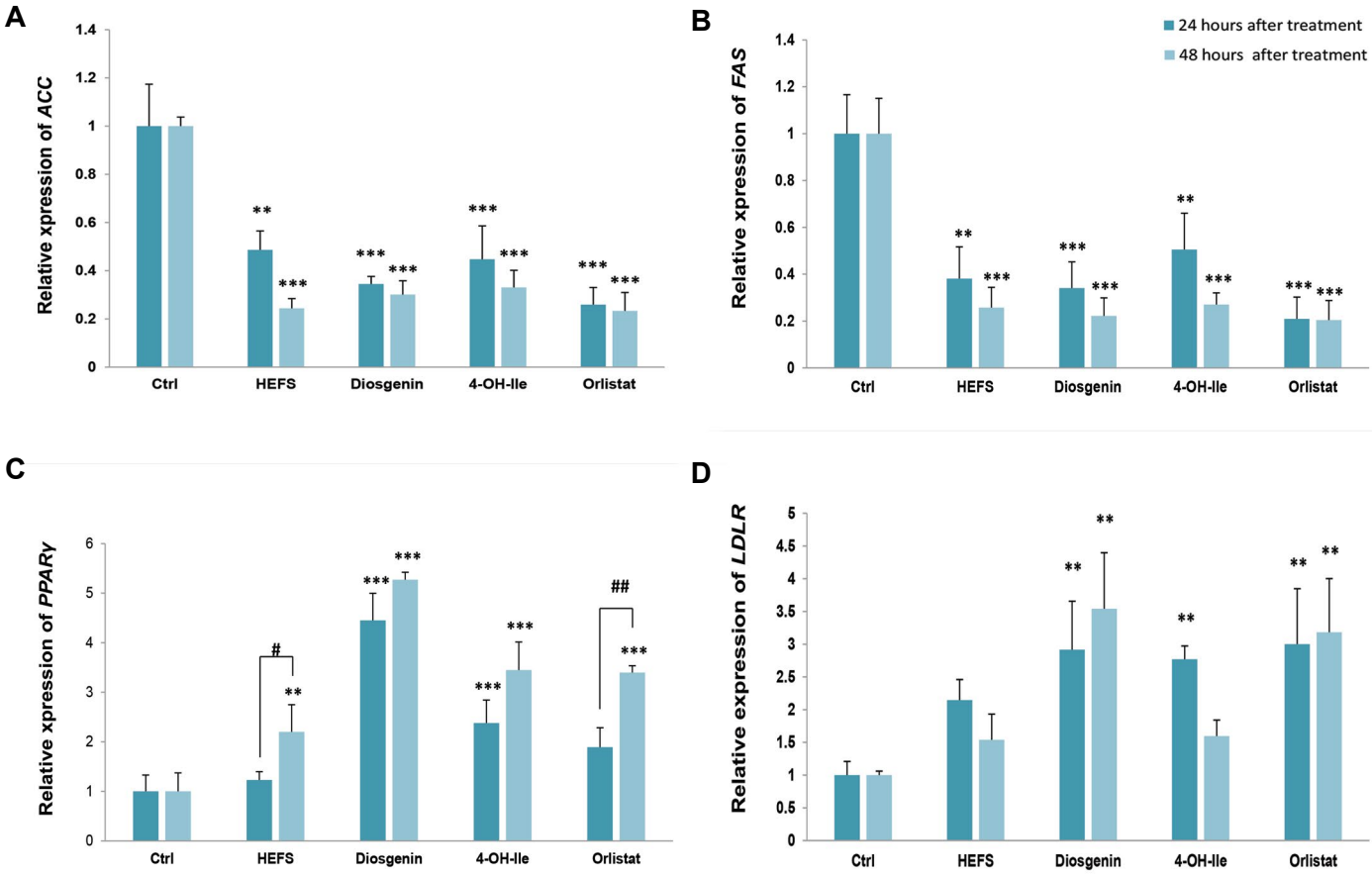

Fig.4: The effects of HFSE, diosgenin, 4-OH-Ile, and orlistat on genes expression in SW480 cells in 24 and 48 hours, respectively. **; P<0.01 and ***; P<0.001 show significant differences compared with the untreated control. #; P<0.05 and ##; P<0.01, and show significant differences between 24 and 48 hours in the indicated groups. **A.** *ACC* (P<0.001, P<0.001), **B.** *FAS* (P<0.001, P<0.001), **C.** *PPARγ* (P<0.001, P<0.001), and **D.** *LDLR* (P=0.005, P=0.001).

Discussion

Excessive fat accumulation which is most often due to overeating, leads to obesity and overweight (20). Obesity and overweight, as major health problems, affect all age groups, especially in developing countries (21). Serious social and clinical burdens are imposed by obesity, as reported by researchers. The association between obesity and metabolic syndrome including insulin resistance, type 2 diabetes, heart disease, dyslipidaemia, hypertension and certain types of cancer varying from breast, colon to prostate, is well defined (13). A large body of evidence showed that colon cancers affect obese people more than those with normal weight (22).

Although the initial step for the obesity therapy is lifestyle modification, several synthetic drugs, including orlistat and sibutramine, were designed for obesity, but the safety and efficacy of these drugs are yet to be established. Some medicinal plants were also examined for controlling obesity (23).

Fenugreek, as a medicinal plant, has long been consumed for treatment of metabolic diseases (11). Investigations suggested that the ethanolic extract of fenugreek seeds was able to significantly reduce the plasma level of cholesterol and attenuate the concentrations of liver cholesterol in hypercholesterolemic rats (24). Recent studies reported that fenugreek can be used as a functional supplement for regulation of glucose and lipid profile. Human and animal studies found that fenugreek seeds are rich in fiber, which gives the feeling of satiety and reduces food intake (25). The beneficial effects of fenugreek seeds on the reduction of total cholesterol, TG and LDL-cholesterol levels and hepatic lipid concentrations, were indicated. These effects are due to saponins and diosgenin which are present in fenugreek seeds (26).

It is believed that if the lipid levels, especially TG and LDL-cholesterol are controlled, the risk of several diseases such as type 2 diabetes, metabolic syndrome, insulin resistance, high blood pressure, dyslipidemia, infertility, cardiovascular disease and others, is significantly reduced.

Our findings for the first time, show that HEFS, diosgenin and 4-OH-Ile significantly downregulate *ACC* and *FAS*, while significant up-regulation of *PPARγ* and *LDLR* genes in SW480 cells was similar to changes induced by orlistat following 24 and 48 hours of treatment. Since there is so far no study on the effect of HEFS, diosgenin, 4-OH-Ile, and orlistat in SW480 cells, here, we refer to similar studies accomplished in other cell lines and animals.

ACC is the downstream target of *AMPK* and has been described as a key enzyme in fatty acid biosynthesis where

it catalyzes the carboxylation of acetyl-CoA to malonyl-CoA. In the present study, HEFS, diosgenin and 4-OH-Ile, all decreased the expression of *ACC* gene. Based on the Pyra et al. (27) study, it can possibly be suggested that HEFS and its two bioactive compounds can lead to phosphorylation of *ACC* through phosphorylation of AMPK. Moreover, by reducing the mRNA expression level of *ACC* gene via further phosphorylation, the activity of *ACC* is inhibited and thereby declines the available substrate for *FAS* and, accordingly, de novo fatty acid synthesis. Also, as a result of reducing the content of malonyl-CoA, carnitine palmitoyltransferase I (*CPT-1*) enzyme, which is the key enzyme in the oxidation of fatty acids, is activated and the beta-oxidation of fatty acids increases (28). These results showed that HEFS and its two bioactive compounds acted in a time-dependent manner, similar to orlistat, and reduced the expression of *ACC* gene. The greatest reduction was related to HEFS in 48 hours. Therefore, it can be said that HEFS probably exerts its hypolipidemic effects via its two bioactive compounds.

One crucial anabolic enzyme required for de novo synthesis of fatty acids is FAS for which, nicotinamide adenine dinucleotide phosphate (*NADPH*) is a cofactor. The present study demonstrated that FAS, as a well-known and important lipogenic enzyme is downregulated in HEFS, 4-OH-Ile, and diosgenin-treated SW480 cells. It was reported that reduced expression of *FAS* inhibited *de novo* synthesis of fatty acids (29). One study reported that diosgenin reduced the abnormal changes in lipid profile including total cholesterol, triglyceride, and LDL-C. Also, the expressions of *SREBP-1* and its target genes, including *FAS*, (*SCD-1*), and *ACC* were inhibited by diosgenin in rats (30). These results are consistent with our study results. So, it can be suggested that probably, HEFS by its diosgenin content, decreases the expression of *ACC* and *FAS* genes via modulation of *SREBP-1C*.

Our findings demonstrated that HEFS, diosgenin and 4-OH-Ile significantly up-regulated the expression of *PPARγ* gene compared to orlistat. *PPARγ* is a member of the nuclear hormone receptor superfamily that regulates gene expression by binding to DNA and plays an important role in lipid homeostasis. It is highly expressed in white and brown adipose tissues, however, it is also expressed by the colon, liver, and muscle (31). Unsaturated fatty acids and their derivatives are endogenous ligands for PPARs. After binding to ligand, PPARs after heterodimerization with retinoic X receptor (*RXR*), bind to *PPAR* response elements (*PPREs*) in the regulatory region of several target genes (32). *PPARγ* is a positive regulator of adiponectin (*ADN*) gene expression. *ADN* increases fatty acid oxidation and limits the endogenous synthesis of lipids by reducing the circulating level of free fatty acids (33). So, HEFS and its two bioactive compounds act like PPAR ligands and upregulate the expression of *PPAR-γ*, hence enhancing the level of ADN by therapeutic agents might be helpful in the treatment of obesity and overweight. A study determined that three phytochemicals namely, kaempferol, curcumin and puerarin moderate the expression and activity of organic anion/cation transporter 2 ($OCTN_2$) by activation of the *PPARg/RXRa* pathway in SW480 cell line. $OCTN_2$ is a member of the solute carrier transporters, which are expressed in human tissues including the kidney, brain, heart, small intestine and colon and it plays a role in the transfer of many endogenous substrates, including carnitine (34). Carnitine is required for mitochondrial β-oxidation of fatty acids (35). Furthermore, we hypothesized that an increase in *PPARγ* leads to an increase in $OCTN_2$ and subsequently an enhancement in carnitine and fatty acids beta-oxidation.

A previous study reported that diosgenin inhibited the differentiation of adipocytes in 3T3-L1 cells by suppressing the expression of *PPARγ* gene and its target genes. In fact, diosgenin increases the expression of estrogen receptor β (*ERβ*), after which ERβ forms a heterodimer with RXRα, and RXRα is separated from PPARγ in the PPARγ/RXRa complex, which reduces PPARγ transcriptional activity. Thus, the expression of *PPARγ* in adipocytes was significantly affected by diosgenin, but in our study, the expression of *PPARγ* in SW480 cells was significantly increased because *PPARγ* in the colon plays a different role from adipose tissue. Its mechanism may be mediated via the liver X receptor *(LXR)*. *LXRs* belong to the nuclear hormone receptor superfamily. Studies showed that *LXRα* with *RXR* forms a heterodimer complex, and then, this complex attaches to the cysteine elements found in the promoter of *SREBP-1C* gene and activates transcription of this gene, so, it regulates lipogenesis. Additionally, like *LXRs*, activated *PPARs* also heterodimerize with the *RXR* and alter the transcription of target genes. Thus, overexpression of *PPARγ* in SW480 cells under the influence of HEFS, diosgenin, 4-OH-Ile, and orlistat competes with *LXRα/RXR* heterodimerization, resulting in a reduction in the transcription of the *SREBP-1C* and its target genes including *ACC* and *FAS* (36). Though considerable attention has been paid to the anti-inflammatory (37) and anti-carcinogenic role of *PPARγ* in the colon (38), *PPARγ* is believed to act as a basic lipid sensor controlling the expression of genes involved in carbohydrate and lipid metabolism, resulting in increased expression of lipoprotein lipase (*LPL*) and decreased expression of apolipoprotein *(apo) C-III*, both key-players in plasma TG metabolism. Moreover, as a downstream target gene of *PPARγ*, *CD36* is known as a mediator in long chain fatty acid (*LCFA*) uptake. Consequently, TG accumulation via *LPL* and rise in beta-oxidation of fatty acids by CD36 in the bowel, can be inhibited by an increase in *PPARy* (39).

We illustrated that HEFS, diosgenin, and 4-OH-Ile treatment significantly increased the expression of the genes coding *LDL* receptor (*LDLR*) in SW480 cells. Reduced cell surface *LDLR* expression leads to an increase in LDL in the circulation. Also, impairment of the *LDLR* activity results in the accumulation of LDL particles in the flow, inducing atherosclerosis development (40). Thus, HEFS and its two bioactive compounds may be beneficial

because of their protective effect on obesity.

The overall results of this study showed that among the groups treated with HEFS, diosgenin, and 4-OH-Ile, the most significant effect was related to diosgenin. Thus, most of the hypolipidemic effects of HEFS are probably caused by diosgenin. Our study showed results similar to those of studies done in the liver cells; so, there is similarity in the effects of fenugreek compounds in the liver and colon cells with respect to fatty acid metabolism. However, HEFS and its derivatives should be further investigated for their effects on dyslipidemia and its complications.

Conclusion

Overall, these results showed significant downregulation of *ACC* and *FAS* alongside upregulation of *PPARγ* and *LDLR* genes at mRNA level in SW480 cell lines treated with HEFS, diosgenin, and 4-OH-Ile. These results present evidence for the hypolipidemic activity of HEFS and its two active substances similar to orlistat. Therefore, according to our findings, they may be suggested as a useful natural remedy for controlling obesity and overweight.

For future studies, studying the effects of the four substances used in this study in other cell lines, in particular the fat cell line (3T3L-1), evaluation of other genes involved in fat metabolism, using other techniques such as western blot and immunohistochemistry to evaluate the protein level of these genes, are recommended by the authors.

Acknowledgements

The authors thank the Molecular Medicine Research Center (MMRC) of Rafsanjan University of Medical Sciences (RUMS) of Iran for providing the equipment necessary to conduct this work. The support of vice chancellor to research of RUMS is acknowledged. This work financially supported by the RUMS (grant No. 20.1094). There is no conflict of interest in this study.

Authors' Contributions

M.M.-S.; Participated in study design, data collection and evaluation, drafting and statistical analysis. M.M.; Contributed to conception and design. Conducted moleculer experiments and drafted the manuscript which was revised by M.N.K, M.R.M.; Conducted molecular experiments and RT-qPCR analysis. M.R.H.; Participated in study design, data collection and evaluation, drafting and statistical analysis and was responsible for overall supervision. All authors performed editing and approved the final manuscript.

References

1. Martin KA, Mani MV, Mani A. New targets to treat obesity and the metabolic syndrome. Eur J Pharmacol. 2015; 763(Pt A): 64-74.
2. Son WM, Kim DY, Kim YS, Ha MS. Effect of obesity on blood pressure and arterial stiffness in middle-aged Korean women. Osong Public Health Res Perspect. 2017; 8(6): 369-372.
3. Executive summary: Guidelines (2013) for the management of overweight and obesity in adults: a report of the American College of Cardiology/American Heart Association Task Force on Practice Guidelines and the Obesity Society published by the Obesity Society and American College of Cardiology/American Heart Association Task Force on Practice Guidelines. Based on a systematic review from the The Obesity Expert Panel, 2013. Obesity (Silver Spring, Md). 2014; 22 Suppl 2: S5-S39.
4. Reis ECD, Passos SRL, Santos MABD. Quality assessment of clinical guidelines for the treatment of obesity in adults: application of the AGREE II instrument. Cad Saude Publica. 2018; 34(6): e00050517.
5. Flegal KM, Carroll MD, Kit BK, Ogden CL. Prevalence of obesity and trends in the distribution of body mass index among US adults, 1999-2010. JAMA. 2012; 307(5): 491-497.
6. Kaplan LM. Pharmacological therapies for obesity. Gastroenterol Clin North Am. 2005; 34(1): 91-104.
7. Sahebkar A, Simental-Mendia LE, Reiner Z, Kovanen PT, Simental-Mendia M, Bianconi V, et al. Effect of orlistat on plasma lipids and body weight: a systematic review and meta-analysis of 33 randomized controlled trials. Pharmacol Res. 2017; 122: 53-65.
8. Pittler MH, Ernst E. Complementary therapies for reducing body weight: a systematic review. Int J Obes (Lond). 2005; 29(9): 1030-1018.
9. Chevassus H, Gaillard JB, Farret A, Costa F, Gabillaud I, Mas E, et al. A fenugreek seed extract selectively reduces spontaneous fat intake in overweight subjects. Eur J Clin Pharmacol. 2010; 66(5): 449-455.
10. Kumar P, Taha A, Kumar N, Kumar V, Baquer NZ. Sodium orthovanadate and Trigonella foenum graecum prevents neuronal parameters decline and impaired glucose homeostasis in alloxan diabetic rats. Prague Med Rep. 2015; 116(2): 122-138.
11. Fuller S, Stephens JM. Diosgenin, 4-hydroxyisoleucine, and fiber from fenugreek: mechanisms of actions and potential effects on metabolic syndrome. Adv Nutr (Bethesda, Md). 2015; 6(2): 189-197.
12. Hao S, Xu R, Li D, Zhu Z, Wang T, Liu K. Attenuation of streptozotocin-induced lipid profile anomalies in the heart, brain, and mRNA expression of HMG-CoA reductase by diosgenin in rats. Cell Biochem Biophys. 2015; 72(3): 741-749.
13. Avalos-Soriano A, De la Cruz-Cordero R, Rosado JL, Garcia-Gasca T. 4-Hydroxyisoleucine from fenugreek (trigonella foenum-graecum): effects on insulin resistance associated with obesity. Molecules. 2016; 21(11). pii: E1596.
14. Bietrix F, Yan D, Nauze M, Rolland C, Bertrand-Michel J, Comera C, et al. Accelerated lipid absorption in mice overexpressing intestinal SR-BI. J Biol Chem. 2006; 281(11): 7214-7219.
15. Gordon SM, Li H, Zhu X, Shah AS, Lu LJ, Davidson WS. A comparison of the mouse and human lipoproteome: suitability of the mouse model for studies of human lipoproteins. J proteome Res 2015; 14(6): 2686-2695.
16. Zaytseva YY, Elliott VA, Rychahou P, Mustain WC, Kim JT, Valentino J, et al. Cancer cell-associated fatty acid synthase activates endothelial cells and promotes angiogenesis in colorectal cancer. Carcinogenesis. 2014; 35(6):1341-1351.
17. Oliva J, French SW, Li J, Bardag-Gorce F. Proteasome inhibitor treatment reduced fatty acid, triacylglycerol and cholesterol synthesis. Exp Mol pathol. 2012; 93(1): 26-34.
18. Song J, Ruan X, Gu M, Wang L, Wang H, Mueck AO. Effect of orlistat or metformin in overweight and obese polycystic ovary syndrome patients with insulin resistance. Gynecol Endocrinol. 2018; 34(5): 413-417.
19. Khorramdelazad H, Bagheri V, Hassanshahi G, Karami H, Moogooei M, Zeinali M, et al. S100A12 and RAGE expression in human bladder transitional cell carcinoma: a role for the ligand/RAGE axis in tumor progression? Asian Pac J Cancer Prev. 2015; 16(7): 2725-2729.
20. Bae J, Kim J, Choue R, Lim H. Fennel (Foeniculum vulgare) and Fenugreek (Trigonella foenum-graecum) Tea drinking suppresses subjective short-term appetite in overweight women. Clin Nutr Res. 2015; 4(3):168-174.
21. Hossain P, Kawar B, El Nahas M. Obesity and diabetes in the developing world-a growing challenge. N Engl J Med. 2007; 356(3): 213-215.
22. Ratke J, Entschladen F, Niggemann B, Zanker KS, Lang K. Leptin stimulates the migration of colon carcinoma cells by multiple signaling pathways. Endocr Relat cancer. 2010; 17(1): 179-189.
23. Bahmani M, Eftekhari Z, Saki K, Fazeli-Moghadam E, Jelodari M, Rafieian-Kopaei M. Obesity phytotherapy: review of native herbs used in traditional medicine for obesity. J Evid Based Complementary Altern Med 2016; 21(3): 228-234.

24. Stark A, Madar Z. The effect of an ethanol extract derived from fenugreek (Trigonella foenum-graecum) on bile acid absorption and cholesterol levels in rats. Br J Nutr. 1993; 69(1): 277-287.
25. Mathern JR, Raatz SK, Thomas W, Slavin JL. Effect of fenugreek fiber on satiety, blood glucose and insulin response and energy intake in obese subjects. Phytother Res. 2009; 23(11): 1543-1548.
26. Yadav UC, Baquer NZ. Pharmacological effects of Trigonella foenum-graecum L. in health and disease. Pharm Biol. 2014; 52(2): 243-254.
27. Pyra KA, Saha DC, Reimer RA. Prebiotic fiber increases hepatic acetyl CoA carboxylase phosphorylation and suppresses glucose-dependent insulinotropic polypeptide secretion more effectively when used with metformin in obese rats. J Nutr. 2012; 142(2): 213-220.
28. Cheng S, Liang S, Liu Q, Deng Z, Zhang Y, Du J, et al. Diosgenin prevents high-fat diet-induced rat non-alcoholic fatty liver disease through the AMPK and LXR signaling pathways. Int J Mol Med. 2018; 41(2): 1089-1095.
29. Auguet T, Berlanga A, Guiu-Jurado E, Martinez S, Porras JA, Aragones G, et al. Altered fatty acid metabolism-related gene expression in liver from morbidly obese women with non-alcoholic fatty liver disease. Int J Mol Sci. 2014; 15(12): 22173-22187.
30. Kumar P, Bhandari U, Jamadagni S. Fenugreek seed extract inhibit fat accumulation and ameliorates dyslipidemia in high fat diet-induced obese rats. Biomed Res Int. 2014; 2014: 606021.
31. Borniquel S, Jadert C, Lundberg JO. Dietary conjugated linoleic acid activates PPARgamma and the intestinal trefoil factor in SW480 cells and mice with dextran sulfate sodium-induced colitis. J Nutr. 2012; 142(12): 2135-2140.
32. Ding Y, Guo ZR, Wu M, Chen Q, Yu H, Luo WS. Gene-gene interaction between PPARδ and PPARγ is associated with abdominal obesity in a Chinese population. J Genet Genomics. 2012; 39(12): 625-631.
33. Padmanabhan M, Arumugam G. Effect of Persea americana (avocado) fruit extract on the level of expression of adiponectin and PPAR-gamma in rats subjected to experimental hyperlipidemia and obesity. J Complement Integr Med. 2014; 11(2): 107-119.
34. Luo J, Qu J, Yang R, Ge MX, Mei Y, Zhou BT, et al. Phytochemicals Mediate the Expression and Activity of $OCTN_2$ as Activators of the PPARgamma/RXRalpha Pathway. Front Pharmacol. 2016; 7: 189.
35. Fujiya M, Inaba Y, Musch MW, Hu S, Kohgo Y, Chang EB. Cytokine regulation of $OCTN_2$ expression and activity in small and large intestine. Inflamm Bowel Dis. 2010; 17(4): 907-916.
36. Wang X, Liu J, Long Z, Sun Q, Liu Y, Wang L, et al. Effect of diosgenin on metabolic dysfunction: Role of ERbeta in the regulation of PPARgamma. Toxicol Appl Pharmacol. 2015; 289(2): 286-296.
37. Fuhr L, Rousseau M, Plauth A, Schroeder FC, Sauer S. Amorfrutins Are Natural PPARgamma Agonists with Potent Anti-inflammatory Properties. J Nat Prod. 2015; 78(5): 1160-1164.
38. Lecarpentier Y, Claes V, Vallee A, Hebert JL. Interactions between PPAR gamma and the canonical Wnt/Beta-catenin pathway in type 2 diabetes and colon cancer. PPAR Res. 2017; 2017: 5879090.
39. Wang Z, Koonen D, Hofker M, Bao Z. Retraction: 5-aminosalicylic acid improves lipid profile in mice fed a high-fat cholesterol diet through its dual effects on intestinal PPARγ and PPARα. PLoS One. 2018; 13(7): e 200947.
40. Temel RE, Brown JM. A new framework for reverse cholesterol transport: non-biliary contributions to reverse cholesterol transport. World J Gastroenterol. 2010;16(47): 5946-5952.

Original Article

Protection against Dextran Sulfate Sodium-Induced Ulcerative Colitis in Mice by Neferine, A Natural Product from *Nelumbo nucifera Gaertn*

Xiangjing Min, B.Sc.[1], Yanling Guo, M.Sc.[1], Yishan Zhou, B.Sc.[1], Xiuping Chen, Ph.D.[1, 2*]

1. Key Lab for Pharmacology of Ministry of Education, Department of Pharmacology, Zunyi Medical University, Zunyi, China
2. State Key Laboratory of Quality Research in Chinese Medicine, Institute of Chinese Medical Sciences, University of Macau, Macao, China

Corresponding Address: State Key Laboratory of Quality Research in Chinese Medicine, Institute of Chinese Medical Sciences, University of Macau, Macao, China
Email: xpchen@umac.mo

Received: 16/April/2019, Accepted: 27/July/2019

Abstract

Objective: Ulcerative colitis (UC) is a long-lasting inflammatory disease of the colon. Epidemiological studies showed that the prevalence and incidence of UC are increasing worldwide in recent years. Neferine is a natural alkaloid isolated from *Nelumbo nucifera* Gaertn that exerts a variety of biological activities. This study was designed to evaluate the protective effect of neferine on dextran sulfate sodium (DSS)-induced experimental UC in mice.

Materials and Methods: In this experimental study, 4% DSS was used to induce a mice model of UC. Neferine (5 and 10 mg/kg) was administered by intraperitoneal injection (ip). Clinical symptoms and disease activity index (DAI) scores were recorded and calculated. Pathological changes of colon tissues were detected by Hematoxylin and Eosin (H&E) staining. The levels of inflammatory mediators were detected by ELISA kits. Western blotting and immunohistochemical analysis were used for the evaluation of protein expressions.

Results: Neferine treatment significantly alleviated DSS-induced UC by inhibiting weight loss, decreasing DAI scores, and alleviating the pathological changes in colon tissues. Furthermore, neferine significantly decreased serum levels of pro-inflammatory cytokines including tumor necrosis factor-alpha (TNF-α), interleukin-1 beta (IL-1β), and IL-6 and increased serum levels of anti-inflammatory cytokine IL-10. The increased myeloperoxidase (MPO) activity and nitric oxide (NO) in colon tissues were also inhibited. In addition, neferine significantly down-regulated inducible NO synthase (iNOS), cyclooxygenase-2 (COX-2), and intercellular cell adhesion molecule-1 (ICAM-1) expression in colon tissues.

Conclusion: These results provided evidence that neferine could protect against DSS-induced UC symptoms in an experimental mice model. This effect might be mediated through inhibition of inflammation.

Keywords: Dextran Sulfate Sodium, Inflammation, Neferine, Ulcerative Colitis

Cell Journal(Yakhteh), Vol 22, No 4, January-March (Winter) 2021, Pages: 523-531

Citation: **Min X, Guo Y, Zhou Y, Chen X. Protection against dextran sulfate sodium-induced ulcerative colitis in mice by neferine, a natural product from nelumbo nucifera gaertn. Cell J. 2021; 22(4): 523-531. doi: 10.22074/cellj.2021.6918.**

Introduction

Ulcerative colitis (UC), a form of inflammatory bowel disease (IBD), is a chronic inflammatory disease (1). UC was first described by Wilks and Moxon in 1875 and officially named by the International Organization Committee of the World Health Organization (WHO) Medical Science Organization in 1973. Clinically, UC is characterized by diarrhea, abdominal pain, mucus pus, bloody stools, and acute diarrhea (2). The lesion site of UC is mostly confined to colon mucosa, including colon mucosa and submucosa, which may involve rectum and distal colon, and spread to the proximal colon and subsequently spread throughout the entire colon, showing a continuous and diffuse distribution (3).

The risk factors and pathogenesis of UC are still unclear (4). It was pointed out that the pathogenesis of the disease is complicated and is related to multiple factors, such as genetic factors, immune factors, infection factors, and inflammatory mediators (5). Epidemiological studies showed that the prevalence and incidence of UC are increasing worldwide in recent years (6). UC has the characteristic of recurrence and there is still a lack of effective and safe therapeutic drugs for treatment of the disease (7). Therefore, finding safe and effective drugs against this serious disease is of particular interest to pharmaceutical companies and researchers.

Traditional Chinese medicines (TCM) has a long history of clinical application for the treatment of various diseases. Especially, documented data demonstrated that TCM and TCM-derived natural products showed protective effects on UC (8, 9). Neferine, a dibenzyl isoquinoline alkaloid (Fig.1), is extracted from the mature seed embryos of *Nelumbo nucifera* Gaertn (Lotus) (10). Numerous studies revealed that neferine possesses various biological activities, such as anti-angiogenesis (11), anti-oxidant (12), anti-cancer (13), anti-diabetic (14, 15), anti-thrombotic, anti-arrhythmic (14), anti-inflammatory (16) and anti-HIV properties (14, 17). We recently reported that neferine significantly inhibited LPS-induced inflammation in Raw264.7 cells and oral administration of neferine improved DSS-induced inflammation in mice (16). However, the underlying

mechanisms remain unclear. Here, neferine protective effects and the underlying mechanism(s) were further investigated following intraperitoneal injection (ip) of neferine in a DSS-induced mice model.

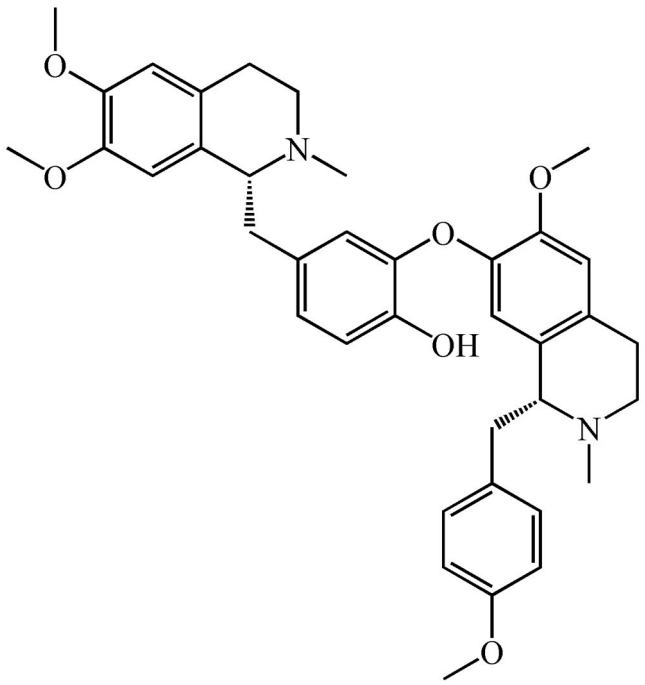

Fig.1: The chemical structure of neferine, a natural alkaloid (10).

Materials and Methods

Reagents

In this experimental study, Neferine (>95%) was provided by Chenguang Herb purify Co., Ltd. (Chengdu, China). Dextran sulfate sodium (DSS, MW 36,000-50,000 Da) was purchased from MP Biomedicals (California, USA). LOX-1, iNOS, COX-2 antibodies were obtained from Abcam (Cambridge Science Park, UK). Antibodies for ICAM-1, VCAM-1, NOSTRIN, β-actin, and GAPDH were purchased from Proteintech (Wuhan, China). ELISA kits for myeloperoxidase (MPO) and NO were purchased from Nanjing Jiancheng Bioengineering Institute Co., Ltd. (Nanjing, China). ELISA kits for tumor necrosis factor-alpha (TNF-α), interleukin-1beta (IL-1β), IL-10, and IL-6 were bought from Shanghai Jianglai Biological Technology Co., Ltd. (Shanghai, China).

Animals and experimental design

C57BL/6J male mice (body weight 22-24 g) purchased from the Chongqing Tengxin Biotechnology Co., Ltd. (Chongqing, China), were maintained in specific pathogen-free (SPF) environment (temperature 24-25˚C, humidity 50-55%，12 hours/12 hours light/dark cycle). Mice were fed with a normal laboratory diet and water ad libitum. They were acclimated to the laboratory environmental conditions for two weeks before the experiments. All protocols were performed upon approval by the Ethics Committee of Zunyi Medical University and were strictly performed in accordance with the "Guide for the Care and Use of Laboratory Animals" (National Research Council, 2011, 81774200).

Induction of UC was conducted as shown in our previous report with minor revisions. Thirty-four mice were randomly divided into four groups: the control group (n=8), the model group (n=10), the low dose (5 mg/kg) group (n=8) and the high dose (10 mg/kg) group (n=8). Mice in the control group received water only while mice in other groups were administered with 4% DSS in drinking water for 7 consecutive days. Mice in neferine-treated groups received neferine ip daily for 10 days, started 3 days before and continued for 7 days after administration of 4% DSS. Neferine was dissolved in 0.8 mM HCl. The colons and serum were collected after mice were sacrificed. The experimental design is summarized in Figure 2.

Disease activity index

The progression of UC was evaluated daily by calculating the scores during the course of treatments as previously described (18), according to the percentage change in body weight, the severity of fecal bleeding and the occurrence of diarrhea.

Hematoxylin and eosin staining

Hematoxylin and eosin (H&E) staining was performed as previously shown (19, 20) with minor revisions. Briefly, colons tissues were immediately fixed in 10% paraformaldehyde overnight and then, embedded in paraffin and sectioned at 4 μm thickness. Slides were then stained with H&E and examined using a microscope for histopathological alterations.

Immunohistochemical assay

The expression of ICAM-1 was investigated using immunohistochemical analysis based on a previous report (16) with minor revisions. Briefly, the colon tissue sections were dried at 60˚C for 45 minutes. Then, the fixed sections were deparaffinized and placed in medium-high heat oven for 18 minutes for antigen unmasking. After inhibition of endogenous peroxidase activity by 3% H_2O_2 solution, non-specific antigens were inhibited by 5% universal blocker for 30 minutes. The slides were incubated with primary antibodies for ICAM-1 (1:200) overnight at 4˚C and then, washed with PBS twice. The slides were incubated for 30 minutes with biotinylated universal link second antibody, stained with 3,3'-Diaminobenzidine (DAB), counterstained with hematoxylin, dehydrated and mounted. Finally, sections were observed under a microscope and images were obtained.

Determination of myeloperoxidase activity and nitric oxide level in colon tissues

MPO activity and NO levels in colon tissues were determined using commercial kits according to the manufacturer's protocol.

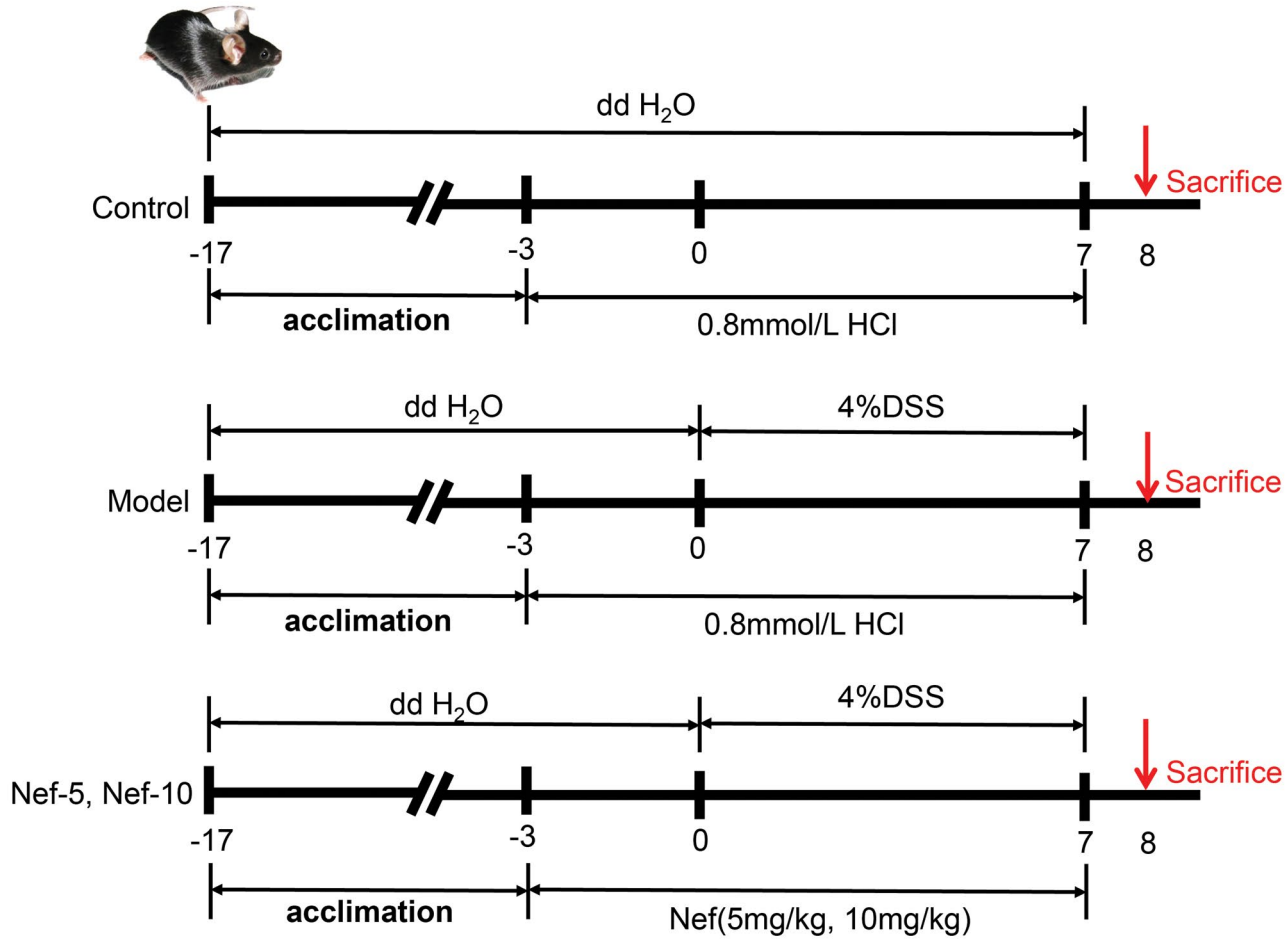

Fig.2: The schematic experimental design of the present study. After 2 weeks of adaptive feeding, mice were randomly divided into groups according to body weights. The experimental period was a total of ten days, including three days of neferine pretreatment by ip followed by co-treatment of 4% dextran sulfate sodium (DSS) and neferine for another 7 consecutive days.

Determination of cytokines

Cytokines (TNF-α, IL-1β, IL-10, and IL-6) levels in serum were determined by commercial ELISA kits following the manufacturer's recommendations.

Western blotting

Colon tissues from different groups were homogenized on ice to extract proteins using protein lysis buffer (containing radio immunoprecipitation assay (RIPA buffer), phenylmethanesulfonyl fluoride (PMSF, 0.1 M), and protease inhibitors). Protein concentrations were determined using BCA protein kit. Equal samples from each group were isolated by 8% sodium dodecyl sulphate-polyacrylamide gel electrophoresis (SDS-PAGE) and then, transferred to the polyvinylidene difluoride (PVDF) membrane. After blocking the PVDF membrane with 5% nonfat milk for 2 hours, primary antibodies (β-actin (1:2000), GAPDH (1:2000), iNOS (1:500), COX-2 (1:500), ICAM-1 (1:1000), VCAM-1 (1:1000), LOX-1 (1:1000) and ROSTRIN (1:1000)) were added. Subsequently, after incubation with the secondary antibody for 1 hour, chemiluminescence signals were detected by ChemiDoc™ Imager image scanner (Bio-Rad Biotech, CA, USA).

Statistical analysis

Results are expressed as means ± standard deviation (SD). Statistical analysis was performed by one-way analysis of variance (ANOVA) by the SPSS 18.0 software software (IBM SPSS, USA). Differences with $P<0.05$ were considered statistically significant.

Results

Neferine alleviated the symptoms of dextran sulfate sodium -induced colitis

Compared with the control group, the body weights of the model group significantly decreased from day 5 to 7. Neferine pretreatment partially inhibited DSS-induced body weights loss (Fig.3A). On the third day after the DSS treatment, diarrhea and bloody stools were observed in some mice. Compared with the control group, DAI scores in model group were significantly increased from day 5 to 7, which was partially reversed by neferine pretreatment (Fig.3B). Furthermore, compared with the control group, the colons from the model group were obviously contracted (Fig.3C, D) and the weights of the colons were also dramatically decreased. These alterations were significantly improved in neferine-administered groups.

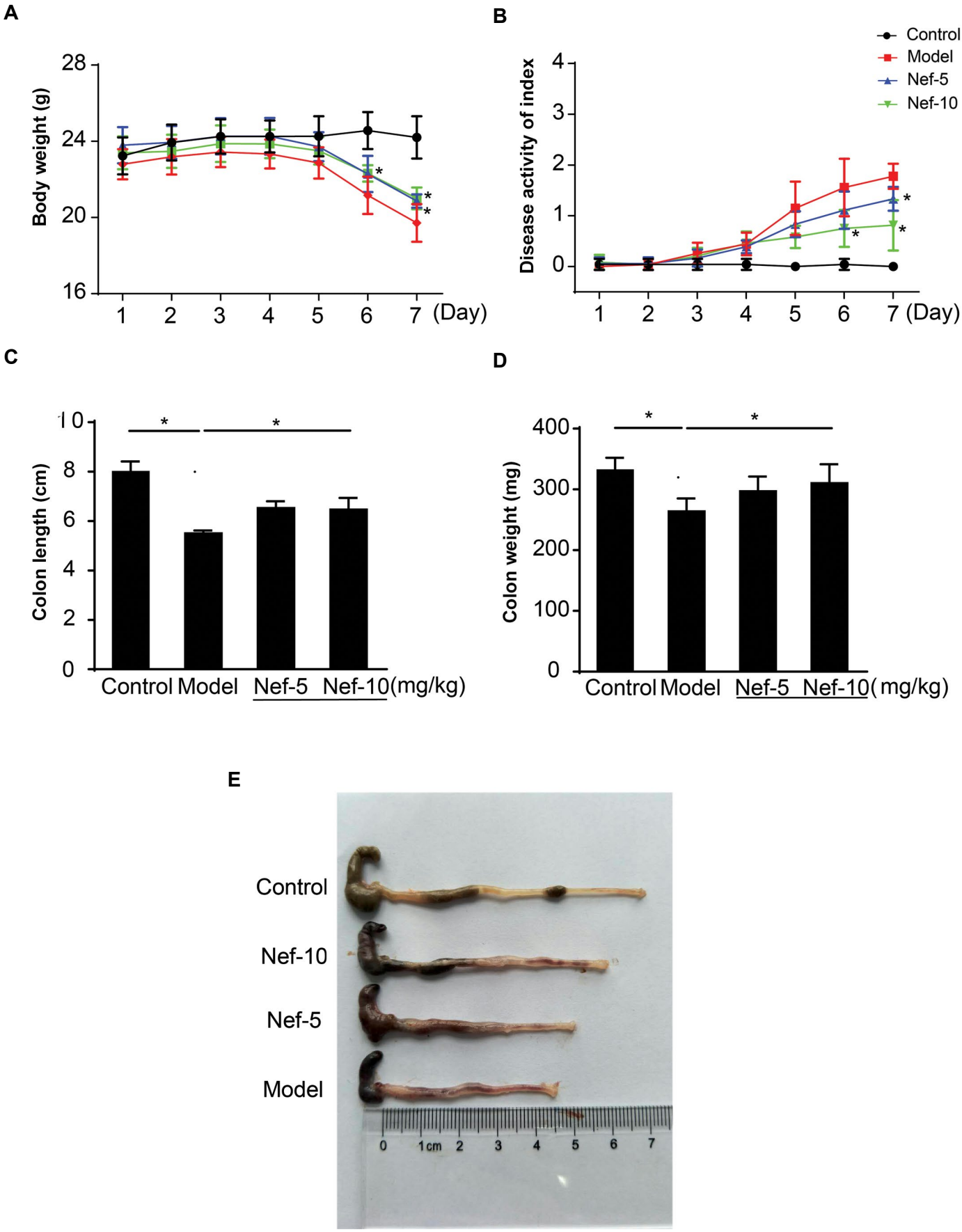

Fig.3: Neferine improved UC induced by DSS in mice. Three days after prophylactic intraperitoneal injection of neferine, mice were challenged with 4% DSS for 7 days of ulcerative colitis modeling. **A.** The average body weights, rectal bleeding and diarrhea were recorded daily. **B.** DAI scores were calculated. **C.** Mean colon lengths. **D.** Average colon weights. **E.** Representative pictures of colon.
*; P<0.05 control versus model, model versus neferine, UC; Ulcerative colitis, DSS; Dextran sulfate sodium, and DAI; Disease activity index.

Neferine improved dextran sulfate sodium -induced pathological changes of colitis

H&E staining showed that the physiological structures of colon tissue from the control group were integral and clear with arranged goblet cells in the mucosa. However, the colon structures in the model group were severely damaged with decreased number of goblet cells, mucosal ulcers, and increased infiltration of neutrophils. These pathological changes were partially improved by neferine administration, especially in the high dose group (Fig.4A).

Neferine decreased myeloperoxidase activity and regulated inflammatory cytokines secretion

The MPO activities in the model group approximately increased 7 folds, which was almost completely inhibited by neferine at both doses (Fig.4B). Similar inhibitory effects were observed in terms of DSS-induced NO increase in colon tissues (Fig.4C). Furthermore, the serum levels of pro-inflammatory cytokines TNF-α, IL-1β, and IL-6 were significantly increased in the model group, which was inhibited by neferine treatment (Fig.4D-F). In addition, the serum levels of IL-10 in the model group were significantly decreased, which was partially reversed by neferine treatment (Fig.4G).

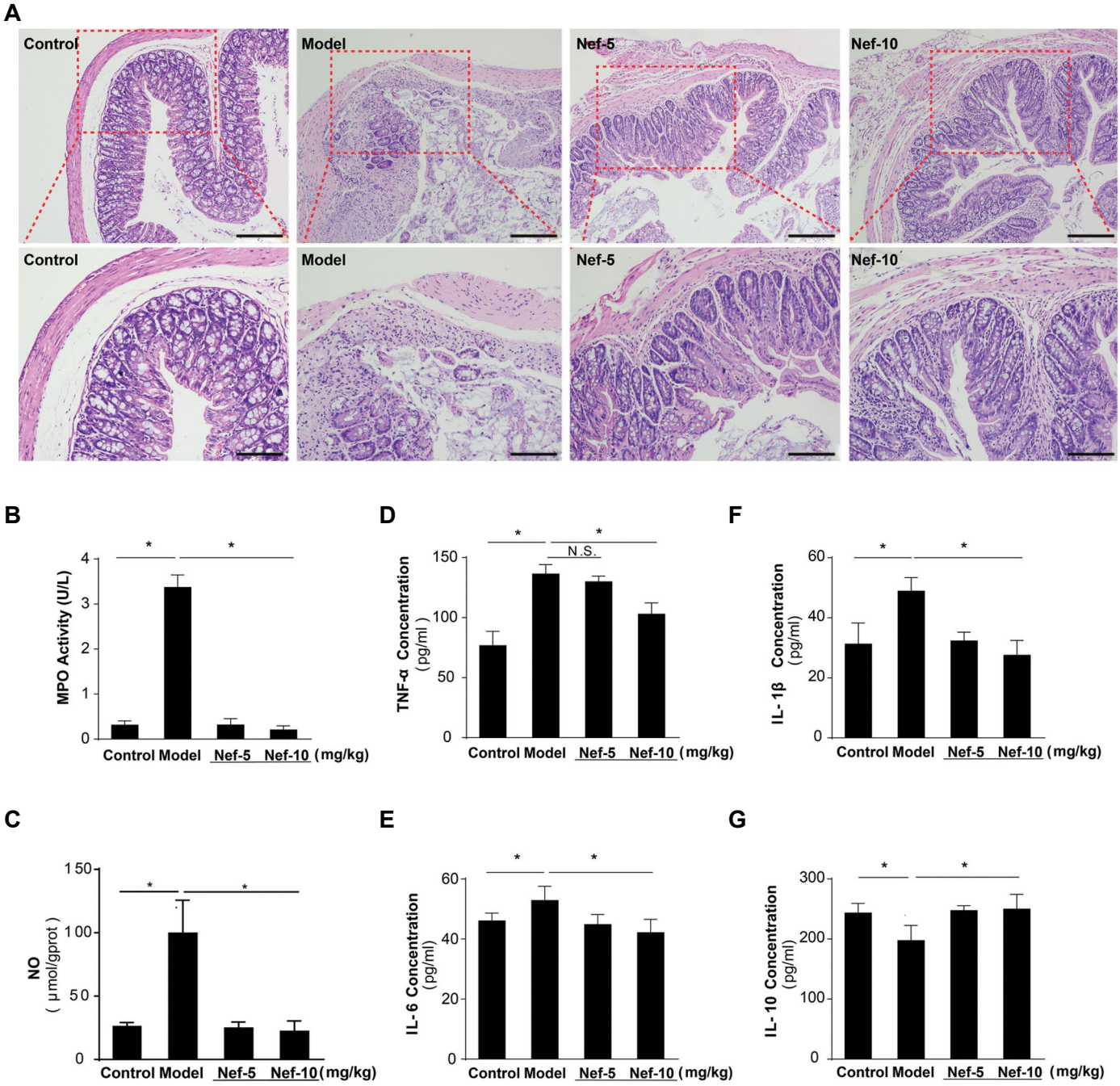

Fig.4: Neferine improved histological changes and restored inflammatory mediators in UC mice. **A.** Representative images of H&E staining of colon tissues are presented [the magnifications of the upper and lower panels are ×100 (scale: 100 μm) and ×200 (scale: 100 μm), respectively]. **B.** The MPO activity and **C.** NO content in colon tissues were determined. Serum levels of **D.** TNF-α, **E.** IL-1β, **F.** IL-6, and **G.** IL-10 were determined.
*; P<0.05, control versus model, model versus neferine, UC; Ulcerative colitis, MPO; Myeloperoxidase, NO; Nitric oxide, TNF-α; Tumor necrosis factor-alpha, and IL; Interleukin.

Neferine inhibited COX-2 and iNOS expression

Western blotting results showed that the protein expression of COX-2 in colon tissues in the model group was significantly increased, which was significantly inhibited by neferine (Fig.5A). Similarly, the protein expression of iNOS in the model group was dramatically increased, which was significantly reversed by neferine (Fig.5B).

Neferine restored dextran sulfate sodium -induced expression of ICAM-1 protein

The protein expression of ICAM-1 in colon tissues in the model group was significantly upregulated, which was completely inhibited by neferine at both doses (Fig.5C). In immunohistochemical analysis, weak brown staining was observed in the control colon tissues while in the model tissues, dramatically enhanced brown staining was observed. Furthermore, treatment with both doses of neferine significantly decreased the brown staining (Fig.5D). However, no difference in the expression levels of VCAM-1, NOSTRIN, and LOX-1 among the groups was found (Fig.5E). These results indicated that the expression of ICAM-1 in the model group was upregulated, but decreased by neferine.

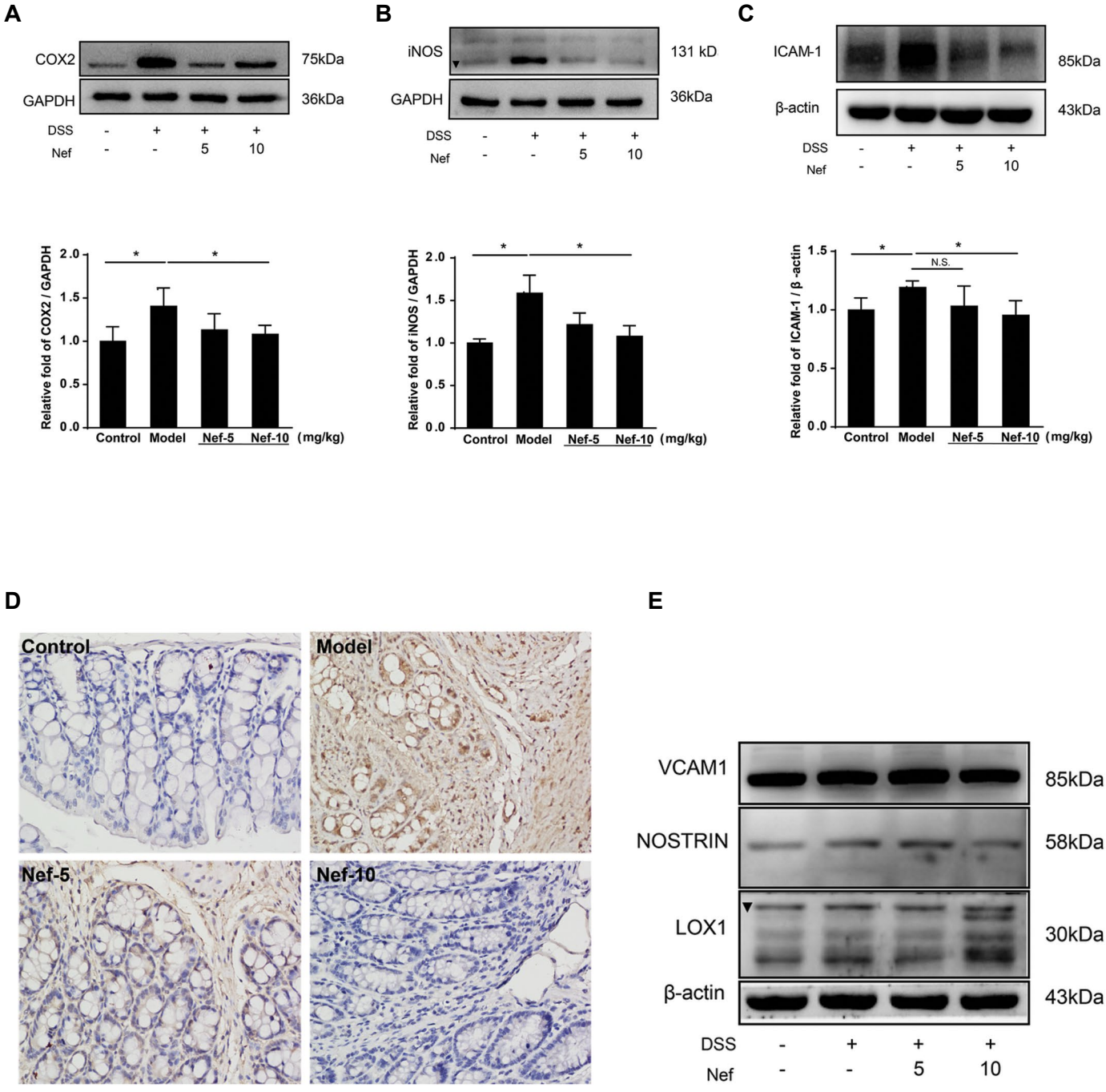

Fig.5: Effect of neferine on protein expression in colon tissues. The protein expression of **A.** COX-2, **B**. iNOS, **C.** ICAM-1 in the colon tissues was determined by Western blotting. **D.** The expression of ICAM-1 in colon tissues was detected by immunohistochemical analysis (×400, scale bar: 50 μm). **E.** The protein expression of VCAM-1, NOSTRIN, and LOX-1 was determined by Western blotting. *; P<0.05, control versus model, model versus neferine.

Discussion

UC is a digestive tract disease characterized by chronic inflammation and ulceration of colonic mucosa and submucosa. Drugs available for UC treatment in clinic are mainly salicylic acid, glucocorticoids, immunosuppressive agents and biological agents (21). Recent studies suggested that many medicinal plants and natural products might have therapeutic potentials for UC (22). Neferine is a natural alkaloid with various pharmacological effects (14) and our recent study showed that oral administration of neferine protects against DSS-induced UC; however, exact mechanism(s) remain unclear (16). In the present study, neferine protective effect on DSS-induced UC and the underlying mechanism were further explored. The main findings of this study were: i. Intraperitoneal injection of neferine significantly protects against DSS-induced UC in mice and ii. This protective effect was mediated via regulation of cytokines secretion and iNOS, COX-2 and ICAM-1 expression.

Many chemicals have been used for induction of experimental UC, such as 2,4,6-trinitro-benzene sulfonic acid (TNBS), oxazolone, DSS and acetic acid (23). Because DSS-induced UC model exhibits similar clinical symptoms and pathological features to those of human IBD, this model has been widely used in basic research (18, 24, 25). In this model of UC, two phases were observed. During the active period, mice had hair erect, weight loss, diarrhea, blood in the stool, and the occurrence of death. Histological changes include changes in mucin depletion, crypt structure, epithelial cell changes, and infiltration of inflammatory cells (25). Here, DSS-treated mice showed decreased body weight, increased DAI scores and decreased colon length and weight. H&E staining showed mucin depletion, epithelial degeneration and infiltration of inflammatory cells. These suggested that the UC model was successfully established. Similar to our previous report and other reports about UC (16, 26), neferine treatment could significantly improve these clinical manifestations and histological alterations. Thus, both oral administration and intraperitoneal injection of neferine showed protective effects in this model. In view of the compliance in clinical, oral administration might be a better choice.

DSS could penetrate the mucosal membrane in the intestine. Lysosomes containing DSS molecules could be found in macrophages in the lamina propria of colon mucosa, and infiltrated inflammatory cells. Under the stimulation by DSS, macrophages on the intestinal surface were activated to produce pro-inflammatory cytokines, including TNF-α, IL-1β, IL-6, which participate in the development of UC. COX-2 and iNOS, two inducible enzymes, produced by macrophages, play important roles in inflammatory responses, including UC (27). Here, neferine treatment significantly inhibited the pro-inflammatory cytokines secretion. Especially, the levels of IL-10, a cytokine with potent anti-inflammatory properties (28), were restored by neferine. Thus, neferine could regulate the balance of pro- and anti-inflammatory cytokines. Neferine decreased NO levels while showed no effect on the colon expression of NOSTRIN, a protein modulating activity, trafficking, and targeting of eNOS. This suggested that increased levels NO were secreted by iNOS. MPO is secreted by neutrophils, and changes in its activity in the colon can indirectly reflect the level of neutrophil infiltration in the colon (29). It could be a useful disease activity biomarker for several diseases, including UC (30). Increased MPO activity was completely inhibited by neferine which suggested that the disease activity could be improved by neferine.

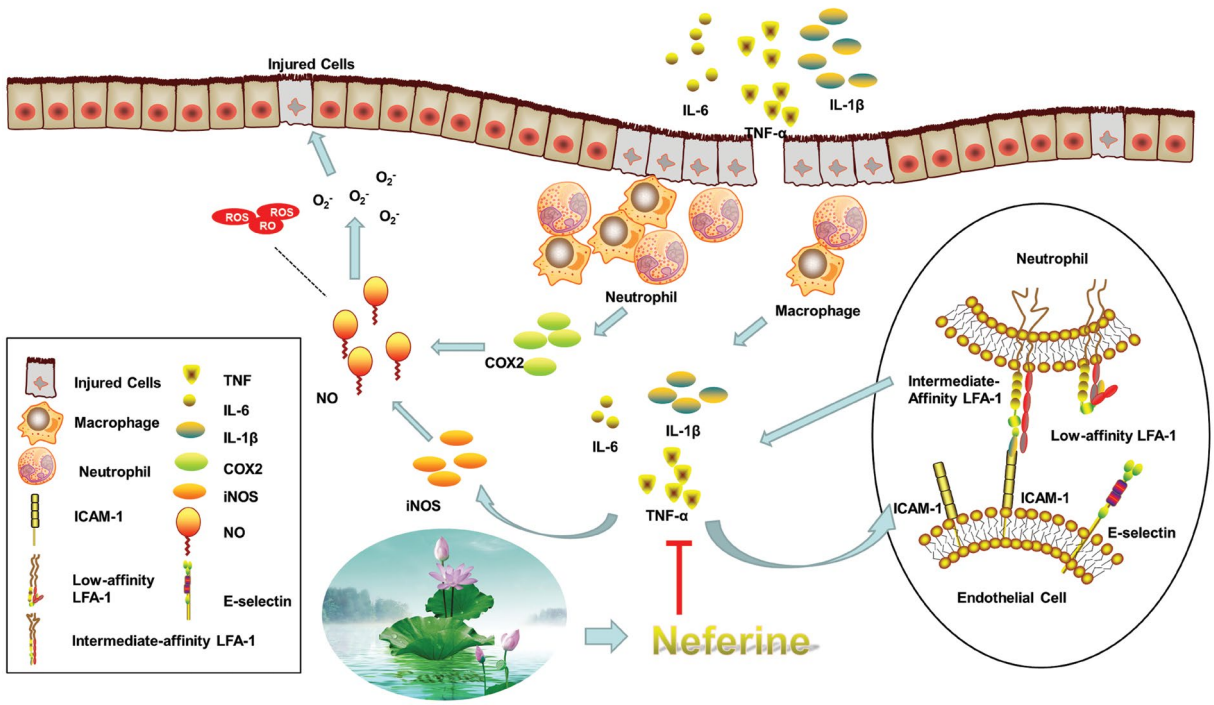

Fig.6: Schematic diagram for protective effect of neferine on UC. Neferine inhibited UC mainly by regulating the secretion of inflammatory cytokines (the pro-inflammatory cytokines TNF-α, IL-1β, and IL-6, and the anti-inflammatory cytokines, IL-10), and inhibiting the expression of COX-2, iNOS, and ICAM-1 proteins. UC; Ulcerative colitis, TNF-α; Tumor necrosis factor-alpha, and IL; Interleukin.

Integrins and adhesion molecules have been attractive targets for the treatment of IBD (31). Previous reports showed increased or unaltered expression of VCAM-1 in mucosa of IBD (32, 33). Here, no enhanced expression of VCAM-1 was observed in DSS-treated colon tissues. Furthermore, the expression of LOX-1, the scavenger receptor mainly found in endothelial cells (34, 35), was not altered by DSS. Thus, these results suggested that neither VCAM-1 nor LOX-1 was actively involved in DSS-induced colitis. ICAM-1, also known as CD54, is a single chain transmembrane glycoprotein. It is an adhesion factor closely related to colon mucosa cells (36). In normal colon tissues, the expression of ICAM-1 in intestinal mucosa lamina propria, monocytes and vascular endothelial cells is very low, and the affinity of its ligand LFA-1 also decreases accordingly (37). Consistent with previous reports in IBD patients (32) and DSS treated mice (38), we found that the protein expression of ICAM-1 was significantly increased in the model group. This result was further confirmed by Western blotting and immunohistochemical analysis. In view of the fact that TNF-α, IL-1β and IL-6 could actively up-regulate ICAM-1 expression and that increased serum levels of these cytokines were detected in DSS model, the increased expression of ICAM-1 might be due to the increased cytokines. Thus, the inhibitory effect of neferine may result in its effect on cytokines secretion. However, the detailed effect and mechanism of ICAM-1 need further investigation. Collectively, the protective effect of neferine was summarized as Figure 6.

Conclusion

According to our results, intraperitoneal injection of neferine had protective effect on UC in a DSS-induced experimental mice model; this effect was mediated through regulating inflammatory responses and COX-2, iNOS, and ICAM-1 expressions.

Acknowledgements

This study financially supported by the National Natural Science Foundation of China (No. 81774200) and Funded by The Science and Technology Development Fund, Macau SAR (Files no.078/2016/A2, 175/2017/A3) and the Research Fund of University of Macau (MYRG2016-00043- ICMS-QRCM). We declare no conflicts of interest in this study.

Authors' Contributions

X.M., X.C.; Designed the study. X.M., Y.Z.; Performed the experiments. Y.G.; Participated in data collection and evaluation. X.M.; Drafted the manuscript and performed statistical analysis. X.C.; Revised the manuscript. All authors read and approved the final manuscript.

References

1. Nanini HF, Bernardazzi C, Castro F, de Souza HSP. Damage-associated molecular patterns in inflammatory bowel disease: From biomarkers to therapeutic targets. World J Gastroenterol. 2018; 24(41): 4622-4634.
2. Olivera P, Danese S, Pouillon L, Bonovas S, Peyrin-Biroulet L. Effectiveness of golimumab in ulcerative colitis: A review of the real world evidence. Dig Liver Dis. 2019; 51(3): 327-334.
3. Yarani R, Mirza AH, Kaur S, Pociot F The emerging role of lncRNAs in inflammatory bowel disease. Exp Mol Med. 2018; 50 (12): 161.
4. Imdad A, Nicholson MR, Tanner-Smith EE, Zackular JP, Gomez-Duarte OG, Beaulieu DB, et al. Fecal transplantation for treatment of inflammatory bowel disease. Cochrane Database Syst Rev. 2018; 11: CD012774.
5. Ordas I, Eckmann L, Talamini M, Baumgart DC, Sandborn WJ. Ulcerative colitis. Lancet. 2012; 380(9853): 1606-1619.
6. Shi L, Dai Y, Jia B, Han Y, Guo Y, Xie T, et al. The inhibitory effects of qingchang wenzhong granule on the interactive network of inflammation, oxidative stress, and apoptosis in rats with dextran sulfate sodium-induced colitis. J Cell Biochem. 2019; 120(6): 9979-9991.
7. Dou YX, Zhou JT, Wang TT, Huang YF, Chen VP, Xie YL, et al. Self-nanoemulsifying drug delivery system of bruceine D: a new approach for anti-ulcerative colitis. Int J Nanomedicine. 2018; 13: 5887-5907.
8. Salaga M, Zatorski H, Sobczak M, Chen C, Fichna J. Chinese herbal medicines in the treatment of IBD and colorectal cancer: a review. Curr Treat Options Oncol. 2014; 15(3): 405-420.
9. Teschke R, Wolff A, Frenzel C, Eickhoff A, Schulze J. Herbal traditional Chinese medicine and its evidence base in gastrointestinal disorders. World J Gastroenterol. 2015; 21(15): 4466-4490.
10. Priya LB, Baskaran R, Huang CY, Padma VV. Neferine ameliorates cardiomyoblast apoptosis induced by doxorubicin: possible role in modulating NADPH oxidase/ROS-mediated NFκB redox signaling cascade. Sci Rep. 2017; 7(1): 12283.
11. Zhang Q, Li Y, Miao C, Wang Y, Xu Y, Dong R, et al. Anti-angiogenesis effect of Neferine via regulating autophagy and polarization of tumor-associated macrophages in high-grade serous ovarian carcinoma. Cancer Lett. 2018; 432: 144-155.
12. Baskaran R, Poornima P, Huang CY, Padma VV. Neferine prevents NF-κB translocation and protects muscle cells from oxidative stress and apoptosis induced by hypoxia. Biofactors. 2016; 42(4): 407-417.
13. Sivalingam K, Amirthalingam V, Ganasan K, Huang CY, Viswanadha VP. Neferine suppresses diethylnitrosamine-induced lung carcinogenesis in Wistar rats. Food Chem Toxicol. 2018; 123: 385-398.
14. Marthandam Asokan S, Mariappan R, Muthusamy S, Velmurugan BK. Pharmacological benefits of neferine - A comprehensive review. Life Sci. 2018; 199: 60-70.
15. Liu X, Song X, Lu J, Chen X, Liang E, Liu X, et al. Neferine inhibits proliferation and collagen synthesis induced by high glucose in cardiac fibroblasts and reduces cardiac fibrosis in diabetic mice. Oncotarget. 2016; 7(38): 61703-61715.
16. Wu X, Guo Y, Min X, Pei L, Chen X. Neferine, a bisbenzylisoquinoline alkaloid, ameliorates dextran sulfate sodium-induced ulcerative colitis. Am J Chin Med. 2018; 46(6): 1263-1279.
17. Zhou H, Jiang H, Yao T, Zeng S. Fragmentation study on the phenolic alkaloid neferine and its analogues with anti-HIV activities by electrospray ionization tandem mass spectrometry with hydrogen/deuterium exchange and its application for rapid identification of in vitro microsomal metabolites of neferine. Rapid Commun Mass Spectrom. 2007; 21(13): 2120-2128.
18. Wirtz S, Popp V, Kindermann M, Gerlach K, Weigmann B, Fichtner-Feigl S, et al. Chemically induced mouse models of acute and chronic intestinal inflammation. Nat Protoc. 2017; 12(7): 1295-1309.
19. Li W, Zhao W, Wu Q, Lu Y, Shi J, Chen X. Puerarin improves diabetic aorta injury by inhibiting NADPH Oxidase-derived oxidative stress in STZ-Induced diabetic rats. J Diabetes Res. 2016; 2016: 8541520.
20. Li J, Kong D, Wang Q, Wu W, Tang Y, Bai T, et al. Niacin ameliorates ulcerative colitis via prostaglandin D2-mediated D prostanoid receptor 1 activation. EMBO Mol Med. 2017; 9(5): 571-588.
21. Maloy KJ, Powrie F Intestinal homeostasis and its breakdown in inflammatory bowel disease. Nature. 2011; 474(7351): 298-306.
22. Sepehrimanesh M, Poorbaghi SL. Ulcerative colitis: a phytomedical technical note. Comparative Clinical Pathology. 2017; 26(6): 1237-1239.
23. Tanideh N, Jamshidzadeh A, Sepehrimanesh M, Hosseinzadeh M, Koohi-Hosseinabadi O, Najibi A, et al. Healing acceleration of ace-

tic acid-induced colitis by marigold (Calendula officinalis) in male rats. Saudi J Gastroenterol. 2016; 22(1): 50-56.
24. Low D, Nguyen DD, Mizoguchi E. Animal models of ulcerative colitis and their application in drug research. Drug Des Devel Ther. 2013; 7: 1341-1357.
25. Perse M, Cerar A Dextran sodium sulphate colitis mouse model: traps and tricks. J Biomed Biotechnol. 2012; 2012: 718617.
26. Dai YC, Zheng L, Zhang YL, Chen X, Chen DL, Wang LJ, et al. Jianpi Qingchang decoction regulates intestinal motility of dextran sulfate sodium-induced colitis through reducing autophagy of interstitial cells of Cajal. World J Gastroenterol. 2017; 23(26): 4724-4734.
27. Sakthivel KM, Guruvayoorappan C. Amentoflavone inhibits iNOS, COX-2 expression and modulates cytokine profile, NF-kB signal transduction pathways in rats with ulcerative colitis. Int Immunopharmacol. 2013; 17(3): 907-916.
28. Iyer SS, Cheng G. Role of interleukin 10 transcriptional regulation in inflammation and autoimmune disease. Crit Rev Immunol. 2012; 32(1): 23-63.
29. Liu X, He H, Huang T, Lei Z, Liu F, An G, et al. Tanshinone IIA protects against dextran sulfate sodium- (DSS-) induced colitis in mice by modulation of neutrophil infiltration and activation. Oxid Med Cell Longev. 2016; 2016: 7916763.
30. Garrity-Park M, Loftus EV Jr, Sandborn WJ, Smyrk TC. Myeloperoxidase immunohistochemistry as a measure of disease activity in ulcerative colitis: association with ulcerative colitis-colorectal cancer, tumor necrosis factor polymorphism and RUNX3 methylation. Inflamm Bowel Dis. 2012; 18(2): 275-283.
31. Bravata I, Allocca M, Fiorino G, Danese S. Integrins and adhesion molecules as targets to treat inflammatory bowel disease. Curr Opin Pharmacol. 2015; 25: 67-71.
32. Nakamura S, Ohtani H, Watanabe Y, Fukushima K, Matsumoto T, Kitano A, et al. In situ expression of the cell adhesion molecules in inflammatory bowel disease. Evidence of immunologic activation of vascular endothelial cells. Lab Invest. 1993; 69(1): 77-85.
33. Koizumi M, King N, Lobb R, Benjamin C, Podolsky DK Expression of vascular adhesion molecules in inflammatory bowel disease. Gastroenterology. 1992; 103(3): 840-847.
34. Chen XP, Zhang TT, Du GH Lectin-like oxidized low-density lipoprotein receptor-1, a new promising target for the therapy of atherosclerosis? Cardiovasc Drug Rev. 2007; 25(2): 146-161.
35. Pothineni NVK, Karathanasis SK, Ding Z, Arulandu A, Varughese KI, Mehta JL. LOX-1 in atherosclerosis and myocardial ischemia: biology, genetics, and modulation. J Am Coll Cardiol. 2017; 69(22): 2759-2768.
36. Bendjelloul F, Rossmann P, Malý P, Mandys V, Jirkovská M, Prokesová L, et al. Detection of ICAM-1 in experimentally induced colitis of ICAM-1-deficient and wild-type mice: an immunohistochemical study. Histochem J. 2000; 32 (12): 703-709.
37. Hamamoto N, Maemura K, Hirata I, Murano M, Sasaki S, Katsu K. Inhibition of dextran sulphate sodium (DSS)-induced colitis in mice by intracolonically administered antibodies against adhesion molecules (endothelial leucocyte adhesion molecule-1 (ELAM-1) or intercellular adhesion molecule-1 (ICAM-1)). Clin Exp Immunol. 1999; 117(3): 462-468.
38. Shin MR, Kim KJ, Kim SH, Kim SJ, Seo BI, An HJ, et al. Comparative evaluation between sulfasalazine alone and in combination with herbal medicine on DSS-induced ulcerative colitis mice. Biomed Res Int. 2017; 2017: 6742652.

Original Article

The Effect of Arbutin on The Expression of Tumor Suppressor *P53*, *BAX/BCL-2* Ratio and Oxidative Stress Induced by Tert-Butyl Hydroperoxide in Fibroblast and LNcap Cell Lines

Shima Ebadollahi, M.Sc.[1, 2], Mahdi Pouramir, Ph.D.[1, 3*], Ebrahim Zabihi, Ph.D.[3], Monireh Golpour, M.Sc.[4], Mohsen Aghajanpour-Mir, M.Sc.[5, 6]

1. Department of Clinical Biochemistry, Faculty of Medicine, Babol University of Medical Sciences, Babol, Iran
2. Student Research Committee, Babol University of Medical Sciences, Babol, Iran
3. Cellular and Molecular Biology Research Center, Health Research Institute, Babol University of Medical Sciences, Babol, Iran
4. Cellular and Molecular Biology Research Center, Student Research Committee, School of Medicine, Mazandaran University of Medical Sciences, Sari, Iran
5. Department of Medical Genetics, School of Medicine, Tehran University of Medical Sciences, Tehran, Iran
6. Department of Genetics, Faculty of Medicine, Babol University of Medical Sciences, Babol, Iran

Corresponding Address: P.O.Box: 4136747176, Department of Clinical Biochemistry, Faculty of Medicine, Babol University of Medical Sciences, Babol, Iran
Email: pouramir@yahoo.com

Received: 16/April/2019, Accepted: 29/July/2019

Abstract

Objective: Arbutin (p-hydroxyphenyl-β-D-glucopyranoside) possesses beneficial functions including antioxidant, anti-inflammatory, and anti-tumoral activities. Due to the important role of oxidative stress and apoptosis in the successful treatment of cancer, understanding mechanisms that lead to apoptosis in cancer cells, is essential. The purpose of the current study was to evaluate the effect of arbutin on tert-butyl hydroperoxide (t-BHP)-induced oxidative stress and the related mechanisms in fibroblast and Lymph Node Carcinoma of the Prostate (LNCaP) cells.

Materials and Methods: In this experimental study, the LNCaP and fibroblast cell lines were pre-treated with arbutin (50, 250 and 1000 μM). After 24 hours, t-BHP (30 and 35 μM) was added to the cells. Viability was measured (at 24 and 48 hours) using MTT assay. The antioxidant effect of arbutin was measured by FRAP assay. The mRNA expression of *P53* and *BAX/BCL-2* ratio were measured using quantitative polymerase chain reaction (PCR). The percentage of apoptotic or necrotic cells was determined using a double staining annexin V fluorescein isothiocyanate (FITC) apoptosis detection kit.

Results: Arbutin pre-treatment increased the total antioxidative power and cell viability in the MTT assay and reduced *BAX/BCL-2* ratio, *P53* mRNA expression and necrosis in fibroblasts exposed to the oxidative agent (P<0.001). In addition, our results showed that arbutin can decrease cell viability, induce apoptosis and increase *BAX/BCL-2* ratio in LNCaP cells at some specific concentrations (P<0.001).

Conclusion: Arbutin as a potential functional β-D-glucopyranoside has strong ability to selectively protect fibroblasts against t-BHP-induced cell damage and induce apoptosis in LNCaP cells.

Keywords: Arbutin, Fibroblast, LNCaP, Oxidative Stress, Tert-Butyl Hydroperoxide

Cell Journal(Yakhteh), Vol 22, No 4, January-March (Winter) 2021, Pages: 532-541

Citation: Ebadollahi Sh, Pouramir M, Zabihi E, Golpour M, Aghajanpour-Mir M. The effect of arbutin on the expression of tumor suppressor P53, BAX/BCL-2 ratio and oxidative stress induced by tert-butyl hydroperoxide in fibroblast and LNcap cell lines. Cell J. 2021; 22(4): 532-541. doi: 10.22074/cellj.2021.6902.

Introduction

Oxidative stress is defined as disequilibrium between production and disposal of reactive oxygen species (ROS) (1). Free radicals and oxidant species can impose irreversible oxidative damage on a variety of indispensable cellular constituents including proteins, lipids, and nucleic acids (2). Oxidative stress causes the dysregulation of oncogenes and tumor suppressor genes such as *P53*. Excessive accumulation of ROS above the homeostatic threshold, is detrimental to cells and disturbs physiological mechanisms related to proliferation, apoptosis, angiogenesis, etc. (3).

Oxidative stress has a prominent role in the pathogenesis of different diseases, such as inflammatory diseases, diabetes, cardiovascular diseases, certain cancers, and neurodegenerative diseases (4). ROS induce DNA damage, genome variability, and cell proliferation. Arbutin (*p*-hydroxyphenyl-β-D-glucopyranoside) extracted from bearberry leaf (*Arctostaphyllos uva-ursi*) possesses various beneficial features (5, 6). Arbutin is broadly utilized as a cosmetic skin whitening agent due to its strong inhibitory effects on hydroxylation of tyrosine in melanin production pathway (7). Alongside its antiseptic, antibacterial, and diuretic features, *in vitro* studies have proven its anti-inflammatory, antioxidant, and anti-tumoral activities (8). The tumor suppressor gene *P53*, the most prevalent mutated gene found in 50% of human cancers, is identified as a genome protector that maintains genome stability. *P53* is mutated through a broad diversity of cellular insults, including DNA damage, oncogene activation, hypoxia, oxidative stress, and DNA-damaging chemotherapy agents (9). *P53* can induce

genes such as pro-apoptotic genes (e.g. *Bax, Caspase-3*, *Apaf-1*, and *P53*-inducible gene) that causes deletion of cells through the incitement of cell mortality or senescence, and inhibit the aggregation of damaged cells (10, 11). The anti-apoptotic mitochondrial protein Bcl-2 and the pro-apoptotic protein Bax are known to be vital regulators of programmed cell death (11). The *BAX/BCL-2* ratio as an index of the mitochondrial apoptotic pathway can control cytochrome c release from mitochondria to cell cytoplasm (12). Tert-butyl hydroperoxide (t-BHP), as a peroxide and an appropriate substitute for H_2O_2, is commonly utilized to investigate several cellular injuries such as oxidative-induced injuries, cell apoptosis, and the fundamental molecular mechanisms which are triggered by ROS (13). To widen the knowledge on the biological effects of arbutin, we investigated the effects of arbutin under oxidative stress conditions induced by t-BHP and evaluated its effects on the expression of tumor suppressor *P53* and the *BAX/BCL-2* ratio which are essential genes involved in programmed cell death.

Materials and Methods

Chemicals and reagents

In this experimental study, Dulbecco's Modified Eagle Medium (DMEM) high glucose and RPMI-1640 were purchased from Biowest (Austria). Fetal bovine serum (FBS) and penicillin-streptomycin were bought from Gibco (Germany). Pure (98%) arbutin powder, 2, 4, 6-tripyridyl-s-triazine (TPTZ), and 3- [4, 5-dimethylthiazol-2-yl]-2, 5-diphenyltetrazolium (MTT) were purchased from Sigma-Aldrich (Germany). Annexin V-FITC apoptosis detection kit was purchased from eBioscience (San Diego, CA, USA). Tert-butyl hydroperoxide (t-BHP) was obtained from MERK (Germany) and cDNA synthesis Kit and YTA qPCR probe MasterMix 2x, were purchased from Yekta Tajhiz (Iran).

Cell lines pretreatment and exposure

The fibroblast cell line was isolated from human newborn foreskin according to Pandamooz et al. (14) method, with the parents' informed consent and upon approval from the local Ethics Committee (Babol University of Medical Sciences, Babol, Iran) and the AR-positive human prostate cancer (PCa) LNCaP cell line was obtained from National Cell Bank of Iran (Pasteur Institute). The fibroblast and LNCaP cells were respectively cultured in DMEM high glucose and RPMI-1640, including 10% FBS, 100 IU/mL penicillin, and 100 µg/mL streptomycin. They were kept at 37˚C in a humidified atmosphere containing 95% air and 5% CO_2. In all tests, cells were permitted to habituate for 24 hours before any treatments.

Arbutin and t-BHP treatment

Oxidative stress was induced by introducing t-BHP into the culture media. The fibroblasts (10^4 cells/well) and LNCaP (7×10^3 cells/well) were cultured in 96- well plates. After 24 hours (60% confluency), the supernatant was replaced with three nontoxic concentrations of pure (98%) arbutin powder in complete medium (50, 250, and 1000 µM) for an additional 24 hours. To evaluate the t-BHP effects, 30 and 35 µM t-BHP were added to the wells containing arbutin in complete medium in fibroblast and LNCaP cells, respectively. The cells without arbutin and t-BHP were considered the control groups. Finally, after 24 and 48 hours of exposure to t-BHP, the supernatant was collected to perform FRAP assays, and the cells were washed twice with phosphate-buffered saline (PBS, pH=7.4) to measure cells viability using MTT assay.

Measuring cell viability using MTT assay

Tetrazolium dye 3- [4, 5-dimethylthiazol-2-yl]-2, 5-diphenyltetrazolium bromide (MTT) is usually used to assess cells viability. The MTT-colorimetric assay is based on the capacity of viable cells to reduce MTT into formazan dye through succinate dehydrogenase in mitochondria. After exposure of the cells to arbutin with/without consequent exposure to t-BHP and incubating for 24 and 48 hours, 50 µL of 5 mg/ml MTT in PBS was added to each well and incubated for another 4 hours. Afterward, the media were aspirated, and the formazan precipitate was dissolved in 150 µl dimethyl sulfoxide (DMSO) to lyse the cells. The color intensity of the solution was measured by Camspec-M501 spectrophotometer (Camspec, UK) at 570 nm with 630 nm as the reference wavelength. The results were reported as the percentage of the control ones (13).

Estimation of ferric reducing antioxidant power

The Ferric Reducing Antioxidant Power (FRAP) assay was done according to Benzie and Strain (15) method. The FRAP assay evaluates the capacity of reduction of total ''antioxidants'' which are capable of reducing "Fe^{+3} 2, 4, 6-tripyridyl-s-triazine (TPTZ) complex" to the blue-colored ferrous form at low pH. The assay mixture is made by adding same volumes of each sample (collected media at t=24 and 48 hours) and standards (50 µl each) in 1.5 ml of FRAP reagent including 10 mM TPTZ in 40 mM hydrochloride acid, 0.3 mM acetate buffer (pH=3.6), and ferric chloride 20 mM. The absorbance was measured (after 15 minutes incubation at 37˚C) at 593 nm of wavelength. Standard graphs were constructed using different concentrations of $FeSO_4$ (125- 1000 µM) (16).

Quantitative reverse transcription polymerase chain reaction assay

Total RNA was extracted from treated cells For quantitative reverse transcription polymerase chain reaction (qRT-PCR), using RNA extraction mini kit (Yekta Tajhiz, Iran) according to the manufacturer's instructions. cDNA synthesis kit was utilized to synthesize the cDNA library. The reaction mixture included 1 µl of the random hexamer, 10 µl of RNA, and 2.4 µl of diethyl pyrocarbonate (DEPC)-treated H_2O. After gentle mixing and brief centrifuging, the mixture was incubated at 70˚C for 5 minutes. Then, while chilling on ice, 4 µl of 5X loading buffer, 1 µl of Moloney Murine Leukemia Virus (MMLV) Reverse Transcriptase, 1 µl dNTPs, and 0.5 µl RNasin were added, and the mixture was incubated for 60 minutes at 37˚C, then heated at 70˚C for 5 minutes.

For *Bax*, *Bcl-2*, and *GAPDH* detection, mRNA PCR primers were designed by Primer 3 software and synthesized by Pishgam company (Iran). Primer sequence homology and total gene specificity were determined by BLAST analysis (http://www.ncbi.nlm.nih.gov/blast) (Table 1).

Table 1: List of primer sequences used for quantification of mRNA expression

Genes	Primer sequence (5′-3′)
Bax	F: GGTTGTCGCCCTTTTCTACTTTGC
	R: ATGTCCAGCCCATGATGGTTCTG
Bcl-2	F: ATGTGTGTGGAGAGCGTCAAC
	R: AGCCAGGAGAAATCAAACAGAGG
GAPDH	F: GGTGGTCTCCTCTGACTTCA
	R: GTTGCTGTAGCCAAATTCGT

Subsequently, 100 ng of cDNA was used as the template in a qRT-PCR reaction using the YTA Super SYBR® Green qPCR Master Mix 2x (Yekta Tajhiz, Iran) kit, according to the manufacturer's instructions. The reaction mixture, including 10 µl of 2 X master mix, 0.4 µl of forward primer, 0.4 µl of reverse primer, 1 µl of cDNA, 7.8 µl of ddH_2O and 0.4 µl of passive reference dye. The PCR thermal cycling situations were set as follows: 40 cycles of denaturation at 95˚C for 10 seconds, annealing at 60˚C for 10 seconds, extension at 72˚C for 20 seconds and a final extension at 72˚C for 7 minutes. For evaluation of *P53* expression, 100 ng of cDNA was used as the template in a qRT-PCR reaction using a TaqMan *TP53* primer and probe was purchased from Applied Biosystems (Foster City, CA, USA). The *TP53* sequence (Assay ID Hs01034249_m1) was amplified in a 20 µl reaction containing 10 µl of qPCR probe Master Mix 2x, 2 µl of cDNA, 1 µl of a TaqMan P53 Gene (primers and probes), and 7 µl of DNase-free water. PCR cycling steps were as follows: 3 minutes at 94˚C, 40 cycles of 15 seconds at 95˚C, and 1 minute at 60˚C. A TaqMan GAPDH (Applied Biosystems, FosterCity, CA, USA, Assay ID Hs03929097-g1) was used as a reference gene (17). The expression level of *P53* and *Bax*, *Bcl-2* genes was evaluated by qRT-PCR using an ABI 7500 Fast Real-Time PCR System (Applied Biosystems). In order to analyze the expression of related genes, we used the formula $2^{-\Delta\Delta CT}$ in which $\Delta\Delta CT = \Delta CT$ sample–ΔCT reference for calculating the fold expression of each transcript relative to *GAPDH*, as a housekeeping gene.

Annexin V-fluorescein isothiocyanate/propidium iodide apoptosis assay

LNCaP and fibroblast cells were cultured in six-well plates (25×10^4 cells/well) for 24 hours and then pretreated with different concentrations of arbutin (50, 250 and 1000 µM) for 24 hours followed by exposure to t-BHP (30, and 35 µM) for extra 24 and 48 hours. Apoptosis was investigated by an annexin V-FITC apoptosis detection kit based on the manufacturer's instructions. After washing the cells twice with cold PBS, cells were collected and centrifuged at 1500 rpm for 5 minutes at 4˚C. Then, they were resuspended in 1 ml binding buffer. The cells were incubated with annexin V-FITC for 5 minutes and then incubated with propidium iodide for 15 minutes in the dark at room temperature 25˚C finally, the percentages of apoptosis and necrosis were observed using FACS Calibur flow cytometer (BD Biosciences, San Jose, CA, USA).

Statistical analysis

All the data obtained under normal and oxidative stress conditions, are presented as mean ± standard error of three separately performed experiment. One-way ANOVA with post-hoc test (Tukey) was used for statistical comparison, and $P<0.05$ were contemplated statistically significant ($0.01<{}^{*}P<0.05$, $0.001<{}^{**}P<0.01$, ${}^{***}P<0.001$).

Results

Dose-response relationship of arbutin and t-BHP toxicity

We first assessed the dose response relationship for t-BHP, a potent pro-oxidant, in fibroblast (Fig.1A) and LNCaP cells (Fig.1B). Toxic effects in fibroblast and LNCaP cells and viability were evaluated after 24 and 48 hours of exposure to varying concentrations of t-BHP, using MTT assay. The viability of the cells significantly reduced after incubation with t-BHP in a dose-dependent manner (30-60 µM, $P<0.001$). The 30 and 35 µM of t-BHP were used for further experiments to determine the effect of arbutin in fibroblast and LNCaP cells, respectively. Moreover, we evaluated the toxicity of arbutin after 24 and 48 hours of exposure. The MTT assay showed that arbutin decreased cell viability at doses above 1000 µM. Then, we used three nontoxic doses (50, 250, 1000 µM) of arbutin for further experiments.

The effect of arbutin pre- treatment on the oxidative stress induced by t-BHP in fibroblast and LNCaP cell lines

Pre-treatment with 250 and 1000 µM arbutin after 24 and 48 hours of exposure to t-BHP, significantly increased cell viability compared to the oxidant group exposed only to 30 and 35 µM t-BHP alone in fibroblasts (Fig.1C) and LNCaP cell lines, respectively ($P<0.001$, Fig.1D).

The effect of arbutin on ferric reducing antioxidant power in fibroblasts and LNCaP cell lines

We found that following treatment of the fibroblast and LNCaP cells with tBHP at 30 and 35 µM for 24 hours, FRAP decreased in the supernatant of the cells compared to the control groups ($P<0.01$, n=3). Also, after 24 and 48 hours of pre-treatment of cells with arbutin 250 and 1000 µM, the antioxidant power increased markedly in the supernatant of fibroblast (Fig.2A) and LNCaP (Fig.2B) cells in t-BHP-induced oxidative stress.

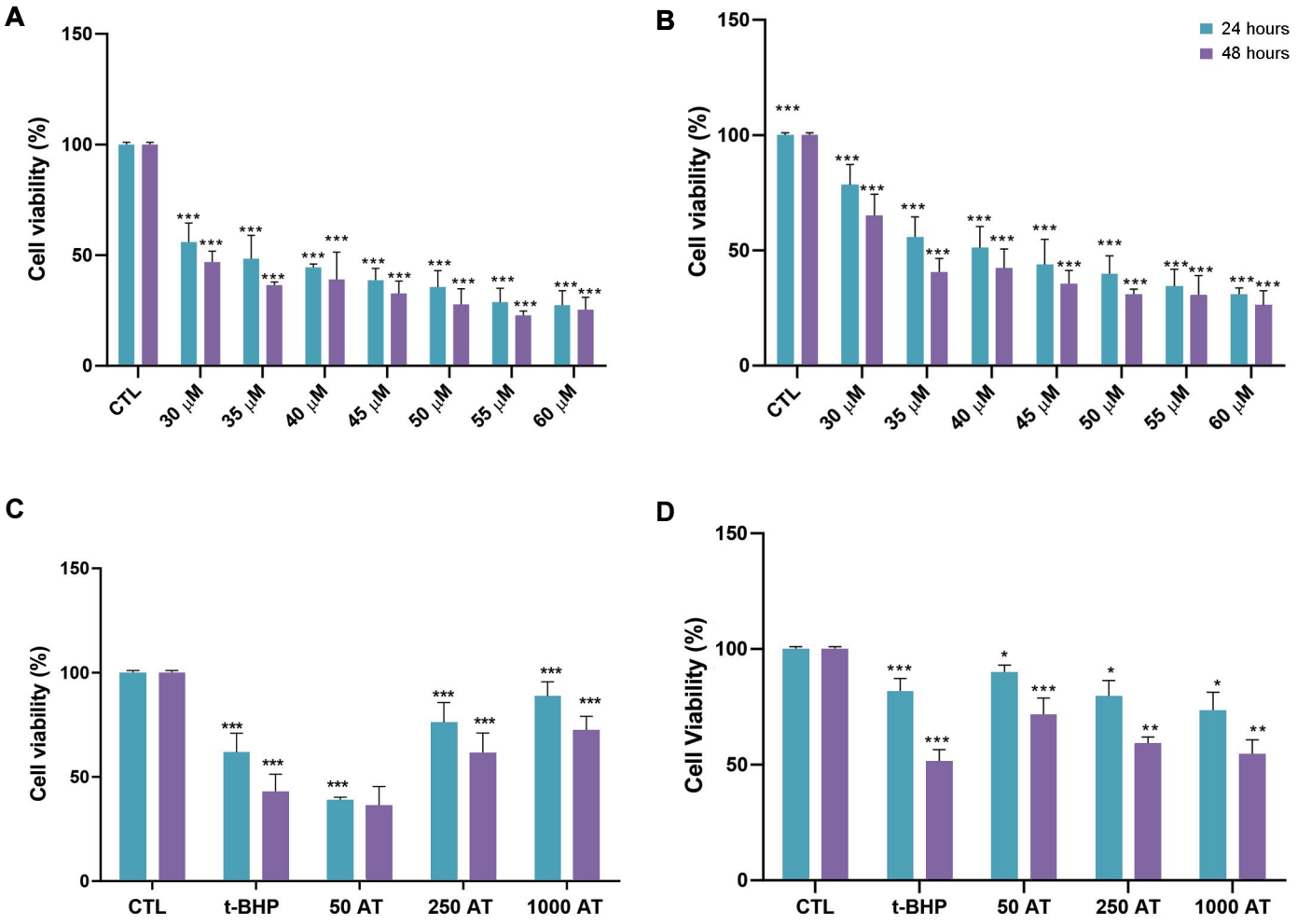

Fig.1: The protective effects of arbutin on t-BHP-induced cytotoxicity in fibroblast and LNCaP cells. **A.** The t-BHP toxicity in fibroblast and **B.** LNCaP cells (*** ; P <0.001 versus control). **C.** The Effect of arbutin pre-treatment on fibroblast and **D.** LNCaP cells viability after 24 and 48 hours of exposure to t-BPH. Data shown represent the mean values of three experiments ± SD (*; P<0.05, **; P<0.01, ***; P<0.001 as compared to oxidant group).
CTL; Control group, t-BHP; Tert-butyl hydroperoxide, 50 AT+t-BHP; Arbutin 50 µM with 30 µM t-BHP, 250 AT; Arbutin 250 µM with 30 µM t-BHP, and 1000 AT; Arbutin 1000 µM with 30 µM t-BHP.

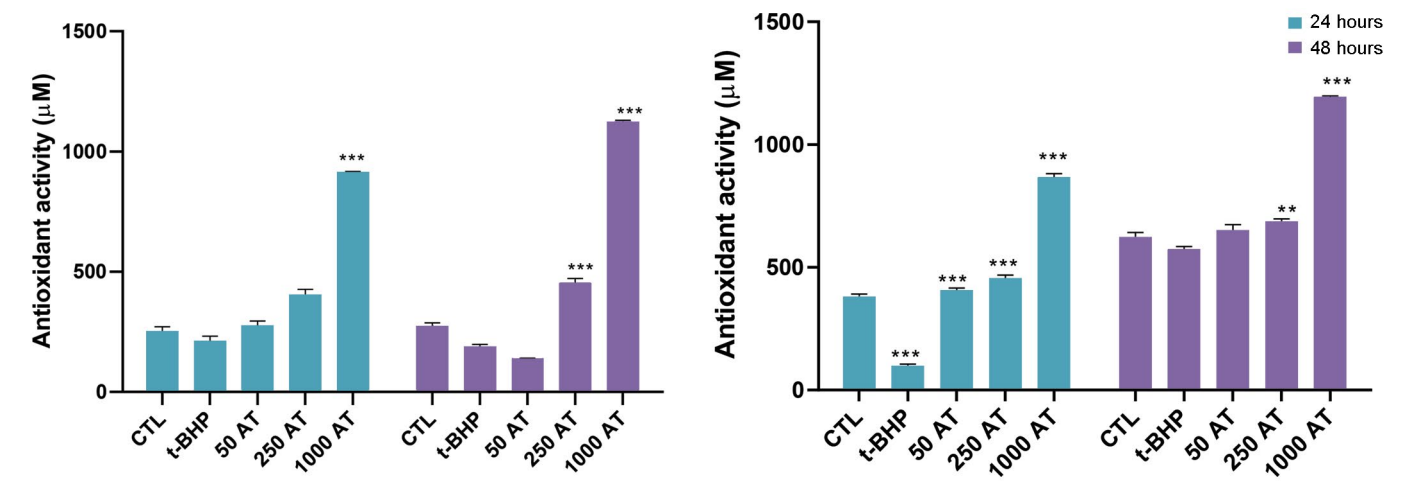

Fig.2: Effect of arbutin on total antioxidant capacity. The ferric reducing antioxidant power (FRAP) after pre-incubation with arbutin in **A.** t-BHP-induced fibroblast and **B.** LNCaP cells. Fibroblast and LNCaP cells were pre-treated with arbutin (50, 250 and 1000 µM) and exposed to t-BHP (30 µM) for 24 and 48 hours. CTL; Control group, t-BHP; Tert-butyl hydroperoxide, 50 AT+t-BHP; Arbutin 50 µM with t-BHP 30 µM, 250 AT; Arbutin 250 µM with t-BHP 30 µM, 1000 AT; Arbutin 1000 µM with t-BHP 30 µM, ** ; P<0.01, and *** ; P<0.001 versus tBHP.

Effect of arbutin pre-treatment on *BAX/BCL-2* ratio and *P53* mRNA expression in t-BHP-induced oxidative stress

The *BAX/BCL-2* ratio (Fig.3A) and *P53* mRNA expression (Fig.3B) was considerably increased after 24 hours of exposure to t-BHP (30 µM) in fibroblasts compared to the control group (P<0.001). Expression of *P53* mRNA in fibroblasts after 24 and 48 hours of pre-treatment with arbutin (50, 250 and 1000 µM) and 30 µM t-BHP, is illustrated in Figure 3B. Pre-treatment with arbutin (250 and 1000 µM) after 24 and 48 hours of exposure to t-BHP, significantly reduced *BAX/BCL-2* level (Fig.3A) and *P53* mRNA (Fig.3B) compared to the oxidant group only exposed to 30 µM t-BHP (P<0.001). Moreover, the ratio of *BAX/BCL-2* mRNA expression was considerably increased after 24 and 48 hours exposure to t-BHP (35 µM) in LNCap cells in comparison to the control group (P<0.05, Fig.3C). As illustrated in Figure 3C, in LNCap cell line, pre-treatment with arbutin (50, 250 and 1000 µM) could significantly decrease the *BAX/BCL-2* ratio compared to the group exposed t-BHP (35 µM, P<0.05). Also, after 48 hours of pre-treatment with 1000 µM arbutin, *BAX/BCL-2* ratio markedly increased compared to the control group in LNCaP cells (P<0.001). Expression of *P53* mRNA increased after 24 hours of exposure to t-BHP compared to the control group in LNCaP cells and pre-treatment with arbutin 50 and 250 µM significantly decreased *P53* mRNA expression compared to both control and oxidant groups (P<0.05, Fig.3D). Moreover, after 48 hours of pre-treatment with arbutin (50, 250 and 1000 µM), *P53* mRNA expression significantly diminished compared to both control and oxidant groups (P<0.05, Fig.3D).

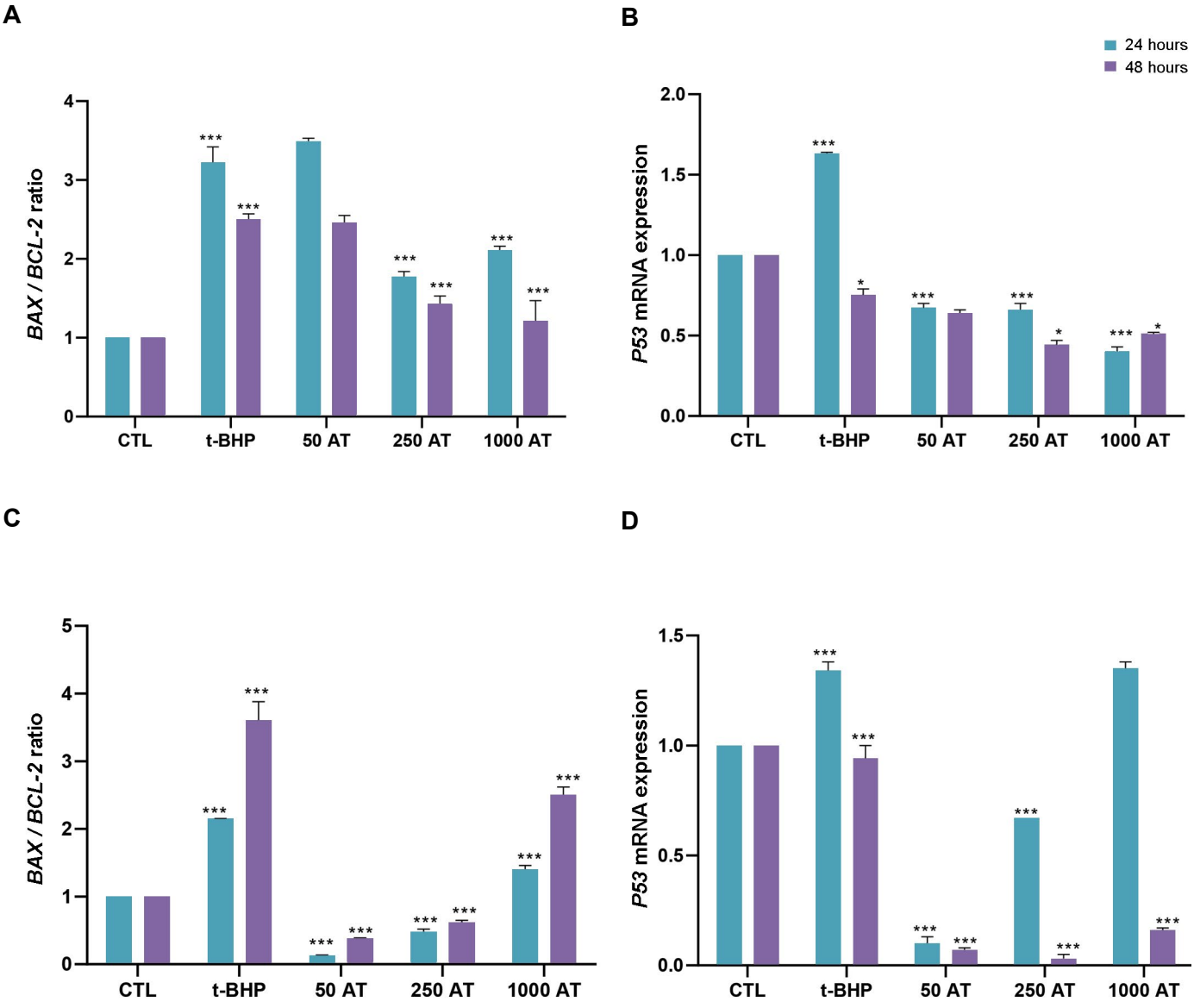

Fig.3: Effect of arbutin on *BAX/BCL-2* ratio and *P53* mRNA expression.The *BAX/BCL-2* ratio and *P53* mRNA expression in **A, B.** t-BHP-induced fibroblast and **C, D.** LNCaP cells. CTL; Control group, t-BHP; Tert-butyl hydroperoxide, 50 AT+t-BHP; Arbutin 50 µM with t-BHP 30 µM, 250 AT; Arbutin 250 µM with t-BHP 30 µM, and 1000 AT; Arbutin 1000 µM with t-BHP 30 µM (0.01<*P<0.05, 0.001<**P<0.01, and ***P<0.001 versus tBHP).

Effect of arbutin pre-treatment on t-BHP induced apoptosis and necrosis in LNCaP and fibroblasts

In fibroblasts, exposure to t-BHP increased the necrosis rate from 0.59% (Fig.4A) to 34.3% (Fig.4B) after 24 hours. The pre-treatment with 50, 250 and 1000 µM arbutin decreased necrosis induced by t-BHP after 24 hours, from 34.3% (Fig.4B) to 26.2% (Fig.4C), 18.4% (Fig.4D) and 7.08% (Fig.4E).

Additionally, after 48 hours exposure to t-BHP increased the necrosis rate from 0.72% (Fig.4F) to 24.8%(Fig.4G). The pre-treatment with 50, 250 and 1000 µM arbutin arbutin decreased necrosis induced by t-BHP in fibroblast cells from 24.8% (Fig. 4G) to 18.7% (Fig. 4H), 11.8% (Fig. 4I) and 4.77% (Fig.4J).

To assess whether arbutin-induced cytotoxicity is indeed due to induction of apoptosis, rather than necrosis in cells, we performed flow cytometry analysis using Annexin V-FITC/PI double-staining method. Conspicuously, LNCap cells exposure to arbutin resulted in enhanced late apoptosis in a dose-dependent manner. As shown in Figure 5, LNCaP cells exposure to t-BHP increased the apoptosis rate from 4.50% (Fig.5A) to 8.68% (Fig.5B) after 24 hours. Also, pre-treatment with 50, 250 and 1000 µM arbutin after 24 hour increased the apoptosis rate to 8.91% (Fig.5C), 11.21% (Fig.5D) and 21.78% (Fig.5E). As illustrated in Figure 5F, t-BHP promoted apoptosis from 4.81% (Fig.5F) to 9.46% (Fig.5G) compared to the control group. Moreover, pre-treatment with 50, 250 and 1000 µM arbutin after 48 hours, increased the percentage of apoptotic cells induced by t-BHP from 9.46% (Fig.5G) to 10.76% (Fig.5H), 13.4% (Fig.5I) and 25.43% (Fig.5J) respectively.

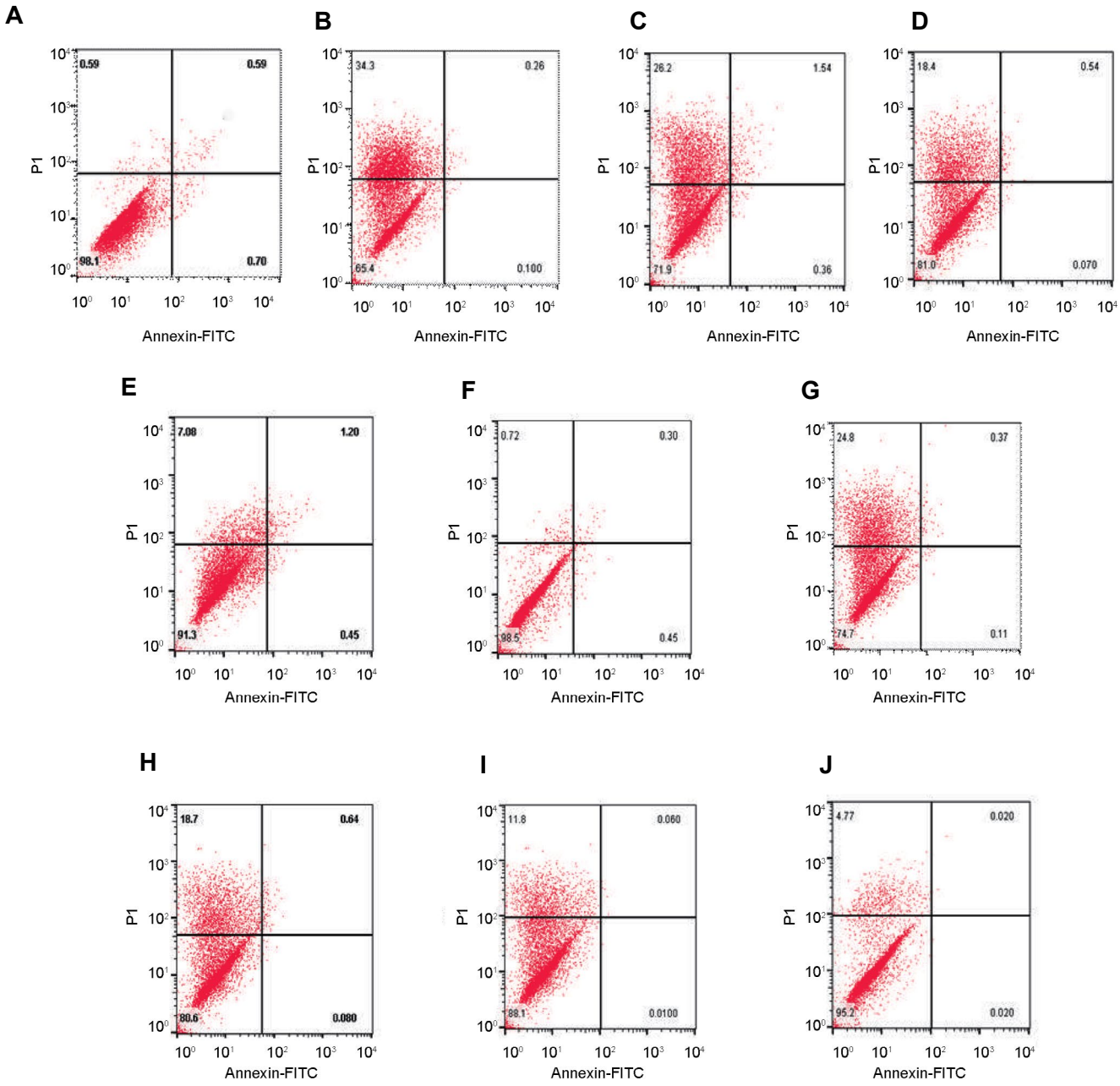

Fig.4: Effect of arbutin on the t-BHP-induced cytotoxicity in fibroblast cells. Arbutin pre-treatment inhibited necrosis of human fibroblast cells in a dose-dependent manner after **A-E.** 24 hours and **F-J.** 48 hours exposure to t-BHP. The necrosis rate of cells cultured in the **A, F.** Control, **B, G.** 30 µM tert-butyl hydroperoxide, **C, H.** 50 µM arbutin+30 µM t-BHP, **D, I.** 250 µM arbutin+30 µM t-BHP, and **E, J.** 1000 µM arbutin+30 µM t-BHP.

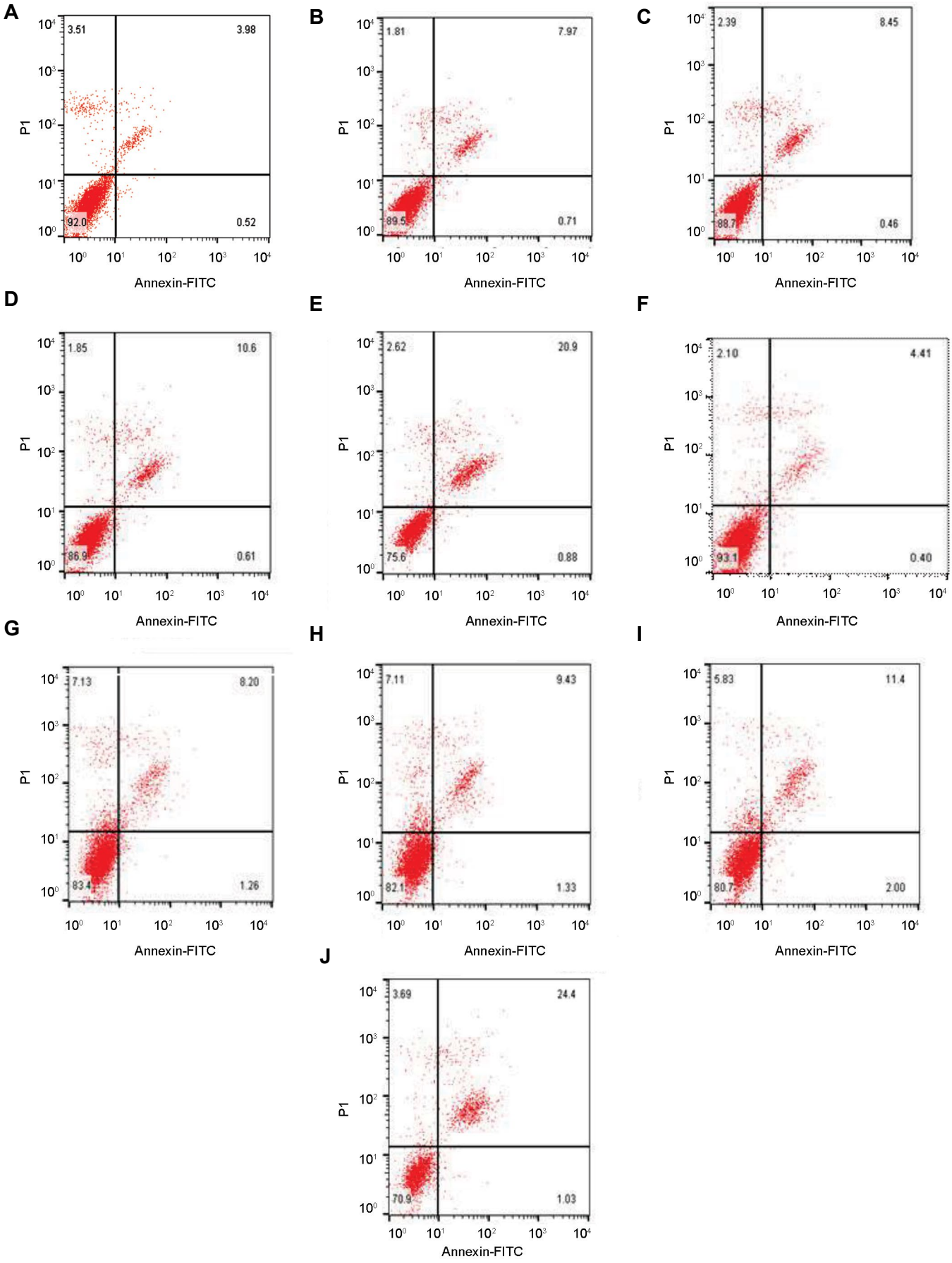

Fig.5: Effect of arbutin on t-BHP- induced cytotoxicity in LNCaP cells. Arbutin induces apoptosis in human LNCaP cells in a dose-dependent manner after **A-E.** 24 hours and **F-J.** 48 hours exposure to t-BHP. The apoptosis rate of cells cultured after 24 hours exposure to t-BHP in the **A, F.** Control, **B, G.** 35 µM tert-butyl hydroperoxide, **C, H.** 50 µM arbutin+35 µM t-BHP and **D, I.** 250 µM arbutin+35 µM t-BHP, and **E, J.** 1000 µM arbutin+35 µM t-BHP.

Discussion

PCa is the most common solid tumor and the sixth main reason for cancer deaths among men, worldwide. It is currently considered one of the foremost important medical issues that the male population faces (18, 19). There has been an enormous interest in using natural agents capable of prompting programmed cell death in cancer cells, which can develop the mechanism-based prevention and treatment approaches for cancer (20). As far as we are concerned, the effect of arbutin has not been evaluated against t-BHP-induced cytotoxicity in LNCaP and fibroblast cells. Besides antiseptic, skin whitening, anti-inflammatory and anti-tussive properties of arbutin, it might have the potential to be an anti-tumor and anti-oxidative agent which could be related to *P53* regulation (8, 21). Tert-butyl hydroperoxide as a potent oxidative stress stimulator has been used to induce oxidative damage *in vitro* and *in vivo* (13). In this experiment, the effect of arbutin was evaluated in LNCaP and fibroblast cells in t-BHP-induced oxidative stress. Due to the vital role of programmed cell death in successful cancer treatment, it is precious to understand the mechanisms that trigger apoptosis, especially *P53*-mediated apoptosis in cancer cells (22). Since apoptotic cell pathways are regulated by the expression level of specific genes, especially the *BAX/BCL-2* ratio, evaluation of the *BAX/BCL-2* ratio can determine the apoptotic pattern in the cells (23).

Results of the current study showed that arbutin decreased *BAX/BCL-2* ratio, and *P53* mRNA expression, increased cell viability and total antioxidant capacity in fibroblast cells and led to diminished t-BHP-induced cell death. Moreover, arbutin induced apoptosis, increased *BAX/BCL-2* ratio, and reduced cell viability in LNCaP cell. There are many documents which illustrated that natural compounds decrease intracellular ROS and protect cells from oxidative stress. It was reported that Turkish propolis rich in phenolic as well as flavonoid contents, significantly decreased t-BHP induced oxidative stress in human fibroblast cells. Moreover, quercetin and rutin protected Caco-2 cells and L6 myoblasts from t-BHP induced oxidative stress (24). It was reported that arbutin in combination with ursolic acid, can act as a strong UV-protector in fibroblast cell (25). However, so far, no study reported the cytoprotective effect of arbutin in fibroblast cells exposed to t-BHP. The protective effect of arbutin (250 and 1000 μM) was illustrated by the substantial increase in fibroblasts viability and FRAP level under stressed conditions (30 μM t-BHP).

On the contrary, in our experiment, arbutin (50 μM) decreased fibroblast cells viability to levels even lower than the t-BHP group. It may be because arbutin at this dose could not resist the oxidant situation and changed to a pro-oxidant substance. Previous studies reported that natural antioxidants like flavonoids and polyphenols, can act as a pro-oxidant when they are exposed to alkali pH, oxygen, and high concentration of transition metals (26). Some antioxidants (resveratrol, coumaric acid, and N-acetylcysteine) could act as pro-oxidant, increased ROS production and led to cell damage in the endothelial cells (27). These investigations raised the possibility that arbutin might have anti-cancer activities for instance against prostate tumor cells. Inconsistent with our data, *in vitro* and *in vivo* experiments confirmed that arbutin induced free radical-scavenging, anti-hyperglycemic, antioxidant, and anti-inflammatory effects and could enhance the level of FRAP in the supernatant of different cells (28-30). Also, pre-treatment of the retinal ganglion cells (RGCs) cells with arbutin (100 μM) had protective effects against oxidative damage induced by H_2O_2 (31). The results of our study declared that pre-treatment with arbutin downregulated *BAX/BCL-2* ratio and *P53* mRNA expression in fibroblast cells compared to the oxidant group. The results support previous reports concerning cytoprotective and antioxidant features of arbutin obtained *in vitro* and *in vivo* (8).

Our findings are consistent with the results showing anti-oxidative effects of arbutin as a potent radical scavenger, in isolated human neutrophils, murine microglial BV2, and Hep G2 cell lines (28, 32, 33). Also, arbutin can reduce oxidative stress derived from the melanogenic pathway within the skin (34). According to previous studies, P53 was significantly up-regulated in an oxidative stress situation and could cause cell cycle arrest, cellular senescence, and apoptosis (35).

Interestingly, we observed a decrease in necrosis and *P53* mRNA expression in fibroblasts in response to arbutin pre-treatment in t-BHP-induced oxidative stress groups. It was shown that arbutin declines radical hydroxyl production and protects U937 cells from *Bax*-mitochondrial pathway apoptosis (36). Our analysis of annexin-v/PI, flow-cytometric results revealed that pre-treatment with 250 μM and 1000 μM of arbutin, increases apoptosis in LNCaP cells exposed to t-BHP (35 μM). Small polyphenols, such as gallic acid, and quercetin, can exhibit peroxidation activity (37). We found that t-BHP treatment increases *BAX/BCL-2* mRNA ratio and pre-treatment with arbutin may counteract *t*-BHP-induced upregulation of *BAX/BCL-2* ratio, however, in comparison to the control group, suggesting that arbutin may trigger *t*-BHP-induced apoptosis in LNCaP cell in a dose-dependent manner. Our results are in consistency with the results of a previous study done on the inhibitory properties of arbutin on the proliferation of cancer cells, including A375 human malignant melanoma cells through up-regulating *P53* expression (38), as well as, HCT-15 and TCCSUP cells (39). Moreover, Jiang et al. reported that arbutin and its acetylated derivative significantly reduce cell viability, promote cell apoptosis, decrease the expression of *Bcl-2* and *Bcl-xL*, and induce a mitochondrial disruption in B16 murine melanoma cells. Treatment with arbutin was shown to induce caspase 9, 3, and PARP, increase *BAX/BCL-2* ratio in cells and cause DNA damage by mitochondrial apoptotic pathway (40). Moreover, the results of this study in terms of *BAX/BCL-*

2 ratio and apoptosis indicated a more intense effect for arbutin in extended periods. According to flow cytometry results, the rate of late apoptosis was higher than early apoptosis in LNCaP cell, which probably reveals the effect of arbutin on DNA damage, and cell membrane changes. This may reflect that arbutin, in addition to its effect on the cell membrane, may disrupt cell cycle. It seems that arbutin is a potent agent to be used against LNCaP cells. The anticancer feature of natural polyphenols is generally attributable to their various pharmacological effects such as anti-inflammatory, anti-oxidative, and anti-proliferation effects. They modulate PCa cell growth by modulating molecular events, and signaling cascades associated with cell survival, proliferation, migration, and differentiation, immune responses, angiogenesis, hormone activities, etc. (18).

Our findings confirmed that arbutin acts as an antioxidant agent, and has anti-proliferative activity in LNCaP cells via induction of apoptosis. Moreover, arbutin caused favorable changes within the fibroblasts, thereby protecting them from oxidative stress conditions. More studies are required to investigate the combined effects of arbutin and chemotherapeutic agents in prostate cancer.

Conclusion

This study indicated, for the first time, that arbutin can increase total antioxidant power leading to significant protective effects on fibroblasts against t-BHP-induced oxidative stress. Also, results of this study revealed that arbutin, which does not show significant toxicity at concentrations up to 1000 µM, could serve as a potential candidate with strong protective effects on t-BHP-induced oxidative stress, by increasing cell viability and decreasing necrosis in fibroblasts. Also, arbutin (1000 µM) can induce apoptosis and increase *BAX/BCL-2* ratio in LNCaP cell line in t-BHP-induced oxidative stress. These findings provide basis for further investigations on arbutin as a novel therapeutic agent to combat oxidative stress for treatment of various diseases.

Acknowledgements

This research financially supported by a grant from the deputy of Research and Technology, Babol University of Medical Sciences. Authors declare their sincere thanks to all staffs in the Cellular and Molecular Biology Research Center at Babol University of Medical Sciences. The authors declare no conflict of interest.

Authors' Contributions

Sh.E., M.P., E.Z.; Participated in study design, data collection and evaluation, drafting, and statistical analysis, contributed extensively in the interpretation of the data and the conclusion. Sh.E., M.G.; Performed cell culture and flow cytometry assay of the study. Sh.E., M.A.-M.; Conducted primer design and molecular experiments and RT-qPCR analysis. All authors participated in finalization of the manuscript and approved the final draft.

References

1. Gyasi-Sarpong C, Ali I, Owiredu WKBA. Oxidative Stress in ghanaians presenting with prostate cancer. British Journal of Medicine and Medical Research. 2016; 14(11): 1-8.
2. Sinha K, Das J, Pal PB, Sil PC. Oxidative stress: the mitochondria-dependent and mitochondria-independent pathways of apoptosis. Arch Toxicol. 2013; 87(7): 1157-1180.
3. Hecht F, Pessoa CF, Gentile LB, Rosenthal D, Carvalho DP, Fortunato RS. The role of oxidative stress on breast cancer development and therapy. Tumour Biol. 2016; 37(4): 4281-4291.
4. Yoon J, Ham H, Sung J, Kim Y, Choi Y, Lee JS, et al. Black rice extract protected HepG2 cells from oxidative stress-induced cell death via ERK1/2 and Akt activation. Nutr Res Pract. 2014; 8(2): 125-131.
5. Pečivová J, Nosáľ R, Sviteková K, Mačičková T. Arbutin and decrease of potentially toxic substances generated in human blood neutrophils. Interdiscip Toxicol. 2014; 7(4): 195-200.
6. Wang S, Fu C, Bilal M, Hu H, Wang W, Zhang X. Enhanced biosynthesis of arbutin by engineering shikimate pathway in pseudomonas chlororaphis P3. Microb Cell Fact. 2018; 17(1): 174.
7. Hong JH, Chen HJ, Xiang SJ, Cao SW, An BC, Ruan SF, et al. Capsaicin reverses the inhibitory effect of licochalcone A/β-Arbutin on tyrosinase expression in b16 mouse melanoma cells. Pharmacogn Mag. 2018; 14(53): 110-115.
8. Migas P, Krauze-Baranowska M. The significance of arbutin and its derivatives in therapy and cosmetics. Phytochem Lett. 2015; 13: 35-40.
9. Ringer L, Sirajuddin P, Tricoli L, Waye S, Choudhry MU, Parasido E, et al. The induction of the p53 tumor suppressor protein bridges the apoptotic and autophagic signaling pathways to regulate cell death in prostate cancer cells. Oncotarget. 2014; 5(21): 10678-10691.
10. Liu J, Zhang C, Hu W, Feng Z. Tumor suppressor p53 and its mutants in cancer metabolism. Cancer Lett. 2015; 356(2): 197-203.
11. Kim GJ, Jo HJ, Lee KJ, Choi JW, An JH. Oleanolic acid induces p53-dependent apoptosis via the ERK/JNK/AKT pathway in cancer cell lines in prostatic cancer xenografts in mice. Oncotarget. 2018; 9(41): 26370-26386.
12. Akef H, Kotb N, Abo-Elmatty D, Salem S. Anti-proliferative effects of androctonus amoreuxi scorpion and cerastes cerastes snake venoms on human prostate cancer cells. J Cancer Prev. 2017; 22(1): 40-46.
13. Lv H, Liu Q, Zhou J, Tan G, Deng X, Ci X, et al. Daphnetin-mediated Nrf2 antioxidant signaling pathways ameliorate tert-butyl hydroperoxide (t-BHP)-induced mitochondrial dysfunction and cell death. Free Radic Biol Med. 2017; 106: 38-52.
14. Pandamooz S, Hadipour A, Akhavan-Niaki H, Pourghasem M, Abedian Z, Ardekani AM, et al. Short exposure to collagenase and coculture with mouse embryonic pancreas improve human dermal fibroblast culture. Biotechnol Appl Biochem. 2012; 59(3): 254-256.
15. Benzie IF, Strain JJ. The ferric reducing ability of plasma (FRAP) as a measure of "antioxidant power": the FRAP assay. Anal Biochem. 1996; 239(1): 70-76.
16. Khadir F, Pouramir M, Joorsaraee SG, Feizi F, Sorkhi H, Yousefi F. The effect of arbutin on lipid peroxidation and antioxidant capacity in the serum of cyclosporine-treated rats. Caspian J Intern Med. 2015; 6(4): 196-200.
17. Piantino CB, Reis ST, Viana NI, Silva IA, Morais DR, Antunes AA, et al. Prima-1 induces apoptosis in bladder cancer cell lines by activating p53. Clinics (Sao Paulo). 2013; 68(3): 297-303.
18. Meng X, Song F, Si H. Mechanisms of anti-prostate cancer by polyphenols compounds. Cancer Cell Research. 2018; 20: 489-495.
19. Cimino S, Russo GI, Reale G, Urzì D, Castelli T, Favilla V, et al. Pharmacological Role of dietary polyphenols in prostate cancer chemoprevention. In: Ullah M, Ahmad A, editors. Critical dietary factors in cancer chemoprevention. Springer; 2016; 239-251.
20. Hastak K, Gupta S, Ahmad N, Agarwal MK, Agarwal ML, Mukhtar H. Role of p53 and NF-kappaB in epigallocatechin-3-gallate-induced apoptosis of LNCaP cells. Oncogene. 2003; 22(31): 4851-4859.
21. Zhou L, Fu X, Jiang L, Wang L, Bai S, Jiao Y, et al. Arbutin increases Caenorhabditis elegans longevity and stress resistance. PeerJ. 2017; 5: e4170.
22. Fulda S. Inhibitor of apoptosis proteins in hematological malignancies. Leukemia. 2009; 23(3): 467-476.

23. TeSlaa T, Setoguchi K, Teitell MA. Mitochondria in human pluripotent stem cell apoptosis. Semin Cell Dev Biol. 2016; 52: 76-83.
24. Misir S, Aliyazicioglu Y, Demir S, Turan I, Yaman SO, Deger O. Antioxidant properties and protective effect of Turkish propolis on t-BHP-induced oxidative stress in foreskin fibroblast cells. Indian J Pharm Educ. 2018; 52(1): 94-100.
25. Chen KC, Chang HH, Ko WS, Wu CL, Chiu WT, Hsieh CL, et al. UV-induced damages eliminated by arbutin and ursolic acid in cell model of human dermal fibroblast WS-1 cells. Egypt Dermatol Online J. 2009; 5(1).
26. Fujimoto A, Sakanashi Y, Matsui H, Oyama T, Nishimura Y, Masuda T, et al. Cytometric analysis of cytotoxicity of polyphenols and related phenolics to rat thymocytes: potent cytotoxicity of resveratrol to normal cells. Basic Clin Pharmacol Toxicol. 2009; 104(6): 455-462.
27. Pasciu V, Posadino AM, Cossu A, Sanna B, Tadolini B, Gaspa L, et al. Akt downregulation by flavin oxidase-induced ROS generation mediates dose-dependent endothelial cell damage elicited by natural antioxidants. Toxicol Sci. 2010; 114(1): 101-112.
28. Seyfizadeh N, Mahjoub S, Zabihi E, Moghadamnia A, Pouramir M, Mir H, et al. Cytoprotective effects of arbutin against tert-butyl hydroperoxid induced toxicity in Hep-G2 cell line. World Appl Sci J. 2012; 19(2): 163-167.
29. Dadgar M, Pouramir M, Dastan Z, Ghasemi-Kasman M, Ashrafpour M, Moghadamnia AA, et al. Arbutin attenuates behavioral impairment and oxidative stress in an animal model of Parkinson's disease. Avicenna J Phytomed. 2018; 8(6): 533-542.
30. Ahmadian SR, Ghasemi-Kasman M, Pouramir M, Sadeghi F. Arbutin attenuates cognitive impairment and inflammatory response in pentylenetetrazol-induced kindling model of epilepsy. Neuropharmacology. 2018; 146: 117-127.
31. Zhao W, Wang S, Qin T, Wang W. Arbutin attenuates hydrogen peroxide-induced oxidative injury through regulation of microRNA-29a in retinal ganglion cells. Biomed Pharmacother. 2019; 112: 108729.
32. Lee HJ, Kim KW. Anti-inflammatory effects of arbutin in lipopolysaccharide-stimulated BV2 microglial cells. Inflamm Res. 2012; 61(8): 817-825.
33. Jurica K, Brčić Karačonji I, Mikolić A, Milojković-Opsenica D, Benković V, Kopjar N. In vitro safety assessment of the strawberry tree (Arbutus unedo L.) water leaf extract and arbutin in human peripheral blood lymphocytes. Cytotechnology. 2018; 70(4): 1261-1278.
34. Tada M, Kohno M, Niwano Y. Alleviation effect of arbutin on oxidative stress generated through tyrosinase reaction with L-tyrosine and L-DOPA. BMC Biochem. 2014; 15: 23.
35. Gnanapradeepan K, Basu S, Barnoud T, Budina-Kolomets A, Kung CP, Murphy ME. The p53 tumor suppressor in the control of metabolism and ferroptosis. Front Endocrinol (Lausanne). 2018; 9: 124.
36. Wu LH, Li P, Zhao QL, Piao JL, Jiao YF, Kadowaki M, et al. Arbutin, an intracellular hydroxyl radical scavenger, protects radiation-induced apoptosis in human lymphoma U937 cells. Apoptosis. 2014; 19(11): 1654-1663.
37. Eghbaliferiz S, Iranshahi M. Prooxidant activity of polyphenols, flavonoids, anthocyanins and carotenoids: updated review of mechanisms and catalyzing metals. Phytother Res. 2016; 30(9): 1379-1391.
38. Nawarak J, Huang-Liu R, Kao SH, Liao HH, Sinchaikul S, Chen ST, et al. Proteomics analysis of A375 human malignant melanoma cells in response to arbutin treatment. Biochim Biophys Acta. 2009; 1794(2): 159-167.
39. Li H, Jeong YM, Kim SY, Kim MK, Kim DS. Arbutin inhibits TCCSUP human bladder cancer cell proliferation via up-regulation of p21. Pharmazie. 2011; 66(4): 306-309.
40. Jiang L, Wang D, Zhang Y, Li J, Wu Z, Wang Z, et al. Investigation of the pro-apoptotic effects of arbutin and its acetylated derivative on murine melanoma cells. Int J Mol Med. 2018; 41(2): 1048-1054.

The Effect of Composol Medium on miR-16 Expression during Platelet Storage up to Day 7 at Room Temperature

Ali Rajabi, Ph.D., Zohreh Sharifi, Ph.D.*, Fatemeh Yari, Ph.D., Mohammadreza Deyhim, Ph.D., Mohammadali Jalili, Ph.D.

Blood Transfusion Research Center, High Institute for Research and Education in Transfusion Medicine, Tehran, Iran

Corresponding Address: P.O.Box 14665-1157, Blood Transfusion Research Center, High Institute for Research and Education in Transfusion Medicine, Tehran, Iran
Email: z.sharifi@ibto.ir

Received: 10/May/2019, Accepted: 3/August/2019

Abstract

Objective: MicroRNAs (miRNAs) are short, noncoding RNAs that play vital roles in gene regulation. It has been shown that storage has an effect on platelet miRNAs. MiR-16 is highly expressed in platelets and it appears to target the genes involved in cell death. It has been shown that platelets could be stored in Composol for a longer period of time. The aim of the present study was to assess and compare the expression pattern of miR-16 in platelet concentrates (PCs) in plasma and Composol media.

Materials and Methods: In an experimental study, ten PC bags were collected and each bag was divided into two separate bags, one with the 70% Composol and the other with only plasma. Both bags were stored for 7 days at 22˚C and tested on days 1, 3, 5, and 7 of storage. For each sample, we performed quantitative real-time polymerase chain reaction (qRT-PCR). The water-soluble tetrazolium salt-1 (WST-1) test was used to assess platelet viability in all of the samples. Statistical analysis was done by SPSS and REST software. A $P<0.05$ was considered statistically significant.

Results: miR-16 was significantly elevated during the storage days, with fold changes of 3.47 (plasma) and 2.77 (Composol). The Composol group had significantly decreased miR-16 expression compared with the plasma group. Results of the WST-1 test showed less decrease in optical density (OD) in the Composol group (0.93 ± 0.4) during the storage days compared with the plasma group (0.75 ± 0.3).

Conclusion: Our finding supported results from previous studies that reported an increase in miR-16 expression during platelet storage. In addition, miR-16 down-regulation in Composol medium implied that Composol might be a good solution for long-term platelet storage because it has the potential to elevate the shelf-life of platelets stored at 22˚C.

Keywords: Blood Platelets, MicroRNAs, miR-16, Platelet Storage

Cell Journal(Yakhteh), Vol 22, No 4, January-March (Winter) 2021, Pages: 542-547

Citation: Rajabi A, Sharifi Z, Yari F, Deyhim MR, Jalili MA. The effect of composol medium on miR-16 expression during platelet storage up to day 7 at room temperature. Cell J. 2021; 22(4): 542-547. doi: 10.22074/cellj.2021.6790.

Introduction

MicroRNAs (miRNAs) are short (20-24 nucleotides), single-strand, noncoding evolutionarily conserved RNAs that mediate post-transcriptional negative regulation of gene expression by recognizing and binding mRNA transcripts (1-3). They were first discovered in the nematode *Caenorhabditis elegans* in 1993 (4). MiRNAs appear to target several mRNAs (4, 5), an average of 307 distinct mRNAs for one particular miRNA (6). More than 60% of mammalian mRNAs are affected by miRNAs (7). They are considered to be negative regulators because they bind to mRNA targets and then silence their translation (8). To date, the number of discovered miRNAs is more than 2000 and they have been investigated more than all other non-coding RNAs (9, 10).

Platelets express high levels of various miRNAs that have been derived from their precursor cells, megakaryocytes (11, 12). There is a lack of knowledge about platelet miRNAs' behaviour under storage conditions (13). It has been shown that storage time has an effect on platelet miRNAs. Some miRNAs have different patterns of expression during storage (14, 15). miRNA-16 (miR-16) appears to have an increased level tendency during platelet storage (15, 16). It was first discovered through profile expression analysis of chronic lymphocytic leukaemia patients. miR-16 binds to and targets a nine base pair sequence in the 3'-UTR region of the anti-apoptotic gene *BCL-2*, which is a crucial gene in programmed cell death. miR-16 negatively regulates *BCL-2* at the posttranscriptional level (17). It is assumed that platelet cell death is mediated by miRNAs, and miR-16 is an apoptotic factor for accelerating cell death.

Platelet additive solutions (PASs) are useful solutions added to platelet concentrates (PCs) to make the cells more viable over longer periods of time. PASs prevent the PC recipients from increased plasma exposure and provide lower risk of transfusion reactions. In these cases, the plasma content of PCs is replaced by PASs. PCs could be stored more than five days under good storage situations that prevent bacterial contamination and with the use of additive solutions (18). There are many PASs that have been introduced, each of which has a different composition that emphasizes multiple aspects of platelet needs. The Composol solution (known as PAS-D) is a third generation PAS salt composed of sodium chloride, sodium gluconate, sodium acetate trihydrase, sodium

citrate dehydrate, potassium chloride, magnesium chloride hexahydrate, HCl, and water. The ingredients, especially magnesium, calcium, potassium and citrate have good effects on platelet membrane function, rate of glycolysis and platelet activation. According to multiple reports, Composol is a potent PAS for long-term PC storage. PCs stored in Composol medium have shown better function with less activated platelets (19-23).

No study has compared platelet miRNAs expression in different PAS media until now. The aim of this study was to investigate platelet miR-16 expression during PC storage periods and the effect of Composol on miR-16 expression.

Materials and Methods

Platelet concentrate collection and sample preparation

This experimental study was approved by the Research Ethics Committee of the High Institute for Research and Education in Transfusion Medicine under the code IR.TMI.REC.1395.010.

Ten single donor PC bags from healthy volunteers were prepared from whole blood bags by the platelet rich plasma method in the Iranian Blood Transfusion Organization. All platelet bags (Macopharma, France) were counted for platelet numbers by a Sysmex K-1000 Hematolgy Analyzer (Sysmex, Japan). Then, the content of each bag was divided equally into two separate bags using a transfer bag and a connective device, CompoDock instrument (Fresenius, Germany). The two bags were separated by a thermic tube sealer device (Fresenius, Germany) and both bags were centrifuged at 5000 g for 6 minutes at 22˚C in a blood bag centrifuge (model 830RS, Hetich, Germany). After removing 70% of the plasma from one of the bags by using a manual plasma extractor, we carefully added Composol solution (Composol-PS, E2083, Fresenius, Germany) and used this bag as the test (Composol) group. We followed aseptic techniques when adding the Composol to the PC bags. The other intact bag contained only plasma and was considered to be the control (plasma) group.

Both the plasma and Composol PC bags were stored with constant agitation on a PC shaker-incubator (Model 48PIAG-93-A, Fajr DP, Iran) at 20-24˚C for seven days. We simultaneously tested both PC groups on storage days 1, 3, 5, and 7. Day zero was the processing day or the day before the onset of testing. Platelet counts and volume of both the plasma and Composol samples were unified. We used the same volume and concentration of platelets for analyses on each of the test days. Less than 24 hours after sample processing, the tests were started with fresh platelets.

In order to detect bacterial contamination, all PC bags were sampled on the first (day 1) and last (day 7) storage day points and cultured on general blood agar and eosin methylene blue (EMB) agar media (Merck, Germany). For minimizing the effect of nucleated cells in molecular testing, both plasma- and Composol-PC tubes were centrifuged at 96 g for 4 minutes in a bench top centrifuge (Sigma, Germany) to reduce the white blood cell numbers.

MicroRNA extraction and analysis by real-time polymerase chain reaction

miRNA was extracted using a SanPrep column microRNA Mini-Prep kit (Bio Basic, Inc., Canada) according to the manufacturer's instructions. mRNA polyadenylation and cDNA synthesis were assessed with BONmiR qPCR kits (Stem Cell Technology, Iran).

Standard curves of miR-16 and U6 snRNA (*RNU6*) were plotted using serial dilutions of the cDNAs to evaluate the quantitative real-time polymerase chain reaction (qRT-PCR) efficiency. qRT-PCR with R2=0.998 and curve slope=3.358 was performed for all samples using a Rotor-Gene Q cycler (Qiagen, Germany) according to the manufacturer's guidelines under the following conditions: 95˚C for 2 minutes (one cycle), 95˚C for 5 seconds and 60˚C for 30 seconds (40 cycles). Melting curve analysis was done by heating from 50˚C to 95˚C at a rate of 0.1˚C/second. The PCR primer for the standard sequence of miR-16-5p according to the miRBase database (mirbase.org) was used as the specific forward primer (5′-GGCATAGCAGCACGTAAAT-3′) in conjunction with the *RNU6* gene forward primer (5′-AACGATACAGAGAAGATTAG-3′) as the internal control and reference housekeeping gene. A common reverse primer was also used for the reactions.

Results were taken as cycles of threshold (CTs) and relative gene expression was obtained using the standard comparative CT (ΔΔCT) method (24). All samples were run in triplicate and the mean CT values were used as the raw and primary results. For relative gene expression and fold change analysis, we used REST software (REST-2009©, rest.gene-quantification.info). *RNU6* CT results were used for gene expression normalization.

Platelet viability assay

The water-soluble tetrazolium salt-1 (WST-1) test was used to assess platelet viability in the two groups with the WST-1 cell proliferation assay kit (Cayman Chemical, Ann Arbor, MI, USA) and a 96-well microplate. All PC samples were centrifuged at 1800 g for 4 minutes and the platelets were re-suspended in phosphate-buffered saline. Platelet concentrations of 5×10^{11} cells/L in a 100 µL suspension were used with the addition of 10 µL of WST-1 reagent mix, followed by incubation for 4 hours in a CO_2 incubator at 37˚C. The absorbance of the reaction was read at 450 nm as the optical density (OD) in a microplate reader (ASYS Expert 96 UV Microplate Reader, UK). Results of the WST-1 analysis were presented as mean ± SD.

Statistical analysis

The data were analysed using IBM SPSS Statistics version 23 (IBM, USA). To compare the results of two

PC groups on corresponding days, we performed the paired t test. Analysis of variance (ANOVA) for repeated measures was done to assess the differences at various storage times. A $P<0.05$ was considered to indicate a statistically significant difference.

Results

Platelet count and microbial analysis

The untreated plasma group samples contained more than 1×10^{12} platelets/L on the first day of storage. The mean ± SD platelet counts on the first day were $1.15 \pm 0.10\times10^{12}$ platelets/L. Upper and lower limits were 1.35×10^{12} platelets/L and 1.03×10^{12} platelets/L, respectively. The Composol bags had slightly less platelet counts than their primary plasma bags because of the centrifugation process. The mean ± SD platelet counts in the Composol group on the first storage day were $0.99 \pm 0.08\times10^{12}$ platelets/L, and the upper and lower limits were 1.15×10^{12} platelets/L and 0.82×10^{12} platelets/L, respectively. However, the count was the same in both paired samples before the start of each testing day. Microbial analyses were conducted on the first and last days of storage before the start of qRT-PCR testing. The analysis of results showed no microbial contamination in any of the samples.

Quantitative real-time polymerase chain reaction results

The qRT-PCR results originally are expressed as raw CTs. All samples were run in triplicate and simultaneously with the control gene, *RNU6*. For reporting the results, we calculated the raw CTs into simple fold changes by REST software to show the amount of *miR-16* gene expression. We found that *miR-16* expression was elevated during the storage days in both the plasma and Composol groups compared with the *RNU6* internal control. Day to day comparison of both group samples against the first storage day (day 1) showed a clear increase in *miR-16* expression during storage. This increase was significant for days 3 and 5 in both groups, but not for day 7 when compared with day 1 (Table 1, Fig.1).

Table 1: Expression of miR-16 in the plasma and Composol groups

Storage days versus storage day 1	Plasma		Composol	
	Mean fold change	P value	Mean fold change	P value
3	2.58	0.027	2.70	0.029
5	4.87	0.037	3.13	0.048
7	2.95	0.124	2.48	0.115

Storage days 3, 5 and 7 were compared to the first storage day. P values were calculated by the t test for paired samples. A $P<0.05$ indicated a statistically significant difference.

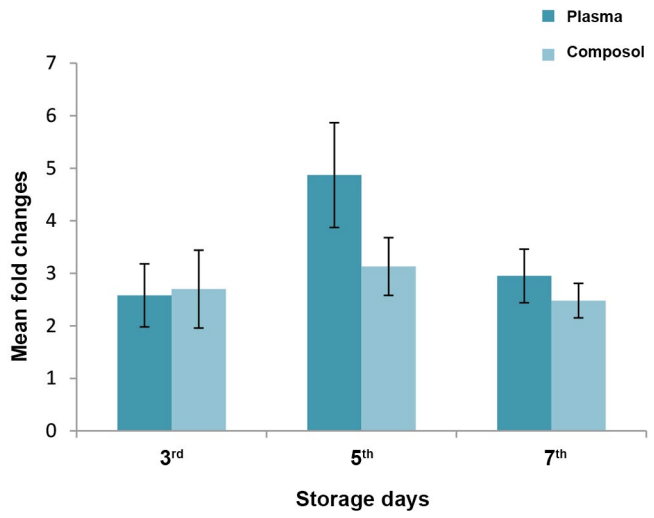

Fig.1: Mean fold changes of miR-16 during the storage days in both platelet concentrates (PCs) groups. Days 3, 5 and 7 were compared to day 1 of storage. Amounts were calculated by REST software, where the raw CT results were converted to fold changes. Fold changes imply the amount of changes in comparison to the baseline level of gene expression.

Fold change analysis

The average fold changes in miR-16 expression in all days in comparison with the first storage day were 3.5 in plasma and 2.8 in Composol group. The most statistically significant increase in miR-16 was seen on day 5 of storage in both PC groups. A fold change of 4.87 ($P=0.037$) was seen in the plasma group and a fold change of 3.13 ($P=0.048$) was observed in the Composol group (Table 1).

Despite the obvious increased expression of miR-16 in both PC groups for all storage days after the third day, miR-16 expression decreased in the Composol group compared with the plasma group (average fold change of 0.356). This expression decrease for all days was statistically significant, except for day 7 of storage (Table 2).

Table 2: Comparison of miR-16 expression in the Composol versus plasma platelet concentrate (PC) group

Storage days	Mean fold change	P value
1	0.382	0.049
3	0.399	0.015
5	0.277	0.045
7	0.365	0.102

P values were calculated by the t test for paired samples. $P<0.05$ was considered statistically significant.

Viability assessment

Results of the WST-1 test for platelet viability revealed that the ODs of WST-1 gradually fell during storage in both groups. This decrease was more obvious from day 3 of storage (Fig.2). We also showed that platelets were

more viable in the Composol samples in comparison with the control plasma samples. The plasma group had an average OD of 0.75 ± 0.3, whereas the Composol group had an average OD of 0.93 ± 0.4 (Table 3, Fig. 2).

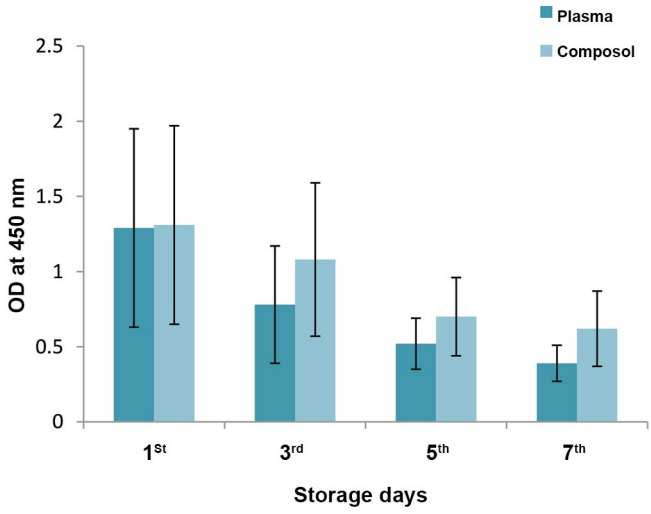

Fig2.: WST-1 assay test with one standard deviation (1SD) in different storage days as optical density (OD) of WST-1 samples at 450 nm. Corresponding days in both group samples were compared and P values were calculated by the t test for paired samples. P<0.05 was considered statistically significant.

Table 3: Results of WST-1 test for the Composol and plasma groups as mean ± SD of the optical density

Storage day	Optical density		P value
	Plasma	Composol	
1	1.29 ± 0.56	1.31 ± 0.66	0.493
3	0.780 ± 0.39	1.08 ± 0.51	0.034
5	0.521 ± 0.17	0.703 ± 0.26	0.049
7	0.394 ± 0.17	0.620 ± 0.25	0.067

Optical density were read at 450 nm. P values were calculated by the t test for paired samples. P<0.05 were considered significant. Comparisons were done between plasma (control) and Composol (test) groups for each of the corresponding storage days.

Discussion

Platelets play very important roles for normal blood haemostasis and effective coagulation function at times of injury. They preserve vascular integrity (25). PCs are used to control bleeding in patients with low platelet counts or impaired platelet functionality. Because of the low (3-5 days) shelf-life of platelets on storage conditions, they are valuable blood components that should be kept for destitute patients.

Platelets lack nucleus, but they have mRNA synthesis (26). miRNAs are involved in fine-tuning control of gene expression (27, 28). They suppress mRNAs by inhibiting translation (29). An attractive issue is that they can put on their regulation in the storage conditions (13). miRNAs have vital roles in essential cellular functions, including cell apoptosis (30, 31). Platelets have several miRNAs and, to date, many studies have researched miRNAs in platelets, each considered one or more aspects of the platelet characteristics, namely their roles in diseases, blood banks, etc.

In this study, we found that miR-16 expression in both the plasma and Composol groups increased during PC storage. The most obvious increase was found on day 5 of storage, with mean fold changes of 4.87 (plasma) and 3.13 (Composol). However, the average increased expression was less in the Composol group (2.8) compared to the plasma group (3.5). To date, no reports have compared miRNA expression in plasma and PAS medium. In 2015, Pontes et al. (14) analysed 16 PC bags in an attempt to characterize the expression profile of platelet miRNAs. They found a total of 1899 miRNAs over six selected storage days and listed the most highly expressed miRNAs in each storage day (until day 7). No information about miR-16 was mentioned in their report. Maués et al. (32) examined the expression profiles of miRNAs from 100 PCs stored for six days at room temperature. They found that nine miRNAs had down-regulated and five had up-regulated profiles. They did not conduct any experiment with miR-16. Kannan et al. (16) reported a change in different apoptosis-associated miRNA levels during storage as assessed by miRNA array. They observed that some of the miRNAs increased, including miR-16 and Let-7b, during storage. In 2014, Yu et al. (15) reported the expression patterns of some apoptosis-associated miRNAs in apheresis platelets. In their study, five miRNA were up-regulated, including miR-16, and five were down-regulated. We also reported the increased expression of miR-16 in all PC bags during the assessed storage days, which supported the results of the above reports.

miR-16 is a marker of apoptosis. It is best known for its role in haematological and non-haematological diseases such as leukaemia, diabetes and solid tumours (17, 33-37), because of the role of platelets in inflammation and other biological processes. The important role of miR-16 in platelet gene regulation has been proven. Therefore, a decreased level of miR-16 is associated with more viable platelets in the PC bags. For this reason, miR-16 is a good predictor of platelet viability in PC bags stored under normal storage conditions. More than 1000 targets have been identified for miR-16, including platelet lipoxygenase and CD151 antigen, which are specific for platelet apoptosis (16).

All unused PC bags in blood banks are discarded after five days of storage (14). This imposes a great expenditure on the country heath system and creates a shortage of PCs for needy patients. It is of great importance to seek a solution. Platelet quality is affected by certain factors, such as the method of preparation, storage media, storage container and donor characteristics (38). It is a good idea to use media for storage of platelets that can increase the shelf-life of cells with better cellular metabolism. Many studies have compared different

PASs and their benefits (18-23, 38). In the current study, we chose the Composol PS solution as an adequate PAS for long-term platelet storage. Advantages of Composol as PAS against plasma include better functional and biochemical parameters, particularly glucose consumption, which improves cellular metabolism and more platelet viability and increased life span. In addition, the use of PASs can saves more plasma for use in other situations, less plasma exposure of PC recipients, and decreased adverse reactions to transfusions (18).

To date, no previous study reported the expression pattern of platelet miRNAs in PCs stored in PAS. The present study was the first that compared the expression of a platelet miRNA (miR-16) in Composol and plasma media. For the comparison between the two PC groups, we replaced the plasma with Composol under sterile conditions. When using PAS, the usual mixture composition is 20-50% plasma and 50-80% PAS (38). In our study, the final mixture in the Composol samples was 30% plasma and 70% Composol solution.

Furthermore, to ensure that adequate platelets existed before the beginning of the miRNA extraction, an original bag with less than 1×10^{12} platelets/L on the preparation day (day zero) was rejected. In addition, centrifugation of PC samples at 96 g for 4 minutes effectively reduced the number of white blood cells and other non-platelet components, and had a minimal effect on reducing platelet counts. We sampled both PC groups simultaneously on days 1, 3, 5 and 7 of storage.

Results of the expression pattern of miR-16 in qRT-PCR cyclers gave raw CT results for each test reaction. However, raw CT results are not reliable and are not good parameters to show the changes in gene expression. We used REST software to analyse the primary results as fold changes according to the comparative CT method. This method is a relative quantification of gene expression in which the amount of target gene is calculated by relative expression of a reference housekeeping gene and is equal to $2^{-\Delta\Delta CT}$. The ΔCT implies the difference between CTs of the target and reference genes, and ΔΔCT is the difference in two ΔCTs such as between the test and calibrator or treated and untreated samples (24). In our study, the ΔΔCT was the difference between the ΔCTs of the Composol (test) group and plasma (control) group samples. *RNU6* was used as the endogenous reference and internal control gene for miR-16 expression normalization for all storage time points. So, the given fold change meant the fold increase or decrease in the expression of the target gene compared to our reference gene. Results of real-time analysis showed an obvious increase in miR-16 expression during storage in both group samples. However, this increase was slower in the Composol group. Furthermore, miR-16 expression was clearly down-regulated in the Composol group for all of the assessed storage days, in comparison to plasma group in corresponding days. Hence, miR-16 is a factor of apoptosis. This finding is of great importance and confirms the results of other studies where PASs, including Composol PS, had positive effects on platelet metabolism and increasing the shelf-life of platelets in storage. However, the previous studies did not compare miRNA expression patterns in plasma and PASs media.

The WST-1 test was used for analysis of platelet viability during PC storage. Viable platelets produce NADH that causes a reduction of cell-impermeable and colourless tetrazolium salt to purple and soluble formazan dye at the cell surface. The greater amount of formazan dye formation indicates a greater number of active and living platelets (39). Our results of WST-1 test support the above mentioned finding about miR-16. The platelets showed more viability in Composol medium than in plasma. This means that the Composol group PCs had more viable platelets than control plasma PCs. Hence, this supports the finding that Composol can be a useful medium for long-term platelet storage.

Conclusion

The present study aimed to determine the effect of a PAS, Composol, on miR-16 expression during platelet storage. miR-16 had an increased expression pattern in all PCs in the control (plasma) and test (Composol) groups during storage. Furthermore, we showed that miR-16 expression decreased effectively in PCs stored in the Composol medium. We concluded that Composol might be a good choice as a PAS for long-term storage of platelets because it has the potential to elevate the shelf-life of platelets stored at 22˚C. Additional, in-depth with more samples integrated are needed to clearly confirm the above results. Analyses of other platelet miRNAs during PC storage would also be important.

Acknowledgements

This study financially supported by the Blood Transfusion Research Center, High Institute for Research and Education in Transfusion Medicine. There is no conflict of interest in this study.

Authors' Contributions

A.R.; Performed the experiments, obtained, analysed and interpreted the results, and conceived, designed and wrote the draft of the manuscript, and final text. Z.Sh.; Conceived and designed the experiments, obtained the funding, revised the manuscript for critically important intellectual content, and approved the manuscript and statistical analysis. F.Y.; Advised the experiments, did the technical support, revised, and approved the manuscript, and statistical analysis. M.R.D., M.A.J.; Advised the experiments and did the technical support. All authors read and approved the final manuscript.

References

1. Haberberger A, Kirchner B, Riedmaier I, Henschler R, Wichmann C, Buhmann R, et al. Changes in the microRNA expression pro-

file during blood storage. BMJ Open Sport Exerc Med. 2018; 4(1): e000354.
2. Liu B, Shyr Y, Cai J, Liu Q. Interplay between miRNAs and host genes and their role in cancer. Brief Funct Genomics. 2018; 18(4): 255-266.
3. Wojciechowska A, Braniewska A, Kozar-Kamińska K. MicroRNA in cardiovascular biology and disease. Adv Clin Exp Med. 2017; 26(5): 865-874.
4. Saliminejad K, Khorram Khorshid HR, Soleymani Fard S, Ghaffari SH. An overview of microRNAs: biology, functions, therapeutics, and analysis methods. J Cell Physiol. 2019; 234(5): 5451-5465.
5. O'Brien J, Hayder H, Zayed Y, Peng C. Overview of microRNA biogenesis, mechanisms of actions, and circulation. Front Endocrinol (Lausanne). 2018; 9: 402.
6. Edelstein LC, Bray PF. MicroRNAs in platelet production and activation. Blood. 2011; 117(20): 5289-5296.
7. Friedman RC, Farh KK, Burge CB, Bartel DP. Most mammalian mRNAs are conserved targets of microRNAs. Genome Res. 2009; 19(1): 92-105.
8. Jonas S, Izaurralde E. Towards a molecular understanding of microRNA-mediated gene silencing. Nat Rev Genet. 2015; 16(7): 421-433.
9. Hammond SM. An overview of microRNAs. Adv Drug Deliv Rev. 2015; 87: 3-14.
10. Sontheimer EJ, Carthew RW. Silence from within: endogenous siRNAs and miRNAs. Cell. 2005; 122(1): 9-12.
11. Sunderland N, Skroblin P, Barwari T, Huntley RP, Lu R, Joshi A, et al. MicroRNA biomarkers and platelet reactivity: the clot thickens. Circ Res. 2017; 120(2): 418-435.
12. Provost P. The clinical significance of platelet microparticle-associated microRNAs. Clin Chem Lab Med. 2017; 55(5): 657-666.
13. Yan Y, Zhang J, Zhang Q, Chen Y, Zhu X, Xia R. The role of microRNAs in platelet biology during storage. Transfus Apher Sci. 2016; 56(2): 147-150.
14. Pontes TB, Moreira-Nunes Cde F, Maués JH, Lamarão LM, de Lemos JA, Montenegro RC, et al. The miRNA profile of platelets stored in a blood bank and its relation to cellular damage from storage. PLoS One. 2015; 10(6): e0129399.
15. Yu S, Deng G, Qian D, Xie Z, Sun H, Huang D, et al. Detection of apoptosis-associated microRNA in human apheresis platelets during storage by quantitative real-time polymerase chain reaction analysis. Blood Transfus. 2014; 12: 541-547.
16. Kannan M, Mohan KV, Kulkarni S, Atreya C. Membrane array-based differential profiling of platelets during storage for 52 miRNAs associated with apoptosis. Transfusion. 2009; 49(7): 1443-1450.
17. Cimmino A, Calin GA, Fabbri M, Iorio MV, Ferracin M, Shimizu M, et al. miR-15 and miR-16 induce apoptosis by targeting BCL2. Proc Natl Acad Sci USA. 2005; 102(39): 13944-13949.
18. van der Meer PF, Pietersz RN, Reesink HW. Storage of platelets in additive solution for up to 12 days with maintenance of good in-vitro quality. Transfusion. 2004; 44(8): 1204-1211.
19. Leitner GC, List J, Horvath M, Eichelberger B, Panzer S, Jilma-Stohlawetz P. Additive solutions differentially affect metabolic and functional parameters of platelet concentrates. Vox Sang. 2016; 110(1): 20-26.
20. Mokhtar MB, Hashim HB, Joshi SR. Assessment of quality of platelets preserved in plasma and platelet additive solution: A Malaysian experience. Asian J Transfus Sci. 2016; 10(1): 84-87.
21. Gulliksson H, AuBuchon JP, Cardigan R, van der Meer PF, Murphy S, Prowse C, et al. Storage of platelets in additive solutions: a multicentre study of the in vitro effects of potassium and magnesium. Vox Sang. 2003; 85(3): 199-205.
22. Cardigan R, Sutherland J, Garwood M, Bashir S, Turner C, Smith K, et al. In vitro function of buffy coat-derived platelet concentrates stored for 9 days in Composol, PASII or 100% plasma in three different storage bags. Vox Sang. 2008; 94(2): 103-112.
23. Tynngård N, Trinks M, Berlin G. In vitro quality of platelets during prolonged storage after washing with three platelet additive solutions. Vox Sang. 2012; 102(1): 32-39.
24. Livak KJ, Schmittgen TD. Analysis of relative gene expression data using real-time quantitative PCR and the 2(-Delta Delta C(T)) method. Methods. 2001; 25(4): 402-408.
25. Deppermann C. Platelets and vascular integrity. Platelets. 2018; 29(6): 549-555.
26. Best MG, Vancura A, Wurdinger T. Platelet RNA as a circulating biomarker trove for cancer diagnostics. J Thromb Haemost. 2017; 15(7): 1295-1306.
27. Sevignani C, Calin GA, Siracusa LD, Croce CM. Mammalian microRNAs: a small world for fine-tuning gene expression. Mamm Genome.2006; 17(3): 189-202.
28. Abbas Q, Raza SM, Biyabani AA, Jaffar MA. A review of computational methods for finding non-coding RNA genes. Genes (Basel). 2016; 7(12). pii: E113.
29. Chen S, Gao G. MicroRNAs recruit eIF4E2 to repress translation of target mRNAs. Protein Cell. 2017; 8(10): 750-761.
30. Harden JT, Krams SM. Micro-RNAs in transplant tolerance. Curr Opin Organ Transplant. 2018; 23(1): 66-72.
31. Voglova K, Bezakova J, Herichova I. Micro RNAs: an arguable appraisal in medicine. Endocr Regul. 2016; 50(2): 106-124.
32. Maués JHDS, Moreira-Nunes CFA, Pontes TB, Vieira PCM, Montenegro RC, Lamarão LM, et al. Differential expression profile of microRNAs during prolonged storage of platelet concentrates as a quality measurement tool in blood banks. OMICS. 2018; 22(10): 653-664.
33. Wang F, Yang L, Sun J, Zheng J, Shi L, Zhang G, et al. Tumor suppressors microRNA-302d and microRNA-16 inhibit human glioblastoma multiforme by targeting NF-κB and FGF2. Mol Biosyst. 2017; 13(7): 1345-1354.
34. Fu X, He Y, Wang X, Peng D, Chen X, Li X, et al. MicroRNA-16 promotes ovarian granulosa cell proliferation and suppresses apoptosis through targeting PDCD4 in polycystic ovarian syndrome. Cell Physiol Biochem. 2018; 48(2): 670-682.
35. Tian C, Li Z, Yang Z, Huang Q, Liu J, Hong B. Plasma MicroRNA-16 is a biomarker for diagnosis, stratification, and prognosis of hyperacute cerebral infarction. PLoS One. 2016; 11(11): e0166688.
36. Guo X, Connick MC, Vanderhoof J, Ishak MA, Hartley RS. MicroRNA-16 modulates HuR regulation of cyclin E1 in breast cancer cells. Int J Mol Sci. 2015; 16(4): 7112-7132.
37. Talari M, Kapadia B, Kain V, Seshadri S, Prajapati B, Rajput P, et al. MicroRNA-16 modulates macrophage polarization leading to improved insulin sensitivity in myoblasts. Biochimie. 2015; 119: 16-26.
38. Gulliksson H. Platelet storage media. Vox Sang. 2014; 107(3): 205-212.
39. Berridge MV, Herst PM, Tan AS. Tetrazolium dyes as tools in cell biology: new insights into their cellular reduction. Biotechnol Annu Rev. 2005; 11: 127-152.

Compression of The Sciatic Nerve May not Contribute to Ipsilateral Hyperalgesia Development in Ovariectomized Female Rats!

Nafissa Telailia, M.Sc.[1]*, Sylvain Fisson, Ph.D.[2, 3, 4], Hacène Frih, Ph.D.[1]

1. Department of Biology, Faculty of Natural Science, University of Badji Mokhtar, Annaba, Algeria
2. National Institute of Health and Medical Research, Joint Research Unit_S951, Evry, France
3. Genethon, National Institute of Health and Medical Research, Joint Research Unit_S951, Evry, France
4. Joint Research Unit_S951, University of Evry Val d'Essonne, Evry, France

Corresponding Address: Department of Biology, Faculty of Natural Science, University of Badji Mokhtar, Annaba, Algeria
Email: naffissa388@gmail.com

Received: 27/April/2019, Accepted: 6 /August/2019

Abstract

Objective: von Frey Filament (vFF) is an aesthesiometer to measure paw withdrawal thresholds. Our aim was to validate the manually von Frey test technique for assessing neuropathic pain behavioral signs in a sciatic nerve ligation model.

Materials and Methods: In this experimental study, peripheral neuropathic pain associated with sciatic nerve chronic ligation (SN-CL) was induced. Filaments used against posterior pad mid-plantar region using a simplified up-down method (SUDO). In addition to baseline withdrawal thresholds, the behavioral test was repeated after surgery thrice more with an interval of ten days. vFF (2 to 26 g) were used in ascending order for hyperalgesia assessment.

Results: In SN-CL rats, the results validate a loss of pain sensation, resulted in, long-lasting ipsilateral allodynia with the development of contralateral allodynia later and an extraterritorial development of neuropathic signs. Variability for the development of ipsilateral and contralateral allodynia over time was noted in sham (SH) control rats. SN-CL group showed a contralateral hyperalgesia development just at the 16th-day after surgery with an absence of ipsilateral hyperalgesia development at the different days of paw withdrawal thresholds measurements.

Conclusion: Manually vFF test technique was successfully used for assessing neuropathic pain behavioral signs in sciatic a nerve ligation model with the absence of ipsilateral hyperalgesia development.

Keywords: Filaments, Injury, Mechanical Allodynia, Mechanical Hyperalgesia Neuropathic Pain

Cell Journal(Yakhteh), Vol 22, No 4, January-March (Winter) 2021, Pages: 548-555

Citation: **Telailia N, Fisson S, Frih H. Compression of the sciatic nerve may not contribute to ipsilateral hyperalgesia development in ovariectomized female rats! Cell J. 2021; 22(4): 548-555. doi: 10.22074/cellj.2021.6907.**

Introduction

Neurological disorders may lead, directly or indirectly, to pain with physiological and physical dimensions that are both essential for its diagnosis and treatment. Daily, pain sensation specifically is evoked by potential or actual noxious (i.e., tissue-damaging) stimuli applied to the body that differs from pain during disease that occurs in the absence of external noxious stimuli (1). “Pain is a mutually recognizable somatic experience that reflects a person’s apprehension of threat to their bodily or existential integrity” (2). This definition was qualified by the Taxonomy Task Force of the association in 1994 (3) "Pain is always subjective. Each individual learns the applications of the word through experiences relating to injuries in early life" (4).

There are three types of pain: acute physiological nociceptive pain, pathophysiological nociceptive pain, also called hyperalgesia and/or allodynia. Hyperalgesia is an extreme pain intensity felt upon noxious stimulation, and allodynia is the sensation of pain elicited by stimuli that are normally below the pain threshold. The sensory system itself can be damaged and become the source of continuous pain. This type of pain is classified as neuropathic. Chronic neuropathic pain has no physical protective role as it continues without obvious ongoing tissue damage. In contrast to nociceptive pain, which is the result of stimulation of primary sensory nerves for pain, neuropathic pain occurs when a lesion or disruption of function occurs in the nervous system. If the cause is located in the central nervous system (CNS) (brain or spinal cord) it gives rise to central neuropathic pain, and if it is located in the peripheral nervous system, it gives rise to peripheral neuropathic pain. Neuropathic pain may be induced by physical injuries of the nervous system, such as surgery (5). Murine models of peripheral nerve injury often target the sciatic nerve which is easy to access, produces behavioral signs of neuropathic pain, including mechanical allodynia (pain perception upon the innocuous tactile stimuli) and hyperalgesia (exaggerated pain sensations by mildly noxious stimuli). Sciatic nerve chronic ligation (SN-CL) allows nociceptive tests on the hind paws that end by studying of neuropathic pain mechanism, pain sensory and for the study of neuropathic pain, treatments using von Frey filaments (vFFs) test. For this aim, sciatic nerve ligation was a target which induces long-lasting mechanical allodynia (6, 7). This last was measured by using vFFs, a highly sensitive test in detecting allodynia in conditions likely to cause

neuropathic pain, and as soon as allodynia is established in the animal, it is easily quantified (8) Von Frey test is a pressure test to detect the perception of light touch. It involves the use of a thin and flexible filament applied to the skin with just enough force to induce a bend in the filament (9). For best comparisons, prior sciatic nerve ligation, we established baselines thresholds values that represent the normal and the beginning thresholds level of nociceptive measurements.

Mechanical allodynia was assessed with the Von Frey test, von Frey monofilaments were utilized for the estimation of paw withdrawal threshold in both hind paws as a measure of mechanical allodynia in our peripheral neuropathic pain model. Hind paw withdrawal thresholds were determined as a measure of ipsilateral and contralateral mechanosensitivity for chronic sciatic nerve ligation (SN-CL) and sham (SH) female rats by the Simplified Up-and-Down Order (SUDO) method, which is more recently developed.

Studying behavioral signs of neuropathic pain in sciatic nerve ligation model compared with SH rats (animal underwent the same surgical procedures without seeing the sciatic nerve ligation) using vFF test technique manually at different days post-surgery was the aim of this study.

Materials and methods

Biological material

In this experimental study, female rats White Wistar Rats from the Pasteur Institute of Algiers were used in our study as the biological material for the reason that female are more sensitive to pain than males because of ovarian hormones (10). Under the environmental conditions of the experiment room (natural photoperiod, humidity, temperature, etc.), the animals were kept in polyethylene cages (8 female rats per cage), given 20 g of food per female rat daily with ad libitum access to water.

After an adaptation period of four weeks, 16 females aged 3 months approximately were randomly selected, they were with an average weight of 214.4 ± 6.389 g and divided into two experimental groups (eight females per group): the rates of the first group were underwent ligation of sciatic nerve in the left hind paws, the second group consists of SH rats (the animal underwent the same surgical procedures without seeing the sciatic nerve ligation in that paws). Contralateral hind paws were always intact in the two groups. Rats weighted one day prior to each test and five days after surgery to determine antibiotic doses.

All applicable international, national, and/or institutional guidelines for the care and use of animals were followed (D01N01UN230120150001).

Surgery procedure for sciatic nerve ligation

Anesthesia

Rats were anesthetized by intraperitoneal injection of ketamine hydrochloride (5 mg⁄Kg i.p., ketamine)+a drop orally of chlorpromazine, and an ophthalmic ointment was applied to the eyes of animals using a cotton swab to avoid increased intra-ocular pressure (11) caused by ketamine. The animals were placed in a calm and quiet place until fully anesthetized. The reflex of rats was checked by pinching the tip of the tail and legs with a pair of tweezers to ensure the immobility of animals before any surgery.

Surgery

According to (12) chronic constriction injury model, surgical area (using an electric razor) was shaved. The animal was placed on its right side, and the left hind limb was put on a small platform in order to keep it high. The leg was fixed with tape. The operative field was disinfected with alternating scrubs of ethanol and betadine outside the surgical site. The knee was located with the thumb of the left hand, and a scalpel was used to make an incision of few centimeters (cm) in the proximal longitudinal direction of the knee. Then, the skin was opened by blunt dissection using the tip of a pair of sterilized scissors. The muscular layer was separated by dissection just next to the visible blood vessel, and we closed the femur (thigh bone). The muscle layers were easily separated without bleeding and then left sciatic nerve below the muscle was revealed. The rat was placed under a stereomicroscope to gently separate the muscles with a pair of tweezers sterilized to visualize the sciatic nerve. The area and the collateral saphenous branches of the sciatic nerve were identified, knowing that the sural nerve is the smallest of the three branches and three tight surgical knots were created around the sciatic nerve. When the first node was done, a contraction of paw's muscle groups supplied by the sciatic nerve that underwent ligation was observed. After that, the suture ends were cut with a pair of micro-scissors and the muscle layer were gently closed. Finally, a drop of lidocaine was added on the wound, and we sutured with surgical knots. The SH control animals were anesthetized, skin and muscles were cut to expose the nerve similar to the ligated animals (except for the ligation). The skin was sutured back to close the opened tissue. For the two groups, contralateral hind paws were intact. SN-CL and sham-operated animals were allowed to recover for five days before testing in their ipsilateral and contralateral hind paws.

Post-surgery period

The sufficiency of eye ointment was checked. Then, the rat was placed in a clean cage under a paper towel in a comfortable posture near to a heat source. Water and food were easily accessible for the animal operated. Finally, intraperitoneal injection of 75000 IU⁄Kg⁄day of benzylpenicillin sodium (Algeria, Saidal, PEN G

Panpharma) for five days after surgery was done.

Nociceptive behavioral test: Von Frey filaments test

Sensory evaluators (Semmes-Weinstein Monofilaments)

In our study, standard esthesiometers set which contains 20 nylon monofilaments have been used to assess mechanical sensitivity. vFFs that are soft nylon hairs of different lengths and calibrated diameters to known forces, providing discrete units of pressure and fixed on hand-held applicators (13) were used to estimate hind paw withdrawal thresholds for SN-CL and SH female rats. The enabling principle of the Von Frey hair methodology for assessing skin sensitivity to crude touch is that a hair (or a plastic monofilament) will exert increasing pressure on the skin as it is pressed harder and harder (14) before the filament starts to bend. However, after bending, the vertical force was constant. The force was directly proportional to the stiffness, directly related to the thickness of the filament and inversely proportional to its squared length (15, 16). Prior to the second and the third tests, two (2) minutes were sufficient for bending filaments to be automatically calibrated and to be straight.

The behavioral assessment was conducted by the same person, time, location, and it was performed in all animals before surgery (day 0), on days 6, 16 and 26 after SN-CL surgery or SH operation for the long assessment of neuropathic pain behavioral signs. The day of surgery was referred to as day1. The testing chamber consisted of an (85×35×35) cm transparent plastic box with wire mesh platform (0.5×0.5 cm grid size) allowing access to the plantar surface of the hind paws, and it was positioned over a support to keep it elevated and to visualize the testing area (the mid-plantar surface just posterior to the footpads: This area is innervated mostly by terminal branches of the sciatic nerve). Each rat was placed in the testing chamber and allowed to acclimate for 15 minutes prior to testing or as soon as the rat stopped exploring and appeared acclimatized to the testing environment and the Von Frey hairs were inserted through the mesh to poke the animal's mid-plantar surface of hind paws, notice that the rat was tested when it was standing quietly on all four paws and was unaware of the experimenter's hand.

Assessment of temporal evolution of tactile paws withdrawal thresholds in sciatic nerve chronic ligation and sham rats

The values of tactical paw withdrawal thresholds in SN-CL and SH rats was performed at basal (day 0), at the 6^{th}, 16^{th}, and 26^{th} days after surgeries in ipsilateral and contralateral hind paws for both SN-CL and SH control rats.

Measurement of mechanical hind paws withdrawal threshold by the SUDO method

The hind paw withdrawal threshold was determined using vFFs and was expressed in Millinewton (mN) by the SUDO method which requires an empirically determined filament force range and starts at the mid-range filament for five consecutive touches (17). In the current study, to assess rat hind paw mechanical allodynia thresholds for SN-CL and sham-operated rats**,** we started with the mid-range filament (2.0 g). The filament was applied at a 90º angle for 2 seconds to the mid-plantar surface just posterior to the footpads of the left hind paw until it was just bent and then withdrawn, the procedure was repeated five consecutive times with an interval of 2 seconds between each stimulation. The response was considered positive if at least three expected responses were observed out of five applications. The expected responses were: Paw withdrawal, sudden flinching, and licking/biting of the stimulated paw. The response was recorded as an "X" for a positive response or an "O" if a negative response was observed.

If a positive response was reached on the first examined filament, then the next lowest filament was chosen. If no response was noted, then the next higher filament was used. This process was repeated until the first transition from the positive response to negative one –or vice versa– was obtained, after which force, was applied to the animal an additional four times following the up and down paradigm. If the last filament caused a response, a set value (0.5) was added to the filament force, whereas if no response was noted, the same value was subtracted from that filament force and was designated as SUDO result.

The force was determined from the newly designated SUDO result:

$$\text{Filament force (mN)} = 0.0016 \times \exp\left[(2.184 - (0.012\,(\text{SUDO result})^2 + 0.429\,(\text{SUDO result}) + 1.359)\right].$$

Once the threshold was determined for the left hind paw, the same testing procedure was repeated on the right hind paw. The baseline withdrawal thresholds of each of the hind paws using von Frey hairs were determined for each rat prior to surgical manipulation (day 0). To assess the long-lasting mechanical allodynia, i.e., a nociceptive response to a normally non-nociceptive stimulus, measurement of the paw withdrawal threshold was repeated next on days 6, 16 and then on day 26 after SN-CL surgery or SH operation. The day of surgery was referred to as day 1.

Mechanical hyperalgesia assessment

For hyperalgesia assessment: 2, 4, 6, 8, 10, 15, and 26 g of vFFs were used until a filament induced a positive response (18). If no filament elicited a

response, then the highest magnitude filament (26 g) was recorded as the threshold.

Data analysis

Graphs were plotted using Graphpad Prism version 7. Statistical analyses were conducted with Past3. The mean hind paw withdrawal thresholds were analyzed using one-way ANOVA (Kruskal Wallis for more than 2 times, in one group between different times and Mann Whitney for 2 times. Student's t test, Fisher's exact test, D-test, and Chi ²-tests were used for comparisons between or within groups of rats following one way ANOVA. The mean (± standard error of the mean) hind paw withdrawal thresholds values between different groups of rats or within the same group at different time points were considered significantly different with a $P<0.05$. For mechanical hyperalgesia assessment, graphs were plotted**,** and statistical analyses were conducted with the Graph-Pad Prism software version 6.

Results

Assessment of temporal evolution of tactile paws withdrawal thresholds in sciatic nerve chronic ligation and sham rats

The values of ipsilateral paw withdrawal thresholds of SN-CL rats are almost identical as illustrated in SH animals from day 6 until day 16 post-surgery (Fig.1). After sixteen -days, the paw withdrawal response in SN-CL remains reduced until twenty -six days when compared with the SH group. For contralateral paw withdrawal thresholds, in SH rats are maintained reduced when compared with SN-CL ones from the 6th to 26th day post-surgery (Fig.1, Table 1).

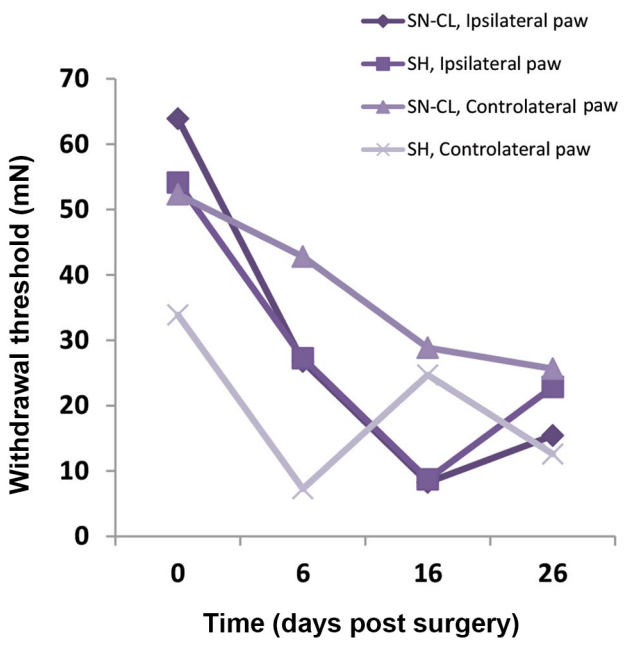

Fig.1: Temporal evolution of ipsilateral and contralateral mechanical paw withdrawal thresholds in sciatic nerve chronic ligation and sham groups (n=8).

Table 1: Sham animals time course of hind paws withdrawal thresholds mean in basal (day 0), at 6th, 16th, and 26th days after surgery

Time (days)	Ipsilateral hind paws withdrawal thresholds mean (mN)	Contralateral hind paws withdrawal thresholds mean (mN)
0	54.13 ± 15.6	33.87 ± 12.64
6	20.45 ± 14.28	19.99 ± 14.25
16	6.548 ± 4.385	21.6 ±14.16
26	22.87 ± 13.84	12.59 ± 4.976

Data are presented as mean ± SE.

Sciatic nerve chronic ligation rats time course of hind paws withdrawal thresholds mean in basal (day 0), at 6th, 16th and 26th days after surgery

In SN-CL rats, the ipsilateral mean paw withdrawal thresholds were reduced in the injured (ipsilateral) hind paw compared to the uninjured (contralateral) hind paw from few days after surgery to the last day of mechanical allodynia's assessment, they were 20.06 ± 14.24, 7.22 ± 4.429, 13.50 ± 4.91 and 37.44 ± 17.65, 25.24 ± 3.985 and 19.22 ± 12.03 mN at the 6th, 16th, and 26th days after surgery, respectively in the ipsilateral paw. In contrast, the mean paw withdrawal thresholds the contralateral one were 7.22 ± 4.429, 37.44 ± 17.65, 19.22 ± 12.03 mM.

Data showed that ipsilateral paw withdrawal thresholds of nociceptive sensitivity were gradually lowered from six until the 16th -day post-surgery, they were varied from 63.91 ± 17 on day 0 to 13.50 ± 4.91 mN in the 16th-day post-surgery. In contrast, the mean withdrawal thresholds were gradually increased to 25.24 ± 3.985 on day 26 after surgery. This variability over time reached the significance from day 6 compared with the pre-operation (day 0) until day 26 (D-test P=0.0097 at 06 day, t test P=0.006 at 16 day, F-test P=0.004 at 26 day).

For contralateral nociceptive sensitivity, the mean paw withdrawal thresholds were reduced over time, they were varied from 52.32 ± 17.66 on day 0 to 19.22 ± 12.03 mN on the 26st day post-surgery. This decrease reached the significance from the 16th day compared with the preoperative (day 0) until the 26th day (t-test P=0.56 at 06 day, F-test P=0.00084 at 16th day, chi ²-test P=0.045 at the 26th day) (Fig.2A).

The analysis of tactile withdrawal threshold using one-way ANOVA, lead to a loss of a significant difference on day 0 (t test P=0.643) and at the 6th after surgery (t test, P=0.45). In contrast, a statistically significant effect of surgery (sciatic nerve ligation) was revealed at the 16th -and 26th days after surgery using Student's t test (P=0.009) and Fisher's exact test (F=6.0081, P=0.03) respectively (Fig.2B).

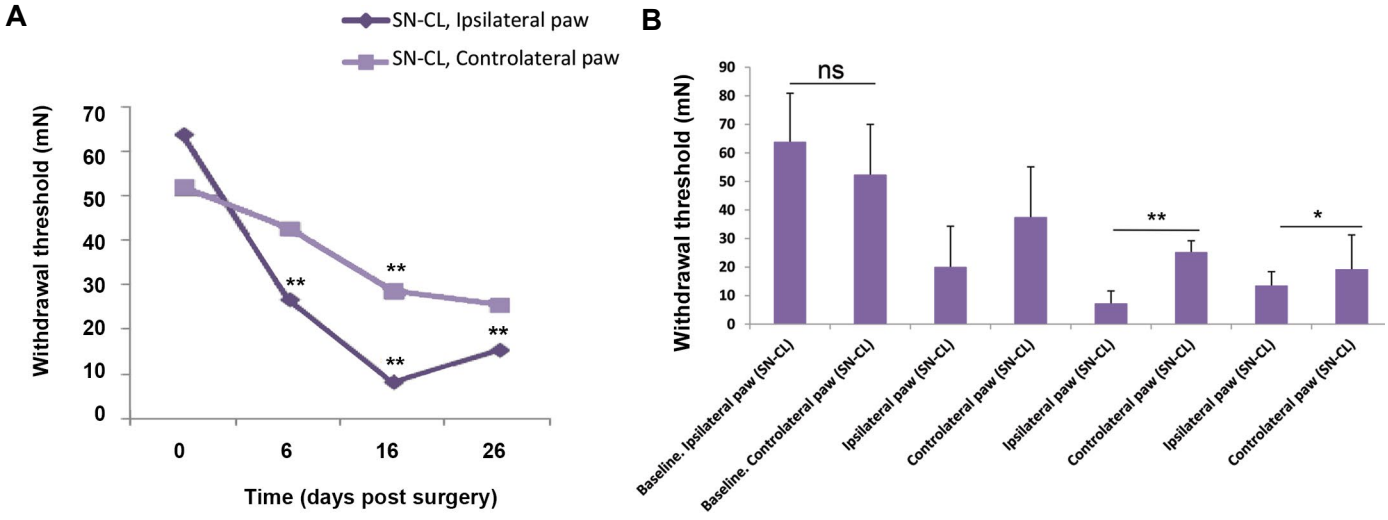

Fig.2: Repeated measurement of- ipsilateral and contralateral mechanical paw withdrawal threshold at 6th, 16th, and 26th days post- surgery in sciatic nerve chronic ligation rats (n=8). Asterisks indicate the significant difference in paw withdrawal threshold. ns; Non significant, *; P<0.05 , and **; P<0.005.

Assessment of mechanical ipsilateral allodynia in sciatic nerve chronic ligation group in six, sixteen, and twenty-six-day post-surgery

At six and sixteen days post-surgery, ipsilateral tactile withdrawal threshold in SN-CL was not significantly different from the SH group (t test, P=0.9). While, at the 26th day after surgery, the mechanical sensitivity was decreased significantly when analyzed by the Fisher's exact test (F=7.94, P=0.01, Fig.3).

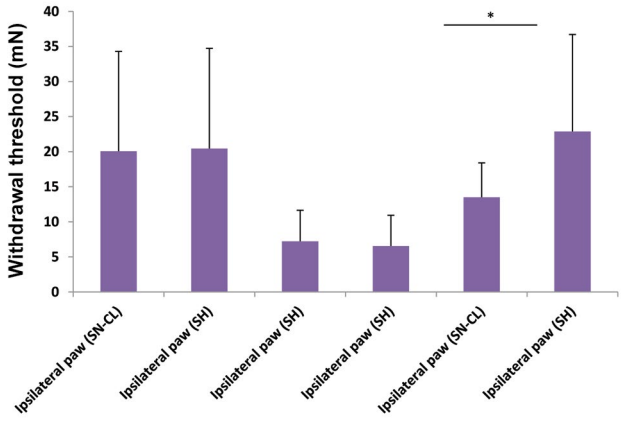

Fig.3: Comparing tactile ipsilateral paw withdrawal threshold of sciatic nerve chronic ligation (SN-CL) rats with sham (SH) group (n=8). Asterisks indicate the significant difference in paw withdrawal threshold. *P<0.05.

Mechanical contralateral allodynia in sciatic nerve chronic ligation rats compared with sham groups

Analysis of changes in sensory paw withdrawal thresholds showed a statistically difference between contralateral paw withdrawal thresholds in SN-CL and SH rats using Fisher's exact test (P=0.0006), (P=0.003) and (P=0.03) at the 6th, 16th, and 26th days after surgery, respectively (Fig.4).

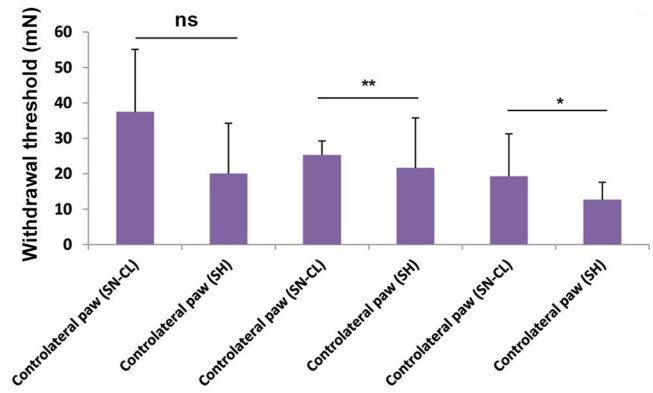

Fig.4: Graph showing compared mechanical contralateral allodynia in sciatic nerve chronic ligation with sham rats at 6th, 16th, and 26th days post- surgery (n=8 Wistar rats). Significant differences in paw withdrawal threshold are indicated by asterisks. ns; Non significant, *; P<0.05, and **; P<0.005.

Hyperalgesia assessment in sciatic nerve chronic ligation and sham rats

Comparing tactile contralateral paw withdrawal thresholds mean in SN-CL rats (8.375 ± 1.133) with SH group ones (10.38 ± 2.632) revealed a significant difference (Fisher's exact test, *P=0.0408, n=8) at the 16th-day post-surgery. However, at the 6th and the 26th days after surgery, the means were higher in SNCL group compared with SH one (14.38 ± 3.615 vs. 11.38 ± 3.520; 11.63 ± 3.495 vs 7.500 ± 2.771, n=8, respectively). For ipsilateral paw withdrawal threshold, the mean paw withdrawal thresholds in SNCL was increased at the 6th, 16th, and 26th days after surgery compared with SH rats (13.50 ± 3.794 vs. 11.75 ± 4.199, 11.125 vs. 9.125, 7.5 vs. 6.875, n=8 respectively) (Fig.5).

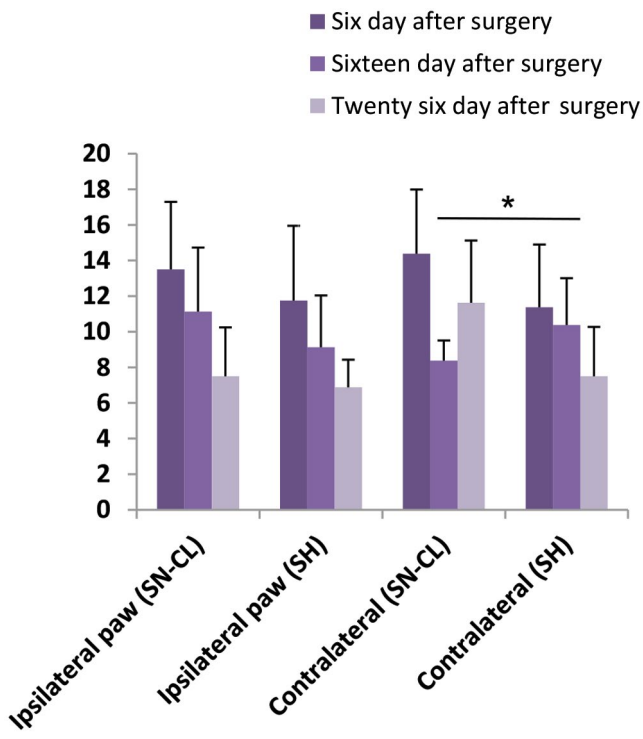

Fig.5: Assessment of mechanical hyperalgesia in sciatic nerve chronic ligation and sham groups at 6th, 16th, and 26th days after surgery. (n=8 Wistar rats). Asterisks indicate the significant difference in paw withdrawal threshold. *; P<0.05.

Discussion

In this study, Von Frey monofilaments which are one of the most non-invasive techniques were used. vFFs are important tools for the study of mechanisms of cutaneous stimulation-induced sensory input (19, 20). To study peripheral neuropathic pain behavior, vFFs which have been exploited for the precise measurement of mechano-sensitivity in most vertebrates in pain research were used (21-24). The filaments were applied at the mid-plantar surface just posterior to the footpads since this area is innervated mostly by terminal branches of the sciatic nerve. Also, applying hairs of different force is done to establish the paw withdrawal threshold (25).

The baseline withdrawal thresholds of each of the hind paws using von Frey hairs were determined for each rat prior to surgical manipulation (day 0). The, unilateral SN-CL of the left sciatic nerve was investigated to assess behavioral signs of peripheral neuropathic pain; however, it should be noted that many experimenters have performed on the right sciatic nerve, with similar pain and behavioral outcomes (26, 27). In this study, the behavioral evaluation was performed on different post-surgical days with an interval of ten days in SN-CL and SH rats in which the left sciatic nerve was exposed but not manipulated (28). On these days, the assessment of pain behavior was performed using Von Frey monofilaments (which are used in both preclinical and clinical assessment of allodynia). There is a limited amount of literature related to the time course measurement of mechanical allodynia using the SUDO method for measuring mechanical allodynia in SN-CL model of chronic neuropathic pain in contrast of the up-and-down method and the first response method for the reason that it was recently developed (29).

The assessment of ipsilateral tactile paw withdrawal thresholds showed that a transitory post-surgical mechanical allodynia was observed in the SH group from the 6th -day until 16th day post-surgery. In contrast, a long-lasting ipsilateral mechanical allodynia was established in SN-CL until twenty-six days after surgery. In the SH group, transitory post-surgical contralateral allodynia was created until day 12 after surgery, in contrast to a long-lasting ipsilateral allodynia until day 22 post-surgery, an assessment of contralateral allodynia was noted from day 22 to 26 post-surgery.

In a SN-CL model, data indicate that ipsilateral allodynia reached the day 6 after surgery and lasted until the 26th day after surgery, the mechanical pain hypersensitivity was maximal at the 16th -day when compared with ipsilateral mean paw withdrawal thresholds in sham-operated rats. In contrast, the contralateral allodynia appeared later on day 16 postoperatively in SN-CL animals.

At the 6th -day after surgery, the absence of significant different determines the loss effect of sciatic nerve ligation, demonstrating that neuropathy was not leaded. In contrast, a very significant and significant statically differences, which observed in day 16 and 26 post-surgery, respectively showed that ipsilateral hind paw becomes more sensitive and gets more pain hypersensitivity at the sixteen-day, with a lower intensity of mechanical allodynia at the twenty-six-day post-operatively witch validate that SN-CL in rats seems to present significant quantitative changes proportional to the external stimulation in mechanical allodynia (30), demonstrated that in mice model of neuropathic pain, neuropathy developed from day 7 postoperatively and in most animals neuropathy, was still observed until day 21-27 post-operatively.

The primary outcome resulted from comparing ipsilateral hind paw withdrawal threshold in SN-CL rats with the SH group demonstrate that ipsilateral allodynia became more intensive on day 16 explained by the loss of sensations (31) resulted from sciatic nerve damage, the mechanical ipsilateral allodynia lasted until day 26 after surgery in SN-CL rats.

When comparing contralateral mean hind paw withdrawal thresholds of SN-CL rats with SH control ones, the significant statically differences showed that contralateral allodynia in SN-CL rats appeared on day 6 and lasted until day 26 postoperatively witch lead to an extraterritorial development of neuropathic signs (32).

For hyperalgesia assessment, data showed an absence of ipsilateral hyperalgesia development at the different days of mechanical paw withdrawal thresholds measurements with the development of contralateral hyperalgesia in SN-CL rats just at the 16th day after surgery.

There are numerous problems with the use of

patients or healthy volunteers in pain research. We can only use a modest stimulus that will not produce any irreversible harm, and we also have to take into account accompanying diseases, malingering, and the placebo effect. It is also very difficult to recruit significant numbers of patients needed for clinical trials. Therefore, pain research is often conducted using animal models. Examination of the pathogenesis of neuropathic pain has been accelerated by the introduction of rodent models of the nerve injury that produce behavior indicative of spontaneous and inducible pain.

We chose SN-CL as a chronic pain model that made a significant contribution in understanding the pathophysiological mechanisms in chronic pain, which is quite distinct from acute noxious pain. The model produces unilateral peripheral mononeuropathy, and it has been observed that symptoms in this rat model correspond to causalgia or complex regional pain syndrome in patients. It induces allodynia in rodents and other symptoms which are similar to those of neuropathic pain in humans.

More work is needed for determination of the most predictive animal models, removal of user bias and, an introduction of more complex outcome measures in behavioral tests. It is important to state that in pain research, the problem is even more pronounced due to the subjective nature of painful experience. Only humans can express and describe the emotional aspect of a painful experience.

Conclusion

Sciatic nerve ligation induces a long-lasting of peripheral neuropathic pain signs with the absence of ipsilateral hyperalgesia development.

Acknowledgements

There is no financially support and conflict of interest in this study.

Authors' Contributions

N.T.; Performed research, analyzed data, and wrote the manuscript. S.F.; Informed reading. H.F.; Project manager, participated in study design. All authors read and approved the final manuscript.

References

1. Michael B, Harald B, Troels SJ, Willem S, Olaitan S, Rolf-Detlef T. Neurological disorders a public health approach. In: Johan AA, Giuliano A, José MB, Hanneke dB, Harald B, Tarun D, Nori G, Aleksandar J, Jürg K, Colin M, Anna M, Leonid P, Benedetto S, Shekhar S, Timothy JS, editors. Neurological disorders: public health challenges. Switzerland: World Health Organization; 2006; 127.
2. Treede RD. The International Association for the Study of Pain definition of pain: as valid in 2018 as in 1979, but in need of regularly updated footnotes. Pain Rep. 2018; 3(2): e643.
3. Merskey H, Bogduk N. Classification of chronic pain: descriptions of chronic pain syndromes and definitions of pain terms. 2nd ed. United States of America: IASP Press; 1994.
4. Michael B, Harald B, Troels SJ, Willem S, Olaitan S, Rolf-Detlef T. Neurological disorders a public health approach. In: Johan AA, Giuliano A, José MB, Hanneke dB, Harald B, Tarun D, et al. editors. Neurological disorders: public health challenges. Switzerland: World Health Organization; 2006; 127.
5. Laird B, Colvin L, Fallon M. Management of cancer pain: basic principles and neuropathic cancer pain. Eur J Cancer. 2008; 44(8): 1078-1082.
6. Bridges D, Thompson SW, Rice AS. Mechanisms of neuropathic pain. Br J Anaesth 2001; 87(1): 12-26.
7. Woolf CJ, Ma Q. Nociceptors--noxious stimulus detectors. Neuron. 2007; 55(3): 353-364.
8. Abelson K, Roughan, John V. Animal models in pain research. In: Hau J, Schapiro SJ, editors. Handbook of laboratory animal. 3rd ed. New York: CRC Press; 2011; 129.
9. Lambert GA, Mallos G, Zagami AS. Von Frey's hairs--a review of their technology and use--a novel automated von Frey device for improved testing for hyperalgesia. J Neurosci Methods. 2009; 177(2): 420-426.
10. Coyle DE, Sehlhorst CS, Mascari C. Female rats are more susceptible to the development of neuropathic pain using the partial sciatic nerve ligation (PSNL) model. Neurosci Lett. 1995; 186(2-3): 135-138.
11. Liu JH, Dacus AC. Intramuscular injection of chlorpromazine decreases intraocular pressure by lowering systemic blood pressure. Curr Eye Res. 1989; 8(12): 1315-1321.
12. Bennett GJ, Xie YK. A peripheral mononeuropathy in rat that produces disorders of pain sensation like those seen in man. Pain. 1988; 33(1): 87-107.
13. Bradman MJ, Ferrini F, Salio C, Merighi A. Practical mechanical threshold estimation in rodents using von Frey hairs/Semmes-Weinstein monofilaments: Towards a rational method. J Neurosci Methods. 2015; 255: 92-103.
14. Victor Pires de Sousa M, Ferraresi C, Carolina de Magalhães A, Mateus Yoshimura E, Hamblin MR. Building, testing and validating a set of home-made von Frey filaments: a precise, accurate and cost effective alternative for nociception assessment. J Neurosci Methods. 2014; 232: 1-5.
15. Fruhstorfer H, Gross W, Selbmann O. von Frey hairs: new materials for a new design. Eur J Pain. 2001; 5(3): 341-342.
16. Mogil JS, Wilson SG, Wan Y. Assessing nociception in murine subjects. In: Kruger L, editor. Methods in pain research. Boca Raton: CRC Press; 2001; 11-39.
17. Bonin RP, Bories C, De Koninck Y. A simplified up-down method (SUDO) for measuring mechanical nociception in rodents using von Frey filaments. Mol Pain. 2014; 10: 26.
18. Liu YT, Chen SD, Chuang YC, Shaw FZ. Pregabalin, duloxetine, and diazepam selectively modulate acid-induced hyperalgesia and anxio-depressive comorbidity in rats. Neuropsychiatry. 2017; 7(6).
19. Chaplan SR, Bach FW, Pogrel JW, Chung JM, Yaksh TL. Quantitative assessment of allodynia in the rat paw. J Neurosci Methods. 1994; 53(1): 55-63.
20. Nirogi R, Goura V, Shanmuganathan D, Jayarajan P, Abraham R. Comparison of manual and automated filaments for evaluation of neuropathic pain behavior in rats. J Pharmacol Toxicol Methods. 2012; 66(1): 8-13.
21. Juszkiewicz-Donsbach J, Levy G. Effect of small variations in heat stimulus temperature on the tail flick response of rats in analgesimetry. J Pharm Sci. 1962; 51: 185-186.
22. Bonnet KA, Peterson KE. Modification of the jump-flinch technique for measuring pain sensitivity in rats. Pharmacol Biochem Behav. 1975; 3(1): 47-55.
23. Pitcher GM, Ritchie J, Henry JL. Paw withdrawal threshold in the von Frey hair test is influenced by the surface on which the rat stands. J Neurosci Methods. 1999; 87(2): 185-193.
24. Kim HT, Kim T, Novotny B, Khan N, Aksamit J, Siegel S, et al. Thermal hyperalgesia assessment for rats after spinal cord injury: developing valid and useful pain index. Spine J. 2014; 14(6): 984-989.
25. Pitcher GM, Ritchie J, Henry JL. Paw withdrawal threshold in the von Frey hair test is influenced by the surface on which the rat stands. J Neurosci Methods. 1999; 87(2): 185-193.
26. Myers RR, Yamamoto T, Yaksh TL, Powell HC. The role of focal nerve ischemia and Wallerian degeneration in peripheral nerve injury producing hyperesthesia. Anesthesiology 1993; 78(2): 308-316.

27. Grace PM, Hutchinson MR, Manavis J, Somogyi AA, Rolan PE. A novel animal model of graded neuropathic pain: utility to investigate mechanisms of population heterogeneity. J Neurosci Methods. 2010; 193(1): 47-53.
28. Polgár E, Hughes DI, Arham AZ, Todd AJ. Loss of neurons from laminas I-III of the spinal dorsal horn is not required for development of tactile allodynia in the spared nerve injury model of neuropathic pain. J Neurosci. 2005; 25(28): 6658-6666.
29. McMackin MZ, Lewin MR, Tabuena DR, Arreola FE, Moffatt C, Fuse M. Use of von Frey filaments to assess nociceptive sensitization in the hornworm, Manduca sexta. J Neurosci Methods. 2016; 257: 139-146.
30. van der Wal S, Cornelissen L, Behet M, Vaneker M, Steegers M, Vissers K. Behavior of neuropathic pain in mice following chronic constriction injury comparing silk and catgut ligatures. Springerplus. 2015; 4: 225.
31. Marchettini P. Painful peripheral neuropathies. Curr Neuropharmacol. 2006; 4(3): 175-181.
32. Pitcher GM, Ritchie J, Henry JL. Nerve constriction in the rat: model of neuropathic, surgical and central pain. Pain. 1999; 83(1): 37-46.

Differentiation Induction and Proliferation Inhibition by A Cell-Free Approach for Delivery of Exogenous miRNAs to Neuroblastoma Cells Using Mesenchymal Stem Cells

Samaneh Sharif, Ph.D.[1, 2*], Mohammad Hossein Ghahremani, Ph.D.[1, 3#], Masoud Soleimani, Ph.D.[4#]

1. Department of Molecular Medicine, School of Advanced Technologies in Medicine, Tehran University of Medical Sciences, Tehran, Iran
2. Medical Genetics Research Center, Mashhad University of Medical Sciences, Mashhad, Iran
3. Department of Toxicology and Pharmacology, Faculty of Pharmacy, Tehran University of Medical Sciences, Tehran, Iran
4. Department of Haematology, Tarbiat Modares University, Tehran, Iran

#The last two authors equally contributed to this work.

Corresponding Address: P.O.Box: 14177-55469, Department of Molecular Medicine, School of Advanced Technologies in Medicine, Tehran University of Medical Sciences, Tehran, Iran
Email: sharif_s@razi.tums.ac.ir

Received: 6/May/2019, Accepted: 30/July/2019

Abstract

Objective: Neuroblastoma (NB) is one of the frequently observed malignant solid tumors of childhood and infancy, accounting for 15% of pediatric cancer deaths. Recently, the approach of differentiation therapy has shown considerable promise in effective treatment of NB patients. MiR-124 belongs to the nervous system-specific miRNAs that is increased during neuronal differentiation and may be one of the potential therapeutic targets for the treatment of NB. However, despite its well-established therapeutic potential, its efficient delivery to the targeted tumor cells is a challenging task. Mesenchymal stem cells (MSCs) are multipotent adult progenitor cells that have antitumor properties, and they can migrate to cancer cells and tumors. This study aimed to assess whether human adipose tissue-derived MSCs (hAD-MSCs) have the potential to deliver exogenous miRNAs to NB cells to induce differentiation and decrease proliferation of cancer cells.

Materials and Methods: In this experimental study, hAD-MSCs were isolated, cultured, and differentiated. The M17 human NB cell line were also cultured. A specific type of miRNAs, i.e., miR-124 was successfully delivered to M17 NB cells with the aid of hAD-MSCs using the direct or indirect (exosome-based) contacts.

Results: It was shown that indirect delivery of miR-124 considerably decreased the proliferation of NB cells and induced their differentiation.

Conclusion: The results suggest the use of delivered exogenous miRNAs by the derived exosomes from hAD-MSCs as a novel cell-free stem cell-based therapy for NB cancer.

Keywords: Differentiation, Exosome, Mesenchymal Stem Cells, MiR-124, Neuroblastoma

Cell Journal(Yakhteh), Vol 22, No 4, January-March (Winter) 2021, Pages: 556-564

Citation: **Sharif S, Ghahremani MH, Soleimani M. Differentiation induction and proliferation inhibition by a cell-free approach for delivery of exogenous miRNAs to neuroblastoma cells using mesenchymal stem cells. Cell J. 2021; 22(4): 556-564. doi: 10.22074/cellj.2021.6928.**

Introduction

Neuroblastoma (NB) is one of the frequently observed malignant solid tumors in children that accounts for nearly 7% of childhood cancers and more than 15% of pediatric cancer deaths. The most commonly used treatments for metastatic NB are powerful chemotherapy or intensive chemotherapy with autologous hematopoietic rescue after the removal of the initial tumor (1). Despite the great advances made in multimodal treatments of NB, its prognosis in metastatic cases is still relatively poor. As widely accepted, NB is caused by imperfect differentiation of neural crest cell precursors of the sympathetic nervous system (2). Therefore, the approach of differentiation therapy could be the most appropriate and effective therapeutic option for NB. The ability of undifferentiated fatal cells in differentiation into mature cells results in arrest of cell growth and apoptosis (3). 13-cis-retinoic acid (RA), as a differentiation-inducing agent, is one of the standard mainstays of therapy in high-risk NB patients (4). This type of treatment leads to a significant increase in patient survival. However, at the same time, more than half of the treated patients develop recurrence. It must also be noted that RA therapy may result in the adverse effects of cell toxicity and inflammation. Therefore, the development of novel therapy for NB is an urgent issue.

MicroRNAs (miRNAs) are noncoding RNAs that play critical roles in the coordinated regulation of gene sets. Indeed, studies performed on the regulatory mechanism of miRNAs have attracted much attention in recent years. They can regulate different cellular processes, such as proliferation, differentiation, apoptosis, invasion, and angiogenesis (5). When miRNAs are expressed in specific tissue types, they can effectively contribute to differentiation. MiR-124 is a member of the nervous system-specific miRNAs regulating neurite outgrowth during neuronal differentiation. The level of miR-124 is increased during neuronal differentiation, and it plays an outstanding role in the development of neurons (6). Its overexpression in human glioblastoma multiforme cells

induces neuronal phenotype (7). It is now known that the overexpression of miR-124 in stem cells leads to terminal neuronal differentiation with reduced malignancy (8). Despite the well-established therapeutic potential of miR-124, its efficient delivery to the targeted tumor cells is a challenging task.

In recent years, studies suggested that mesenchymal stem cells (MSCs) have tropism to tumor sites and produce antitumor effects (9). They can also act as delivery vehicles for therapeutic miRNAs to transfer them into the region of cancer cells. The *in vivo* experiments indicated that MSCs promote NB differentiation and suppress tumor proliferation (10). As we reported previosly (11), MSCs derived from Wharton's jelly have the capability to deliver miR-124 to glioblastoma multiforme cells and decrease cell migration and proliferation as well as indicing chemosensitivity. Based on the mentioned evidence, it can be expected that the use of MSCs for transferring miR-124 to cancer cells holds great promise for the treatment of NB.

In this study, we reported the transfer of miR-124 to NB cells with the aid of MSCs. It was shown that human adipose tissue-derived MSCs (hAD-MSCs) can deliver miR-124 to NB cells and this delivery system regulates the transcription profile and changes the function of cancer cells. It was demonstrated that indirect delivery of miR-124 in the form of secreting exosomes from hAD-MSCs significantly decreases the proliferation of NB cells and induces their differentiation.

Materials and Methods

In this section, the preparation of the cell samples and the methods used for characterizations are fully described.

Ethical considerations

All procedures performed in studies involving human participants were in accordance with the ethical standards of the Research Ethics Committee of Tehran University of Medical Sciences (No. 92-01-87-21665-85626).

Isolation, cell culture, and cell differentiations of human adipose tissue-derived mesenchymal stem cells

hAD-MSCs were obtained from healthy donors undergoing esthetic surgery. The isolation of hAD-MSCs was performed as descrived previosly (12). The digestion of adipose tissue was conducted at 37˚C with 1 mg/ml collagenase type I (Gibco, USA). After centrifugation of the suspension, hAD-MSCs were cultured in DMEM (Invitrogen, USA) supplemented with 10% fetal bovine serum (FBS, Gibco, USA), 100 g/ml streptomycin (Invitrogen, USA), 100 U/ml penicillin (Invitrogen, USA), and 2 mM L-glutamine (Invitrogen, USA). Replacement of the medium of the cultured cells and removal of the non-adherent cells were carried out after 48 hours. After 3 weeks, detachment of hAD-MSCs was performed when the cells reached 70-80% confluence. hAD-MSCs were characterized by the positive expression of CD73, CD105, and CD90 (Abcam, UK) markers and the negative expression of hematopoietic stem cell markers, namely HLA-DR (Abcam, UK), CD34 and CD45 (PE, eBiosciences). In order to study the multipotential differentiation of cells, particular cell culture media were utilized for the induction of the differentiation of hAD-MSCs into osteocytes and adipocytes. Dexamethasone (10 M) and insulin (6 ng/ml) were added to the cell culture medium to induce adipogenic differentiation in the plated cells. Similarly, for osteogenic differentiation, ascorbic acid (50 µg/ml), dexamethasone (10 M) and sodium β-glycerophosphate (10 mM) were applied. After 3 weeks, the plates were washed, and the cells were stained with Alizarin Red (13) and Oil Red O (14) to confirm their osteogenic and adipogenic differentiation, respectively.

The cell culture of M17 cell line

In this experimental study, the cloned M17 human NB cell lines derived from the SK-N-Be (2) NB cell line were used (ATCC manassas, VA). HEK T293 and human M17 NB cell lines were purchased from the Pasteur Institute of Iran.

M17 cells were cultured in the culture medium containing a mixture of DMEM and F12 medium at a ratio of 50:50 supplemented (to final concentration) with 10% FBS, 100 U/mL penicillin, 0.1 mg/mL streptomycin, 2 mM L-glutamine and 1% nonessential amino acids (Invitrogen, USA) (15).

miR−124 Transfection

Cy3 (Life Technologies, Invitrogen, USA) was used for labeling RNA duplexes corresponding to has-miR-124. The transfections of hAD-MSCs, at passeges 3-4, was conducted using the Lipofectamine 3000 kit (LifeTechnologies, Inc., Invitrogen, USA) according to the manufacturer's instructions (16).

Preparation of exosomes

The cell culture of the transfected hAD-MSCs with miR-124-Cy3 and control miR was performed in the MSC medium using Gibco™ Exosome-Depleted FBS (Thermo Fisher Scientific, USA). After incubating for four days, the isolation of the exosomes from the supernatants of the hAD-MSC culture medium was carried out using the exosome precipitation solution, ExoQuick (System Biosciences). The protein content was evaluated by the Micro BCA assay kit (Sigma-Aldrich, Sweden) (17).

Co−culturing human adipose tissue-derived mesenchymal stem cells with M17 NB Cells

Following the manufacturer's protocols, M17 NB cells were labeled with green fluorescence CMFDA Cell Tracker (Molecular Probes). After labeling the cells, they were mixed at a ratio of 50:100 by hAD-MSCs transfected with miR-124 and plated in 8-well plates. After 72 hours, flow cytometric analysis was performed for confirming the delivery of miR-124 to M17 cells.

To check the delivery of miR-124 mimetic with an indirect contact (i.e., via the secreted exosomes from hAD-MSCs), membranes with 0.4 μm-pore diameter were used in a transwell chamber to inhibit cell infiltration (hAD-MSCs-miR-124-Cy3 and M17 cells). Plating hAD-MSCs transfected with with miR-124-Cy3 was carried out in the transwell inserts. At the same time, seeding M17 NB cells was performed in the lower well. After 72 hours, M17 NB cells were collected, and the flow cytometric analysis was applied to ensure that miR-124-Cy3 was delivered to M17 cells.

Quantitative real-time polymerase chain reaction

The QIAzol reagent (Qiagen, Germany) was used for the extraction of the total RNA. The synthesis of complementary DNA (cDNA) was also performed by reverse transcriptase (Fermentas, Germany) and random hexamers for gene primers. Triplicate real-time polymerase chain reaction analysis with SYBR Premix Dimer EraserTM (TaKaRa, Japan) was used, and the results were analyzed using the REST and the Rotor-Gene 6.1 (Corbett, Australia) software. The PCR primers and their respective reverse complements were as follows:

h-Tubullin beta III-
F: 5′-GGA GTA TTT GGA TGA CAG AAA C-3′
R: 5′-GAT TAC CAC TGG AGT CTT C-3′ (product length: 238 bps)

MAP2-
F: 5′-AGT TCC AGC AGC GTG ATG-3′(product length: 164 bps)
R: 5′-TAGTCTAAGCTTAGC TGAGAATCTACCGA-3′

GAPDH-
F: 5′-GAC AAG CTT CCC GTT CTC AG-3′
R: 5′-GAG TCA ACG GAT -TTG GTC GT-3′ (product length: 132 bps).

GAPDH mRNA was used as the internal control. The real-time PCR protocol was as follows: 2 minutes at 95˚C, 5 seconds at 95˚C for denaturation, 30 seconds at 60˚C for annealing, 10 seconds at 72˚C for amplification, and 40 cycles of extension (18).

Cell viability and apoptosis assay

In order to investigate the cell viability, M17 cells were seeded at a density of 5×10^3 in 96-well plates and incubated overnight while keeping the temperature constant at 37˚C. The addition of the exosomes derived from control-miR and hAD-MSC-miR-124-Cy3 to M17 cells was carried out after 24 hours. The flow cytometry analysis was performed to detect the delivery of exosomes containing miR-124. Upon the assurance of the delivery of miR-124 to the M17 cells, the viability of M17 cells transfected with miR-124 and control miR was examined by the MTT assay after 24, 48 and 72 hours. The rate of apoptosis in M17 cells transfected with miR-124 and control miR was assayed using terminal deoxynucleotidyltransferase dUTP nick-end labeling (TUNEL) assay performed by the In Situ Death Detection kit (Roche Diagnostics, Indianapolis, IN) according to the manufacturer's instructions. The cultured M17 NB cells with the secreted exosomes from hAD-MSCs-Con-miR (M17-hAD-MSCs-Con-miR) were treated with derived exosomes from hAD-MSCs-miR-124 (M17-hAD-MSCs-miR-124). The cultured M17 NB cells were also directly transfected with miR-124 (M17-miR-124) and its control (M17-con-mir).

In this study, the data were analyzed by the Statistical Package for Social Sciences version 11 software (SPSS, IBM, USA).

Results

As shown in Figures 1A-C, the flow cytometry analysis indicated the expression of CD73, CD90, and CD105 in hAD-MSCs. Furthermore, the cells were negative for HLA-DR, CD34, and CD45 (Fig.1D-F). The multipotency of hAD-MSCs was also confirmed by adipogenic and osteogenic differentiation (Fig.1G, H). Transfection efficiency was estimated about 80% by fluorescence microscopy (Fig.2A, B). In the following sections, the delivery of hAD-MSCs to M17 NB cells and their subsequent effects on inducing apoptosis and neuronal differentiation in NB cells is indicated.

Delivery of miR-124 mimetic to M17 NB cells

According to previous reports (19, 20), MSCs have the ability of cell-to-cell communication via gap-junctional intercellular channels (direct contact) or by secreting different factors, such as cytokines, vesicles, and extracellular matrix molecules (indirect contact) that promote neurogenesis. Furthermore, MSCs can also be genetically modified to be able to release specific growth factors, cytokines, and miRNAs in the form of exosomes (21). In this paper, the potential of hAD-MSCs to deliver exogenous miRNA mimetics to M17 NB cells was examined. Specifically, the focus of this study was on miR-124 delivery because this miRNA has already been reported to have a significant role in differentiation of NB cells (8). For this aim, two days after the co-culture period of hAD-MSCs-miR-124 with M17 NB cells (direct contact), the combination was studied with the aid of the two-channel flow cytometry technique. The direct transfer of miR-124 from hAD-MSCs-miR-124 into M17 NB cells was confirmed by the detection of Cy3 in M17 NB cells (Fig.2C). Moreover, in transwell-cultured hAD-MSCs, the detection of miR-124-Cy3 indicated that M17 cells were Cy3-positive, and hence, miR-124-Cy3 was indirectly transferred from hAD-MSCs into M17 NB cells (Fig.2D). Figure 2C corroborates that miR-124 was indirectly transferred with exosomes derived from hAD-MSCs into M17 NB cells. The bi-color flow cytometry dot plots in Figure 2 represent the percentage of the co- and the transwell-cultured cells.

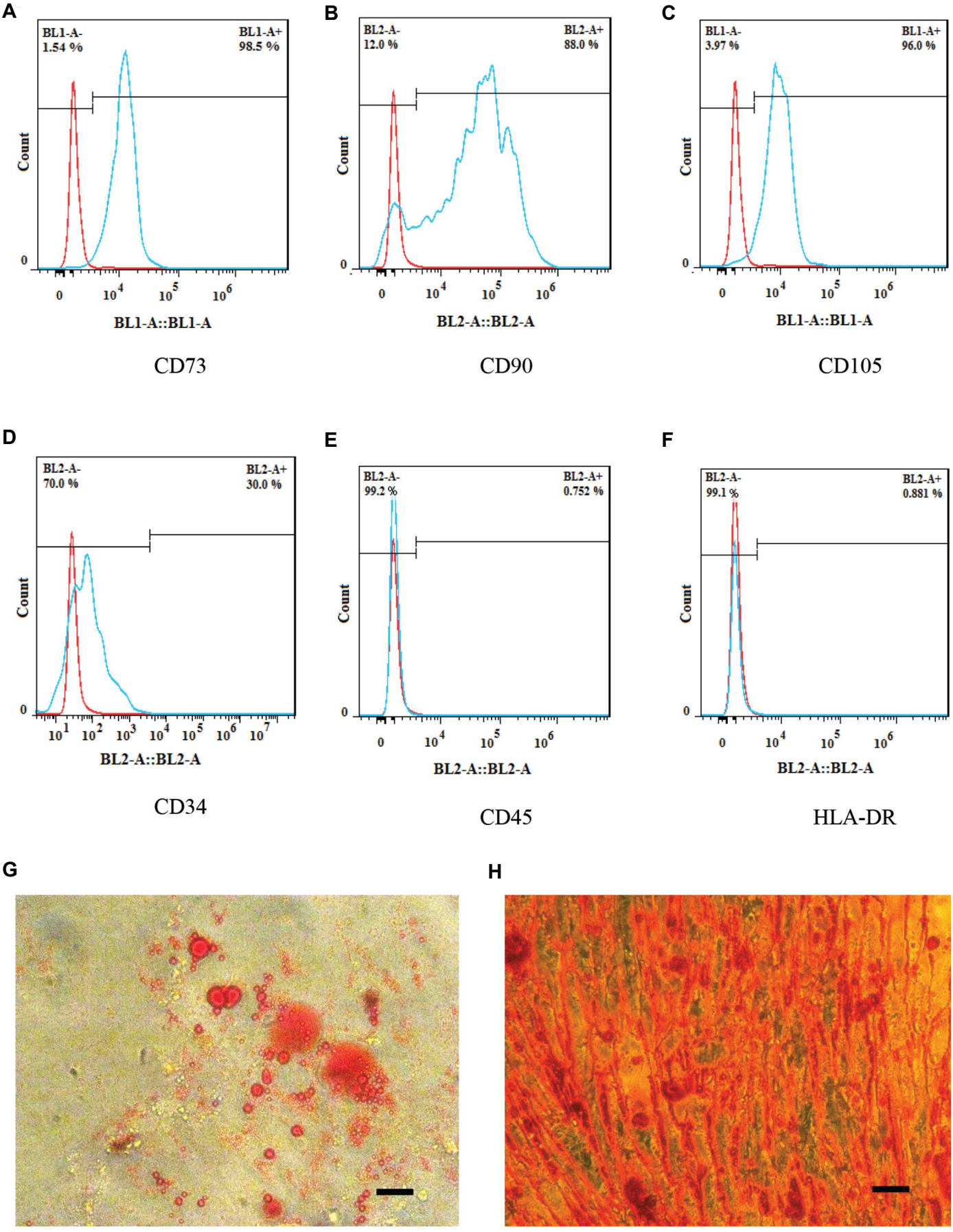

Fig.1: Characterization of human adipose tissue-derived mesenchymal stem cells (hAD-MSCs) by flow cytometry and light microscopy. The flow cytometry analysis of hAD-MSCs for the detction of **A.** CD73, **B.** CD90, **C.** CD105 (positive markers), **D.** CD34, **E.** CD45, **F.** HLA-DR (negative markers). Light microscopy images show **G.** Adipogenic and **H.** Osteogenic differentiation of hAD-MSCs (scale bar: 200 µM).

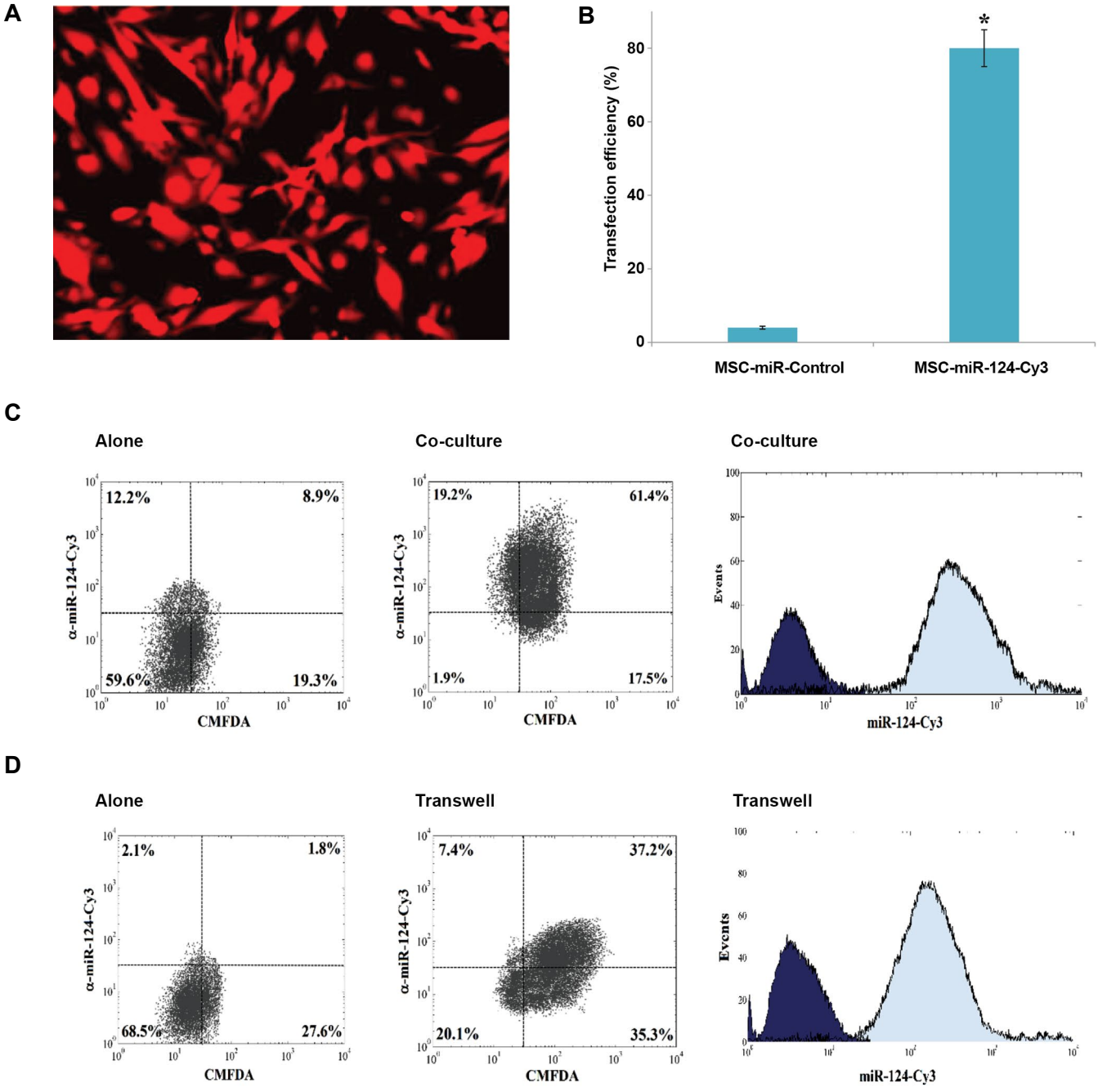

Fig.2: The results of flow cytometry confirmed the delivery of miR-124 to M17 NB cells by human adipose tissue-derived mesenchymal stem cells (hAD-MSCs). HAD-MSCs were transfected with Cy3-labeled miR-124. After 24 hours, the labeled M17 NB cells with Green Cell Tracker CMFDA were added to the ceulture medium of hAD-MSCs. The expression of the fluorescent miR-124 in M17 NB cells was analyzed after 24 hours by flow cytometry. The results indicated the transfer of miR-124-Cy3 from hAD-MSCs into M17-CMFDA cells. **A.** hAD-MSCs were transfected with cy3-labllled miR-124. **B.** Transfection efficiency was estimated about 80% by fluorescence microscopy (P<0.05). **C.** M17 NB cells co-cultured with hAD-MSCs-miR-124-Cy3, left panel: NB cells alone; middle panel: analysis of NB cells and hAD-MSCs for CMFDA and Cy3; right panel: Cy3 in co-cultured cells. **D.** Exosomes derived from hAD-MSCs were added to NB cells with transwell, left panel: NB cells alone; middle panel: the analysis of M17 NB cells for CMFDA and Cy3; right panel: Cy3 alone in M17 NB cells. *; P<0.05.

Concomitant decreased proliferation and apoptosis induction in M17 NB cells through the delivery of miR-124 by hAD-MSCs

To determine whether transferring miR-124 to M17 NB cells by hAD-MSCs may have an effect on proliferation in addition to induction of apoptosis, the derived exosomes from hAD-MSC-miR-124 cells were used for treating M17 cells. The result of the MTT assay showed that the delivery of miR-124 reduced the proliferation of M17 cells (Fig.3A). In order to further check whether the delivery of miR-124 can induce apoptosis in M17 NB cells, the TUNEL assay was carried out, as well. As indicated in Figure 3B, it was demonstrated that miR-124 induced apoptosis in M17 NB cells.

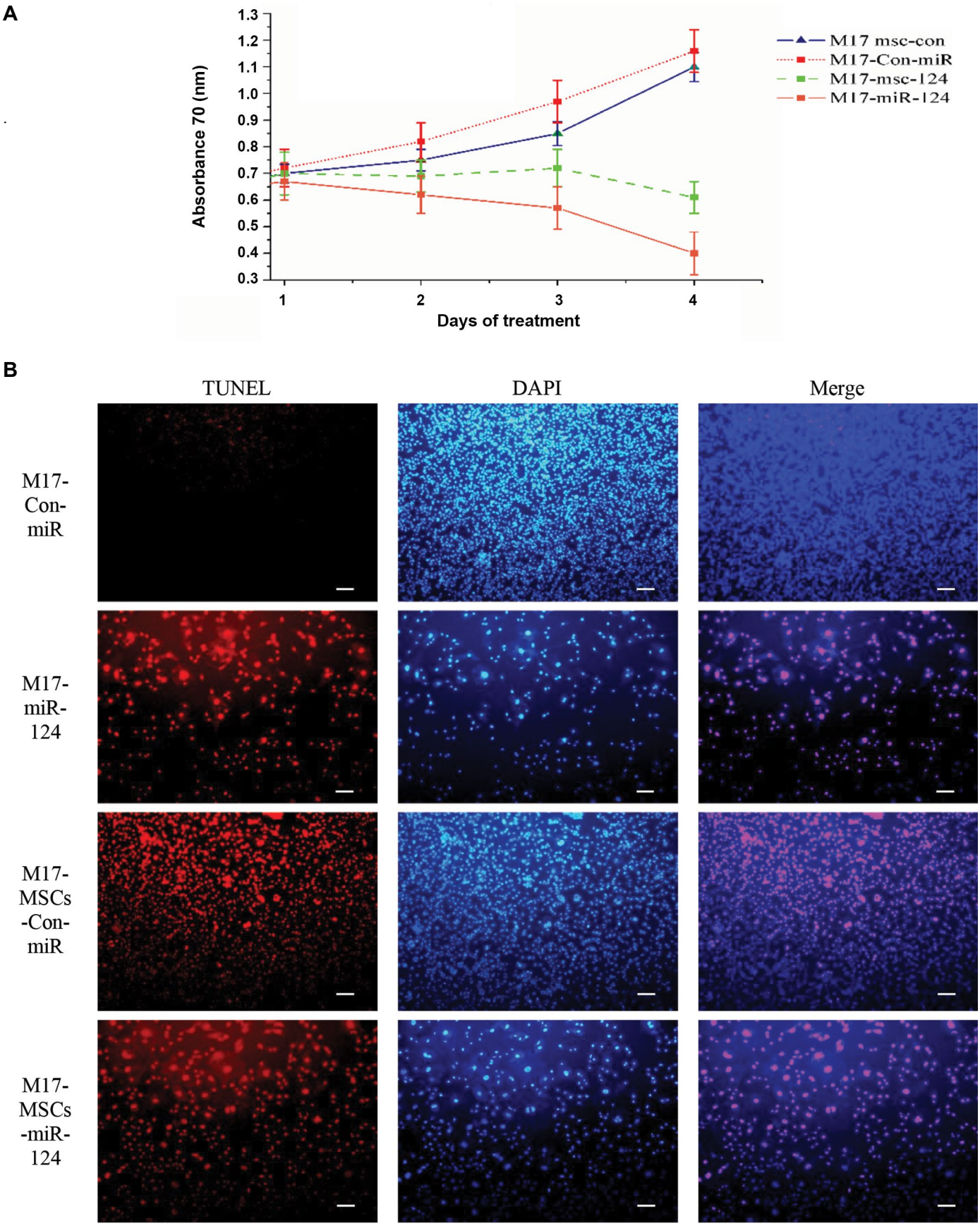

Fig.3: The results of inducing differentiation in M17 NB cells after delivery of miR-124 by hAD-MSCs. **A.** The MTT assay represents the cell proliferation in miR-124-treated cells in every 24 h interval and **B.** TUNEL staining results indicating that the delivered miR-124 induced considerable apoptosis 24 hours after exposure. The nuclei of TUNEL-positive cells show that most of the cells underwent apoptosis. The cultured M17 NB cells with exosomes secreted from hAD-MSCs-Con-miR (M17-hAD-MSCs-Con-miR) were treated with exosomes derived from hAD-MSCs-miR-124 (M17-hAD-MSCs- miR-124). The directly transfected M17 NB cells with miR-124 (M17-miR-124) and its control (scale bar: 50 µM).

MiR-124 mimetic delivery by hAD-MSCs stimulates the neuronal differentiation of M17 NB cells

As mentioned earlier in previous sections, the sole delivery of miR-124 to NB cells without any intermediate element has been reported to induce differentiation in cells (8, 22). The goal of this study was to examine the role of MSCs, as intermediate carriers, in facilitatating the delivery of miR-124 to M17 NB cells and inducing further differentiation. In order to investigate this, M17 cells were treated with the exosomes derived from hAD-MSCs-miR-124 and showed that the expression of β-tubulin III and MAP2 significantly enhanced in comparison with the control (Fig.4). This results confirm that miR-124 delivery induced the differentiation of M17 NB cells. Additionally, as depicted in Figure 3, M17 cells treated with exosomes derived from hAD-MSCs-Con-miR also induced cell differentiation. In the same manner, the induction of differentiation was rather spectacular in M17 cells treated with exosomes secreted from hAD-MSCs-miR-124. The increased differentiation in this case can be ascribed to synergistic effect of neurotropic factors secreted from both hAD-MSCs and miR-124. Furthermore, compared with the undifferentiated cells, the morphology of neuron-like cells was more pronounced in differentiated M17 cells . This is consistent with previous findings that the overexpression of miR-124 noticeably induces differentiation of NB cancer cells (8, 22).

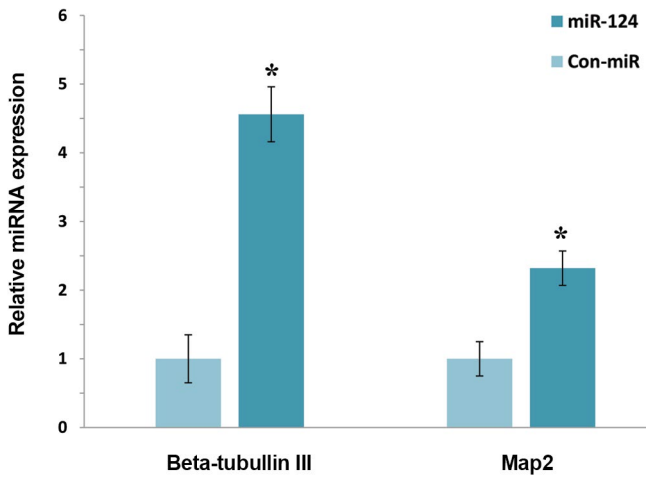

Fig.4: The qRT-PCR analysis results, showing the increase of mRNA level of β-Tubulin III and MAP2 (P<0.05). The results indicate that hAD-MSCs delivered miR-124 and induced differentiation in M17 NB cells in comparison with the control cells. *; P<0.05 and qRT-PCR; Real-time quantitative reverse transcription polymerase chain reaction.

Discussion

Recently, miRNAs have been appeared as the main potential therapeutic targets in cancers (23) and expression alternation of miRNAs in different neurological disorders have been the subject of several studies (24, 25). Indeed, it is already shown that administration of miR-based therapy will provide therapeutic approaches in pathological conditions of the central nervous system cancers (26). However, despite their therapeutic potential, the existing problems in the way of controlled delivery of therapeutic agents to targeted neural cells are mostly considered as the major reasons for the poor outcomes of treatment.

In regenerative medicine, MSCs are known to be hopeful sources for cell therapy since they have immunomodulation, trophic factor secretion and transdifferentiation properties (27). Furthermore, the secreted exosomes from MSCs that assist in restraining tissue injuries, lead to re-entry of cell cycle in resident cells and induce tissue self-repair, are being examined for various applications in neural, musculoskeletal or cardiac repair (28). In recent years, various studies have indicated that MSCs can be effectively used for treating different disorders in the central nervous system, including Parkinson's disease, multiple sclerosis, amyotrophic lateral sclerosis (ALS) and stroke (29, 30). MSCs show tropism to malignant cells, migrate to tumor microenvironments, exert antitumor effects and also have this ability to act as delivery vectors for anticancer agents (31). MSCs and neural stem cells are also considered as promising candidates for overcoming the blood-brain barrier by delivering drugs and RNAs to tumours or neurodegenerative disorders (32).

In this study, the ability of hAD-MSCs to act as a delivery vector for transferring miR-124 to co-cultured NB cancer cells has been demonstrated, and they are proposed as a promising approach for the targeted delivery of miRNA-based therapy to NB cancer cells. Previously, Bianchi et al. reported that functional cross-talks between hMSCs and NB cell lines can be effective only within short range interaction and showed that intravenously inoculated hMSCs in different NB models did not reach the tumor sites (10). Nevertheless, they also showed that intratumorally injected hMSCs in a subcutaneous NB model decreased tumor growth and enhanced the survival time. On the contrary, Kimura et al. have reported that intraperitoneally administered hMSCs can migrate and affect tumor cells in a TH-MYCN mouse model (33). In a recent clinical study, the efficiency of the inhibition of bone marrow metastasis in NB was shown by menas of the infected autologous MSCs with ICOVIR-5. Excellent treatment tolerance and full clinical response were reported for this new type of treatment (34). It was also shown in our previous work (11) that MSCs of Wharton's jelly deliver exogenous miRNAs to glioblastoma multiform cells and their functional effects were fully elucidated. It has been demonstrated that the labeled miR-124 can be delivered effectively by MSCs of Wharton's jelly to U87 glioblastoma multiform cells through exosome-dependent or independent manners. Consistent with these reports, in this study, it was also found that hAD-MSCs can successfully deliver miR-124 to the co-cultured M17 NB cells by localizing the Cy3-labeled miR-124. Furthermore, it was revealed that miR-124 delivery by exsosomes secreted from hAD-MSCs to M17 NB cells holds great promise for delivery of miRNAs to target cells.

It is now know that miR-124 is a neuron-specific miRNA that has a great impact on neurogenesis and differentiation of neuronal cells (35). According to previous reports, miR-124 has the ability to act as proliferation inhibitor, and thereby the suppression of CDk6, can induce cell differentiation (36, 37). Also shown in our previous work, the overexpression of miR-124 increased the the expression levels of MAP2, β-Tubulin III, NF-M, SYN and Nestin markers and induced the functional differentiation in M17 NB cells (22). In this study, it was indicated that exosomes secreted from hAD-MSCs-miR-124 promotes miR-124 delivery to M17 NB cells and reduces their proliferation. The proliferation control is a critical step in terminal differentiation program in tumor cells (38). Therefore, in the current work, after successful delivery of miR-124 with exosomes secretd from hAD-MSCs to the M17 NB cells and approving their proliferation decrease, the induction of differentiation in these cells was also investigated. The obtained results confirmed that exosome delivery of miR-124 to M17 NB cancer cells can be an efficient cell-free approach for differentiation of NB cancer. In a previously published report, it was demonsrtrated that secreted neurotrophic factors from MSCs can solely induce differentiation in neuronal progenitor cells (39). Furthermore, exosome secreted from MSCs, as a novel cell-free stem cell-based therapy and the genetically modified exosomes, have yielded positive therapeutic results (40). In the present study, it was shown that the induction of differentiation in the M17 NB cells treated with exosomes secreting from hAD-MSCs-miR-124, compared with the control (M17 NB cells treated with exosomes secreted from hAD-MSCs-Con-miR), is the outcome of two distinct factors, i.e., miR-124 and hAD-MSCs. Considering these results, using hAD-MSCs as a vector for miR-124 delivery to NB cells seems very useful for the treatment of NB cancer.

Conclusion

In this study, it was demonstrated hAD-MSCs can efficiently deliver exogenous miR-124 to NB cells which, in turn, decrease their proliferation and stimulate the induction of their differentiation. The obtained results suggest the opportunity to use the delivered exogenous miRNAs by hAD-MSCs, as a novel cell-free stem cell-based therapy, for the treatment of NB cancer. Future studies can be directed towards more investigations on allogeneic MSCs by murine tumor models, which are necessary for the confirmation of the antitumor potential of MSCs.

Acknowledgements

This work is a part of Ph.D. thesis of Samaneh Sharif that fiancially supported by the Department of Molecular Medicine, School of Advanced Technologies in Medicine, Tehran University of Medical Sciences, Tehran, Iran. There is no conflict of interest in this study.

Authors' Contributions

S.S.; Participated in study design, data collection, evaluation, manuscript drafting, and revision. M.H.G., M.S.; Participated in study design and data evaluation. They were responsible for overall supervision and provided critical revision of the manuscript. All authors read and approved the final manuscript.

References

1. Garcia-Castro J, Alemany R, Cascallo M, Martinez-Quintanilla J, del Mar Arriero M, Lassaletta A, et al. Treatment of metastatic neuroblastoma with systemic oncolytic virotherapy delivered by autologous mesenchymal stem cells: an exploratory study. Cancer Gene Ther. 2010; 17(7): 476-483.
2. Brodeur GM. Neuroblastoma: biological insights into a clinical enigma. Nat Rev Cancer. 2003; 3(3): 203-216.
3. Cruz FD, Matushansky I. Solid tumor differentiation therapy-is it possible? Oncotarget. 2012; 3(5): 559-567.
4. Park JR, Eggert A, Caron H. Neuroblastoma: biology, prognosis, and treatment. Hematol Oncol Clin North Am. 2010; 24(1): 65-86.
5. Shamsara J, Sharif S, Afsharnezhad S, Lotfi M, Raziee HR, Ghaffarzadegan K, et al. Association between MGMT promoter hypermethylation and p53 mutation in glioblastoma. Cancer Invest. 2009; 27(8): 825-829.
6. Ko HY, Lee J, Lee YS, Choi Y, Ali BA, Al-Khedhairy AA, et al. Bioimaging of transcriptional activity of microRNA124a during neurogenesis. Biotechnol Lett. 2015; 37(11): 2333-2400.
7. Tavakoli R, Vakilian S, Jamshidi-Adegani F, Sharif S, Ardeshirylajimi A, Soleimani M. Prolonged drug release using PCL-TMZ nanofibers induce the apoptotic behavior of U87 glioma cells. International Journal of Polymeric Materials and Polymeric Biomaterials. 2018; 67(15): 873-878.
8. Samaraweera L, Grandinetti KB, Huang R, Spengler BA, Ross RA. MicroRNAs define distinct human neuroblastoma cell phenotypes and regulate their differentiation and tumorigenicity. BMC Cancer. 2014; 14: 309.
9. Shah K. Mesenchymal stem cells engineered for cancer therapy. Adv Drug Deliv Rev. 2012; 64(8): 739-748.
10. Bianchi G, Morandi F, Cilli M, Daga A, Bocelli-Tyndall C, Gambini C, et al. Close interactions between mesenchymal stem cells and neuroblastoma cell lines lead to tumor growth inhibition. PLoS One. 2012; 7(10): e48654.
11. Sharif S, Ghahremani MH, Soleimani M. Delivery of exogenous miR-124 to glioblastoma multiform cells by Wharton's jelly mesenchymal stem cells decreases cell proliferation and migration, and confers chemosensitivity. Stem Cell Rev. 2018; 14(2): 236-246.
12. Gojanovich AD, Gimenez MC, Masone D, Rodriguez TM, Dewey RA, Delgui LR, et al. Human adipose-derived mesenchymal stem/stromal cells handling protocols. Lipid droplets and proteins double-staining. Front Cell Dev Biol. 2018; 6: 33.
13. Paul H, Reginato AJ, Schumacher HR. Alizarin red S staining as a screening test to detect calcium compounds in synovial fluid. Arthritis Rheum. 1983; 26(2): 191-200.
14. Koopman R, Schaart G, Hesselink MK. Optimisation of oil red O staining permits combination with immunofluorescence and automated quantification of lipids. Histochem Cell Biol. 2001; 116(1): 63-68.
15. Andres D, Keyser BM, Petrali J, Benton B, Hubbard KS, McNutt PM, et al. Morphological and functional differentiation in BE (2)-M17 human neuroblastoma cells by treatment with Trans-retinoic acid. BMC Neurosci. 2013; 14: 49.
16. Li Y, Shao G, Zhang M, Zhu F, Zhao B, He C, et al. miR-124 represses the mesenchymal features and suppresses metastasis in Ewing sarcoma. Oncotarget. 2017; 8(6): 10274-10286.
17. Momen-Heravi F, Balaj L, Alian S, Mantel PY, Halleck AE, Trachtenberg AJ, et al. Current methods for the isolation of extracellular vesicles. Biol Chem. 2013; 394(10): 1253-1262.
18. Hosseini S, Dehghani-Mohammadabadi M, Ghafarri Novin M, Haji Molla Hoseini M, Arefian E, Mohammadi Yeganeh S, et al. Toll-like receptor4 as a modulator of fertilization and subsequent pre-implantation development following in vitro maturation in mice. Am J Reprod Immunol. 2017; 78(5).
19. Greco SJ, Rameshwar P. Mesenchymal stem cells in drug/gene delivery: implications for cell therapy. Ther Deliv. 2012; 3(8): 997-

1004.
20. Park HJ, Shin JY, Lee BR, Kim HO, Lee PH. Mesenchymal stem cells augment neurogenesis in the subventricular zone and enhance differentiation of neural precursor cells into dopaminergic neurons in the substantia nigra of a parkinsonian model. Cell Transplant. 2012; 21(8): 1629-1640.
21. Mittelbrunn M, Gutiérrez-Vázquez C, Villarroya-Beltri C, González S, Sánchez-Cabo F, González MÁ, et al. Unidirectional transfer of microRNA-loaded exosomes from T cells to antigen-presenting cells. Nat Commun. 2011; 2: 282.
22. Sharif S, Ghahremani MH, Soleimani M. Induction of morphological and functional differentiation of human neuroblastoma cells by miR-124. J Biosci. 2017; 42(4): 555-563.
23. Peng Y, Croce CM. The role of MicroRNAs in human cancer. Signal Transduct Target Ther. 2016; 1: 15004.
24. Junn E, Mouradian MM. MicroRNAs in neurodegenerative disorders. Cell Cycle. 2010; 9(9): 1717-1721.
25. Mouradian MM. MicroRNAs in Parkinson's disease. Neurobiol Dis. 2012; 46(2): 279-284.
26. De Smaele E, Ferretti E, Gulino A. MicroRNAs as biomarkers for CNS cancer and other disorders Brain Res. 2010; 1338: 100-111.
27. Dominici M, Le Blanc K, Mueller I, Slaper-Cortenbach I, Marini F, Krause D, et al. Minimal criteria for defining multipotent mesenchymal stromal cells. The International Society for Cellular Therapy position statement. Cytotherapy. 2006; 8(4): 315-317.
28. Biancone L, Bruno S, Deregibus MC, Tetta C, Camussi G. Therapeutic potential of mesenchymal stem cell-derived microvesicles. Nephrol Dial Transplant. 2012; 27(8): 3037-3042.
29. Harraz MM, Dawson TM, Dawson VL. MicroRNAs in Parkinson's disease. J Chem Neuroanat. 2011; 42(2): 127-130.
30. Junn E, Mouradian MM. MicroRNAs in neurodegenerative diseases and their therapeutic potential. Pharmacol Ther. 2012; 133(2): 142-150.
31. Chulpanova DS, Kitaeva KV, Tazetdinova LG, James V, Rizvanov AA, Solovyeva VV. Application of mesenchymal stem cells for therapeutic agent delivery in anti-tumor treatment. Front Pharmacol. 2018; 9: 259.
32. Aleynik A, Gernavage KM, Mourad YSh, Sherman LS, Liu K, Gubenko YA, et al. Stem cell delivery of therapies for brain disorders. Clin Transl Med. 2014; 3: 24.
33. Kimura K, Kishida T, Wakao J, Tanaka T, Higashi M, Fumino S, et al. Tumor-homing effect of human mesenchymal stem cells in a TH-MYCN mouse model of neuroblastoma. J Pediatr Surg. 2016; 51(12): 2068-2073.
34. Melen GJ, Franco-Luzón L, Ruano D, González-Murillo Á, Alfranca A, Casco F, et al. Influence of carrier cells on the clinical outcome of children with neuroblastoma treated with high dose of oncolytic adenovirus delivered in mesenchymal stem cells. Cancer Lett. 2016; 371(2): 161-170.
35. Visvanathan J, Lee S, Lee B, Lee JW, Lee SK. The microRNA miR-124 antagonizes the anti-neural REST/SCP1 pathway during embryonic CNS development. Genes Dev. 2007; 21(7): 744-749.
36. Li KK, Pang JC, Ching AK, Wong CK, Kong X, Wang Y, et al. miR-124 is frequently down-regulated in medulloblastoma and is a negative regulator of SLC16A1. Hum Pathol. 2009; 40(9): 1234-1243.
37. Pierson J, Hostager B, Fan R, Vibhakar R. Regulation of cyclin dependent kinase 6 by microRNA 124 in medulloblastoma. J Neurooncol. 2008; 90(1): 1-7
38. Matushansky I, Radparvar F, Skoultchi AI. CDK6 blocks differentiation: coupling cell proliferation to the block to differentiation in leukemic cells. Oncogene. 2003; 22(27): 4143-4149.
39. Hardy SA, Maltman DJ, Przyborski SA. Mesenchymal stem cells as mediators of neural differentiation. Curr Stem Cell Res Ther. 2008; 3(1): 43-52.
40. Vishnubhatla I, Corteling R, Stevanato L, Hicks C, Sinden J. The development of stem cell-derived exosomes as a cell-free regenerative medicine. J Circ Biomark. 2014; 3: 1-14.

Original Article

Astaxanthin Reduces Demyelination and Oligodendrocytes Death in A Rat Model of Multiple Sclerosis

Alireza Lotfi, M.Sc., Mitra Soleimani, Ph.D., Nazem Ghasemi, Ph.D.*

Department of Anatomical Sciences, School of Medicine, Isfahan University of Medical Sciences, Isfahan, Iran

Corresponding Address: Department of Anatomical Sciences, School of Medicine, Isfahan University of Medical Sciences, Isfahan, Iran
Email: n_ghasemi@med.mui.ac.ir

Received: 8/June/2019, Accepted: 3/August/2019

Abstract

Objective: Astaxanthin (AST) is a carotenoid with anti-oxidative, anti-inflammatory, and anti-apoptotic properties. It has also been reported that AST exerts protective effects against neurodegenerative diseases and reduces oxidative stress-induced the central nervous system (CNS) injury. In this study, we aimed to evaluate the protective potential of AST in inhibiting demyelination and oligodendrocyte death in a rat model of multiple sclerosis (MS).

Materials and Methods: In this experimental study, forty Wistar rats were randomly assigned to four experimental groups: control group (with normal feeding), cuprizone (CPZ group) that daily received 0.6% CPZ for 4 weeks, sham group that daily received 0.6% CPZ plus dimethyl sulfoxid (DMSO) for 4 weeks, and AST group that daily received 0.6% CPZ and after 12 hours were treated with AST (3 mg/kg), for 4 weeks. Muscle strength was evaluated by the behavioral basket test at the end of every week for 4 weeks. Luxol Fast Blue (LFB) staining was utilized for the identification of myelination and demyelination. Myelin density was evaluated by the ImageJ software. The expression of A2B5 (oligodendrocyte precursor protein) and myelin oligodendrocyte protein (MOG) were assessed by immunohistochemistry (IHC) and the expression of myelin basic protein (*MBP*), *MOG,* and platelet-derived growth factor-alpha (*PDGFR-α*) genes was examined by the real-time polymerase chain reaction (RT-PCR) technique.

Results: The administration of AST reduced the oligodendrocyte damage and myelin sheath disruption in a rat model of MS. The basket behavioral test showed the improvement of muscle strength in the AST group compared with CPZ and sham groups. Besides, the results of real-time PCR and IHC indicated the beneficial effects of AST in declining demyelination and oligodendrocyte death in a rat model of MS.

Conclusion: AST reduces damages to the myelin sheath and oligodendrocyte death in a rat model of MS.

Keywords: Astaxanthin, Cuprizone, Multiple Sclerosis, Oligodendrocyte

Cell Journal(Yakhteh), Vol 22, No 4, January-March (Winter) 2021, Pages: 565-571

Citation: **Lotfi A, Soleimani M, Ghasemi N. Astaxanthin reduces demyelination and oligodendrocytes death in a rat model of multiple sclerosis. Cell J. 2021; 22(4): 565-571. doi: 10.22074/cellj.2021.6999.**

Introduction

Neurodegeneration is a feature of several debilitating and progressive disorders characterized by chronic loss of neurons in the nervous system. Demyelination is one of the most important causes of neurological disability (1, 2). Multiple sclerosis (MS) is a chronic inflammatory disease characterized primarily by demyelination and progressive neurodegeneration in the central nervous system (CNS). Oligodendrocyte death due to focal immune cell infiltration is the primary cause of demyelination and has an important role in the pathogenesis of MS (3). Hence, the prevention of oligodendrocyte death by the use of natural compounds, such as curcumin (4) and AST may decrease the adverse complications developed in demyelinating disorders.

AST (3, 3'-dihydroxy-ß, ß'-carotene-4, 4'-dione) is a natural red fat-soluble xanthophyll carotenoid produced by marine microorganisms, gaining considerable attention by researchers in recent years. Studies examined the protective properties of AST indicate that its protective roles are due to three main effects: anti-oxidative, anti-inflammation, and anti-apoptotic effects. It has been reported that AST has anti-oxidative properties ten times more than some carotenoids, such as lutein, canthaxanthin, and zeaxanthin, as well as a hundred times more than vitamin E (5).

In addition, other experiments demonstrated that AST has a protective impact against primary brain damages, as well as the destruction of neurons and blood-brain barrier (BBB) disruption, cerebral edema, and impaired nerve function through suppressing brain inflammation (6).

Additional works also demonstrated other effects of AST, including anti-lipid peroxidation and anticancer activity (7, 8).

These protective properties mostly pertain to the unique chemical structure of AST, the presence of hydroxyl and keto moieties on each ion ring. This unique nature confers the ability to AST to be esterified, posing a higher antioxidant activity and a more polar nature than other carotenoids (9). Neuroprotective properties of AST have been evaluated in animal models, and its protective roles have been addressed

by several research groups (5, 10-13). Some parts of these beneficial roles are attributed to the ability of AST in crossing the BBB (10).

Utilizing animal models of neurodegenerative diseases has been enhancing the knowledge of molecular pathogenesis which is responsible for the onset and development of MS and other potentially disabling neurodegenerative disorders (14). Among different protocols that have been introduced for producing an animal model of MS, CPZ is the well-stablished one to study demyelination and remyelination in rodent models of MS (15).

In this study, we designed an experiment to assess the impact of AST in the amelioration or prevention of demyelination in a rat model of MS.

Materials and Methods

Ethics statement

This experimental study was performed at the Isfahan University of Medical Sciences (Isfahan, Iran). All experimental procedures were conducted in compliance with the guidelines of the Iranian Committee of Animal care and approved by the Ethics Committee of Isfahan University of Medical Sciences (Ethics#IR.MUI.MED.REC.1398.037).

Animals

Forty male Wistar rats, weighing 150-200 g, were purchased from the Royan Institute, Isfahan, Iran. Rats were housed for seven days, before the start of the experiment, in constant environmental conditions, at a temperature of 22 ± 2˚C with free access to food and water and a 12:12 light/dark cycle.

Behavioral test

The Basket behavioral test evaluates motor coordination and sensorimotor deficits in rodent models of CNS disorders (4). For this purpose, rats were placed in the center of a rectangular basket (60 cm in length and 50 in width), and then the basket was overturned and the delay in dropping rats from the ceiling of the basket was determined over 180 seconds, and eventually the mean of these times (seconds) were recorded. The experiment was conducted triplicate.

Production of a rat model of multiple sclerosis

Animals were randomly divided into four groups. The number of rats per group was determined by ten rats, by means of the power analysis calculations. To produce a rat model of MS, the CPZ suspension was prepared by the use of CPZ powder (Sigma-Aldrich, USA) and 1% methylcellulose (Sigma-Aldrich, USA). To prepare AST (Sigma-Aldrich, USA), AST powder were dissolved in dimethyl sulfoxid (DMSO, Gibco, USA) to reach a homogenous solution. Rats were fed as planned per group. The control group was fed with normal chow for four weeks. The CPZ group was treated with 2 ml CPZ (0.6%), by gavage, daily for 4 weeks (16). The sham group was first treated with 2 ml CPZ (0.6%) and after 12 hours treated with 2 ml DMSO, by gavage, daily for 4 weeks (this was done to reject any possibility of repairmen effects of DMSO as the solvent of AST). The AST group first received CPZ 0.6% and after 12 hours received 2 ml AST (3 mg/kg/day) (17), daily for 4 weeks. Animals in all groups were weighed 3 times per week during chemical administrations until they were sacrificed. Tissue samples from all groups were processed at the same time within the same experiment.

Craniotomy and dissection of the corpus callosum

Animals were sacrificed by performing deep anesthesia using ketamine/xylazine (100/10 mg/kg, Sigma-Aldrich, Germany) and decapitated. The brains were removed by craniotomy of the vertex, weighed precisely and then immersed in the fixative solution of formaldehyde and formalin (10%, Sigma-Aldrich, USA) for more than 24 hours. After washing with a 0.1 M phosphate buffer (Sigma-Aldrich, USA), the brains were sectioned at the coronal plane and using its natural cleavage plane, the corpus callosum identified and dissected, removing samples of the mid-body. After tissue processing, the blocks were cut in sections of 5- and 6-µm of thickness, and these sections were used for Luxol Fast Blue (LFB) staining and immunohistochemistry technique.

Immunohistochemistry

After tissue processing by use of ethanol, xylene and paraffin (Asia Pajohesh, Iran), serial sections (5-µm thick) of the brain samples were prepared using a microtome. After de-paraffinization and rehydration, the slices were pre-treated using the method of heat-induced epitope retrieval with sodium citrate buffer (pH=6) and 1 mM EDTA buffer (pH=8) (Gibco, USA) for 20 minutes, washed-out three times with PBS (Gibco, USA). Then, the slices were incubated with special antibodies against A2B5, a marker of oligodendrocyte precursor cells (Abcam, USA) and MOG, a myelin oligodendrocyte glycoprotein (Abcam, USA), and then washed-out with PBS. Then, goat anti-mouse -FITC (2 µg/ml, Abcam, USA) and rabbit anti-goat-FITC (Sigma-Aldrich, USA) were used as the secondary antibody at room temperature for 1 hour. Finally, nuclear counterstaining was conducted using 4, 6 Diamino-2-phenylindole, dilactate (DAPI) and in order to quantitative analysis, the total numbers of positive cells were counted in a minimum total of 200 cells per slide in six sections per sample using fluorescence microscope (Olympus bx51, Japan). Meanwhile, all IHC analyses were repeated at least three times.

Luxol Fast Blue staining

After deep anesthesia, perfusion fixation was done by use of cold PBS and 4% paraformaldehyde. In the following, corpus callosum dissection was performed, and in order to post-fixation, formalin solution (10%) was used at 4˚C overnight. Subsequently, paraffin slices (6 µm) were prepared. Then sections were dewaxed and cleared in 100% and 95% ethanol and then were stained in a solution of LFB (0.1% w/v, Sigma-Aldrich, USA), 10% acetic acid and ethanol (95%, Asia Pajohesh, Iran) overnight at 56˚C. Sections then were differentiated by rinsing in 95 % ethanol, 0.05% lithium chloride solution (Asia Pajohesh, Iran) followed by 70 % ethanol. Differentiation continued in distilled water until unmyelinated tissue appeared white (18).

Gene expression analysis

In order to evaluate gene expression, real-time polymerase chain reaction (RT-PCR) analysis of *MOG*, *MBP*, and *PDGFR-α* was performed according to the SYBR Green master mix protocol. According to our previous study, Total RNA was extracted from the brain corpus callosum by using RNeasy micro kit (Qiagen, GmBH, Germany) and then, 2 µg of RNA was used for cDNA synthesis using RevertAid First Strand cDNA Synthesis Kit (Fermentas, Germany) (19). Finally, quantitative real-time PCR was done using Thermal Cycler Rotor-Gene in a total volume of 20 µl containing Power SYBR Green master mix (2x), forward and reverse Primers (0.5 µM), cDNA (30 ng/µl) and H_2O with the following cycling conditions: 1 cycle of denaturation (95˚C for 5 minutes) which followed by a 40 cycle amplification (at 95˚C for 15 seconds) and the extension cycle (at 60˚C for 40 seconds). The primer sequences used for RT-PCR analysis in this study are listed in Table 1.

Table 1: Primer sequences

Gene primers	Primer sequence (5′-3′)
PDGFR-α	F: tccagtcactgtgctgcttc
	R: gcaagggaaaagggagtctt
MOG	F: gaggttctcggatgaaggag
	R: cagggttgatccagtagaagg
MBP	F: tcacagaagagaccctcacag
	R: ggtgtacgaggtgtcacaatg
GAPDH	F: tgcaccaccaactgcttagc
	R: ggcatggactgtggtcatgag

Data analysis

Immunohistochemistry, behavior test, RT-PCR, and LFB results were analyzed using the SPSS software version 25.0 (SPSS Inc., Chicago, IL, USA). One-way ANOVA was conducted, followed by Tukey's post hoc test. In addition, all data were shown as mean ± standard error of the mean (mean ± SEM).

Results

Basket behavior test

The basket behavioral test was performed at the end of every week for a total of 4 weeks. During this study, the comparison of behavioral results demonstrated that the use of AST increases the average latency to fall compared to sham and CPZ groups. Unlike the AST group, in CPZ and sham groups, the average latency to fall was decreased significantly from the first week ($P \leq 0.05$, Fig.1).

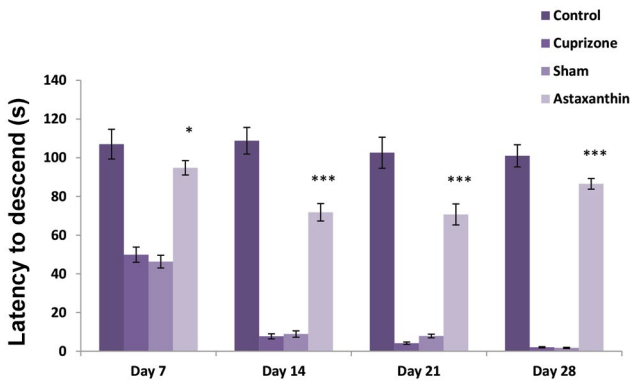

Fig.1: The comparison of latency to fall in different groups. In the Cuprizone and sham groups, the average latency to fall was decreased significantly from the first week in comparison with the Astaxanthin group (P<0.05). *; P<0.05 and ***; P<0.001.

Histological observation of cuprizone-induced demyelination in rats

LFB staining of coronal sections of corpus callosum observed under ×40 magnification. Myelinated axons were stained blue. Achievement of MS induction in rat models was confirmed by prominent demyelination in CPZ group and vehicle group. While the control group represented blue colored bands indicating the presence of myelinated axons (Fig.1). In the AST group, majority of axons stained blue, while few axons were stained pink, confirming the inhibitory effects of AST in demyelination.

Moreover, calculating the myelin density by the ImageJ software, revealed that the myelin density of corpus callosum in tissue sections of the AST group was significantly higher than that of CPZ and sham groups (Fig.2).

Immunohistochemistry

IHC results indicated that the mean percentage of positive cells for MOG and A2B5 proteins were significantly higher in the AST group compared with the CPZ group, 56 ± 2.7 and 59.7 ± 5.2, respectively (Figs.3, 4).

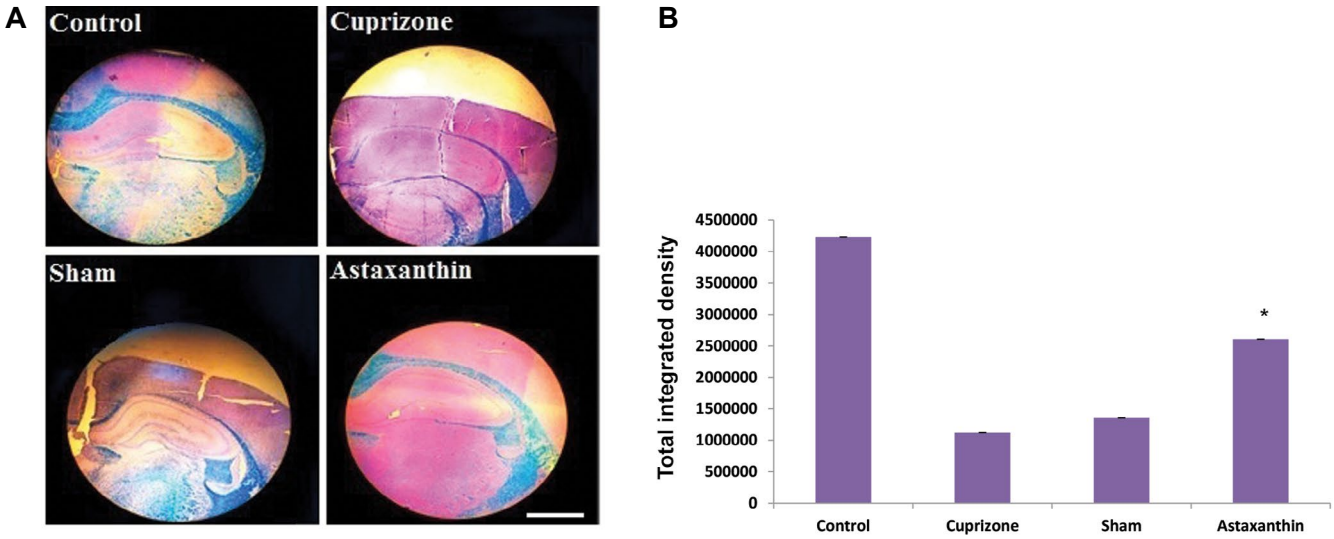

Fig.2: Illustration of LFB in coronal sections of the brain of Wistar rats to assess myelin status, after treatment with CPZ. **A.** The blue colured region indicates the presence of myelin. In the control group, a distinct delineated pattern of areas without (pink) and with stained myelin (blue) is observable. In CPZ and sham groups, there is a significant reduction in the myelin contents in the corpus callusom, indicated by an asterisk. In the AST group, induced with CPZ and treated with AST, a sharply delineated pattern is identifiable. **B.** The total integrated density of myelin calculated by ImageJ software (scale bar: 200 µm). LFB; Luxol Fast Blue, CPZ; Cuprizone, AST; Astaxanthin, and *; P<0.05.

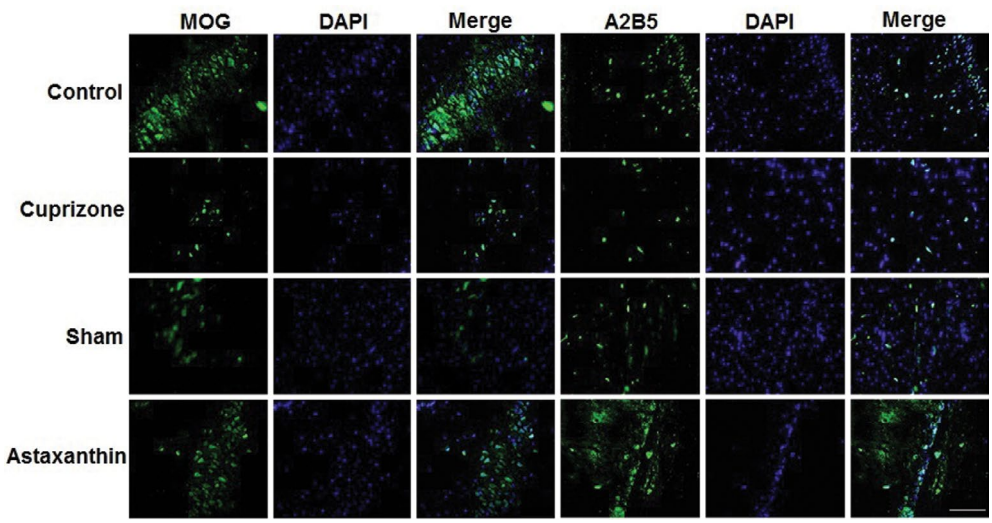

Fig.3: MOG and A2B5 stained of the corpus callosum in control, Cuprizone, sham, and Astaxanthin groups. The statistical analysis of MOG and A2B5 staining according to the relative optical density. The presence of MOG-positive cells (green) and A2B5 positive cells (green) were significantly higher in Astaxanthin group as compared to Cuprizone and sham groups. Astaxanthin alleviated demyelination in Cuprizone-induced rat corpus callosum (scale bar: 200 µm).

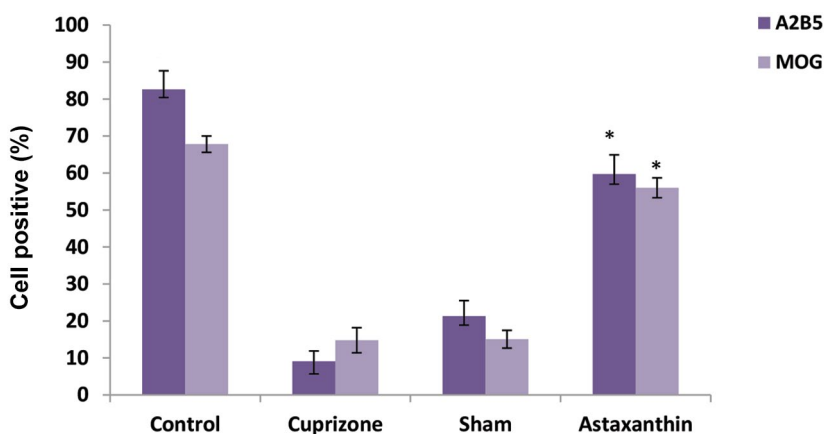

Fig.4: The comparison of A2B5 and MOG expression in all experimental groups. In the Astaxanthin group, the mean percentage of cells which express A2B5 and MBP markers was statistically significant in comparison with Cuprizone and sham groups (P<0.05). *; P<0.05.

Gene expression analysis

Real-time PCR results of gene expression analysis in four experimental groups indicated that mRNA expression of the *MOG*, *MBP*, and *PDGFR-α* genes were higher in AST group compared to CPZ group and the sham group that represented similar expression pattern for these genes (Fig.5).

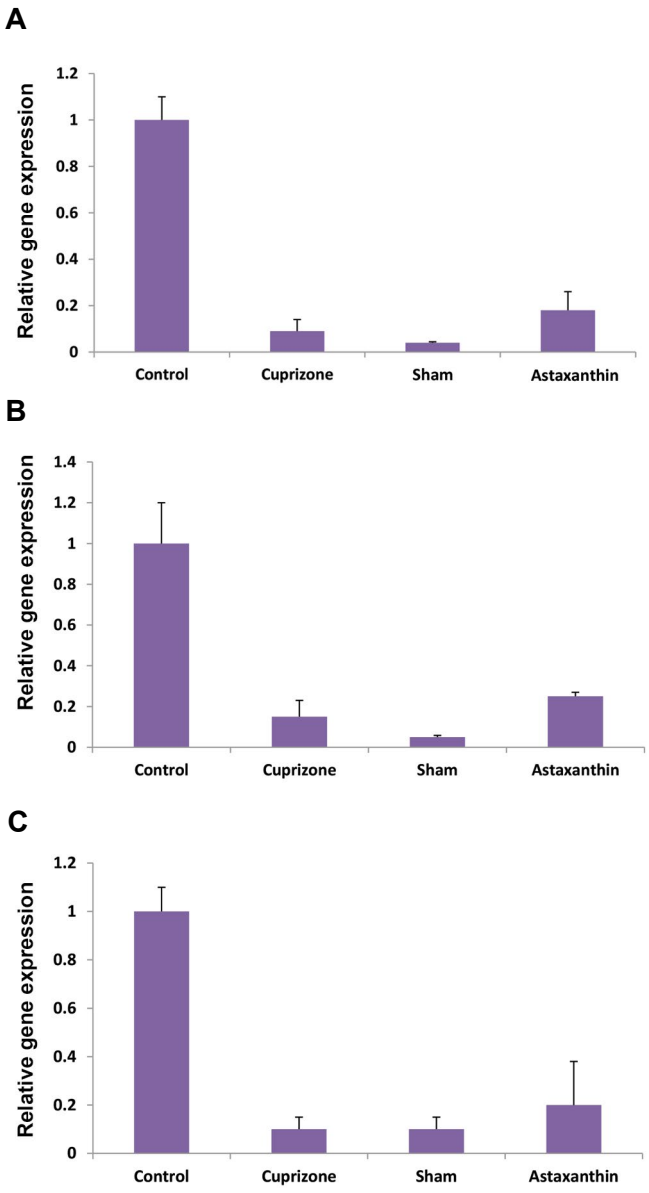

Fig.5: Comparative analysis of *MBP*, *MOG* and *PDGFR-α* markers in different groups. The relative expression levels of **A.** *MBP*, **B.** *MOG*, and **C.** *PDGFR*-α genes that were evaluated by the real-time polymerase chain reaction. The expression of all three genes increased significantly in the Astaxanthin group compared to Cuprizone and sham groups.

Discussion

We concluded that consumption of AST modulated demyelination and oligodendrocyte death as well as muscle weakness in CPZ-induced rat model of MS. MS is a chronic inflammatory CNS disease leading to primary demyelination is featured with focal plaques (20). Some natural products already have been suggested to contribute to the alleviation of demyelination in demyelinating diseases (21). However, the mechanism of their effects rarely confirmed scientifically. AST is a natural product of aquatic microorganisms that recently has gained strong attention from medical and life science research (5). It is a lipophilic terpene and a metabolite of zeaxanthin. The presence of the hydroxyl and keto moieties on each ionone ring explains some of its unique features, namely, the ability to be esterified, higher antioxidant activity and a more polar nature than other carotenoids and so, AST is considered as a suitable multi-target pharmacological agent (9, 22). Due to its unique chemical structure, AST can cross the BBB (23). This property has conferred AST particular attention in research implementing in the realm of neurodegenerative disorders. Moreover, since the late onset of extensive neuronal death in neurodegenerative diseases is related to oxidative damage, and due to proven anti-oxidative effects of AST (11), CNS is considered one of its key target organs and has been as particular interest as co-treatments in neurodegenerative diseases. Therefore, in the present study, in order to investigate the neuroprotective effects of AST, the composition of the CPZ was used for induce a toxic model of MS and finally, the laboratory tests were performed on brain tissue.

CPZ (oxalic acid bis-cyclohexylidene hydrazide), is a copper chelator that induces highly reproducible demyelination in the CNS and extensively used to create a model of demyelinating disease (24). By the third week of CPZ treatment, consistent demyelination can be observed in the corpus callosum, the largest white matter tract in the rodent brain (25). So, in order to induce MS in rats, we treated male Wistar rats with 0.6% CPZ, daily for four weeks.

LFB stained sections displayed corpus callosum with defined borders of the corpus callosum, and there was a sharply delineated differentiation between white (blue) and gray matter (pink) in the control group. However, in CPZ-induced groups, CPZ and Sham, the myelin density, evaluated with the ImageJ software was shrunk, and no defined borders were observable in the stained samples. Four weeks after treatment with AST, the sections of LFB staining represented a corpus callosum that was significantly well- delineated and with cohesive texture compared to the shrunk texture were seen in CPZ group and Sham group. In justifying this result, it can be said that AST due to cross the BBB is able to carry out its neuroprotective effects at high levels and thus prevent myelin destruction. Another relevant finding of the current study was that AST is able to induce a significant delay in climbing down the basket wire wall in comparison to CPZ and sham groups. This result is consistent with a recent study which has also shown that AST can improve sensory-motor function through modulating specific cell signaling pathways in a rat model of spinal cord injury (26). For justifying this outcome, it can be said that AST is capable of improving the neural dysfunction, caused by CPZ by preventing demyelination and increasing the transmission of neural impulses. Finally,

we evaluated the influences of CPZ and AST on oligodendrocytes. Progenitor cells of oligodendrocytes are widely scattered in CNS and are a constant reservoir for oligodendrocyte replacement and remodeling. To detect impairment effects of CPZ, and repairment influences of AST on rat model of MS, we stained corpus callosum section, in all our four groups, with two oligodendrocyte proteins, MOG and A2B5. MOG, myelin oligodendrocyte glycoprotein, expressed on the outer membrane of myelin sheath and oligodendrocytes, and exclusively found within the CNS. Giving the late commencement of MOG expression in myelination, it is believed that MOG plays a role in the maintenance of the myelin sheath and may serve as a potential marker in oligodendrocyte maturation. Therefore, MOG could potentially function as a cell surface marker of matured oligodendrocytes (27). During OPC differentiation, cells sequentially express A2B5, PDGFR-α, and MBP (28). Our stained sections of corpus callosum for MOG and A2B5 represented significant positive staining for both antibodies in the AST group than CPZ and sham groups. This may underpin the ameliorative effects of AST on oligodendrocyte death or even its oligodendrogenic effects. To confirm the obtained IHC results, we assessed the real-time PCR expression of *MOG*, *MBP*, and *PDGFR-α* genes in the corpus callosum in all groups. The results demonstrated that the expression of all three genes decreased significantly in CPZ and sham groups than the control group, indicating the destructive effects of CPZ in a rat model of MS.

Moreover, the expression of all three genes was higher in AST group compared to the CPZ and sham groups. This may represent that AST due to its antioxidant and neuroprotective effects, is capable of preventing the death of oligodendrocytes which induced by CPZ. Besides, since MOG and PDGFR-α have a sequential expression pattern in oligodendrocyte maturation, it could be suggested that AST may infuse oligodendrogenesis from progenitors to mature oligodendrocytes.

Conclusion

AST may reduce demyelination and oligodendrocyte death in MS rat model. Either AST stimulates the proliferation of oligodendrocytes, or it prohibits death of pre-existing oligodendrocyte is an issue to be confirmed.

Acknowledgements

This research financially supported by the research center of Isfahan University of Medical Sciences. The authors have no conflict of interest.

Authors' Contributions

A.L., M.S., N.Gh.; Participated in study design, data collection, evaluation, and statistical analysis. All authors performed editing and approving the final version of this manuscript for submission, also participated in the finalization of the manuscript and approved the final draft.

References

1. Gao HM, Hong JS. Why neurodegenerative diseases are progressive: uncontrolled inflammation drives disease progression. Trends Immunol. 2008; 29(8): 357-365.
2. Gitler AD, Dhillon P, Shorter J. Neurodegenerative disease: models, mechanisms, and a new hope. Dis Model Mech. 2017; 10(5): 499-502.
3. Haider L, Zrzavy T, Hametner S, Höftberger R, Bagnato F, Grabner G, et al. The topograpy of demyelination and neurodegeneration in the multiple sclerosis brain. Brain. 2016; 139(Pt 3): 807-815.
4. Bagheri E, Marandi SM, Ghasemi N. Evaluation of curcumin effects on improvement of muscle strength, prevention of oligodendrocytes and myelin damage in brain, in an animal model of multiple sclersosis (MS). Scientific Journal of Kurdistan University of Medical Sciences. 2018; 23(5): 55-64.
5. Chen X, Chen R, Guo Z, Li C, Li P. The preparation and stability of the inclusion complex of astaxanthin with ß-cyclodextrin. Food Chem. 2007; 101(4): 1580-1584.
6. Zhang XS, Zhang X, Wu Q, Li W, Wang CX, Xie GB, et al. Astaxanthin offers neuroprotection and reduces neuroinflammation in experimental subarachnoid hemorrhage. J Surg Res. 2014; 192(1): 206-213.
7. Kamath BS, Srikanta BM, Dharmesh SM, Sarada R, Ravishankar GA. Ulcer preventive and antioxidative properties of astaxanthin from Haematococcus pluvialis. Eur J Pharmacol. 2008; 590(1-3): 387-395.
8. Fathi E, Farahzadi R, Charoudeh HN. L-carnitine contributes to enhancement of neurogenesis from mesenchymal stem cells through Wnt/β-catenin and PKA pathway. Exp Biol Med (Maywood). 2017; 242(5): 482-486.
9. Ekpe L, Inaku K, Ekpe V. Antioxidant effects of astaxanthin in various diseases-a review. J Mol Pathophysiol. 2018;7(1): 1-6.
10. Speranza L, Pesce M, Patruno A, Franceschelli S, de Lutiis MA, Grilli A, et al. Astaxanthin treatment reduced oxidative induced pro-inflammatory cytokines secretion in U937: SHP-1 as a novel biological target. Mar Drugs. 2012; 10(4): 890-899.
11. Grimmig B, Daly L, Subbarayan M, Hudson C, Williamson R, Nash K, et al. Astaxanthin is neuroprotective in an aged mouse model of Parkinson's disease. Oncotarget. 2018; 9(12): 10388-10401.
12. Grimmig B, Kim SH, Nash K, Bickford PC, Shytle RD. Neuroprotective mechanisms of astaxanthin: a potential therapeutic role in preserving cognitive function in age and neurodegeneration. Geroscience. 2017; 39(1): 19-32.
13. Wu H, Niu H, Shao A, Wu C, Dixon BJ, Zhang J, et al. Astaxanthin as a potential neuroprotective agent for neurological diseases. Mar Drugs. 2015; 13(9): 5750-5766.
14. Mix E, Meyer-Rienecker H, Zettl UK. Animal models of multiple sclerosis for the development and validation of novel therapies–potential and limitations. J Neurol. 2008; 255 Suppl 6: 7-14.
15. Silvestroff L, Bartucci S, Pasquini J, Franco P. Cuprizone-induced demyelination in the rat cerebral cortex and thyroid hormone effects on cortical remyelination. Exp Neurol. 2012; 235(1): 357-367.
16. Adamo AM, Paez PM, Escobar Cabrera OE, Wolfson M, Franco PG, Pasquini JM, et al. Remyelination after cuprizone-induced demyelination in the rat is stimulated by apotransferrin. Exp Neurol. 2006; 198(2): 519-529.
17. Mehani RS, Yadav V. Effect of Astaxanthin in animal models of anxiety and depression. Int J Pharm Bio Sci. 2014; 5(2): 12-18.
18. Ek CJ, Habgood MD, Dennis R, Dziegielewska KM, Mallard C, Wheaton B, et al. Pathological changes in the white matter after spinal contusion injury in the rat. PLoS One. 2012; 7(8): e43484.
19. Ghasemi N. The evaluation of astaxanthin effects on differentiation of human adipose derived stem cells into oligodendrocyte precursor cells. Avicenna J Med Biotechnol. 2018; 10(2): 69-74.
20. Popescu BF, Pirko I, Lucchinetti CF. Pathology of multiple sclerosis: where do we stand? Continuum (Minneap Minn). 2013; 19(4 Multiple Sclerosis): 901-921.

21. Yadav V, Shinto L, Bourdette D. Complementary and alternative medicine for the treatment of multiple sclerosis. Expert Rev Clin Immunol. 2010; 6(3): 381-395.
22. Fakhri S, Abbaszadeh F, Dargahi L, Jorjani M. Astaxanthin: a mechanistic review on its biological activities and health benefits. Pharmacol Res. 2018; 136: 1-20.
23. Galasso C, Orefice I, Pellone P, Cirino P, Miele R, Ianora A, et al. On the neuroprotective role of astaxanthin: new perspectives? Mar Drugs. 2018; 16(8). pii: E247.
24. Zhen W, Liu A, Lu J, Zhang W, Tattersall D, Wang J. An alternative cuprizone-induced demyelination and remyelination mouse model. ASN Neuro. 2017; 9(4): 1759091417725174.
25. Stidworthy MF, Genoud S, Suter U, Mantei N, Franklin RJ. Quantifying the early stages of remyelination following cuprizone-induced demyelination. Brain Pathol. 2003; 13(3): 329-339.
26. Fakhri S, Dargahi L, Abbaszadeh F, Jorjani M. Effects of astaxanthin on sensory-motor function in a compression model of spinal cord injury: involvement of ERK and AKT signalling pathway. Eur J Pain. 2019; 23(4): 750-764.
27. Ramya L. Role of N-glycan in the structural changes of myelin oligodendrocyte glycoprotein and its complex with an antibody. J Biomol Struct Dyn. 2019: 1-10.
28. Ma Z, Cao Q ,Zhang L, Hu J, Howard RM, Lu P, et al. Oligodendrocyte precursor cells differentially expressing Nogo-A but not MAG are more permissive to neurite outgrowth than mature oligodendrocytes. Exp Neurol. 2009; 217(1): 184-196.

Hardy Weinberg Equilibrium Disturbances in Case-Control Studies Lead to Non-Conclusive Results

Jose Luis Royo, Ph.D.

Department of Surgery, Biochemisty and Immunology, School of Medicine, University of Malaga, Boulevar Louis Pasteur s/n, Málaga, Spain

Corresponding Address: Department of Surgery, Biochemisty and Immunology, School of Medicine, University of Malaga, Boulevar Louis Pasteur s/n, Málaga, Spain
Email: jlroyo@uma.es

Received: 1/October/2019, Accepted: 30/November/2019

Abstract

Recently, it has been proposed the association of a common deletion affecting toll-like receptor 2 promoter (-196 to -177) to type 2 diabetes mellitus risk. However, genotyping results show a significant deviation from the Hardy-Weinberg Equilibrium (HWE). The law of Hardy-Weinberg shows that for an autosomal biallelic marker with allele frequencies f_A=p and f_a=q, the proportion of subjects with genotypes AA, Aa, and aa should follow the following: $f_{AA}=p^2$, $f_{Aa}=2pq$, and $f_{aa}=q^2$. Departure from HWE or Hardy-Weinberg Disequilibrium (HWD) in a human control population can be caused by natural factors such as selective pressure against a certain genotype. However their prevalence is scarce and magnitude of effect over the HWE are small. Other factors such as inbreeding caused by consanguinity, population stratification, or technical problems in genotyping are more usual. Nevertheless, if the control population follows a perfect HWE, the presence HWD among patients might be explained by the genetic association and evidencing a real link between the locus and the trait under study. However, HWD affecting both cases and controls, such as the one reported might be explained by one of the aforementioned issues.

Cell Journal(Yakhteh), Vol 22, No 4, January-March (Winter) 2021, Pages: 572-574

Citation: Royo JL. Hardy weinberg equilibrium disturbances in case-control studies lead to non-conclusive results. Cell J. 2021; 22(4): 575-574. doi: 10.22074/cellj.2021.7195.

Genetic case-control studies have been proven as a powerful strategy to decipher the biochemical pathways underlying complex diseases. The basis of this approach is to find whether patients share an ancestral haplotype harboring either a common risk factor or directly a causative mutation. This implies sharing a determined genotype due to the fact of being patients (identical by state) rather than being relatives (identical by descent). Geneticists determine the genotypes and then compare allele frequencies in unrelated patients and control series. Whenever the mutant allele is in linkage disequilibrium with the causative mutation, we observe a statistically significant increase on its allele frequency among cases. However, independent of the allele frequency and the locus under analysis, any genetic marker mapping the autosomal chromosome shall follow the Hardy-Weinberg Equilibrium (HWE) (1, 2). This apparently simple rule states that for a biallelic locus with frequencies p and q respectively, genotypic frequencies must follow the p^2, 2pq and q^2. Disturbances of the Hardy-Weinberg Equilibrium (HWD) occur when natural selection operates over a particular genotype giving a differential fitness to any of them, such in the case of the hemoglobin (Hb) locus, associated to sickle cell anemia and resistance to *Plasmodium falciparum* infection (3). However, these cases arescarce in the literature, and large series are required to find statistically significant results. More often, HWD evidences population stratification. If a study series comprises subjects with different genetic background differing in their allele frequencies, their mix would exhibit a HWD. This is the called Wahlund effect and happens when each population, independently, fit HWE (4). Alternatively, HWD might be due to the existence of inbreeding in the series. This is evidenced by a reduction of the heterozygosity within a population (5). Finally, the HWD might be consequence of genotyping problems. A cross contamination typically pops up due to an excess of heterozygotes, while a reduced sensitivity of the mutant allele results in a lower mutant homozygotes frequency. Alternatively, the inclusion of duplicates in the genotyping series might also be associated to HWD.

Recently, Ermiş Karaali et al. (6) studied the role of a common Toll-like receptor 2 promoter deletion (-196 to -177) in type 2 diabetes risk (T2DM). The rational underlying work roots on the contrasted role of TLR2 on human innate immunity. They performed a case-control study determining the presence of this promoter deletion among 100 cases and 98 age-matched controls, and concluded that the deletion allele was associated to T2DM risk. However, this conclusion should betaken with caution. Both cases and controls show a remarkable HWD (X^2 $P=4.99\times10^{-8}$ and 1.4×10^{-4} for cases and controls, respectively). The nature of this HWD relies on an underrepresentation of heterozygotes in both cases and controls that can be illustrated in the De Finetti diagram (Fig.1). The observed heterozygotes among controls only represent 61% from what expected according to HWE (3 vs. 4.87) and this effect was more accused within the

T2DM series with only 45.5% from what expected (14 vs. 30.78). Therefore inbreeding coefficient estimates range between F=0.545 and F=0.384 (cases and controls, respectively). *TLR2* -196 to -177 has been extensively determined in different studies with no evident HWD and, whenever reported, this was constrained to cases (Table 1). It has been recently reported that besides using the information from 2,405 subjects available from the 1,000-genome project release 3, no HWD is found for control populations of Europe, Africa, Asia or America at this locus (7). This suggests that Ermiş Karaali et al. (6) might have fallen in at least one of the aforementioned problems associated to HWD. It should be highlighted that we cannot rule out the possibility that functional variants affecting TLR2 physiology might be associated to T2DM. However, this potential role of *TLR2* -196 to -177 deletion shall be repeated following the adequate controls in order to determine its potential implication in T2DM risk.

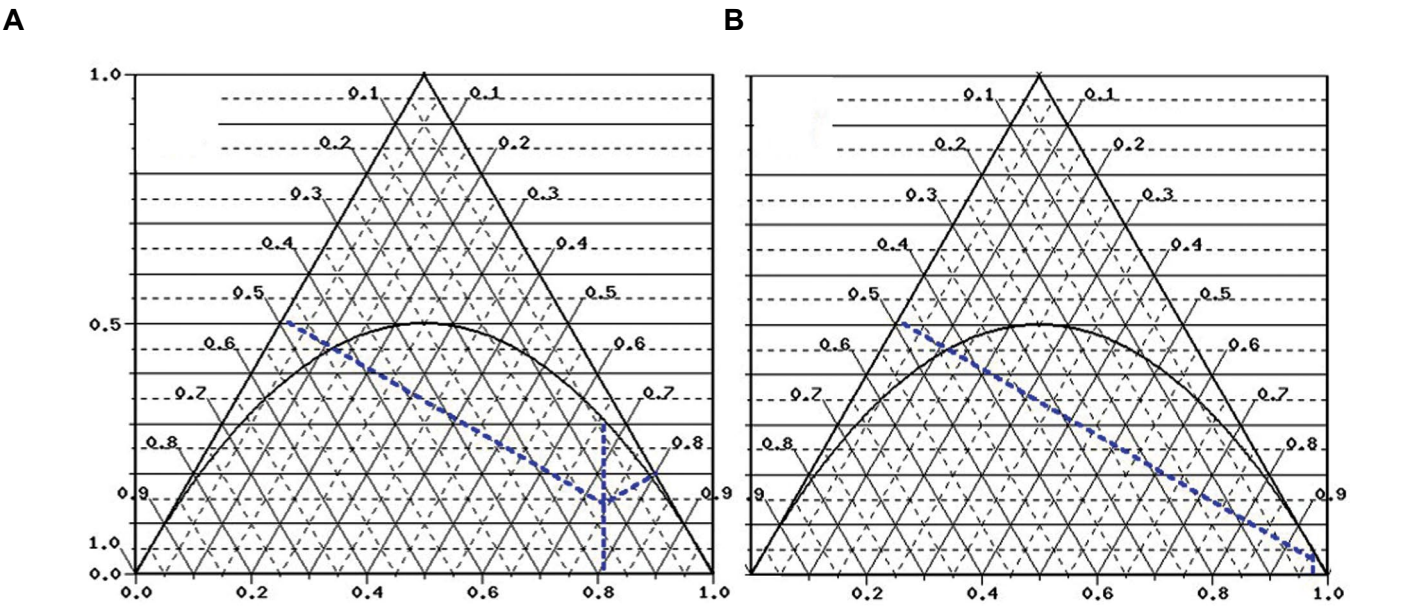

Fig.1: De Finetti representation of Ermiş Karaali et al. (6) results of TLR2 -196 to -177 variant on T2DM risk. De Finetti representation (8) of **A.** Both cases and **B.** Controls from Ermiş Karaali et al. (6). The X-axis represents the frequency of the Ins allele. The intersection of the parabola and vertical line represents the frequency of genotype Ins/Del under f Hardy-Weinberg Equilibrium.

Table 1: HWE was assayed using the freely available resource at https://ihg.gsf.de/cgi-bin/hw/hwa2.pl from the University of Munich. P values were calculated using Pearson's goodness-of-fit chi-square with one degree of freedom

Disease	Subjects	Ins/Ins	Ins/Del	Del/Del	MAF	HWE P value	Country	Reference
T2DM	Controls	94	3	1	0.03	1.42×10^{-4}	Turkey	(6)
	Cases	74	14	12	0.19	4.99×10^{-8}		
Parkinson's disease	Controls	95	21	2	0.11	0.511	Greece	(9)
	Cases	156	52	7	0.15	0.309		
VIH susceptibility	Controls	189	65	3	0.14	0.318	Spain	(7)
	Cases	160	18	0	0.05	0.477		
General population	Controls	208	85	11	0.18	0.531	Poland	(10)
Gastric cancer	Controls	75	65	8	0.27	0.202	Japan	(11)
	Cases	126	112	51	0.37	4.1×10^{-3}		
Alzheimer's disease	Controls	172	168	60	0.36	0.077	China	(12)
	Cases	150	161	89	0.42	4.37×10^{-4}		

Acknowledgments

The author has no financial support to disclose with respect to this manuscript and declares no conflict of interest. The author would like to thank Dr. Bravo for critically reading this letter.

References

1. Hardy GH. Mendelian proportions in a mixed population. Science. 1908; 28 (706): 49-50.
2. Weinberg W. About proof of heredity in humans. Germany: The association for national natural history in württemberg; 1908; 64: 368-382.
3. Piel FB, Adamkiewicz TV, Amendah D, Williams TN, Gupta S, Grosse SD. Observed and expected frequencies of structural hemoglobin variants in newborn screening surveys in Africa and the Middle East: deviations from Hardy-Weinberg equilibrium. Genet Med. 2016; 18(3): 265-274.
4. Wahlund S. Composition of population and correlation phenomenon from the viewpoint of heredity. Hereditas. 1928; 11: 65-106.
5. Falconer DS, Mackay TFC. Introduction to quantitative genetics. Oxford: Blackwell's Oxford; 1996.
6. Ermiş Karaali Z, Candan G, Aktuğlu MB, Velet M, Ergen A. Toll-like receptor 2 (TLR-2) gene polymorphisms in type 2 diabetes mellitus. Cell J. 2019; 20(4): 559-563.
7. Royo JL, Alarcón-Martín E, Díaz-Fuentes J, Colmenero JD, Bravo MJ. Discordance in TLR2 (-196 to -174) polymorphism effect on HIV infection risk. J Gene Med. 2018; 20(10-11): e3051.
8. Cannings C, Edwards AW. Natural selection and the De Finetti diagram. Ann Hum Genet. 1968; 31(4): 421-428.
9. Kalinderi K, Bostantjopoulou S, Katsarou Z, Fidani L. TLR9 -1237 T/C and TLR2 -194 to -174 del polymorphisms and the risk of Parkinson's disease in the Greek population: a pilot study. Neurol Sci. 2013; 34(5): 679-682.
10. Lewandowska M, Garczyńska P, Jędrychowska-Dańska K, Kopczyńska P, Masłowska A, Witas H. Frequency of P2RX7 A1513C and TLR2 -196 to -174 ins/del in healthy Polish individuals. Int J Immunogenet. 2015; 42(3): 195-199.
11. Tahara T, Arisawa T, Wang F, Shibata T, Nakamura M, Sakata M, et al. Toll-like receptor 2 -196 to 174del polymorphism influences the susceptibility of Japanese people to gastric cancer. Cancer Sci. 2007; 98(11): 1790-1794.
12. Yu JT, Mou SM, Wang LZ, Mao CX, Tan L. Toll-like receptor 2 -196 to -174 del polymorphism influences the susceptibility of Han Chinese people to Alzheimer's disease. J Neuroinflammation. 2011; 8: 136.

Advisory Board of Cell Journal(Yakhteh)
Vol 22, No 1-4, 2020-2021

Inanloo K

J

Jafari F
Jafarian A
Jafarinia M
Janati Esfahani A
Javan M
Javeri A
Javid A
Jitpean S

K

Kafi M
Kalantar K
Kathem S
Kumar Kaushik N
Kavianpour M
Kazemi B
Khademi F
Khalili S
Khamisipour G
Khazaei M
Kheiripour N
Khochbin S
Khodababandehloo H
Khodadi E
Khoei S
Khoshzaban A
Kido T
Koruji M
Kraus A
Kumar V
Kumar M
Kumar Mageswaran S

L

Larti F
Li Y
Li M
Lotti F
Lu G
Lu H

M

Maali A
Mahmoud K
Mahmoudi A
Mahmoudi F
Mahmoudzadeh-Sagheb M
Mansouri V
Mashadi Sh
Maziar A
Mehrabani M
Mehrabi S
Memar R
Mirdrikvand M
Mirfakhraie R
Mirnajafi-Zadeh J
Mirzaee R
Mirzaei L
Mobasher P
Mobini GR
Moghadasali R
Mohammadali F
Mohammadi M
Mohammadi S
Moharamzadeh S
Moharrami T
Mokaram P
Montazeri L
Moradi S
Moshkdanian G
Motalleb G
Motevaseli E
Movaghar B
Mozdarani H

N

Nabavi SM
Najafi A
Naji M
Najjari M
Nasiri S
Nasr-Esfahani MH
Nazemalhosseini-Mojarad E
Nejad Dehbashi F
Nejatbakhsh R
Nikanfar S
Nikbakht M
Nematollahi-Mahani SN
Nourbakhsh M

O

Obeidi N
Ohkawara B
Okada S
Omrani D

P

Parham A
Parian M
Pergialiotis V
Peymani M
Pourabolii I
Pourhoseingholi MA
Pourkhodadad S
Pourhasan-Moghaddam M
Pourtahmasebi V

Q

Qie S

R

Rafieemehr H
Rahbarghazi R
Rahbarizadeh F
Rahim F
Rahimipour A
Rajabzadeh A
Ramezani M
Ranjbar A
Ranji N
Rasouli H
Razavi S
Razban V

Index by Authors in Cell Journal(Yakhteh)
Vol 22, No 1-4, 2020-2021